

NO-A191 284

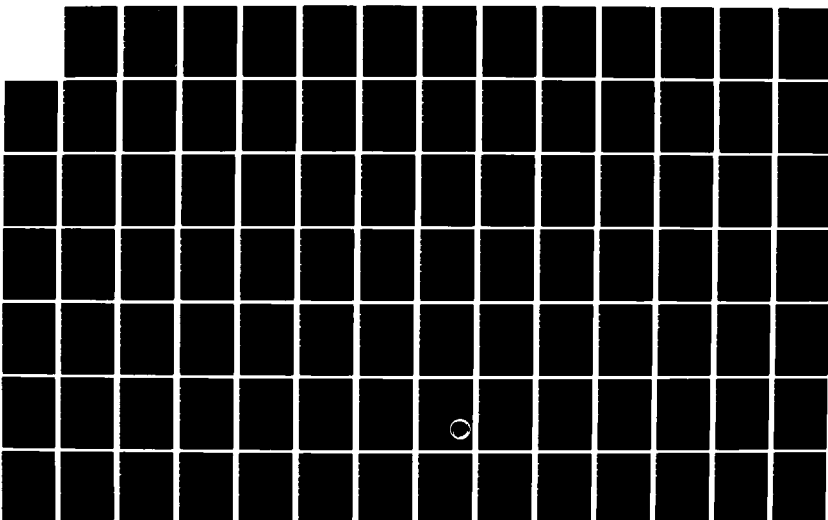
UNITED STATES AIR FORCE SUMMER FACULTY RESEARCH PROGRAM
(1987) PROGRAM TE. (U) UNIVERSAL ENERGY SYSTEMS INC
DAYTON OH R C DARRAH ET AL DEC 87 AFOSR-TR-88-0213
F49628-85-C-0013

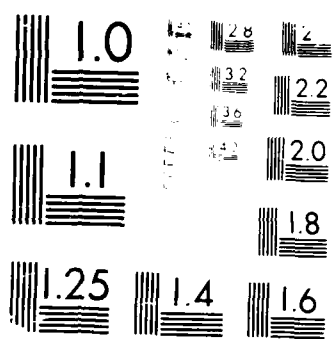
1/11

UNCLASSIFIED

F/G 5/1

NL





MICROCOPY RESOLUTION TEST - HART

AD-A191284

UNITED STATES AIR FORCE
SUMMER FACULTY RESEARCH PROGRAM
1987
PROGRAM TECHNICAL REPORT
UNIVERSAL ENERGY SYSTEMS, INC.
VOLUME II of III

Program Director, UES
Rodney C. Darrah

Program Manager, AFOSR
Major Richard Kopka

Program Administrator, UES
Susan K. Espy

Submitted to
Air Force Office of Scientific Research
Bolling Air Force Base
Washington, DC

December 1987

DTIC
ELECTE
MAR 01 1988
H

DISTRIBUTION STATEMENT A

Approved for public release
Distribution Unlimited

WFO 101 A-1A

TABLE OF CONTENTS

<u>SECTION</u>	<u>PAGE</u>
Preface	i
List Of Participants	ii
Participant Laboratory Assignment	xxviii
Research Reports	xxxiii



Accession For	
NTIS GRA&I	<input checked="" type="checkbox"/>
DTIC TAB	<input type="checkbox"/>
Unannounced	<input type="checkbox"/>
Justification	
By	
Distribution/	
Availability Codes	
Dist	Avail and/or Special
A-1	

REPORT DOCUMENTATION PAGE

Form Approved
OMB No. 0704-0188

1a. REPORT SECURITY CLASSIFICATION			1b. RESTRICTIVE MARKINGS		
2a. SECURITY CLASSIFICATION AUTHORITY			3. DISTRIBUTION / AVAILABILITY OF REPORT Approved for public release; distribution unlimited.		
2b. DECLASSIFICATION / DOWNGRADING SCHEDULE					
4. PERFORMING ORGANIZATION REPORT NUMBER(S)			5. MONITORING ORGANIZATION REPORT NUMBER(S) AFOSR-TK- 88-0213		
6a. NAME OF PERFORMING ORGANIZATION Universal Energy Systems Inc.		6b. OFFICE SYMBOL (If applicable)		7a. NAME OF MONITORING ORGANIZATION AFOSR/XOT	
6c. ADDRESS (City, State, and ZIP Code) 4401 Dayton-Xenia Road Dayton, OH 45432			7b. ADDRESS (City, State, and ZIP Code) Building 410 Bolling AFB DC 20332-6448		
8a. NAME OF FUNDING / SPONSORING ORGANIZATION Same as #7		8b. OFFICE SYMBOL (If applicable)		9. PROCUREMENT INSTRUMENT IDENTIFICATION NUMBER F49620-85-C-0013	
8c. ADDRESS (City, State, and ZIP Code) Same as #7			10. SOURCE OF FUNDING NUMBERS		
			PROGRAM ELEMENT NO 61102F	PROJECT NO 3396	TASK NO D5
11. TITLE (Include Security Classification) USAF Summer Faculty Research Program - Volume 2 - 1987					
12. PERSONAL AUTHOR(S) Rodney C. Darrah, Susan K. Espy					
13a. TYPE OF REPORT Annual		13b. TIME COVERED FROM _____ TO _____		14. DATE OF REPORT (Year, Month, Day) December 1987	
15. PAGE COUNT					
16. SUPPLEMENTARY NOTATION					
17. COSATI CODES			18. SUBJECT TERMS (Continue on reverse if necessary and identify by block number)		
FIELD	GROUP	SUB-GROUP			
19. ABSTRACT (Continue on reverse if necessary and identify by block number) See Attached					
20. DISTRIBUTION / AVAILABILITY OF ABSTRACT <input checked="" type="checkbox"/> UNCLASSIFIED/UNLIMITED <input type="checkbox"/> SAME AS RPT <input type="checkbox"/> DTIC USERS			21. ABSTRACT SECURITY CLASSIFICATION UNCLASSIFIED		
22a. NAME OF RESPONSIBLE INDIVIDUAL LT. COL. CLAUDE CAVENDER			22b. TELEPHONE (Include Area Code) 202-767-4970		22c. OFFICE SYMBOL XOT

1. INTRODUCTION

Universal Energy Systems, Inc. (UES) was awarded the United States Air Force Summer Faculty Research Program on August 15, 1984. The contract is funded under the Air Force Systems Command by the Air Force Office of Scientific Research.

The program has been in existence since 1978 and has been conducted by several different contractors. The success of the program is evident from its history of expansion since 1978.

The Summer Faculty Research Program (SFRP) provides opportunities for research in the physical sciences, engineering, life sciences, business, and administrative sciences. The program has been effective in providing basic research opportunities to the faculty of universities, colleges, and technical institutions throughout the United States.

The program is available to faculty members in all academic grades: instructor, assistant professor, professor, department chairman, and research facility directors. It has proven especially beneficial to young faculty members who are starting their academic research programs and to senior faculty members who have spent time in university administration and are desirous of returning to scholarly research programs.

Beginning with the 1982 program, research opportunities were provided for 17 graduate students. The 1982 pilot student program was highly successful and was expanded in 1983 to 53 students; there were 84 graduate students in the 1984 program.

In the previous programs, the graduate students were selected along with their professors to work on the program. Starting with the 1985 program, the graduate students were selected on their own merits. They were assigned to be supervised by either a professor on the program or by an engineer at the Air Force Laboratories participating in the program. There were 92 graduate students selected for the 1985 program.

Again in the 1986 program, the graduate students were selected on their own merits, and assigned to be supervised by either a professor on the program or by an engineer at the participating Air Force Laboratory. There were 100 graduate students selected for the 1986 program.

Follow-on research opportunities have been developed for a large percentage of the participants in the Summer Faculty Research Program in 1979-1983 period through an AFOSR Minigrant Program.

On 1 September 1983, AFOSR replaced the Minigrant Program with a new Research Initiation Program. The Research Initiation Program provides follow-on research awards to home institutions of SFRP participants. Awards were made to approximately 50 researchers in 1983. The awards were for a maximum of \$12,000 and a duration of one year or less. Substantial cost sharing by the schools contributes significantly to the value of the Research Initiation Program. In 1984 there were approximately 80 Research Initiation awards.

PREFACE

The United States Air Force Summer Faculty Research Program (USAF-SFRP) is a program designed to introduce university, college, and technical institute faculty members to Air Force research. This is accomplished by the faculty members being selected on a nationally advertised competitive basis for a ten-week assignment during the summer intersession period to perform research at Air Force laboratories/centers. Each assignment is in a subject area and at an Air Force facility mutually agreed upon by the faculty members and the Air Force. In addition to compensation, travel and cost of living allowances are also paid. The USAF-SFRP is sponsored by the Air Force Office of Scientific Research, Air Force Systems Command, United States Air Force, and is conducted by Universal Energy Systems, Inc.

The specific objectives of the 1987 USAF-SFRP are:

- (1) To provide a productive means for Scientists and Engineers holding Ph.D. degrees to participate in research at the Air Force Weapons Laboratory;
- (2) To stimulate continuing professional association among the Scholars and their professional peers in the Air Force;
- (3) To further the research objectives of the United States Air Force;
- (4) To enhance the research productivity and capabilities of Scientists and Engineers especially as these relate to Air Force technical interests.

During the summer of 1987, 159-faculty members participated. These researchers were assigned to 25 USAF laboratories/centers across the country. This three volume document is a compilation of the final reports written by the assigned faculty members about their summer research efforts.

LIST OF 1987 PARTICIPANTS

NAME/ADDRESS	DEGREE, SPECIALTY, LABORATORY ASSIGNED
Dr. Suresh K. Aggarwal Assistant Professor Dept. of Mechanical Eng. Univ. of Illinois at Chicago P O Box 4348 Chicago, IL 60680 (312) 996-2235/5317	<u>Degree:</u> Ph.D., Aerospace Eng., 1979 <u>Specialty:</u> Aerospace Engineering <u>Assigned:</u> APL
Dr. Gurbux S. Alag Associate Professor Dept. of Electrical Eng. Western Michigan University 1940 Howard Street, #410 Kalamazoo, MI 49008 (616) 383-1538	<u>Degree:</u> Ph.D., Systems Eng., 1976 <u>Specialty:</u> Systems Engineering <u>Assigned:</u> RPL
Dr. John W. Amoss Associate Professor Dept. of Systems Science University of West Florida Pensacola, FL 32514 (904) 474-2547	<u>Degree:</u> Ph.D., Electrical Eng., 1972 <u>Specialty:</u> Electrical Engineering <u>Assigned:</u> AL
Dr. Victor H. Appel Associate Professor Dept. of Educational Psychology Univ. of Texas at Austin Austin, TX 78712 (512) 471-4155	<u>Degree:</u> Ph.D., Psychology, 1959 <u>Specialty:</u> Psychology <u>Assigned:</u> HRL/MO
Dr. Xavier J.R. Avula Associate Professor Dept. of Engineering Mechanics University of Missouri-Rolla Rolla, MO 65401 (314) 341-4585	<u>Degree:</u> Ph.D., Engineering Mechanics 1968 <u>Specialty:</u> Engineering Mechanics <u>Assigned:</u> HRL/MO
Dr. Francesco L. Bacchialoni Associate Professor Dept. of Electrical Engineering University of Lowell 1 University Avenue Lowell, MA 02173 (617) 452-5000	<u>Degree:</u> Ph.D., Ingegneria, 1946 <u>Specialty:</u> Engineering Mechanics <u>Assigned:</u> HRL/MO

Dr. Praphulla K. Bajpai
Professor
Dept. of Biology
University of Dayton
300 College Park
Dayton, OH 45469
(513) 229-3029

Degree: Ph.D., Immunophysiology,
1965
Specialty: Immunology
Assigned: AAMRL

Dr. Vernon L. Bakke
Associate Professor
Dept. of Math. Science
University of Arkansas
Fayetteville, AR 72701
(501) 575-4531

Degree: Ph.D., Mathematics, 1971
Specialty: Mathematics
Assigned: AL

Dr. Shankar S. Bale
Professor
Dept. of Science and Math
Saint Paul's College
Lawrenceville, VA 23868-1299
(804) 848-3111

Degree: Ph.D., Genetics, 1971
Specialty: Genetics
Assigned: AAMRL

Dr. William W. Bannister
Professor
Dept. of Chemistry
University of Lowell
Lowell, MA 01824
(617) 452-5000

Degree: Ph.D., Organic Chemistry,
1961
Specialty: Organic Chemistry
Assigned: ESC

Prof. Beryl L. Barber
Assistant Professor
Dept. of Electronic Eng. Tech.
Oregon Institute of Technology
3201 Campus Drive
Klamath Falls, OR 97601-7791
(503) 882-6321

Degree: MS, Electronic Eng., 1961
Specialty: Electrical Engineering
Assigned: RADC

Dr. William M. Bass
Professor
Dept. of Anthropology
The University of Tennessee
252 South Stadium Hall
Knoxville, TN 37996
(615) 974-4408

Degree: Ph.D., Physical Anthropology
1961
Specialty: Physical Anthropology
Assigned: ESC

Dr. Bryan R. Becker
Associate Professor
Dept. of Mechanical Engineering
Rose-Hulman Institute
5500 Wabash Avenue
Terre Haute, IN 47803
(812) 877-1511

Degree: Ph.D., Engineering Science,
1979
Specialty: Engineering Science
Assigned: APL

Dr. Charles Bell
Professor
Dept. of Engineering
Arkansas State University
P O Drawer 1080
State University, AR 72467-1080
(501) 972-2088

Degree: Ph.D., Mechanical Eng.,
1965
Specialty: Mechanical Engineering
Assigned: AD

Prof. Kweku K. Bentil
Associate Professor
School of Building Construction
University of Florida
Gainesville, FL 32611
(904) 392-5965

Degree: M.S., Building Construction,
1975
Specialty: Building Construction
Assigned: LMC

Dr. David E. Betounes
Associate Professor
Mathematics Department
Univ. of Southern Mississippi
S.S. Box 5045
Hattiesburg, MS 39406-5045
(601) 266-4293

Degree: Ph.D., Mathematics, 1978
Specialty: Mathematics
Assigned: AD

Prof. Phillip A. Bishop
Assistant Professor
Area of HPER
University of Alabama
Tuscaloosa, AL 35487-9909
(205) 348-8370

Degree: Ed.D., Exercise Physiology,
1983
Specialty: Exercise Physiology
Assigned: SAM

Dr. Jerome W. Blaylock
Associate Professor
Dept. of Computing & A.S.
Texas Southern University
3100 Cleburne Avenue
Houston, TX 77004
(713) 527-7011

Degree: Ph.D., Computer Science,
1982
Specialty: Computer Science
Assigned: LMC

Dr. John W. Bopp
Assistant Professor
Dept. of Chemistry
Nazareth College
4245 East Avenue
Rochester, NY 14610
(716) 586-2525

Degree: Ph.D., Chemistry, 1984
Specialty: Computer Science
Assigned: AD

Dr. Kevin Bowyer
Assistant Professor
Dept. of Computer Sci. & Eng.
University of South Florida
4202 E. Fowler Avenue
Tampa, FL 33620
(813) 974-3032

Degree: Ph.D. Computer Science, 1980
Specialty: Computer Science
Assigned: RADC

Mr. Lee I. Britt
Instructor
Dept. of Physics
Grambling State University
Grambling, LA 71245
(318) 274-2575

Degree: M.S., Physics, 1978
Specialty: Physics
Assigned: AEDC

Mr. Richard H. Brown
Associate Professor
Dept. of Biology
Ouachita Baptist University
Box 3686
Arkadelphia, PA 71923
(501) 246-4531

Degree: M.S., Physiology, 1963
Specialty: Physiology
Assigned: OEHL

Dr. Robert A. Buchl
Assistant Professor
Dept. of Physics & Astronomy
Univ. of Wisconsin-Eau Claire
Eau Claire, WI 54702-4004
(715) 836-2272

Degree: Ph.D., Physics, 1971
Specialty: Physics
Assigned: AD

Dr. Charles M. Bump
Assistant Professor
Dept. of Chemistry
Hampton University
P O Box 6483
Hampton, VA 23668
(804) 727-5330

Degree: Ph.D., Organic Chemistry,
1979
Specialty: Organic Chemistry
Assigned: FJSRL

Dr. Allan R. Burkett
Associate Professor
Dept. of Chemistry
Dillard University
2601 Gentilly Blvd.
New Orleans, LA 70122
(504) 283-8822

Degree: Ph.D., Inorganic Chemistry,
1972
Specialty: Inorganic Chemistry
Assigned: RPL

Dr. Ronald V. Canfield
Professor
Dept. of Applied Science
Utah State University
UMC 42002601 Gentilly Blvd.
Utah State University, UT 84233
(801) 750-2434

Degree: Ph.D., Statistics, 1975
Specialty: Statistics
Assigned: RADC

Dr. Patricia A. Carlson
Professor/Director
Dept. of Humanities
Rose-Hulman Inst. of Technology
5500 Wawash Avenue
Terre Haute, IN 47803
(812) 877-1511

Degree: Ph.D., Literature/Language,
1973
Specialty: Literature/Language
Assigned: HRL/LR

Dr. Kwo-Sun Chu
Chairman
Dept. of Physics & Comput. Sci.
Talladega College
Talladega, AL 35160
(205) 362-0206

Degree: Ph.D., Theoretical Physics,
1974
Specialty: Theoretical Physics
Assigned: ML

Dr. David Y. Chung
Professor
Dept. of Physics
Howard University
Washington, DC 20059
(202) 636-7903

Degree: Ph.D., Physics, 1966
Specialty: Theoretical Physics
Assigned: FJSRL

Dr. Robert W. Courter
Associate Professor
Dept. of Mechanical Engineering
Louisiana State University
CEBA 2513D
Baton Rouge, LA 70803
(504) 388-5891

Degree: Ph.D., Aerospace Eng., 1965
Specialty: Aerospace Engineering
Assigned: AD

Dr. Bruce A. Craver
Associate Professor
Dept. of Physics
University of Dayton
300 College Park
Dayton, OH 45469
(513) 229-2219

Degree: Ph.D., Physics, 1976
Specialty: Physics
Assigned: ML

Prof. William K. Curry
Assistant Professor
Dept. of Computer Science
Rose-Hulman Inst. of Technology
5500 Wabash Ave.
Terre Haute, IN 47803
(812) 877-1511

Degree: M.S., Computer Sci., 1976
Specialty: Computer Science
Assigned: AL

Dr. Phanindramohan Das
Professor
Dept. of Meteorology
Texas A&M University
College Station, TX 77843
(409) 845-0633

Degree: Ph.D., Meteorology, 1963
Specialty: Meteorology
Assigned: ESD

Dr. Bruce A. DeVantier
Assistant Professor
Dept. of Civil Eng. & Mechanics
S. Illinois University
Carbondale, IL 62901
(618) 536-2368

Degree: Ph.D., Civil Eng., 1983
Specialty: Civil Engineering
Assigned: ML

Dr. Elvis E. Deal
Assistant Professor
Dept. of Industrial Engineering
University of Houston
4800 Calhoun
Houston, TX 77004
(713) 749-4487

Degree: Ph.D., Industrial Eng., 1985
Specialty: Industrial Engineering
Assigned: OEHL

Dr. Suhrit K. Dey
Professor
Dept. of Mathematics
Eastern Illinois University
Charleston, IL 61920
(217) 581-3217

Degree: Ph.D., Aerospace Eng., 1970
Specialty: Aerospace Engineering
Assigned: AEDC

Dr. Ronna E. Dillon
Professor
Depts. of Educational Psychology
and Psychology
Southern Illinois University
Carbondale, IL 62901
(618) 536-7763

Degree: Ph.D., Educational
Psychology, 1978
Specialty: Educational Psychology
Assigned: HRL/MO

Dr. Ravinder Diwan
Professor
Dept. of Mechanical Engineering
Southern University
Baton Rouge, LA 70813
(504) 771-4701

Degree: Ph.D., Metallurgy, 1973
Specialty: Metallurgy
Assigned: ML

Dr. Verlynda S. Dobbs
Assistant Professor
Dept. of Computer Science
Wright State University
414 Fawcett
Dayton, OH 45435
(513) 873-2491

Degree: Ph.D., Computer Sci., 1985
Specialty: Computer Science
Assigned: AL

Dr. F. Carroll Dougherty
Assistant Professor
Dept. of Aerospace Engineering
University of Colorado
Campus Box 429
Boulder, CO 80309
(303) 492-8464

Degree: Ph.D., Aeronautical/
Astronautical Engr., 1985
Specialty: Aerospace Engineering
Assigned: AEDC

Dr. John M. Dunn
Assistant Professor
Dept. of Elec. & Compt. Eng.
University of Colorado
Campus Box 425
Boulder, CO 80309
(303) 492-5487

Degree: Ph.D., Applied Physics, 1984
Specialty: Applied Physics
Assigned: RADC

Dr. Thomas A.W. Dwyer
Associate Professor
Dept. of Aero & Astro Eng.
University of Illinois
104 S. Mathews Avenue
Urbana, IL 61801
(217) 244-0720

Degree: Ph.D., Mathematics, 1971
Specialty: Mathematics
Assigned: WL

Dr. Kiah Edwards
Professor
Dept. of Biology
Texas Southern University
3100 Cleburne Street
Houston, TX 77004
(713) 527-7829

Degree: Ph.D., Molecular Biology,
1974
Specialty: Molecular Biology
Assigned: OEHL

Dr. Marco A. Egoavil
Associate Professor
Dept. of Mechanical Engineering
University of Puerto Rico
Mayaguez, PR 00709
(809) 834-4040

Degree: Ph.D., Mechanical Eng., 1981
Specialty: Mechanical Engineering
Assigned: AEDC

Dr. Ira Elder
Professor
Dept. of Mathematical Sciences
Eastern New Mexico University
Portales, NM 88130
(505) 356-6208

Degree: Ph.D., Applied Mathematics
1979
Specialty: Applied Mathematics
Assigned: WL

Dr. Ramez Elmasri
Assistant Professor
Dept. of Computer Science
Univ. of Houston
Houston, TX 77036
(713) 749-2630

Degree: Ph.D., Computer Science,
1980
Specialty: Computer Science
Assigned: RADC

Dr. John E. Erdei
Assistant Professor
Dept. of Physics
University of Dayton
Dayton, OH 45469
(513) 229-2318

Degree: Ph.D., Condensed Matter,
1983
Specialty: Physics
Assigned: APL

Dr. Joseph J. Feeley
Associate Professor
Dept. of Electrical Engineering
University of Idaho
Moscow, ID 83843
(208) 885-7482

Degree: Ph.D., Electrical Eng., 1980
Specialty: Electrical Engineering
Assigned: AD

Dr. Wilton Flemon
Associate Professor
Dept. of Chemistry
Metropolitan State College
Denver, CO 80204
(303) 556-2838

Degree: Ph.D., Physical Organic
Chemistry, 1970
Specialty: Physical Organic Chemistry
Assigned: RPL

Dr. Dennis R. Flentge
Associate Professor
Dept. of Math/Science
Cedarville College
Box 601
Cedarville, OH 45314-0601
(513) 766-2211

Degree: Ph.D., Physical Chemistry,
1974
Specialty: Physical Chemistry
Assigned: APL

Dr. Luther D. Flippen, Jr.
Assistant Professor
Dept. of Mechanical and
Nuclear Engineering
Mississippi State University
P O Drawer ME
Mississippi State, MS 39759
(601) 325-3412

Degree: Ph.D., Mechanical Eng., 1982
Specialty: Mechanical Engineering
Assigned: RPL

Dr. Lee A. Flippin
Assistant Professor
Dept. of Chemistry
San Francisco State Univ.
San Francisco, CA 94132
(415) 469-1627

Degree: Ph.D., Organic Chemistry,
1980
Specialty: Organic Chemistry
Assigned: AFGL

Dr. Lionel R. Friedman
Professor
Dept. of Electrical Eng.
Worcester Polytechnic Inst.
100 Institute Road
Worcester, MA 01609
(415) 469-1627

Degree: Ph.D., Physics, 1961
Specialty: Physics
Assigned: RADC

Dr. John W. Gilmer
Assistant Professor
Polymer Science Program
Penn State University
University Park, PA 16802
(814) 863-1487

Degree: Ph.D., Physical Chemistry,
1984
Specialty: Physical Chemistry
Assigned: ML

Dr. Stephen J. Gold
Associate Professor
Dept. of Electrical Engineering
South Dakota State University
P O Box 2220
Brookings, SD 57007
(605) 688-4419

Degree: Ph.D., Electrical Eng., 1969
Specialty: Electrical Engineering
Assigned: FJSRL

Dr. Michael R. Gorman
Assistant Professor
Dept. of Engineering Mechanics
Univ. of Lincoln-Nebraska
216 Bancroft Hall
Lincoln, NE 68588-0347
(402) 472-2397

Degree: Ph.D., Physics, 1981
Specialty: Physics
Assigned: RPL

Dr. Benjamin Gottlieb
Professor
Dept. of Science
Bishop College
3837 Simpson Stuart Road
Dallas, TX 75042
(214) 372-8773

Degree: Ph.D., Physics, 1964
Specialty: Physics
Assigned: AFGL

Dr. Gary M. Graham
Assistant Professor
Dept. of Mechanical Engineering
Ohio University
261 Stocker
Athens, OH 45701
(614) 593-1556

Degree: Ph.D., Mechanical Eng., 1985
Specialty: Mechanical Engineering
Assigned: FDL

Mr. William M. Grissom
Assistant Professor
Dept. of Physics
Morehouse College
630 Westview Dr., S.W.
Atlanta, GA 30314
(404) 681-2800

Degree: M.S., Mechanical Eng., 1978
Specialty: Mechanical Engineering
Assigned: AEDC

Dr. Timothy A. Grogan
Assistant Professor
Dept. of Electrical and
Computer Engineering
University of Cincinnati
ML#30 898 Rhodes Hall
Cincinnati, OH 45245
(513) 475-2349

Degree: Ph.D., Electrical Eng., 1983
Specialty: Electrical Engineering
Assigned: RADC

Dr. David Ludwig
Assistant Professor
Dept. of Mathematics
Univ. of North Carolina
Greensboro, NC 27412-5001
(919) 334-5749

Degree: Ph.D., Mathematics, 1971
Specialty: Mathematics
Assigned: SAM

Dr. Mohammed Maleque
Associate Professor
Dept. of Pharmacology
Meharry Medical College
Nashville, TN 37208
(615) 327-6510

Degree: Ph.D., Pharmacology, 1976
Specialty: Pharmacology
Assigned: SAM

Dr. Robert Masingale
Professor
Dept. of Sciences and Math
Jarvis Christian College
Hawkins, TX 75765
(214) 769-2174

Degree: Ph.D., Chemistry, 1966
Specialty: Chemistry
Assigned: FJSRL

Dr. Michael Matthews
Assistant Professor
Dept. of Behavioral Sciences
Drury College
Springfield, MO 65802
(417) 865-8731

Degree: Ph.D., Psychology, 1984
Specialty: Psychology
Assigned: HRL/MO

Dr. Alastair McAulay
Professor
Dept. of Electrical Engineering
Wright State University
Dayton, OH 45440
(513) 873-2167

Degree: Ph.D., Electrical Eng., 1974
Specialty: Electrical Engineering
Assigned: AL

Dr. Barry McConnell
Assistant Professor
Dept. of Computer & Info Sci.
Florida A&M University
Tallahassee, FL 32307
(904) 599-3022

Degree: Ph.D., Computer Sci., 1984
Specialty: Computer Science
Assigned: WL

Mr. Oliver McGee
Sr. Research Associate
Dept. of Civil Engineering
Ohio State University
Gahanna, OH 43230
(614) 476-5035

Degree: M.S., Eng. Mechanics, 1983
Specialty: Engineering Mechanics
Assigned: FDL

Dr. Daniel Mihalko
Associate Professor
Dept. of Math & Statistics
Western Michigan University
Kalamazoo, MI 49008
(616) 383-6165

Degree: Ph.D., Math Statistics, 1977
Specialty: Math Statistics
Assigned: SAM

Mr. Augustus Morris
Mathematics Instructor
Dept. of Natural Sciences
Wilberforce University
Wilberforce, OH 45426
(513) 376-2911

Degree: B.S., Biomedical Eng., 1981
Specialty: Biomedical Engineering
Assigned: AAMRL

Dr. Mary Morton-Gibson
Associate Professor
Dept. of Chemistry/Physics
Lock Haven University
Lock Haven, PA 17745
(717) 893-2054

Degree: Ph.D., Physiology, 1970
Specialty: Physiology/Biophysics
Assigned: SAM

Dr. Lena Myers
Professor
Dept. of Sociology/Social Psych.
Jackson State University
Jackson, MS 39217
(601) 968-2591

Degree: Ph.D., Sociology, 1973
Specialty: Sociology
Assigned: DEOMI

Dr. James Nail
Associate Professor
Dept. of Engineering
Mississippi State Univ.
Mississippi State, MS 39762
(601) 325-3665

Degree: Ph.D., Electrical Eng., 1976
Specialty: Electrical Engineering
Assigned: AD

Dr. Henry Nebel
Associate Professor
Dept. of Physics
Alfred University
Alfred, NY 14802
(607) 871-2208

Degree: Ph.D., Physics, 1967
Specialty: Physics
Assigned: AFGL

Dr. Maurice Neveu
Associate Professor
Dept. of Chemistry
State University College
Fredonia, NY 14063
(716) 673-3285

Degree: Ph.D., Chemistry, 1959
Specialty: Physical/Organic Chemistry
Assigned: FJSRL

Dr. James Noyes
Associate Professor
Dept. of Math & C.S.
Wittenberg University
Springfield, OH 45501
(716) 673-3285

Degree: Ph.D., Computer Sci., 1977
Specialty: Computer Science
Assigned: AL

Dr. Noel Nussbaum
Associate Professor
Dept. of Biology
Wright State University
Dayton, OH 45401-0927
(513) 426-8935

Degree: Ph.D., Biology, 1964
Specialty: Biology
Assigned: AAMRL

Dr. Thomas Nygren
Associate Professor
Dept. of Psychology
Ohio State University
Columbus, OH 43221
(614) 486-7931

Degree: Ph.D., Psychology, 1975
Specialty: Psychology
Assigned: AAMRL

Dr. Kurt Oughstun
Assistant Professor
Dept. of Electrical/Computer
Engineering
University of Wisconsin
Madison, WI 53705
(608) 231-3126

Degree: Ph.D., Optics, 1979
Specialty: Optical Sciences
Assigned: SAM

Dr. Surgounda Patil
Professor
Dept. of Math
Tennessee Technical University
Cookeville, TN 38501
(615) 528-6924

Degree: Ph.D., Math Stat., 1966
Specialty: Math Statistics
Assigned: AEDC

Dr. Martin Patt
Associate Professor
Dept. of Electrical Engineering
University of Lowell
Lowell, MA 01854
(617) 452-5000

Degree: M.S., Electrical Eng., 1964
Specialty: Electrical Engineering
Assigned: AFGL

Dr. William Patten
Assistant Professor
Dept. of Mechanical Eng.
University of Iowa
Iowa City, IA 52242
(319) 335-5675

Degree: Ph.D., Mechanical Eng., 1986
Specialty: Mechanical Engineering
Assigned: FDL

Dr. Ralph Peters
Associate Professor
Dept. of Biology
Wichita State University
Wichita, KS 67217
(316) 943-8762

Degree: Ph.D., Zoophysiology, 1975
Specialty: Zoology
Assigned: SAM

Dr. Randall Peters
Associate Professor
Dept. of Physics
Texas Tech University
Lubbock, TX 79409
(806) 742-3757

Degree: Ph.D., Physics, 1968
Specialty: Physics
Assigned: WL

Dr. Gerald Pollack
Professor
Dept. of Physics/Astronomy
Michigan State University
East Lansing, MI 48823
(517) 353-9590

Degree: Ph.D., Physics, 1968
Specialty: Physics
Assigned: SAM

Dr. Spencer Porter
Professor
Dept. of Chemistry
Capital University
Columbus, OH 43209
(614) 236-6107

Degree: Ph.D., Phys. Chemistry, 1968
Specialty: Physical Chemistry
Assigned: ML

Dr. Leonard Price
Chairman
Dept. of Chemistry
Xavier Univ. of Louisiana
New Orleans, LA 77012
(504) 486-7411

Degree: Ph.D., Org. Chemistry, 1962
Specialty: Organic Chemistry
Assigned: SAM

Dr. Stephen Pruett
Assistant Professor
Dept. of Biological Sciences
Mississippi State University
Mississippi, MS 39762
(601) 325-3120

Degree: Ph.D., Immunology, 1980
Specialty: Immunology
Assigned: SAM

Dr. Panapkkam Ramamoorthy
Associate Professor
Dept. of Electrical/Computer Eng.
University of Cincinnati
Cincinnati, OH 45221
(513) 475-4247

Degree: Ph.D., Digital Signal
Process, 1977
Specialty: Electrical Engineering
Assigned: RADC

Dr. Gandikota Rao
Professor
Dept. of Meteorology
St. Louis University
St. Louis, MO 63156
(314) 658-3115

Degree: Ph.D., Meteorology, 1965
Specialty: Meteorology
Assigned: AFGL

Dr. Donald Robertson
Associate Professor
Dept. of Psychology
Indiana University of PA
Indiana, PA 15705
(412) 357-4522

Degree: Ph.D., Psychology, 1981
Specialty: Psychology
Assigned: AAMRL

Dr. Kenneth Roenker
Associate Professor
Dept. of Electrical/Computer Eng.
University of Cincinnati
Cincinnati, OH 45221
(513) 475-4461

Degree: Ph.D., Solid State Physics,
1973
Specialty: Solid State Physics
Assigned: AL

Dr. Ramendra Roy
Professor
Dept. of Nuclear Engineering
Arizona State University
Mesa, AZ 85202
(602) 838-0551

Degree: Ph.D., Nuclear Engr., 1975
Specialty: Nuclear Engineering
Assigned: APL

Dr. Paul Rybski
Assistant Professor
Dept. of Physics
University of Wisconsin
Whitewater, WI 53190-1790
(414) 472-5766

Degree: Ph.D., Astronomy, 1972
Specialty: Astronomy
Assigned: AFGL

Dr. Joseph Saliba
Assistant Professor
Dept. of Civil Engineering
University of Dayton
Dayton, OH 45469
(513) 229-3847

Degree: Ph.D., Solid Mechanics, 1983
Specialty: Solid Mechanics
Assigned: FDL

Dr. Richard Schori
Professor
Dept. of Mathematics
Oregon State University
Corvallis, OR 97331
(503) 754-4686

Degree: Ph.D., Mathematics, 1964
Specialty: Mathematics
Assigned: SAM

Dr. Lawrence Schovanec
Assistant Professor
Dept. of Mathematics
Texas Tech University
Lubbock, TX 79409
(806) 742-1424

Degree: Ph.D., Mathematics, 1964
Specialty: Mathematics
Assigned: RPL

Dr. William Schulz
Associate Professor
Dept. of Chemistry
Eastern Kentucky University
Richmond, KY 40475
(606) 622-1463

Degree: Ph.D., Chemistry, 1975
Specialty: Chemistry
Assigned: ESC

Dr. Nisar Shaikh
Assistant Professor
Dept. of Engr. Mechanics
Univ. of Nebraska
Lincoln, NE 68588-1347
(402) 472-2384

Degree: Ph.D., Mechanics, 1983
Specialty: Mechanics
Assigned: ML

Dr. Shiva Singh
Professor
Dept. of Mech. Engineering
Univ. of Kentucky
Lexington, KY 40506
(606) 257-3825

Degree: Ph.D., Mathematics, 1959
Specialty: Mathematics
Assigned: FDL

Dr. Gary Slater
Professor
Dept. of Aerospace Engineering
University of Cincinnati
Cincinnati, OH 45221
(513) 475-6287

Degree: Ph.D., Aerospace Engr., 1971
Specialty: Aerospace Engineering
Assigned: FDL

Dr. Timothy Su
Professor
Dept. of Physical Chemistry
Southeastern Massachusetts Univ.
North Dartmouth, MA 02790
(617) 999-8235

Degree: Ph.D., Physical Chem., 1971
Specialty: Physical Chemistry
Assigned: AFGL

Dr. David Sumberg
Associate Professor
Dept. of Electrical Engr.
Rochester Institute of Tech.
Rochester, NY 14618
(716) 475-6067

Degree: Ph.D., Physics, 1972
Specialty: Physics
Assigned: RADC

Dr. Wesley Tanaka
Associate Professor
Dept. of Chemistry
University of Wisconsin
Eau Claire, WI 54701
(715) 836-5388

Degree: Ph.D., Biochemistry, 1974
Specialty: Biochemistry
Assigned: SAM

Dr. Richard Tankin
Professor
Dept. of Mechanical Engr.
Northwestern University
Evanston, IL 60201
(312) 491-3532

Degree Ph.D., Mechanical Eng., 1960
Specialty: Mechanical Engineering
Assigned: APL

Dr. Joseph Tedesco
Assistant Professor
Dept. of Civil Engineering
Auburn University
Auburn, AL 36849
(205) 826-4320

Degree Ph.D., Civil Engr., 1982
Specialty: Civil Engineering
Assigned: ESC

Dr. Forrest Thomas
Professor
Dept. of Chemistry
University of Montana
Missoula, MT 59812
(406) 549-8205

Degree Ph.D., Chemistry, 1959
Specialty: Chemistry
Assigned: FDL

Dr. Howard Thompson
Professor
Dept. of Mechanical Engineering
Purdue University
W. Lafayette, IN 47907
(317) 494-5624

Degree Ph.D., Mech. Engr., 1965
Specialty: Mechanical Engineering
Assigned: FJSRL

Dr. David Townsend
Associate Professor
Dept. of Psychology
Montclair State College
Upper Montclair, NJ 07043
(201) 783-9407

Degree Ph.D., Cog. Psychology, 1972
Specialty: Cognitive Psychology
Assigned: HRL/LR

Dr. Michele Trankina
Assistant Professor
Dept. of Biology
St. Mary's University
San Antonio, TX 78284
(512) 436-3241

Degree Ph.D., Nutrit. Physiology
1982
Specialty: Nutritional Physiology
Assigned: SAM

Dr. Robert Trenary
Assistant Professor
Dept. of Computer Sci. & Math
Western Michigan University
Kalamazoo, MI 49008
(616) 383-6151

Degree Ph.D., Computer Science/Math
1987
Specialty: Computer Science
Assigned: AL

Dr. Dennis Truax
Assistant Professor
Civil Engineering
Dept. of Civil Engineering
Mississippi State University
Mississippi State, MS 39762
(601) 325-3050

Degree Ph.D., Civil Eng., 1986
Specialty: Civil Engineering
Assigned: ESC

Dr. John Uhlarik
Professor
Dept. of Psychology
Kansas State University
Manhattan, KS 66506
(913) 532-6850

Degree Ph.D., Psychology, 1970
Specialty: Psychology
Assigned: HRL/OT

Dr. P. Vaidya
Associate Professor
Dept. of Mechanical Engineering
Washington State Univ.
Pullman, WA 99164
(509) 335-7436

Degree Ph.D., Acoustics, 1969
Specialty: Acoustics
Assigned: ESC

Dr. Joseph Verducci
Assistant Professor
Dept. of Statistics
Ohio State University
Columbus, OH 43210
(614) 292-3886

Degree: Ph.D., Statistics, 1982
Specialty: Statistics
Assigned: OEHL

Dr. Robert Voigt
Associate Professor
Metallurgy
Dept. of Mechanical Engr.
University of Kansas
Lawrence, KS 66045
(913) 864-3181

Degree: Ph.D., Metallurgical Engr.,
1981
Specialty: Metallurgical Engineering
Assigned: ML

Dr. Keith Walker
Professor
Dept. of Physics
Point Loma College
San Diego, CA 92106
(619) 221-2374

Degree: Ph.D., Physics, 1971
Specialty: Physics
Assigned: AFGL

Dr. Richard Walker
Assistant Professor
Dept. of Mathematics
Fort Lewis College
Durango, CO 81302
(303) 247-7147

Degree: Ph.D., Math/Geophysics, 1979
Specialty: Mathematics
Assigned: AFGL

Dr. Jacob Weinberg
Professor
Dept. of Mathematics
University of Lowell
Lowell, MA 01854
(617) 727-9820

Degree: Ph.D., Mathematics, 1961
Specialty: Mathematics
Assigned: RADC

Dr. Howard Weiss
Associate Professor
Dept. of Management
Temple University
Philadelphia, PA 19122
(215) 787-6829

Degree: Ph.D., Industrial Eng., 1975
Specialty: Industrial Engineering
Assigned: LC

Dr. Charles Wells
Associate Professor
Dept. of Decision Sciences
University of Dayton
Dayton, OH 45469
(513) 229-3332

Degree: Ph.D., Management Sci., 1982
Specialty: Management Science
Assigned: HRL/LR

Dr. Ward Wells
Assistant Professor
Human Performance
Dept. of Physical Education
University of Alaska
Fairbanks, AL 99775-0240
(907) 479-5115

Degree: Ph.D., Human Performance,
1981
Specialty: Human Performance
Assigned: SAM

Dr. John Westerkamp
Assistant Professor
Dept. of Electrical Engr.
University of Dayton
Dayton, OH 45469
(513) 229-3611

Degree: Ph.D., Electrical Eng., 1985
Specialty: Electrical Engineering
Assigned: AAMRL

Dr. Robert Wetherhold
Assistant Professor
Mechanical & Aerospace Eng.
State University of New York
Buffalo, NY 14260
(716) 636-2593

Degree: Ph.D., Applied Science, 1983
Specialty: High Temperature Composite
Materials
Assigned: ML

Dr. William Wheless
Assistant Professor
Dept. of ECE
New Mexico State University
Las Cruces, NM 88003
(505) 646-3214

Degree: Ph.D., Electrical Eng., 1985
Specialty: Electrical Engineering
Assigned: WL

Dr. Stanley Whidden
Researcher
Hyperbaric Medicine
Dept. of Hyperbaric Medicine
JESM Baromedical Research Inst.
New Orleans, LA 70115
(504) 363-7656

Degree: M.D., Hyperbaric Medicine,
1984
Specialty: Hyperbaric Medicine
Assigned: SAM

Dr. Andrew Whipple
Associate Professor
Dept. of Biology
Taylor University
Upland, IN 46989
(317) 998-5333

Degree: Ph.D., Cell Biology, 1979
Specialty: Cell Biology
Assigned: AAMRL

Dr. Sharon Williams
Instructor
Dept. of Chemistry
Southern University
Baton Rouge, LA 70813-0572
(504) 771-3990

Degree: M.S., Cell Biology, 1979
Specialty: Biochemistry
Assigned: SAM

Dr. Frank Witzmann
Assistant Professor
Dept. of Biology
IUPUI Columbus
Columbus, OH 47203
(614) 372-8266

Degree: Ph.D., Biology, 1981
Specialty: Biology
Assigned: AAMRL

Dr. William Wolfe
Associate Professor
Dept. of Civil Engineering
Ohio State University
Columbus, OH 43210
(614) 292-0790

Degree: Ph.D., Engineering, 1979
Specialty: Engineering
Assigned: FDL

Dr. Lawrence Wolpert
Associate Professor
Dept. of Psychology
Ohio State University
Columbus, OH 43210
(614) 267-9328

Degree: M.S., Psychology, 1983
Specialty: Psychology
Assigned: AAMRL

Dr. Cheng-Hsiao Wu
Associate Professor
Solid State Physics
Dept. of Electrical Engineering
Univ. of Missouri
Rolla, MO 65401
(314) 341-4677

Degree: Ph.D., Solid State Physics,
1972
Specialty: Solid State Physics
Assigned: APL

Dr. Joan Wyzkoski
Associate Professor
Dept. of Math & Computer Sci.
Fairfield University
Fairfield, CT 06430-7524
(203) 254-4000

Degree: Ph.D., Mathematics, 1979
Specialty: Mathematics
Assigned: WL

Dr. Melvin Zandler
Associate Professor
Physical Chemistry
Dept. of Chemistry
Wichita State Univ.
Wichita, KS 67204
(316) 689-3120

Degree: Ph.D., Physical Chemistry,
1966
Specialty: Physical Chemistry
Assigned: FJSRL

Dr. George Zobrist
Professor
Dept. of Computer Science
University of Missouri
Rolla, MO 65401
(314) 341-4492

Degree: Ph.D., Electrical Eng., 1965
Specialty: Electrical Engineering
Assigned: ESMC

C. PARTICIPANT LABORATORY ASSIGNMENT (Page 1)

1987 USAF/UES SUMMER FACULTY RESEARCH PROGRAM

AERO PROPULSION LABORATORY (AFWAL/APL)
(Wright-Patterson Air Force Base)

- | | |
|--------------------|-------------------|
| 1. Suresh Aggarwal | 5. Thomas Lalk |
| 2. Bryan Becker | 6. Ramendra Roy |
| 3. John Erdei | 7. Richard Tankin |
| 4. Dennis Flentge | 8. Cheng-Hsiao Wu |

ARMAMENT LABORATORY (AD)
(Eglin Air Force Base)

- | | |
|-------------------|---------------------|
| 1. Charles Bell | 6. Joseph Feeley |
| 2. David Betounes | 7. Elmer Hansen |
| 3. John Bopp, Jr. | 8. James Hoffmaster |
| 4. Robert Buchl | 9. James Nail |
| 5. Robert Courter | |

ARMSTRONG AEROSPACE MEDICAL RESEARCH LABORATORY (AAMRL)
(Wright-Patterson Air Force Base)

- | | |
|---------------------|----------------------|
| 1. Xavier Avula | 8. Thomas Nygren |
| 2. Praphulla Bajpai | 9. Donald Robertson |
| 3. Shankar Bale | 10. John Westerkamp |
| 4. Gwendolyn Howze | 11. Andrew Whipple |
| 5. Charles Kimble | 12. Frank Witzmann |
| 6. Augustus Morris | 13. Lawrence Wolpert |
| 7. Noel Nussbaum | |

ARNOLD ENGINEERING DEVELOPMENT CENTER (AEDC)
(Arnold Air Force Station)

- | | |
|----------------------|--------------------|
| 1. Lee Britt | 4. Marco Egoavil |
| 2. Suhrit Dey | 5. William Grissom |
| 3. Carroll Dougherty | 6. Surgounda Patil |

AVIONICS LABORATORY (AFWAL/AL)
(Wright-Patterson Air Force Base)

- | | |
|-------------------|---------------------|
| 1. John Amoss | 6. Alastair McAulay |
| 2. Vernon Bakke | 7. James Noyes |
| 3. William Curry | 8. Kenneth Roenker |
| 4. Verlynda Dobbs | 9. Robert Trenary |
| 5. Narayan Halder | |

DEFENSE EQUAL OPPORTUNITY MANAGEMENT INSTITUTE (DEOMI)
(Patrick Air Force Base)

1. Dan Landis
2. Lena Myers

EASTERN SPACE AND MISSILE CENTER (ESMC)
(Patrick Air Force Base)

1. George Zobrist

C. PARTICIPANT LABORATORY ASSIGNMENT (Page 2)

ELECTRONICS SYSTEMS DIVISION (ESD)
(Hanscom Air Force Base)

1. Phanindramoha Das

ENGINEERING AND SERVICES CENTER (ESC)
(Tyndall Air Force Base)

- | | |
|----------------------|-------------------|
| 1. William Bannister | 5. William Schulz |
| 2. William Bass | 6. Joseph Tedesco |
| 3. Peter Jeffers | 7. Dennis Truax |
| 4. Yong Kim | 8. P. G. Vaidya |

FLIGHT DYNAMICS LABORATORY (AFWAL/FDL)
(Wright-Patterson Air Force Base)

- | | |
|-------------------|-------------------|
| 1. Gary Graham | 6. Shiva Singh |
| 2. David Hart | 7. Gary Slater |
| 3. Oliver McGee | 8. Forrest Thomas |
| 4. William Patten | 9. William Wolfe |
| 5. Joseph Saliba | |

FRANK J. SEILER RESEARCH LABORATORY (FJSRL)
(USAF Academy)

- | | |
|----------------------|--------------------|
| 1. Charles Bump | 6. Henry Kurtz |
| 2. David Chung | 7. Maurice Neveu |
| 3. Stephen Gold | 8. Howard Thompson |
| 4. Albert Hirschberg | 9. Melvin Zandler |
| 5. Lawrence Koons | |

GEOPHYSICS LABORATORY (AFGL)
(Hanscom Air Force Base)

- | | |
|--------------------------|--------------------|
| 1. Francesco Bacchialoni | 8. Martin Patt |
| 2. Lee Flippin | 9. Gandikota Rao |
| 3. Benjamin Gottlieb | 10. Paul Rybski |
| 4. Robert Hoffman | 11. Timothy Su |
| 5. Mayer Humi | 12. Keith Walker |
| 6. Steven Leon | 13. Richard Walker |
| 7. Henry Nebel | |

HUMAN RESOURCES LABORATORY/LR (HRL/LR)
(Wright-Patterson Air Force Base)

1. Patricia Carlson
2. David Townsend
3. Charles Wells

C. PARTICIPANT LABORATORY ASSIGNMENT (Page 3)

HUMAN RESOURCES LABORATORY/MO (HRL/MO)
(Brooks Air Force Base)

1. Victor Appel
2. Ronna Dillon
3. Michael Matthews

HUMAN RESOURCES LABORATORY/OT (HRL/OT)
(Williams Air Force Base)

1. Terence Hines
2. John Uhlarik

LOGISTICS COMMAND (LC)
(Wright-Patterson Air Force Base)

1. Howard Weiss

LOGISTICS MANAGEMENT CENTER (LMC)
(Gunter Air Force Base)

1. Kweku Bentil
2. Jerome Blaylock
3. William Kauder

MATERIALS LABORATORY (AFWAL/ML)
(Wright-Patterson Air Force Base)

- | | |
|---------------------|-----------------------|
| 1. Kwo-Sun Chu | 8. Gordon Johnson |
| 2. Bruce Craver | 9. William Jordan |
| 3. Bruce DeVantier | 10. Spencer Porter |
| 4. Ravinder Diwan | 11. Nisar Shaikh |
| 5. John Gilmer | 12. Robert Voigt |
| 6. Vijay Gupta | 13. Robert Wetherhold |
| 7. Kenneth Halliday | |

OCCUPATIONAL AND ENVIRONMENTAL HEALTH LABORATORY (OEHL)
(Brooks Air Force Base)

- | | |
|------------------|---------------------|
| 1. Richard Brown | 4. Robert Masingale |
| 2. Elvis Deal | 5. Joseph Verducci |
| 3. Kiah Edwards | |

ROCKET PROPULSION LABORATORY (RPL)
(Edwards Air Force Base)

- | | |
|-------------------|-----------------------|
| 1. Gurbux Alag | 5. Michael Gorman |
| 2. Allan Burkett | 6. John Kenney |
| 3. Wilton Flemon | 7. Lawrence Schovanec |
| 4. Luther Flippen | |

C. PARTICIPANT LABORATORY ASSIGNMENT (Page 4)

ROME AIR DEVELOPMENT CENTER (RADC)
(Griffiss Air Force Base)

- | | |
|--------------------|---------------------------|
| 1. Beryl Barber | 7. Timothy Grogan |
| 2. Kevin Bowyer | 8. Louis Johnson |
| 3. Ronald Canfield | 9. Panapakkam Ramamoorthy |
| 4. John Dunn | 10. David Sumberg |
| 5. Ramez Elmasri | 11. Jacob Weinberg |
| 6. Lionel Friedman | |

SCHOOL OF AEROSPACE MEDICINE (SAM)
(Brooks Air Force Base)

- | | |
|-----------------------|----------------------|
| 1. Phillip Bishop | 9. Leonard Price |
| 2. David Ludwig | 10. Stephen Pruett |
| 3. Mohammed Maleque | 11. Richard Schori |
| 4. Daniel Mihalko | 12. Wesley Tanaka |
| 5. Mary Morton-Gibson | 13. Michele Trankina |
| 6. Kurt Oughstun | 14. Ward Wells |
| 7. Ralph Peters | 15. Stanley Whidden |
| 8. Gerald Pollack | 16. Sharon Williams |

WEAPONS LABORATORY (WL)
(Kirtland Air Force Base)

- | | |
|--------------------|--------------------|
| 1. Thomas Dwyer | 5. Randall Peters |
| 2. Ira Elder | 6. William Wheless |
| 3. Jerome Knopp | 7. Joan Wyzkoski |
| 4. Barry McConnell | |

RESEARCH REPORTS

RESEARCH REPORTS
1987 SUMMER FACULTY RESEARCH PROGRAM

<u>Technical Report Number</u>	<u>Title</u>	<u>Professor</u>
Volume I		
1	Vaporization Behavior of Multicomponent Fuel Droplets in a Hot Air Stream	Dr. Suresh K. Aggerwal
2	Large Space Structure Parameter Estimation	Dr. Gurbux S. Alag
3	Correlation and Simulation Studies of GaAs Microwave MESFET Power Devices	Dr. John W. Amoss
4	Air Force Officer Selection Revisited: Entertaining The Possibilities for Improvement	Dr. Victor H. Appel
5	Evaluation of Three-Dimensional Kinetics Analysis Methods of Robotics for the Study of Human Articulated Motion	Dr. Xavier J.R. Avula
6	Pointing Control Systems for Balloon-Flown Instruments	Dr. Francesco Bacchialoni
7	Sustained Delivery of Volatile Chemicals by Means of Ceramics	Dr. Praphulla K. Bajpai
8	Frequency Estimation in the Analysis of Radar Signals	Dr. Vernon L. Bakke
9	Invitro Cytotoxic Effects of Perflurodecanoic Acid on L5178Y Mouse Lymphoma Cells	Dr. Shankar S. Bale
10	Fire Technology of Jet Fuels (JP-8 vs. JP-4)	Dr. William W. Bannister
11	Microwave Measurements	Prof. Beryl L. Barber
12	Identification Techniques Using Fragmentary Human Bone	Dr. William M. Bass
13	A Numerical Simulation of the Flow Field and Heat Transfer in a Rectangular Passage with a Turbulence Promoter	Dr. Bryan R. Becker
14	Synergistic Effects of Bomb Cratering	Dr. Charles Bell

15	Construction Contract Administrator's Technical Handbook	Prof. Kweku K. Bentil
16	Least Squares Estimation Theory and Geometrical Smoothers	Dr. David E. Betounes
17	Increasing Work Capacity of Personnel Wearing Protective Clothing in Hot Environments	Prof. Phillip A. Bishop
18	User-System Interface Standards	Dr. Jerome W. Blaylock
19	Fourier Transform Infrared Studies of Ethylenediammonium Dinitrate and 1,4-Butanediammonium Dinitrate	Dr. John M. Bopp, Jr.
20	A "Form and Function" Knowledge Representation for Reasoning about Classes and Instances of Objects	Dr. Kevin W. Bowyer
21	An Analysis of Infrared Light Propagation in Hollow Metallic Light Pipes	Mr. Lee I. Britt
22	Phytotoxicity of Soil Residues of JP-4 Aviation Fuel	Mr. Richard. H. Brown
23	Dynamics of a Metallic Jet	Dr. Robert A. Buchl
24	Reactions of Nitryl Chloride with Aromatic Substrates in Chloraluminum Melts	Dr. Charles M. Bump
25	Chemistry for the Space Program	Dr. Allan R. Burkett
26	Bayesian Testability Demonstration	Dr. Ronald V. Canfield
27	Hypertext and the Integrated Maintenance Information System (IMIS)	Dr. Patricia Carlson
28	Dopant Diffusion in NIPI Semiconductor Superlattices	Dr. Kwo-Sun Chu
29	Nonlinear Optical Effects in Fibers and Small Crystals	Dr. David Y. Chung
30	The Effect of Model Flexibility on the Accuracy of Aerodynamic Coefficients Determined from Free-Flight Ballistic Tests	Dr. Robert W. Courter
31	Tunable Absorption in Superlattices	Dr. Bruce A. Craver

- | | | |
|----|--|--------------------------|
| 32 | Computer Simulation of Adaptive Resource Management in Real-Time | Prof. William K. Curry |
| 33 | Effect of Wind and Turbulence on an Artificially Generated Strato-Mesospheric Plasma | Dr. Phanindramoha Das |
| 34 | Analysis and Modeling of the Thermal Response of an Autoclave for Expert System Control of Carbon-Epoxy Composite Fabrication | Dr. Bruce A. DeVantier |
| 35 | A Study of Service Demand Distribution and Task Organization for the Analysis of Environmental Samples and Associated Support Services at the USAF Occupational and Environmental Health Laboratory-Brooks AFB, San Antonio, Texas | Dr. Elvis Deal |
| 36 | Vectorized Perturbed Functional Iterative Scheme (VPFIS) for Numerical Solution of Nonlinear Partial Differential Equations | Dr. Suhrit K. Dey |
| 37 | An Eight-Domain Framework for Understanding Intelligence and Predicting Intelligent Performance | Dr. Ronna F. Dillon |
| 38 | Microstructural Developments in Titanium Aluminides: A Study of Dynamic Material Modeling Behavior | Dr. Ravinder Diwan |
| 39 | Ada and Artificial Intelligence Applications for Electronic Warfare | Dr. Verlynda S. Dobbs |
| 40 | Computational Simulation of Transonic Store Separation | Dr. F. Carroll Dougherty |
| 41 | Guided Waves in Millimeter Wave Circuit Design | Dr. John M. Dunn |
| 42 | Slew-Coupled Structural Dynamics Identification and Control | Dr. Thomas A.W. Dwyer |
| 43 | The Effects of Metal Mutagens on the Synthesis and Accumulation of Macromolecules | Dr. Kiah Edwards |
| 44 | Project 1 - Scaling Laws of Two-Dimension Nozzle Plumes; Project 2 - Design of a Mechanism to Control Turbulence Levels in Wind Tunnels | Dr. Marco A. Egoavil |

45	Computation of Rutherford Scattering Cross Sections	Dr. Ira T. Elder
46	Database Processing in Real-Time Systems	Dr. Ramez A. Elmasri
47	Non-Uniform Spatial Systems and the Transition to Turbulence	Dr. John E. Erdei
48	Bank-To-Turn Control of Air-To-Air Missiles	Dr. Joseph J. Feeley
49	Borazine Reactions	Dr. Wilton Flemon
50	Chemical and Spectroscopic Evaluation of Antimony Sulfides	Dr. Dennis R. Flentge
51	The Evaluation of a Thermal-Hydraulic Design of a Fixed Particle Bed Reactor and Suggested Model Revisions	Dr. Luther D. Flippen
52	Sift Studies of Gas Phase Ion-Molecule Reactions	Dr. Lee A. Flippin
53	Silicon Junction-Difet Electrooptic Modulator	Dr. Lionel R. Friedman

Volume II

54	Phase Behavior of Poly(p-phenylene benzobisthiazole) Molecular Composites	Dr. John W. Gilmer
55	Design of an Omnidirectional Torquer	Dr. Stephen J. Gold
56	Acoustic Emission and the Fracture Behavior of 2 D Carbon Carbon	Dr. Michael R. Gorman
57	No Report Submitted	Dr. Benjamin Gottlieb
58	High Amplitude Airfoil Motion Using Point Vortices	Dr. Gary M. Graham
59	Liquid Film Cooling of Rocket Engines	Mr. William M. Grissom
60	Cellular Logic Image Processor Evaluationn	Dr. Timothy A. Grogan
61	Thermal Decomposition Investigations of Candidate High Temperature Base Fluids II. Silahydrocarbons	Dr. Vijay K. Gupta
62	Effect of Surface States on the Electronic Transport Properties in Semi-Insulating GaAs	Dr. Narayan C. Halder

63	The Surface Primitive Method of Feature Based Computer Aided Design for Manufacture	Dr. Kenneth R. Halliday
64	Gun Gas Diversion	Dr. Elmer C. Hansen
65	Multi-Block Grid Optimization	Dr. David Hart
66	Encoding in Less than 100 Milliseconds Demonstrated Using a Reaction Time Task	Dr. Terence M. Hines
67	Nitrated Heterocyclic Compounds: A Synthetic Study	Dr. Albert I. Hirschberg
68	A Human Factors Approach to the Process of Developing the Advanced Meteorological Processing System	Dr. Robert R. Hoffman
69	Pressure Attenuation in Solids: A Computer Model	Dr. James S. Hoffmaster
70	In Situ Detection of Osteoprogenitor Cells in an Actively Growing Bone System	Dr. Gwendolyn B. Howze
71	Non-local Turbulance Theories	Dr. Mayer Humi
72	Leaching and Hydrolysis of some Chlorinated Solvents	Dr. Peter M. Jeffers
73	Cholesteric Liquid Crystals of Bio-molecules for Use as Optical Filters	Dr. Gordon O. Johnson
74	Contribution of the Value Assignment Problem to the Complexity of Test Generation in Combinational Logic Circuits and Power Line Testing of CMOS Digital Logic Circuits	Dr. Louis G. Johnson
75	Effect of Stacking Sequence Upon Delamination Fracture Toughness	Dr. William M. Jordan
76	"Generic" Credit Card Feasibility Study	Dr. William F. Kauder
77	High Energy Metastable Species in Cryogenic Matrices: Preparation, Photophysics, and Photochemistry	Dr. John W. Kenney
78	Development of a Geotechnical Centrifuge Facility at Tyndall Air Force Base	Dr. Yong S. Kim

79	Emergent Leadership and Team Effectiveness on a Team Resource Allocation Task	Dr. Charles E. Kimble
80	Experimental Testing of Imaging Correlography	Dr. Jerome Knopp
81	A Study of the Electrochemical Behavior of Trihalide Ions Containing Bromine and Chlorine in Melts Composed of Aluminum Chloride and 1-Methyl-3-Ethylimidazolium Chloride	Dr. Lawrence F. Koons
82	Semiempirical Calculation of Non-Linear Optical Properties	Dr. Henry A. Kurtz
83	Mathematical Removal of Low Frequency Fluctuations From Experimental LDV Data	Dr. Thomas R. Lalk
84	Construction of a Preliminary Validation of an Equal Opportunity Climate Assessment Instrument	Dr. Dan Landis
85	A Hyperbolic Interpolation Algorithm for Modelling Radiance Data and Exponential Inversion	Dr. Steven J. Leon
86	Experimental Protocols for Investigating the Physiology of Orthostatic Intolerance in Humans	Dr. David A. Ludwig
87	Effect of Repeated Low Dose Soman On Acetylcholinesterase Activity	Dr. Mohammad A. Maleque
88	Disposal of Chemotherapeutic Wastes	Dr. Robert E. Masingale
89	Assessing Costs and Benefits of Personnel Research: Application of Utility Concepts to Military Programs	Dr. Michael D. Matthews
90	Investigation of New Luminescent Rebroadcasting Devices for Optical Information Processing	Dr. Alastair D. McAulay
91	Automated Extraction of Knowledge-Based Object Tuples from Domain Documents	Dr. Barry A. McConnell
92	Automated Design of Large-Scaled Frame Structures with Multiple Frequency Constraints	Mr. Oliver G. McGee

93	Statistical Methodology for Assessing Group Health Differences	Dr. Daniel Mihalko
94	A Comparison of Tracking with Active Stick Controllers with an Optimal Control Model	Mr. Augustus Morris
95	Examination of the Point Spread Function in the Retinal Thermal Model	Dr. Mary L. Morton-Gibson
96	Developing Models for Empirical Research on Women in the Military	Dr. Lena W. Myers
97	Multi-Mode Sensing in Air-to-Air Missiles	Dr. James B. Nail
98	Night-Time CO ₂ (001) Vibrational Temperatures and Limb-View Integrated Radiances in the 50 to 150 KM Altitude Range	Dr. Henry Nebel
99	A Kinetic Study of Thermal Decomposition by TNT By High Performance Liquid Chromatography	Dr. Maurice C. Neveu
100	Evaluating Expert Systems	Dr. James L. Noyes
101	Isolation of Osteoprogenitor Cells from the Trauma-Activated Periosteum	Dr. Noel S. Nussbaum
102	Assessing the Attributes of Expert Judgment: Measuring Bias in Subjective Uncertainty Estimates	Dr. Thomas E. Nygren
103	On the General Existence of Precursor Fields in a Casually Dispersive Medium	Dr. Kurt E. Oughstun
104	Estimation of Spectal Density by Random Samples	Dr. Surgounda A. Patil
105	Computer Skeleton Program Generator	Prof. Martin A. Patt
106	A Suboptimal Feedback Control for Wing Rock	Dr. William N. Patten
Volume III		
107	Release of Dynorphin B From Mossy Fiber Synaptosomes	Dr. Ralph I. Peters
108	Momentum Transfer and Mass Loss for a C.W. Laser Irradiated Target	Dr. Randall D. Peters

109	Raman Spectrum of Acetanilide	Dr. Gerald L. Pollack
110	X-Ray Diffraction by Superconducting Oxides	Dr. Spencer K. Porter
111	A New Sensitive Fluorometric Method for the Analysis of Submicrogram Quantities of Cholesterol	Dr. Leonard Price
112	A Model System for Examining Macrophage-Lymphocyte Interactions	Dr. Stephen B. Pruett
113	Digital Optical Computing Potentials and Problems	Dr. Panapakkam A. Ramamoorthy
114	A Critical Review of Some Recent Remotely Sensed Studies of Typhoons in the North West Pacific	Dr. Gandikota V. Rao
115	Ambiguity and Probabilistic Inference in a Missile Warning Officer Task	Dr. Donald U. Robertson
116	A Test Chip for Evaluation of MBE Epitaxial Layers for Novel Device Applications	Dr. Kenneth P. Roenker
117	Heat Removal from High Heat Flux/Large Area Surfaces by Single-Phase and Two-Phase Flow of Water	Dr. Ramendra P. Roy
118	Late Appointment No Report Submitted at this time	Dr. Paul M. Rybski
119	Three-Dimensional Finite Element Program Elastic Viscoplastic	Dr. Joseph E. Saliba
120	A Case for Neural Networks	Dr. Richard M. Schori
121	Fracture in Damaged Media: An Inhomogeneous Material Approach	Dr. Lawrence E. Schovanec
122	Characterization of Fire Training Facility Wastewater	Dr. William D. Schulz
123	Leaky Rayleigh Waves on Surfaces With Laminar Microstructures	Dr. Nisar Shaikh
124	Radiation Hypersonic Aerodynamics	Dr. Shiva N. Singh
125	Robustness and Control/Structure Design Integration for Flexible Dynamic Systems	Dr. Gary L. Slater

126	Theoretical and Experimental Investigations of Ion-Polar Molecule Interactions	Dr. Timothy C. Su
127	A Balanced Fiber Optic Distribution Network for Phased Array Antennas	Dr. David A. Sumberg
128	Use of High Performance Molecular Exclusion Chromatopography to Separate Lippoproteins	Dr. Wesley K. Tanaka
129	Visualization, Velocity and Frequency Measurements of a Two-Dimensional Jet	Dr. Richard S. Tankin
130	Pressure Waves in Foam and Foam-Sand Samples	Dr. Joseph W. Tedesco
131	High Velocity Projectiles	Dr. Forrest D. Thomas
132	The Effect of Transient Shock Waves in a Mach 3 Flow	Dr. Howard D. Thompson
133	A Computational Model of Resource Allocation in Experts and Novices	Dr. David J. Townsend
134	Development of an Animal Model for G-Induced Loss of Consciousness	Dr. Michele L. Trankina
135	An Advanced Vision System Testbed	Prof. Robert G. Trenary
136	Ozonation of Firefighter Training Facility Wastewater and its Effect on Biodegradation	Dr. Dennis D. Truax
137	Effects of Adaptation to Fourier Descriptor Stimuli on Discrimination Thresholds for Visual Form	Dr. John J. Uhlarik
138	Prediction of Structural Response to Sonic Booms: An Assessment of Technological Gaps	Dr. P. G. Vaidya
139	Model-free Statistical Analyses of Contaminated Ground Water	Dr. Joseph S. Verducci
140	Microstructure and Mechanical Properties of Titanium Aluminides	Dr. Robert C. Voigt
141	Excitation Cross Sections of Atomic Oxygen by Electron-Impact Dissociative Excitation of O ₂	Dr. Keith G. Walker
142	Fifth Force Studies for a Layered Earth	Dr. Richard C. Walker
143	Magnetostatic Waves Studies	Dr. Jacob Weinberg

144	Lateral Resupply of Spare Parts	Dr. Howard J. Weiss
145	Design Optimization of Complex Systems by Goal Decomposition	Dr. Charles E. Wells
146	Thermal Physiology: Selected Field Study Problems and Methodology	Dr. Ward T. Wells
147	Adaptive Filtering of Evoked Brain Potentials	Dr. John J. Westerkamp
148	Thermal Fatigue of Ceramic Matrix Composite (CMC) Materials	Dr. Robert C. Wetherhold
149	Mode Extraction from an Electromagnetic Slow Wave System	Dr. William P. Wheless
150	Hyperbaric (3ATA) Oxygen 100% Therapy as an Adjuvant in the Treatment of Resuscitated (Lactated Ringer' and Dextrose 5%) Guinea Pigs' Burn (3°, 50 BSA) Shock	Dr. Stanley J. Whidden
151	Perfluorodecanoic Acid Interactions with Mouse Lymphoma Cells and Primary Rat Hepatocytes	Dr. Andrew P. Whipple
152	Polyunsaturated Omega-3 Fatty Acids As A Risk Predictor of Coronary Artery Disease	Ms. Sharon Williams
153	In Vitro Cytotoxicity Assessment Via Two-Dimensional Polyacrylamide Gel Electrophoresis	Dr. Frank A. Witzmann
154	Low Velocity Impact of Graphite/Epoxy Plates	Dr. William E. Wolfe
155	The Active Control of Altitude Over Differing Texture	Mr. Lawrence Wolpert
156	The Interface Contribution to GaAs/Ge Heterojunction Solar Cell Efficiency	Dr. Cheng-Hsiao Wu
157	Parallel Processing and Numerical Linear Algebra	Dr. Joan P. Wyzkoski
158	Semi-Empirical Molecular Orbital (MOPAC) Studies of Energetic Materials: Nitrogen Heterocyclics and Nitroenamine	Dr. Melvin E. Zandler
159	Specification of a Computer Aided Design System	Dr. George W. Zobrist

1987 USAF-UES SUMMER FACULTY RESEARCH PROGRAM
GRADUATE STUDENT SUMMER SUPPORT PROGRAM

Sponsored by the
AIR FORCE OFFICE OF SCIENTIFIC RESEARCH

Conducted by the
Universal Energy Systems, Inc.

FINAL REPORT

Prepared by: John W. Gilmer
Academic Rank: Assistant Professor of Polymer Science
Department and Department of Materials Science and Engineering
University: The Pennsylvania State University
Research Location: AFWAL/MLBP
Wright-Patterson Air Force Base, OH 45433
USAF Researcher: W. Wade Adams
Date: 28 September 1987
Contract No: F49620 - 85 - C - 0013

Phase Behavior of Poly(p-phenylene benzobisthiazole) Molecular Composites

by

John W. Gilmer

Abstract

New high strength, high modulus molecular composite materials are being fabricated by utilizing a rigid rod polymer molecule as the fiber which is molecularly dispersed in a flexible coil matrix. As phase separation proceeds, the rod is no longer molecularly dispersed and its ability to reinforce the flexible coil matrix is decreased. The phase behavior of poly(p-phenylene benzobisthiazole)(PBT) containing molecular composites was characterized in this study by small angle light scattering (SALS). In characterizing these materials, accomplishments were made in three areas: development of light scattering software and instrumentation; preparation of a prospectus for future studies of molecular composites by neutron scattering; and SALS measurements during phase separation for molecular composites containing PBT in benzocyclobutene and PBT in amorphous nylon.

Acknowledgements

For the opportunity to participate in this program, I wish to thank the Air Force Systems Command, The Air Force Office of Scientific Research , and The Wright Aeronautical Laboratory. Special thanks are extended to Drs. W. Wade Adams and Hoe H. Chuah for their assistance in carrying out this study and to the Air Force Institute of Technology for the use of their OMA III console.

I Introduction

The purpose of this report is to summarize the accomplishments by the author during the 1987 summer faculty research program (SFRP) spent in the Polymer Branch of the Materials Laboratory at Wright-Patterson Air Force Base. The primary focus of this project was to characterize the morphology and phase behavior of rigid-rod molecular composites. This study was carried out in collaboration with W. W. Adams, the Effort Focal Point, and H. H. Chuah, a staff scientist of the University of Dayton Research Institute (UDRI). This SFRP study was part of an ongoing program at Wright Aeronautical Laboratories to develop and optimize rigid-rod molecular composite materials.

A molecular composite is a polymeric material which contains rigid-rod molecules individually dispersed in a flexible coil matrix. The tendency of rigid-rod molecules not to mix with flexible coil polymers was first pointed out by Flory^{1,2} in his study on the phase equilibria of rod-like particles. It was clearly demonstrated that a thermodynamically miscible mixture of rods and coils would be extremely difficult to produce. Moreover, only small percentages of rods and coils of sizeable molecular weight are predicted to codissolve in an isotropic phase when placed in a common solvent. This means that conventional methods of blending polymers, e.g. solvent casting, cannot be utilized to form molecular composite materials.

To form the molecular composites investigated in this study, the method which was implemented to blend rigid-rod poly(p-phenylene benzobisthiazole) (PBT) molecules with a flexible coil component, either Zytel 330 or benzocyclobutene (BCB), was to wet spin fibers of the materials in a process similar to that used for single component PBX materials.³ Dilute dopes of the rigid-rod and flexible coil materials are prepared using a strong acid solvent. The dope is then wet spun into a film or fiber using a deionized water

nonsolvent. The process of quickly removing the acid solvent by coagulation does not allow sufficient time for extensive phase separation or clustering of rods to occur. Whether a truly molecular composite has been formed by coagulation is being investigated by S. Krause with both scanning and transmission electron microscopy.

Several different materials including ABPBI, Nylon-6,6, BCB, and Zytel 330 (an amorphous Nylon) have been blended together with PBT to form molecular composites.⁴ Of primary interest in this study are the PBT/Zytel 330 and PBT/BCB blend systems. These materials are formed by wet spinning a methane sulfonic acid dope of the two blend components with deionized water serving as nonsolvent. The Zytel 330 Nylon was chosen because it forms a tough flexible matrix material which is noncrystallizable. Also, since Zytel 330 is partially aromatic and can hydrogen bond with PBT, the dominating tendency toward phase separation may be somewhat lessened. The BCB component was utilized to determine whether it might be possible to thermally set the matrix material before any phase separation had occurred and thus keep the rod in its molecularly dispersed state.

The presence of the Nylon in the PBT/Zytel 330 system causes this blend system, unlike the parent PBT, to exhibit a glass transition (T_g). Raising the temperature above the T_g , in addition to making the material mechanically more pliable, introduces mobility at the molecular level. As the overwhelming tendency of rods and coils to demix was suppressed by the rapid coagulation process used to form the molecular composite materials, the introduction of any mobility into the blend allows the sample to undergo spontaneous phase separation. It is quite unlikely that the formation of critical sized nuclei is necessary for the phase separation of these materials to proceed. Thus the rate of phase separation for PBT/Zytel 330 at a given temperature would be

anticipated to be controlled by the mutual rate of diffusion of each component in the blend.

The initial portion of the phase separation process for such a molecular composite material has the greatest effect in lowering the strength and modulus of this material. Since any degree of bundling exhibited by the rod-like molecules greatly decreases the effective aspect ratio of the rod, the reinforcing ability of the rigid-rod component is therefore quickly reduced with the onset of phase separation. To describe the initial process of diffusion controlled phase separation of isotropic, binary mixtures, the theory of spinodal decomposition has been developed by Cahn and Hilliard.^{5,6} This theory is based on the assumption that the free energy for a binary mixture depends on the free energy per unit volume (a function of the concentration) and a concentration gradient term. The phase separation behavior of blended polymers can be characterized by utilizing small angle light scattering to follow changes in the blend morphology as a function of time. For a blend undergoing spontaneous phase separation, both the shape of the light scattering peak and its initial rate of growth at a given temperature are predicted by the spinodal theory. The angle of maximum intensity is then determined by the initial coarseness of the phase separated structure. This theory was originally applied to polymer blends by Hashimoto, Kumaki, and Kawai⁷ for the poly(vinyl methyl ether)/polystyrene blend system. The only previous study conducted on the phase separation of rigid-rod molecular composites was undertaken by Chuah, Kyu, and Helminiak⁸ on PBT/Nylon-6,6 molecular composites. Although the initial phase separation kinetics appeared to approximately follow the predictions of the spinodal theory, the complication of simultaneous crystallization of the Nylon and phase separation of the molecular composite made an exact interpretation of the light scattering data difficult.

II. Objectives of the Research Effort

Several objectives have helped determine the motivation and specific direction of this project. In fabricating a molecular composite material, the rigid rod must be molecularly dispersed in the flexible coil matrix to achieve the maximum reinforcement from the rigid component. Light scattering methods are being developed as a way of monitoring the extent of phase separation in these materials during either processing or annealing. Also by careful analysis of the light scattering profile, an understanding is desired of the exact mechanism of phase separation in rod/coil mixtures, an understanding which shall then be extended to more complicated copolymer molecular composites. Development of small angle light scattering (SALS) software and instrumentation has allowed us to make considerable progress toward meeting these objectives. Finally, in future characterization of molecular composite copolymers currently being developed at Wright-Patterson Air Force Base, we plan to employ small angle neutron scattering (SANS), X-ray diffraction, electron microscopy, and small angle X-ray scattering (SAXS) to effectively determine the phase behavior, rod orientation, and the role of the flexible coil component in these materials. With the author's experience in neutron scattering, a final objective of the SFRP was to begin planning how SANS could be most effectively utilized in the further development of molecular composite polymers.

Accomplishments in three major areas will be described in this report. First of all, a characterization by small angle light scattering (SALS) of the phase behavior of PBT containing molecular composites was initiated. Secondly, to aid in the light scattering analysis, optimizations were made with the SALS instrumentation in the Polymer Branch, and computer programs in the Hemmingway Basic language were written which allowed one dimensional

scattering from isotropic samples, measured by the OMA III apparatus to be scaled to absolute intensity, stored on disk, and plotted. The third area of endeavor involved formulating a prospectus on how small angle neutron scattering (SANS) could be utilized with current and future molecular composite materials.

III. System Changes

The light scattering system initially in use at the Materials Laboratory was the OMA II apparatus developed by R. J. Tabar, R. S. Stein and M. B. Long.⁹ This system utilized a vidicon camera with a PAR model 1216 controller. The controller then communicated with a PDP 11/23 plus computer via a homemade interface board designed by M. Long. At the start of the summer, the light scattering unit did not function, apparently due to an interface problem. After extensive futile attempts to repair the interface, the decision was made to upgrade the light scattering system to an OMA III, a system where all the electronic components comprise a light scattering system offered commercially by PAR (without any homemade modifications).

Two modifications were made to the light scattering optics in an attempt to optimize the scattering pattern obtained. Firstly, to decrease the internal reflections in the system, lenses with quarter wave coatings were utilized and the beam stop was placed immediately in front of the first lens, instead of on the analyzer. Secondly, in addition to the main optical bench, a second bench was placed beside the first to allow access to wider angles by diverting the main beam with mirrors. The major hardware need remaining for the SALS system is the development of a quenching cell which allows rapid quenching from one temperature to another, thus enhancing our capability of examining the early

stages of phase separation in rod/coil systems. This cell is being developed as part of the continuation of this summer's project.

The OMA III SALS system allows programming in Basic in addition to the system software which is in binary. Two programs were constructed in Basic to allow the light scattering results to be more easily presented and analyzed. The program SALS.BAS takes the background corrected one dimensional data from the OMA III system and calculates the scattering intensity, log intensity, scattering vector, and scattering angle for each data point. These data can then be plotted on the console or on a Houston Instruments plotter, printed out on a line printer, or stored for further analysis. The program PLOT.BAS utilizes the Houston Instruments plotter to produce single curve or multicurve plots of data which have been stored in the SALS program.

IV. Light Scattering from PBT Molecular Composites

SALS was utilized to follow the phase separation behavior of two molecular composite systems PBT/BCB and PBT/Zytel 330. Both of the materials had been synthesized in the Polymer Branch and wet spun into films by H. Chuah. For the PBT/BCB system, blends of 50/50 composition were studied. For the PBT/Zytel 330 system blends with a 30/70 and a 50/50 composition were characterized.

The PBT/BCB molecular composite system did not exhibit a clear change in the light scattering profile when annealed between its T_g and its curing temperature. Although SALS may not be able to detect phase separation, the embrittlement of the material with annealing is a good indication that some phase separation did occur. Any changes occurring in the x-ray diffraction profile of this material will allow any clustering of rods into PBT domains during phase separation to be characterized.

The PBT/BCB molecular composite had been prepared with the hope that the BCB could be crosslinked prior to the occurrence of phase separation, and thus that the rigid-rod component would remain molecularly dispersed in the flexible coil thermoset matrix. Different samples of 50% PBT in BCB were annealed 170°C, 200°C, 240°C and 260°C, all temperatures between the glass transition of the blend and the curing temperature of the BCB. It was observed that the blend samples became quite brown, shriveled, and crumbled easily as a result of heating. However, no significant changes were observed in the light scattering profiles of these materials.

The PBT/Zytel 330 system was investigated by small angle light to observe its phase separation behavior. When this material is heated to temperatures above its glass transition, phase separation immediately begins to occur at essentially all compositions. The real time phase separation for blends of 30% and 50% PBT in amorphous Zytel 330 nylon was followed by placing samples in a FP-2 Mettler Hotstage mounted in the SALS which had been preheated to the temperature of interest. Like the PBT/Nylon-6,6 system,⁸ the light scattering patterns from these materials exhibited a ringlike pattern, which grew in intensity and, after the initial stages of phase separation, moved to smaller angles.

An example of a typical scattering pattern from these materials is shown in figure 1. The scattering from these materials occurring at quite low angles results from the presence of voids caused by the spinning process used to form films; this low angle scattering contribution can often make a precise interpretation of the SALS pattern quite difficult. The light scattering maximum exhibited at moderately wider angles as these materials undergo phase separation is quite broad and is observed to initially grow exponentially with time. Figure two presents the log of the light scattering intensity at q_{max} as a

function of time. As has been observed with blends of polystyrene and poly(vinyl methyl ether) undergoing phase separation in the unstable region, the exponential growth of the light scattering maximum occurs only during the initial stages of phase separation. In Figures 3 and 4 the initial rates of growth for the 30% and 50% blends of PBT in amorphous nylon are shown as a function of temperature. As one might expect, the initial rate of phase separation increases with increasing temperature for both compositions. In a publication currently being prepared to describe the phase separation behavior of the PBT / Zytel 330 molecular composite system, an attempt is being made to analyze to what extent the existing theories of phase separation can be applied to these materials.

The theory of spinodal decomposition^{5,6} was derived to describe the early stage phase separation behavior of any two component mixture of materials where initial composition lies in the spinodal or unstable region of the phase diagram. Several important assumptions were made in this derivation, some of which may not apply as rigorously to molecular composite materials. First of all, the two materials are assumed to be homogeneously mixed at a molecular level. Secondly, the Gibbs free energy at a given location in the sample is taken to be comprised of two main contributions: the free energy per unit volume, which depends on the local blend composition, and a second term, which depends on the square of the gradient of the composition at a given location in the blend. Secondly, both the initial and final states of the blend are also assumed to be isotropic in structure. If a lattice is formed as part of the phase separation process, then it must be identical in structure in the x, y, and z directions, e.g. a simple cubic lattice. Thirdly, since only the initial stages of phase separation are considered in the Cahn-Hilliard theory of spinodal

decomposition, terms of higher order and degree for the concentration and the concentration gradient are assumed to be negligible.

As a result of the preceding assumptions, the light scattering profile of intensity versus q (the scattering vector) for a spinodally demixing system is predicted to exhibit an intensity maximum which remains at a constant angle but grows exponentially with time. A specific shape is also predicted for this scattering peak. This shape is not predicted to change as the peak grows in amplitude during the phase separation process. The kinetics of the initial stages of phase separation and resulting morphology are predicted entirely in the spinodal theory from the mobility of the material, the coefficient of the gradient contribution to the free energy density, and $\delta f(c)/\delta c$ where $f(c)$ is the free energy density contribution of homogeneous material of composition c .

For PBT containing molecular composites several deviations may result from the spinodal theory. The well-mixedness of a rigid-rod molecular composite is difficult to characterize below a certain size scale. It is thus quite possible in blends of high rod content, that some bundling of the rigid-rod component is present. Secondly, in the free energy expression used for the spinodal theory, no term is included which describes the orientational correlation of the rigid-rod component. Thirdly, molecular composites comprised of large percentages of rigid rods would probably exhibit liquid crystalline like order instead of being isotropic. This departure from isotropic morphology will likely become noticeable as a wider range of PBT compositions are examined in the continuation of this summer's study. As liquid crystalline order begins to be exhibited by the molecular composites being studied, an ellipsoidal halo of scattered light, instead of a scattering ring, would be expected to form.

Finally, after the phase separation process is initiated, it is difficult to conceive of a single mobility, M , describing both the rigid-rod rich regions and the remainder of the rod/coil blend. Although this extreme difference in mobility between the rod rich and the coil rich phases may not invalidate the application spinodal theory to molecular composites, it may be responsible for the rather short duration of phase separation which follows Cahn-Hilliard kinetics.

V. Future SANS Experiments

A SANS prospectus was prepared entitled "SANS of High Temperature Stable Order Polymers" was written to aid in planning future experiments involving neutron scattering from rigid-rod and molecular composite polymers. The main contents of this prospectus shall be included in an Air Force technical report.¹⁰ The primary utility of neutron scattering for polymeric materials is that by isotopic substitution of deuterium for hydrogen, scattering contrast can be imparted to two materials which in all other respects are chemically identical. By careful deuterium labeling, the single chain structure for either whole molecules or portions of molecules can be determined.

With rigid-rod polymers in the solution and in the bulk, small angle neutron scattering can be utilized to determine the average length and orientation of each rigid-rod molecule. In these materials, SANS can thus be used to verify information already readily obtainable by light scattering and X-ray diffraction. Two extremely useful areas for the application of SANS are those of *in situ* rod polymerization¹¹ and copolymer molecular composite materials. With the synthesis of *in situ* rod materials, SANS could be used as a method of determining to what extent the flexible coils have been converted into rigid rods. A second area in which SANS could be very useful is that of copolymer molecular composites. Questions such as the degree of extension in

the flexible coil portion of the molecule, the average orientation of each rod, and that of what region is occupied by the flexible component of the molecule could be addressed by neutron scattering.

VI. Recommendations

The most promising system from which to develop a basic understanding of rod coil phase behavior is the PBT/Zytel 330 blend system. Since the Zytel 330 is noncrystallizable, we avoid with these materials the additional complication of crystallization accompanying phase separation process. By examining a broad range of PBT/Zytel 330 compositions, the phase behavior of both isotropic and anisotropic molecular composites can be characterized. Since the oriented molecular composites are of greater interest than the isotropic materials as a high strength material, obtaining a complete experimental characterization of these materials should initiate theoretical endeavor to understand the process by which they phase separate.

An excellent technique to follow the initial bundling of PBT molecules into fibrous domains is wide angle x-ray diffraction (WAXD). Since the initial bundling serves to decrease the aspect ratio of the reinforcing fiber, it is quite important to be able to follow this behavior in its early stages. To augment the information obtained by the light scattering experiments, changes in the x-ray diffraction profile accompanying phase separation will be followed. Initial diffraction patterns for ABPBI/PBT/ABPBI triblock copolymers developed in the Polymer Branch indicate that the diffraction of the molecular composite is distinctly different from that exhibited by the two parent materials¹². By annealing the PBT/Zytel 330 samples in an oil bath at the phase separation temperature and then quenching them below their T_g at various stages during the phase separation process, samples exhibiting various degrees of clustering

could be obtained. A photographic X-ray camera could then be utilized to obtain the x-ray diffraction profiles of these materials.

Unfortunately, since higher order diffraction peaks are not present in the zeroth order layer from the rigid-rod polymers, it would be impossible to separate the broadening of the diffraction peaks due to crystallite size as analyzed by the Scherrer equation ^{13,14} from broadening due to crystallite imperfection and paracrystalline disorder. ^{15,16} The most effective way to analyze for crystallite size would still be to naively assume that the disorder of the rigid rod crystal is constant during the phase separation process. For a quantitative determination of the width of the diffraction peaks, the wide angle Huber or Picker diffractometer could be utilized.

Since the molecular composite materials used in this study were formed by coagulation of a methane sulfonic acid dope in water, all sample films contain ellipsoidal shaped voids. These voids gave rise to considerable light scattering at low angles near the beamstop when the SALS experiments on these materials were performed. Several steps could be implemented to minimize void formation. Firstly, the dope should be degassed before coagulation. Secondly, instead of utilizing water as a nonsolvent, a dilute acid bath could be utilized to help slow down the coagulation process. Thirdly, the spinning process could be carried out under pressure so that when shrinking occurs as the acid is drawn off by the water bath, the pressure compensates for this change in volume and prevents gas bubble formation.

Since the mechanical properties of the molecular composite deteriorate quite rapidly during the initial stages of phase separation, this portion of the phase separation process is the most critical to understand. Thus it is crucial that a rapid, well defined temperature quench can be carried out on these

materials. Thus the design and fabrication of a quenching cell is recommended to replace the Mettler FP-1 hotstage currently being used.

In future endeavors two basic approaches to fabricating molecular composites should be pursued. First of all copolymeric structures should be used for molecular composites to prevent phase separation from occurring and to make the orientation of these materials easier. The most promising design for a molecular composite copolymer appears to be the multigraft or comb copolymer. Secondly, in discovering the specific role fulfilled by the flexible component in molecular composite materials, small angle neutron scattering should be utilized to follow the structure of the flexible coil component at the molecular and submolecular level.

REFERENCES

1. Flory, P. J., Proc. R. Soc., London, Ser.A, **234**, 73 (1956).
2. Flory, P. J., Macromolecules, **11**, 1138 (1978).
3. Helminiak, T. E., W.-F. Hwang, D. Wiff, C. Benner, G. Price, U.S. Air Force Technical Report AFWAL-TR-82-4039, October 1982.
4. Chuah, H. H., Private Communication.
5. Cahn, J. W. and J. E. Hilliard, J. Chem. Phys., **31**, 688 (1959).
6. Cahn, J. W. , J. Chem. Phys., **42**, 93 (1965).
7. Hashimoto, T., J. Kumaki, and H. Kawai, Macromolecules, **16**, 641 (1983).
8. Chuah, H. H., T. Kyu, T. E. Helminiak, Submitted to Polymer.
9. Tabar, R. J., R. S. Stein, and M. B. Long, "A Two Dimensional Position Sensitive Detector for Small Angle Light Scattering," presented at the American Chemical Society, New York, August, 1981.
10. Gilmer, J. W. and S. J. Bai, in preparation.
11. Wallace, J. S., F. E. Arnold, and L. S. Tan, Polymer Preprints, **28**(2), 316 (1987).
12. Adams, W. W., Private Communication.
13. Scherrer, P., Goettinger Nachrichten, **2**, 98 (1918).
14. Klug, H. P. and L. E. Alexander, X-Ray Diffraction Procedures, Wiley, New York, 1954, Chapter 9.
15. Hosemann, R., Z. Physik, **128**, 1, 464 (1950).
16. Alexander, L. E., X-Ray Diffraction Methods in Polymer Science, Wiley, New York, 1969, Chapter 7.

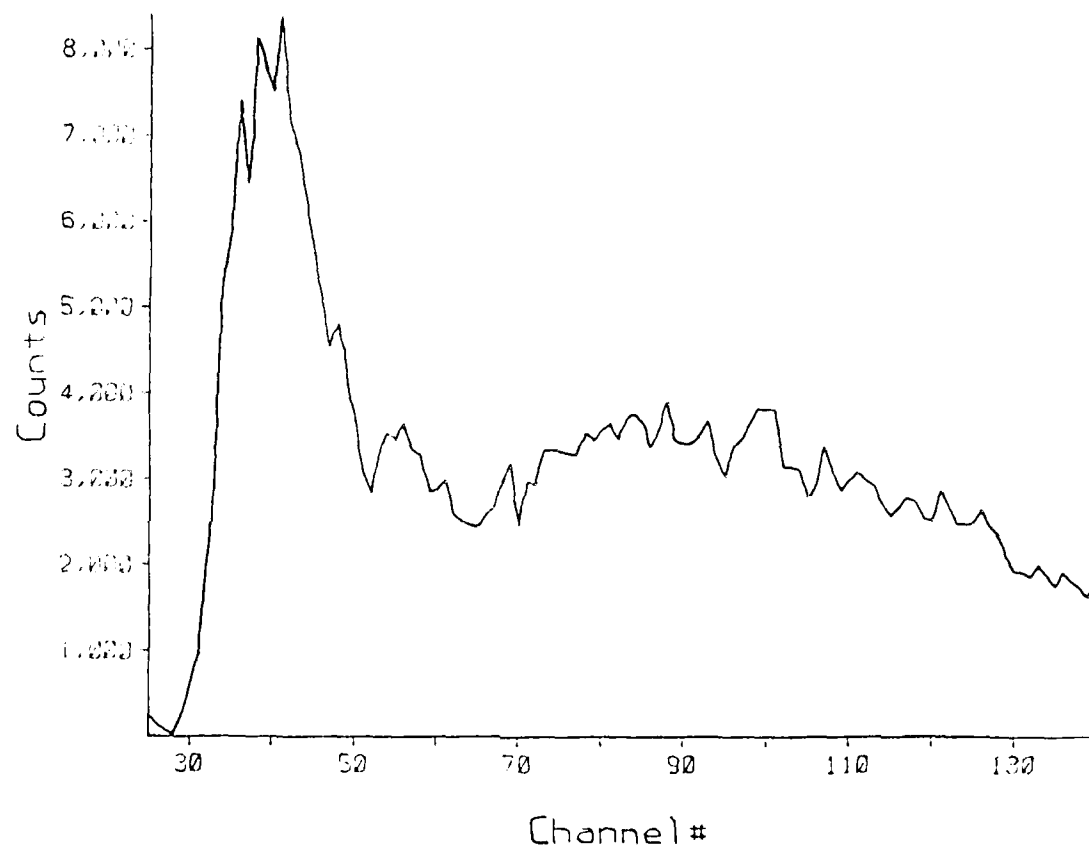


Fig. 1. 30% PBT in Zytel 330 at 245°C.

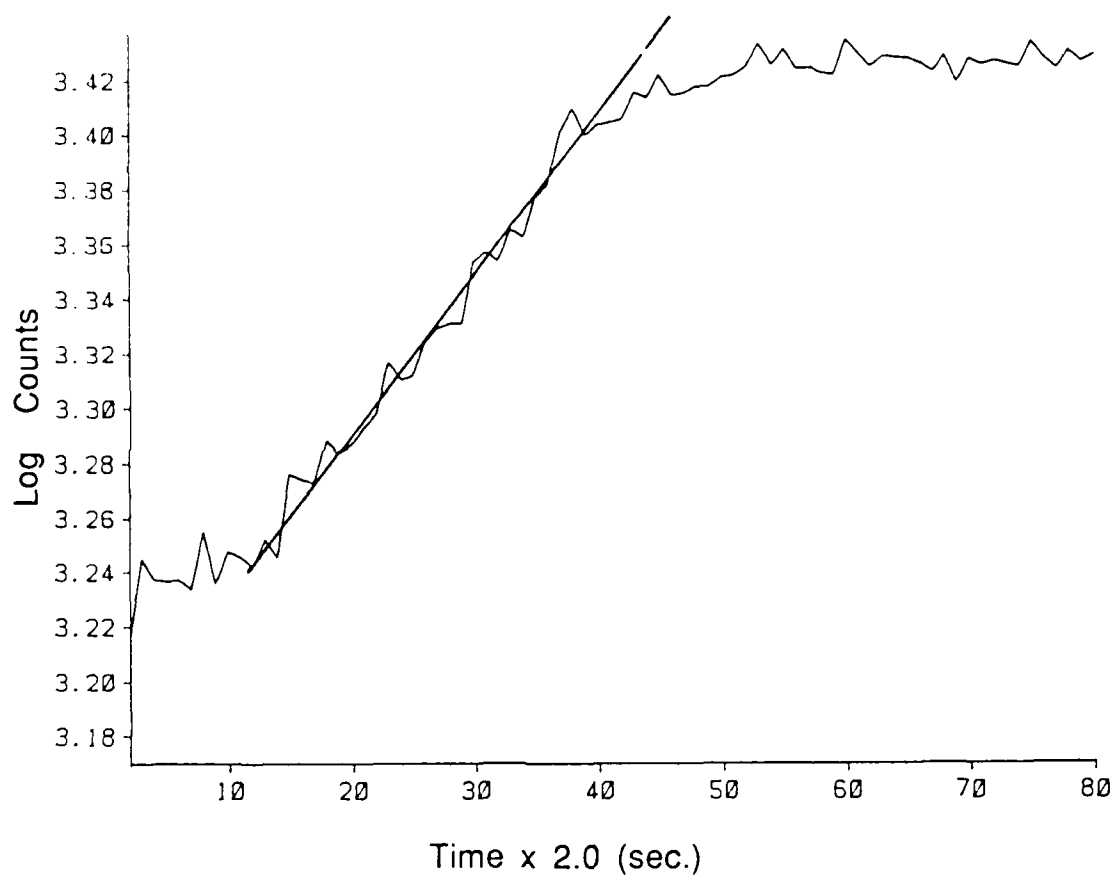


Fig. 2. Growth of Intensity at Scattering Maximum for 30% PBT in Zytel 330 at 265° C.

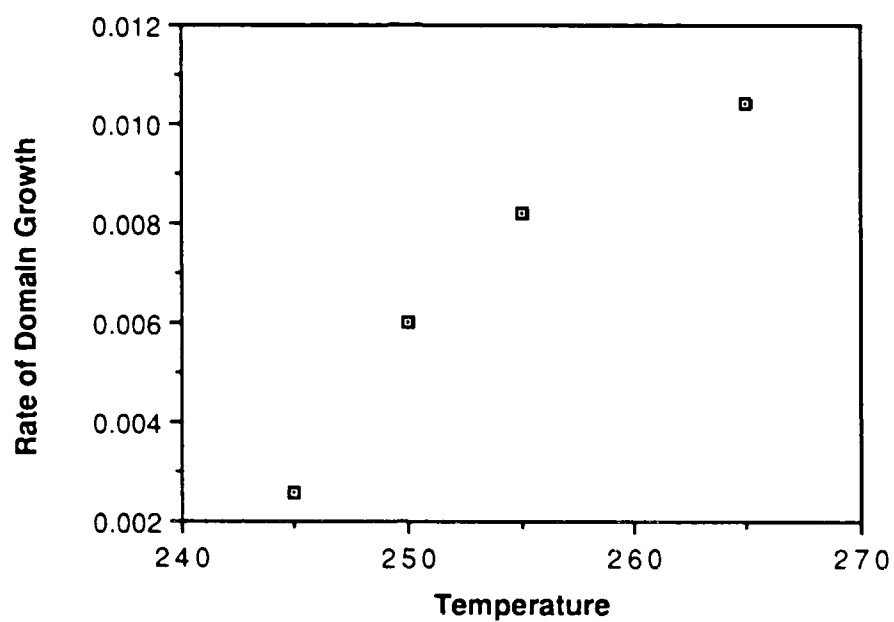


Fig. 3. Phase Separation of 30% PBT in Nylon

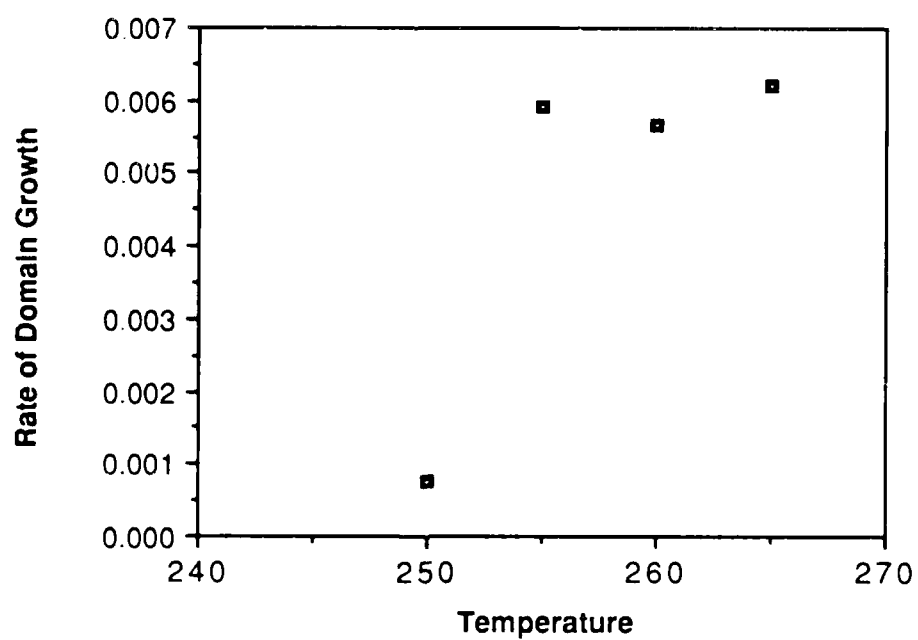


Fig. 4. Phase Separation of 50% PBT in Nylon

1987 USAF-UES SUMMER FACULTY RESEARCH PROGRAM/

GRADUATE STUDENT SUMMER SUPPORT PROGRAM

Sponsored by the
AIR FORCE OFFICE OF SCIENTIFIC RESEARCH

Conducted by the
Universal Energy Systems, Inc.

FINAL REPORT:

"DESIGN OF AN OMNIDIRECTIONAL TORQUER"

Prepared by: Stephen J. GOLD, PhD.

Academic Rank: Associate Professor

Department and Department of Electrical Engineering

University: South Dakota State University

Research Location: United States Air Force Academy

F. J. Seiler Research Laboratory

Department of Engineering Mechanics

Colorado Springs, Colorado

USAF Researcher: Major Steven Lamberson, PhD.

Date: 7 August, 1987

Contract No: F49620 - 85 - C - 0013

Stephen J. Gold

ABSTRACT

This paper describes the design and performance expectations of an Omnidirectional Torquer, which is a special kind of induction motor. The rotor is a sphere, and the useful output is the countertorque that the rotor exerts on the stator while the rotor is being accelerated. The machine has three distributed stator windings surrounding orthogonal axes. Quadrature currents in the form of $i_1(t) = I_m \cos(\omega t)$ and $i_2(t) = I_m \sin(\omega t)$ flowing in any two of these windings will create a rotating magnetic field whose pattern is a spherical surface zonal harmonic of order 1. This moving field induces currents in the rotor's silver surface conductors, which interact with the magnetic field to create torque. To make the machine work in 1 g. environments, the rotor is suspended with neutral buoyancy in a dense ZnBr_2 solution.

A computer simulation was done. Results show that torques of up to 2.7 Newton-meters are possible, in any direction. The torque produced by this machine is in most cases very nearly parallel to the axis of the rotating stator field, even when the rotor is initially rotating at nearly right angles to that axis.

Acknowledgements

My thanks is extended to the Air Force Systems Command and the Air Force Office of Scientific Research for their sponsorship of this effort. Thanks is also due to Universal Energy Systems, Inc. for good instructions and prompt handling of the administrative details of the 1987 Summer Faculty Research Program. My stay from June-August at the United States Air Force Academy was made pleasant by all I encountered, from those who set me up with a parking permit, to those who served me in the cafeteria; and most especially those capable librarians who helped me find or obtain thru interlibrary loans several important references.

The immediate sponsor of this work was F. J. Seiler Research Laboratory's Control of Large Space Structures project. Major Steven Lamberson, the Technical Focal Point and Director of large space structures research, did a good job of focusing my attention on the vibration problems and on instrumentation and experimental methods available to address them. I had some useful discussions with John Duke of the Engineering Mechanics Department about gyroscopic dynamics, and with Major Michael DeLorenzo of the Astronautics Department concerning various methods of attitude control currently being used on satellites. Captain David Bannerman and Major Anthony Nunez were very helpful in getting me going on the computer.

Also, I wish to here acknowledge the support and encouragement received from South Dakota State University: the Electrical Engineering Department Head, Virgil Ellerbruch and the Dean of the College of Engineering, Ernest Buckley - for their interest and letters of recommendation. Wayne Knabach, Director of the Center for Power System Studies, for his interest and critique of proposed work, and for funding one undergraduate and one graduate student (Jim Dykstra and A. Prabhakar) who have worked with me on the Omnidirectional Torquer. Finally, thanks to Christopher Sword, Dean of the Graduate School, for providing a Faculty Development Grant that paid me while I worked on the project during May 1987.

I. INTRODUCTION

The author of this report, Stephen J. Gold, PhD. is an electrical engineering professor with sixteen years of teaching experience, mostly at the University of Southwestern Louisiana in Lafayette, but more recently at South Dakota State University in Brookings. He has taught the Electrical Machinery Course almost every one of those sixteen years, and also teaches Circuits, Control Systems, Electronics, Numerical Methods, and Power Systems as the occasion demands.

The idea for the Omnidirectional Torquer first occurred to Dr. Gold in the fall of 1985, and he has been actively seeking a sponsoring organization since December, 1986. The Air Force Summer Faculty Research Program provided an opportunity for the author to visit the Air Force Academy for a couple of days in March 1987; when he talked with the Officers in Charge and convinced them of the possible relevance of this proposed new 3-dimensional spherical rotor electromagnetic machine to satellite attitude control and active vibration damping in large space structures.

II. OBJECTIVES

It was agreed in March that the ultimate objective of this research should be to make/demonstrate a working prototype of an Omnidirectional Torquer. Design was to be done during the summer of 1987, with procurement of parts to be begun later in 1987 (pending approval of further funding), with assembly and testing to be done in 1988. The Goals and Objectives document filed with Universal Energy Systems, Inc. in the spring of 1987 included these points:

- 1) Find a suitable commercial product that can be used as the stator inside boundary. By May we had obtained from EuroCon some 100 mm dia. translucent polyethelene spheres with dimensional tolerances such that they could be used for this critical part. The size of this part dictates the size of the other parts that will be used for the prototype.
- 2) Design the ferromagnetic core material and conductor bars for the rotor sphere to fit inside 1) above.
- 3) Study stator winding configurations to arrive at a workable layout of semi-distributed windings, together with stator yoke pieces that will complete the magnetic circuit.

- 4) Specify the electric currents necessary in the stator windings to establish the design magnetic flux required by the Torquer.
- 5) Use a computer to predict how much torque (and its 3-dimensional orientation) will be created by the currents of 4) above.
- 6) Set up the rotor dynamics in a form suitable for a computer to simulate the action of the rotor as it accelerates and precesses under various transient excitation drive signals.
- 7) Investigate ways to measure the three angular velocities ω_x , ω_y , and ω_z . These constitute the mechanical state of the rotor.
- 8) Show how the State Measurements in 7) above, and the dynamical equations in 6) above can be used to form a closed loop digital control system for the torquer.

Most of this report is about items 2), 3), 4), and 5), of the above list; item 1) having been already accomplished. Items 6), 7), and 8) are discussed briefly at the end of the report.

III. HISTORICAL BACKGROUND

The idea of a spherical rotor electromagnetic machine to be used for satellite control is not new. It was considered in the early '60's by several individuals and companies. In (1), R.D. Ormsby describes a large 0.25 m dia. hollow aluminum sphere that is held in place by electrostatic forces. The sphere is surrounded by three orthogonal coils excited by sinusoidal voltages and currents. Two of the coils are supplied by voltages $V_m \sin(\omega t)$ and $V_m \cos(\omega t)$, resulting in a 2ϕ induction motor action on/by the sphere. By energizing a chosen pair of coils, the sphere can be made to rotate around either the x-, y-, or z-axis. Hering and Hufnagel (2), present a similar idea, but their sphere is centered by controlled magnetic fields. Both of these concepts required a zero-gravity environment to keep the sphere from scraping bottom. Neither design employed ferromagnetic parts to allow concentration of the magnetic field, so the operating magnetic flux density was low: $.002 \text{ W/m}^2$. Ormsby's paper described how the sphere would be slowed down by interaction with the Earth's magnetic field. Walter Haessermann, who was Tech Chief of the U.S. Army Missile Command during that era, was quite impressed with the possibilities inherent in using a single sphere instead of three separate reaction wheels, seeing that the sphere could result in significant weight saving (3).

In 14, Hans Schropl asserts that "...attitude control and stabilization of satellites by means of rotating masses shows several advantages over reaction jet control. The disturbance torques of space environment are partially cyclic and thus can be averaged out over orbit against reaction jet control; finer resolution and larger range of available torque can be achieved. There are no valve problems and power consumption is smaller by approximately one order of magnitude compared to ion or plasma jets. If the bearing problems can be solved, rotating inertia control will be more reliable - especially for applications involving long mission times - than other types of control. The free reaction sphere offers an optimum way of rotating inertia control. Gyroscopic cross-coupling inherent in combinations of three reaction wheels is negligible with the spherical rotor. Moreover, the weight penalty for angular momentum storage is smaller by a factor of 1.8." These views were being promulgated in the period between 1960 and 1965; thereafter, the literature is silent on the subject of Reaction Spheres. James R. Wertz, author/editor of a modern textbook on attitude control for satellites 15, told this author in a phone conversation that he is unaware of any such system being employed on a satellite since 1975, and probably none were actually used before then.

One big problem in these early designs was How to Keep the Sphere Centered. The preoccupation was to have a sphere that was free to turn with essentially zero friction. In this report we examine some designs that no longer try for a free sphere; there is appreciable friction caused by a liquid filling the space between rotor and stator. The liquid provides several benefits: 1) A hydrodynamic centering force similar to what happens in cylindrical journal bearing. 2) Lubrication to prevent/minimize damage caused by contact of the rotor with the stator. 3) A gravity-cancellation mechanism; the composite rotor's specific gravity is designed to match the fluid, so it is suspended with neutral buoyancy. This enables terrestrial testing. 4) A heat-transfer medium to keep the rotor conductors from overheating. 5) A fluid brake that automatically and smoothly recovers angular momentum from the sphere and restores it to the spacecraft as a whole. 6) Vibration damping; this occurs to some extent even if the Torquer's stator windings are not excited at all. The fluid in the gap means that there will be a terminal speed at which the friction torque equals the driving torque, and no further useful output in that direction can be obtained until the rotor has been slowed down or reoriented.

A new problem for spacecraft has arisen as they become larger, approaching Space Station size. The earlier satellites were typically regarded as rigid bodies; but if something large is assembled in space using slender structural members, low-frequency vibration (in the range from less than 0.1 to about 10 Hz) becomes a problem, especially after slewing maneuvers. A active damping actuator is desirable; and it is known that torque-producing machines are more effective at this than linear force-producing machines would be in vibration-supression service.

IV. DESCRIPTION OF THE TORQUER AND ITS PARTS

The Omnidirectional Torquer is a machine designed for transient rather than steady-state service. Its useful output is the counter-torque that the rotor exerts on the stator while the rotor is being accelerated. 'Accelerated' is to be interpreted in the general vector sense of gyroscopic precession as well as changing the magnitude of the angular velocity while holding its orientation fixed.

The Torquer operates on the principles of a polyphase induction motor: The stator windings are excited by periodic currents whose fundamental components are strongly dominant (pure sinusoids would work best, but other waveforms with a strong 1st harmonic will also work). There is a phase shift of 90° between currents in a pair of coils, which creates a rotating magnetic field as in a 2 ϕ motor. The rotor is spherical, with a ferromagnetic core and the best conductive material - silver - near the surface, either as discrete rotor bars or a thin spherical shell. Because there is relative velocity between the rotating stator field and the rotor, there are large eddy currents induced in the silver on the rotor surface. The magnetic field is mostly radial as it passes across the rotor-stator gap, through the conductor-surface and into the core, and the induced currents are parallel to the surface perpendicular to the magnetic field. By the Laurentz Magnetic Force law, there will be a force on these rotor-surface currents, which is mutually perpendicular to both the radial field and the tangential currents:

$$d\vec{F} = i d\vec{L} \times \vec{B} \quad \text{Eq(1)}$$

This force is also tangential to the surface of the sphere; and since it acts at the end of a radial lever arm, it produces a torque which can accelerate the rotor. In most practical cases the speed of stator magnetic field greatly exceeds the rotor's mechanical speed, and the torque is almost alligned with the axis of rotation of the stator field.

The Rotor Core

The ferromagnetic rotor core needs to have the following properties:

- 1) High magnetic permeability.
- 2) Low eddy current and hysteresis losses.

Making the core of solid iron would result in core losses in excess of 1 KW. Solid exotic magnetic materials such as Vanadium Permendur, while capable of sustaining high flux densities, would have core losses in excess of 1 watt. The two best candidate materials are those commonly used in cores in high audio frequency inductors: 1) ZnMn Ceramic Ferrite, Type MN-67, which saturates at a flux density of 0.52 W/m^2 , or 2) Pressed Powdered Iron with a relative permeability of 125, which begins to saturate at 1.1 W/m^2 . The powdered iron core would have losses of about 27 watts/lb if driven to 1 W/m^2 at a frequency of 400 hz, which is about what the core losses would be in the core shown in Fig. 1 below if it were standing still in a 400 Hz rotating field. The ceramic ferrite has a density of 4.8 g/cm^3 , and the pressed powdered iron's density is 6.9 g/cm^3 . In electromagnetic machines, it is generally true that the output power is proportional to B_{max}^2 , so the powdered iron is more attractive from that standpoint; however, the core loss in a ferrite core would be less than 1 watt. {6}, {7}

To attain neutral bouyancy, it is necessary that the rotor core be hollow. Manufacturability considerations dictate that it be fabricated using several identical sections which could be cemented together with epoxy; such as the Octant Sectors shown below in Fig. 1:

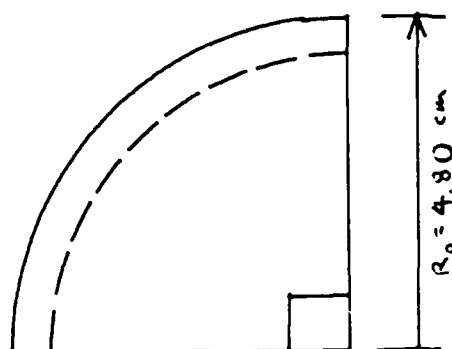
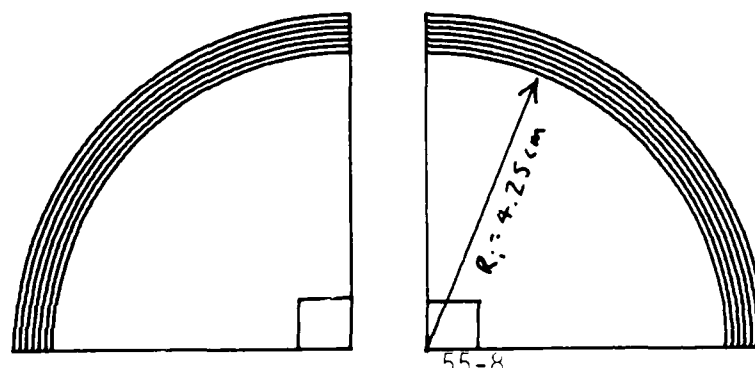


Fig. 1. Orthographic Views of a Rotor Octant Sector

Mat'l: Carbonal Pressed Powdered Iron
Relative Permeability, 125.



The rotor core of Fig. 1 is designed to be suspended in ZnBr_2 solution. The density of such a solution can be $2.4 \pm \frac{2}{\text{cm}^3}$, which is what determines the allowable thickness of the core wall. An alternative design which utilizes a solid ferrite core surrounded by a silver spherical shell 0.377 in. thick was also considered. This alternate rotor has a composite density of $9.5 \frac{\text{g}}{\text{cm}^3}$, and could be suspended in liquid gallium. It would also be possible to have a solid pressed iron core surrounded by a gold shell, with composite density of $13.6 \frac{\text{g}}{\text{cm}^3}$ such that it could be suspended in mercury; but mercury is hard to contain.

The Conductor Bars on the Rotor Surface

While it is possible to make a rotor with an outer shell of silver or copper, it was decided to investigate a configuration of finite rotor bars as a recommended design. The bars divide the surface up into triangles, as shown in Fig. 2 at right. The analysis of motionally induced electromotive forces and the resultant current flow pattern then becomes a sort of Finite Element Analysis. The result would also be indicative of what would happen with a rotor surface shell. Two practical benefits accrue from using finite bars instead of a solid shell:

- 1) A Lubricant Step Pressure Boost occurs on the leading edge of a bar as it slides, tending to push the rotor toward the center of its cavity-10*, Gross.
- 2) The increased volume of fluid is capable of absorbing more heat.

There is also an argument that a dimpled surface turns with less friction than a smooth one: "Total drag on a body can often be reduced by causing a laminar boundary layer to become turbulent. To accomplish this transition the surface can be artificially roughened or projections mounted upon it.*" 8

The layout of the rotor bars is begun by establishing where on the surface of a unit sphere the vertices of a regular dodecahedron, which has 12 pentagonal faces, are. There are a total of 20 such vertices, and a tabulation of their rectangular cartesian coordinates is in Table I.

* This applies to linear motion through a fluid; it's not clear whether it applies to rotating-in-place. It's only significant at rare higher speeds.

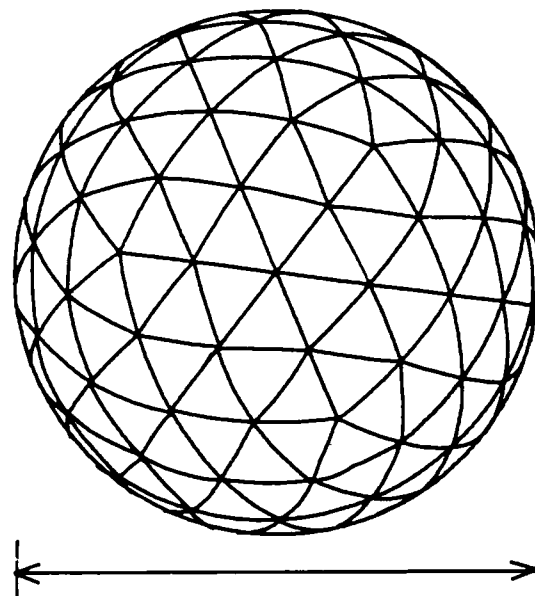


Fig. 2. A Perspective View of the Rotor and Surface Bars.

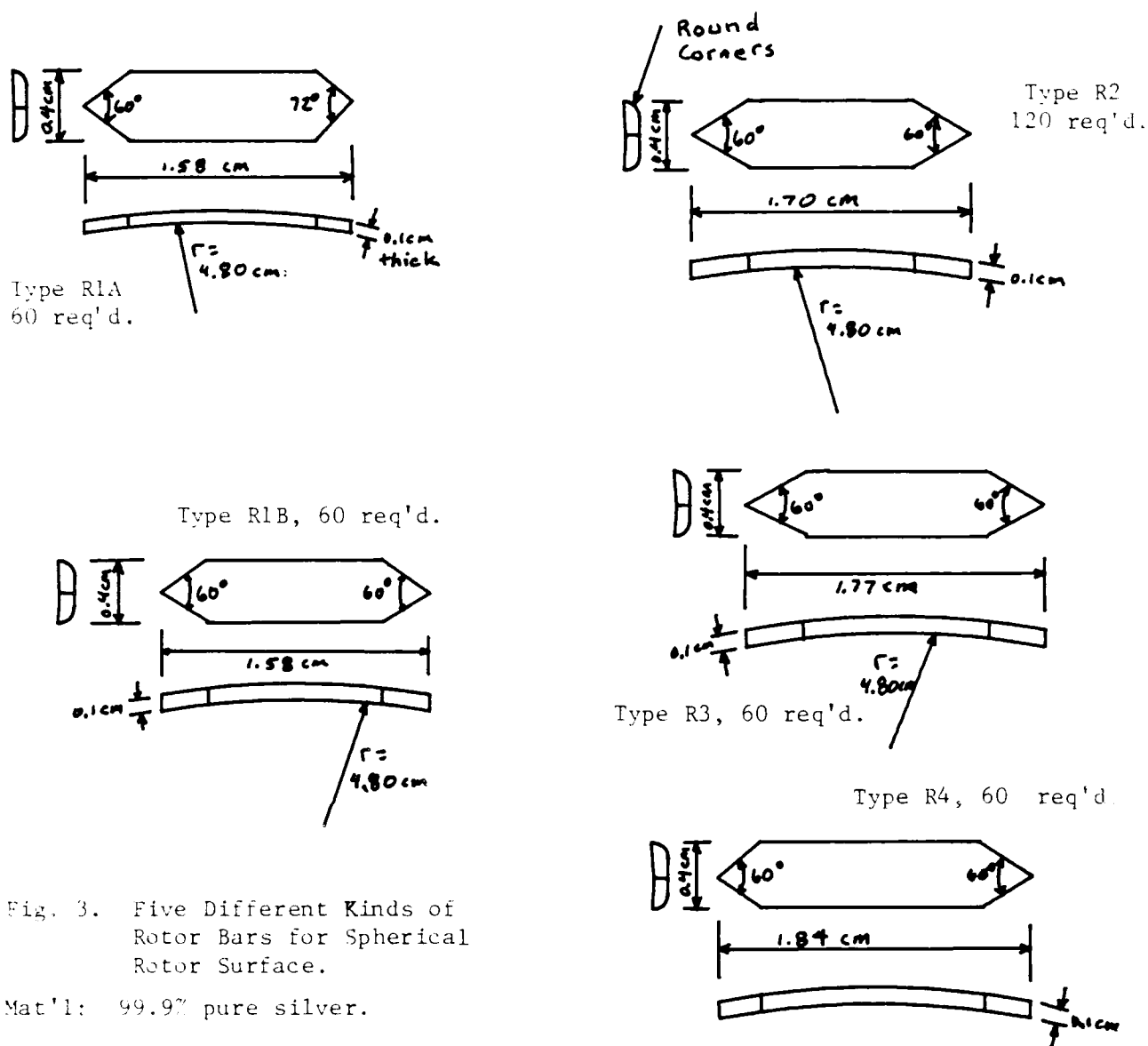


Fig. 3. Five Different Kinds of Rotor Bars for Spherical Rotor Surface.

Mat'l: 99.9% pure silver.

(0.00000, 0.00000, 1.00000)	(0.57735, 0.74535, 0.33333)
(0.00000, 0.66667, 0.74535)	(-0.57735, 0.74535, 0.33333)
(-0.57735, -0.33333, 0.74535)	(-0.93417, 0.12732, 0.33333)
(0.57735, -0.33333, 0.74535)	(-0.35682, -0.87268, 0.33333)
(0.93417, 0.12732, 0.33333)	(0.35682, -0.87268, 0.33333)

Table 1. The X-, Y-, and Z- Coordinates of the Vertices of a Dodecahedron.

The other ten vertices of the dodecahedron are diametrically-opposed to the ten tabulated above, with opposite algebraic signs.

Next, the center points of the twelve faces of the dodecahedron are found. This can be done by averaging the individual components of the coordinates. The vector from the origin through each face-center point is

normalized to unit length. The 20 vertices and the 12 face-center points divide the sphere surface up into 60 almost-equilateral triangles. Each of these triangles can be further subdivided, joining the midpoints of their sides; this results in 240 triangles covering the sphere surface. All connections are made using great circle arc segments. The resulting rotor bar configuration consists of 360 individual rotor bars with four different lengths (see Fig. 3). Viewed as an electric network, it has 121 independent nodes and 239 independent loops. The network can be stretched and laid flat on a plane; that is done below in Fig. 4. Also shown on Fig. 4 are the numbers that were assigned to some of the nodes to facilitate computer analysis of the network. Adjacent node voltages differed by less than 0.1 volts, and most of the currents in the bars were about 30-90 amperes.

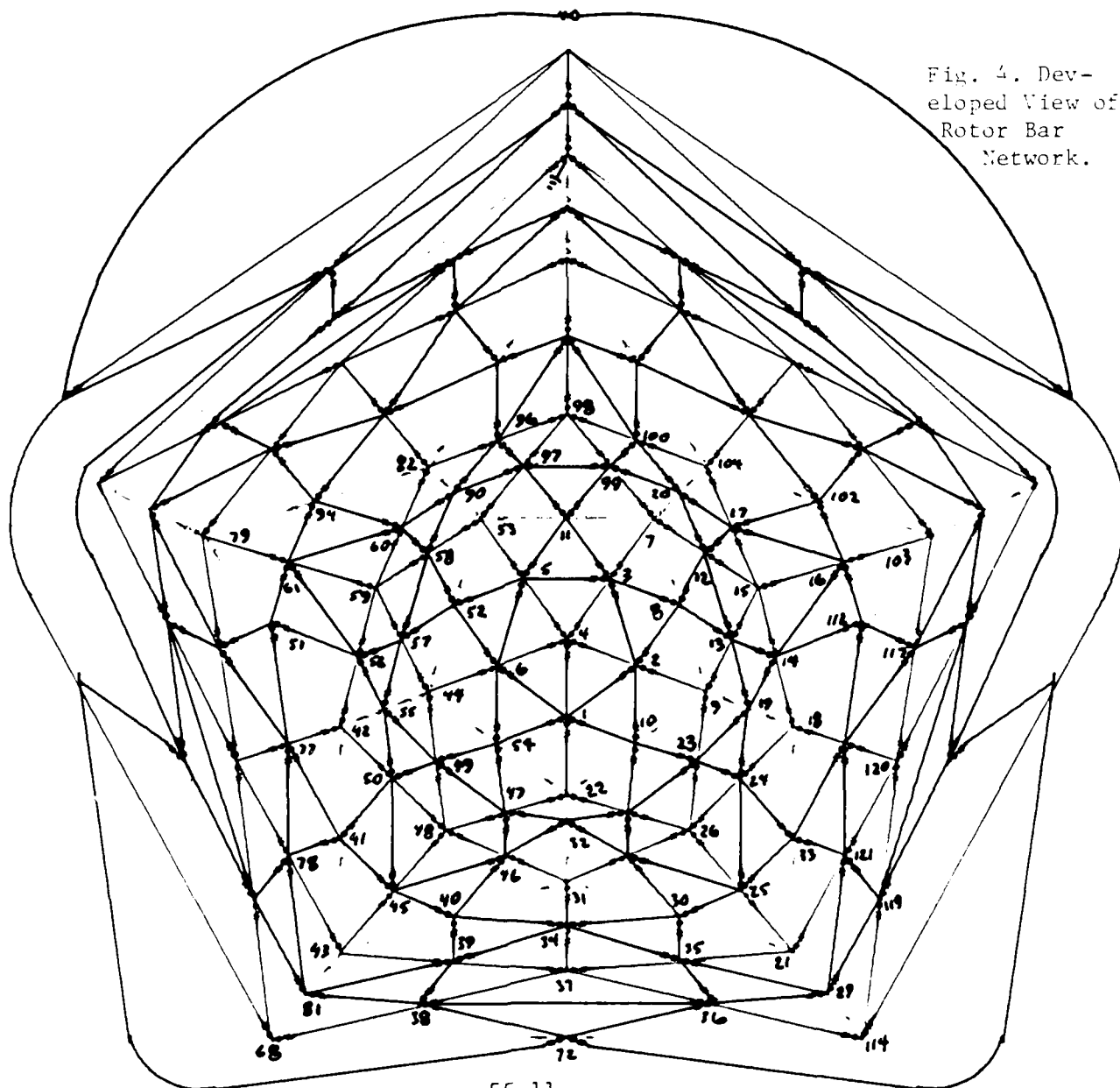


Fig. 4. Developed View of Rotor Bar Network.

Composite Rotor Parameters

The spherical rotor described in the foregoing paragraphs has a combined mass of 1151 grams (978 grams in core + 173 grams of silver rotor bars). Its density is

$$\rho_r = \frac{1151}{4 \cdot 4.84^3/3} = 2.42 \text{ g/cm}^3.$$

The polar moment of inertia of this rotor would be $1.61 \times 10^{-3} \text{ kg-m}^2 = \text{J}$.

Liquid for the Gap

The primary requirement for the liquid that fills the spacing gap between the stator and rotor is that it must be dense enough to lift the rotor off the bottom so earth-bound testing in a 1 g field is possible. There are surprisingly few liquids that will meet that primary requirement. One fair candidate is zinc bromide solution in water. It is possible to dissolve up to 447 grams of this salt in cold water, to get a solution whose density is 2.45 g/cm^3 at 20°C (9). For most purposes, we can regard the density to be proportional to the number of grams dissolved in a given volume of H_2O ; so ZnBr_2 solution is a clear, almost colorless liquid whose density can be adjusted over the range from 1.0 to $2.4+ \text{ g/cm}^3$.

The viscosity of this liquid is about the same as water's viscosity, but its kinematic viscosity is less than water's because of the higher density of ZnBr_2 solution. Assuming that for closely spaced concentric spheres the Reynolds Number separating laminar from turbulent flow is about 1000 (10) we deduce that for the 0.1 cm spacing between rotor and stator, turbulence in the boundary layer will commence at a speed of about 2 m/sec , which corresponds to a rotational angular velocity of 40 rad/sec . For rotational speeds in excess of 100 rad/sec , we can expect turbulence in this particular liquid even if both inner and outer surfaces were smooth.

Friction torque when the rotor is turning at 30 rad/sec was estimated using integration of the viscous shear forces over the surface of the sphere. The result was that at this speed, $T_f = 1.6 \times 10^{-3} \text{ Newton-Meters}$. This is a rather uncertain result, as it depends on the temperature of the liquid, how well the sphere is centered, and possibly roughage-induced turbulence. However, it is an order of magnitude smaller than the drive torque available so we conclude that it will be possible to accelerate the rotor to some point beyond the inception of turbulence, probably beyond 100 rad/sec , but to get up to speed may take 1-2 seconds of acceleration. If the Torquer were to be used to damp low frequency vibrations of say 0.1 Hz, then it would be desirable to drive it in one direction for five seconds, reverse it for the next five seconds, etc. Rapid acceleration causes turbulence early.

When a sphere is immersed in a liquid while it is being turned inside a slightly larger spherical cavity, there is a hydrodynamic centering force given by

$$F_x = \frac{\Lambda \pi}{(4+\epsilon^2) \epsilon^2} \left[(1+\epsilon^2) \ln\left(\frac{1+\epsilon}{1-\epsilon}\right) - 2\epsilon \right] \sin(\phi) , \quad \text{Eq(2)}$$

from Matsch (10)

To use Eq(2), first find the center offset from $c = h - e \cos(\phi)$ Eq(3)

where h = average fluid gap spacing when spheres are centered

e = distance between the spheres' centers at point in question

ϕ = angle between a line drawn from the center of the inner sphere to the center of the outer sphere and the axis of rotation of the inner sphere; $0 < \phi < \pi$ radians.

Then c can be used to evaluate the 'Bearing Number' Λ from

$$\Lambda = 6 \mu \omega r^2 / (c p_a) \quad \text{Eq(4)}$$

here μ = Viscosity

ω = Angular Velocity

r = Spheres' radius (almost the same for both)

c : defined above in Eq(3).

p_a = Average absolute pressure in liquid

F_x is not collinear with the line joining the centers, but in nearly all cases it has a positive component along that line. The exception is when the inner sphere is rotating around the line joining the spheres' centers, such as a heavy metal ball turning around a vertical axis in a round cavity; in that case there is no hydrodynamic force to lift the ball off the bottom. It is of interest to estimate the size of this hydrodynamic force for the 100 mm dia. Omnidirectional Torquer:

using $e = .05 \text{ cm} = .000164 \text{ ft}$ and $h = .1 \text{ cm} = .000328 \text{ ft}$

$\cos(\phi) = .7071 = \sin(\phi)$ then $e \cos(\phi) = 1.16 \times 10^{-4} \text{ ft}$

so $c = h - e \cos(\phi) = 2.12 \times 10^{-4} \text{ ft}$

$p_a = 1440 \text{ lb/ft}^2$

$\omega = 100 \text{ rad/sec}$

$r = .165 \text{ ft.}$

$\mu = .00002$

Values are normalized by a factor of $p_a r^2$.

from which $\Lambda = 1.07 \times 10^{-3}$

and $\epsilon = e/c = .774$; $\epsilon^2 = .598$

Putting these values in the formula for F_x yields $F_x = 0.06 \text{ lb}$ or about .27 newtons. This value is less than 10% as big as the tangential forces produced by the rotating magnetic field, mostly because the viscosity of ZnBr_2 solution is much less than typical lubricants.

Stator Windings

The ideal flux distribution for a 2-pole spherical machine is the aforementioned Surface Zonal Harmonic of Order 1 [2], [11]. If such a flux distribution moves past a great circle coil, it will generate a sinusoidal voltage in the coil. The converse is also true; quadrature currents of the form $I_m \cos(\omega t)$ and $I_m \sin(\omega t)$ flowing in orthogonal coils properly distributed over the stator surface will set up a rotating magnetic flux whose spatial form is a spherical surface zonal harmonic of order 1.

One way to create such a flux distribution is to wind a single layer of wire on the stator inner sheath as shown in Fig. 5 below. The turns are as close as possible near the equatorial bulge, but the space between turns increases as the sine of the latitude. This layout has the virtue that the space allocated for windings is a simple spherical shell. For AWG#16 wire, Phase A would be 74 turns around a 10.2 cm diameter sphere. Phase B would also have 74 turns, and it is set at right angles to Phase A. Phase C is on a slightly larger 10.72 cm diameter sphere oriented at right angles to both of the other phases. The outside diameter after all three windings are in place would be 10.98 or nearly 11 cm. The flux gap from the rotor core surface to the outside of the third stator winding would be $5.5 - 4.8 = 0.7$ cm, and it would be uniform all around.

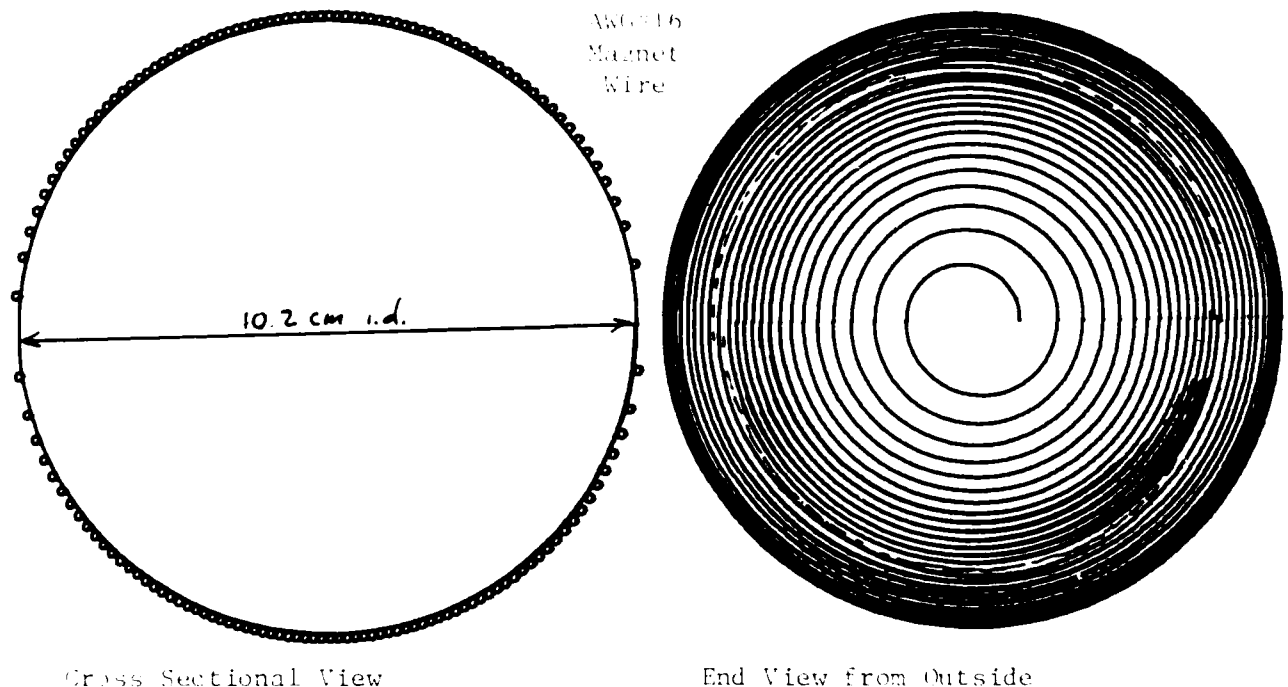


Fig. 5 Two Views of a Single Layer Winding whose Space-Between-Wires Varies as the Sine of the Latitude. 3 Concentric Windings Req'd.

The current required in the stator coils to establish a peak flux density of 0.216 W/m^2 at the poles (which would mean that the flux density in rotor core midway between the poles would be $1. \text{ W/m}^2$) is 23 Amps_{rms}. This is nearly 7x the steady state rated current of AWG #16 magnet wire, and could be tolerated only briefly (one second or so) if followed by a much longer (1 minute) period of almost no current. The long air gap assures the the machine will be linear with no saturation of the ferromagnetic parts over a wide range of stator currents. To protect the stator windings from overheating and burning their insulation, there should be a Slow Blow fuse with a steady-state pass through current rating of 4.0 A. in series with each of the three stator coils.

Stator Yoke

The ferromagnetic piece on the outside of the Torquer is very similar to the innermost rotor core: both are spherical shells that must be made of isotropic, low loss, high permeability material. Both are about 0.6 cm thick and would probably be made by the same vendor out of the same substance: powdered iron compress or ZnMn ferrite. In each part, there are several pieces to put together to make the whole; however, the stator yoke would be banded rather than glued so disassembly will be possible. Also the stator yoke needs some holes designed into it to allow the wires to pass out, and also allow for tubes carrying the gap liquid to/from an external heat exchanger.

V. COMPUTER SIMULATION PROGRAM AND RESULTS

Two computer programs were written using a TurboPASCAL software development disk that runs on Zenith 248 and other IBM-PC compatible microcomputers; two separate programs were necessary because of the 64Kbyte storage capacity limitation of TurboPASCAL. The intermediate data had to be put to and read from random access disk files, which slowed the running time so it took 53 minutes to complete a single simulation run through both programs.

The two programs compute 3-dimensional torque at a given instant for any user-specified rotor velocity vector, and any size and orientation of rotating magnetic field. The first program finds the voltages generated by the motion of each bar relative to the field. Each branch voltage is then converted to an equivalent Norton-type current source. The second program uses an accelerated Gauss-Siedel algorithm to solve 121 simultaneous equations for the Node Voltages. Then it finds the branch currents and computes their interaction with the field to produce torque.

Both programs use data files which specify the location on the rotor surface of the 122 nodes together with their interconnections and reference polarities to form 360 individual branches.

Surface points' coordinates are transformed to get their locations at $t = t_1$. The first program then computes the 1st Zonal Harmonic flux density that will exist at each point when $t = t_1$, using

$$B_s = B_m \sin(\phi) \quad \text{Eq(5)}$$

where ϕ is the latitude angle.

The flux of Eq(5) is radially oriented, and must be resolved into x-, y-, and z- components. Also the inertial frame velocity vector of the flux density wave as it moves along the rotor surface is calculated and resolved into cartesian coordinates. The \vec{B} and $\dot{\vec{B}}$ vectors are computed for each of the 122 nodes plus three intermediate points equally spaced along the 360 rotor bar branches, so a total of 7212 numbers must be stored.

The first program uses the computed positions to find the velocities of the rotor surface points from

$$\vec{V} = \vec{\omega}_r \times \vec{P} \quad \text{Eq(6)}$$

The velocity vectors are then transformed into a coordinate frame whose x-axis coincides with the axis of rotation of the stator field, where they can be subtracted from the field's velocity to get a relative velocity, \vec{U}_r .

The voltage induced in each rotor bar is computed by using Bode's 5-point numerical integration formula to evaluate the expression

$$E_{\text{bar}} = \int_{-\pi}^{+\pi} (\vec{U}_r \times \vec{B}) \cdot d\vec{L} \quad \text{Eq(7)}$$

Finally, the first program uses the rotor circuit topology specified in the input data file to convert the Thevinin-type voltages sources (a generator in series with a resistor) to equivalent Norton-type current sources in parallel with resistors. Signed sums of all current sources feeding toward each of the 121 independent nodes are then computed.

The second program begins with the final results of the first program; the current source sums are incorporated into Kirchhoff-current-law equations for each node. The equations are rearranged to a form where the voltage in question appears by itself on the left side of '=':

$$V_n = I_{sn}/g_t + \frac{g_b V_b}{g_t} + \frac{g_c V_c}{g_t} + \frac{g_d V_d}{g_t} + \frac{g_e V_e}{g_t} + \frac{g_f V_f}{g_t} \quad \text{Eq(8)}$$

where g_b is the conductance of the element between node \underline{n} and node \underline{b} and g_t is the sum of all conductances attached to node \underline{n} . Eq (8) is

the form required by Gauss-Siedel iterative methods; such methods will eventually converge from any set of initial guesses for unknown values; faster convergence can be obtained in this case by using an acceleration factor of $a = .4$ in

$$(V_n)_{i+1} = (1+a) \left(\frac{I_{sn}}{g_t} + \frac{g_b V_b}{g_t} + \frac{g_c V_c}{g_t} + \frac{g_d V_d}{g_t} + \frac{g_e V_e}{g_t} + \frac{g_f V_f}{g_t} \right) - a(V_n)_i \quad \text{Eq(9)}$$

even with the acceleration factor, several hundred iterations were required to obtain answers to 6-significant-digit accuracy.

Using simple algebraic equations instead of differential equations to model the rotor circuit is justified because the size of the rotor inductance parameters is so small: the self-inductance of one of the triangular loops can be computed from $L = l^2/R_m$ where l is the number of turns and R_m is the magnetic reluctance of the air gap, $R_m = g/\mu_0 A$. This yields a value of 2.3×10^{-9} Henries, so a radian frequency in excess of 10^4 rad/sec would have to exist before inductance of the rotor would be important. The highest frequency considered in any simulation was 2513 rad/sec for 400 Hz operation.

When the Gauss-Siedel iterations are finished, the current in each branch is found by dividing the potential difference between the ends by the particular resistance of that branch ($r_1 = 7.08 \times 10^{-5}$ ohms, $r_2 = 7.44 \times 10^{-5}$ ohms, $r_3 = 7.93 \times 10^{-5}$ ohms or $r_4 = 8.25 \times 10^{-5}$ ohms).

The torque is computed by first finding the vector forces from Eq(1) at each end, at the mid-point, and at the quarter-points of each rotor bar

$$d\vec{F} = i d\vec{L} \times \vec{B} \quad \text{Eq(1)}$$

The x-, y-, and z- components of the tangential unit vector \vec{L} which runs along the length of the rotor bar was computed/saved in the first program, where they were used to find the voltages generated in a bar. Finally, differential torque can be computed using the vector cross product

$$d\vec{T} = \vec{P} \times d\vec{F} \quad \text{Eq(10)}$$

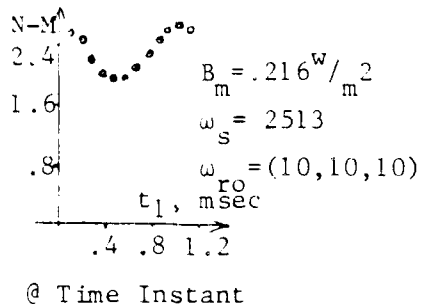
the three components of such torques were computed at each of the five points in each rotor bar. Each component was then numerically integrated using Bode's formula to get the total torque due to current in that bar

$$T_x = \int dT_x \approx \frac{\text{length}}{90} (7 T_{0x} + 32 T_{1x} + 12 T_{2x} + 32 T_{3x} + 7 T_{4x}) \quad \text{Eq(11)}$$

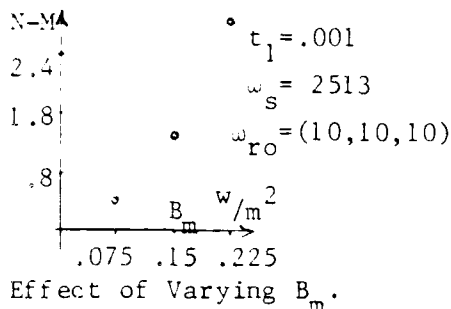
There are similar equations for the y- and z- components. Torque components for all 360 bars were added together to find the total torque acting on the rotor.

Some Results from Simulation Test Runs

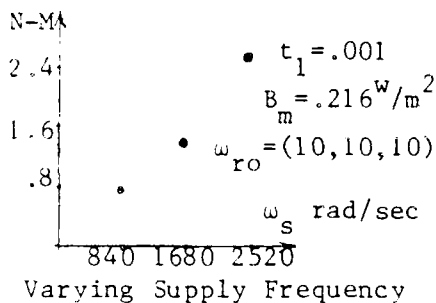
Shown below in Fig. 6 are a few data points showing the magnitude of torque predicted for the Omnidirectional Torquer as supply parameters vary.



The top graph shows the effect of varying the time instant, t_1 . It shows the effect of finite element modelling. A solid spherical shell rotor would have the same torque for any t_1 . The 800 Hz variation is 2x the supply frequency; Similar rapid torque variations occur in cylindrical machines, particularly 1 \emptyset models.



The middle graph displays the expected property that torque varies as the square of the air gap flux density. The rotor core would begin to saturate at a flux density of 0.216 W/m^2 .



The bottom graph shows that the torque increases almost quadratically as the stator frequency is increased--as expected. For all 17 cases whose torque magnitudes are plotted in Fig. 6, the direction cosine of that torque was $(.998+, 0, 0)$ so the torque is essentially aligned with the axis of the rotating field. Other test showed that when the rotor velocity was $3/4$ as big as and nearly at right angles to the rotating field the torque produced was still within 7.7° of the rotating field axis. Simulation also showed braking torque with d-c excitation.

Fig. 6 Plots Showing How Torque Varies With t_1 , B_m , and ω_s .

VI. CONCLUSIONS

The simulations show the torquer will work reasonably well, producing torque of about .25 N-M when the drive frequency is 100 Hz. That much torque could accelerate the rotor from standstill to 100 rad/sec in about 1.5 sec. Going faster than that is not recommended because of turbulence in the gap liquid. The torque available from the Omnidirectional Torquer is somewhat less than one gets from similar-size 1-degree-of-freedom cylindrical machines for three reasons:

- 1) The total flux through and density of the Omnidirectional Torquer rotor is limited by what can be supported in a liquid whose maximum density is only 2.45 g/cm^3 . This limit is imposed by the desire to test the Torquer in a laboratory instead of in space; in a weightless environment the rotor

density could be as high as $7 \frac{g}{cm^3}$ and the liquid could be chosen for its lubricant properties rather than its buoyant properties.

2) The stator currents are uncomfortably large. This would be partially overcome by the fact that only two of the three windings would be energized at a time; and also because the machine is designed to produce torque transients, so no mode of operation would persist for more than a few seconds. If the stator is wound with fewer turns of thicker wire, say 59 turns of AWG #14 instead of 74 turns of AWG #16, that would increase the length of the air gap from 0.7 to 0.8 cm; so a 25% increase in wire space would only result in a 10% increase in flux. An external cooling fan would help, as would increasing the circulation rate of $ZnBr_2$ solution through the gap. Allowable stator currents, rather than rotor flux density, are the limiting factor in a machine of this design.

3) The isotropic ferromagnetic material used in the torquer saturates at a lower level than the electrical steel laminations used in cylindrical machines does (1.0 vs $1.5 \frac{W}{m^2}$). Restriction 2) above still dominates.

VII. RECOMMENDATIONS

A Proposal for a follow-on Mini Grant to build and test a prototype of the Torquer will be submitted about Sept. 30. The proposal will describe torque measuring techniques and a way to estimate the 3-dimensional velocity of the rotor. Further work on a larger, faster computer can expand the present program so it can simulate acceleration/precession transients. When the applied torque is not collinear with the axis of rotation of the rotor, it can be resolved into a collinear component and a perpendicular component. The collinear component T_c increases or decreases the speed of the rotor according to

$$\frac{d\omega}{dt} = \frac{1}{J} T_c - f \omega \quad \text{Eq(12)}$$

The perpendicular component T_p will cause precession, governed by

$$\frac{d\vec{\omega}}{dt} = \frac{1}{J \omega} \vec{T}_p \quad \text{Eq(13)}$$

The differential eqns(12,13) can be simulated using a Runge-kutta method.

Finally, a control scheme will be developed that uses microprocessors to receive and interpret measurement information; compare the measured condition to what is desired, and use the difference(s) to control the voltage and current waveforms - which should be nearly sinusoidal - coming from a power supply to the stator windings.

REFERENCES

1. Ormsby, R.D. and Smith M.C. "Capabilities and Limitations of Reaction Spheres for Attitude Control" in American Rocket Society Journal, pgs. 808-812 June 1961.
2. Hering, K.W. and Hufnagel, R.E. "An Inertial Sphere System for Complete Attitude Control of Earth Satellites" in American Rocket Society Journal Vol. 31 pgs. 1074-79 August, 1961.
3. Haeussermann, Walter "Comparison of Some Actuation Methods for Attitude Control of Space Vehicles" In Proceedings of Space Stations Symposium, sponsored by International Astronomics Society (Los Angeles, 1960).
4. Schropl, Heinz "Attitude Stabilization of Satellites using a Free Reaction Sphere" in Raumfahrtforschung (German) Vol. 9 pgs 112-117 July-Sep. '65. English abstract appears as entry A65-30319 in the 1965 International Aerospace Abstracts.
5. Wertz, James R. editor of Spacecraft Attitude Determination and Control (written by members of the technical staff Attitude Systems Operations, Computer Sciences Corp.) Dordrecht: Boston: Reidel, 1978.
6. Ceramic Magnetics, Inc. Engineered Ferrites informational brochure available from Ceramic Magnetics, 87 Fairfield Rd. Fairfield, N.J. 07006
7. Magnetics Div. of Spang and Co. Powder Cores, Molypermalloy and High Flux Cores for Filter and Inductor Applications copyright 1986 by Magnetics 900 E. Butler Rd. P.O. Box 391 Butler, Pennsylvania 16003
8. Plapp, John E. Engineering Fluid Mechanics pg. 454 Prentice-Hall, 1968
9. Chemical Rubber Company Handbook of Chemistry and Physics, 83rd Ed. pg. B-158 Cleveland, Ohio 1983
10. W.A. Gross, L.A. Matsch, V. Castelli, A Eshel, J.H. Vohr, & M. Wiklmann Fluid Film Lubrication, pgs 298-301 Wiley Interscience, 1980
11. A.N. Miliakh, V.A. Barabanov, & D.V. Dvoynikh Three-Degree-of-Freedom Electrical Machines (in Russian) published in Kiev, U.S.S.R. 1979

1987 USAF-UES SUMMER FACULTY RESEARCH PROGRAM/
GRADUATE STUDENT SUMMER SUPPORT PROGRAM

Sponsored by the
AIR FORCE OFFICE OF SCIENTIFIC RESEARCH
Conducted by the Universal Energy Systems, Inc.

FINAL REPORT

Acoustic Emission and the Fracture Behavior of
2-D Carbon-Carbon

Prepared by:	Michael R. Gorman, Ph.D.
Academic Rank:	Assistant Professor
Department and	
University:	University of Nebraska-Lincoln
Research Location:	AFAL/MKBC Edwards AFB, California
USAF Researcher:	James Koury
Date:	September 30, 1987
Contract No.:	F49620-85-C-0013

Acoustic Emission and the Fracture Behavior of 2-D Carbon-Carbon

Dr. Michael R. Gorman

Abstract

Very limited data on the acoustic emission behavior of C-C material can be found in the literature.

Tensile coupons 10" x 1" x 1/4" were machined from flat plates made of 2-D Carbon-Carbon material and subjected to uniaxial loading in either the warp or fill directions. The specimens showed a notch sensitive fracture behavior when quasistatically loaded to failure. The quality of the material was documented by photomicrographs. The average density was approximately 1.6 g/cc and the strength values in the warp direction were about 14 ksi for the unnotched specimens. The AE parameters recorded included counts, duration, amplitude, and energy. They are being studied for correlations with the observed fracture behavior.

Acknowledgements

The author would like to thank Jim Koury, Jim Wanachek, Peter Pollock, and Frank Fair of the Components lab for giving so freely of their time and talents to make this short summer effort successful, enjoyable, and to teach me about carbon-carbon material. Thanks also to Wayne Roe for helping me to understand the paper requirements of Universal Energy Systems. I would particularly like to thank Jim Koury for being such a good carpool companion. I would like to acknowledge the sponsorship of the Air Force Systems Command, the Air Force Office of Scientific research, and the Air Force Astronautics Laboratory.

I. Introduction

The detection and assessment of defects in Carbon-Carbon material (C-C) is an important goal of the USAF. Acoustic emission (AE) has been shown to be an effective Nondestructive Evaluation (NDE) technique in graphite/epoxy structures and has been proposed as a candidate technique for evaluating C-C structures such as exit cones.

The intent of this project was to begin to develop a database on AE in 2-D C-C from which a technology assessment could be made. Before it can be decided on how to apply this method, basic studies need to be carried out on the material itself in the form of simple tensile coupons.

The author has considerable experience with the AE technique and was instrumental in guiding programs in the aerospace industry using graphite/epoxy from basic studies through to final applications for real structures. This contributed to being assigned to the Components group at AFAL.

II. Objectives

The primary objectives for the work this summer were as follows:

1. To become more familiar with the activities at the Air Force Astronautics Laboratory, Edwards Air Force Base, California, particularly the goals of the Components Group.
2. To begin preliminary tests on 2-D C-C to determine the AE response, to observe its fracture behavior by studying notched tensile coupons, and to correlate the fracture behavior with the AE response.
3. To help direct the Master's thesis research of a co-op student funded by the AFAL.

Other objectives developed during the course of the summer and are summarized as follows:

1. To evaluate the acoustic emission (AE) equipment residing at the lab and to recommend upgrades.
2. To discuss the needs in acoustic emission and ultrasonic studies of carbon-carbon (C-C) materials and graphite/ matrix materials and to assist in preparing plans for research.
3. To evaluate the software needs for driving a UT scanner and graphics displays and to make recommendations to the Components lab personnel after discussing the options with AFAL computer personnel and Boeing Aerospace participants.

This last objective stemmed from the author's recommendations, given earlier in the year, on ultrasonic (UT) C-scan equipment to be purchased by the Components lab.

III.

A test matrix for the experimental work was produced and is exhibited below.

Two flat plates made of 2-D C-C were acquired and a cutting plan for the machine shop was drawn up. This plan showed the number of specimens to be cut in either the warp or the fill directions. These types of specimens had not been produced in the AFAL machine shop before, so the PI worked closely with the machinist to ensure that specimens suitable for AE research resulted.

Each specimen was tabbed with aluminum tabs. A twenty four hour cure epoxy manufactured by 3M (DP 110) was used to bond the tabs. This glue had been tested previously for enough shear strength by the author in his lab at the university. The proper test procedures and the theory behind acoustic emission (AE) transducer connected directly to an oscilloscope. Lead breaks (Pentel 2-H) were used for linear location calibration after the two transducers (PAC R15, 150 KHz resonant) were taped to either end of each specimen. Vacuum grease was used as the acoustic couplant.

The acoustic emission analyzer at the AFAL (Physical Acoustics Corp. Spartan/3000) was calibrated on channels four and five by using arbitrary/function generator (Kronn-Hite 59103 Programmable). Some dips in the analyzer software were discovered and documented. These were corrected by the application of a patch program. The results

cost upgrade which took care of some of the bugs. The manufacturer also pointed out that new hardware upgrades were also available, which would significantly increase the speed and accuracy of data acquisition. This is important information since one of the goals of the Components Lab (MKBC) is to set the standards for composites and NDE testing.

The specimens produced from the flat plates were loaded quasistatically in tension to failure. The grips for the MTS mechanical test machine in the Components Lab had to be replaced with smaller ones suitable for testing Carbon-Carbon coupons. These grips were mounted on rotatable spherical surfaces which allow them to automatically align the specimen with the load. This is done in order to ensure uniaxial, centric tensile loading. Several reject specimens were tested for a system "shakedown." The extensometer used allowed the strains on the front and back of the specimen to be measured. The difference between the front and back readings is a measure of the amount of bending present due to misalignment of the load train. Very little was observed. After all test instrumentation was working properly actual testing commenced.

Load and strain were digitized simultaneously with the MTS data. The computer was set up to collect data at a rate of 1000 samples per second. The data was then processed and plotted. The results were then compared to the results of the other tests. The results were then compared to the results of the other tests.

the digitizer used were sufficient for the fracture and AE studies. A significant amount of time was spent calibrating the AE analyzer, which had not been accomplished for some time. Recommendations for equipment upgrades will be given in a section below. The load was measured by the load cell on the MTS machine and the strain was measured with an extensometer. The AE data recorded include counts, events, event amplitude, duration, and energy.

The AE data has only been checked to ensure that it was well recorded and documented so that analysis could be carried out at a later date. Due to the short time nature of this program, much of the period was spent photographing, measuring, weighing, and otherwise documenting the specimens, calibrating the AE analyzer, directing the student's study of fracture mechanics, and running the tests. Even the precise machining of these specimens was something that AFAL machinists had never accomplished before, and thus it had to be learned through trial and error. Fortunately they had a good selection of surface grinders and were willing to experiment till the right one was found.

About two thirds of the test matrix was executed, primarily the notched, quasistatic to failure specimens. Significantly, it appears that the material does exhibit a size sensitivity. This assessment comes from a peak plot of the test results. The peak plot is a plot of the peak load versus the notch radius. The peak load is the maximum load recorded during the test. The notch radius is the radius of the notch in the specimen. The peak plot shows that the peak load decreases as the notch radius increases. This is a clear indication of size sensitivity.

In addition to the planned work, several seminars and discussions about Air Force programs were attended. These broadened my view of the scope of the Air Force's research needs. My perspective on the research needs of the AFAL has definitely expanded because I am now aware of more of the details of many of their programs. Now I will be able to concentrate on them and think more about how my own knowledge and experience can contribute to AFAL's efforts. I am confident that a mutually beneficial and fruitful relationship will continue to develop.

Other scientific discussions with AFAL personnel included scaling theories, fracture theories, finite element modeling requirements for NDE, and wave propagation in anisotropic media. Plans are being formulated for research using the ultrasonic C-scan instrument when it comes on line. A research program for acoustic emission studies of graphite/matrix coupons during impact has been proposed. It will take advantage of the impact testing facilities at the AFAL. Wave studies on certain idealized specimens containing different material constituents have been discussed informally and would involve AFAL facilities and researchers.

IV Recommendations

The basic AE parameters and mechanical data were recorded and are currently being analyzed for trends which can be attributed to the fracture behavior of the material and the loading pattern. Differences in the emission characteristics of the tensile coupons loaded uniaxially in both the warp and fill directions will be studied in a follow on effort to this summer program. A different pattern would allow the cracking direction in a C-C part such as a rocket nozzle to be determined which would be very valuable information to a stress analyst. Currently, exit cones do not undergo a proof test by mechanical loading or pressurization thus making it difficult to apply the AE technique to the manufactured part. Also to evaluate the quality, some AE studies will have to be done at elevated temperatures to really see the performance of the C-C part. But there will also be room temperature measurements which yield AE signatures which correlate with processing parameters. The processing parameters will correlate with part performance. Thus, as a result of these studies, it will be possible in the future to establish an acceptable nondestructive method for C-C structures. This would provide a much lower reject rate than the present costly one of around 50%.

As can be seen in the test matrix, a few specimens were used for study under cyclic loading to progressively

higher loads. The load was cycled beginning at forty percent of ultimate and then increased in ten percent increments up to ninety percent of failure load. In analyzing the data, particular attention should be paid to any observable Kaiser Zone phenomena. This has been important in other composites for detecting and assessing the level of damage.

The loading/unloading portion of the test matrix will be finished under a follow on program so that a model can be developed which relates the change in modulus, i.e., "damage", after each cycle to the size of the measured Kaiser Zone (or the so called "Felicity Ratio").

As was mentioned before, the manufacturer of the AE equipment used by the Components Lab makes available both an hardware and a software upgrade, which it claims can significantly increase the speed and accuracy of data acquisition. However there exists on the market a competing instrument which has garnered some good reviews. I suggest that both companies be allowed to bring their instruments to the AFAL lab. There real tests can be run on actual specimens. This will make the results independent of the manufacturer's simulated data which is usually what they present in a demonstration. This procedure worked well in the past when I helped to select equipment for an aerospace company.

TEST MATRIX

2-D CC 10" X 12" Plates

Monotonic Tension to Failure - Spec. dim. 10" x 1" x 1/4"				
a/w*	0.0	0.05	0.1	0.15
Warp	3	2	2	1
Fill	3	1	1	1

Loading/Unloading - Spec. dim.

	10" x 1" x 1/4"	10" x 1/2" x 1/4"
Warp	3	2
Fill	2	0

Loading 50, 60, 70, 80% of P* (ultimate)

Total # Spec. = 21

* a/w = notch 1/2 length/specimen width

DR. BENJAMIN GOTTLIEB

FINAL REPORT NUMBER 57

NO REPORT SUBMITTED

1987 USAF-UES SUMMER FACULTY RESEARCH PROGRAM

Sponsored by the
AIR FORCE OFFICE OF SCIENTIFIC RESEARCH

Conducted by the
Universal Energy Systems, Inc.

FINAL REPORT

HIGH AMPLITUDE AIRFOIL MOTION USING POINT VORTICES

Prepared by: Gary M. Graham
Academic Rank: Assistant Professor
Department and
University: Mechanical Engineering Dept
Ohio University
Research Location: AFWAL/FIGC
Wright-Patterson AFB, Ohio 45433-6553
USAF Researcher: Jerry Jenkins
Date: 1 September 1987
Contract No: F49620-85-C-0013

80-R191 284

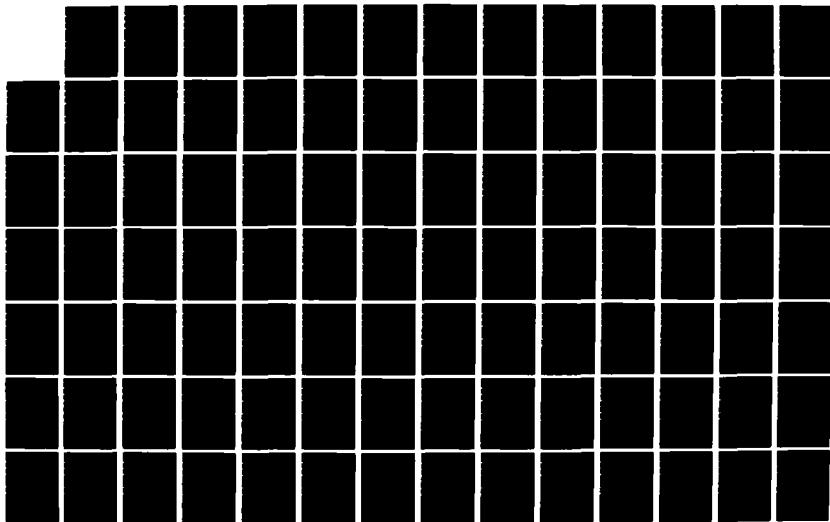
UNITED STATES AIR FORCE SUMMER FACULTY RESEARCH PROGRAM
(1987) PROGRAM TE (U) UNIVERSAL ENERGY SYSTEMS INC
DAYTON OH R C DARRAH ET AL DEC 87 AFOSR-TR-88-0213
F49620-85-C-0013

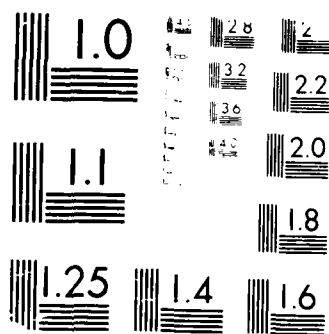
2/7/

UNCLASSIFIED

F/G 5/1

NL





MICROCOPY RESOLUTION TEST CHART
NBS 1010-A

High Amplitude Airfoil Motion Using Point Vortices

by

Gary M. Graham

ABSTRACT

An analytical model which predicts the aerodynamics of a two-dimensional airfoil experiencing a rapid pitch-up maneuver has been developed. The model is based on simulating the vortex shedding of an airfoil as it moves in an otherwise quiescent fluid. The onset of leading edge flow separation which occurs at high angles of attack is predicted using an empirical correlation for the case of constant pitch rate. The aerodynamic loads are computed using a momentum approach based on an unsteady Blasius integral. The results of these calculations may be useful in applications such as the concept of enhanced maneuverability of fighter aircraft.

ACKNOWLEDGMENTS

I wish to thank the Air Force Systems Command and the Air Force Office of Scientific Research for sponsorship of this research. In addition, I thank Universal Energy Systems for their support in the administrative aspects of this program.

I also want to thank Mr. Jerry Jenkins and the other members of the FDL Design Prediction Group for their technical support and friendship.

I. INTRODUCTION

The key to the development of highly maneuverable fighter aircraft lies in the utilization of the large transient loads which occur when an airfoil experiences a rapid pitching motion. Some researchers have coined the word "supermaneuverability" to describe such aircraft capability. Herbst [1] defines supermaneuverability as "the capability of fighter aircraft to execute tactical maneuvers with controlled side slipping and at angles of attack beyond maximum static lift." Flight simulations have indicated that an aircraft with supermaneuverability, in a close-quarters encounter with a conventional fighter aircraft, will have an advantage in weapon exchange ratio of 2 to 1. This is primarily due to the fact that the aircraft would be able to outmaneuver its opponent and thus be in a position to deliver weapons first and for a longer period of time. While executing a supermaneuver an aircraft may experience reduced pitching rates ($\dot{\alpha}C/2U_{\infty}$) in excess of 0.1 and angles of attack greater than 45° . Such motions may give rise to aerodynamic flow separation and complex time dependent flow geometries. There is presently a need for the development of analytical techniques which can predict the aerodynamics of such radical flightpaths. One such approach, albeit two-dimensional, is discussed herein. Other approaches are described in references [2-4].

In the past, my research interests have been in the area of unsteady separated flows over airfoils experiencing time dependent motions. This has included experimental studies of the flow associated with a Darrieus wind turbine and experimental studies of an airfoil experiencing rapid pitch-up motions. I have also had experience in using discrete vortex models to predict these flows. These factors contributed to my assignment to the Flight Dynamics Laboratory at Wright-Patterson for this research period.

II. OBJECTIVES OF THE RESEARCH EFFORT

Several approaches have been taken with regard to the prediction of unsteady separated flows on pitching airfoils. These approaches range from methods for numerically solving the Navier-Stokes equations [2] to methods which simulate the vortical shedding of a body as it moves through a fluid [4]. The Navier-Stokes solvers consume enormous amounts of computer time and are usually limited to Reynolds numbers below 10^5 . This Reynolds number limitation may be attributed to the lack of a turbulence model for the Reynolds stresses. The vortex models are computationally efficient, however, problems are encountered predicting flow separation and reattachment. To date, none of these approaches has been shown to be completely adequate for predicting the flow associated with a body of arbitrary geometry experiencing arbitrary motions.

The objective of the research during my participation in the 1987 Summer Faculty Research Program was to develop a vortex model which would be capable of predicting the aerodynamics associated with a two-dimensional airfoil experiencing a rapid pitch-up motion at a constant pitch rate. The motion under consideration included very high angles of attack which are beyond the aerodynamic stall threshold. Therefore, one particular requirement was that the analysis include the capability of handling the potential occurrence of leading edge separation. An empirical correlation that predicts the onset of leading edge separation which has been shown to be applicable to the constant pitch rate motion was incorporated into the numerical model. In general, the approach outlined herein is directly applicable to arbitrary motions without separation and to motions involving separation if such a correlation exists.

Within the general framework of the "vortex" approach exist a number of questions which have potentially, more than one answer. As many of these questions as was possible within the limits of this program were addressed. However, the work described in this report is not exhaustive. Some parts of this analysis could be replaced with alternative formulations which may improve the accuracy of the results.

III. ANALYTICAL METHODS

The major components of the analytical model are described in the following sections. These include the representations of the airfoil and wake region, the flow separation model, calculation of bound vorticity, and calculation of lift and drag forces.

Airfoil and Wake Model

The airfoil and wake region may be represented as in Figure 1. Here the airfoil is shown pitching about its quarter chord while moving into a motionless fluid at a constant velocity. As is depicted, the airfoil surface is modeled as a set of elements or "panels" each consisting of a "control point" located at the quarter chord of the panel and a discrete "bound" vortex placed at the three-quarter chord of the panel. The term bound implying that the vortex is confined to move with the airfoil. The strength of the bound vorticity is discussed in a latter section. Let it suffice to say here that the strength of each bound vortex is sufficient to maintain a zero normal velocity component at each control point on the airfoil surface.

The wake region is composed of a number of "free" vortices which originate continuously from the airfoil trailing edge and also the leading edge if the flow has separated. Once free, each vortex remains constant in strength and is convected downstream at its local velocity which is induced by all the other vortices in the flow. The velocity which a 2-D vortex induces at some point located

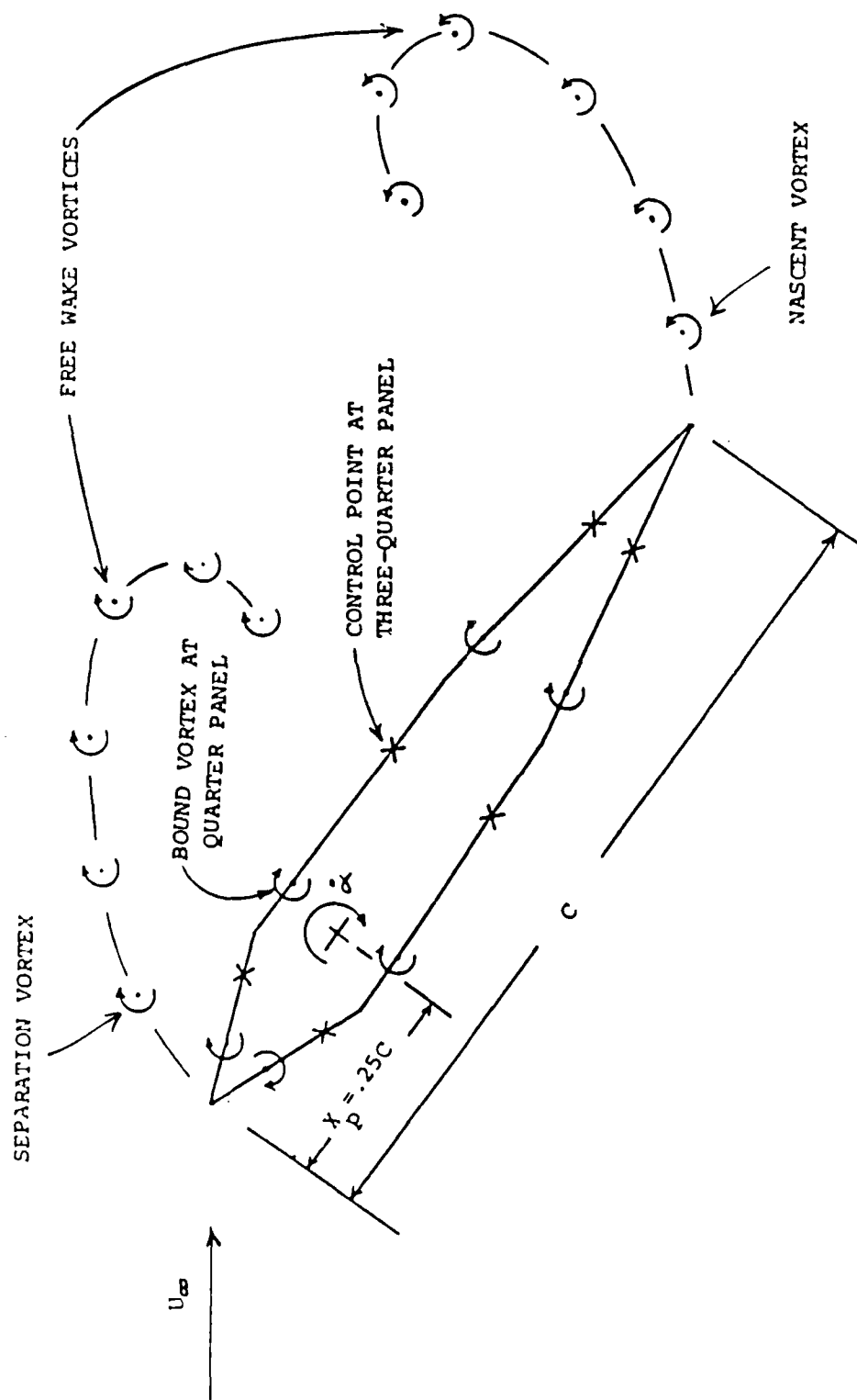


FIGURE 1. REPRESENTATION OF AIRFOIL AND WAKE REGION

a distance r from the vortex center is given by the Biot-Savart law

$$V_I = \bar{C} \Gamma \quad (1)$$

where

$$\bar{C} = (\sin \theta \hat{e}_2 - \cos \theta \hat{e}_1) / (2\pi r)$$

$$\tan \theta = (y_2 - y_1) / (x_2 - x_1)$$

$$r = [(x_2 - x_1)^2 + (y_2 - y_1)^2]^{1/2}$$

and Γ is the vortex strength, (x_1, y_1) is the location of the vortex, and (x_2, y_2) is the location of the point in a rectangular coordinate system, and the vector \bar{C} is called the "influence" coefficient.

Flow Separation Model

At Reynolds numbers in excess of 1×10^6 boundary layer separation tends to occur near the leading edge for steady flow conditions. Leading edge stall is even more prevalent at low pitching rates and low Reynolds numbers. Therefore, a reasonable approximation is to assume that the boundary layer separation occurs at the leading edge.

For the dynamic situation, separation occurs suddenly at the leading edge and at angles of attack which may, depending upon the pitching rate, greatly exceed the static stall angle of attack. Shown in Figure 2 are data for dynamic stall inception angles from several workers. Here $\Delta \alpha_M$ is the difference between the effective angle of attack at the leading edge at which dynamic stall occurs and the angle of

a distance r from the vortex center is given by the Biot-Savart law

$$V_{\text{induced}} = \bar{C} \Gamma \quad (1)$$

where

$$\bar{C} = (\sin \theta \hat{i} - \cos \theta \hat{j}) / (2\pi r)$$

$$\tan \theta = (y_2 - y_1) / (x_2 - x_1)$$

$$r = [(x_2 - x_1)^2 + (y_2 - y_1)^2]^{1/2}$$

and Γ is the vortex strength, (x_1, y_1) is the location of the vortex, and (x_2, y_2) is the location of the point in a rectangular coordinate system, and the vector \bar{C} is called the "influence" coefficient.

Flow Separation Model

At Reynolds numbers in excess of 1×10^6 boundary layer separation tends to occur near the leading edge for steady flow conditions. Leading edge stall is even more prevalent at low pitching rates and low Reynolds numbers. Therefore, a reasonable approximation is to assume that the boundary layer separation occurs at the leading edge.

For the dynamic situation, separation occurs suddenly at the leading edge and at angles of attack which may, depending upon the pitching rate, greatly exceed the static stall angle of attack. Shown in Figure 2 are data for dynamic stall inception angles from several workers. Here $\Delta \alpha_N$ is the difference between the effective angle of attack at the leading edge at which dynamic stall occurs and the angle of

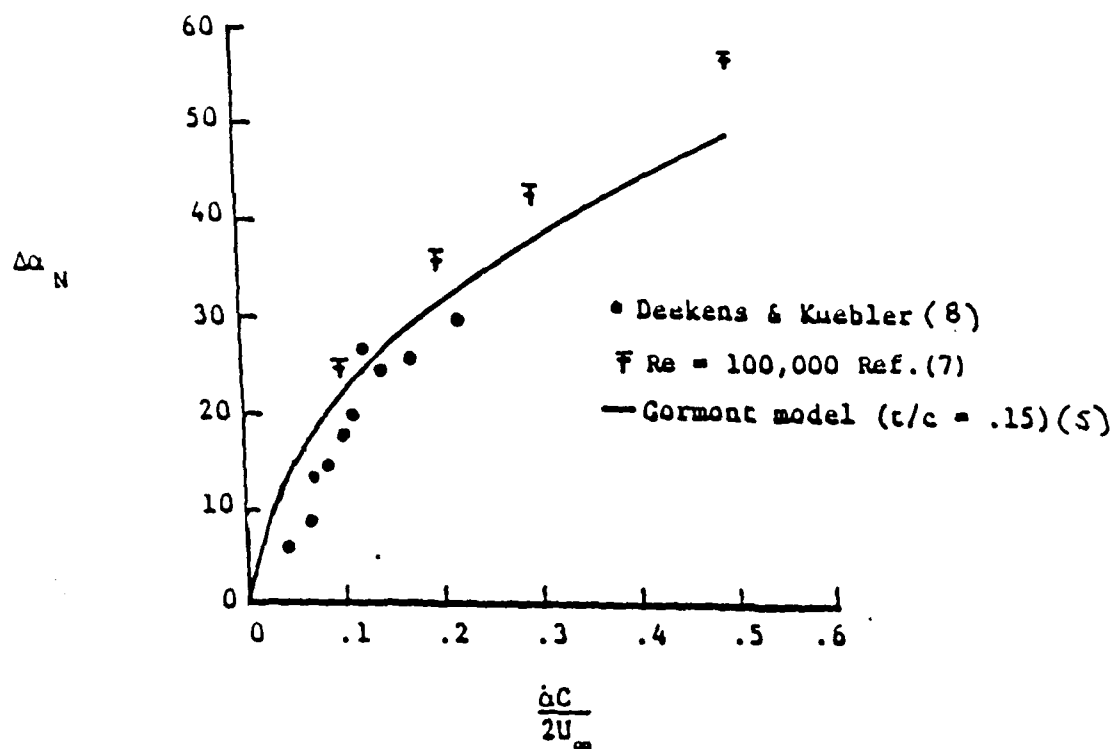


FIGURE 2. THE GORMONT CORRELATION FOR LEADING EDGE SEPARATION

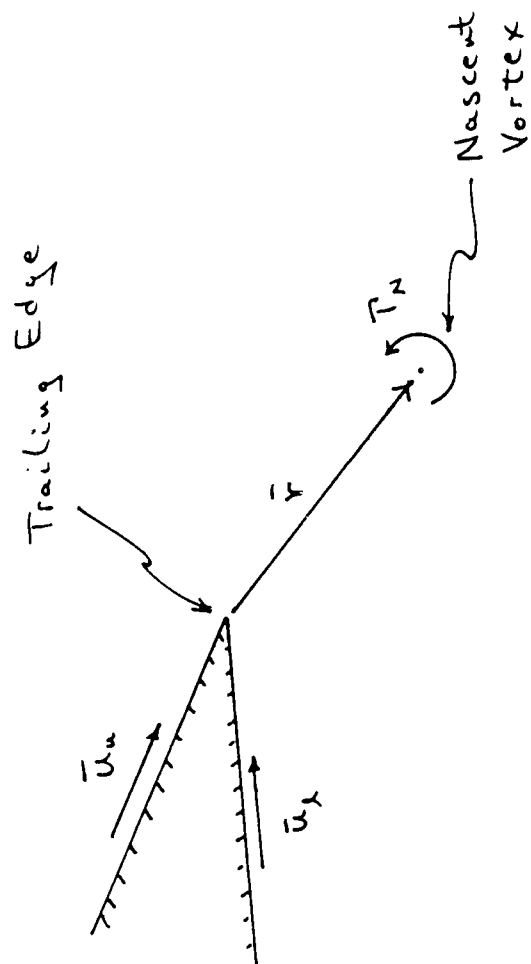
attack at which static stall occurs. These data represent flow visualization data taken on NACA 0012 and NACA 0015 airfoils at Reynolds numbers in the range 5×10^3 to 3×10^5 undergoing constant pitch rate motions. With the exception of a few data points, the stall delay angle $\Delta\alpha_N$ is reasonably well correlated with the nondimensional pitching rate $\dot{\alpha}C/2U_\infty$. It is interesting to note that the correlation by Gormont [5], which is based on oscillating airfoil data, tends to fit the experimental data reasonably well. The Gormont model is applicable to airfoils operating over a wide range of Mach numbers and contains a correlation for various airfoil maximum thickness ratios. It therefore seems applicable to use the Gormont model to predict the inception of leading edge stall. Calculation of the strength of the separating shear layer is discussed in the next section.

Calculation of Bound Vorticity

At some instant in time the flowfield may be depicted as shown in Figure 1. The strengths of the bound vortices can be uniquely determined by forcing the fluid velocity at the control points to be tangent to the airfoil surface. At each control point at a time step k the surface tangency condition may be expressed as

$$\left[\sum_{i=1}^{NB} \bar{C}_{Bi} T_{Bi}^k + \sum_{i=1}^{NW} \bar{C}_{Wi} T_{Wi}^k + \bar{V}_M^k + \bar{U}_\infty^k + \bar{C}_N^k T_N^k + \bar{C}_s^k T_s^k \right] \cdot \hat{n}_{\text{control point}}^k = 0 \quad (2)$$

where NB is the number of bound vortices and NW^k is the number of vortices in the free wake. In Equation 2, the first term is the downwash due to the bound vorticity, the second term is the downwash due to the wake, the third term is the downwash due to the motion of the body (pitching, etc.), the fourth term is the downwash due to the freestream, the fifth term is the downwash due to a nascent vortex near the trailing edge, and the sixth term is the downwash due to a separation vortex near the leading edge. The influence coefficients may be computed from the Biot-Savart law and the geometry of the flowfield as discussed earlier. There are essentially $NB+2$ unknowns in Equation 2; namely, the NB bound vortex strengths, the nascent vortex strength (Γ_N^k), and the separation vortex strength (Γ_s^k). The strength of the nascent vortex is determined in a fashion illustrated in Figure 3. Here u_u is the fluid velocity relative to the airfoil on the upper surface and u_l is the relative velocity on the lower surface. The appropriate position of the nascent vortex is also shown in Figure 3. Since the strength of the bound vorticity and the separation vortex have yet to be determined at the current time step, the upper and lower fluid velocities must be computed using the flowfield at the previous time step. Therefore, in order to expect adequate results small time steps must be used. As an improvement to the current model a predictor-corrector scheme might be employed here. The strength of the separation vortex may be related to the nascent vortex strength and the change in



$$\Gamma_N = \frac{1}{2}(\bar{u}_u^2 - \bar{u}_x^2) \Delta t$$

$\Delta t = \text{time step}$

$$\bar{r} = \frac{1}{2}(\bar{u}_u + \bar{u}_x)$$

Figure 3. Strength and Position of Nascent Vortex

bound vortex strength at time step k through application of Kelvins theorem and is given by

$$\Gamma_S^k = - \left[\Gamma_N^k + \sum_{i=1}^{NB} (\Gamma_{Bi}^k - \Gamma_{Bi}^{k-1}) \right] \quad (3)$$

Substitution of Equation 3 into Equation 2 yields

$$\left[\sum_{i=1}^{NB} (\bar{C}_{Bi}^k - \bar{C}_S^k) \Gamma_{Bi}^k + \sum_{i=1}^{NW^k} \bar{C}_{wi}^k \Gamma_{wi}^k + \bar{V}_M^k + \bar{U}_\infty^k + (\bar{C}_N^k - \bar{C}_S^k) \Gamma_N^k + \bar{C}_S^k \sum_{i=1}^{NB} \Gamma_{Bi}^{k-1} \right] \cdot \hat{n}_{\text{control point}}^k = 0 \quad (4)$$

where the nascent vortex strength is determined as illustrated in Figure 3. An equation of the form of Equation 6 may be written at each control point resulting in a system of NB linear equations for the NB unknown bound vortex strengths. This may be expressed in matrix notation by

$$[D]^k \{ \Gamma_B \}^k = \{ E \}^k \quad (5)$$

where, for the j^{th} control point

$$D_{ji}^k = (\bar{C}_{Bji}^k - \bar{C}_{sj}^k) \cdot \hat{n}_j^k$$

$$E_j^k = - \left[\sum_{i=1}^{NW^k} \bar{C}_{wi}^k \Gamma_{wi}^k + \bar{V}_{Mj}^k + \bar{U}_\infty^k + (\bar{C}_{Nj}^k - \bar{C}_{sj}^k) \Gamma_N^k + \bar{C}_{sj}^k \sum_{i=1}^{NB} \Gamma_{Bi}^{k-1} \right] \cdot \hat{n}_j^k$$

This system may be solved using a number of methods. Once the bound vortex strengths are known the separation vortex strength is computed using Equation 3.

Calculation of Lift and Drag Forces

The airfoil lift and drag forces are computed at each time step after the strengths of each vortex in the flow has been determined as outlined in the previous sections. The lift and drag on the airfoil are computed using an unsteady Blasius integral [6] and are given by

$$L = -e \sum_{i=1}^{NV} \left(x_i \frac{d\Gamma_i}{dt} + v_i \Gamma_i \right) \quad (6)$$

$$D = e \sum_{i=1}^{NV} \left(y_i \frac{d\Gamma_i}{dt} + u_i \Gamma_i \right)$$

where NV is the number of vortices in the flow.

IV. RESULTS

The lift coefficient for the steady unseparated case was computed using the approach outlined above. The analytical results are in close agreement with the potential flow solution based on a symmetrical Joukowski airfoil. These results are not shown here for brevity.

The lift and drag force results for the case of constant pitch rate with nondimensional pitch rates of .088 and .19 are shown in Figures 4 and 5. In both cases the model overpredicts the lift and underpredicts the drag.

V. RECOMMENDATIONS

The results of this project have shown this analytical approach to, at this point in time, be moderately successful. There are a number of things which might be done

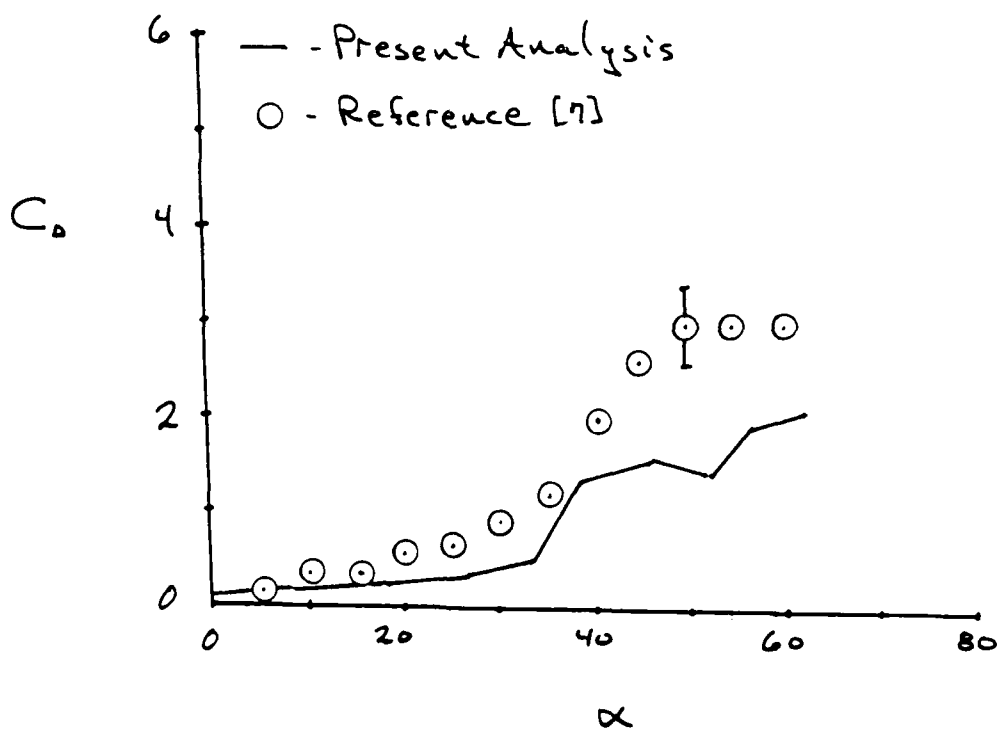
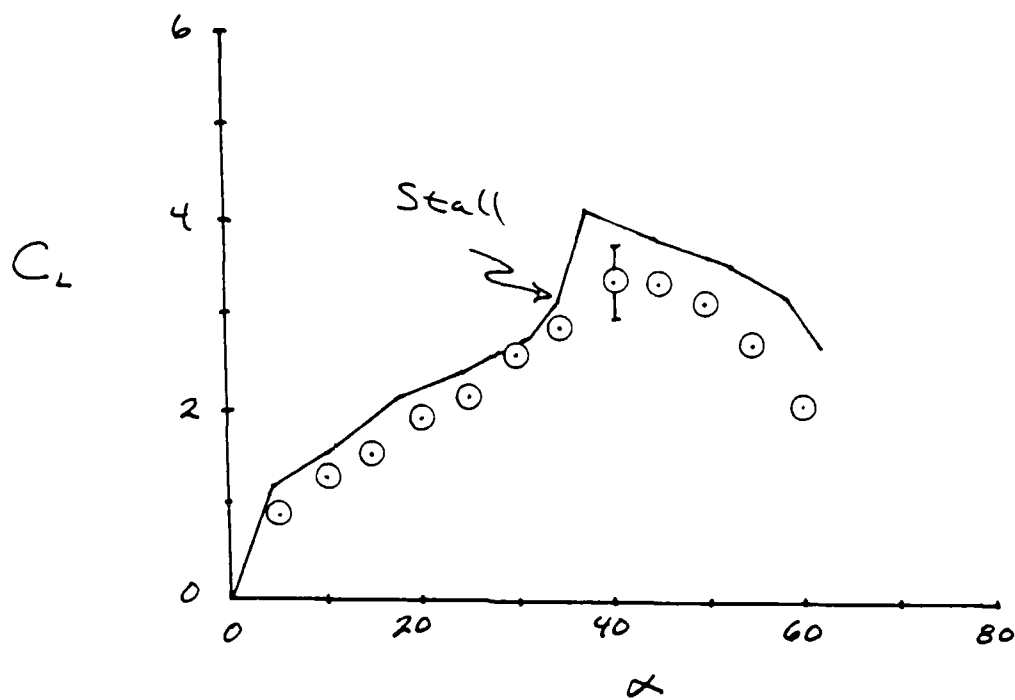


Figure 4. Force Coefficients for a Nondimensional Pitch Rate of $\dot{\alpha}C/2U_\infty = .088$

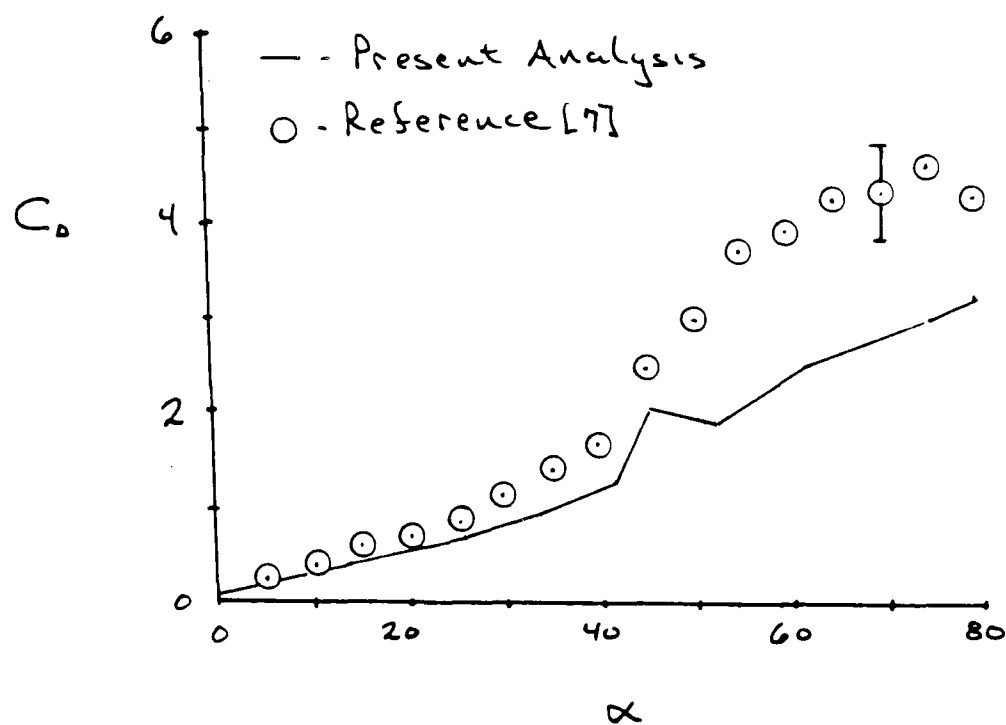
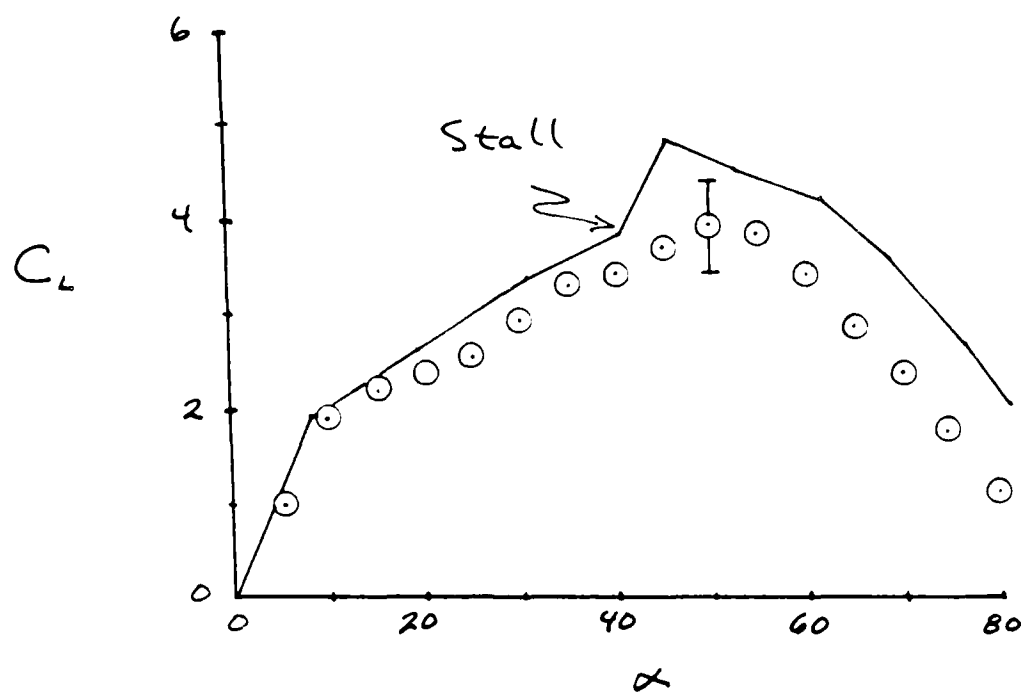


Figure 5. Force Coefficients for a Nondimensional Pitch Rate of $\dot{\alpha} c / 2U_{\infty} = .19$

to improve the model. A few of these are listed below.

a. Inspection of Equation 6 indicates that the lift and drag forces as computed in this model are intimately related to the wake convection. Therefore, in order to improve these results a study could be undertaken as to what method of wake convection, if any, might be employed to obtain closer agreement with the experimental data. For instance, as mentioned before a predictor-corrector scheme might be employed with regard to the calculation of the bound vorticity. Also some type of weighted time averaging of the local wake convection velocities might prove useful.

b. An alternate method of computing the force coefficients would be to apply the unsteady Bernoulli equation and integrate the resulting pressure distributions. This method would require somewhat more computer time but might prove to be more accurate.

c. In the opinion of the author, some empirical work might provide information which would be of use within the framework of this analysis. For example, the success of this analysis, to a large part, relies on the accuracy of Equation 1 (Biot-Savart law). Inspection of Equation 1 shows that the velocity induced by a point vortex is infinite at the vortex center. This is obviously a departure from reality. An experiment could be performed to study the range of applicability of Equation 1. Another interesting subject would be to study the applicability of the Gormont model to the pitch-down and arbitrary motion cases.

REFERENCES

1. Herbst, W., "Supermaneuverability," Proc. of the Workshop on Unsteady Separated Flows, USAF Academy, Colo. Sprgs., Aug. 10-11, 1983.
2. Visbal, M.R. and Shang J.S., "Numerical Investigation of the Flow Structure Around a Rapidly Pitching Airfoil," Proc. of the Workshop on Unsteady Separated Flows, USAF Academy, Colo. Sprgs., July 28-30, 1987.
3. Maskew, B. and Dvorak, F.A., "Calculation of Unsteady Flow Characteristics on Complex Configurations in Arbitrary Motion," Proc. of the Workshop on Unsteady Separated Flows, USAF Academy, July 28-30, 1987.
4. Chow, C. and Sheen, Q., "Unsteady Vortical Flows Around an Airfoil," Proc. of the Workshop on Unsteady Separated Flows, USAF Academy, Colo. Sprgs., July 28-30, 1987.
5. Gormont, R.E., A Mathematical Model of Unsteady Aerodynamics and Radial Flow Application to Helicopter Rotors," U.S. Army AMRDL Tech. Report 72-67, 1973.
6. Theodorsen, T., "Impulse and Momentum in an Infinite Fluid," Theodore von Karmen Anniversary Volume, published by the friends of Theodore von Karmen, Pasadena, Ca., May 1941.
7. Strickland, J.H. and Graham, G.M., "Force Coefficients on a NACA 0015 Airfoil Undergoing Constant Pitch Rate Motions," AIAA Journal, Vol. 25, No. 4, p. 622, Ap., 1987.
8. Deekins, A.C. and Kuebler, W.R., "A Smoke Tunnel Investigation of Dynamic Separation," Aeronautics Digest, USAF A-TR-79-1, pp. 2-16, F. 1972.

1987 USAF-UES SUMMER FACULTY RESEARCH PROGRAM

GRADUATE STUDENT SUMMER SUPPORT PROGRAM

Sponsored by the
AIR FORCE OFFICE OF SCIENTIFIC RESEARCH

Conducted by the
Universal Energy Systems, Inc.

FINAL REPORT

LIQUID FILM COOLING OF ROCKET ENGINES

Prepared by: William M. Grissom
Academic Rank: Assistant Professor
Department: Physics Department
University: Morehouse College
Research Location: Arnold Engineering
Development Center,
Sverdrup Technology,
Plume Diagnostics Group
SvT Researcher: Chad Limbaugh
Date: August 7, 1987
Contract no: F49620-85-C-0013

LIQUID FILM COOLING OF ROCKET ENGINES

by

William M. Grissom

ABSTRACT

The cooling of the combustion chamber walls in a rocket engine by a liquid film is analyzed. The evaporation rate is calculated from the dry-wall heat flux modified by a transpiration correction due to the blowing vapor generated. The mixing of the vapor with mainstream gases in the boundary layer above and downstream of the liquid film is studied. The convection rate of coolant into the mainstream is also inferred from this analysis. Estimates of the radiant heat transfer show that it can account for the difference between the convective calculations and experimental measurements. Radiant heat can also cause problems such as burnout of the liquid film.

I. INTRODUCTION

A number of liquid rocket engines employ a liquid film of fuel as thermal protection for the combustion chamber walls. This process was experimentally studied in the 1950's and 1960's, however no general analysis procedure was established at that time. Since then various heat transfer analyses have arisen which can be applied to study the mechanisms occurring as the liquid film evaporates and mixes with the freestream gases.

My M.S. thesis in mechanical engineering dealt with the evaporation of liquid droplets on a surface. This initially appeared quite similar to the situation of liquid film cooling in rockets. The mechanism actually involved considerations of convective and radiative heat transfer. My background in aerospace engineering and spectroscopy proved useful in studying these concerns. The USAF is presently interested in the effects of the liquid film upon the plume signature. To analyze this it is necessary to determine the evaporation process and subsequent mixing of the vapor when liquid film cooling is used in a rocket.

II. OBJECTIVES OF THE RESEARCH EFFORT

The initial goal was to determine the evaporation rate of the liquid film. Very little information concerning this was located in the general literature. Contact with Michael Powell of AFAL, with whom I had worked on a previous SFRP appointment, provided many obscure references. These references allowed comparison of the calculation procedure developed here with actual rocket data, which showed the need for radiative considerations. With the evaporation rate of the film determined, an additional task was undertaken to analyze the vapor mixing with the hot freestream gases.

These various analyses will be summarized in the following. A more thorough reporting of the research and comparison with experimental data is available in a separate technical report available from AEDC.

III. Liquid Film Evaporation

Dry-wall heat flux:

To interpolate between the standard $1/7$ power law boundary layer results [1] and that for fully-developed flow [6] define a new variable, x' :

$$x'/D = -C_i \ln\{\exp(-3.53/C_i) + \exp(-x/[C_i D])\}$$

with $C_i = 0.5$ suggested.

The convective heat transfer is then calculated, (with properties evaluated at the mean temperature):

$$St = 0.023 Ca Rex'^{-0.2} Pr^{-0.6} \quad (1)$$

$$\text{where: } Ca = \begin{cases} 1.25 & \text{if } x < 3.53 D \\ 1 + 0.25(3.53 D/x) & \text{if } x > 3.53 D \end{cases}$$

Blowing corrections:

The vapor is transpired into the boundary layer and decreases the skin friction and heat transfer to the wall. Transpiration solutions are normally expressed as the heat transfer reduction versus a parameter:

$$H = \frac{\dot{m}_v}{\rho_g U_g St} = \frac{C_{pg} \Delta T}{\lambda^*}$$

The simplest result is that resulting from a Couette flow model [5,8]:

$$\frac{h}{h_o} = \frac{1}{H} \ln(1+H)$$

To account for different molecular weight injectants the parameter H is replaced by:

$$Z = \left(\frac{M_g}{M_v} \right)^a H \quad \begin{array}{l} a=0.6 ; \quad M_v < M_g \\ a=0.35 ; \quad M_v > M_g \end{array} \quad [12]$$

These relations are not useful if the liquid flow-rate exceeds a critical value given by Knuth [14] for the onset of large waves:

$$\Gamma_{cr} = 1.01 \cdot 10^{-5} (\mu_v / \mu_l)^2 \mu_l$$

Calculation of film-cooled length:

Combining the above relations with $x=L_c$:

$$L_c = \frac{61.62 \bar{\mu}_g}{\rho_g U_g} \left[\frac{\lambda^* \Gamma}{\bar{c}_p g \Delta T \bar{\mu}_g (h/h_o)} \right]^{1.25} Pr^{0.75} \quad (2)$$

II. Vapor Film Mixing

The cooling effectiveness is defined:

$$\eta \equiv \frac{T_g - T_w}{T_g - T_c} = \frac{1}{1 + (m_g C_{pg} / m_c C_{pc})}$$

and a dimensionless distance:

$$X = \left[\frac{\bar{\rho}_g U_g \bar{\mu}_g^{0.25}}{\dot{M}_c^{1.25}} \right] x$$

where: \dot{M}_c = coolant vapor mass flow per width

Using the 1/7 power law boundary layer equations as per ref.32:

$$\eta = [1 + C_{pc}/C_{pg}(0.325[X+4.08]^{0.8} - 1)]^{-1} \quad (3)$$

A suitable correction for freestream turbulence is to multiply X by a correction term (1+Ct). Applying this to Eq. and analyzing the data of ref. 27 and 29:

$$Ct = 10.2 e ; \text{ where: } e = \text{turb. intensity fraction}$$

The results with helium coolant are well fit by the empirical Eq. 12 of ref [32]. This can be put into the

form of Eq.3 by adding a multiplier of 0.76 to the C_{pc}/C_{pg} ratio. Assuming that this is due to the density ratio a scaling factor of molecular weight to the 0.14 power can be used.

The effects of centripetal accelerations at the throat turns can be corrected by generalizing the results of Rousar [30]. This suggests using a scaling factor K_t which divides the unturned effectiveness value:

$$K_t = \left(0.5 + 3.46 \left[2 \left(\frac{p-1}{p+1} \right) + 0.38 \right]^2 \right)^{[0.727 / \bar{R}]}$$

where: \bar{R} = avg of in- and out-turning radii of throat

$$\bar{R} = \left[\frac{1}{R_{in}} + \frac{1}{R_{out}} \right]^{-1} = 0.727 \text{ in [30]}$$

$$p = \frac{p_g}{p_w} = \left(\frac{M_g}{M_c} \right) \left(\frac{T_w}{T_g} \right) = \frac{M_g}{M_c} \left[1 - \eta \left(1 - \frac{T_c}{T_g} \right) \right]$$

Final vapor film correlation equation:

$$\eta = \frac{1}{K_t [1+F]}$$

where:

$$F = \frac{C_{pc}}{C_{pg}} \left(\frac{M_c}{M_g} \right)^{0.14} \{ [1 + 0.245(1 + 10.2e)X]^{0.8} - 1 \} \quad (4)$$

Applications to liquid film evaporation:

Equation 4 can be extended to the case of continuous injection from the liquid film by calculating the total mass injected upstream of a point x . Subst. into the definition for x gives:

$$x = \frac{\bar{p}_g U_g}{\dot{m}_v^{1.25}} \left(\frac{\mu_g}{L_c} \right)^{0.25}$$

which predicts a constant cooling effectiveness over the liquid film. Downstream of the film:

$$\dot{M}c = \dot{m}_v Lc$$

with X calculated as before.

Coolant convection into freestream:

The film mixing derivation assumed that the concentration across the boundary layer was uniform and that no gases from the boundary layer went into the freestream. These assumptions gave a good comparison with the measured wall temperatures. In actuality there is a temperature and concentration profile across the boundary layer [32].

The boundary layer mixing is controlled by masses not molar fractions. The mass fraction of coolant is:

$$c = \frac{m_c}{m_c + m_g} = \frac{1 + n_g M_g}{n_c M_c} = \left[1 + \left(\frac{1}{N} - 1 \right) \frac{M_g}{M_c} \right]^{-1}$$

If the temperature variation across the boundary is neglected the average concentration may be expressed as 0.35 times the vapor concentration at the wall [32].

Further approximate the mass fraction:

$$\frac{\bar{c}}{c_w} \approx \frac{\bar{N}}{N_w} \left(\frac{M_c}{M_g} \right)$$

The film mixing model assumed that the mass fraction was c_w over the entire boundary layer. In actuality a mass of coolant $\Delta \dot{M}_c$ has migrated into the freestream, accounting for the actual profile. The mass lost is:

$$\begin{aligned}\Delta \dot{M}_c &= c_w \dot{M}_{bl} - \bar{c} \dot{M}_{bl} \\ &= c_w \left(1 - \frac{\bar{c}}{c_w} \right) \dot{M}_{bl}\end{aligned}$$

Substituting the 1/7 power law result for \dot{M}_{bl} :

$$\frac{\Delta \dot{M}_c}{\dot{M}_c} = \frac{0.325(X+4.08)^{0.8} (1 - 0.035Mc/Mq)}{1 + C_{pc}/C_{pg}(1/\eta - 1)} \quad (5)$$

III. RADIATIVE HEAT TRANSFER

Radiation from high temperature, high density,combusting gases can be a difficult subject to analyze due to the poorly known high pressure molecular spectra, the importance of carbon particles and transient species in the flame, and the variable path length over the viewing angle. However, for gases which are sufficiently thick a number of simplifications are possible.

The complicated molecular spectra are best handled by using total emissivity values for the entire spectra. These are direct measurements of the total gas radiation relative to that of a black-body source. The two most important gases are H₂O and CO₂. These are given in ref.10 .

At high enough optical densities the emissivities become constants of 0.90 for H₂O and 0.23 for CO₂. Neither becomes unity because there are regions in each spectra where no

spectral lines are found. At no wavelength can the intensity radiated exceed that for a black body. For this reason when determining the emissivity of a mixture of gases the regions of overlap must be subtracted. For CO₂ and H₂O this overlap is 13% at high densities.

In applying this method to rocket engines consideration must be made of the fact that the sight path through the gas varies over the viewing angle. The chord distance across an axial section is: $C = D \cos \theta$. The total distance also varies with the angle from this section plane as: $L = C / \cos \phi$. One must also consider the light reflected from a surface in the background view. Perhaps the simplest correction, due to Egletti [34], is to increase the geometric path length by the factor $L' = A_w^{-0.85} L$; where A_w is the absorptivity of the wall.

For rockets with high optical densities a simple approximation is to evaluate the emissivity at an effective length:

$$L_{\text{eff}} = \int_0^{\pi/2} \int_0^{\pi/2} L' \cos \theta \cos \phi d\theta d\phi = 1.23 D A_w^{-0.85}$$

Assuming $A_w = E_w$, the radiant heat flux is calculated:

$$\dot{q}_{\text{rad}} = \sigma E_w E_g [T_g^4 - T_w^4]$$

$$\text{where: } \sigma = 5.67 \text{ E-8 W/m}^2\text{-K}^4$$

Transpiration Effects:

This radiant heat vaporizes a mass flux of vapor:

$$\dot{m}_{\text{rad}} = \dot{q}_{\text{rad}} / \lambda^*$$

This in turn decreases the convective heat transfer, as discussed in section I.A.2 . The total vapor generated will be:

$$\dot{m}_v = \dot{m}_{rad} + \dot{m}_{conv}$$

The blowing correction for convection becomes:

$$Z = Z_{conv} + C1/h$$

$$h = \frac{h_0 \ln(1+Z)}{Z}$$

$$\text{where: } Z_{conv} = \frac{C_{pg} \Delta T}{\lambda^*} \left(\frac{M_g}{M_v} \right)^a$$

$$C1 = \dot{m}_{rad} C_{pg} \left(\frac{M_g}{M_v} \right)^a$$

Note that the correction factor now depends upon the heat transfer rate so that an iterative solution is necessary.

Liquid Film Burnout:

The radiant heat is different than the convective heat in that the radiant heat can penetrate the thin liquid film and be absorbed directly at the combustion chamber walls. It is then conducted into the liquid film by boiling heat transfer. At a high enough heat flux the surface can become covered with a poorly conducting vapor film which causes the wall temperature to rapidly rise, usually with catastrophic results. This transition point is rather abrupt and is termed "burnout".

Almost the same geometry of a thin liquid film flowing across a heated surface has been studied by Katto et al

[35,36]. They found a dimensionless correlation from measurements with water, freon 113, and trichlor. Their result can be written:

$$\dot{q}_{bo} = 0.0164 \lambda \rho_l^{0.534} \left(\frac{U_l \delta_l}{l} \right)^{1/3} \rho_v^{0.133}$$

It was noted that at the burnout point the liquid film was deflected from the surface. With water this deflection occurred at the first contact with the plate, whereas for freon and trichlor the liquid was deflected only near the end of the plate.

Since we are concerned mostly with organic liquids we will assume that the burnout occurs at a downstream position. As mentioned, Ziebland [34] measured the maximum radiation flux to occur somewhat downstream of the injector. For this reason we might use $l = 5$ cm as the most likely burnout point.

The interface velocity will be taken as 3 m/s for most cases, giving an average velocity $U_l = 1.5$ m/s in the liquid film.

The burnout heat flux for several fuels can now be estimated at a pressure of 100 psia [properties from ref. 37]:

Liquid	Tsat	λ	ρ_l	ρ_v	δ	\dot{q}_{bo}
	(K)	(E03 J/kg)	(kg/m ³)	(kg/m ³)	(E-3 N/m)	(kW/m ²)
MMH	433	663	720	9.79	20.2	419
AZ50	413	990	778	9.50	18	624
H2	29	335	70	5.75	0.6	17.6

The fact that the liquid is usually subcooled can be accounted for by multiplying the previous burnout heat flux by a factor [35]: $1+C_{sub}$

where:

$$C_{sub} = 2.7 (\rho_l / \rho_v)^{0.5} [C_{pl}(T_{sat}-T_c/\lambda)]^2$$

One should note that the maximum value of C_{sub} in ref. 35 was 0.41 . Extrapolating past this value is uncertain. Indeed, a similar term for pool boiling predicts much smaller corrections. In view of this it might be more reasonable to simply replace λ with λ^* in calculating \dot{q}_{bo} .

A final consideration is that a number of liquids would absorb much of the incident radiation before it reaches the wall. At 3500 K the radiation would peak at 830 nm. Unfortunately, the absorption spectra for this range is not easily found for most fuels. It is known, however that H₂ would provide little absorption since it has no dipole moment. Given the very low burnout heat flux it is almost certain that H₂ would not provide effective cooling as a liquid film.

With the unknowns of spectral absorption by the liquids and the proper correction for subcooling it is difficult to say other than the burnout heat fluxes of the liquid films are of the same order of magnitude as the heat flux reaching the wall and hence burnout may be a limit to the protective ability of a liquid film.

V. RECOMMENDATIONS:

Comparison was made with the data in references 13,14,18,20,22,and 23. For all cases in which Knuth's stability criterion was not exceeded the calculations were within the uncertainty in the data. The results are omitted for brevity.

In the high temperature environment of most liquid rocket engines the evaporation due to radiant heat is dominant. This vapor is transpired from the liquid film and greatly decreases the convective heat transfer by decreasing the wall shear stress. The radiation from high temperature gases is a complicated subject. More research is needed to allow more accurate calculations. Additionally, the optical absorption properties of the liquid films need to be studied to determine how much of a barrier they can provide to radiantly induced film burnout. It is hoped that as a follow on project the infrared spectroscopy resources at AEDC will be utilized to provide this data. Fluid mechanics calculations will be needed to determine the liquid film thickness.

The vapor mixing process has been well characterized in lower temperature flows without any turns. Data in both positive and negative turns is needed to charac-

terize the phenomenon at the throat of a rocket engine. Additional analysis needs to be made to determine the concentration and temperature profiles in the boundary layer, especially in supersonic flows and with chemical reactions.

Acknowledgements

Research sponsored by Air Force Office of Scientific Research/AFSC under Contract F49620-85-C-0013 (Summer Faculty Research Program). Appreciation is due CC.Limbaugh and WK.McGregor of AEDC for suggesting the topic, MH.Simmons of AEDC for running the NASA eqil. code, and M.Powell of AFAL for providing numerous obscure references.

REFERENCES

- 1.Schlichting,H.;Boundary Layer Theory, McGraw-Hill, 1981.
- 2.Cebeci,T.and P. Bradshaw;Phys. and comp. asp. of Convective Heat Transfer, Springer-Verlag, 1984.
- 3.Landis,R.B.;"Num. sol. of var. prop. turb. boundary layers with foreign gas inj.", Phd Thesis, UCLA, 1971.
- 4.Reynolds,W.C. et al;NASA Memo 12-1-58W, 1958.
- 5.Kays,W.M.;Convective Heat and Mass Transfer, McGraw-Hill, 1966.
- 6.Humble,L.V. et al; NACA Rep. 1020, 1951.
- 7.Bartz,D.R., Jet Prop.-ARS J., Jan 19
- 8.Hartnett,J.P. et al in Heat and Mass Transf Boundary Layers, Vol.1, N. Afgan,ed. Pergamon, 1972.

9. Hartnett, J.P. et al in Handbook of Heat Transfer, W.M. Rosenhow, ed., McGraw-Hill, Ch.17, Fig.69, 19
10. Eckert, E.R.G. et al; Analysis of Heat and Mass Transfer, McGraw-Hill, 1972.
11. Brunner, M.J.; ASME Paper no.64-WA/HT-50.
12. Rubesin, M.W. et al in Handbook of H.T. op cit in [8], Ch.8, p.171.
13. Kinney, G.R. et al; NACA rep.1087, 1952.
14. Knuth, E.L., The Mechanics of Film Cooling, JPL Memo 20-85, Sept 1953.
15. Gater, R.A. et al; Jet Prop. Center TM-69-1, Purdue Univ., contract Nonr 1100(21), 1969.
16. Zucrow, M.J. et al; Jet Prop.-ARS J., June 1957, p. 650.
17. Zucrow, M.J. et al; ARS J., May 1961, p.668.
18. Warner, C.F. et al; Trans. ASME J. of Heat Transfer, May 1964, p. 271.
19. Gater, R.A.; Jet Prop. Center TM-65-6, Purdue Univ., contract Nonr 1100(21), Oct. 1965.
20. Shembharkar, T.R. and B.R.Pai, Int.J.Heat and Mass Transfer, Vol.29, No.6, 1986, p.899.
21. Economos, C; "The comp. turb. b.l. with mass transfer", Phd thesis, Polytechnic Inst. of Brooklyn, 1968.
22. Morrell, G.; NACA RM E51E04, July 1951.
23. Kesselring, R.C. et al; "Boundary cooled rocket engines for space storable prop.", NAS7-767, NASA-CR-129260, June 1972, (Rocketdyne).
24. Kutateladze, S.S. et al; High Temperature (Soviet), Vol.1, Sept-Oct 1963.
25. Stollery, J.L. et al; Int. J. Heat and Mass Transfer, Vol.8, 1965, p.55 .
26. Librizzi, J. et al; AIAA J., Vol.2, no.4, April 1964.

27. Carlson, L.W. et al; Gas film cooling at var. accel. and turb. levels", in Heat and Mass T. in B.L. op cit [8].
28. Goldstein, R.J. et al; Trans. ASME J. of Heat Transfer, Aug 1965, p.353 .
29. Marek, C.J. et al; NASA TN D-7958, June 1975.
30. Rousar, D.C. et al; "Comb. eff. on film cooling", NASA CR-135052, Feb 1977, (Aerojet).
31. Ko, S.Y. et al; AIAA J., vol.18, no.8, Aug 1980, p.907 .
32. Goldstein, R.J. et al; Int. J. of Heat and Mass Transfer, Vol. 9, 1966, p.1341
33. Lucas, J.G. et al; NASA TN D-1988, Oct 1963.
34. Ziebland, H. et al; "Heat Transfer in Rocket Engines", AGARD-AG-148-71, Sept 1971.
35. Monde, M. et al; Int.J.of Heat and Mass Transfer, vol.21, 1978, p.295.
36. Katto, Y. et al; 7th Int. Heat Transfer Conf., vol.4, Toronto, 1978, p.435.
37. CPIA Liquid Propellants Manual, Chem. Prop. Inform. Ag. Laurel, Md.

Nomenclature

- a = $0.6 Mv < Mg, 0.35 Mv > Mg$
- A_w= absorptivity of chamber walls
- C = circumference or mass fraction
- C_l= radiative transpiration constant
- C_f= skin friction factor= $2(\text{tang. shear}) / \rho g U_g$
- C_i= interpolation rate constant
- C_p= specific heat per mass
- C_{sub}= subcooling correction to burnout
- C_t= correction constant for turbulence

D = diameter of comb. chamber at position x
 e = freestream turbulence intensity
 E = emissivity
 h = convective heat transfer coeff.
 $H = C_{pg} \Delta T / \lambda^*$
 K = thermal conductivity
 K_t = correction factor for turning
 L = optical path length
 L_c = film-cooled length
 L_{eff} = average optical path length
 m = mass entrained in b.l.
 \dot{m} = mass flow per area
 M = molecular weight
 \dot{M} = mass flow per circumference
 n = no. of moles
 N = mole fraction of coolant
 Nu_D = Nusselt no based on $D = hD/k$
 Pr = Prandtl no of gas = $\mu_g C_{pg} / K_g$
 P = absolute pressure
 P_g = partial pressure of species
 \dot{q} = heat flux
 Re_D = Reynold's no based on diameter = $\rho_g U_g D / \mu_g$
 Re_x = Reynold's no based on position = $\rho_g U_g x / \mu_g$
 St = Stanton no = $h / (\rho_g U_g C_{pg})$
 T = absolute temperature
 $\Delta T = T_g - T_w$
 U = axial velocity
 x = axial position

x' = corrected x for developing pipe flow

x = dimensionless distance

y = distance from wall

z = $H(Mg/Mv)$ (convection)

Greek:

Γ = coolant mass flow per circumferential length

δ = boundary layer thickness

λ = latent heat of vaporization of coolant

$\lambda^* = \lambda + Cpl(T_v - T_c)$

η = film cooling effectiveness

ρ = mass density

ρ_{opt} = optical density = PgL

σ = surface tension of coolant or Stephan's const.

μ = dynamic viscosity

subscripts:

bl- boundary layer

bo- burnout point

c - coolant

conv- convective

g - freestream gas

l - coolant liquid

o - initial position or dry-wall heat flux

rad- radiative

w - evaluated at wall

superscript:

(\quad) - properties evaluated at mean temperature

$(T_g + T_w)/2$

1987 USAF-UES SUMMER FACULTY RESEARCH PROGRAM

Sponsored by the

AIR FORCE OFFICE OF SCIENTIFIC RESEARCH

Conducted by the

Universal Energy Systems, Inc.

FINAL REPORT

Cellular Logic Image Processor Evaluation

Prepared by:	Timothy A. Grogan, Ph.D.
Academic Rank:	Assistant Professor
Department and	Electrical and Computer Engineering
University:	University of Cincinnati
Research Location:	RADC/IRRE Griffiss AFB, NY 13441
USAF Researcher:	Paul Hagerty
Date:	26 September, 1987
Contract No.:	F49620-85-C-0013

Cellular Logic Image Processor Evaluation

by

Timothy A. Grogan

ABSTRACT

Benchmark operations were performed on the British-built Stonefield Mark I 32x32 element cellular logic image processor (CLIP). A comparison was made to benchmark results reported in the literature for other parallel computers with specialized architectures for image processing. Performance estimates of the 128x128 element Stonefield Mark III CLIP design were obtained. The Mark III design has a price-performance ratio exceeding the MPP by a factor of five. A subjective evaluation of the Mark I CLIP software was also performed.

Recommendations are made for the benchmark testing of the Mark III. In addition, issues regarding the integration and utility of the Mark III as part of an imagery exploitation system are discussed.

ACKNOWLEDGEMENTS

I would like to express my gratitude to the Rome Air Development Center and Air Force Office of Scientific Research for the opportunity to participate in this program. My appreciation is also extended to Universal Energy Systems for their competent and congenial administration of the program.

Several people made my experience enjoyable and stimulating. Paul Hagerty was a valuable help in focusing on the pertinent issues and generous in his hospitality. Lee Ruiu was invaluable in performing much of the necessary programming. The technical discussions with Capt. Michael Richard were informative and thought provoking. The support of Branch Chief Arnie Lanckton was very much appreciated. The interactions with other members of the Imaging Branch were beneficial in increasing my understanding of the mission of RADC.

My brief but informative conversations with Dr. Michael J.B. Duff, the originator of the CLIP, are also gratefully acknowledged.

I INTRODUCTION

Parallel processing is being used to meet the enormous computational requirements of automated exploitation of digital imagery. The Imaging Systems Division of the Intelligence and Reconnaissance Directorate of the Rome Air Development Center, USAF, at Griffiss Air Force Base are investigating the use of this technology for the automated exploitation of reconnaissance imagery. Under the Foreign Weapons Evaluation (FWE) Program, RADC has acquired a 32x32 element cellular logic image processor (CLIP) from Stonefield Vision Systems, Great Britain. A 128x128 element CLIP is to be delivered in early 1988.

It is important to determine which of many proposed specialized parallel architectures will be most appropriate to image exploitation tasks.

My research interests have been in the development of algorithms for image analysis: shape and texture analysis, in particular. Some of my work utilizing Fourier descriptors for shape analysis is currently in use at RADC.

II OBJECTIVES

The objectives of my assignment were to measure the performance of the Stonefield Mark I 32x32 element array CLIP and to recommend a course of action for the evaluation of the 128x128 Mark III CLIP. In addition, I was to make recommendations on the integration of the CLIP into a larger image exploitation system.

The Stonefield CLIP is a commercial version of a system developed at

the University College of London led by Dr. Michael J.B. Duff. This was a 96x96 element array of processors. The evaluation of the 32x32 Mark I CLIP was to be made by implementing and running a suite of benchmark algorithms. A subjective evaluation of the software, the documentation, and the programming environment was also desired.

The 128x128 Mark III CLIP will utilize the same chip containing the processing elements as the 32x32 Mark I CLIP. The design of the rest of the 128x128 CLIP system is very different from the standpoint of both hardware and software. Some preliminary estimates of its performance based on information from Stonefield were to be made.

III RESULTS

The benchmark results for the Abingdon cross operations have been published for more than 20 computers for image processing.

The Abingdon cross is a $N \times N \times 8$ bit image of a cross shape. The amplitude of both the arms of the cross is 160 except for the central overlapping square which has value 192. All the background values are set to 128. White Gaussian noise having zero mean and standard deviation 32 is added at all points of the image. This noisy cross image was generated on the INTEL System 310/286 which hosts the CLIP. The image was loaded into the external memory of the CLIP.

The benchmark operations consist of performing a 3x3 averaging filter twice followed by a thresholding operation. Then, 8-connected Levialdi thin-

Image Size	Time (msec)	FOM
32x32	19.2	1,663
64x64	74.6	858
128x128	266.4	480

Table 1: Abingdon benchmark: Stonefield Mark I 32x32 CLIP

ning is performed to obtain the skeleton of the cross.

The Image Management Software (IMS) manages the processing of images a power of 2 larger than the processing array. The benchmark was performed on images of sizes $N = 32, 64$, and 128 . Table 1 contains the results of the Abingdon cross benchmark. The table values do not include the time necessary to transfer the image in and out of the staging memory.

The figure-of-merit (FOM) is the size of the image (N) divided by the time to perform the benchmark (T) or N/T . These results indicate that as the image size increases over the fixed size of the processing array, the computation becomes increasingly inefficient. This is because a significant amount of time is required to transfer small sections of the image into the processing elements local memory. In addition, the mean filter requires that overlapped sections of the processor array size be computed. Then a merging operation must be performed at the edges of these sections covering the full image size. The IMS, however, manages this overlap and block mapping automatically when a user invokes one of the image processing functions loaded previously into the CLIP controller program memory. However, there is a side-effect of this capability to process images of size greater than the

array size. It is necessary for the IMS to load, process, and then unload the internal processor memory. Because of this, intermediate results are swapped in and out of memory reducing efficiency. The IMS does not attempt to optimize the use of the internal processor memory by retaining intermediate results of a sequence of operations in the local processor memory.

The 8-neighborhood gating and global parallel propagation circuitry provides for efficient computation of local masking and global transmission of information across the array. This leads to better performance on these types of operations than would be expected from this early architecture. The figure-of-merit for the 32x32 Stonefield Mark I can be compared with already published results for other parallel processors. (See Table 2.) It should be noted that the cost of the computers differ considerably. For example, the Massively Parallel Processor (MPP) is a \$5 million computer, where the Mark I and Mark III computers together cost less than \$500 thousand. The price-performance ratio $(N/T)/\text{cost}$ for the Mark III exceeds that of the MPP by a factor of five. There are, however, some proprietary systems now under development which will exceed that of the Mark III. This is most directly a result of the design constraints imposed by the integrated circuit processing technology of the middle and late 1970's. The instruction cycle time is 480 nsec. compared to the 100 nsec. cycles times becoming common in current designs. Modern chip designs have enhanced functionality and improved data paths. In addition, the 32 bit internal memory per processing element are surpassed by design now having 128 to 1024 bits of on chip

Machine	Time (sec)	FOM	Notes
UCL 96x96 CLIP4	0.0132	7.273	96x96x6 bit image
Stonefield Mark I CLIP4	0.019	1.684	32x32x8 bit image
Stonefield Mark III CLIP4	0.019	13.472	128x128x8 bit image estimated
ERIM Cytocomputer	5	102	512x512x8 bit image
VICOM/CYTO	0.075	6.827	512x512x8 bit image
MPP		26,283	512x512x8 estimated
Warp	7.8	65.6	estimated

Table 2: Abingdon benchmark for some other parallel architectures.

memory per processor or up to 32K of off-chip memory. The insertion of a chip having a more modern architecture and processing technology into the Mark III system would have truly impressive performance.

Included in the figures of Table 2 is an estimate of the FOM for the 128x128 element Mark III CLIP. This estimate is based on the increase in the number of processors in the array. This is a conservative estimate. Changes in the partitioning of the external memories will provide the ability to transfer data in and out of the internal processor memories of the array in one-fourth the time. In addition, the total system throughput will be increased due to the 20-fold speed-up in the time required to transfer an image between the video I/O buffers and the external array memories. The external array memories are to be dual-ported allowing overlapped input & output operations.

Benchmarks for two other image processing operations were also per-

Operation	Time (sec)
Sobel	0.00864
zcLoG	0.195
Hough	2.1

Table 3: Benchmark results for other image processing operations

formed. These were the 3x3 sobel edge detector and the zero-crossings of the Laplacian of the Gaussian (zcLoG) using an 11x11 window. An estimate for computing the Hough transform was also obtained. These results are shown in Table 3.

The programming of the Stonefield Mark I CLIP was performed on the INTEL 310/286 host running the XENIX operating system. The CLIP resources: external memory, video I/O, and array controller program execution are managed using C language callable routines. The use of these functions by the novice programmer was somewhat hindered by inconsistent terminology in the documentation. Once the system functions were mastered, it was relatively painless to utilize the large number of boolean, arithmetic, and neighborhood processing routines. These routines are called from C, via the IMS which performs the block-mapping of images of size larger than the array. Missing from the system routines were utilities for printing the image values of intermediate results for debugging the C programs.

The development of assembly language routines was accomplished using an interpreted assembler. However, the syntax for register label conventions were different than those required by the assembly language compiler. This had the tendency to frustrate the use of the interpreter for debugging

large assembler routines. In addition, the register operations in the interpreter were carried out in the host and not in the array controller. This could lead to unpredictable results when the routines are compiled and executed.

Assembly language routines were written for computing the zero-crossings of the Laplacian of the Gaussian, grey-scale morphological erosion and dilation. Some arithmetic and boolean functions were modified to be maskable. Progress was made in programming a general image rotation routine. However, difficulties encountered in completing this task emphasized the need for the conditional execution masking. Conditional execution masking is discussed in the following recommendations.

IV RECOMMENDATIONS

The same benchmarks that were performed on the 32x32 Mark I CLIP should be repeated after delivery on the 128x128 Mark III, i.e. Abingdon cross, sobel edge, zero-crossings of the Laplacian of the Gaussian. This will require some minor modifications to the assembler routines. In addition, the Hough transform should be coded and executed. The 8-connected Levialdi thinning required in the Abingdon cross benchmark will require more extensive revision. The global propagation used in the thinning must be scanned over the entire image (a multiple of the array size.) This includes the proper manipulation of the edge stores as each array size sub-image is processed. This requirement is likely to effect the design and operation of the Image Management System. In fact, all routines making use of global propagation

will also require this modification.

In order to obtain more accurate timing statistics with fewer iterations, a real-time clock having more precision than the INTEL host clock (having 20 msec ticks) would be desirable.

The throughput of the 128x128 Mark III as part of a larger image exploitation system is likely to be limited by the bus and/or disk transfer rate of the IBM PC host. The throughput of the system could be optimized by the addition of a disk with its high-speed data channel connected to the ADX bus. The disk controller could then be another processor on the Mark III system buss controlled by another concurrent OCCAM process on the Transputer. If necessary, this disk could be dual-ported to the host computer of the exploitation system.

The IBM PC will provide an ETHERNET connection between the larger image exploitation system (a VAX) and the Transputer controlling the CLIP array and the associated I/O processors. To make the CLIP useful to the image exploitation system, the ETHERNET software controller should be required to permit remote process initiation and control on the CLIP control processor.

Three classes of image processing/analysis routines are noticeably missing from the list of routines supplied with the Mark I. These are the geometric operations, the decision theoretic operations, and the global transformations. The geometric operations include rotation, scaling, resampling, map projections, and mosaicing/registration. Among the common global transforma-

tions are Fourier, Walsh, and Hough transforms. It should be noted that many of the geometric operations and the global transformations require either global transmission of information across the array or are spatially variant operations. It is exactly these types of operations that are relatively inefficient on mesh-connected parallel computers. The decision theoretic operations or pixel classifiers often make use of multi-channel images. The extremely limited local memory of the CLIP4D processor chip (32 bits per processor) will likely be a bottleneck for these types of operations.

A high-order language for the array controller would be desirable to facilitate the programming of complex algorithms. To be compatible with the programming of the other system processors, an extension to the OCCAM language might be a good choice. The conditional execution is a programming language structure that is extremely useful in programming SIMD machines. (The statement: **where** \langle array condition is true \rangle **do** \langle perform operation 1 \rangle **else** \langle perform operation 2 \rangle .) This allows each processor, depending on the condition of a logical array variable, to ignore an instruction and so not modify its memory. The MPP and some of the newer processing chip designs implement the conditional execution masking in hardware. The CLIP4D chip does not. Therefore, this capability would have to be implemented in software. This would require modifications to most of the low-level Boolean and arithmetic assembler routines.

The limited array size of the 32x32 element Mark I as well as its slow I/O transfers greatly reduces its utility for routine image processing operations. It

is probably most useful for training in the fundamentals of parallel computing for image processing.

Limitations in the types of operations the mesh-connected SIMD machine can perform efficiently necessitate the investigation of alternative architectures which provide a solution to image exploitation problems. The mesh-connected parallel machines are efficient at most of the iconic-to-iconic operations required for image processing. Global array output information provided by the array-all-zeroes signal and the array histogramming functions augmenting most mesh-connected machines provide efficient computations of some iconic-to-symbolic operations. However, most image exploitation paradigms now incorporate iconic-to-iconic, iconic-to-symbolic, as well as symbolic-to-symbolic processes operating in parallel. More advanced architectures having richer interconnections between processors and a hierarchy of control will be necessary. One of the more promising architectures are those based on image pyramids. Here, planes of processors are connected in a mesh with its neighboring sibling processors on the same plane. In addition, each processor is connected to four children processors in the plane below and a parent processor in the plane above. Information flows up and down the pyramid as hypotheses are proposed at the upper levels of the pyramid and verified by the data processed by the lower levels.

The image pyramid is only one of many possible advanced architectures. Other possibilities are architectures having hypercube and reconfigurable interconnections among processors. As a follow-on to this activity, it

would be useful to determine the general classes of algorithms used for image exploitation. Then, determine alternative processor control strategies and interconnection networks required to efficiently support the flow of both data and control among the processors.

REFERENCES

1. V. Cantoni & S. Levialdi (eds.), **Pyramidal Systems for Computer Vision**, Springer-Verlag, Berlin, 1986.
2. M.J.B. Duff (editor), **Computing Structures for Image Processing**, Academic Press, London, 1983.
3. M.J.B. Duff and T.J. Fountain, **Cellular Logic Image Processing**, Academic Press, Orlando, 1986.
4. T.F.J. Fountain, "Array Architectures for Iconic and Symbolic Image Processing," IEEE Publ. No. CH2342-4/86, pp. 24-33, 1986.
5. T.J. Fountain, M. Postranecky, G.K. Shaw, "The CLIP4S System," *Pattern Recognition Letters*, Vol. 5, pp. 71-79, 1987.
6. R.P. Gabriel, "Massively Parallel Computers: The Connection Machine and NON-VON," *Science*, Vol. 231, Feb.28, pp. 975-978, 1986.
7. W.D. Hillis and G.L. Steele, "Data Parallel Algorithms," *Comm. of the ACM*, Vol.29, no. 12, December, 1986, pp. 1170-1183.
8. M.E.C. Hull, "OCCAM- A Programming Language for Multiprocessor Systems," *Computer Languages*, Vol.12, no. 1, pp. 27-37, 1987.
9. K. Hwang, "Computer Architectures for Image Processing," *Computer*, pp. 10-12, 1983.
10. J.J. Little, G. Blelloch, T. Cass, "Parallel Algorithms for Computer

Vision," *First Intl. Conf. on Computer Vision*, London, England, June 8-11, 1987, pp. 587-591.

11. C.F. Neveu, C.R. Dyer, and R.T. Chin, "Two-Dimensional Object Recognition Using Multiresolution Models," *Computer Vision, Graphics, and Image Processing*, Vol.34, 1986, pp.52-65.
12. T.J. Olson, L. Bukys, and C.M. Brown, "Low Level Image Analysis on a MIMD Architecture," *First Intl. Conf. on Computer Vision*, London, England, June 8-11, 1987, pp. 463-475.
13. J.L. Potter, "Image Processing on the Massively Parallel Processor," *Computer*, pp.62-67, January, 1983.
14. K. Prazdnay, "Position-, Rotation-, and Scale-Invariant Pattern Recognition using Parallel Distributed Processing," *First Intl. Conf. on Computer Vision*, London, England, June 8-11, 1987, pp. 587-591.
15. K. Preston, "Cellular Logic Computers for Pattern Recognition," *Computer*, January, pp. 36-47, 1983.
16. K. Preston & M.J.B. Duff, **Modern Cellular Automata: Theory and Applications**, Plenum Press, New York, 1984.
17. A.P. Reeves, "Survey: Parallel Computer Architectures for Image Processing," *Computer Vision, Graphics, and Image Processing*, Vol.25, pp. 68-88, 1984.

18. A. Rosenfeld, "Parallel Image Processing Using Cellular Arrays,," *Computer*, pp. 14-20, 1983.
19. A. Rosenfeld, J. Ornelas, and Y. Hung, "Hough Transform Algorithms for Mesh-Connected SIMD Parallel Processors," (preprint), January, 1986.
20. A. Rosenfeld, "A Report on the DARPA Image Understanding Architectures Workshop," pp. 298-302.
21. T.M. Silberberg, "The Hough Transform on the Geometric Arithmetic Parallel Processor," *IEEE Computer Pub. No. CH2229-3/85*, pp.387-391.
22. L. G. Shapiro, R.M. Haralick, and M.J. Goulish, "INSIGHT: A Dataflow Language for Programming Vision Algorithms," in *Proc. of IEEE Computer Conf. on Computer Vision & Pattern Recognition*, Miami Beach, FL, June 22-26, 1986, pp. 375-380.
23. L. Snyder, L.H. Jamieson, D.B. Gannon, and H.J. Siegal (eds.), **Algorithmically Specialized Parallel Computers**, Academic Press, Orlando, 1985.
24. S.R. Sternberg, "Biomedical Image Processing," *Computer*, January, pp.22-34 1983.
25. T. Toffoli and N. Margolus, **Cellular Automata Machines**, MIT Press, Cambridge, Mass., 1987.

26. L. Uhr, K. Preston, S. Levialdi, & M.J.B. Duff (eds.), **Evaluation of Multicomputers for Image Processing**, Academic Press, Boston, 1986.

1987 USAF-UES SUMMER FACULTY RESEARCH PROGRAM

GRADUATE STUDENT SUMMER SUPPORT PROGRAM

Sponsored by the

AIR FORCE OFFICE OF SCIENTIFIC RESEARCH

Conducted by the

Universal Energy Systems, Inc.

FINAL REPORT

THERMAL DECOMPOSITION INVESTIGATIONS OF CANDIDATE HIGH TEMPERATURE

BASE FLUIDS II. SILAHYDROCARBONS

Prepared by:	Vijay K. Gupta	and	Mark Prazak
Academic Rank:	Professor of Chemistry		Graduate Student
Department and	Chemistry Deaprtment		Chemistry Department
University:	Central State University		Wright State University
	Wilberforce, OHio 45384		Dayton, Ohio 45435
Research Location:	Materials Laboratory (AFWAL/MLBT)		
	Wright Patterson Air Force Base		
	Dayton, Ohio 45433		
USAF Researcher:	Mr. Carl E. Snyder Jr.		
Date:	September 4, 1987		
Contract No.:	F49620-85-C-0013		

Thermal Decomposition Investigations of Candidate High Temperature
Base Fluids II. Silahydrocarbons

by

Vijay K. Gupta and Mark Prazak

ABSTRACT

The effect of molecular structural variations in novel candidate base stocks such as silahydrocarbons on tribological properties such as thermal stability was investigated. The silahydrocarbons chosen for these studies contain a silicon atom and three n-octyl groups and another substituent group which provides the structural variation. The structural variations in the substituent group are the size, branching, the position of the branching, the presence of double bond, and the variation in the position of the double bond. The thermal stability of the above compounds was determined, and the extent of degradation was measured using gas chromatography, viscosity change, and mass spectroscopic analysis. Interesting trends were found and the rationale for these trends is presented.

ACKNOWLEDGEMENTS

The author would like to thank the Air Force Systems Command and Universal Energy Systems for providing an opportunity to work as Visiting Scientist at Materials Laboratory, Wright Patterson Air Force Base, Dayton, Ohio 45433. Thanks are also due to Nonstructural Materials Branch of the laboratory for their hospitality and excellent working conditions. The author is thankful to Mr. Lee D. Smithson of the Analytical Services Branch, and Dr. Jeff Workman and Dr. Chin Yu of the Technical Services Inc. for providing GC/MS analysis. Thanks to all the members of the Nonstructural Materials Branch and UDRI lubricants group specially to Mr. Daniel Miller for providing GPC analysis. Finally, the author would like to thank Mr. Carl E. Snyder Jr. and Lois J. Gschwender for suggesting this area of research and for their collaboration and helpful suggestions.

Thermal Decomposition Investigations of Candidate High Temperature

Base Fluids II. Silahydrocarbons

INTRODUCTION

In order to understand the effect of molecular structural variations in novel candidate base stocks such as silahydrocarbons on tribological properties such as thermal stability, micro-thermal stability studies have been conducted. The thermal stability investigations were conducted on pure and well defined compounds the structures of which were selected specifically to establish their structure-property relationships. The synthesis and characterization of silahydrocarbon base fluids and the performance properties of typical formulations have been previously reported (1-4). The experimental silahydrocarbon fluids that were investigated are shown in table 1. It may be noted that all of the fluids contain a silicon atom and three n-octyl groups and another substituent group which provides the structural variation. The fluid A contains an n-pentyl group, whereas fluids B, C, and D contain a branched pentyl group with branching in the α , γ , and β positions respectively. The fluids E, F, and G all three contain a C_5H_9 . The fluid E has double bond in the α position of the substituent group with respect to the silicon atom. Fluid F has double bond in the δ position of the substituent group with respect to the silicon atom. Fluid G is a mixture of the fluid where part of the fluid contains a double bond in γ position and part of the fluid contains a double bond in the β position of the substituent group with respect

to the silicon atom. The fluid H containing a CH_3 group has been included as a typical silahydrocarbon fluid for comparison with earlier investigations (4). The above silahydrocarbon compounds have been chosen to provide the structure-property relationships with respect to the position of the branching in C_5H_{11} substituent group, and the position of the double bond in C_5H_9 substituent group on the thermal stability of these fluids.

RESULTS AND DISCUSSION

The silahydrocarbon fluids shown in table 1 were analyzed for their purity on a Hewlett-Packard Model 5710A Gas Chromatograph using a capillary column. Specific GC conditions used during the analysis are given in table 2. The purity data for fluids A through G is given in table 3, and the data for fluid H is reported in table 8 under the column labelled 'unstressed'. From the data given in table 3 and table 8, it is clear that the concentration of the major component in all the fluids A through H was in the range of 94.9% to 98.7%. All of the fluids contained other silahydrocarbons as impurities. The presence of these specific impurities was considered to be acceptable for this program as none of these impurities are likely to bias the thermal stability data on the compounds of interest.

The viscosity-temperature properties of of the fluids A through H are given in table 4. Typical of silahydrocarbons, they all demonstrated good viscosity characterisites at low and high temperatures. From the viscosity values at 37.8°C , it appears that the

branching in the substituent group C_5H_{11} tends to increase the viscosity and the presence of a double bond in the C_5H_9 group tends to lower the viscosity as compared to $n-C_5H_{11}$ group. The viscosity of fluid H at $37.8^\circ C$ is significantly lower than the viscosity of fluids A through G at $37.8^\circ C$. The lower viscosity of fluid H is consistent with the lower molecular weight of fluid H as compared to fluids A through G.

The thermal stability of the silahydrocarbon fluids was determined using the following procedure. The thermal stability test bombs were made of 304 stainless steel tubing with 316 stainless steel Swagelok end caps. The bombs were 20 cm (8") long X 6 mm (0.25") outside diameter (unless otherwise specified). The bombs were cleaned with a suitable solvent (usually naphtha) and dried in an oven at $100^\circ C$ for one hour. Approximately 2.00 cc of the test fluid was added to the partially assembled bomb (one Swagelok end fitting attached), and 99.9% pure nitrogen was bubbled through the fluid for 5 minutes to remove the air. The bomb was then quickly capped with the top Swagelok fitting and the whole assembly weighed to the nearest mg. The bomb was then placed in an oven at the specified temperature (controlled within $2^\circ C$) for the specified time. The bomb was then removed, allowed to cool to ambient temperature, and then re-weighed. If the weight of the assembly changed by more than 0.1 g, the test was considered invalid and rerun. The bomb was then opened and the liquid sample was transferred to a glass vial and analyzed using capillary column gas chromatography and then viscosities at $37.8^\circ C$ were measured. All eight silahydrocarbon fluids listed in table 1 were investigated using the above procedure.

The thermal stability data for the specific silahydrocarbon fluids is given in table 5. The data in table 5 shows the concentration of the unstressed fluid remaining after heating the sample for 6 hours at the specified temperature. These concentrations represent the amount of a specific component as determined by gas chromatographic analysis using area percentage of the peak as percent concentration. The viscosity data in table 5 represents the viscosities of the fluids at 37.8°C before and after thermal stressing. The % change columns represent the changes in concentration and viscosity of the fluid during the stress test. The fluids A, B, C, D, and H were stressed at 371.1°C for 6 hours, and the % concentration values for these fluids represent the area percentage of the peaks as stated above. Sample chromatograms for fluids A and F unstressed and A stressed at 371.1°C and F stressed at 343.3°C for 6 hours are given in figure 1. The chromatograms of unstressed fluids A and F show some low and high molecular weight impurities as pointed out in table 3. The comparison of the chromatograms of stressed and unstressed fluid shows the formation of degradation products. It is observed that degradation products with molecular weights lower and higher than the parent silahydrocarbon compound are present. For the fluids A, B, C, and D which contained a saturated C_5H_{11} substituent, the change in concentration varied from -11.67% to -20.22%. The change in viscosity varied from -10.51% to -20.90%. The changes in viscosity agree very well with changes in concentration. The fluid A which contains the n-pentyl group appeared to be more stable as compared to the fluids B, C, and D which contained a branched pentyl group. In fluids B, C, and D, the position of branching in the pentyl group did not seem to make any difference in the

thermal stability of the fluid. It is clear that the branching in the silahydrocarbon's alkyl substituent results in lowering of the thermal stability of the silahydrocarbon molecule. This finding is consistent with the results reported previously (1). The thermal stability for the fluid H is comparable to the fluid A. This indicates that increasing the size of the substituent group from CH_3 to C_5H_{11} has not noticeably affected the thermal stability of the silahydrocarbon molecule.

The unsaturated silahydrocarbon fluids E, F, and G were stressed at 343.3°C for 6 hours, because stressing these fluids at 371.1°C resulted in excessive degradation. The % concentration values for stressed fluids E, F, and G as determined by capillary column gas chromatography were obtained using an internal standard method (n-tridecane was used as an internal standard). For the fluids E, F, and G containing an unsaturated C_5H_9 substituent group, the change in concentration varied from -32.68% to -76.93%, and the change in viscosity varied from +16.87% to +454.9%. From the above results, it is clear that the presence of a double bond in the side chain of the silahydrocarbon molecule has a significant effect on thermal stability. It is also evident that fluid F where the double bond was present at the end of the side chain was less thermally stable than fluids E and G where the double bond was not located in the terminal position of the side chain. The increase in viscosity observed in fluids E, F, and G is not consistent with the degradation of the molecule. The above increase in viscosity may be attributed to the polymerization of the molecule. In order to determine if the polymerization occurred during thermal stressing of the fluid, the stressed and unstressed samples of fluids E, F, and G were examined by

Gel Permeation Chromatography. The stressed samples exhibited slight band broadening, which indicates a change in molecular weight distribution had occurred which probably resulted from a combination of thermal degradation and thermally induced polymerization.

In order to determine any chemical changes in the silahydrocarbon fluids, infrared spectra of the stressed and unstressed fluids were recorded. Sample spectra of fluid F are given in figure 2 (unstressed sample) and figure 3 (sample stressed at 343.3°C for 6 hours). In figure 2 the absorptions at 1830 cm^{-1} and 910 cm^{-1} represent the vinyl group $-\text{CH}=\text{CH}_2$, the band at 1640 cm^{-1} represents the double bond, and the band at 970 cm^{-1} represents the symmetrical stretching of the double bond. In fluid F the trans form appears to be more prevalent than the cis form. On comparison of the spectrum of the stressed fluid in figure 3 with spectrum of unstressed fluid in figure 2, the absorption at 1830 cm^{-1} has disappeared and the intensities of the absorptions at 1640 cm^{-1} and 910 cm^{-1} are significantly reduced. The above observation indicates that significant amount of the major component of the fluid containing the double bond has decomposed during thermal stressing. A new absorption at 2100 cm^{-1} has been observed in stressed fluid F as well as in other stressed fluids indicating the formation of a Si-H bond. The band at 1830 cm^{-1} was not observed in fluids E and G as the substituent group C_5H_9 in these fluids did not contain the double bond at the end of the chain.

Using gas chromatography coupled with mass spectrometry, the degradation components present in the liquid phase of the stressed

samples were identified and the data is given in tables 6, 7, and 8. The hydrocarbons with 5 carbon atoms to 8 carbon atoms were found. Based on the previous work(4), it is believed that hydrocarbons with four or less carbon atoms were in the gas phase and hence not detected in the liquid phase. Many silahydrocarbon compounds with less than 29 carbon atoms were also found. Silahydrocarbon compounds with more than 29 carbon atoms and up to 34 carbon atoms were found in increasing concentrations compared to their concentration in the unstressed fluid. The data in tables 6 to 8 do not reveal any significant difference in the mode of degradation of one silahydrocarbon molecule from another. Within limits of the method, what is observed is primarily random carbon-carbon bond breaking with silicon carbon-bond breaking to a significantly lesser extent.

CONCLUSIONS

The structure-property relationships of silahydrocarbon compounds have been studied with respect to the position of the branching in one of the substituent groups C_5H_{11} , the effect of the double bond in the substituent group C_5H_9 , and the effect of the position of the double bond in the C_5H_9 substituent group. The following conclusions are derived.

1. When the substituent group in the silahydrocarbon molecule is branched, it tends to increase the viscosity slightly, and the presence of a double bond in the substituent group tends to decrease the viscosity slightly.

2. Branching in the substituent group C_5H_{11} reduces the thermal stability of the silahydrocarbon molecule, but the position of branching does not appear to have any effect on the thermal stability.

3. A double bond in the side chain reduced the thermal stability significantly.

4. The double bond at the end of the side chain reduced thermal stability more than when the double bond was present in the middle of the side chain.

5. The double bond in the side chain appears to have caused polymerization of the molecule as indicated by the increase in post-thermal stress viscosity and Gel Permeation Chromatography analysis.

Finally, it may be concluded that both branching and double bonds in the side chain should be avoided if good thermal stability characteristics are an important requirement for the silahydrocarbon fluid.

REFERENCES

1. Snyder, C. E. Jr., Gschwender, L.J., and Tamborski, C., "Synthesis and Characterization of Silahydrocarbons - A Class of Thermally Stable Wide-liquid Range Functional Fluids", ASLE Trans. 25, 299-308 (1981).
2. Snyder, C.E. Jr., Tamborski, C. Gschwender, L.J. and Chen, G.J., "Development of High Temperature (-40°C to 288°C) Hydraulic Fluids for Advanced Aerospace Applications", Lubrication Engineering, 38, 173-178 (1982).
3. Tamborski, C., Chen, G.J. Anderson, D.R., and Snyder, C.E. Jr., "Synthesis and Properties of Silahydrocarbons, a Class of Thermally Stable Wide Liquid Range Fluids", Ind. Eng. Chem. Prod. res. Dev., 22, 172-178 (1983).
4. Gupta, V. K., Snyder, C. E. Jr., Gschwender, L. J., and Fultz, G. W., "Thermal Decomposition Investigations of Candidate High Temperature Base Fluids I. Silahydrocarbons", 41st Annual meeting of The American Society of Lubrication Engineers, Toronto, Canada, May 11-14, 1986 (To be published in ASLE Transactions).

Table 1. Structures of Various Silahydrocarbon Fluids

Fluid	Structure
A	$n\text{-C}_5\text{H}_{11}\text{-Si-(n-C}_8\text{H}_{17})_3$
B	$(\text{CH}_3)_2\text{CHCH}_2\text{CH}_2\text{-Si-(n-C}_8\text{H}_{17})_3$
C	$\text{CH}_3\text{CH}_2\text{CH}_2\underset{\text{CH}_3}{\text{CH}}\text{-Si-(n-C}_8\text{H}_{17})_3$
D	$\text{CH}_3\text{CH}_2\underset{\text{CH}_3}{\text{CH}}\text{CH}_2\text{-Si-(n-C}_8\text{H}_{17})_3$
E	$\text{CH}_3\text{CH}_2\text{CH}_2\text{CH=CH-Si-(n-C}_8\text{H}_{17})_3$
F	$\text{H}_2\text{C=CHCH}_2\text{CH}_2\text{CH}_2\text{-Si-(n-C}_8\text{H}_{17})_3$
G*	$\text{CH}_3\text{CH=CHCH}_2\text{CH}_2\text{-Si-(n-C}_8\text{H}_{17})_3$ + $\text{CH}_3\text{CH}_2\text{CH=CHCH}_2\text{-Si-(n-C}_8\text{H}_{17})_3$
H	$\text{CH}_3\text{-Si-(n-C}_8\text{H}_{17})_3$

* This fluid is a mixture of the above two isomers.

Table 2. Gas Chromatographic Conditions.

Model: Hewlett-Packard 5710A
Detector: FID
Column: Fused Silica Capillary Column
Length: 12 meters
Diameter: 0.22 mm
Liquid Phase: Methyl Silicone Carbowax Deactivated
Carrier Gas: 1 ml/min He
Auxiliary Gas: 40 ml/min
Chart Speed: 10 cm/hr.
Attenuation: 10 x 32
Temperatures:
Injector: 300 °C
Detector: 350 °C
Column: 70 °C to 270 °C
Program Rate: 8 °C/min
Initial Hold: 2 min
Final Hold: 32 min
Sample Size: 1 Microliter

Table 3. Analysis of Various Silahydrocarbon Fluids (Unstressed).

Component	No. of C Atoms	% Concentration						
		A	B	C	D	E*	F*	G*
H-Si(n-C ₈ H ₁₇) ₃	24	0.107		0.062				
CH ₃ -Si-(n-C ₈ H ₁₇) ₃	25			0.196	0.056			0.135
C ₂ H ₅ -Si-(n-C ₈ H ₁₇) ₃	26	0.094		0.125	0.178	0.247	0.108	0.430
(C ₅ H ₁₁) ₂ -Si-(n-C ₈ H ₁₇) ₂	26	0.072			0.157			
C ₃ H ₇ -Si-(n-C ₈ H ₁₇) ₃	27			1.178	0.168	0.089		0.066
C ₅ H ₁₁ -Si-C ₆ H ₁₃ (n-C ₈ H ₁₇) ₂	27		0.096					
C ₄ H ₉ -Si-(n-C ₈ H ₁₇) ₃	28	0.031	0.144	0.894		0.079	0.084	0.324
C ₅ H ₁₁ -Si-(n-C ₈ H ₁₇) ₃	29	98.49	98.47	96.82	98.45	97.30	98.74	94.90
C ₆ H ₁₃ -Si-(n-C ₈ H ₁₇) ₃	30	0.443	0.453	0.260	0.310	0.411	0.327	1.961
C ₇ H ₁₅ -Si-(n-C ₈ H ₁₇) ₃	31	0.225	0.158	0.470	0.098	0.850	0.242	1.164
Si-(n-C ₈ H ₁₇) ₄	32	0.297	0.168	0.360	0.583	0.799	0.377	0.569
Si-(n-C ₈ H ₁₇) ₃ C ₁₀ H ₂₁	34		0.510					0.211

* In fluids E, F, and G, C₅H₁₁ group is C₅H₉.

Table 4. Viscosities of Various Fluids as a Function of Temperature.

Fluid Viscosity Values at Different Temperatures (cSt)

	98.9°C	37.8°C	-40.0°C	-53.9°C
A	2.97	11.36	790	3184
B	3.14	12.56	1007	4602
C	3.30	13.83	1456	5833
D	3.04	11.95	832	3450
E	2.92	11.09	708	2659
F	2.87	10.72	654	2529
G	2.92	10.56	733	2823
H	2.37	7.99	443	1529

Table 5. Thermal Stability Data for Various Silahydrocarbon Fluids.

Fluid	% Concentration			Viscosity cSt at 37.8°C		
	Unstressed	Stressed	% Change	Unstressed	Stressed	% Change
371.1°C-6Hr						
A	98.49	87.00	-11.67	11.36	10.08	-11.28
B	98.47	78.56	-20.22	12.56	10.08	-19.74
C	96.82	78.17	-19.26	13.83	10.94	-20.90
D	98.45	80.83	-17.90	11.95	9.74	-18.49
H	98.42	88.65	- 9.93	7.99	7.15	-10.51
343.3°C-6Hr						
E	97.30	65.50*	-32.68	11.09	12.96	+16.87
F	98.74	22.78*	-76.93	10.72	59.49	+454.9
G	94.90	59.72*	-37.71	10.56	13.89	+31.53

* Values obtained using internal standard method.

Table 6. GC/MS Analysis of Silahydrocarbon Fluids Stressed at 371.1°C for 6 Hours.

Component	No. of C Atoms	% Concentration of Components in Fluids			
		A	B	C	D
C_5H_{10}	5	0.520	1.799	3.205	2.637
C_6H_{12}	6	0.183	0.468		
C_7H_{14}	7	0.185	0.811	0.260	0.627
C_8H_{16}	8	1.184	2.933	1.404	1.350
$(CH_3)_2Si(C_8H_{17})_2$	18		0.275		
$C_2H_5SiC_3H_7C_5H_{11}C_8H_{17}$	18				0.123
$HSiC_2H_5(C_8H_{17})_2$	18			0.193	0.092
$C_2H_5Si(C_4H_9)_2C_8H_{17}$	18				0.113
$CH_3SiC_2H_5(C_8H_{17})_2$	19		0.202	0.123	0.097
$HC_3H_7Si(C_8H_{17})_2$	19			0.157	
$CH_3SiC_3H_7(C_8H_{17})_2$	20			0.048	
$(C_2H_5)_2Si(C_8H_{17})_2$	20			0.066	0.145
$C_2H_5SiC_3H_7(C_8H_{17})_2$	21			0.106	
$CH_3SiC_4H_9(C_8H_{17})_2$	21		0.184	0.058	
$HSiC_5H_{11}(C_8H_{17})_2$	21	1.463	1.990	1.443	2.001
$CH_3SiC_5H_{11}(C_8H_{17})_2$	22	0.801	1.167	1.097	0.523
$C_2H_5SiC_5H_{11}(C_8H_{17})_2$	23	0.586	0.729	0.573	0.449
$(C_4H_9)_2Si(C_8H_{17})_2$	24			0.185	
$C_3H_7SiC_5H_{11}(C_8H_{17})_2$	24	0.457	0.689	0.431	0.222
$HSi(C_8H_{17})_3$	24	0.629	0.405	2.786	3.104
$C_4H_9SiC_5H_{11}(C_8H_{17})_2$	25	0.363	1.154	0.225	0.296
$CH_3Si(C_8H_{17})_3$	25	0.369	2.721	0.908	0.694
$(C_5H_{11})_2Si(C_8H_{17})_2$	26	0.899	1.146		0.923
$C_2H_5Si(C_8H_{17})_3$	26	0.211	0.270	1.650	0.454
$C_3H_7Si(C_8H_{17})_3$	27	0.142		1.248	0.756
$C_5H_{11}SiC_6H_{13}(C_8H_{17})_2$	27	0.350	0.442		
$C_5H_{11}SiC_7H_{13}(C_8H_{17})_2$	28	0.442	0.611		
$C_4H_9Si(C_8H_{17})_3$	28	0.122	0.237	2.051	0.565
$C_5H_{11}Si(C_8H_{17})_3$	29	87.00	78.56	78.17	80.83
$C_6H_{13}Si(C_8H_{17})_3$	30	0.481	0.462	0.432	0.519
$C_7H_{15}Si(C_8H_{17})_3$	31	0.458	0.413	0.498	0.422
$Si(C_8H_{17})_4$	32	1.018	1.489	2.845	2.866
$Si(C_8H_{17})_3C_{10}H_{21}$	34		0.939		

Table 7. GC/MS Analysis of Silahydrocarbon Fluids Stressed at 343.3°C for 6 Hours.

Component	No. of C Atoms	% Concentration of Components in Fluids		
		E	F	G
C_5H_{10}	5	0.229	0.049	0.396
C_6H_{12}	6	0.133	0.063	0.170
C_7H_{14}	7	0.148	0.087	0.267
C_8H_{16}	8	0.578	0.581	0.708
$(CH_3)_2Si(C_8H_{17})_2$	18		0.049	0.097
$HSiC_5H_9(C_8H_{17})_2$	21		0.049	
$CH_3SiC_4H_7(C_8H_{17})_2$	21			0.088
$CH_3SiC_5H_9(C_8H_{17})_2$	22			0.134
$C_2H_5SiC_5H_9(C_8H_{17})_2$	23			0.102
$HSiC_7H_{11}C_8H_{15}C_8H_{17}$	23	0.133		
$HSiC_8H_{13}(C_8H_{17})_2$	24	0.179		
$HSi(C_8H_{17})_3$	24	0.718	0.208	0.385
$C_4H_9SiC_5H_9(C_8H_{17})_2$	25			0.142
$CH_3Si(C_8H_{17})_3$	25	0.218	0.267	0.624
$CH_3SiC_8H_{13}(C_8H_{17})_2$	25	0.425		
$C_2H_5Si(C_8H_{17})_3$	26	0.224	0.275	0.488
$C_3H_7Si(C_8H_{17})_3$	27	0.318	0.291	0.239
$C_4H_9Si(C_8H_{17})_3$	28	0.567	0.166	0.330
$C_5H_9Si(C_8H_{17})_3$	29	65.50	22.78	59.72
$C_6H_{13}Si(C_8H_{17})_3$	30	0.112	0.210	0.164
$C_7H_{15}Si(C_8H_{17})_3$	31	0.258	0.161	0.528
$Si(C_8H_{17})_4$	32	0.493	0.325	0.523
$Si(C_8H_{17})_3C_{10}H_{21}$	34		0.106	0.078

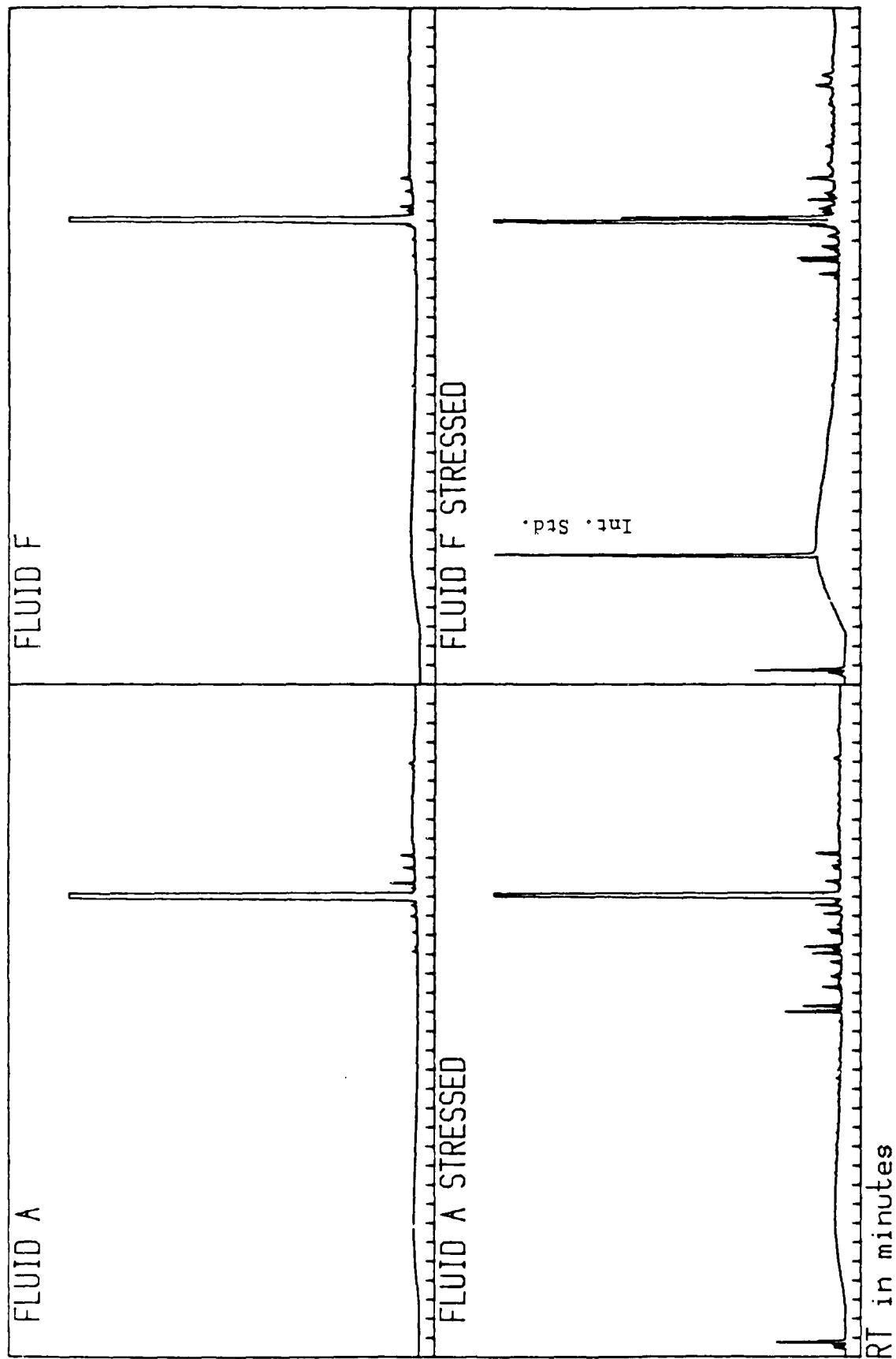


Fig. 1. Capillary GC for Fluid A Stressed at 371.1°C and Fluid F Stressed at 343.3°C for 6 Hours.

Sample: Fluid F Cell: NaCl Path: 0.05 mm Solvent: None

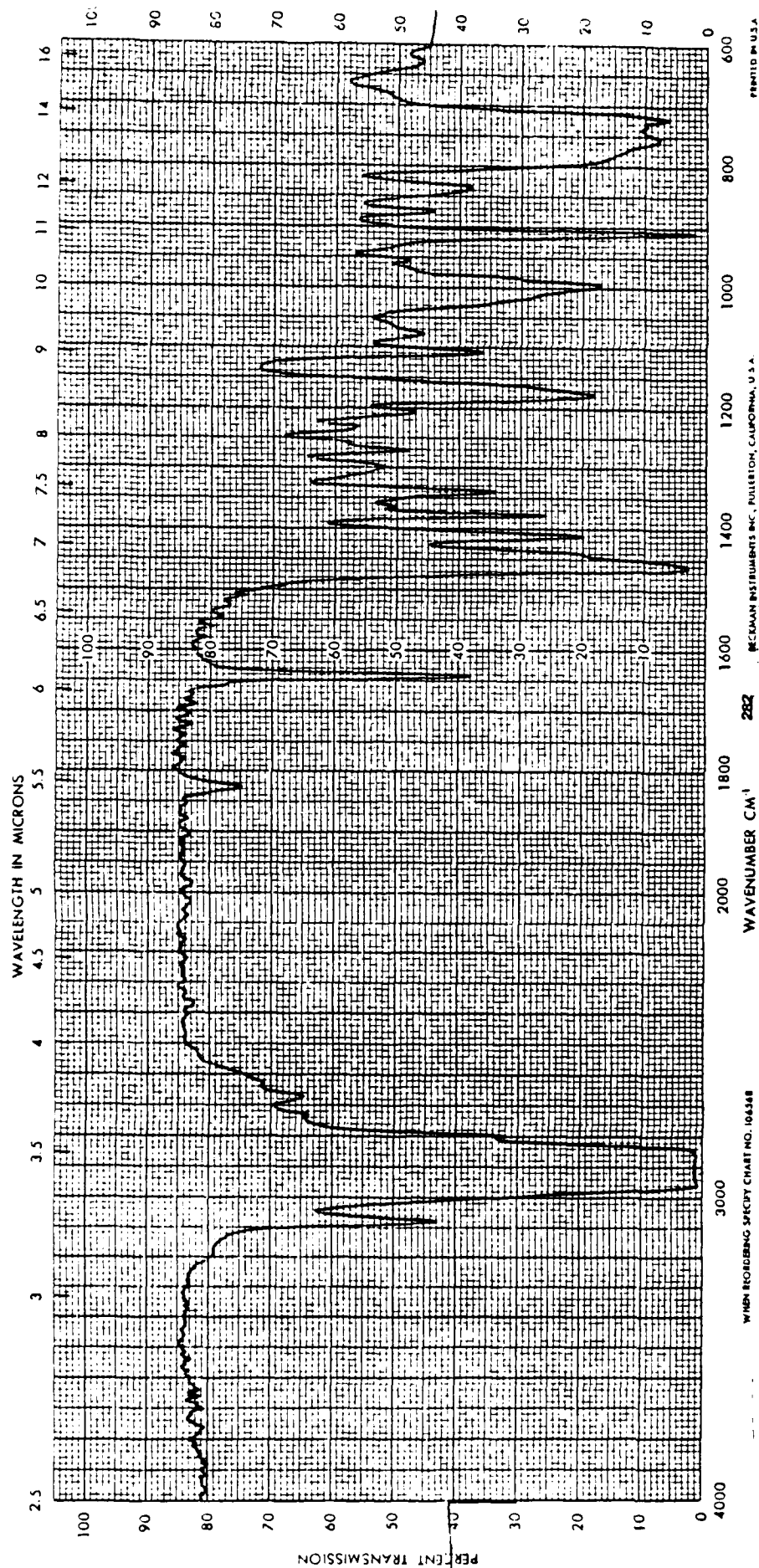


Fig. 2. Infra-red Spectrum of Fluid F (Unstressed).

Sample: Fluid F (Stressed) Cell: NaCl Path: 0.05 mm Solvent: None

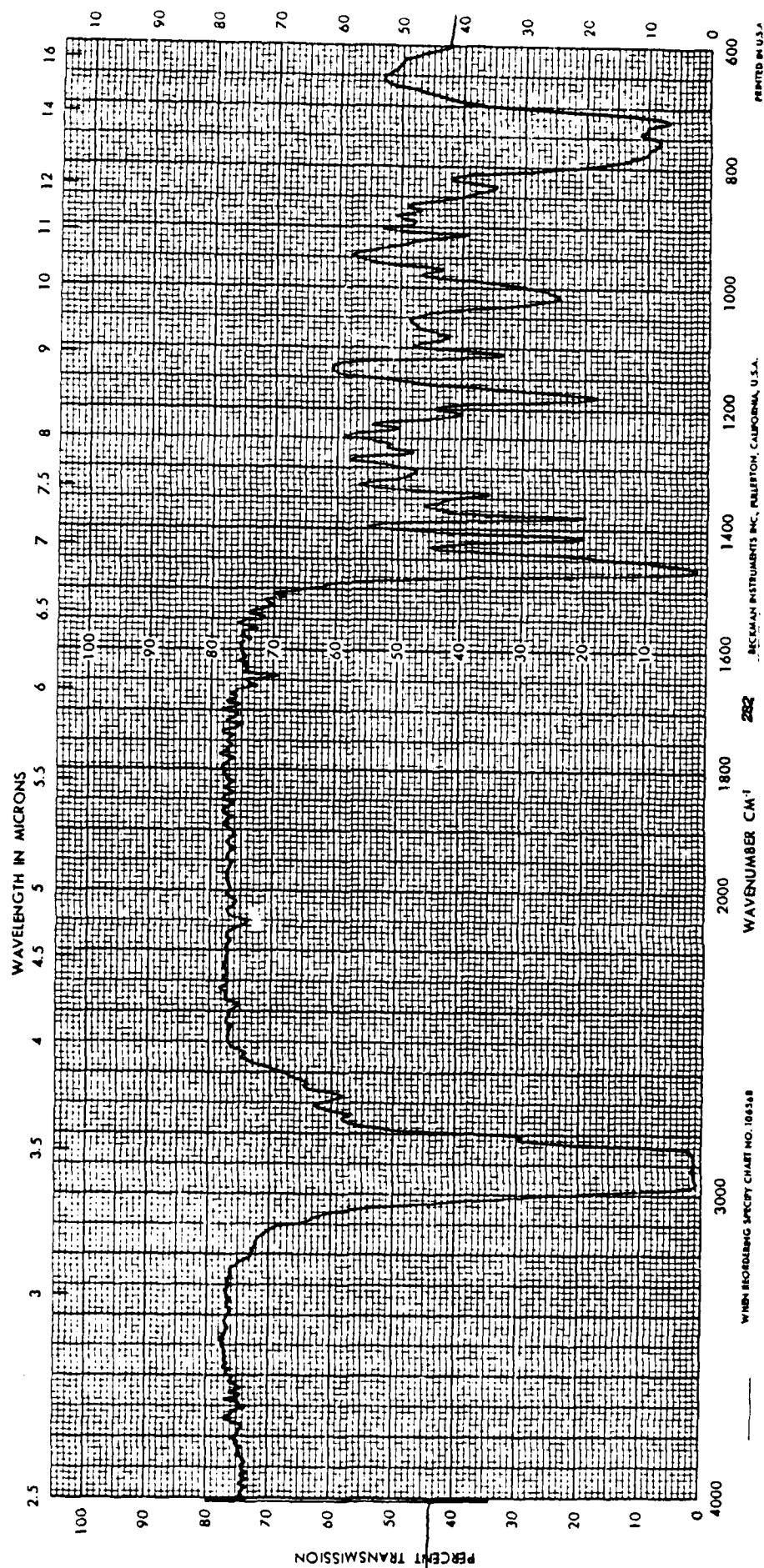


Fig. 3. Infra-red Spectrum of Fluid F Stressed at 343.3°C for 6 Hours.

1987 USAF-UES SUMMER FACULTY RESEARCH PROGRAM/

GRADUATE STUDENT SUMMER SUPPORT PROGRAM

Sponsored by the
AIR FORCE OFFICE OF SCIENTIFIC RESEARCH

Conducted by the
Universal Energy Systems, Inc.

FINAL REPORT

Prepared by: Narayan C. Halder
Academic Rank: Professor
Department and Physics
University: University of South Florida, Tampa, FL 33620
Research Location: Avionics Laboratory
AFWAL/AADR
Wright-Patterson AFB, OH 45433
USAF Researchers: D.C. Look
T.A. Cooper
D. Elsaesser
K.K. Bajaj
Date: July 14, 1987
Contract No: F49620-85-C-0013
Project No: 760

EFFECT OF SURFACE STATES ON THE ELECTRONIC TRANSPORT

PROPERTIES IN SEMI-INSULATING GaAs

by

Narayan C. Halder

ABSTRACT

The electronic transport properties (electrical conductivity, mobility and carrier concentration) have been measured in semi-insulating (SI) GaAs samples as functions of temperature from 250 to 390°K. Several gas ambients (N_2 , He, air, and vacuum) were considered to detect any possible effect of the surface states and/or charge accumulation on the surface that might influence the layers immediately below the surface of the samples. Four samples were selected for this study. The results of the present study indicate that there is a marked effect of the conductivity, mobility and concentration data, especially in the low temperature region, in that the slopes of the corresponding temperature dependence plots were different. These results are interpreted in terms of variations of the surface states on the samples due to various gas ambients.

ACKNOWLEDGEMENTS

I would like to thank the Air Force Office of Scientific Research and Universal Energy Systems for the award of a summer faculty research fellowship, which made this research work possible at the Avionics Laboratory, Wright-Patterson Air Force Base. I am grateful to Drs. K.K. Bajaj and D.C. Look for their cooperation and support, in particular making available to me all laboratory facilities. Finally, I wish to acknowledge the technical and computational help I received from Tim Cooper and David Elsaesser respectively throughout the progress of my experimental work.

1. INTRODUCTION

In GaAs, the midgap donor level, called EL2, is the most dominant level¹⁻³. It is the most important native defect that plays a major role in compensating residual impurities in undoped semi-insulating GaAs substrates. Many papers have been published⁴ on the study of this EL2 level and its role on various properties of the material pertinent to devices that use GaAs, but still there are many unanswered questions.

A summary of recent publications⁵ indicates that there are as many as twelve hole traps (H1-H12) and fifteen electron traps (E1-E15), plus the level EL2 at the midgap in GaAs grown by various techniques. There could be more, but these are well recognized and have been reported more than once. These are again characterized⁶ by the method of preparation (MBE, LPE, LEC, and VPE) and nature of transition metal dopants (Fe, Cu, Cr). It has been further seen that most defects are observed in bulk samples, while LPE samples show the least. It is also known that their concentrations change markedly with temperature, and radiations⁷ (especially, electrons and neutrons) add further new types of defects such as EL6, U-band, etc. For example, the broad DLTS band present^{6,7} in neutron irradiated GaAs appears near the midgap, which is very similar to EL2 and antisite As_{Ga} in as-grown GaAs. This is stable up to about 300°C. This is not found in electron irradiated GaAs. Why? The similarities between EL2 and As_{Ga} have not been looked into in great detail. However, it has been mentioned⁸⁻¹² that it is

incorrect to identify EL2 with undistorted antisite As_{Ga} . The microscopic nature and existence of the very distortions are still open to discussion. Why is there no support for impurity interaction with As_{Ga} in one study against the evidence of support in another study, etc.? There are three major questions, however, which are still not answered: (i) the relationship between EL2 and As_{Ga} defect, and (ii) the unusual optical properties of EL2 at $T < 140\text{K}$ which manifest as persistent optical bleaching and photocapacitance quenching, and (iii) identification and significance of another new defect EL0 which reportedly occurs at the same energy as EL2 ($\sim 0.75\text{eV}$).

Recent studies¹³⁻¹⁵ of the conductivity on semi-insulating GaAs indicate some interesting results. For example, the ac conductivity results show that the conductivity is frequency dependent even at high temperatures. Normally, amorphous semiconductors and dielectrics show a strong frequency dependent conductivity, but crystalline semiconductors show somewhat smaller effect at relatively low temperatures. On the other hand, dc conductivity measurements have been explained in terms of quantum mechanical tunneling between localized states in the bandgap. These states are separated by potential barriers which are found to fluctuate with the thermal expansion of the lattice. Other studies¹³ indicate that the temperature dependence of the dc conductivity, especially in the low temperature region, is given by the Berthelot equation

$$\log \sigma = aT + b$$

where σ is the surface conductance, whereas the bulk

conductance obeys the Arrhenius-type behavior

$$\sigma = \sigma_0 e^{-E/kT}$$

For the ac conductivity, as well, there are some recent developments. Abdalla and Pistoulet¹⁵ proposed a model based on Gaussian distribution of potential fluctuation suggesting

$$\sigma \propto \omega^s$$

where $s < 1$ for the intermediate range of $\omega < 10^6$ Hz, but $s = 2$ for $\omega > 10^6$ Hz under some approximations. However, their model depends on a number of unknown input parameters whose justification may be questionable.

II. OBJECTIVES OF THE RESEARCH EFFORT

We will first review some of the important papers relevant to our present investigation. Kristofik et al. measured¹³ the temperature and frequency dependence of electrical conductivity of SI-GaAs and concluded that the surface conductivity is explained by the Berthelot equation, whereas the bulk conductivity has the Arrhenius-type behavior. This type of investigation was followed¹⁵ by Abdalla and Pistoulet, and Pistoulet and Hamamdjian. They suggested that the long range potential fluctuations can give rise to mixed conductivity due to the accumulation of electrons in potential wells separated in space from holes accumulated in potential hills. They have further carried out a theoretical analysis of the problem by assuming a potential fluctuation with truncated Gaussian distributions, which depended on a number of input parameters (as many as eight parameters). On the other hand, Look¹⁶ had already pointed out earlier the existence of mixed conduction in Cr-doped SI-GaAs from his study of Hall-effect and

magnetoresistance. Later on, he has developed¹⁷ an appropriate theory to represent the mixed conduction effect in semiconductors in general. Most recently, Lo et al.¹⁸ have demonstrated by a surface property study using cw-electro-optic probing that the EL2 concentration on the surface of SI-GaAs is nonuniform across the wafer, which tends to be depleted near the surface after thermal annealing. This surface depletion of EL2 defect can cause a very leaky substrate surface promoting a serious backgate effect.

The purpose of this research is to investigate the surface states and/or surface defects in semi-insulating GaAs (SI-GaAs) to understand the role they play in influencing the electronic transport properties; when SI-GaAs is used as substrate material in making devices, after MBE layers are grown, it is believed¹⁷ the characteristics of the devices will heavily depend on the properties of the substrate. The surface states or defects could arise in the samples from adsorbed or absorbed gas molecules. The ionized molecules, in the presence of electric field, could thermally diffuse into the layers immediately below the surface and might interfere with the conduction band electrons. Yeo et al.¹⁹ have investigated the surface effect on Si-implanted GaAs (n-type) and concluded that this surface states could also result from the abrupt termination of the lattice or defects at the semiconductor surface, and therefore, they can pin²⁰ the Fermi energy within the forbidden gap at the surface, creating a carrier depletion in the region just below the surface. The long range potential fluctuation is a real possibility due to a nonuniform distribution of the impurities.

We have made a series of experimental measurements to investigate this problem. The results so obtained have been analyzed and examined in the light of most recent theoretical predications and other relevant experiments.

III. EXPERIMENTAL

In this report we will include the experimental measurements of two SI-GaAs samples (R158-6-65 and TI-EB31S 41-65). These samples are part of the research "Advanced GaAs Growth Program", and were obtained^{21,22} from Rockwell International and Texas Instruments respectively. The last number in each of the samples identifies the location on the wafer, which happens to be in the central portion, in this case. More detailed description of sample growth and characterization are available elsewhere.^{21,22} The sample TI31-41-65 is a low-pressure, liquid-encapsulated Czochralski (LEC), near-tail-end sample of the boule, which was undoped, but R158-6-65 is a high pressure LEC, near-seed-end sample, and doped with In($9.23 \times 10^{20}/\text{cm}^3$ in the melt). For this reason these two are contrasting samples. The methods of sample preparation, polishing and etching, etc. are also described in the above two reports.^{21,22}

The three important transport properties - electrical conductivity, carrier concentration and the Hall mobility have been measured in the standard van der Pauw configuration. The property mobility is a very important parameter, along with the other two, and very sensitive to the material quality and existence of defects. The experimental arrangement of the measuring system is shown in Fig. 1,

which is identical to the system published by Look and Farmer.²³ It is a computer-controlled system capable of measuring all the above three properties simultaneously in the temperature range 4.2 to 600°K in a magnetic field up to 1.8T.

IV. RESULTS AND DISCUSSIONS

The results of our measurement are presented in Table I and Table II. The corresponding plots are shown in Figs. 2-3. Since this investigation is far from being complete at this stage, as will be seen in the next section, we will only summarize the main features of the data. The resistivity of the samples is quite high $\sim 10^8 \Omega\text{cm}$, concentration $10^6/\text{cm}^3$ and mobility $10^3 \text{cm}^2/\text{V-s}$. The conductivity σ is linear with $1/T$ when plotted on logarithmic scale in the high temperature region, but there is some nonlinearity in the low temperature region, particularly below room temperature. The slopes of the $\log \sigma$ vs $1/T$ plots are different for different gas ambients, especially below room temperature. The behavior of the concentration plots, i.e., $\log n$ vs $1/T$ is the same as that of $\log \sigma$ vs $1/T$ plots, since μ is not nearly as temperature-dependent as n . The mobility μ , as expected, increased with $1/T$ in the high temperature region. Once again these plots show some marked effect not only from sample to sample but also from one gas ambient to another. Apparently, at this point we need more data and extensive measurement as functions of temperature. Therefore no attempt is being made in this report to fit these data with any model or make any conclusion with regard to the role of surface states. However, the present data suggest two

important conclusions: (i) the ambient gas, in general, does affect the magnitude of σ , n , and μ and, thus, must be considered or at least mentioned in the routine measurement of SI-GaAs, (ii) the bulk model of Pistoulet et al.¹⁴ is not sufficient to explain the temperature dependence of SI-GaAs.

V. RECOMMENDATIONS

From the preliminary results of the present research work it appears that future efforts should be directed in two directions: (i) more SI-GaAs samples, both of Rockwell International and Texas Instruments-type should be investigated for various wafer numbers across the wafer sections, and the (ii) low temperature data, which could only be recorded down to 250°K due to very high resistivity ($\sim 10^{11} \Omega\text{cm}$) of the samples with the present measuring system, should be expanded to measure much higher resistivity at considerably lower temperatures. This research project could be further extended to the measurement of ac conductivity and Hall parameters especially in the frequency range $\omega=1$ to 100MHz and temperature range 77 to 400°K. The effect of surface states or defects then can be explored in various gaseous ambients. Finally, a theoretical analysis of the present and future data based on of various models, such as long range fluctuation of the potentials and the surface states contributing to the conduction band electrons, will provide more physical understanding of the surface effects in SI-GaAs.

VI. REFERENCES

1. J.F. Wager and J.A. Van Vechten, Phys. Rev. B 35, 2330(1987).
2. M. Skowronski, J. Lagowski and H.C. Gatos, Phys. Rev. B 32, 4264(1985).
3. P. Dzwig, V. Crum and A. Chantre, J. Phys. C: Solid State Phys., 15, L1177(1982).
4. For example, see Ref. 1 for a good review of most recent works on this subject.
5. A. Mitonneau, G.M. Martin, and A. Mircea, Electron Lett. 13, 667(1977); Inst. Phys. Conf. Ser. No. 33a, 73(1977).
6. D. Pons, H. Mircea, A. Mitonneau, and G.M. Martin, Inst. Phys. Conf. Ser. No. 46, 352(1979).
7. G.M. Martin, E. Esteve, P. Langlade, and S. Makram-Ebeid, J. Appl. Phys. 56, 2655(1984); H.J. Bardelben, D. Steivenard, and J.C. Bourgoin (preprint).
8. R.J. Wagoner, J.J. Krebs, G.H. Strauss, and A.M. White, Solid State Commu. 36, 15(1980).
9. D. Pons and J.C. Bourgoin, Phys. Rev. Lett. 47, 1293(1980); D. Pons, Physica 116B, 388(1983); D. Pons and J.C. Bourgoin, J. Phys. C: Solid State Phys. 18, 3839(1985).
10. J.A. Van Vechten, J. Electrochem. Soc. 122, 423(1975).
11. Z. Yuenxi, Z. Jicheung, L. Yian, W. Kyangyu, H. Binghua, L. Bingfang, L. Cuncai, L. Liansheng, S. Jiuan, and S. Chi, Proc.

- Thirteenth Int. Conf. on Defects in Semiconductors, Coronado, CA, p1021(1981).
12. E.R. Waber, Proc. Thirteenth Int. Conf. in Defects in Semiconductors, p77(1981).
 13. J.J. Mares, J. Kristofik, V. Smid, and J. Zeman, Sol. State Commu. 60, 275(1986); J. Kristofik, J.J. Mares, V. Smid, and J. Zeman, Phys. Stat. Sol. (a) 88, K187(1985).
 14. B. Pistoulet, P. Girad, and G. Hamamdjian, J. Appl. Phys. 56, 2268(1984); J. Appl. Phys. 56 2275(1984); B. Pistoulet, F.M. Roche, and S. Abdalla, Phys. Rev. B 59, 5987(1984).
 15. S. Abdalla and B. Pistoulet, J. Appl. Phys. 58 2646(1985); B. Pistoulet and G. Hamamdjian, Phys. Rev. B 35, 6305(1987).
 16. D.C. Look, J. Phys. Chem. Solids 36, 1311(1975).
 17. D.C. Look, Phys. Rev. B 25, 2920(1982); D.C. Look, Semiconductors and Semimetals, 19, 127 (1983), Editors R.K. Williardson and A.C. Beer, Academic Press, New York.
 18. Y.H. Lo, Z.H. Zhu, C.L. Pan, S.Y. Wang, and S. Wang, Appl. Phys. Lett. 50, 1125(1987).
 19. Y.K. Yeo, R.L. Hengehold, and D.W. Elsaesser, J. Appl. Phys. 61, 5070(1987).
 20. W.E. Spicer, I. Lindau, P. Skeath, C.Y. Su, and P. Chye, Phys. Rev. Lett. 44, 420(1980).
 21. Advanced GaAs Growth, Interim Technical Report Final, No. 10 for Contract No. F33615-83-C-5072, Sept. 1986.
 22. Advanced GaAs Growth, Interim Report No. 11 for Contract No.

F33615-83-C-5134, Oct. 1986.

23. D.C. Look and J.W. Farmer, J. Phys. E: Sci. Instrum. 14,
472(1981).

Table I. Experimental data for SI-GaAs sample TI31-41-65

Ambients	T °K	ρ ($\Omega \cdot \text{cm}$)	σ ($\Omega \cdot \text{cm}$) ⁻¹	μ (cm ² /V-s)	n (cm ⁻³)
N ₂ gas	253.90	245.6 x10 ⁸	0.004x10 ⁻⁸	- x10 ³	0.0568x10 ⁶
	274.88	7.457	0.13	5.585	1.501
	295.39	0.7428	1.35	5.398	15.59
	297.61	0.5373	1.86	5.372	21.65
	313.48	0.08461	11.82	4.969	148.7
	333.33	0.01726	57.94	4.644	779.8
	350.87	0.004170	239.81	4.389	3416.0
	370.37	0.001103	906.62	4.143	13670.0
Vacuum	253.90	16.49	0.061	-	1.928
	274.73	2.235	0.45	5.233	5.344
	274.88	2.100	0.48	-	6.010
	289.86	0.4618	2.17	5.246	25.80
	295.39	0.2657	3.76	5.179	45.43
	307.69	0.07508	13.32	4.942	168.5
	325.20	0.01645	60.79	4.660	815.2
	338.98	0.003717	296.03	4.353	3863.0
	353.98	0.001008	992.06	4.141	14970.0
He gas	274.88	10.71	0.093	-	1.066
	289.86	2.050	0.49	-	4.698
	295.39	1.095	0.913	5.498	10.39
	303.03	.5494	1.82	5.242	21.70
	320.00	.09080	11.01	4.939	139.4
	338.98	.01882	53.13	4.663	712.2
	357.14	.004574	218.63	4.399	3107.0
	373.83	.001228	814.33	4.175	12190.0
Air	297.87	1.838	0.54	5.346	6.362
	310.38	0.5108	1.96	5.176	23.64
	330.89	0.07803	12.82	4.915	163.0
	351.39	0.01494	66.93	4.626	904.4
	371.89	0.00344	290.70	4.359	4168.0
	392.40	0.0009765	1024.07	4.102	15600.0

Table II. Experimental data for SI-GaAs sample R158-6-65

Ambients	T °K	ρ ($\Omega \cdot \text{cm}$)	σ ($\Omega \cdot \text{cm}$) ⁻¹	μ ($\text{cm}^2/\text{V}\cdot\text{s}$)	n (cm^{-3})
N ₂ gas	274.88	37.430x10 ⁸	0.27x10 ⁻⁸	- x10 ³	0.4127x10 ⁶
	285.14	8.352	0.12	5.793	1.292
	295.39	2.626	0.38	5.792	4.109
	296.43	2.790	0.36	5.635	3.975
	310.38	0.6807	1.47	5.393	17.03
	330.89	0.1136	8.80	4.983	110.4
	351.39	0.02330	42.92	4.649	577.0
	371.89	0.00549	182.15	4.401	2583.0
	392.40	0.00146	884.93	4.148	10330.0
Vacuum	253.90	298.3	0.003	-	0.07138
	274.88	23.69	0.042	-	0.8475
	295.39	2.194	0.46	-	5.436
	296.74	2.272	0.44	5.552	4.954
	310.38	0.6814	1.47	5.411	16.95
	330.89	0.1115	8.97	5.037	111.3
	351.39	0.0253	39.53	4.729	586.5
	371.89	0.005519	181.19	4.445	2548.0
	392.40	0.001532	652.74	4.184	9752.0
He gas	253.90	523.8	0.002	-	0.02762
	274.88	23.94	0.042	-	0.6444
	291.97	2.798	0.36	-	3.989
	295.39	1.936	0.52	5.691	5.672
	305.34	0.6861	1.46	5.430	16.78
	322.58	0.1158	8.64	5.089	106.1
	344.82	0.02412	41.46	4.734	547.3
	362.32	0.005968	167.56	4.441	2358.0
	380.95	0.001683	594.18	4.189	8862.0
Air	296.64	2.664	0.38	5.662	4.14
	310.38	0.6988	1.43	5.459	16.38
	330.89	0.1184	8.45	5.079	103.9
	351.39	0.02433	41.10	4.772	638.3
	371.89	0.005812	172.06	4.483	2399.0
	392.40	0.001498	667.56	4.201	9.927.0

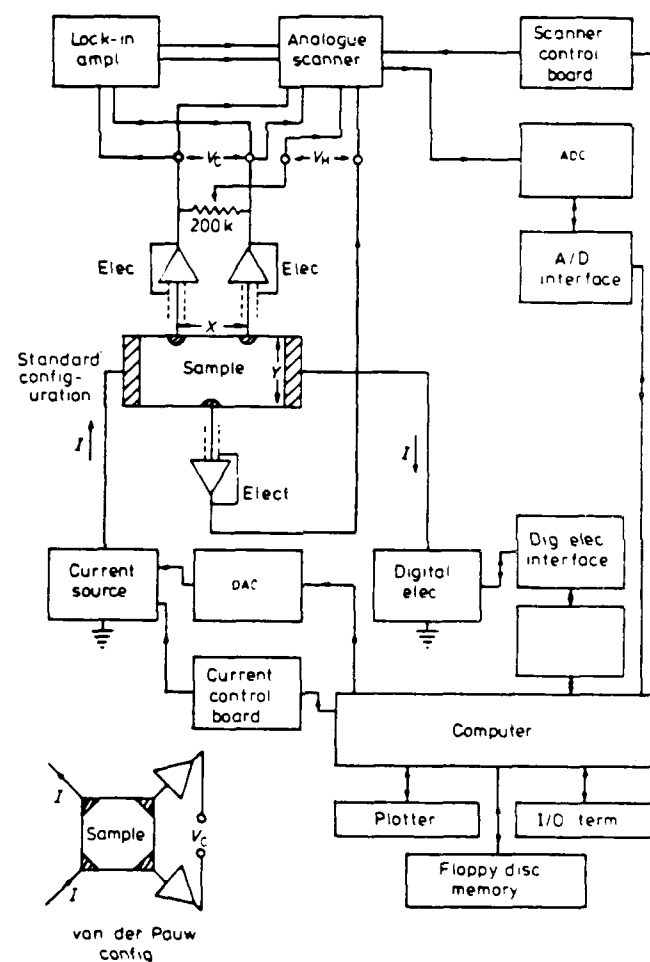


Figure 1

Schematic diagram of the automatic, high resistivity Hall-effect apparatus. A standard van der Pauw configuration is also shown in the diagram. See Ref. 23 for details.

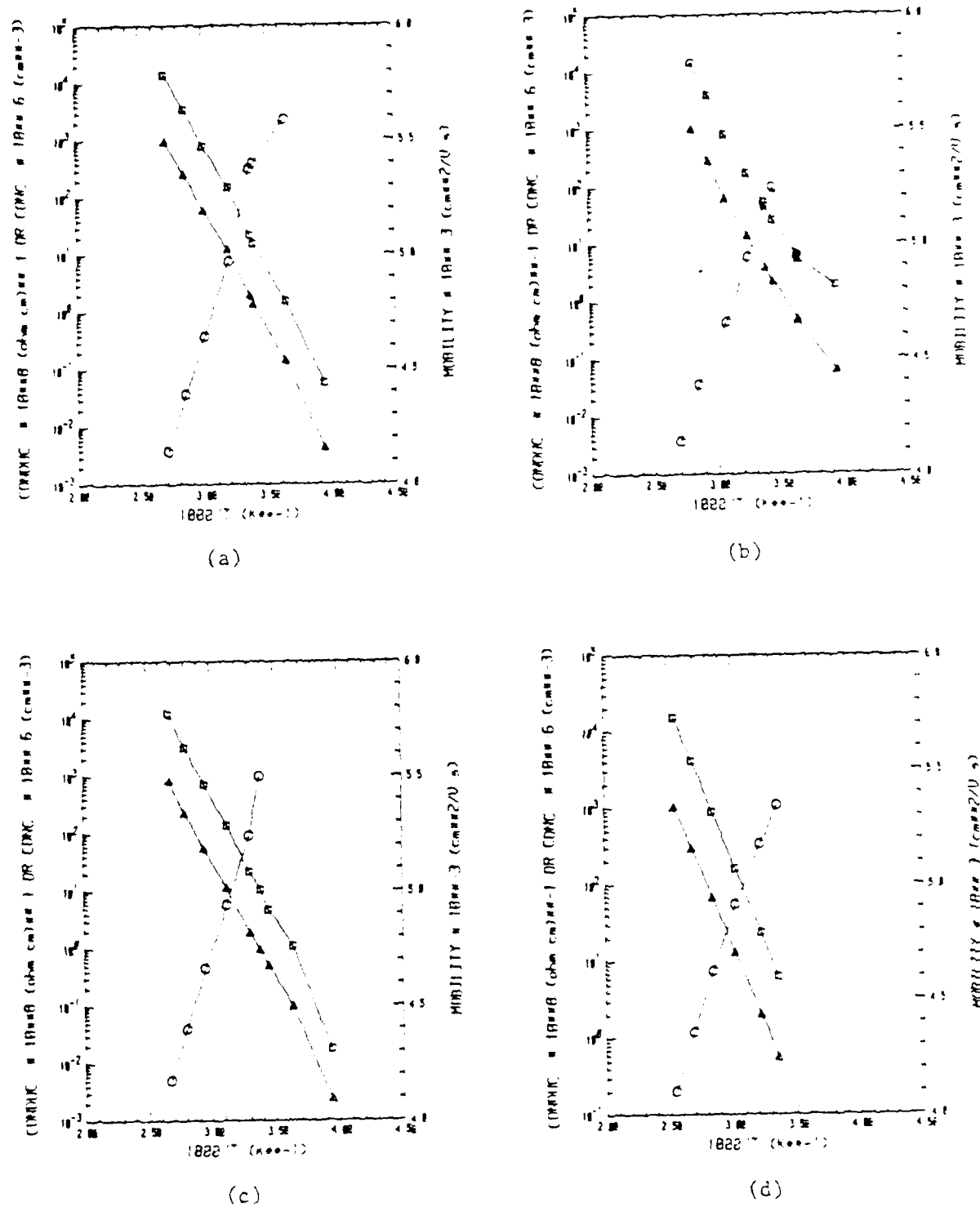


Figure 2

The plots of electrical conductivity (σ) carrier concentration (n) and Hall mobility (μ) for Si-GaAs (sample T131-41-65) in (a) N_2 gas, (b) vacuum, (c) He gas and (d) air. The symbols on the plots are: \circ -conductivity; Δ -concentration; and \square - mobility.

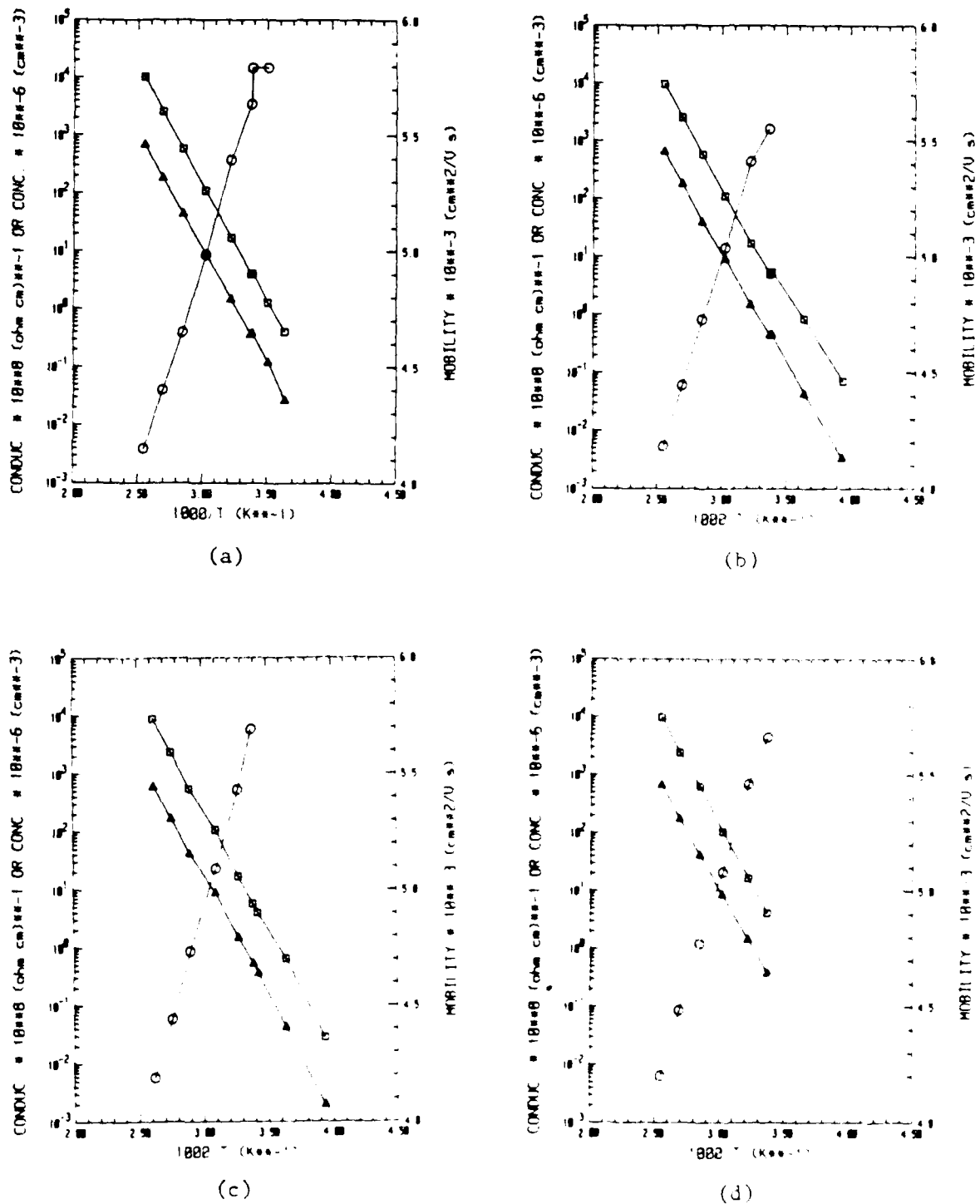


Figure 3

The plots of electrical conductivity (σ), carrier concentration (n) and Hall mobility (μ) for SI-GaAs (sample R158-6-65) in (a) N_2 gas, (b) vacuum, (c) He gas and (d) air. The symbols on the plots are: Δ -conductivity; \square -concentration; \circ -mobility.

NO-A191 284

UNITED STATES AIR FORCE SUMMER FACULTY RESEARCH PROGRAM
(1987) PROGRAM TE. (U) UNIVERSAL ENERGY SYSTEMS INC
DAYTON OH R C DARRAH ET AL. DEC 87 AFOSR-TR-88-0213

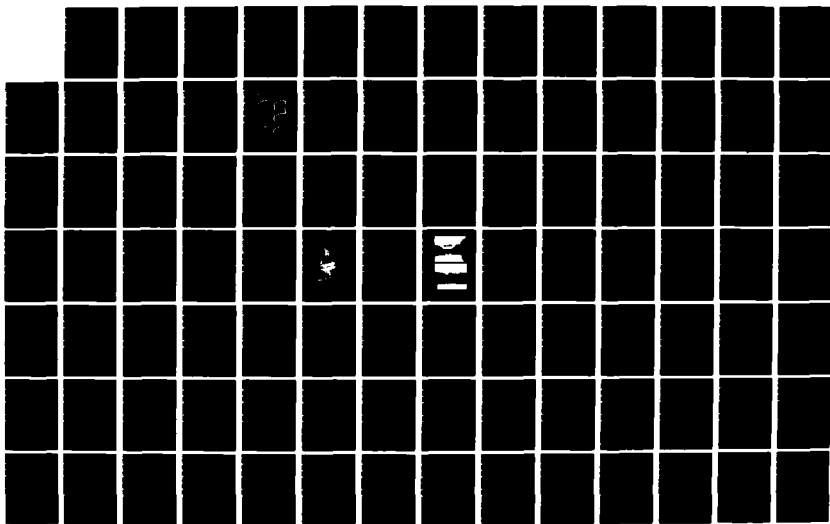
3/11

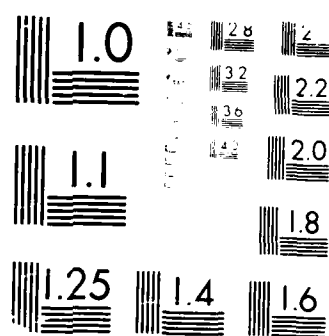
UNCLASSIFIED

F49620-85-C-0013

F/G 5/1

NL





MICROCOPY RESOLUTION TEST CHART
NBS 1963-A

1987 USAF-UES SUMMER FACULTY RESEARCH PROGRAM/
GRADUATE STUDENT SUMMER SUPPORT PROGRAM

Sponsored by the
AIR FORCE OFFICE OF SCIENTIFIC RESEARCH

Conducted by the
Universal Energy Systems, Inc.

FINAL REPORT

The Surface Primitive Method of Feature Based Computer Aided
Design for Manufacture

Prepared by:	Kenneth R. Halliday, Ph.D.
Academic Rank:	Associate Professor
Department and	Mechanical Engineering
University:	Ohio University, Athens, Ohio
Research Location:	AFWAL/MLTC, Wright-Patterson AFB, Ohio.
USAF Researcher:	Major Steven R. LeClair, Ph.D.
Date:	August 28, 1987
Contract No:	F49620-85-C-0013

The Surface Primitive Method
of Feature Based Computer Aided
Design for Manufacture

by

Kenneth R. Halliday, Ph.D.

Abstract

A new method is presented in this paper for structuring the design features which can be used in knowledge based expert systems for the Computer Aided Design, CAD, of mechanical components. This technique, called the surface primitive method, uses information about the properties of the surfaces of a feature in order to explicitly embed manufacturing knowledge into the definition of the feature.

The ideas which are fundamental to the surface primitive method are introduced in this paper. Furthermore, an example of using the method to construct a common CAD feature, a cylindrical through hole, is presented, and the methods used to extract the information about manufacturing from the model are illustrated. In particular, a demonstration program is presented which evaluates the production time and the production cost of the feature from the basic feature definition. Future extensions for this work are discussed.

Acknowledgements

I would like to take this opportunity to thank the Air Force Systems Command and the Air Force Office of Scientific Research for providing the financial support which has allowed me to initiate this research. I am particularly grateful to the people of the Materials Laboratory, Manufacturing Technology Division who worked with me this summer. Major Steven LeClair, of the CIM branch, provided the main motivation for this work. Lts. C. Wright and C. Madden contributed their considerable expertise in formulating the nature of the solution. Finally I would like to thank UES, Inc. for the administrative help which they provided throughout the summer.

1. Introduction:

Traditional Computer Aided Design, CAD, systems are structured to assist the designer in the process of graphical presentation of a design configuration. Virtually all commercial CAD systems allow the designer to create either a wire-frame or a "true solids" model of the part which is being designed and then allow manipulation of this model in order to display the results of graphical operations such as hidden line suppression, rotation and shading. More sophisticated CAD systems perform additional design operations such as the preparation of parts lists, the automatic generation of shop drawings or the evaluation of inertial properties. Additional functionality can be found in CAD/CAM software which further extends the capability of these systems to allow, for example, the evaluation of stresses and the preparation of media for the CNC machining of the part.

In recent years there has been a growing interest in extending the capabilities of CAD systems to incorporate the techniques of artificial intelligence, AI, which would allow these programs to evaluate crucial aspects of the design as it evolves. In particular, numerous investigators have been interested in the possibility of using intelligent CAD systems to evaluate the producibility of a proposed design. Halliday [1.] discusses a possible architecture for this type of system.

In addition, a number of investigators have been interested in developing "design with features" based computer programs [2-7.] This software has been created in order to provide a simple yet meaningful method of representing the geometry of mechanical components in CAD systems. When coupled with the basic concepts of group technology feature based design systems provide an organized way of dealing with manufacturing knowledge.

For the most part, "design with features" programs properly represent the geometry of the design facets, however, the manufacturing and service aspects of the design feature must either be defined a priori for each feature, on an ad hoc basis, or they must be inferred within the context of the specific

computer program in which these features are used. Both of these approaches impose severe limitations on the usefulness of feature based modeling.

The ad hoc method of describing the manufacturability of a design, for example, requires that the designer deal with a number of nearly identical design features in order to select that one which best satisfies the design criteria. A simple through hole becomes a much more complex entity if the sequence of manufacturing operations is attached to the definition of the hole as a basic attribute. In fact, the feature "cylindrical through hole" might become a variety of holes - drilled hole, reamed hole, bored hole, or ground hole, to name a few - in order to properly model the characteristics of the manufactured design feature. If the designer is to be responsible for choosing a feature from among this variety then the purpose of the expert system has been severely compromised. On the other hand, the bewildering variety of design characteristics which are possible for a moderately complex feature such as a counter-bored hole, or an internal spline would make it prohibitively difficult to automate the process of selecting design features.

Most investigators have circumvented the difficulties posed by this complexity by constructing expert designers which either neglect the manufacturing issue completely [8,9], or which only operate in a specific manufacturing domain. Libardi et al., for example, have created an expert system for the design of parts which are to be extruded [2.] Dixon and co-workers have also created a separate, completely different, expert system for the design and analysis of castings [3.]

While these programs are interesting in and of themselves, they have side stepped the main issue which must be solved in constructing a generally applicable knowledge based design system. This issue is structuring both the data and the knowledge available to the expert system in such a way that it allows the human designer to investigate the implications of using a variety of manufacturing methods and a variety of materials so that he or she might select the design solution which best satisfies some performance criteria.

The greatest economy of resources; manpower, money and time, is realized by accepting the broadest possible definition of manufacturing in constructing the expert knowledge base. Suh [10] recommends that the concept of manufacturing be extended to include every operation performed

on a component from materials extraction, through design and production up to final disposal of the discarded machine. At the very least, the expert designer should have knowledge about a variety of related topics including: production techniques, methods of parts handling, assembly, and quality control procedures. Furthermore, it should be able to treat the issues of maintainability and repair. Each of these topics forms an important part of the general concept of "Total Life Cycle Costing."

It is the purpose of this current research project to explore the possibility of developing an expert system which is capable of making decisions about aspects of the proposed design solution using knowledge which crosses the boundaries of the various manufacturing technologies.

II. Objectives of the Research Effort:

The summer research effort started with two major objectives. The first goal of this research effort was to formulate the correspondence between the properties of design features and those of the surface primitives of which they are composed. The second goal was to construct a small scale design system which could be used to demonstrate the efficacy of this approach to provide the CAD process with the rudiments of manufacturing knowledge.

A third major research theme emerged from this preliminary work. This is the need to structure the vast amount of "design for manufacture knowledge" into an appropriate, workable knowledge base which will support future CIM operations. These three research goals are discussed in more detail in the following sections.

III. The Surface Primitive Method:

The purpose of the surface primitive method of "feature based" computer aided design is to provide an explicit method for incorporating knowledge about manufacturing into the fundamental definition of the design features. The first issue which must be treated regards the nature of this manufacturing information. In particular the question arises as to exactly which surface attributes must be included in the basic definition of a feature

in order to provide sufficient manufacturing information to support a knowledge based expert system which acts as an enhancement of the normal CAD operations. The purpose of this research project was to find a preliminary answer to this question.

The following research method is developed in this project: First, a common design feature, the through hole, is studied. This feature can be constructed from three occurrences of two different surface primitives, the surface perforation and the internal bore. The specific attributes of each of these surfaces are defined in the first section of this report. The logical process of combining the surfaces into the "through hole" design feature is then demonstrated in the second section of the report. Once the operational definition of a hole has been established some aspects of performance relevant to the use of this feature in a CAD program are developed. In particular, an example of a proposed CAD user interface is demonstrated. The methods of inferring the production processes, costs and times are also shown. Further, the relationships between the geometry of the design and the properties of the design feature are explored. Finally, the interrelationships between the feature based design algorithms and the supporting manufacturing and design data bases are discussed.

IV. Definition of the Primitive Surfaces:

In order to illustrate the use of the surface primitive method, a single design feature, the cylindrical through hole, will be considered. This is one of the most common features in mechanical components. The through hole is composed of three occurrences of two of the basic surface primitives. These are shown in Figure 1.

The surface perforation provides a curve of connection between the surface of origin and the matching primitive surface. In essence, this primitive is used to connect features to parts which have already been created in the CAD system.

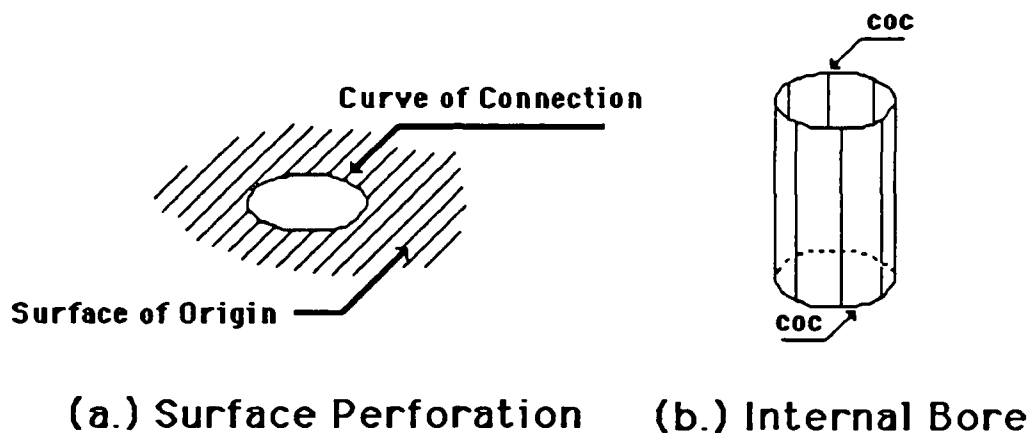


Figure 1. Two Basic Surface Primitives

The bore, shown in Figure 1b., is a cylindrical surface which is bounded by material around the outside, and which can be attached to other surfaces by means of the two circular "curves of connection" at the top and the bottom of the surface. In addition to these qualitative descriptions, there is the need to create precise quantitative definitions for these primitives in order to support the variety of logical, algorithmic and graphical operations which the expert design system is intended to perform. This is a two step process.

First, a geometric model can be formulated. The parameters required to describe the surface perforation are shown in Figure 2:

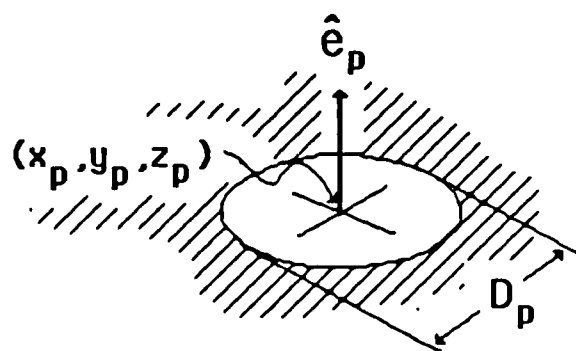


Figure 2. The Parameters Which Define The Perforation Surface Primitive

As seen in this figure, the geometry of the perforation is specified by three parameters: the location of the origin, the diameter of the curve of connection and the outward normal vector. While the geometry of this primitive is referenced to the global, or "design space" coordinate system, it is also bound to the definition of the surface of origin. In particular, the origin of the perforation must lie in this surface and the outward normal vector of the primitive must be the same as that of the surface which is perforated.

The geometric and logical descriptions of a number of primitive surfaces can be established in a similar manner. Those attributes which are required in order to define a general surface can then be abstracted from these descriptions. This has been done in a preliminary manner for a group of over twenty possible primitives. The results of this survey are summarized in Table 1. Those attributes which are specifically required to define the surface perforation are highlighted in this table.

It is fairly straight forward to define the geometric and logical parameters of the bore and then use these characteristics to create a table of attributes for the bore similar to Table 1. Since the bore is a more complex surface than the perforation additional information is required to define it. For example, if the bore extends through a part then it has a destination surface as well as an origin, and this further implies that the bore has a length. The bore is an actual surface and, therefore, possesses surface texture which must be described. Finally, a bore may be used to locate features in the design of a component in which case the bore would have reference status. This must also be indicated in the attribute based description of the primitive. Those additional attributes which are required to define a bore are displayed in italics in Table 1.

In addition to those attributes required to define the perforation and the bore, Table 1 contains a number of other characteristics which are needed in order to define additional surface primitives. Exactly what constitutes a complete list of surface attributes, suitable for general CAD applications, has not been determined yet. It is expected that the final list of attributes will be based upon both the operations that will be carried out with the features models as well as the geometry of the features themselves. However, this is still an active area of research.

1. IDENTIFIER:	Name or Number
2. POSITION OF ORIGIN:	x_0, y_0, z_0
3. OUTWARD NORMAL VECTOR:	e_x, e_y, e_z
4. SURFACE OF ORIGIN:	Identifier
5. DESTINATION SURFACE :	Identifier
6. LENGTH:	L_s
7. TOP DIAMETER:	D_{st}
8. BOTTOM DIAMETER:	D_{sb}
9. SURFACE FINISH:	R_{a_s}
10. SURFACE LAY:	ANSI Descriptor
11. REFERENCE STATUS:	T or Nil
12. CONNECTS TO:	Identifier List
13. MATES WITH:	Identifier
14. FIT TYPE:	ANSI Descriptor
15. WRAP ORIGIN VECTOR:	W_x, W_y, W_z
16. WRAP ANGLE:	ϕ_w
17. THREAD SYSTEM:	UNC or UNF
18. THREAD PITCH:	P_s

Table 1. The Attribute List for a Surface Perforation

V. Construction of A Design Feature

Having defined a restricted set of surface primitives, the next step is to combine them to form one or more design features. As shown in Figure 3, instances of the perforation and the bore can be combined into the design feature of the through hole.

The definition of the feature "through hole" involves five separate surfaces. First, there are the two surfaces of the component which is being designed. The first surface the designer selects determines the origin of the hole feature. The expert design system will interpret this origin as the starting point for the actual hole generating manufacturing operation. That is, the program will check the parameters which describe the component's current design in order to assess whether there are proper provisions for work holding and tool clearance. It is also necessary that the expert system insure

that the physical characteristics of the origin surface are able to support the feature which is to be manufactured.

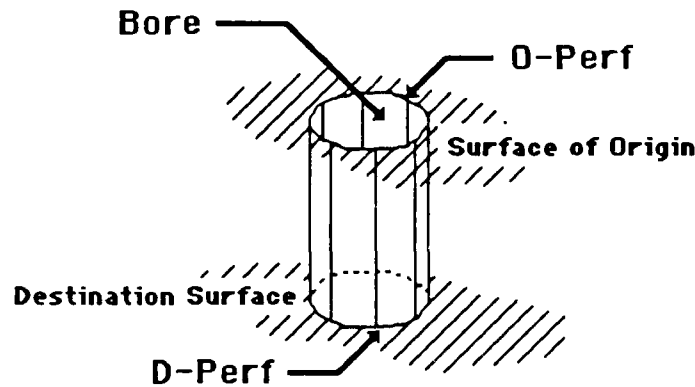


Figure 3. Combining Surface Primitives into a Through Hole

The designer will also need to specify the destination surface for the feature. Depending upon the choice of material for the part as well as the process which has been selected in order to manufacture the feature the destination surface may also require special production operations such as deburring. Again, the expert designer must alert the human designer to these possibilities, and at the same time the expert must keep track of the implications which might apply to the design of other parts of the system.

In addition to the surfaces of the component in which it is to be placed, the design feature is itself composed of surfaces. The through hole shown in Figure 3, for example, is composed of the three surface elements designated as O-Perf, Bore, and D-Perf. It is a basic design premise of the surface primitive method that the nature of the design feature is determined through inheritance from the surface elements from which it has been constructed.

Table 2 illustrates the manner in which the properties of the individual surface primitives are combined to form the properties of the complete design feature, in this case the through hole shown in Figure 3.

Identifier:	<u>O-Perf</u>	<u>Bore</u>	<u>D-Perf</u>
Position of Origin:	USER	$\{xyz\}_B = \{xyz\}_O$	$\{xyz\}_D = \{xyz\}_O + L_b e_D$
Outward Normal Vector:	Expert	$e_B = e_O$	$e_D = -e_B$
Surface of Origin:	USER	Expert	NA
Destination Surface:	NA	Expert	USER
Length:	NA	USER/Expert	NA
Top Diameter:	USER	$D_B = D_O$	$D_D = D_O$
Surface Finish:	NA	USER	NA
Surface Lay:	NA	USER/Expert	NA
Reference Status:	NA	USER	NA
Connects To:	Bore	O-Perf, D-Perf	Bore

Table 2. Combining The Attributes of Surface Primitives to Create a Design Feature.

As shown in this table, there are three methods of specifying the combination of attributes which are used to define the "through hole" design feature. First, some of the attributes will be combined by means of simple algorithms derived from the geometrical descriptions of the feature and surface primitives. For example, the global coordinates of the points of origin of the bore and the perforation of the starting surface must be equal since these points have to coincide. The other two possibilities are that the user specifies the type and magnitude of the combination, or alternatively that the expert designer infers the nature of the combination from knowledge about either the feature or the perceived intent of the human designer.

Considering the data shown in Table 2, if the user specifies the surface of origin for the hole then the expert program should infer that the normal vector for the hole coincides with that of the surface since a through hole should be placed perpendicular to it's starting surface to eliminate expensive jigs and other production tooling. Similarly, if the user selects the destination surface then the expert program should be able to calculate the length of the feature. It is very important that the program enforce the basic rules of compatibility to prevent the development of erroneous or ambiguous

situations from the redundant specification of component dimensions. This is a common error encountered in "dumb" CAD applications.

An attribute combination list, such as that displayed in Table 2, will have to be constructed for each feature which is to be included in the CAD system under development. These lists will then suggest the nature of the user interface which should be implemented in that system. For example, to place a hole into a design model which is being constructed the user would select the generic feature "Through Hole" from some type of menu. He or she would first be instructed to select the starting surface, then the point of origin in that surface, next either the length of the hole, or, alternatively, the destination surface and finally the diameter of the hole. The CAD system could be designed to provide both graphical feed-back and prompting between each of these operations.

While the user was constructing this hole the program would reconcile any ambiguities which might be encountered by either investigating some rule of thumb heuristics included in the design knowledge base or by querying the user about the specific intent of the design. As an example of a design rule of thumb it is generally accepted that the center of a hole which is to be drilled into a plate like component should not be any closer than two and a half diameters from the edge.

The allowable surface roughness of the bore of the hole is a critical design parameter. The expert system should be configured to estimate this value independently by polling a number of different sources of information in order to be certain that the roughness is chosen properly. The program might, for example, ask the user for the value of the roughness directly. By also questioning the user about the tolerances of any linked dimensions, the intended use of the feature, expected service conditions and the expected production history of the component the program should be able to either verify the users choice, or suggest a more appropriate alternative.

As shown in the next section, the value of surface roughness when combined with other information about the configuration of the feature is sufficient to estimate the manufacturing methods required to construct the feature. Knowing the manufacturing technique allows the expert system to estimate the "Total Life Cycle Cost" of including the feature in the design. The

expert should also be able to check the other features incorporated into the design and resolve any conflicts which become apparent at this point in the design evolution.

VI. Estimating the Manufacturing Sequence from The Feature Definition:

The major impetus for the development of surface primitive based design features is the need to provide generic information about manufacturing in the basic structure of the feature itself. It is a primary axiom of the surface primitive method that:

" A component is material bounded by manufactured surfaces "

It is this emphasis on the nature of the surfaces of the component which distinguishes this approach from other "design with features" CAD systems. A second axiom of the surface primitive method is:

" The nature of the surfaces of a feature and the geometric details of the feature determine how the feature will be manufactured."

Too often, the manufacturability of a component is determined by the decisions made by the designer in an incorrect, or at least an inappropriate, context. That is, the designer often locks certain manufacturing difficulties into the design of a part because of decisions about the geometry used to represent that part in the CAD system rather than the true operational, or surface, geometry of the part which describes the configuration of the component at various stages in the actual sequence of operations used to manufacture the part.

For example, if we consider the through hole as an exemplar of a design feature, then we must reach the conclusion that if the feature is to have any meaning in an operational sense it is necessary to select each given instance of the feature "through hole" which occurs in a design from a variety of "through hole" features. There are a number of methods which could be used in order to construct such a collection of features, however, the most direct would be to select each of these features on the basis of the sequence of operations required to manufacture them.

A partial listing of these variants is shown in Table 3. As shown in this table the design situation is complicated by two facts. First, there are a number of basic technologies which might be used in order to construct the basic component itself. For example, the component might be cast, or machined from stock or perhaps bent from sheet metal. The ultimate choice of manufacturing methods for the component is determined by the gross characteristics of the component as well as the characteristics of the features associated with the part. The ultimate choice of any of these primary production methods limits the manufacturing opportunities which remain available for the minor features associated with the part. The hole, for example, cannot be cast into a part which is machined from stock.

Through Hole Cast In Place - Suspended Cores
Through Hole Cast In Place - Through Core
Through Hole, Machined - Twist Drill
Through Hole, Machined - Drilled then Reamed
Through Hole, Machined - Drilled then Ball Sized
Through Hole, Punched

Table 3. Variations of the "Through Hole" CAD Feature

A second complication is the fact that manufacturing a given feature might require a variety of operations. Precision holes, for example, require an operation to initiate them and another operation to refine their inner surface. These processes may not be carried out in direct sequence. There may be costly intermediate steps required which contribute to the value added to the part and therefore, must be accounted for.

An example of a component whose cost is increased dramatically by interstage handling is shown in Figure 4. Here, if the bores are produced in numerical order, then the disk shaped workpiece must be reversed in the tooling in between the operations which create bores 2 and 3. This handling of the workpiece will either require a slow operation to reestablish the concentricity of the spin axes for each face, or a relatively expensive jiggling

and therefore, must be accounted for.

An example of a component whose cost is increased dramatically by interstage handling is shown in Figure 4. Here, if the bores are produced in numerical order, then the disk shaped workpiece must be reversed in the tooling in between the operations which create bores 2 and 3. This handling of the workpiece will either require a slow operation to reestablish the concentricity of the spin axes for each face, or a relatively expensive jiggling procedure. In addition, there are potential quality control problems presented by the two machined faces of the work piece.

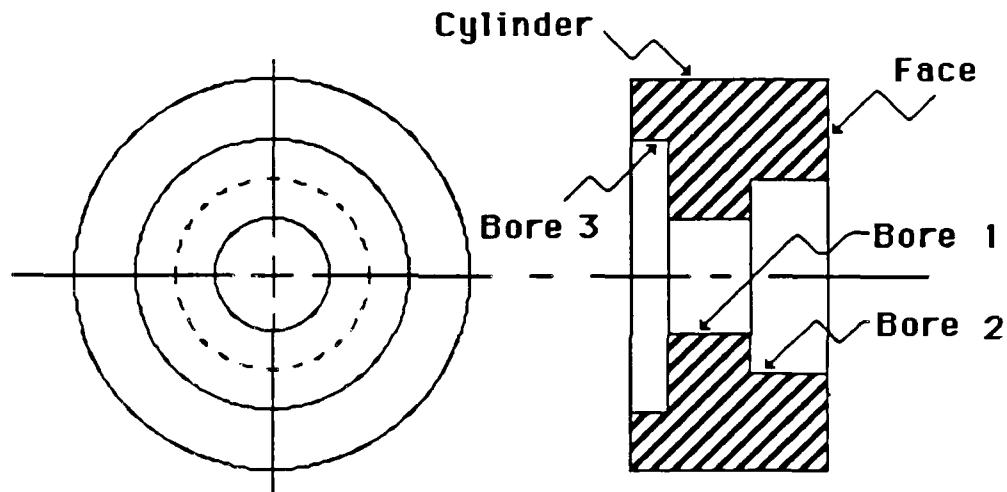


Figure 4. A Component With "Value Added" By Intermediate Handling

The CAD tools, developed in this project must be cognizant of the manufacturing, work handling and quality control aspects of the design. One possible technique for utilizing the manufacturing knowledge embedded in the surface primitive definition of a design feature is to develop an expert system which can extract this knowledge during the evolution of the design. A simple demonstration of this type of system was developed during this research period. The source code is attached to this document as Appendix A. This demonstration used a relatively simple IF - THEN - ELSE rule structure in order to determine the primary manufacturing process, the surface refining

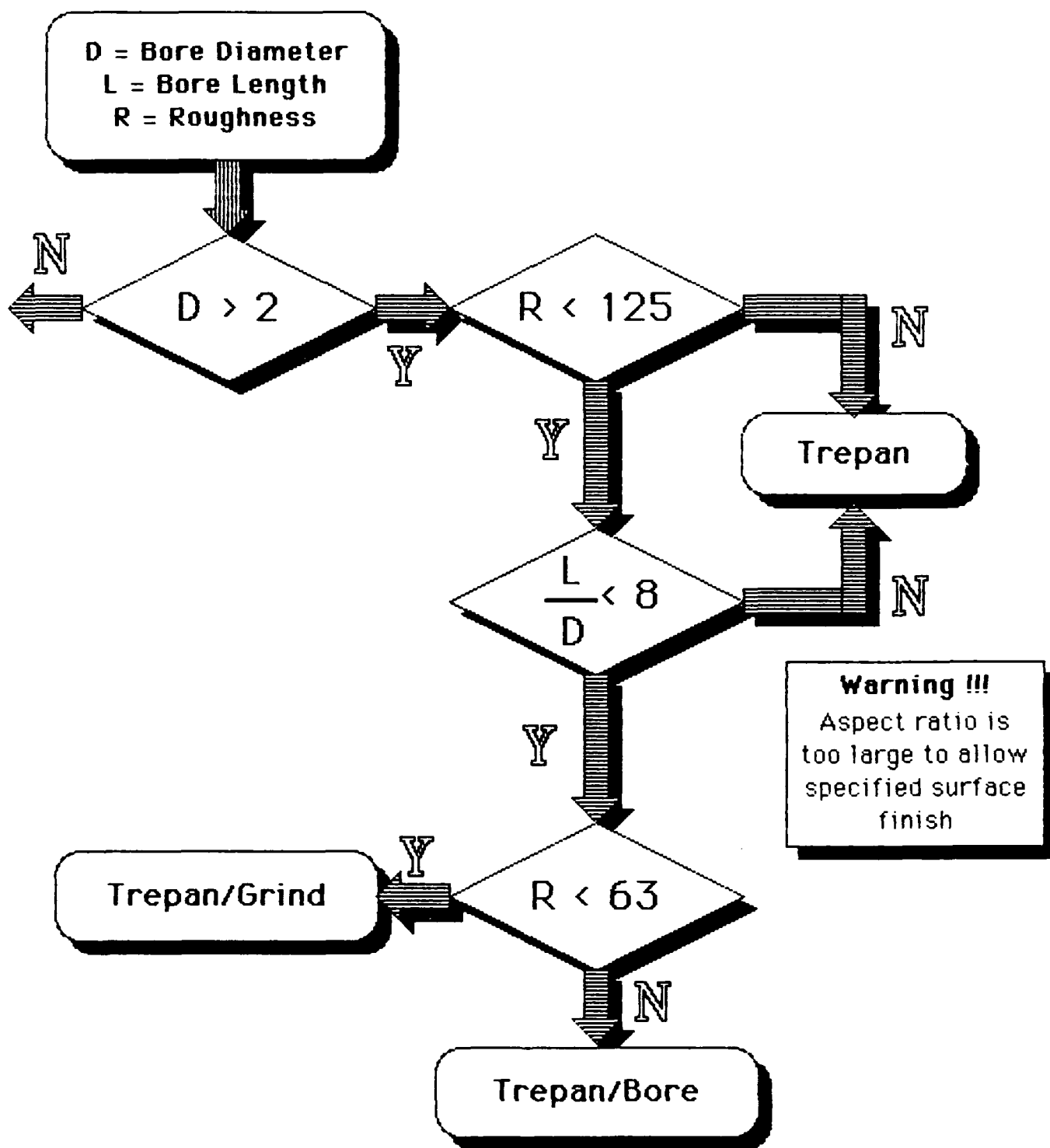


Figure 5. Hole Generation Processes

process and the type of production conditions required in order to produce a feature, in this case a through hole, in a specified part, a prismatic slab.

The structure of a portion of the rule base is shown in Figure 5. As shown in the figure the program was able to determine the production sequence from the basic properties of the feature itself. In addition to the production sequence, the program was also able to compute the production time and the production cost required to place this feature into the current configuration of a specific part, for a range of materials. This programming work not only demonstrates the potential power of the Surface Primitive formulation but it also provided the research team with a great deal of knowledge about how to structure the associated design data bases which must also be developed in order to support this work

VII. Recommendations:

This work represents the beginning of a promising line of research into techniques of representing and manipulating knowledge to support the computer evaluation of design. The preliminary assessment demonstrates that the Surface Primitive approach is potentially very useful in both representing knowledge from the variety of solution domains required by a designer, and in providing the linkage to that knowledge which will allow CAD based expert systems to infer the intent of the designer. Additional work is required in three areas.

First, the knowledge representation of design features has to be made more efficient in order to prevent the inordinate memory size requirements which plague other CAD systems. One of the great virtues of the surface primitive technique is that it provides a generic way of creating these features as they are required. Second, the knowledge base embedded in the definition of the feature must be completely defined. In part this is a matter of anticipating the CIM applications for this type of representation, however there is also some fundamental theoretical work which will have to be done in this area. Finally, the demonstration CAD system should be expanded both in depth and in breadth. It should handle a wider range of features in a more robust fashion.

The ultimate goal of this proposed research is to provide artificial intelligence tools which will support the development of computer generated designs. To this end one of the critical issues which will have to be addressed is the treatment of design alternatives as they cross technological boundaries. A major challenge is to create CAD tools which can move from castings, to forgings to machined features while properly assessing the features encountered in each technological domain so that the program can properly instruct the designer on the truly optimal approach to the design.

VIII. References:

- [1.] Halliday, K.R., "Computer Aided Design for Manufacture," TRANS. IASTED Conference on CAD and Applications, Montreal, pp 6-10, 1985.
- [2.] Libardi, E.C., Dixon, J.R. and Simmons, M.K., "Designing with Features: Design and Analysis of Extrusions as an Example," ASME Paper # 86-DE-4, National Design Engineering Conference, Chicago, March 1986.
- [3.] Luby, S.C., Dixon, J.R., and Simmons, M.K., "Designing With Features: Creating and Using a Features Data Base for Evaluation of Manufacturability of Castings," Proceedings ASME Computers in Engineering Conference, Chicago, July 1986.
- [4.] Vaghul, M., Dixon, J.R., Zinsmeister, G.E., and Simmons, M.K., "Expert Systems in a CAD Environment: Injection Molding Part Design as an Example," Proceedings ASME Computers in Mechanical Engineering Conference, Boston, August, 1985.
- [5.] Hummel, K.E., and Brooks, S.L., "Symbolic Representation of Manufacturing Features for an Automated Process Planning System," Knowledge-Based Expert Systems for Manufacturing, ASME, PED-Vol. 24, pp. 233-243, 1986.
- [6.] Hayes, C. and Wright, P., "Automated Planning in the Machining Domain," Knowledge-Based Expert Systems for Manufacturing, ASME, PED-Vol. 24, pp. 221-232, 1986.
- [7.] Hardwick, M. and Spooner, D.L., "Comparison of Some Data Models for Engineering Objects," IEEE Computer Graphics and Applications, pp. 56-66, March 1987.
- [8.] Brown, D.C., and Chandrasekaran, B., "Knowledge and Control for a Mechanical Design Expert System," IEEE Computer, Vol. 19, No. 7, pp. 92-102, July 1986.

[9.] Dixon, J.R. and Simmons, M.K., "Expert Systems for Design: Standard V-Belt Drive Design as an Example of the Design - Evaluate - Redesign Architecture," Proceedings ASME Computers in Engineering Conference, Las Vegas, August, 1984.

[10.] Suh, N.P., Bell, A.C., and Gossard, D.G., "On an Axiomatic Approach to Manufacturing and Manufacturing Systems," ASME Journal of Engineering for Industry, Vol. 100, No. 2, May 1978.

Appendix A: The Source Code for the CAD Demonstration Program

```

***** Feature Based CAD Demo *****

K.R. Halliday, Ph.D.
August 11, 1987

LIBRARY "3dLib","MenuLib"
! - Initialize Material and Tool Data
DIM Material$(10), MatProp(10,10)
DIM Tool$(10), ToolProp(10,10)
CALL Load_Material_Data(Material$,MatProp)
CALL Load_Tool_Data(Tool$,ToolProp)
LET MatFlag = 0
! - Initialize Menu Data
DIM choice$(7), master$(7), part$(7)
MAT READ master$
DATA Shape, View, Material, Production
DATA Feature, Plot, Quit
MAT READ choice$
DATA Top_View, Side_View, Front_View, Iso_View
DATA Four_VIEWS, ---, Exit
MAT READ part$
DATA Set-Up, Slab, Disk, ---, ---, ---, Exit
LET where$="Right"
LET col$=""
LET maxent=7
LET maxlen=10
LET nchoices=7
CALL Menu_set(where$,col$,maxent,maxlen,menu$,#9)
! - Initialize Graphics Data
LET xmax,ymax,zmax=12
OPEN #1: Screen 0,0.7,0,1
OPEN #2: Screen 0,.35,.5,1
OPEN #3: screen 0,.35,0,.5
OPEN #4: screen .35,0.7,0,.5
OPEN #5: screen .35,0.7,.5,1
LET Object$ = "Nil"
LET Feature$ = "Nil"
LET Warning_Number = 0
LET message$ = "Normal Production Methods"
DO ! - Begin Main Menu Loop
  CLEAR
  CALL Menu_all(Master$,nchoices,"Master",ans1,menu$,#1,#9)
  SELECT CASE ans1
  CASE 1 ! - Get Shape
    DO
      CALL Menu_all(part$,nchoices,"Part",PartType,menu$,#1,#9)
    SELECT CASE PartType
    CASE 1 ! - Set-Up
      CLEAR

```

```

SET cursor 3,10
PRINT "Default Dimensions of the Workspace:"
SET cursor 5,18
PRINT " X-max - ";xmax;" inches."
SET cursor 6,18
PRINT " Y-max - ";ymax;" inches."
SET cursor 7,18
PRINT " Z-max - ";zmax;" inches."
SET cursor 9,12
INPUT PROMPT "DO YOU WISH TO CHANGE THIS ?":SetUpAns$
LET SetUpAns$ = Ucase$(SetUpAns$)
IF SetUpAns$ = "YES" or SetUpAns$ = "Y" THEN
  CLEAR
  SET cursor 3,10
  PRINT "Enter New Dimensions of the Workspace:"
  SET cursor 5,18
  INPUT PROMPT " X-max - ":xmax
  SET cursor 6,18
  INPUT PROMPT " Y-max - ":ymax
  SET cursor 7,18
  INPUT PROMPT " Z-max - ":zmax
ELSE
  CLEAR
END IF
CASE 2          ! - Slab
  LET object$ = "SLAB"
  CLEAR
  SET cursor 7,10
  INPUT PROMPT "Length of slab, x: ":xslab
  SET cursor 8,10
  INPUT PROMPT "Width of slab, y: ":yslab
  SET cursor 9,10
  INPUT PROMPT "Height of slab, z: ":zslab
  LET xmax = 0
  IF xmax < xslab THEN LET xmax = xslab
  IF xmax < yslab THEN LET xmax = yslab
  IF xmax < zslab THEN LET xmax = zslab
  LET ymax = xmax
  LET zmax = xmax
CASE 3          ! - Disk
CASE ELSE
  CLEAR
  EXIT DO
END SELECT
LOOP
CASE 2          ! - View Design
DO
  CALL Menu_all(choice$,nchoices,"Choice",ans2,menu$,#1,#9)
  SELECT CASE ans2
  CASE 1
    WINDOW #1
    CLEAR
    CALL ParaWindow(0,xmax,0,ymax,0,zmax,work$)
    LET xview = xmax/2

```

```

    LET yview = ymax/2
    LET zview = zmax*100
    CALL SetCamera3(xview,yview,zview,work$)
    CALL drawing(work$)
CASE 2
    WINDOW #1
    CLEAR
    CALL ParaWindow(0,xmax,0,ymax,0,zmax,work$)
    LET xview = xmax/2
    LET yview = -ymax*100
    LET zview = zmax/2
    CALL SetCamera3(xview,yview,zview,work$)
    CALL drawing(work$)
CASE 3
    WINDOW #1
    CLEAR
    CALL ParaWindow(0,xmax,0,ymax,0,zmax,work$)
    LET xview = xmax*100
    LET yview = ymax/2
    LET zview = zmax/2
    CALL SetCamera3(xview,yview,zview,work$)
    CALL drawing(work$)
CASE 4
    WINDOW #1
    CLEAR
    CALL ParaWindow(0,xmax,0,ymax,0,zmax,work$)
    CALL drawing(work$)
CASE 5
    CLEAR
    WINDOW #2
    CALL ParaWindow(0,xmax,0,ymax,0,zmax,work$)
    LET xview = xmax/2
    LET yview = ymax/2
    LET zview = zmax*100
    CALL SetCamera3(xview,yview,zview,work$)
    CALL drawing(work$)
    WINDOW #3
    CALL ParaWindow(0,xmax,0,ymax,0,zmax,work$)
    LET xview = xmax/2
    LET yview = -ymax*100
    LET zview = zmax/2
    CALL SetCamera3(xview,yview,zview,work$)
    CALL drawing(work$)
    WINDOW #4
    CALL ParaWindow(0,xmax,0,ymax,0,zmax,work$)
    LET xview = xmax*100
    LET yview = ymax/2
    LET zview = zmax/2
    CALL SetCamera3(xview,yview,zview,work$)
    CALL drawing(work$)
    WINDOW #5
    CALL ParaWindow(0,xmax,0,ymax,0,zmax,work$)
    CALL drawing(work$)
CASE ELSE

```

```

        CLEAR
        EXIT DO
    END SELECT
LOOP
CASE 3                ! - Choose Material
    CLEAR
    SET CURSOR 3,10
    PRINT "Select Material for Component:"
    PRINT
    LET NumMat = Ubound(Material$)
    FOR i=1 to NumMat
        SET cursor i+4,25
        IF material$(i)<>" " THEN PRINT i;".  ";material$(i)
    NEXT i
    PRINT
    INPUT PROMPT"                Option Number? ":Mat_ID
    LET MatFlag = 1
CASE 4                ! - Estimate Production Parameters
    IF Feature$ = "Nil" then
        CLEAR
        SET cursor 7,10
        PRINT "You must define a FEATURE before"
        SET cursor 8,10
        PRINT "  you can use this module."
        SET cursor 10,10
        PRINT " Press any key to continue ..."
        GET KEY Save_Screen
    ELSE
        IF MatFlag = 0 THEN
            CLEAR
            SET cursor 6,10
            PRINT "You must select a Material in order to"
            SET cursor 7,10
            PRINT "  run this module..."
            SET cursor 9,10
            PRINT " Press any key to continue ..."
            GET KEY Save_Screen
        ELSE
            !
            !          ***** Process Selection Algorithm *****
            !
            IF diameter_bore > 2 THEN
                LET finish$ = "nil"
                LET process$ = "trepanning"
                IF roughness < 125 THEN
                    IF aspect_ratio < 4 THEN
                        LET finish$ = "bore"
                    ELSE
                        LET warning_number = 1
                    END IF
                ELSEIF roughness < 32 THEN
                    IF aspect_ratio < 4 THEN
                        LET finish$ = "grind"
                    ELSE

```

```

        LET warning_number = 1
    END IF
ELSEIF roughness < 16 THEN
    LET finish$ = "grind"
    LET warning_number = 2
END IF
ELSE
    ! Bore diameter is less than 2
    LET finish$ = "nil"
    IF aspect_ratio > 8 THEN
        LET process$ = "gun drilling"
    ELSEIF aspect_ratio > 5 THEN
        IF roughness > 125 THEN
            LET message$ = "Coolant Hole Drilling"
            LET process$ = "twist drill"
        ELSE
            LET message$ = "Coolant Hole Drilling"
            LET process$ = "twist drill"
            LET finish$ = "bore"
            IF roughness < 80 THEN
                LET warning_number = 1
            END IF
        END IF
    ELSEIF aspect_ratio > 4 THEN
        LET message$ = "Drill at Reduced Speed, Feed"
        LET process$ = "twist drill"
        IF roughness < 125 THEN
            LET finish$ = "bore"
            IF roughness < 63 THEN
                LET warning_number = 1
            END IF
        END IF
    ELSE
        ! aspect ratio is less than 4
        LET process$ = "twist drill"
        IF roughness < 32 THEN
            LET finish$ = "grind"
            LET warning_number = 2
        ELSEIF roughness < 63 THEN
            LET finish$ = "bore"
        ELSEIF roughness < 125 THEN
            LET finish$ = "ream"
        END IF
    END IF
END IF
END IF
PRINT
PRINT "Selected Hole Generation Process is: ";process$
PRINT "Selected Finishing Process is: ";finish$
PRINT "Note: ";message$
PRINT
    IF warning_number <> 0 THEN CALL Warning(warning_number)
PRINT "          PRESS ANY KEY TO CONTINUE ..."
GET KEY Screen_Save
    LET ProdTime, ProdCost = 0
CALL Process_Cost
    LET FinTime, FinCost = 0

```

```

    IF Finish$ <> "nil" THEN CALL Finish_Cost
    LET TotalTime = ProdTime + FinTime
    LET TotalCost = ProdCost + FinCost
    PRINT
    PRINT "Production Time is: ";ProdTime;" Minutes."
    PRINT "Finish Time is: ";FinTime;" Minutes."
    PRINT "Total Time is: ";TotalTime;" Minutes."
    PRINT
    PRINT "Production Cost is: ";ProdCost;" Dollars."
    PRINT "Finish Cost is: ";FinCost;" Dollars."
    PRINT "Total Cost is: ";TotalCost;" Dollars."
    PRINT
    PRINT "  Press any key to continue ..."
    GET KEY Save_Screen
  END IF
END IF
CASE 5          ! - Select Feature
  LET Object$ = Ucase$(Object$)
  IF Object$ = "NIL" then
    CLEAR
    SET cursor 7,10
    PRINT "You must define a component to place "
    SET cursor 8,10
    PRINT " a feature ..."
    SET cursor 10, 10
    PRINT "PRESS ANY KEY TO CONTINUE ."
    GET KEY Save_Screen
  ELSEIF Object$ = "SLAB" then
    LET Feature$ = "HOLE"
    CLEAR
    SET cursor 4,10
    PRINT "The Only Feature Currently Supported"
    SET cursor 5,10
    PRINT "      is the THROUGH HOLE:"
    SET cursor 7,10
    INPUT PROMPT" Diameter of Hole? ":diameter_bore
    SET cursor 8,10
    INPUT PROMPT" Roughness? ":roughness
    LET length_bore = zslab
    SET cursor 9,10
    PRINT " The length of the bore of a through hole"
    SET cursor 10,10
    PRINT " is the same as the thickness of the slab"
    SET cursor 11,10
    PRINT " Length of bore = ";length_bore;" inches."
    SET cursor 13, 13
    PRINT "PRESS ANY KEY TO CONTINUE ..."
    GET KEY Save_Screen
    LET aspect_ratio = length_bore/diameter_bore
  END IF

CASE 6          ! - Plot Design
CASE ELSE
  STOP

```

```
END SELECT
LOOP
```

```
SUB Process_Cost
```

```
! ***** Internal Subroutine Calculates Time to Machine *****
! ***** and Cost to Machine the Primary Hole of the *****
! ***** Feature *****
```

```
SELECT CASE Process$
```

```
CASE "twist drill"
```

```
LET Tool_Name$ = "Drill"
```

```
CALL ID_Tool
```

```
LET LW = length_bore + (diameter_bore/3) + (1/16)
```

```
LET sfpm = MatProp(Mat_ID,1)
```

```
LET rpm = 3.8*sfpm/(diameter_bore)
```

```
LET a=MatProp(Mat_ID,3)
```

```
LET b=MatProp(Mat_ID,4)
```

```
IF diameter_bore < 0.25 THEN
```

```
LET feed = a
```

```
ELSEIF diameter_bore > 1 THEN
```

```
LET feed = a+b
```

```
ELSE
```

```
LET feed = a+(4*b*(diameter_bore - 0.25)/3)
```

```
END IF
```

```
!
```

```
! ***** De-Rate Speeds and Feeds According to *****
```

```
! ***** Schedule in SME Handbook p. 3-20 *****
```

```
!
```

```
IF aspect_ratio < 4 THEN
```

```
LET sf=1
```

```
LET ff=1
```

```
ELSEIF aspect_ratio < 5 THEN
```

```
LET sf=0.85
```

```
LET ff=0.90
```

```
ELSEIF aspect_ratio < 6 THEN
```

```
LET sf=0.72
```

```
LET ff=0.81
```

```
ELSEIF aspect_ratio < 7 THEN
```

```
LET sf=0.61
```

```
LET ff=0.73
```

```
ELSE
```

```
LET sf=0.52
```

```
LET ff=0.66
```

```
END IF
```

```
LET feed = ff*feed
```

```
LET rpm = sf*rpm
```

```
LET TimeMachine = LW/(feed * rpm)
```

```
LET m= 1/ToolProp(Tool_ID,5)
```

```
LET vr = MatProp(Mat_ID,2)
```

```
LET num_tools = TimeMachine*((sfpm/vr)^m)
```

```
LET ProdTime=TimeMachine+num_tools*ToolProp(Tool_ID,4)
```

```
LET work_sta_cost=(ToolProp(Tool_ID,1)+ToolProp(Tool_ID,2))/60
```

```
LET ToolCost=ToolProp(Tool_ID,3)
```

```

    LET ProdCost = ProdTime*work_sta_cost+num_tools*ToolCost
CASE "gun drilling"
    LET Tool_Name$ = "GunDrill"
    CALL ID_Tool
    LET LW= length_bore + 1/16
    LET penetration_rate = MatProp(Mat_ID,5)
    IF aspect_ratio > 15 THEN
        LET speed_factor = 0.4+(0.16*(75-aspect_ratio)/60)
    ELSEIF aspect_ratio > 4 THEN
        LET speed_factor = 1.05 - 0.03*aspect_ratio
    ELSE
        LET speed_factor = 0.95
    END IF
    LET ProdTime = LW/(speed_factor*penetration_rate)
    ! ***** Assume 100 deep holes per tool edge *****
    LET ProdTime = ProdTime + ToolProp(Tool_ID,4)/100
    LET work_cost = (ToolProp(Tool_ID,1)+ToolProp(Tool_ID,2))/60
    LET ProdCost = ProdTime*work_cost + ToolProp(Tool_ID,3)/100
CASE "trepanning"
    LET Tool_Name$ = "TrepanDrill"
    CALL ID_Tool
    LET LW= length_bore + 1/16
    LET penetration_rate = MatProp(Mat_ID,5)
    IF aspect_ratio > 15 THEN
        LET speed_factor = 0.4+(0.16*(75-aspect_ratio)/60)
    ELSEIF aspect_ratio > 4 THEN
        LET speed_factor = 1.05 - 0.03*aspect_ratio
    ELSE
        LET speed_factor = 0.95
    END IF
    LET ProdTime = LW/(speed_factor*penetration_rate)
    ! ***** Assume 100 deep holes per tool edge *****
    LET ProdTime = ProdTime + ToolProp(Tool_ID,4)/100
    LET work_cost = (ToolProp(Tool_ID,1)+ToolProp(Tool_ID,2))/60
    LET ProdCost = ProdTime*work_cost + ToolProp(Tool_ID,3)/100
END SELECT
END SUB

SUB ID_Tool
    LET Tool_Num = Ubound(Tool$)
    FOR i=1 to Tool_Num
        IF Tool$(i) = Tool_Name$ THEN
            LET Tool_ID = i
            EXIT FOR
        END IF
    NEXT i
END SUB

SUB Finish_Cost
    !
    ! ***** Internal Subroutine Calculates Cost *****
    ! ***** And Time to Refina an Existing Hole *****
    !
    LET Finish$ = Ucase$(Finish$)

```



```

SELECT CASE Finish$
CASE "REAM"
    LET Tool_Name$ = "StraightReam"
    CALL ID_Tool
    LET ream_sfp = MatProp(Mat_ID,6)
    LET ream_rpm = 3.8*ream_sfp/(diameter_bore)
    LET finish_length = length_bore+1/16
    LET ream_feed = 0.019*diameter_bore
    LET ream_time = finish_length/((ream_feed)*(ream_rpm))
    LET m = 1/ToolProp(Tool_ID,5)
    LET vr = MatProp(Mat_ID,2)
    LET num_reams=ream_time*((ream_sfp/vr)^m)
    LET FinTime = ream_time + num_tools*ToolProp(Tool_ID,4)
    LET work_cost=(ToolProp(Tool_ID,1)+ToolProp(Tool_ID,2))/60
    LET ToolCost = ToolProp(Tool_ID,3)
    LET FinCost=FinTime*work_cost+num_reams*ToolCost
CASE "BORE"
CASE "GRIND"
END SELECT
END SUB

!
SUB drawing(work$)
    ! - Start Application Program Here
    SELECT CASE Object$
    CASE "SLAB"
        CALL Box3(0,xslab,0,yslab,0,zslab,work$)
        IF Feature$ = "HOLE" then
            CALL zhole(xslab/2,yslab/2,0,diameter_bore/2,zslab,work$)
        END IF
    CASE "DISK"
    CASE ELSE
    END SELECT
    ! - End Application Program Here
END SUB

END ! - End of Main Program

!
SUB Xcylinder(xc,yc,zc,r,l,work$)
    FOR theta = 0 to 360 step 45
        LET dth=(theta*pi)/180
        LET y1=yc-r*cos(dth)
        LET z1=zc+r*sin(dth)
        CALL LineOn3(xc,yc,zc,xc,y1,z1,work$)
        LET x2=xc+l
        CALL LineOn3(xc,y1,z1,x2,y1,z1,work$)
        CALL LineOff3(x2,y1,z1,x2,yc,zc,work$)
    NEXT theta
    LET ymin=yc-r
    LET ymax=yc+r
    LET zmin=zc-r
    LET zmax=zc+r
    CALL CircleX3(xc,ymin,ymax,zmin,zmax,work$)

```

```

    CALL CircleX3(x2,ymin,ymax,zmin,zmax,work$)
END SUB

```

```

SUB Ycylinder(xc,yc,zc,r,l,work$)
  FOR theta = 0 to 360 step 45
    LET dth=(theta*pi)/180
    LET x1=xc+r*cos(dth)
    LET z1=zc+r*sin(dth)
    CALL LineOn3(xc,yc,zc,x1,yc,z1,work$)
    LET y2=yc+l
    CALL LineOn3(x1,yc,z1,x1,y2,z1,work$)
    CALL LineOff3(x1,y2,z1,xc,y2,zc,work$)
  NEXT theta
  LET xmin=xc-r
  LET xmax=xc+r
  LET zmin=zc-r
  LET zmax=zc+r
  CALL CircleY3(yc,xmin,xmax,zmin,zmax,work$)
  CALL CircleY3(y2,xmin,xmax,zmin,zmax,work$)
END SUB

```

```

SUB Zcylinder(xc,yc,zc,r,l,work$)
  FOR theta = 0 to 360 step 45
    LET dth=(theta*pi)/180
    LET y1=yc-r*cos(dth)
    LET x1=xc+r*sin(dth)
    CALL LineOn3(xc,yc,zc,x1,y1,zc,work$)
    LET z2=zc+l
    CALL LineOn3(x1,y1,zc,x1,y1,z2,work$)
    CALL LineOff3(x1,y1,z2,xc,y1,zc,work$)
  NEXT theta
  LET ymin=yc-r
  LET ymax=yc+r
  LET xmin=xc-r
  LET xmax=xc+r
  CALL CircleZ3(zc,xmin,xmax,ymin,ymax,work$)
  CALL CircleZ3(z2,xmin,xmax,ymin,ymax,work$)
END SUB

```

```

SUB YHole(xc,yc,zc,r,l,work$)
  FOR theta = 0 to 360 step 45
    LET dth=(theta*pi)/180
    LET x1=xc+r*cos(dth)
    LET z1=zc+r*sin(dth)
    LET y2=yc+l
    CALL LineOff3(x1,yc,z1,x1,y2,z1,work$)
  NEXT theta
  LET xmin=xc-r
  LET xmax=xc+r
  LET zmin=zc-r
  LET zmax=zc+r
  CALL CircleY3(yc,xmin,xmax,zmin,zmax,work$)
  CALL CircleY3(y2,xmin,xmax,zmin,zmax,work$)
END SUB

```

```

SUB XHole(xc,yc,zc,r,l,work$)
  FOR theta = 0 to 360 step 45
    LET dth=(theta*pi)/180
    LET y1=yc-r*cos(dth)
    LET z1=zc+r*sin(dth)
    LET x2=xc+l
    CALL LineOff3(xc,y1,z1,x2,y1,z1,work$)
  NEXT theta
  LET ymin=yc-r
  LET ymax=yc+r
  LET zmin=zc-r
  LET zmax=zc+r
  CALL CircleX3(xc,ymin,ymax,zmin,zmax,work$)
  CALL CircleX3(x2,ymin,ymax,zmin,zmax,work$)
END SUB

SUB ZHole(xc,yc,zc,r,l,work$)
  FOR theta = 0 to 360 step 45
    LET dth=(theta*pi)/180
    LET y1=yc-r*cos(dth)
    LET x1=xc+r*sin(dth)
    LET z2=zc+l
    CALL LineOff3(x1,y1,zc,x1,y1,z2,work$)
  NEXT theta
  LET ymin=yc-r
  LET ymax=yc+r
  LET xmin=xc-r
  LET xmax=xc+r
  CALL CircleZ3(zc,xmin,xmax,ymin,ymax,work$)
  CALL CircleZ3(z2,xmin,xmax,ymin,ymax,work$)
END SUB

SUB Load_Material_Data(Material$(),MatProp(.))
  LET NumProp = 6
  LET i=1
  DO while more data
    READ Material$(i)
    FOR j=1 to NumProp
      READ MatProp(i,j)
    NEXT j
    LET i=i+1
  LOOP
  !   Name      sfpm  vr   a    b   gun  ream
  !           fpm      ipm  fpm
  DATA "Aluminum", 650, 900, 0.005, 0.030, 8.2, 150
  DATA "Brass",    200, 500, 0.008, 0.020, 2.6, 120
  DATA "Cast Iron", 80, 300, 0.005, 0.012, 3.6, 66
  DATA "Magnesium", 300, 700, 0.004, 0.030, 5.0, 140
  DATA "Mild Steel", 110, 350, 0.008, 0.020, 2.2, 96
  DATA "Stainless", 20, 200, 0.003, 0.008, 1.2, 45
  DATA "Titanium", 30, 250, 0.003, 0.008, 0.8, 40
END SUB

```

```

SUB Load_Tool_Data(Tool$( ),ToolProp(,))
  LET NumProp = 5
  LET i=1
  DO while more data
    READ Tool$(i)
    FOR j=1 to NumProp
      READ ToolProp(i,j)
    NEXT j
    LET i=i+1
  LOOP
  !   Tool      Op  Mach Tool Tool Tool
  !           Cost Cost Cost Time Expon.
  !
  DATA "Drill",      22.5, 25,   3.5, 0.5, .125
  DATA "GunDrill",   22.5, 37.5, 25,   3,   .125
  DATA "TrepanDrill", 22.5, 37.5, 40,   2,   .125
  DATA "StraightReam",22.5, 25,   8,   0.5, .125
END SUB

```

```

SUB Warning(warning_number)
  PRINT
  PRINT "          WARNING !!!"
  PRINT
  SELECT CASE warning_number
  CASE 1
    PRINT "      The aspect ratio is too large to support"
    PRINT "      the finishing operation(s) required by the"
    PRINT "      surface finish you have specified."
  CASE 2
    PRINT "      This value of surface finish is very hard"
    PRINT "      to produce and inspect because of the size"
    PRINT "      and type of component."
  CASE ELSE
    PRINT "          Option - ";warning_number;" has not yet"
    PRINT "          been implemented."
  END SELECT
  PRINT
END SUB

```

1987 USAF-JES SUMMER FACULTY RESEARCH PROGRAM/

GRADUATE STUDENT SUMMER SUPPORT PROGRAM

Sponsored by the

AIR FORCE OFFICE OF SCIENTIFIC RESEARCH

Conducted by the

Universal Energy Systems, Inc.

FINAL REPORT

GUN GAS DIVERSION

Prepared by:	Elmer C. Hansen
Academic Rank:	Assistant Professor
Department and	Mechanical Engineering
University:	University of Florida
Research Location:	Air Force Armament Laboratory
	Munitions Division
	Guns and Projectiles Branch
USAF Researcher:	LT Kenneth J. Welzyn
Date:	7 August 1987
Contract No:	F49620-85-C0013

GUN GAS DIVERSION

by

Elmer C. Hansen

ABSTRACT

The process of gun gas diversion using a single hole perforated disk diverter was investigated with a steady state apparatus. The efficiency of diversion was found to depend on the distance between the muzzle and the diverter disk and the ratio of muzzle pressure to diverter exit pressure. Diversion efficiencies of up to 98% were obtained. A diverter was designed in a multibarrel configuration and tested at the muzzle of two different 20mm guns. Measured diverter pressures were in the range predicted by the original design. High speed motion pictures showed that the great majority of flash and secondary flash was diverted.

ACKNOWLEDGEMENTS

This research was sponsored by the Air Force Office of Scientific Research/AFSC, United States Air Force, under Contract F49620-85-C-D013 with Universal Energy Systems. I would like to thank the Air Force Office of Scientific Research and Universal Energy Systems for this effort.

This project was successful because of the many people who helped by bringing their energy and expertise to bear on the problem. I was given excellent support by Branch Chief Lanny Burdge and the staff of the Guns and Projectiles Branch. Most notable was Nunzio Zummo, who helped me understand the existing hardware and construct new hardware. The Air Force Armament Laboratory provided personnel in the Model Shop who constructed precision hardware for me. Finally, I would like to give due respect to God for giving the insight and understanding of the physical processes upon which this work is based.

I. INTRODUCTION

After a projectile leaves the muzzle of an aircraft cannon, the gun gas inside the barrel blows down escaping into a region 20 to 40 feet in front of the muzzle. When multiple firings occur in flight, the concentration of gun gas can increase to a level that will cause unwanted further combustion called secondary flash. It is desired to be able to divert gun gas away from the front of the gun and out in a direction away from the aircraft and its engines. References 1-4 describe the muzzle devices for guns which are most pertinent to this work.

II. OBJECTIVES

Diversion of gun gas is governed by the geometry of the diversion device and the amount of underexpanded pressure at the nozzle. The geometry in this experiment is the distance between the muzzle and the perforated disk diverter. The first objective of this work was to determine the fraction of the mass flow rate diverted for a range of underexpanded pressure ratios and a range of nozzle to disk distances. The second objective was to design, build, and test a diverter on a 20mm single shot gun.

III. STEADY STATE GAS DIVERSION

a. APPROACH

A test fixture was built to simulate the flow of gas from a muzzle into a single hole perforated disk diverter. The muzzle was a 0.0625 inch diameter sonic nozzle. The test gas, nitrogen, was supplied at 2400 psi from standard cylinder. The sonic nozzle was placed at the center of one inch diameter disk as shown in Figure 1. Down stream of and in line with the sonic nozzle was a one inch diameter disk with a 0.078 inch hole. This hole is slightly larger than the sonic nozzle. The one inch disks were each connected to 6-inch diameter plates. These plates were held together and adjusted by four threaded rods.

The mass flow rate through the sonic nozzle and through the perforated plate were treated as flows through a sonic nozzle. The mass flow rate through such a nozzle is a function of the specific heat ratio, the stagnation pressure, the throat area, and the stagnation temperature. For a constant specific heat ratio, the mass flow rate is

$$\dot{m} = \frac{P_c \sqrt{\gamma} A}{\sqrt{RT_c}} \left(\frac{2}{\gamma+1} \right)^{\frac{\gamma+1}{2(\gamma-1)}}$$

The stagnation pressure in the larger diameter pipe in front of the sonic nozzle was measured by a 5000 psi Gould-Statham PA-4099-5M strain gage type transducer. The area ratio of the large pipe to the sonic nozzle was 41.5 to 1. The stagnation pressure of the fluid passing through the 0.078 inch hole was measured using a 0.028 diameter stagnation tube connected to another Gould-Statham transducer. The ratio of the downstream hole area to the sonic nozzle area was 1.357, when a deduction was made for the stagnation tube cross sectional area. The stagnation pressure of the diverted flow was measured by a Bourns ± 3 psid pressure transducer and a 0.028 inch diameter stagnation tube positioned at a radial distance of 0.5 inch from the axis of flow and midway between the one inch diameter disks. Because a ratio of mass flow rates was desired and because the stagnation temperature, T_o , is the same through both holes, T_o was not measured.

The three pressure measurements were taken as a function of time using a Nicolet digital oscilloscope as the nitrogen bottle emptied its contents through the test fixture. Data was taken at a rate of 5 milliseconds per point at the highest pressure ratios (80+) and at 50 milliseconds per point at lower pressure ratios.

5. RESULTS

The mass fraction diverted, the mass flow rate of the diverted gas over the total flow rate, was called the diversion efficiency, D .

$$D = 1 - \frac{(\text{mass flow rate out last plate})}{(\text{mass flow rate out sonic nozzle})} \quad (2)$$

Diversion efficiency was governed by the two parameters, pressure ratio and distance (Figure 2). The pressure ratio is the ratio of the static pressure at the sonic nozzle exit to the stagnation pressure at the exit of the diverter. The distance is the ratio of the length between disks to the diameter of the sonic nozzle.

At pressure ratios greater than 50, the diversion efficiency is greater than 90%. Below a pressure ratio of 50, the diversion efficiency falls off dramatically. The length ratio has a significant effect in raising and lowering the curve. At the high value of $L/D=7$, there is only 2% of the flow remaining to be diverted.

When the pressure ratio was greater than 50 and $L/D=2$, the pressure transducer measuring the diverted flow stagnation pressure did not have enough range to make useful measurements. The measured diversion efficiency of 93-94% at pressure ratios above 50 and $L/D=2$ was not

plotted on Figure 2 because of the uncertainty of the pressure ratio. There seems to be some oscillation that occurs at a pressure ratio near 50 when the disk spacing is close, $L/D=2$, because a variation of at least 10% diversion efficiency occurred consistently in that collected data. The physical effect of the pressure ratio on the diversion can be seen in Figure 3. The shock bottle (shown by the dark lines) is larger at higher pressure ratios and smaller at lower pressure ratios.

IV. DESIGN OF GUN DIVERTER

Steady state experimental data showed that downstream of an under-expanded sonic nozzle the flow accelerated to supersonic and then decelerated across a shock wave. This shock dissipated the stagnation pressure. The process was adiabatic so that the stagnation temperature remained constant. The equations used to describe the process are the conservation of mass, the conservation of momentum, the equation of state, and the isentropic relationship between static and stagnation densities.

$$\rho_1 V_1 A_1 = \rho_2 V_2 A_2 \quad (1)$$

$$T_1 + V_1^2 / (2 C_p) = T_2 + V_2^2 / (2 C_p) = T_c \quad (2)$$

$$P = \rho R T \quad (3)$$

$$\rho / \rho_c = \left(1 - V^2 / (2 C_p T_c) \right)^{\frac{1}{\gamma-1}} \quad (4)$$

State 1 refers to the muzzle exit and state 2 refers to the diverter exit. The four previous equations can be combined to give

$$A_2 = \frac{A_1 P_{01} V_1 D}{P_2 V_2} \left[\left(1 - V_1^2 / (2 C_p T_0) \right)^{\frac{1}{\gamma-1}} \left(1 - V_2^2 / (2 C_p T_0) \right) \right] \quad (7)$$

When A_1 , V_1 , P_{01} , and T_0 are known and D , P_2 , and V_2 are established for a particular diverter design, the required cross-sectioned area of the diverter can be found. A representative graph of equation 7 is shown in Figure 4. The design used in this work had a cross-sectional area of 49 square inches. The design of the diverter assembly used in this work is shown in Figure 5.

V. DIVERTER TEST

a. GUN POD TEST

An opportunity was available to instrument a GPU-5/A gun pod which has a perforated disk diverter. The pressure time trace is shown in Figure 6. With an estimation of the stagnation temperature, the mass

flow rate could be calculated by assuming choked flow through the diverter exit area. The mass flow rate was integrated over time as the gun gas left the diverter and compared to the charge mass. The charge mass was 0.338 lb. and the integrated mass was .42 lb.

b. 20mm Tests.

The diverter (Fig. 5) was attached to two 20mm guns, an M61 and a higher velocity gun. Tests were run to observe the operation of the diverter. Interior diverter pressures were measured using piezoelectric transducers and high speed photos were taken of the flash and expulsion of gun gas.

The M61 test was run first to check the integrity of operation and the instantaneous pressures within the diverter housing. Tests showed that even though there was occasional secondary flash, this did not proceed out the peanut hole through which the projectile traveled.

The test of the higher velocity 20mm gun was run with and without venturi plates. Because of triggering problems, no pressure data was obtained for the three shots without venturi plates. Good pressures were obtained for two of the three shots with venturi plates. Pressures were measured with a piezoelectric transducer and a strain gage transducer. The piezoelectric transducer has a faster rise time and

gave a better indication of the instantaneous pressures. The results of both transducers were combined to estimate a reasonable pressure time trace for the blow down. The peak pressure was about 600 psig and the average pressure over the 6 millisecond blow down was 200 psig. Based on the pressure profile, the mass flow was integrated over time to give a mass of .233 lb as compared to the charge of .286 lb.

The similarities between the pressure time traces of the single shot 20mm tests and the multiple shot 30mm indicate that single shot testing is useful for determining flow characteristics of multiple firings.

VI. RECOMMENDATIONS

a. Additional Physical Understanding

Understanding of the diversion process should be extended using a steady gas flow apparatus. A larger range of pressure ratios and L/D ratios should be studied. Asymmetric geometries should also be included. Velocity measurements should be taken at the exit of the diverter to indicate the nonuniformity of the velocity distribution.

b. Multiple Shot Diverter

A gun gas diverter should be designed, built and tested in a multiple shot configuration. Once tested the design strategy can be refined to minimize secondary flash. This will then provide a sound basis for diverter designs of advanced guns.

REFERENCES

1. WITKIN, S. G., "30MM Operable Prototype Diverter", AFATL-TR-84-40, 1984.
2. Ranum, G. L., Evaluation of the GPU-5/A 30mm Full-Scale Engineering Development (FSED) Gun Pod, AD-TR-86-45, 1986.
3. Yates, J., Robinson, R. E., and J. C. Kennedy, Test Report for XPD Gun-Gas Diverter, A-10 SPO 19, 1983.
4. Engineering Design Handbook, Gun Series, Muzzle Services, AD 838748, AMCP 706-251, 1968.

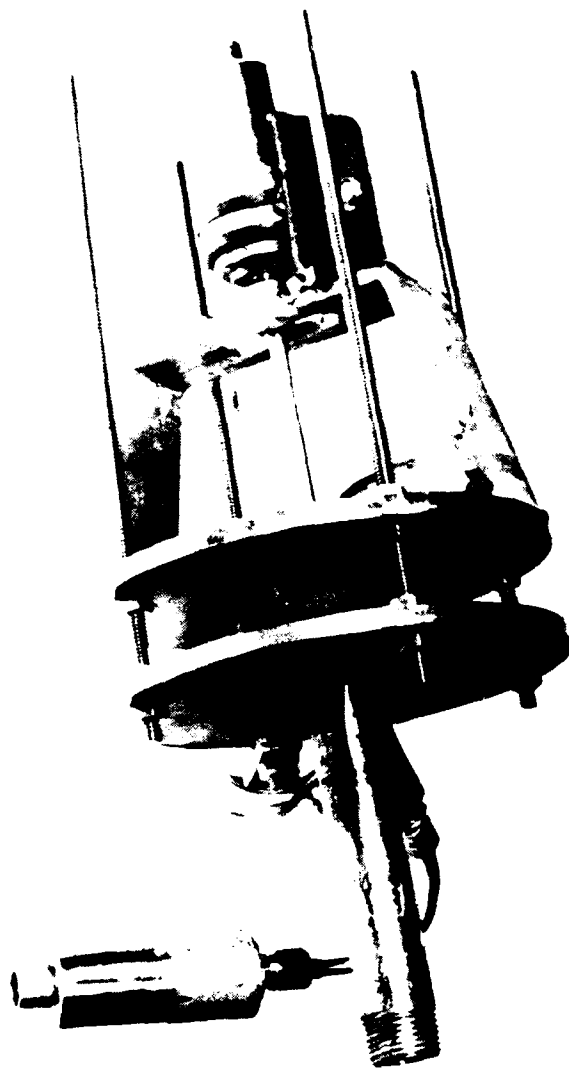


Figure 1. Steady state flow diverter apparatus.

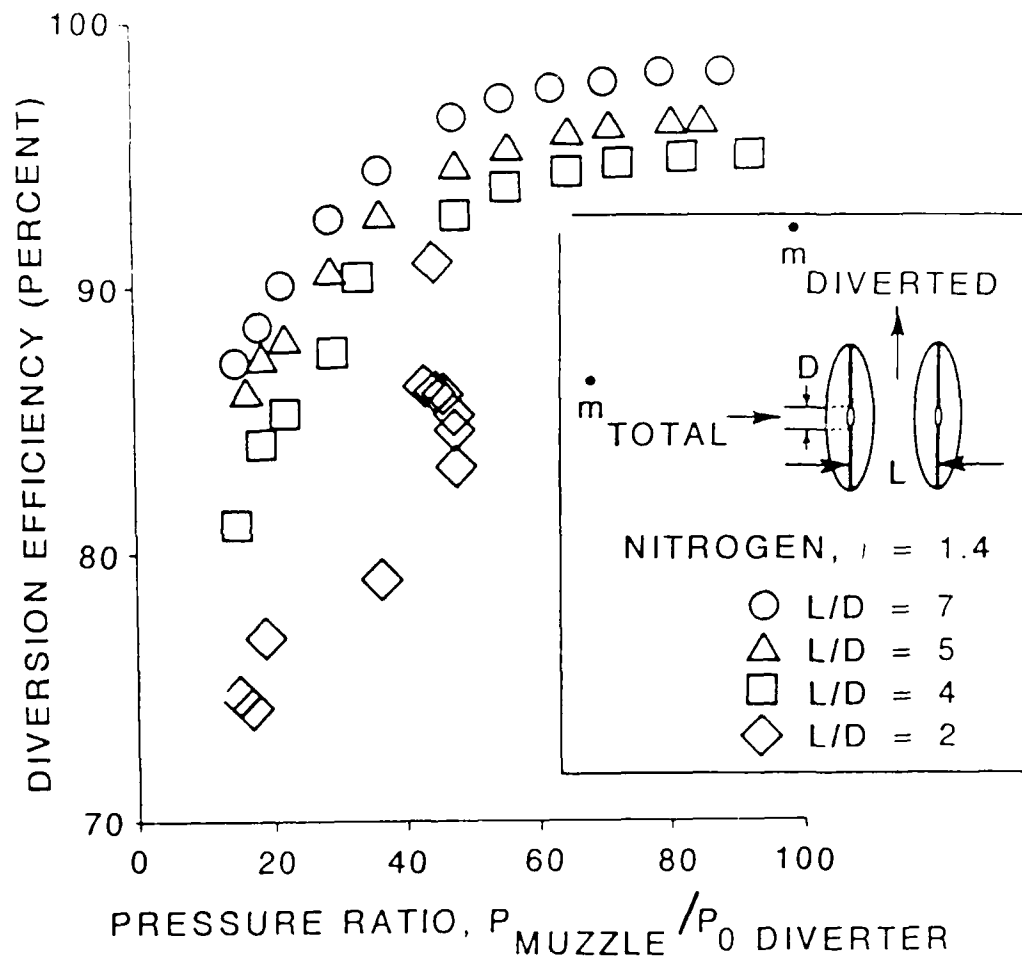


Figure 2. Diversion efficiency of a single hole perforated disk under steady flow conditions.



Figure 3. Shadowgraph of the Flow Within the Single Hole Perforated Plate Diverter

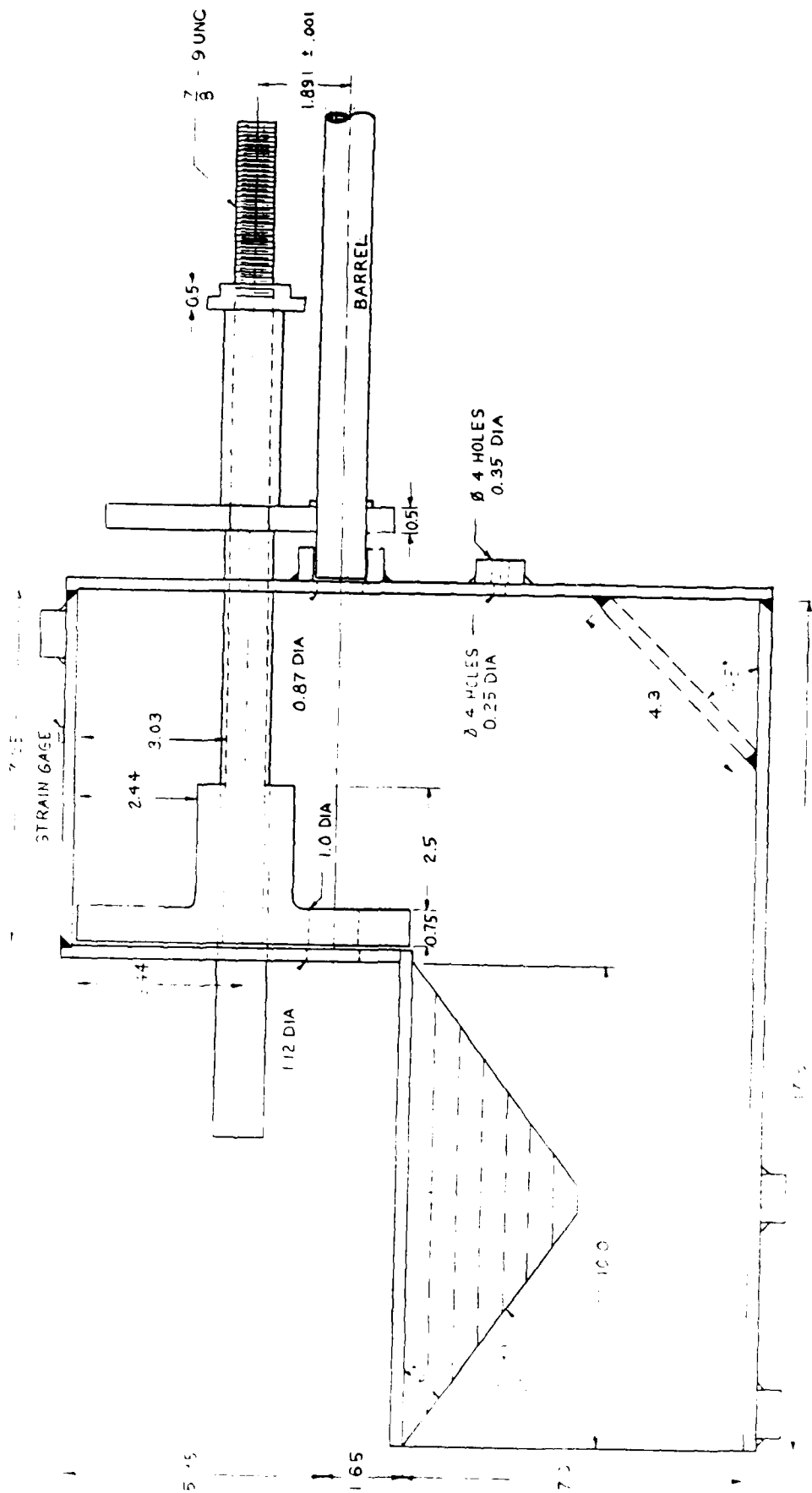


Figure 5. Gas diverter designed for high speed 20mm gun.

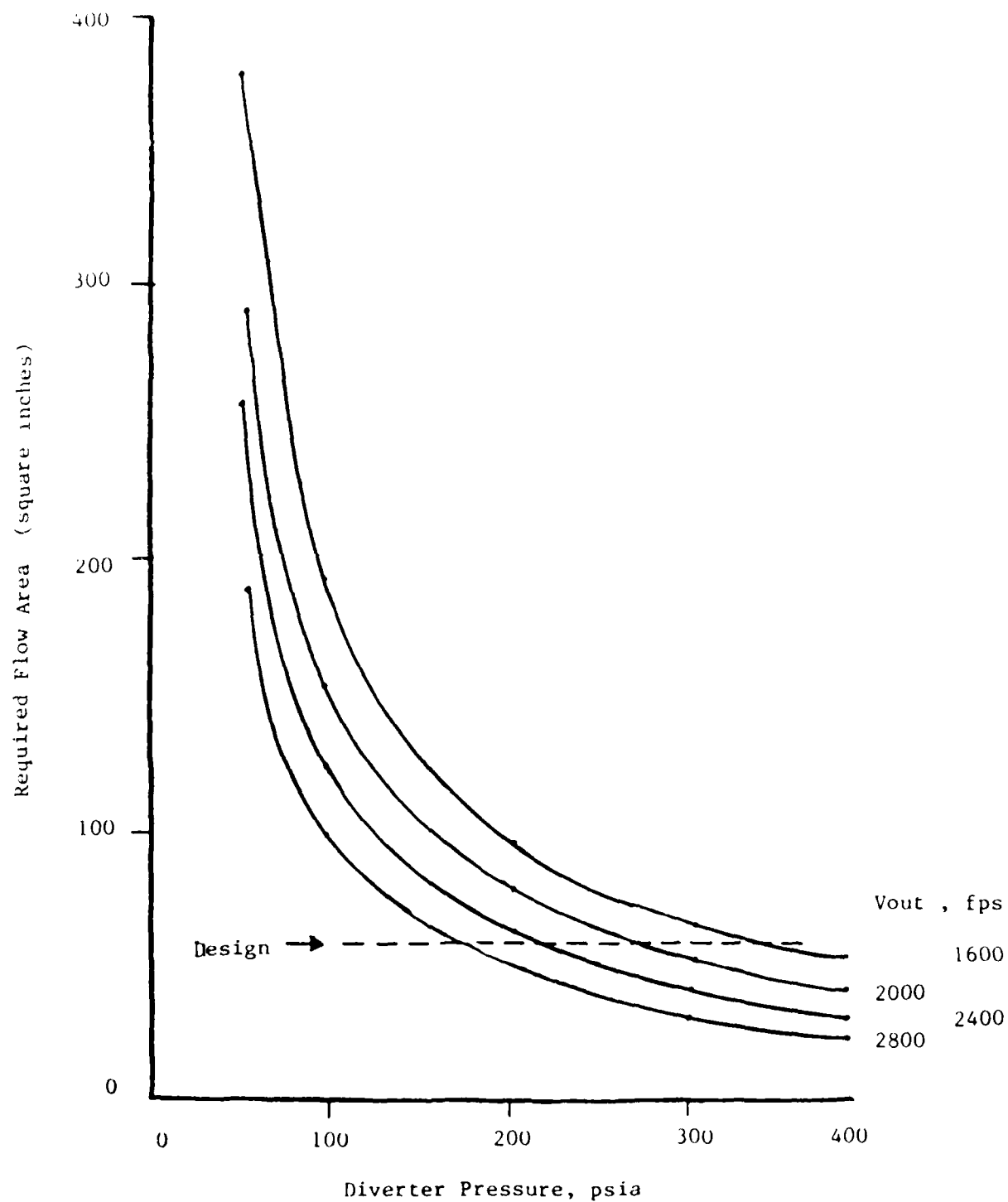


Figure 4. Design of diverter cross sectional area based on pressure and velocity.

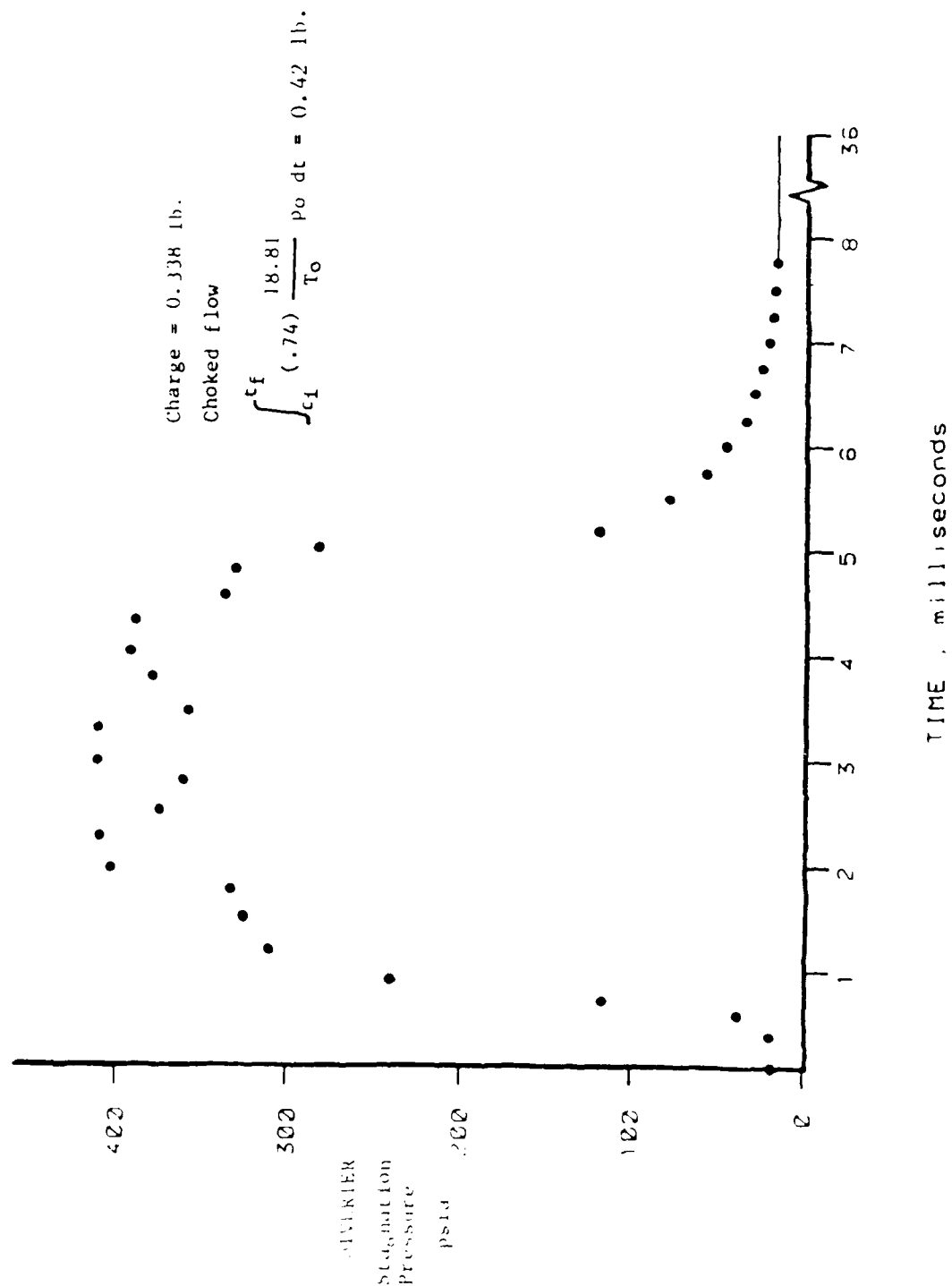


Figure 6. Experimental diverter pressure of gun pod GPU-5/A during multiple firing.

1987 USAF-UES SUMMER FACULTY RESEARCH PROGRAM

Sponsored by the
AIR FORCE OFFICE OF SCIENTIFIC RESEARCH

Conducted by the
Universal Energy Systems, Inc.

FINAL REPORT

Multi-block Grid Optimization

Prepared by:	David C. Hart
Academic Rank:	Assistant Professor
Department and	Mathematical Sciences
University:	University of Cincinnati
Research Location:	USAFWAL/FIMMA
	Wright-Patterson AFB
	Dayton, OH
USAF Researcher:	Dennis Sedlock
Date:	18 Sep 87
Contract No:	F49620-85-C-0013

Multi-block Grid Optimization

by

David C. Hart

ABSTRACT

A major obstacle in obtaining a numerical solution for the flow around a geometrically complex object is the generation of an adequate coordinate grid. An approach which might minimize this obstacle is decomposition of the flow domain into subdomains, in each of which a grid is generated separately, and recombination of these multiple blocks into a single global grid. A program has been developed for revising a crudely joined grid into one suitable for computation, by maximizing overall smoothness and orthogonality.

ACKNOWLEDGEMENTS

I wish to thank the Air Force Systems Command and the Air Force Office of Scientific Research for their sponsorship of this effort, and Wright Aeronautical Laboratories at Wright-Patterson Air Force Base for the excellent facilities and support provided.

Particular thanks are due to Dr. Keith Richey, Mr. Dennis Sedlock, and the men and women of the Aerodynamic Methods Group, for their warmth, advice, and encouragement throughout a rewarding and enjoyable experience.

I. INTRODUCTION

Computational approaches to fluid dynamics require the use of a body-fitted, curvilinear coordinate system. Generating these coordinates is generally regarded as one of the primary obstacles to more widespread use of computational methods in aeronautical engineering. Inadequate grids lead to slow convergence, or even lack of convergence, of flow solutions, and grids for even relatively simple configurations may involve a tremendous investment of time and talent.

The Aerodynamic Methods Group of the Flight Dynamics Laboratory at Wright-Patterson Air Force Base is involved in a continuing effort to develop reliable and efficient computational tools for general engineering application. Grid generation has been identified as an important component of this effort, especially as complex objects such as complete aircraft begin to be modelled by realistic mathematical equations. Such objects have traditionally been subjected to expensive and time-consuming wind-tunnel testing. A fast and reliable method for creating computational grids would therefore be of great practical value.

The problem of grid generation is essentially mathematical. It is the computational aspect of differential topology, the author's thesis area. The author has been involved with this problem for several years, first developing a scheme for generating a grid for the entire F-16 aircraft (similar to those later developed at General Dynamics and NASA/Ames), and later studying the cavity/inlet problem for NASA/Langley.

II. OBJECTIVES OF THE RESEARCH EFFORT

Computational grids are subject to a great many demands, in order that they serve the goal of computing a fluid flow well. They should be orthogonal to solid surfaces, to handle the associated boundary conditions. To minimize the development and growth of error, they should be as nearly orthogonal as possible overall, concentrated in regions of high velocity gradients, and have minimal second derivatives. In the interests of economy, they should be parsimonious, and the "coordinate domain" geometrically simple; and they should be easily constructed.

An approach which minimizes these difficulties is the use of a multiple-block grid. The multi-block approach decomposes the flow domain into a number of smaller, simpler subdomains. Of particular value with this approach would be to minimize the constraints the global system puts upon the construction in the smaller blocks. These must, however, be patched back together to obtain the flow in the entire domain. My task was to develop a method for converting such patched or overset grid blocks into a smoothly compatible unit.

III. RESULTS

The idea of "improving" a given grid by some automatic process has been entertained by several investigators (for example, [BS], [CKD], and [ND]). Given a grid $\underline{R} = R(i,j,k)$, one defines a measure, $F(\underline{R})$, of the deficiency of that grid. A new grid is then found, which is less defective.

Although spectacular results have been obtained along these lines in [BS], theirs is primarily an adaptive method for simple configurations, and it is very expensive. This has led to several attempts to find a more tractable scheme. We follow the outline of [CKD], but attempt a more direct and rigorous evaluation of the input grid. Our defect function measures two items: the size of the second derivatives (departure from "smoothness"), as indicated by the variation in line spacing; and skewness (departure from orthogonality), as indicated by the cosines of the angles formed by the edges incident at a grid point. Provision is made for varying the relative weight accorded these factors; their leading role, in the effect of the grid upon the flow calculation, has been discussed in [TM].

The grid is updated by the conjugate gradient method; that is, the new grid $\underline{R}' = \underline{R} + w\underline{P}$, where \underline{P} is chosen, first as $-\text{grad}(F(\underline{R}))$, and then with successive updates orthogonal to all previous ones. The parameter w determines the amount of change along the line $\{\underline{R} + t\underline{P}, t \text{ arbitrary}\}$ thus determined; we define $f(t) = F(\underline{R} + t\underline{P})$, and choose w to minimize the resulting function. This may be done quite precisely, since $f(t)$ is a polynomial. We use the homotopy (or, continuation) method to solve $f'(t) = 0$, which is deformed (or, continued) from the easily solved $t^3 - q^3 = 0$, " q " a particular complex number. Newton's method is used to follow the path determined by each of the three roots. The values of f at the real roots are then compared, to determine the optimal solution, w .

The final Fortran code is about 1100 lines (900 for the 2D version), half of which, however, are documentation. The program involves $O(n)$ arithmetic operations, per global iteration, and $O(n)$ storage; both are optimal.

IV. RECOMMENDATIONS

The program developed and tested during the 1987 SFRP provides an efficient and reliable method for enforcing smoothness and orthogonality, hence for joining crudely "glued" blocks together. However, it does not include terms for clustering points into regions which are expected to have high velocity gradients for the flow, which is a highly desirable feature. Addition of such terms could also be easily extended to an adaptive capability, the ability to regenerate the grid during the course of the flow calculation, to improve both accuracy and convergence rate.

If n is the number of grid points, the defect function, F , depends upon $3n$ variables (many). The present algorithm tends to slow down substantially as the optimum solution is approached. The program could be improved by the incorporation of a predictor-corrector scheme, to speed convergence. (This would be possible both in the overall revision of the grid and also in the Newton method loop of the polynomial solution subroutine). This should greatly accelerate convergence.

REFERENCES

Brackbill, J., and J. Saltzman, "Adaptive zoning for singular problems in two dimensions," Jnl. Comp. Physics, 46, 1982, 342-368.

Carcaillet, R., S. Kennon and G. Dulakravitch, "Optimization of three dimensional grids," AIAA paper 85-4087.

Nakahashi, K. and G. Deiwert, "A three dimensional adaptive grid method," AIAA paper 85-486.

Thompson, J., and C.W. Mastin, "Order of difference expressions in curvilinear coordinate systems," Advances in Grid Generation, FED-Vol. 5, ed. K.N. Ghia and U. Ghia, ASME Applied Mechanics, Bioengineering and Fluids Engineering Conference, Houston, 1983.

1987 USAF-UES SUMMER FACULTY RESEARCH PROGRAM

Sponsored by the
AIR FORCE OFFICE OF SCIENTIFIC RESEARCH

Conducted by the
Universal Energy Systems, Inc.

FINAL REPORT

ENCODING IN LESS THAN 100 MILLISECONDS DEMONSTRATED USING
A REACTION TIME TASK

Prepared by:	Terence M. Hines
Academic Rank:	Assistant Professor
Department and	Psychology Department
University:	Pace University, Pleasantville, NY
Research Location:	AFHRL, Williams AFB, AZ
USAF Researcher:	Don Lyon
Date:	September 15, 1987
Contract No.:	F49620-85-C-0013

ENCODING IN LESS THAN 100 MILLISECONDS DEMONSTRATED USING

A REACTION TIME TASK

by

Terence M. Hines

ABSTRACT

The encoding task of Posner and Boies (1971) was modified to allow the examination of the build up of information in short (117 msec. or less) intervals following stimulus presentation. Significant encoding was demonstrated as early as 67 msec. post stimulus onset. This result shows that the Posner and Boies (1971) task is a useful and valid measure of the time course of encoding even at very short intervals following stimulus presentation. An additional issue investigated was whether there are age differences in the time course of encoding. No evidence for such age differences was found.

Acknowledgements

I wish to thank the Air Force Systems Command and the Air Force Office of Scientific Research for sponsorship of this research. Universal Energy Systems must be mentioned for their concern and help to me in all administrative and directional aspects of this program. I also want to thank Drs. Don Lyon, Elizabeth Martin, and Mary Lou Cheal for their help, guidance and comments. Special thanks are due Chris Voltz who wrote the program that ran the experiment reported herein.

I. INTRODUCTION:

When a stimulus is presented it automatically begins to activate its representations in memory (Posner, 1978). In terms of Morton's (1969, 1979) logogen model, information about the stimulus begins to build up in the appropriate logogen(s). This process of information build up continues over time, more information accruing as the longer the stimulus is present. Posner and Boies (1971) have termed this build up of information "encoding". The use of the term encoding in this context does not imply any permanent storage of information about the stimulus in the memory system. It refers only to the process of the build up of information which, depending on the circumstances, may or may not be followed by more permanent storage.

A question of considerable theoretical interest is how quickly information builds up following stimulus presentation and whether it builds up at different rates for different types of stimuli. Posner and Boies (1971) developed a methodology that permits the study of such questions. In their method, a subject is presented with a pair of visual stimuli and must decide whether the two members of the pair are the same or different. The time between the onset of the two stimuli in a pair, termed stimulus onset asynchrony (SOA) is varied. The dependent measure is reaction time, which is measured from the onset of the second stimulus in each pair. Since both stimuli must be encoded before a correct response can be made, as SOA increases, reaction time (RT) decreases. This occurs because longer SOAs permit more information about the first stimulus in the pair to build up before the second member of the pair is presented. In the limiting case, an SOA of zero (simul-

taneous presentation), both stimuli must be encoded before a decision can be made. Longer SOAs permit part or, if long enough, all of the encoding of the first stimulus to be done before the second appears. Since RT is measured from the onset of the second stimulus, processing that takes place before the second stimulus appears will not contribute to RT. At some time, X, after presentation of the first stimulus its encoding will be complete. Giving additional time, in the form of SOAs greater than X, will not further reduce RT as the system is simply waiting for the presentation of the second stimulus and no longer accumulating information about the first. Thus, the SOA at which the function relating RT to SOA reaches asymptote is a measure of the time taken to fully encode the first stimulus.

II. OBJECTIVES OF THE RESEARCH EFFORT:

In their initial study Posner and Boies (1971) used SOAs of 0, 150 and 500 msec. and found that the encoding function had asymptoted by 150 msec. As far as is known, no investigators have used SOAs of less than 150 msec. in this paradigm. However, evidence from other paradigms indicates that encoding can take place in less than 150 msec., perhaps considerably less. Fischler and Goodman (1978) used a lexical decision task and found evidence of what is termed encoding in this report as little as 40 msec. following presentation of a word stimulus. In the electrophysiological literature cortical evoked potentials have been found, in both humans and animals, at 90 to 100 msec. following stimulus onset. These findings suggest that there can be enough build up of information to influence RT or evoked potentials at intervals of less than 150 msec. It does not necessarily indicate that this build up represents the completion of encoding by such short intervals.

If the paradigm developed by Posner and Boies (1971) is a valid and accurate measure of the time course of the build up of information following stimulus presentation, it should be able to demonstrate such build up at SOAs of less than 150 msec. The present experiment was designed to examine this question.

III. METHOD:

Subjects. Subjects were 25 professional laboratory and support personnel from the Air Force Human Resources Laboratory at Williams Air Force Base who volunteered to participate in the study. They ranged in age from 21 to 68 years. The mean age was 39 years.

Apparatus. Subjects sat in front of an XX inch closed circuit television monitor which was used for stimulus presentation. Subjects sat in front of the screen but not at any fixed distance. They were allowed to adjust their distance from the screen to what was the most comfortable viewing distance. Responses were made by pressing one of two buttons on a response box subjects held in front of them. The left button was to be pressed to indicate a "same" response. The right button was to be pressed to indicate a "different" response. Subjects were instructed to respond as fast as possible but to be as accurate as possible. Control of stimulus presentation and response recording was handled on-line by an IBM compatible AT computer.

The stimuli consisted of pairs of upper case letters. A trial began when a visual warning signal in the form of a plus sign ("+") was displayed at the center of the screen. This was followed 501 msec. later by the first letter, which was presented slightly to the left of the plus. After a random SOA the second letter was presented to the right of the plus. SOAs of 0, 33, 67, 88 and 117 msec. were used.

Both the plus and the letter pair remained on the screen until the subject made his or her response. The screen was then blanked and feedback about the speed and accuracy of the response was displayed. The feedback consisted of the reaction time and the word "CORRECT" or "INCORRECT" as appropriate. The feedback was displayed for 1000 msec. There was then a blank 752 msec. intertrial interval before the presentation of the plus sign that signaled the beginning of the next trial. There were 30 practice trials followed by 300 actual trials. On half the trials the letters in a pair were the same and on half the letters were different. Since there were five different SOAs, this resulted in 10 different trial types, same and different pairs for each of the five SOAs. These ten trial types were randomly distributed over the course of the experiment with the restriction that 15 of each type occur in the first 150 non-practice trials and in the second 150 non-practice trials. The letters used were all the letters of the alphabet except the vowels and "Y". Reaction times of over 1000 msec. were excluded from data analysis, as were error responses.

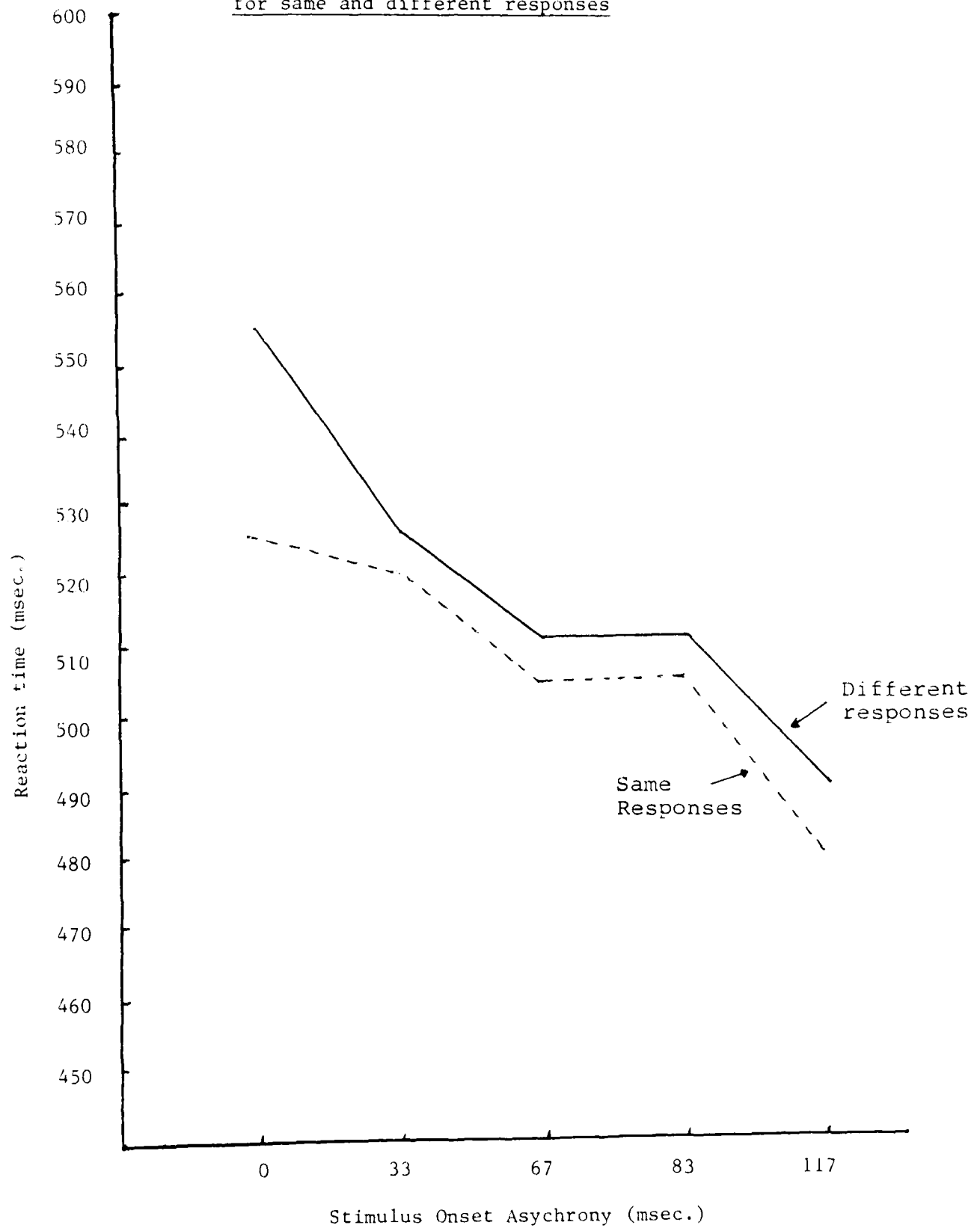
IV. RESULTS:

The results are shown graphically in Figure 1. A two way analysis of variance with both SOA and Response Type (same vs. different) as within subject factors revealed a significant main effect of SOA ($F(4, 96) = 39.04, p < .001$) and an insignificant effect of Response Type ($F(1, 24) = 3.17; p = .084$). The interaction between the two factors did reach significance ($F(4, 96) = 3.57; p = .009$).

Because the ANOVA reported above includes data from both same and different trials, it can not be used to reach conclusions

FIGURE 1.

Reaction time as a function of SOA
for same and different responses



about the time course of encoding. This is because reaction times on different trials are a function of two factors. One is the amount of information that has built up about the first stimulus in the pair. If this were the only factor operating, there would be no problem in using different trials to determine the time course of encoding. However, because internal noise is much more likely to make two same stimuli appear different than it is to make two different stimuli appear to be the same, subjects engage in a rechecking procedure much more frequently on different than on same trials (Kruger, 1978; Kruger and Shapiro, 1982). This rechecking procedure probably also varies as a function of SOA, subjects being more likely to recheck at short than at long SOAs. Because of this confounding of the different RTs with a non-encoding process, it is best to use only the RTs from same trials to plot an encoding function (see Hines, Poon, Cerella and Fozard, 1982 for further discussion). Thus, a one way ANOVA with SOA as the single, within subjects, factor was performed on the mean RTs for same trials. These means are shown in Table 1. There was a significant main effect of SOA ($F(4, 96) = 20.15; p < .001$). The main effect only indicates that RT dropped as SOA increased. It does not indicate which SOAs were different from one another. To determine this a Tukey Test was performed. With a df of 96 and an r of 5, the critical difference between means needed to reach the .01 level of significance was 19 msec. The critical difference at the .05 level was 15 msec. Using these critical differences, there is not a significant drop in RT from 0 to 33 msec. SOA. There is a significant drop from 33 to 67 msec. SOA. Thus, some encoding has

taken place as soon as 67 msec. following the presentation of the first stimulus. Encoding continues after 67 msec., however. This is seen in the significant further drop in RT between the 67 and the 117 msec. SOAs.

TABLE I

	SOA (msec.)				
	000	33	67	83	117
Mean RT (msec.)	526	521	505	506	481

Another issue was addressed in the present experiment, the issue of age differences in the time course of encoding. Hines, Poon, Cerella and Fozard (1982) used an encoding paradigm with SOAs of 0, 250, 500, 750 and 1000 msec. and reported finding a small but significant slowing of encoding in their elderly subjects. Because the subjects in the present experiment spanned a wide range of ages, it was possible to analyze the data for age effects. To do this another ANOVA was run on only the same responses but with age added as a between subjects variable. Age was dichotomized with one group (N = 13) consisting of all subjects below age 40 and the other group (N=12) consisting of all subjects aged 40 or above. The mean ages of these two groups were 28 and 51, respectively. The ANOVA revealed a main effect of SOA ($F(4, 92) = 20.56$; $p < .001$) and a main effect of Age ($F(1, 23) = 9.66$; $p = .005$) but no interaction between these two factors ($F(4, 92) = 1.35$; $p = .257$). The lack of an interaction indicates that the functions relating RT and SOA were parallel for both age groups. That is, RT dropped as a function of SOA at the same rate for both groups. Thus, information was building up in the memory systems of both groups at the same rate and there was no difference in encoding speed.

V. RECOMMENDATIONS:

The results of the present experiment demonstrate that the encoding paradigm developed by Posner and Boies (1971) is sensitive to build up of information that takes place at sub-100 msec. intervals following stimulus presentation. A significant decline in RT was found 67 msec. following stimulus presentation. This finding is in line with findings from other paradigms reviewed briefly in section II that showed early build up or presence of information. It is possible that the encoding paradigm could demonstrate build up of information even earlier than 67 msec. but it was not possible, because of the hardware used, to examine SOAs between those used. Nonetheless, the present results help to validate the encoding paradigm as a useful tool in examining factors affecting the speed of build up of information. The results dovetail nicely with those of Hines (1987) that show that the encoding task is sensitive to changes in the cognitive and perceptual aspects of a task, but not to its motor aspects. Hines (1987) showed that a manipulation, visually degrading a stimulus, known to slow encoding does result in an encoding slowing as indicated by the encoding function relating RT to SOA. The encoding function is also altered by the specific nature of the cognitive task the subject must perform. Encoding was faster when subjects had to decide whether two words were physically the same (ROBIN ROBIN) than when the decision required a category level decision (ROBIN SPARROW). The encoding function is not sensitive to motoric aspects of the task. Although increasing the probability of a same response resulted in overall faster RTs for same than for different responses, this manipulation did not change the speed of encoding in conditions

where same responses were common (70%) or rare (30%).

The results of the present experiment also have implications for the study of aging. As noted above Hines, Poon, Cerella and Fozard (1982) did find a small slowing of encoding in their elderly subjects. No such slowing was found in the present study. Of the several differences between these two studies, one stands out as the most likely reason for the difference in findings. In the Hines et al. (1982) study, the two age groups differed to a greater degree in age than they did in the present study. Hines et al. (1982) used a young group with a mean age of 21 and an older group with a mean age of 71. They also had more subjects (22 and 27, respectively) in each group than were used in the present experiment. These differences gave the Hines et al. (1982) experiment greater power to detect small differences.

REFERENCES

- Cowey, A. (1985). Aspects of cortical organization related to selective attention and selective impairments of visual perception: A tutorial review. In M. Posner and O. Marin (Eds.), Attention and performance XI. Hillsdale, NJ: Erlbaum, pp. 41-62.
- Fischler, I., and Goodman, G. (1978). Latency of associative activation in memory. Journal of Experimental Psychology: Human Perception and Performance, 4, 455-470.
- Hines, T. (1987). Do changes in stimulus-onset-asynchrony manipulate what we think they do? Paper presented at the first annual Cognitive Aging Conference, Atlanta, GA, 1987.
- Hines, T., Poon, L., Cerella, J., and Fozard, J. (1982). Age-related differences in the time course of encoding. Experimental Aging Research, 8, 175-178.
- Kruger, L. (1978). A theory of perceptual matching. Psychological Review, 85, 278-304.
- Kruger, L., and Shapiro, R. (1982). Search for a matching of mismatching letter pair. Perception and Psychophysics, 31, 484-492.
- Morton, J. (1969). Interaction of information in word recognition. Psychological Review, 76, 165-178.

Morton, J. (1979). Facilitation in word recognition: Experiments causing changes in the logogen model. In P. Kolars, W. Wrolstad, and M. Bouma (Eds.), Processing of visible language, vol. 1. New York: Plenum, pp. 259-268.

Posner, M. (1978). Chronometric explorations of mind. Hillsdale, NJ: Erlbaum.

Posner, M., and Boies, S. (1971). Components of attention. Psychological Review, 78, 391-408.

1987 USAF-UES SUMMER FACULTY RESEARCH PROGRAM
GRADUATE STUDENT SUMMER SUPPORT PROGRAM

Sponsored by the
AIR FORCE OFFICE OF SCIENTIFIC RESEARCH

Conducted by the
Universal Energy Systems, Inc.

FINAL REPORT

NITRATED HETEROCYCLIC COMPOUNDS: A SYNTHETIC

STUDY

Prepared by:	Albert Hirschberg, Ph.D.
Academic Rank:	Professor
Department and	Chemistry
University:	Long Island University
Research Location:	FJSRL/NC Air Force Academy Colorado Springs, Colorado 80840-6528
USAF Researcher:	Capt. Jon Swanson
Date:	August 11, 1987
Contract No:	F49620-85-C-0013

Nitrated Heterocyclic Compounds: A Synthetic
Study

by

Albert Hirschberg

ABSTRACT

Laboratory syntheses of 1,2,4-triazolin-3-one, 2-imidazolone-4-carboxylic acid, and 2-imidazolone are described. Attempts at converting these compounds to nitro derivatives are also described.

The characterization of 5-nitro-1,2,4-triazolin-3-one and its potassium and ammonium salts was carried out to resolve the mass spectrum anomaly demonstrated by the parent compound.

3,6-Diamino-1,2,4,5-tetrazine was synthesized and oxidation of the amino groups to yield 3,6-dinitro-1,2,4,5-tetrazine was attempted.

Acknowledgements

I wish to thank the Air Force Systems Command and the Air Force Office of Scientific Research for sponsorship of this work. The warm reception by the staff of the Frank J. Seiler Chemical Research Laboratory where this work was performed is also gratefully acknowledged.

I particularly wish to thank Major Stephen Lander, Laboratory Director, and Major Kenneth M. Dieter, Deputy Director, for their warm hospitality and cooperation. The help, direction, and background material provided by Capt. Jon Swanson is greatly appreciated. Thanks also to Mr. Lloyd Pflug and Mr. Fred Kibler for their help in making my laboratory experience productive. Finally, I would like to thank Dr. Norman Heimer, a URRP Fellow, returning to the University of Mississippi after a two year stay at the Seiler Laboratories. Dr. Heimer's invaluable help in solving various logistical and technical problems contributed greatly to every aspect of this research project.

I INTRODUCTION

One of the aims of the Energetic Materials Division of the Seiler Research Laboratories has been the synthesis and study of organic compounds containing nitro groups as potential explosives or propellants.

The prediction as to which nitro derivatives have promise as high energy materials has been studied on a theoretical basis at the Seiler Laboratories by means of molecular orbital calculations and computer modeling, which allow for estimation of heats of reaction, bond energies, and detonation pressures and velocities. This information, coupled with the study of reaction mechanisms and kinetic determinations, has led to an interest in the synthesis of heterocyclic nitro derivatives as models for confirmation of theoretical predictions as well as serving as a source of materials which may have practical use.

Some of my research interests have been in the area of heterocyclic synthesis and nitrations. These interests accordingly, contributed to my being selected for the SFRP program and assigned several projects involving synthesis of potential high energy heterocyclic nitro compounds.

II OBJECTIVES

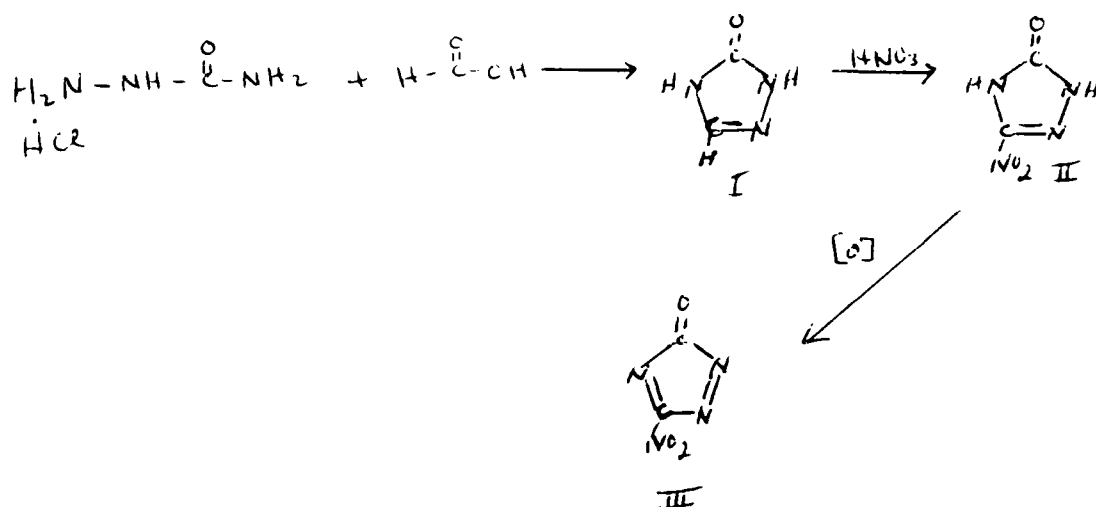
My assignment in the Summer Faculty Research Program

for 1987, at the Seiler Chemical Research Laboratories (FJSRL/NC) was to synthesize potentially useful heterocyclic nitro compounds. These would possibly be useful high energy materials, and would also serve as compounds for verification of theoretical predictions based on structural elements possessed by these substances. Accordingly, the synthesis of several nitro heterocyclic compounds was to be attempted, involving the preparation of 5-nitro-1,2,4,-triazolin-3-one and its oxidation products, nitro derivatives of 2-imidazolone, and 3,6-dinitro-1,2,4,5-tetrazine.

III 5-NITRO-1,2,4-TRIAZOLIN-3-ONE

5-Nitro-1,2,4,-triazolin-3-one II, while known¹, was needed for confirmation of some theoretical calculations, and also presented some literature discrepancies regarding its melting point behavior which we hoped to resolve. Oxidation of II to its "dehydro" derivative III, was also to be attempted.

In order to prepare II, the synthesis of 1,2,4-triazolin-3-one I, from semicarbazide hydrochloride and formic acid, in a modification by Lee and Coburn², of a procedure reported in the Russian literature³, was carried out. Nitration of I using 90% nitric acid (d. 1.95) as also described by Lee and Coburn², yielded II.



The melting point behavior of II confirmed the previous report¹ that the compound melted at various temperatures depending on the rate of heating. In our experience, no melting was observed up to a temperature of 360°, if the melting point was taken very slowly, although the compound did darken and presumably decompose. Examination of the melting point capillary revealed deposition of material on the cooler portions of the capillary. A moderate rate of heating resulted in a melting point of 268-270° which compared reasonably well with that reported by the Russian workers³.

The mass spectrum of the nitro derivative II, revealed a parent ion peak of 130 consistent for the compound as well a mass ion peak of 85 which could be ascribed to some unreacted triazolin-3-one I, being present to the extent of about twenty percent. Several

recrystallizations from water did not change this value or the melting point of the product, but we were still not certain of the purity of the material.

HPLC analysis, using a U.V. detector, revealed only one peak. However, since I was subsequently shown to be transparent in the ultraviolet, while the nitro derivative II absorbed at 319 nm, the purity of the sample was still uncertain.

It was then decided to prepare the known ammonium² and potassium³ salts of the nitro-triazolin-3-one II. Since 1,2,4-triazolin-3-one I, did not form such salts, the formation of the salts free of the presumed triazolin-3-one I impurity would allow for isolation of the pure nitro derivative II, from the salts by treatment with acid.

Accordingly, the preparation of the ammonium and potassium was carried out to give substances whose melting points compared well with those reported^{2,3}. The proton and carbon-13 NMR data for the ammonium salt were consistent for those reported².

Liberation of the nitrotriazolin-3-one II, by treating each salt with dilute acid, afforded material whose spectral characteristics and melting point were identical to the original nitrated material. It thus appears that the original nitrated product, although possessing a curious mass spectrum, is pure. In light

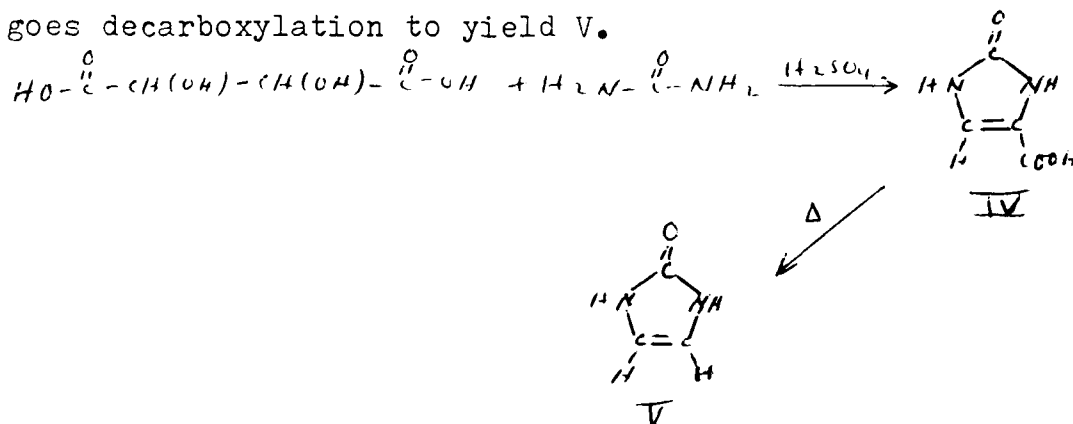
of the strange melting and decomposition behavior of this substance, the mass spectral anomaly is perhaps, not surprising.

Attempts to oxidize II to the "dehydro" derivative III, a compound of theoretical and practical interest, was attempted using several oxidizing agents, such as 3% H_2O_2 , 45% H_2O_2 , Br_2 in H_2O , and Iodine. In each case either unreacted starting material was obtained or decomposition occurred.

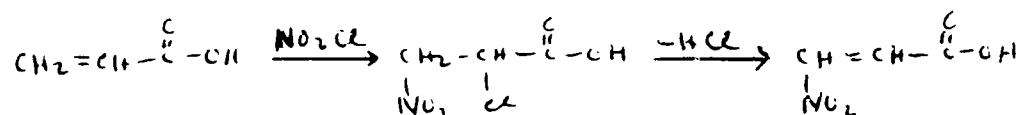
IV NITRO DERIVATIVES OF 2-IMIDAZOLONE

Nitro derivatives of 2-imidazolone V, represent compounds closely analogous to the nitrotriazolin-3-one II, and for purposes of comparison should be of some interest.

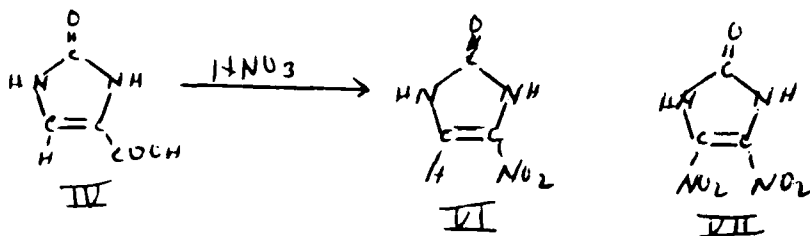
Accordingly V was to be synthesized following the procedure described by Hilbert⁴, which involved treating tartaric acid with fuming sulfuric acid and urea to yield 2-imidazolone-4-carboxylic acid IV, which undergoes decarboxylation to yield V.



First attempts at nitration involved treating IV with nitryl chloride, NO_2Cl ⁵, in the hope that IV would undergo an addition-elimination reaction across the double bond conjugated with the carboxyl group in a manner similar to that reported for acrylic acid⁶. Due largely to the low temperatures required and the insolubility of IV in the reagent, no reaction occurred.



Nitration of IV was then attempted using fuming nitric acid, nitric acid-sulfuric acid mixtures, and nitric acid in glacial acetic acid. It was hoped that nitration and decarboxylation would occur leading to the mononitro VI, or dinitro VII derivatives.

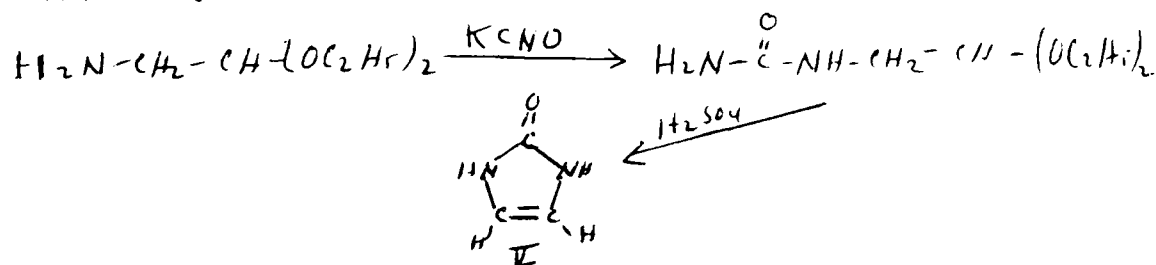


In all cases only a few milligrams of tacky, oily material was obtained which could not be characterized.

While the preparation of 2-imidazolone-4-carboxylic acid IV, and subsequent decarboxylation to 2-imidazolone V, was successful, it was not the most convenient method of preparation due to the long and tedious nature of

the steps involved and the overall small yield obtained.

Accordingly, a somewhat more convenient method of preparing V was carried out which involved treatment of aminoacetaldehyde diethyl acetal with potassium cyanate to produce ureidoacetal VIII. Subsequent treatment of this product with dilute sulfuric acid afforded 2-imidazolone V⁷.



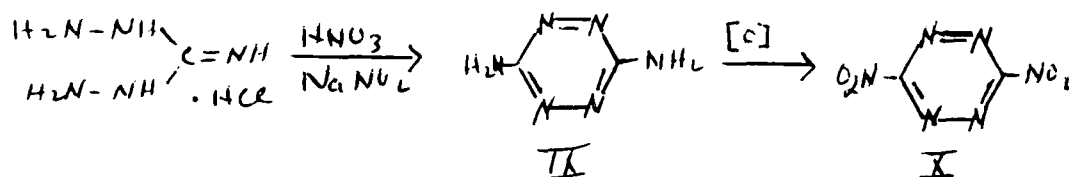
Since V has been reported to undergo Friedel-Crafts acylation⁷, a typical aromatic substitution process, it was hoped that nitration of V would also be successful. Unfortunately, all attempts at nitration using a variety of nitrating mixtures, led only to decomposition of the starting material.

V 3,6-DINITRO-1,2,4,5-TETRAZINE

3,6-Dinitro-1,2,4,5-tetrazine X, is another compound which would appear to be of potential interest for theoretical as well as practical reasons. X was to be synthesized by the attempted oxidation of 3,6-diamino-1,2,3,5-tetrazine IX.

The diamine IX, was synthesized by a modification of a procedure reported by Lin, Lieber, and Horwitz⁶,

which involved the treatment of a dilute nitric acid solution of 1,3-diaminoguanidine hydrochloride with dilute sodium nitrite solution, which yielded the diamine IX, in about 10% yield. Attempts to oxidize IX using 30% H_2O_2 mixed with 30% fuming H_2SO_4 ⁹ were unsuccessful, leading only to decomposition.



VI EXPERIMENTAL DETAILS

1,2,4-Triazolin-3-one I- To 45 ml of 85% formic acid was added 46.03 g (0.39 mole) of semicarbazide hydrochloride slowly with stirring. After the addition was complete the mixture was refluxed for five hours after which, the mixture was distilled and concentrated to about one half volume. Water (50ml) was then added and the mixture was distilled until about 70 ml of distillate was collected. The material in the distillation flask was then chilled and the resulting precipitate filtered, and dried in an oven at 95°C overnight. The material was recrystallized from ethanol yielding 24.4 g (70%) of product, which melted at 234-236°C. Lit.² 234-235°C.

5-Nitro-1,2,4-triazolin-3-one II- To a mixture of 8 ml of H_2O and 17 ml of 90% HNO_3 (d 1.49) at 50°C was added slowly 7.82 g (0.09 mole) of 1,2,4-triazolin-3-

one I, with stirring. The temperature was maintained at 50°C as addition progressed by careful heating on a hot plate. After the addition was complete, the mixture was heated to 80°C, at which time brown fumes were given off and the mixture continued boiling even after removal from the hot plate. After a period of time a heavy white precipitate formed. Ice water (10 ml) was then added and the mixture filtered. The precipitate was then washed with two 10 ml portions of ice water and the remaining solid was recrystallized from water to yield 7.39 g (67%) of product melting at 268-270°C. Lit.³ 265-268°C. NMR: Observed- ¹H NMR (DMSO-d6) 12.76 ppm and 10.92 ppm. Lit.² 12.7 ppm. Observed- ¹³C NMR (DMSO-d6) 147.96 ppm. and 154.37 ppm. Lit.² 148.0 ppm. and 154.4 ppm.

Ammonium salt of 5-nitro-1,2,4-triazolin-3-one-

To a solution of 1.30 g (0.01 mole) of 5-nitro-1,2,4-triazolin-3-one II, in 40 ml of methanol was added 1 ml of 30% ammonium hydroxide. Evaporation of the solvent yielded 1.47 g (100%) of the ammonium salt melting at 195-197°C. Lit.² 190°C. NMR: Observed- ¹³C NMR (DMSC-d6) 159.58 ppm. and 164.94 ppm. Lit.² 159.4 and 164.6 ppm. One gram of the ammonium salt (0.006 mole) was dissolved in 40 ml of water and the resulting solution was acidified with 12N HCl to a pH of 2. Chilling of the solution yielded 0.24 g (30%) of 5-nitro-1,2,4-

triazolin-3-one II, melting at 267-269°C. Lit.³ 265-268°C.

Potassium salt of 5-nitro-1,2,4-triazolin-3-one-

To a solution of 1.30 g (0.01 mole) of 5-nitro-1,2,4-triazolin-3-one II, in 30 ml of 95% ethanol was added 10 ml of ethanol containing 0.66 g of potassium hydroxide. The resulting yellow precipitate obtained weighed 1.64 g (98%) and melted at 232-234°C. Lit.³ 228-230°C. The free nitro-triazolin-3-one was obtained from the potassium salt in the same manner as described above for the ammonium salt.

2-Imidazolone-4-carboxylic acid IV- To 80 ml of 15% fuming sulfuric acid at 0°C was slowly added 22.2 g (0.15 mole) of tartaric acid with stirring. The temperature was kept below 10°C during the addition.

The ice bath was then removed and 20 g (0.33 mole) of urea was added, during which time the temperature rose to 70°C. By use of a heating mantle the temperature of the mixture was maintained at 80°C and the mixture bubbled vigorously and turned black. After all bubbling ceased the mixture was poured onto 250 g of ice and chilled overnight in a refrigerator. Filtration yielded a dark brown solid which was recrystallized from a large quantity of water using decolorizing carbon, to yield 3.48 g of the product (18%) as a whitish yellow solid melting at 247-249°C. Further recrystallization

from water, using carbon, yielded a white solid which melted at 255-257°C. Lit.⁴ 260-261°C. The product from the first recrystallization was essentially pure enough for further use.

Ureidoacetal VIII- To a mixture of 35 g (0.26 mole) of aminoacetaldehyde diethylacetal and 55 g of crushed ice was 53 ml of 5N HCl (0.26 mole) previously cooled to -40°C. Immediately afterward a solution of 32 g (0.39 mole) of potassium cyanate in 70 ml of water was added, and the mixture refluxed for 90 minutes. After cooling, the solution was evaporated under vacuum to 75 ml and then chilled to yield 37.60 g of product (82%) melting at 109-110°C, pure enough for the next step to 2-imidazolone V. Lit.⁷ 107-108°C.

2-Imidazolone V- (Procedure A): 2-Imidazolone-4-carboxylic acid IV (1.00 g, 0.008 mole) was decarboxylated by sublimation at 240°C and 0.5 torr, to yield 0.21 g (31%) of 2-imidazolone V, which melted at 240-245°C. Lit.⁷ 243-245°C.

2-Imidazolone V- (Procedure B): To a solution of 9.37 g (0.053 mole) of ureidoacetal VIII, in 150 ml of water was added 0.49 g (0.01 equiv.) of concentrated sulfuric acid. The mixture was allowed to stand at room temperature for 72 hours after which time enough solid barium hydroxide octahydrate was added to bring the pH of the resulting solution to about 7. The barium

sulfate precipitate was filtered from the solution and the resulting clear filtrate was concentrated, under vacuum, to about 40 ml and then chilled to yield 1.24 g of product melting at 245-248°C. A second crop yielded 1.53 g of product melting at 248-253°C. The combined yield was 62%. Further purification was not necessary but could be effected by sublimation.

3,6-Diamino-1,2,4,5-tetrazine IX- To a solution of 4.8 g (0.038 mole) of 1,3-diaminoguanidine hydrochloride in 50 ml of 1N HNO₃, was added dropwise with stirring, over a period of about five hours, a solution of 5.5 g of sodium nitrite in 50 ml of water. The resulting reddish mixture was chilled in a refrigerator over night and 0.21 g of a red solid collected. The mass spectrum of the solid indicated a molecular weight of 112, consistent for the product, which did not melt up to a temperature of 355°C. The yield was 10%.

VI RECOMMENDATIONS

A thorough study of the thermal decomposition products from 5-nitro-1,2,4-triazolin-3-one II, should be undertaken in light of the unique melting point and decomposition behavior this compound demonstrates.

Those nitrations and oxidations that were unsuccessful should be more fully investigated as they may be successful under different sets of conditions.

Time constraints also precluded investigating several other combinations of reagents leading to oxidation and nitration.

Some thoughts might be given to synthesizing nitro heterocyclics by using condensation techniques involving nitro group containing reactants such as nitrourea and nitroguanidine derivatives.

REFERENCES

1. A. Nanchot and G. Noll, Ann., 343, 24 (1905).
2. K. Lee and M.D. Coburn, Tech. Report, LA-10302-MS, Feb. 1985.
3. G. Cipens, R. Bokaldser, and V. Grinsteins, Khim. Geterosikl. Soedin., 1, 110 (1966). Chem. Abst., 65, 705 (1966).
4. G.E. Hilbert, J. Amer. Chem. Soc., 54, 3414 (1932).
5. Kindly supplied by Dr. Charles Bump, a fellow SFRP participant.
6. H. Schechter, F. Conrad, A.L. Daulton, and R.B. Kaplan, J. Amer. Chem. Soc., 74, 3052 (1952).
7. R. Duschinsky and L.A. Dolan, J. Amer. Chem. Soc., 68, 2350 (1946).
8. C.H. Lin, F. Lieber, and J.P. Horwitz, J. Amer. Chem. Soc., 76, 427 (1954).
9. R.H. Wiley and J. Hartman, J. Amer. Chem. Soc., 73, 494 (1951).

1987 USAF-UES SUMMER FACULTY RESEARCH PROGRAM/
GRADUATE STUDENT SUMMER SUPPORT PROGRAM

Sponsored by the
AIR FORCE OFFICE OF SCIENTIFIC RESEARCH
Conducted by the
Universal Energy Systems, Inc.

FINAL REPORT

A HUMAN FACTORS APPROACH
TO THE PROCESS OF DEVELOPING
THE ADVANCED
METEOROLOGICAL PROCESSING SYSTEM

Prepared by:	Robert R. Hoffman, Ph.D.
Academic Rank:	Associate Professor
Department and	Department of Psychology
University:	Adelphi University
Research Location:	Air Force Geophysics Laboratory Atmospheric Prediction Branch Atmospheric Sciences Division
USAF Researcher:	Mrs. Rosemary Dyer
Date:	27 July 1987
Contract No.:	F49620-85-0013

A HUMAN FACTORS APPROACH
TO THE PROCESS OF DEVELOPING
THE ADVANCED
METEOROLOGICAL PROCESSING SYSTEM

by
Robert R. Hoffman

ABSTRACT

This is a report on the process used in deriving design specifications for the Advanced Meteorological Processing System (AMPS). The AMPS project has as a goal the development of a workstation environment for the support of meteorological forecasting and research. A major aspect of the AMPS project will be the attempt to integrate Artificial Intelligence (AI) techniques with forecasting procedures. The process used in deriving design specifications involved reliance on human factors principles, structured interviews with meteorologists, and observations of forecasting deliberations. The resulting specifications involve such things as the design of a "user friendly" interface and an answer to the question of how many video displays the workstation will need in order to support the activities of meteorologists. A number of recommendations also derived from this work, involving the follow-up research that will be needed to refine the design specifications, and the qualifications of the support personnel who will be needed to carry out the development phase of the AMPS project.

ACKNOWLEDGMENTS

This work was supported by the US Air Force Office of Scientific Research, Summer Faculty Research Program. I would like to thank, and congratulate, Mr. Rodney Darrah and the people at Universal Energy Systems, Inc., for their highly effective management of the Program. Mr. A.S. Jursa and Dr. Agnes Bain served as the AFGL coordinators for the SFRP and were very helpful in a number of ways.

Special thanks go to Mrs. Rosemary Dyer and Mr. Donald Chisholm of the Atmospheric Prediction Branch of the AFGL. Mr. Chisholm, the Branch Chief, was very supportive and amiable, and it was a real pleasure to work under his guidance. My efforts involved close interaction with Mrs. Dyer, and I regard the opportunity to work with her as a distinct privilege.

Thanks also to the AFGL meteorologists and researchers whose expertise and patience enabled me to develop the design specifications for AMPS: Dr. Al Bohne, Mr. Robert d'Entremont, Dr. Ralph Donaldson, Lt. Jerry Freeman, Lt.Col. Gordon Hammond, Mr. Arthur Jackson, Mr. Thomas Kleespies, Dr. Stuart Muench, Mr. Keith Roberts, and Dr. Larry Thomason.

Finally, I would like to express my appreciation to the Commander and all the administrators at the AFGL, for providing an atmosphere in which important basic meteorological research can be conducted, and for their openness to the contributions that can be made by experimental psychologists.

I. INTRODUCTION

Human factors psychology is concerned with the design of man-machine systems in such a way as to make the machine fit with the skills and abilities of the human operator. The human factors approach involves applying methods from experimental psychology in order to assess operator characteristics and to bring design specifications in line with those characteristics.

The Atmospheric Prediction Branch of the Air Force Geophysics Laboratory (AFGL) is just beginning to design the "Advanced Meteorological Processing System" (AMPS), which will be a workstation environment that can support a number of related activities: (1) Networked forecasting, (2) Single station forecasting, (3) Meteorological research, (4) Artificial Intelligence-based use of weather data and data sources, to assist in the proper interpretation of data, and for the integration of new data types into forecasting and research operations.

Human factors psychology can provide useful input with regard to the design of the workstation and the design of the AI component of AMPS. As an experimental psychologist with an interest in meteorological remote sensing (Hoffman, 1987a), and with some experience in the development of AI systems (Hoffman, 1987b), I attempted to contribute to the initial stages of AMPS development by spelling out some of the relevant human factors considerations.

II. OBJECTIVES OF THE RESEARCH EFFORT

The main purpose of this effort was to provide guidance for the process of developing the AMPS, in the form of design specifications. Furthermore, since the AMPS will be a highly complex system, there will have to be an overall design strategy or guiding philosophy, according to which the separate components are researched and designed in an integrated way. An alternative would be to design the system piecemeal, which for a system of the complexity of AMPS would almost certainly result

NO-A191 284

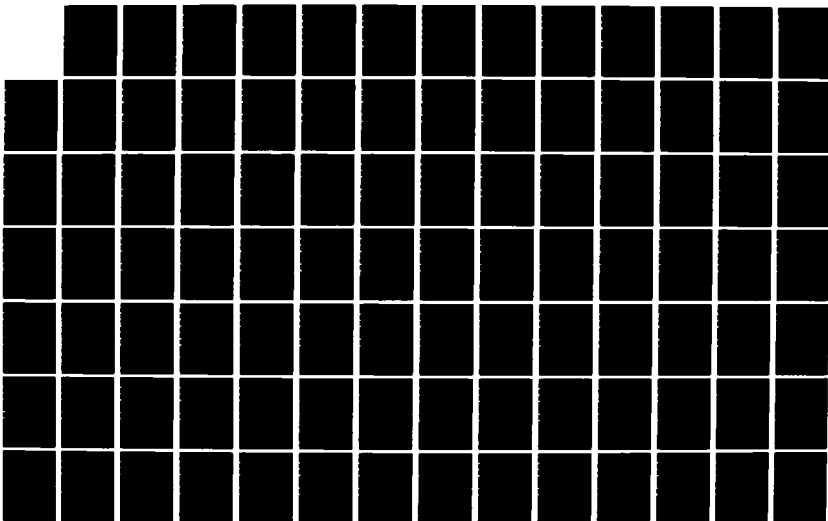
UNITED STATES AIR FORCE SUMMER FACULTY RESEARCH PROGRAM
(1987) PROGRAM TE (U) UNIVERSAL ENERGY SYSTEMS INC
DAYTON OH R C DARRAH ET AL DEC 87 AFOSR-TR-88-0213
F49620-85-C-0013

4711

UNCLASSIFIED

F/G 5/1

NL



THE FOLLOWING RESULTS ARE THEOREMS OF THE AUTHOR

In problems when the various components get put together.

In the following sections of this Final Report I describe the human factors principles that form the guiding design philosophy, I describe the research method I used in deriving the detailed design specifications, and then I provide some examples of the specifications. The Report concludes with some recommendations and ideas about the research that will be needed to develop the AMPS.

III. THE HUMAN FACTORS APPROACH TO SYSTEM DESIGN

According to Monk (1985), the factors that significantly contribute to workload in workstation-like environments are: (a) The display of information in a form the user cannot work with, (b) The display of too much information, (c) The display of insufficient information, (d) The display of irrelevant information, and (e) The display of important information in the wrong places. These are all "human factors," and all relate to the display and processing of information.

It is sometimes assumed that human factors considerations are not significant relative to engineering considerations. It is typically assumed that human factors considerations, when they are important, can be easily taken into account after a system has been engineered and built. For instance, in the Boston Area NEXRAD Demonstration (Forsyth, et al., 1985), it was asserted that "interpretation of products is expected to be mostly a problem of training and not one of . . . display" (p.7).

This design strategy can result in specifications for a system with inherent weaknesses, requiring some "backpedaling." For example, here is a passage from Giraytys' (1975) report on the AFOS (Automation of Field Operations and Services) workstation. After building the system, it was given a trial run, and then the participating meteorologists were then given a questionnaire:

"Most of the negative reactions concerned the layout of the workstation controls. The elements

of the forecaster console (function keyboard, graphic displays, etc.) had been studied extensively from the human factors standpoint . . . However, the forecasters' work procedures had not been documented as extensively. As a result, several design changes were recommended (p.113) [emphasis added].

The designers had not begun their design process with an empirical characterization of exactly what meteorologists do and what their needs are. It turned out that what the designers thought the meteorologists needed was not always what the meteorologists actually needed or wanted. AFOS has small CRT displays, restricted use of color, confusing command acronyms, and the need for users to type in many lines of commands in order to operate the system.

HUMAN FACTORS PRINCIPLE #1: The AMPS needs to be human-factored from the very beginning of the design process, taking both user needs and user capabilities into account.

Tapping into the available literature on human factors during the initial design phases is helpful, and can be critical. However, available principles are not sufficient. Research is necessary to refine available human factors design principles, to adapt them to the specific situation at hand, in this case, the needs of meteorological forecasters and researchers (Chisholm, et al., 1983). Thus, another principle that is axiomatic in human factors engineering (Buck, 1983) is:

HUMAN FACTORS PRINCIPLE #2: The design process should be based on a functional analysis of tasks, activities, and human-machine communication patterns.

Along with the increased use of information processing systems in meteorological forecasting, meteorologists have had to spend more time communicating with the information processing systems and less time doing actual forecasting:

"The volume of guidance can inundate the forecaster, who then has no time to properly assimilate the

information, let alone determine an optimal tailored forecast . . . the forecaster is the bottleneck. The computer is driving the man rather than vice versa" (Boehm, 1979, p.4).

The basic reason for the information processing systems is to accomodate the needs and capabilities of meteorologists, and to support their rapid understanding of the physical dynamics that underlie a given atmospheric situations. Thus,

HUMAN FACTORS PRINCIPLE #3: The AMPS system should be adaptable to human needs, and not the other way around.

HUMAN FACTORS PRINCIPLE #4: The AMPS system should optimize the user's activities and ability to do work.

Although humans are, in general, more adaptable than machines, both the machine and the human component of the AMPS system will have to adapt to one another. As is widely recognized in the human factors literature (Hutchingson, 1981), machines are good at processing, storage and display of data. People are good at perceiving and interpreting patterns, at generalizing and inferring, at dealing with the unexpected, and at making decisions. Thus,

HUMAN FACTORS PRINCIPLE #5: The workstation design should support the interaction of machine and human as a complementary pair, a single system that capitalizes on the capabilities of each component.

Over its development and operational phases, AMPS will have to be able to accomodate and manage new data and new data types, new user activities or tasks, new hardware, new software, new graphics, and new AI systems. While on the one hand the AMPS system will have to be very flexible,

HUMAN FACTORS PRINCIPLE #6: AMPS systems to be used in operational forecasting will have to be standardized in many ways, including graphics displays, user interfacing, and hardware.

The spirit of these six general human factors principles manifested in the detailed assumptions and design specifications

that resulted from my research.

IV. RESEARCH METHOD

The method used in deriving the design specifications was to begin by surveying the available literatures on workstation design and display design, and the relevant human factors literature. Especially helpful was Kelly & Sauer's (1985) report on the design of the US Air Force Advanced Integrated Workstation, and the Technology Systems, Inc. (1984) report on the specifications for the AFGL Meteorological Data Acquisition, Management, and Processing System.

The literature survey yielded a preliminary set of 148 assumptions and specifications. That preliminary set (plus nine Figures) was then used as the basis for "structured interviews" (Hoffman, 1987b) with meteorologists at the AFGL and at the AFGL Sudbury NEXRAD (NEXt generation weather RADar) installation. The interviews had three purposes: (1) To determine whether or not each of the assumptions and specifications was reasonable, (2) To generate refinements of the assumptions and specifications, and (3) To generate ideas about additional assumptions and specifications.

In all, ten meteorologists were interviewed. Most were research meteorologists, although three had previous experience in forecasting. In addition, three had extensive experience with meteorological information processing systems (i.e., hardware integration and software development). The interviewees went through the preliminary set of assumptions and specifications, commenting on each one. For some of the assumptions and design specifications, interviewees had no comments. For example, an operational forecaster with little experience with the details of information processing systems would be expected to have little to say about specifications for the information processing system's file structure. In general, however, agreement with the assumptions and specifications was very strong. Indeed, the most frequent responses were: "Yes, I

agree," "Absolutely essential," "Yes, definitely," "Yes, that is often overlooked," and "Yes, good idea." Table 1 presents a summary of the results in terms the number of agreement responses, disagreement responses, elaborative comments, and "no comment" responses.

TABLE 1

Summary of the results from the interviews. The total number of propositions involved was 148 times the ten interviewees (1,480). The percentages do not sum to 100 since a given response could be commented upon whether agreed with or disagreed with.

	NUMBER OF AGREEMENT RESPONSES	NUMBER OF DISAGREEMENT RESPONSES	NUMBER OF ELABORATIVE COMMENTS	NUMBER OF "NO COMMENT" RESPONSES
<u>TOTAL NUMBER</u>	1,352	62	384	66
<u>PERCENT OF TOTAL</u>	92.60	4.25	26.30	4.52
<u>AVERAGE (N = 10)</u>	135.20	6.20	38.40	6.60
<u>RANGE (N = 10)</u>	119-146	0-26	20-75	1-21

The overall high rate of agreement suggests that the initial set of assumptions and design specifications did indeed form a reasonable starting point. The interviews satisfied the goals stated above in that they also resulted in suggested

modifications of many of the assumptions and specifications.

Having introduced the goals of the AMPS project, the human factors approach to design, and the method used in generating the design specifications, I can now present some examples of the design specifications that resulted. (The full final set of set of specifications is too extensive to be presented here. It can be made available upon request.)

V. EXAMPLE DESIGN SPECIFICATIONS

Design specifications can be categorized in terms of their reference to one of the three main components of the AMPS: The Information Processing (IP) component, the graphics component, and the workstation itself.

The Information Processing and Artificial Intelligence Component

AMPS will need an advanced IP/AI system for rapid processing and efficient storage of data, and for the application of mathematical forecasting analyses. The IP/AI component of AMPS will have to serve as an effective "manager" of information and "intelligent assistant" to the user in that it will have to support the meteorologist's familiar methods and reasoning strategies. At the same time, AMPS should also encourage learning and refinement of the user's knowledge and activities.

It is now possible to create automated decision aids using methods from AI. Knowledge that is represented in the form of "if-then" rules and other logical forms, can be programmed, enabling the information processing system to operate as an "expert system." As has been demonstrated (GEOMET, 1987), such decision aids can be created that focus on important and recurring weather events of the kind that meteorologists and forecasters need to predict and analyze, such as fog, isolated severe storms, microbursts, wind shear, hail, precipitation, rain/snow line, temperature highs and lows, and lightning. The

AMPS IP component will have to contain an AI system, which will reason about synoptic-scale weather situations on the basis of a knowledge base of rules and facts gleaned from expert meteorologists.

Here are some examples of the design specifications for the AMPS IP component.

DESIGN SPECIFICATION: To facilitate development and maintenance, all AMPS IP systems should be designed in a "modular" fashion (Norman, 1984).

DESIGN SPECIFICATION: Most of the systems maintenance functions and hardware-dependent aspects of AMPS operation should be "invisible" to the user.

DESIGN SPECIFICATION: The AMPS interface should be "user friendly."

A friendly user interface is one that is designed on the basis of a functional analysis of the task domain in which the interface is embedded. A friendly user interface makes system operation (i.e., sequences of prompts, commands, inputs, etc.) approximate a natural dialog. Indeed, the more that the human-machine interactions reflect a naturalistic dialog, the better (Hollan, 1984). Four examples of the design specifications for a user friendly interface are:

DESIGN SPECIFICATION: All prompts, menus, and error messages should be meaningful (even if long), and as simple as possible.

DESIGN SPECIFICATION: User operation should involve graphic interfacing (i.e., use of menus and icons) in order to minimize the need for key-ins.

DESIGN SPECIFICATION: There should be "easy navigation" through the menu hierarchy. Windows should show the level of the hierarchy at which the user is currently operating, and various commands such as "Go back," "Return to start," "Escape," "Undo," "Where am I?," and "Help."

DESIGN SPECIFICATION: Users should be able to select menu items through use of either a keyboard, a keypad, or a mouse.

The Graphics Component

In general, the AMPS graphics component will combine product displays with a robust graphics "display engine" (Hollan, 1984) to permit the construction of representations of changes of state in a complex dynamic physical system, the atmosphere. AMPS graphics will have to display a large number of data types and data products: meteorological observations, radar imagery, satellite imagery, and various forecast products, such as the forecasts produced by the National Oceanic and Atmospheric Administration.

In terms of the human factors approach, displays should be as simple as possible given what they have to do; they should present data clearly and unambiguously; they should take a minimum amount of time to interpret; they should require minimal display-reading skills, granted that "minimal" may require considerable training in the case of meteorological displays.

Specifications for this component involve the nature of the cathode ray tube (CRT) display devices, the format of the displays, graphics symbols, graphics colors, and graphics manipulations options. Here are some examples of the specifications:

DESIGN SPECIFICATION: AMPS should use high-resolution 19-inch diagonal color CRTs of the highest available quality.

DESIGN SPECIFICATION: CRTs must be mounted in the workstation on adjustable height/angle mounts.

DESIGN SPECIFICATION: Each graphics CRT should be able to display individual products (i.e., imagery) and sets of observations (i.e., data tables), and should be able to be sectorized to display more than one product or set of observations.

DESIGN SPECIFICATION: AMPS displays should ultimately have the capability of portraying three spatial dimensions as well as a temporal dimension.

DESIGN SPECIFICATION: If possible, AMPS displays should have as an option the presentation of data in the form of function graphs rather than in the form of data tables.

DESIGN SPECIFICATION: Alphanumeric and other symbols should generally be at least 0.20 inches in height, and probably larger (i.e., as large as the capitalized letters that appear in this manuscript).

DESIGN SPECIFICATION: AMPS graphics displays should have the capability of displaying symbols, lines, areas, etc. in color.

DESIGN SPECIFICATION: AMPS color graphics should rely on a "standard" color set for each of the display products, with the number of hues in any one display restricted to 7 to 9 (i.e., blue, green, desaturated yellow, red, light gray, black, indigo).

DESIGN SPECIFICATION: Users should be able to manipulate (via software) all the color sets and color coding schemes, including hue, brightness, and saturation variations.

DESIGN SPECIFICATION: The AMPS graphics component should permit a number of graphics manipulations: Overlays, enhancements, pan and zoom, time series looping, and manipulations of coordinate systems.

Workstation Design

All the displays, keyboards, shelf space, etc. should be located in a central workstation-like environment. One of the first issues to be addressed is the question of how many CRT displays the workstation should have. To get a tentative answer to this question, I observed a number of the bi-weekly forecasting deliberations held at the AFGL and conducted by meteorological researchers, some of whom had operational forecasting experience. The mean duration of the deliberations was 16 minutes (Range = 10 to 21 minutes), and the average number of displays or charts referred to (including repeated references to some charts and displays) was 41 (Range = 31 to 60). This works out to about 2.6 charts/displays per minute. In the individual gestural acts in which they referred to charts and displays, the forecasters would generally point to between one and four charts or displays. It thus seems likely that the

AMPS workstation would need three or four CRTs.

With regard to other aspects of workstation design, I broke workstation design into the following categories: Manipulanda, operational modes, workstation configuration, and room layout. Here are some example specifications for the workstation:

DESIGN SPECIFICATION: Keyboards, graphics pads w/ mice, and other manipulanda should be commercially available and of standard design (i.e., "off the shelf").

DESIGN SPECIFICATION: The workstation should be able to operate in a distinct "mode" for each functionally distinct activity or task.

DESIGN SPECIFICATION: The general workstation configuration should have a "wrap-around" or parabolic design. Dimensions of the parabola, desk space, chairs, etc. will be derivable from known rules of anthropometry (cf. Davis & Swezey, 1983; Kantowitz & Sorkin, 1983, Ch.15).

DESIGN SPECIFICATION: For seated users and a narrow workstation parabola, CRTs should be placed between 35 and 98 centimeters above the seating surface; the optimal viewing distance is 46 centimeters; the optimal vertical angle for viewing CRTs ranges from 65 degrees above the horizontal line-of-sight and 35 degrees below it; and the optimal parabola should place all CRTs within plus or minus 60 degrees of the user's straight-ahead line-of-sight.

DESIGN SPECIFICATION: The workstation room configuration should support the discussions and interactions of small groups.

DESIGN SPECIFICATION: Ambient room illumination should be indirect and incandescent.

DESIGN SPECIFICATION: Dark shades of color should not be used on ceilings, walls, or consoles; pastels or light gray with a dull matte finish are preferable.

DESIGN SPECIFICATION: Optimal room temperature is between 72 and 78 degrees Farenheit with humidity between 20 and 60 percent. The temperature of the air at the floor and at the ceilings should not differ by more than 10 degrees Farenheit.

DESIGN SPECIFICATION: The AMPS rooms that contain hardware (i.e., printers, the workstation, and the computer room) should have a raised floor under which cables and ventilation ducts can be placed, in order to facilitate development work, maintenance, and ventilation.

VI. RECOMMENDATIONS FOR FURTHER RESEARCH

The AMPS system will require a great deal of research and development work. There should, of course, be a well thought-out research and development plan. Each of the AMPS components (i.e., hardware systems, software interface systems, graphics systems, AI systems, workstation design) and sub-components (e.g., IP system for data ingest) will need the following general development phases:

STAGE 1. Refinement of specifications.

STAGE 2. Generation and testing of initial mock-up or prototype.

STAGE 3. Refinement of specifications.

STAGE 4. Generation of working prototype.

STAGE 5. Testing and refinement of working prototype.

STAGE 6. Field testing.

While human factors research has yielded many principles and much advice, human factors engineers are always careful to point out that the design of human-computer systems is as much an art as it is a science. Any principles that come from basic research will need to be adapted, modified, and even rejected, in the light of research on the specific domain at hand. Since the AMPS system will be very complex and is of such great potential importance,

RECOMMENDATION #1: I recommend that the AFGL contract with a leading human factors engineer for comments on the design specifications. Ideally, such a consultant would be familiar with Air Force activities and needs, with meteorology, and with the design of workstations that contain more than one CRT.

RECOMMENDATION #2: I recommend that the design specifications be analyzed and revised in light of visits to operational forecast

stations (i.e., Logan Airport, Global Weather Central, the National Meteorological Center), interviews of the forecasters there, and observations of their workstation systems.

RECOMMENDATION #3: I recommend that the design specifications be compared with those of existing meteorological workstations (both operational ones and ones in the design stage), such as MCIDAS (The University of Wisconsin "Man-Computer Interactive Data Acquisition System"), AFOS ("Automation of Field Operations and Services" workstation for airport forecasting operations), PROFS (the NOAA "Program for Regional Forecasting and Observing Services"), and AWDS ("Automated Weather Distribution System," the Air Force operational AFOS stations).

The various workstation systems that are either operational or are in the development phase are each intended to support either research or forecasting. Although each has (apparently) not taken into consideration some of the design specifications that the present work has generated, they are nevertheless all fairly similar to this tentative AMPS design, with the important exception of the AI component. Therefore,

RECOMMENDATION #5: Coordinate workstation development efforts and avoid duplication of workstation systems. This may require the establishment of a cross-branch, cross-agency "study team."

RECOMMENDATION #6: In its development phase, the AMPS project will require a number of full-time, in-house, experienced personnel: (1) A Ph.D.-level expert in AI systems, expert systems, and information processing system integration, (2) A computer hardware Systems Manager, ideally an individual with a knowledge of meteorology, FORTRAN, and LISP, (3) At least two full-time, in-house, experienced programmers, ideally individuals with a knowledge of meteorology and a proficiency in both FORTRAN and LISP, (4) At least one full-time, in-house experienced forecaster, and (5) At least one forecaster who is intimately familiar with the needs of the various Air Force stations where AMPS will eventually be located.

Needed Research on Display Design

A host of questions about display design need to be addressed. For example, should display backgrounds be pastel or gray? Are all the colors to be used of equal subjective magnitude? How should the flags and windows be formatted? Research will also be needed to develop the color manipulations options, and all the other graphics manipulations.

Needed Research on Workstation Design

A host of questions about workstation design need to be addressed. For example, can the height-adjustable CRTs accommodate standing forecasters? Will a "standing user" configuration best suit the needs of forecasters and a "sitting user" configuration best suit the needs of researchers? How can the keyboard and mouse be positioned so as to accommodate both right-handed and left-handed users?

Needed Research on Expert Knowledge

While the AI component of AMPS can conceivably operate effectively in the form of semi-autonomous modules, each of the modules will have to rely on a knowledge base containing general and specific principles of physics and meteorology. Thus, from the perspective of the AI system engineer, there will be a need for a shared "knowledge base."

In order to generate such a knowledge base, one must specify the knowledge and reasoning of expert meteorologists, requiring the application of methods from experimental psychology (Hoffman, 1987b). Research on the reasoning of meteorologists is in its infancy. Many studies have examined meteorologists' forecasting "hit rate" and "degrees of belief" in specific predictions (e.g., Daan & Murphy, 1982), but there has been little research on the ongoing reasoning of meteorologists. Two exceptions to this are Schlatter's (1985) study of "A day in the life of a mesoscale forecaster," and Moninger & Stewart's (1986) analysis of forecasters' deliberations. There is a need for research on

this topic (Murphy & Brown, 1984, p.396).

There are many different ways to represent knowledge in AI systems---scripts, frames, object-oriented representations, networks, etc.--and it is not yet clear which format or formats will work best for the various domains of meteorological knowledge. The knowledge acquisition process "drives" other aspects of developing and implementing an expert system in that it yields ideas about the appropriate representational format. Therefore, the task of extracting the knowledge of expert meteorologists can be initiated at the outset of the AMPS project. Also, a thorough functional analysis will have to be performed on tasks and operations. Precisely what (in terms of console or computer commands) do meteorological researchers and forecasters do? How can their job be made easier by the AMPS?

- Hutchingson, R.D. (1981). New horizons for human factors in design. New York, NY: McGraw-Hill.
- Kantowitz, B.H., & Sorkin, R.D. (Eds.) (1983). Human factors: Understanding people-system relationships. New York, NY: John Wiley and Sons.
- Kelly, S. & Sauer, D.W. (1986). "Advanced integrated workstation evaluation, Vols. 1 - 3." Systems Research Laboratories, Dayton, OH.
- Moninger, W.R. & Stweart, T.R. (1986). "A proposed study of human information processing in weather forecasting." Report, Environmental Sciences Group, National Oceanic and Atmospheric Administration, Boulder, CO.
- Monk, D.L., & Kelly, S. (1985). "Survey of human factors affecting the requirements for the Military Airlift Command Crisis Action Team Workstations." Air Force Aerospace Medical Research Laboratory, Wright-Patterson AFB, OH.
- Murphy, A.H., & Brown, B.G. (1984). A comparative evaluation of objective and subjective probability forecasters in the United States. Journal of Forecasting, 3, 369-393.
- Norman, D.A. (1984). Cognitive engineering principles in the design of human-computer interfaces. In G. Salvendy (Ed.) Human-computer interaction. Amsterdam, The Netherlands: Elsevier Science Publishers.
- Schlatter, T.W. (1985). A day in the life of a modern mesoscale forecaster. ESA Journal, 9, 235-256.
- Technology Systems, Inc. (1984). "Meteorological data acquisition, management, and processing system." Technology Systems, Inc., Lexington, MA.

VIII. REFERENCES

- Boehm, A.R. (1979). "The rank input method and probability variation guides." Environmental Technical Applications Center Report TN-80-004. Air Force Environmental Technical Applications Center, Scott AFB, IL.
- Buck, J.R. (1983). Visual displays. In B. Kantowitz & R. Sorkin (Eds.) Human factors: Understanding people-system relationships. New York, NY: John Wiley and Sons. 137-143.
- Chisholm, D.A., Jackson, A.J., Niedzielski, M.E., Schechter, R., and Ivaldi, C.F. (1983). "The use of interactive graphics processing in short-range terminal weather forecasting: An initial assessment." Report AFGL-83-0093. Air Force Geophysics Laboratory, Hanscom AFB, MA.
- Daan, H., & Murphy, A.H. (1982). Subjective probability forecasting in the Netherlands: Some operational and experimental Results. Meteorological Research, 35, 99-112.
- Davis, E.G., & Swezey, R.W. (1983). Human factors guidelines in computer graphics: A case study. International Journal of Man-machine Studies, 18, 113-133.
- GEOMET (1987). "Report on the expert system for predicting fog in the vicinity of Cape Canaveral." Report, GEOMET, City, Maryland.
- Giraytys, J. (1975). AFOS experimental Program. IEEE Transactions on Geoscience Electronics, Vol. GE-13, 111-115.
- Hoffman, R.R. (1987a). "Remote perceiving: Charting a new area of applied science." Manuscript, Department of Psychology, Adelphi University, Garden City, NY.
- Hoffman, R.R. (1987b). The problem of extracting the knowledge of experts from the perspective of experimental psychology. The AI Magazine, 8, 53-67.
- Hollan, J.D. (1984). Intelligent object-based graphical interfaces. In G. Salvendy (Ed.) Human-computer interaction. Amsterdam, The Netherlands: Elsevier Science Publishers.

1987 USAF-UES SUMMER FACULTY RESEARCH PROGRAM/

GRADUATE STUDENT SUMMER SUPPORT PROGRAM

Sponsored by the

AIR FORCE OFFICE OF SCIENTIFIC RESEARCH

Conducted by the

Universal Energy Systems, Inc.

FINAL REPORT

PRESSURE ATTENUATION IN SOLIDS: A COMPUTER MODEL

Prepared by:	James Steven Hoffmaster, Ph.D.
Academic Rank:	Associate Professor
Department and	Physics Department
University:	Gonzaga University
Research Location:	Air Force Armament Laboratory Munitions Division Energetic Materials Branch Dynamics Laboratory Eglin AFB FL 32542-5434
USAF Researcher:	David R. Wagnon
Date:	28 July 1987
Contract No.:	F49620-85-C-0013

PRESSURE ATTENUATION IN SOLIDS: A COMPUTER MODEL

by

James Steven Hoffmaster

ABSTRACT

The peak pressure in a material produced by a shock wave decreases as the wave passes through the object. The rate of decrease depends on the size, shape, and molecular structure of the object. Pressure is a key consideration when evaluating insensitive high explosive candidate materials. Current state-of-the-art computer codes are extremely complex and are difficult, time consuming affairs to apply. A simpler, user friendly computer program is described in this report. It is capable of giving peak shock wave pressure at interfaces as well as pressure attenuation as a function of distance in selected materials. Numerical approximation techniques employed are the least squares polynomial fit and Newton's method of iterative solutions for polynomial equations. The results obtained, although less accurate than those of the more complex codes, are far easier to obtain and are sufficiently accurate to be useful in choosing experimental parameters in IHE evaluative testing.

Acknowledgements

I wish to thank the Air Force Systems Command and the Air Force Office of Scientific Research for sponsorship of this research, as well as Universal Energy Systems for their assistance in facilitating the administrative aspects of the program.

Many people are responsible for making this summer at Eglin AFB an enjoyable and rewarding research experience. I would first like to thank Dr Sam Lambert for his efforts on my behalf in the initial selection process. Mr James D. Aplin, Mr Mark Grimmponpre', and TSgt Bobby Cole of the Dynamics Laboratory at the High Explosive Research and Development Facility are to be commended for their patience while listening to my questions and for their clarity when answering them. Likewise, my conversations with Capt Anthony Taliancich were quite helpful. Finally, and most significantly, I am pleased to thank Mr David Wagnon, Chief of the Dynamics Laboratory, for his suggestions and guidance. They were always constructive and informative.

I. INTRODUCTION:

Insensitive high explosives (IHEs) have been an area of major interest in the armed services. Because of the tremendous energy releases associated with even conventional explosives, the safe handling, storage, and transportation of high explosives is literally a matter of life and death to those involved in these processes. IHEs are those whose behavior is such that they have passed certain cookoff, impact, and sympathetic detonation tests. Tests which in essence try to ensure that IHEs do not detonate by accident or under enemy attack, but at the same time are reliable and effective in times of military action (Corley, 1986).

For the past two summers in a similar faculty research program run by the US Navy, I was involved in the investigation of effective armoring of Navy and Marine facilities and equipment. In evaluating armoring, many threats must be considered and, of course, one of these is conventional explosives. Because of the destructive nature of the process and the expense associated with sacrificing facilities to destructive testing, much of the evaluation is done by computer simulation and modeling. Many of the techniques used in the modeling of effective armoring can also be applied to similar modeling of the IHEs themselves. These procedures involve the use of state-of-the-art techniques, such as finite differences and finite elements analysis as well as more traditional but still useful methods involving least squares curve fitting and other numerical analysis techniques. The success of these models varies with the problem analyzed and with the type of analysis.

II. OBJECTIVES OF THE RESEARCH EFFORT:

The problems associated with the understanding and prediction of detonation characteristics are extremely complex. They involve several fields of both chemistry and physics and often several states of matter within those fields (Fickett and Davis, 1979). As such, they have not lent themselves to a simple tractable solution (Davis, 1987). The most successful approach is one that has developed over the last thirty years and has increasingly involved the use of rather sophisticated computer analysis. The software associated with this analysis started with a "SIN" code and led to several spin-offs. All of these are finite difference approximations. Differences between; burning and detonation, heterogeneous and homogeneous materials, and various geometries can all be approximated by additions to the original program, such as Forest Fire and Sharp-Shock Burn (Mader, 1979). This, of course, adds to the complexity of the analysis.

Currently, the situation is such that in the ordinary day-to-day operations of the laboratory, these models are far too complex to be of any use. Typically, they will take an expert in the field several months to enter the appropriate initial and boundary conditions, run the program, and then check to see if the results make sense. Hence, these computer codes are really viable only at the large research facilities such as Los Alamos and Sandia.

At the smaller laboratories, there is a need for a more simple approach to obtain reasonably accurate predictions for explosive parameters as new IHEs are developed and tested. The major objective of this summer's research was to begin development of one such model.

III.

a. It was decided that the most reasonable procedure would permit a shock wave to be transmitted between two different materials and then look at pressure attenuation of that shock wave in the second material as a function of the thickness of this second substance. Such a strategy would then, with some minor modifications, allow analysis of shock transmission and pressure attenuation in several materials in contact with one another.

The starting point for the model developed is the Hugoniot curve for the material being considered. This curve is the set of all possible shock states in the material. There are several such curves for each material just as there are several interrelated parameters that can describe a particular state. One can experimentally determine the shock wave speed in the material with a standard streak photograph, pressure pins, or some other similar technique. If the density is known, one can then obtain the corresponding pressure and particle velocity (Fickett and Davis, 1979).

In the current research, material density, ρ_0 and shock wave speed, U_s , were assumed. Then, from the relationship in equation (1)

$$P = \rho_0 U_s U_p \quad (1)$$

one can find the slope of the straight line extending from the origin to the Hugoniot Curve of Pressure, P , vs particle speed, U_p , for the material in question. In this case, it is the material through which the shock wave initially travels. The analytical form for the Hugoniot curve was obtained from a least squares curve fitting analysis for experimental data in Marsh (1980). In all

cases, it was found that the best fit for pressure versus particle speed was quadratic and of the general form given by equation (2)

$$P = a + bU_p + cU_p^2 \quad (2)$$

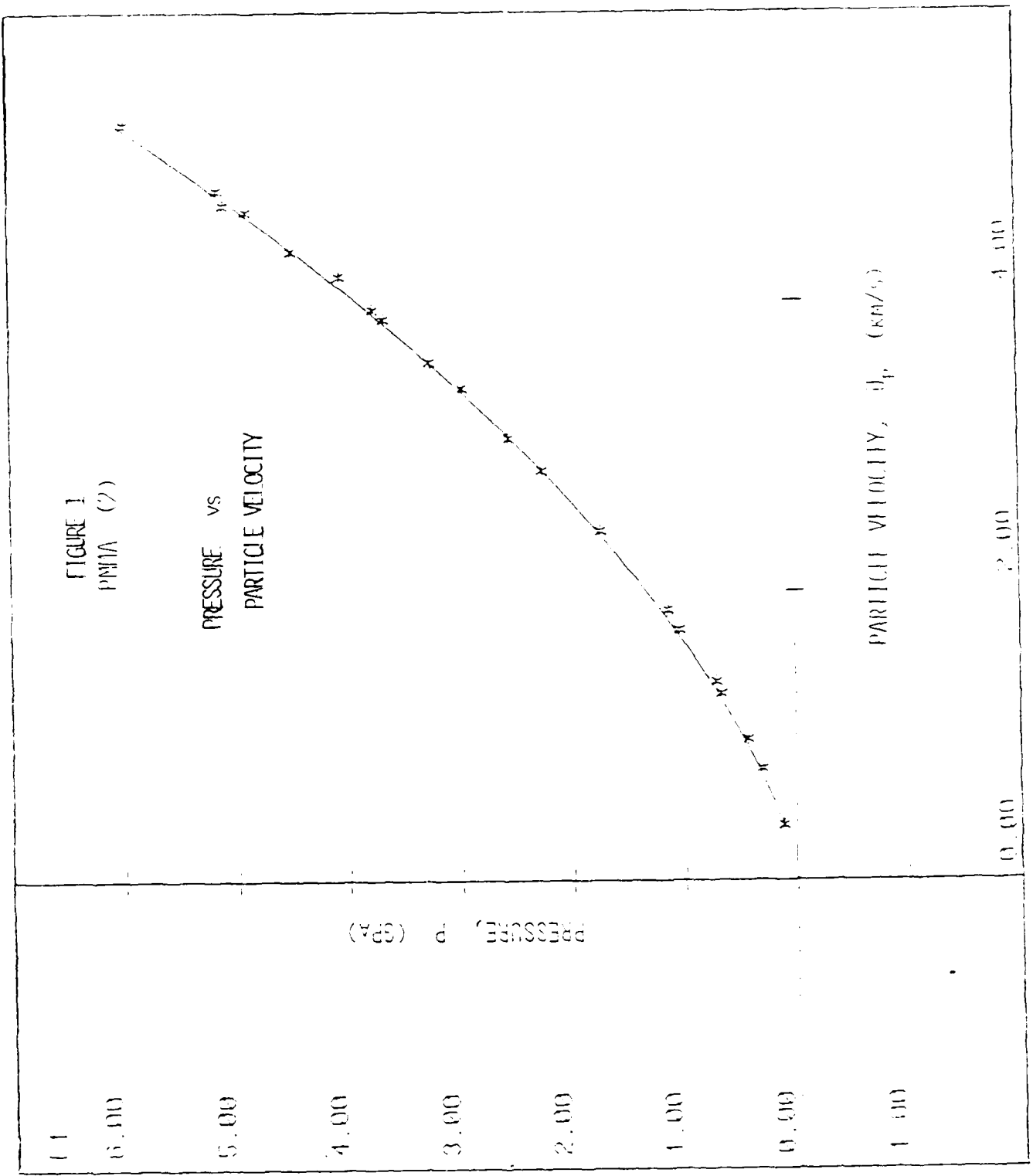
where each material will have its own unique a, b, and c values. The least squares quadratic fit is given for PMMA in Figure (1) and the results for the other materials are presented in Table (1). All such graphs are similar to that of Figure (1).

TABLE 1

COEFFICIENTS OF EQUATION (2)			
Material	a	b	c
Aluminum	-0.99	15.96	3.21
Beryllium	0.23	14.45	2.17
Brass	0.01	31.74	11.91
Calcium	-0.12	5.79	1.44
Cesium	-1.58	2.57	2.20
Copper	0.17	34.58	13.43
Lithium	0.25	2.21	0.65
Magnesium	0.46	7.34	2.31
PMMA	-0.57	4.06	1.46
Silver	2.46	29.33	18.10
Sodium Chloride	0.28	6.93	2.95
Titanium	-0.16	23.17	4.24
Tungsten	-2.04	81.99	21.31
Water	-1.14	3.32	1.17
Zinc	1.38	19.44	11.58

The units associated with the quantities mentioned are density (gm/cm³), speeds (km/s), and pressure (GPa).

The point of intersection of the straight line of equation (1) and the Hugoniot curve of equation (2) represents the incident pressure at the boundary between two materials. At this point, the



Hugoniot of material one must be "flipped" (rotated 180 degrees around a vertical axis passing through this point). Then the point of intersection of the Hugoniot curve for material one with the corresponding curve for material two will give the pressure in the second material, the one the shock wave enters. Boundary conditions require that transmitted pressure be equal to the reflected pressure in the first material.

The flipped curve for material one is given by equation (3)

$$P = (a + 2bU_p^* + 4cU_p^{*2}) - (b + 4cU_p^*)U_p + cU_p^2 \quad (3)$$

where U_p^* represents the particle velocity at the intersection of equations (1) and (2).

The second material can be represented by equation (2) with appropriate values for a, b, and c as given by equation (4) and table 1.

$$P = a_2 + b_2U_p + c_2U_p^2 \quad (4)$$

When equations (2) and (4) are solved simultaneously the value for P will be the pressure in material two as the shock wave enters. A straightforward but algebraically unpleasant process will yield two answers. One will typically make no physical sense and can be eliminated.

b. The second part of this summer's research was to investigate the attenuation of the pressure once the shock wave is in the second material. It was found that for PMMA, the best smooth curve fit corresponded to a fourth order least squares fit of the form

$$P = A + Br + Cr^2 + Dr^3 + Er^4 \quad (5)$$

where r is the distance the shock wave has traveled into the PMMA in millimeters. Table 2 gives the values of the coefficients of equation (5) for PMMA, when pressure is expressed in kbar.

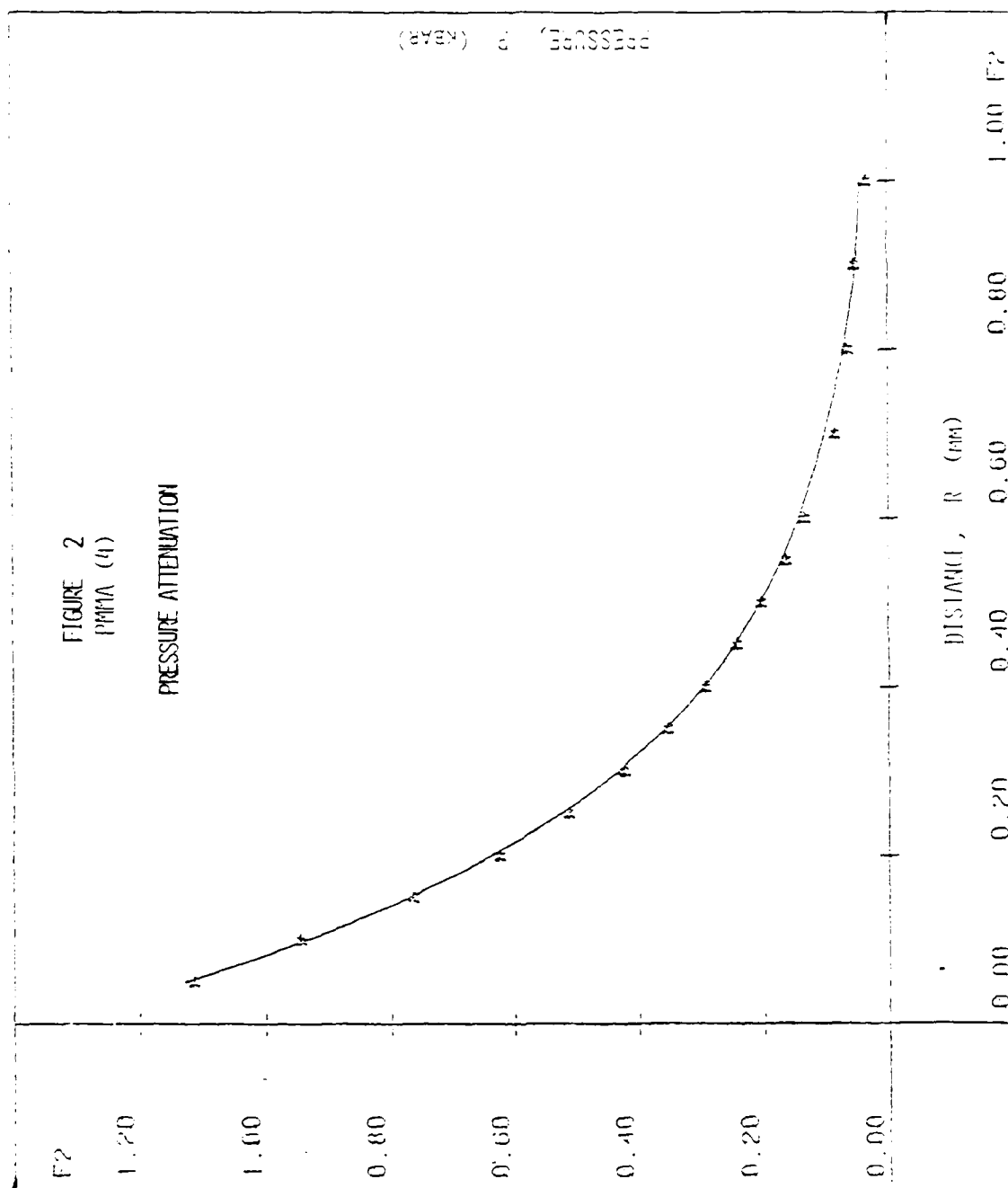
TABLE 2

COEFFICIENTS OF EQUATION (5)	
PMMA	5 m < r < 100 mm
A	13.5
B	-0.492
C	7.86E-3
D	-6.23E-5
E	1.98E-7

Unfortunately experimental data for pressure attenuation is not easily found in the literature, if indeed it exists, so that equation (5) was only evaluated for PMMA (Jaffe et al, 1965). Figure (2) represents the fourth order least squares fit of pressure versus attenuation distance.

c. Both equations (2) and (5) can be generalized to any number of materials by evaluating the coefficients. The data for equation (2) is readily available, that for equation (5) is not. There are some limitations on the generality of the results obtained. The major one pertains to the fact that the PMMA results for equation (5) are for samples two inches in diameter. It would seem reasonable to expect different coefficients for samples of different diameter.

This particular analysis although rather limited in scope offers the opportunity to quickly and accurately approximate peak pressure values in different materials. The program can be run on any common personal or scientific computer and gives immediate results. Although clearly not of the accuracy of the complex computer codes using finite difference methods, it is far easier to use and its accuracy is good enough for choosing masses and



geometries that are useful in testing new explosives, their effects, and their suitability as IHEs.

IV. RECOMMENDATIONS:

a. There are a number of directions that one might pursue the research just described. Probably the most apparent is the acquisition of pressure attenuation data for materials other than PMMA. In addition then to allowing more applications of the predictive model, we could also use it to do multiple reflections. That is, the model could then apply to a pressure wave that attenuated in several materials and passed through more than one interface.

b. The data that is available for pressure attenuation in PMMA applies to two-inch thick cylinders. Similar data should be obtained for cylinders of different thickness. Since pressure attenuation is a process involving both axial and side effects, the diameter of the cylinder should significantly affect pressure changes.

c. With different diameter cylinders of different materials, the time required for peak pressures to reach certain points in the cylinders could be measured and would provide insight into the relationship between side reflections and pressure waves.

All three of the preceding research suggestions could be carried out in a set of experiments. These experiments would involve time and pressure measurements on cylinders of different materials (steel 304, aluminum 6061, PMMA and glass) of different diameters (2, 4, 6, and possibly 8 inches). A series of measurements would record the pressure and time-of-arrival of peak pressure at points along the axis of each cylinder and at points

$r/4$, $r/2$, and $3r/4$ off axis. A proposal to this effect will be submitted to Universal Energy Systems as a Research Initiation Program request. As a spin-off from such research, the results obtained might provide insight into the physical phenomena involved in pressure attenuation and, hence, help to clarify what is already known.

d. Further refinement of analysis includes a computation of the errors associated with the least squares approximations so that a more explicit confidence level for the results could be obtained.

e. A start could be made on determining if the model developed could also be applied to explosives in which pressure would not attenuate but, at least near detonation, would increase. Such an improvement would significantly increase the usefulness of the results.

In conclusion, let me restate that the computer model developed was at no time meant to replace the more sophisticated, more accurate, and more detailed computer codes that now exist. Instead, it is intended as one that is easier to use and, hence, can be used by scientists and technicians in related fields who might not have the time or expertise to use the more complex programs.

The computer program, when completed, will provide appropriate data, pressure values, both forward and backward in space, and will give them quickly. It is this data that is useful in the design and testing of IHEs. And, it is the ease with which this data will be available that will make it a useful research tool.

REFERENCES

Corley, John D., 1Lt, USAF. "Insensitive High Explosives Evaluation Techniques." Internal Report, Eglin Air Force Base, Florida, AD-PA-86-233, 1986.

Davis, William C. "The Detonation of Explosives." Scientific American, May 1987, pp 106-112.

Fickett, Wildon, and Davis, William C. Detonation, Berkeley, California, University of California Press, 1979.

Jaffee, I., et al. "The NOL Large Scale Gap Test. Compilation of Data for Propellants and Explosives II." NOLTR 65-177, White Oak, Maryland, Naval Ordnance Laboratory Technical Report, 1965, pp 35-42.

Mader, Charles L. Numerical Modeling of Detonations, Berkeley, California, University of California Press, 1979.

Marsh, Stanley P. (editor). LASL Shock Hugoniot Data, Berkeley, California, University of California Press, 1980.

1987 USAF-UES SUMMER FACULTY RESEARCH PROGRAM/
GRADUATE STUDENT SUMMER SUPPORT PROGRAM

Sponsored by the
AIR FORCE OFFICE OF SCIENTIFIC RESEARCH

Conducted by the
Universal Energy Systems, Inc.

FINAL REPORT

IN SITU DETECTION OF OSTEOPROGENITOR CELLS
IN AN ACTIVELY GROWING BONE SYSTEM

Prepared by:	Gwendolyn B. Howze
Academic Rank:	Associate Professor
Department and	Biology
University:	Texas Southern University
Research Location:	AAMRL/BBD/Biodynamic Effects Branch WRIGHT-PATTERSON AFB W-P AFB, OHIO 45433
USAF Researchers:	Clarence M. Oloff and Leon Kazarian
Date:	24 Sept. 87
Contract No:	F49620-85-C-0013

IN SITU DETECTION OF OSTEOPROGENITOR CELLS
IN AN ACTIVELY GROWING BONE SYSTEM

by

Gwendolyn B. Howze

ABSTRACT

Rats of the weight range 412 to 496 grams and 135 days old were injected with hydroxyurea (HU) in order to inhibit DNA synthesis in "S" phase cells and to block cells in the "G1"/"S" transition. Preosteoblasts synthesize DNA on the pathway to becoming osteoblast. Preosteoblast should therefore be caught in the HU "net". If HU inhibits osteoblast formation through inhibition of DNA synthesis by preosteoblast the indirect effect should be inhibition of bone formation (osteogenesis).

Histology and light microscopy were used to assay the cytological effects. Labeling with the fluorochromes, tetracycline, calcein, xylenol orange, and histomorphometry were used to assay the effects upon osteogenesis.

The putative preosteoblast population is identified if there is a conjunction of three conditions: HU treatment, the appearance of an abnormal cell population, and inhibition of labeling as detected by histomorphometry. The inference being that the HU inhibited DNA synthesis in the osteoprogenitors, thereby preventing them from developing into osteoblast and consequently inhibiting osteogenesis.

The treatment regimen, collection of the specimen and a subset of the histology was completed during the summer research period. All of the histomorphometry and two-thirds of the histological assays remain to be done.

In the histological specimens which have been studied a definite cellular effect has been observed. It is not possible to correlate the cellular effect with the effect on osteogenesis because the histomorphometry has not been done.

ACKNOWLEDGEMENTS

I wish to thank the Air Force Systems Command, the Air Force Office of Scientific Research, and the Biodynamic Effects Branch of the Biodynamics and Bioengineering Division, Armstrong Aerospace Medical Research Laboratory for sponsorship of this research. Universal Energy Systems did an excellent job of managing the program. They were available, and interested in solving any administrative problem.

Mr. Clarence M. Oloff, effort focal point, and Mr. Leon E. Kazarian, Branch Chief, were responsible for having me on board for the summer research effort. They were supportive and interested in every aspect of the project.

I wish to thank the following people for major contributions which enabled me to finish the project in the allotted time. The names are in alphabetical order, each person gladly contributed the support which was needed at a critical point of the project. I am profoundly grateful to each person: Major James Cooper, Ph.D., Mr. Edward Everland, Ms. Nadia Greenidge, Mr. Douglass Hilton, Dr. David Mattie, Ms. Gloria Neely, Mr. Marvin Souder, Mr. Anthony Stuart, Ms. Sharon Wagner.

I. Introduction

The best known cells of bone are the osteocytes, osteoblasts and osteoclasts. The osteoblasts manufacture the bone matrix, change state and become osteocytes. The osteocytes are the mature bone cells which reside in the lacunas of the bone matrix. The osteoclasts which function in resorption are multinucleated giant cells derived from blood monocytes. Other cell types which have been described include : bone lining cells (13) and fibroblast (unpublished SEM studies).

The origins of the osteocytes and osteoclasts are agreed upon, the proposed origins of the osteoblast are, however, controversial. The proposed precursors to the osteoblasts, the so called osteoprogenitor cells include the following : undifferentiated mesenchymal cells (17), fibroblast (19), bone lining cells (13), and epithelium in certain experimental systems (7,8). If it is accepted that all of the cells in the list are indeed osteoprogenitors, it still is not clear whether they are all equally important in all systems. Nor is it clear whether there is a relationship between activating conditions and cell type.

In order to study this problem we utilized a continuously growing bone system, in which osteoblast are continuously manufacturing matrix. Presumably the osteoprogenitor population constantly generates osteoblasts according to some endogenous program. The experimental design should allow us to determine where in the bone the stem cells

(osteoprogenitors) reside; and answer the question as to whether any or all of the cells referred to above act as stem cells in the system under study. According to this design the stem cells were both tagged and incapacitated. Thus if the incapacitated stem cells were not able to generate osteoblasts, bone matrix could not be produced, i.e., osteogenesis will be inhibited. By definition an osteoblast is a cell which lays down the osteoid which subsequently mineralizes to form bone matrix .

In many systems which are regenerated or restored from a stem cell line, the stem or precursor cells follow a relatively set sequence of events after activation. One of the earliest events in the consecution is DNA synthesis, which is usually closely followed by mitosis. After their activation, at least one amplifying cell division (mitosis) is required of the precursors so as not to exhaust the stem cell line. In eukaryotic cells, mitosis is always preceded by DNA synthesis. There is evidence that osteoprogenitor cells follow the same pattern (3); for example, certain substances which induce bone formation (osteogenesis) in preosteoblast cultures also induce DNA synthesis in those cultures (4,3).

The basic assumption of this research proposal is that the following sequence of events will occur in the stem cell population: 1) activation, 2) DNA synthesis, 3) at least one amplifying cell division or mitosis, 4) the differentiation of at least one the progeny cells into the osteoblast cell line, 5) osteogenesis by osteoblast. Events one through four are ascribed to the osteoprogenitor/stem cell line. The osteoblasts generated by those processes manufacture bone matrix, i.e., osteogenesis.

Because the osteoprogenitors should be sensitive to DNA synthesis inhibitors, if the inhibitors were carefully selected, it should be possible to effect an in situ visualization of the osteoprogenitors engaged in the events which lead to the formation of osteoblasts. Hydroxyurea was used in these experiments. It is an inhibitor of DNA synthesis, which : 1) reversibly inhibits entry into the DNA synthetic period of the cell cycle, and 2) kills cells engaged in DNA synthesis at the time the drug arrives at the site of action. These two features of hydroxyurea are expected to : 1) tag the activated osteoprogenitors by killing cells which are in the process of DNA synthesis, 2) prevent the osteoprogenitor from generating osteoblast (the DNA synthesis being a required event in this process), 3) inhibit new bone formation (osteoblast are required for new bone formation). Hydroxyurea (HU) is a simple compound with the formula : H NCONHOH (16). It is relatively nontoxic at effective concentrations, and its effects are reversible by discontinuation of the dosing (16).

In order to monitor the effect of (HU) on osteogenesis (the manufacture of new bone matrix); tetracycline, calcein and xlenol orange labeling was used. Tetracycline and similar chemicals are deposited in vivo at the site of active bone formation (21b). Tetracycline chelates calcium and is deposited at the mineralization front in newly forming bone matrix (10,18,19,21b). The incorporation of tetracycline, etc., at the mineralization front, permanently labels, and points out the bone that was manufactured during the tetracycline dosing period (10,18,21b). The label can be visualized by fluorescence microscopy of the undecalcified bone sections (2,10,18,21b). It will be possible to study both patterns of activity and rate of osteogenesis in these experiment.

Because of the focus on the osteoprogenitor cells, the results from this project should be relevant to the general problem of repair of bone after injury. Many USAF activities put bone at risk. Such activities as high speed flight and ejection from aircraft expose bone to the risk of fracture from impact and strong vibrations. Potential risks are implied due to the prospects of space flight and residence in low G-force space stations in the future. It is well known that exposure to low G-force and hypokinesia induce loss of bone mass and imply the risk of spontaneous fracture. The Biodynamic Effects Branch (of the Biodynamics and Bioengineering Division of The Armstrong Aerospace Medical Research Laboratory at Wright-Patterson AFB) has a long history of studies on the mammalian skeleton and development of devices for protecting the human skeleton from the hazards of high speed flight. My background as a cell biologist with interest in the organization of cell and cell products in bone meshes with that of the Biodynamic Effects Branch by virtue of our common interest in the relationship between organization at the microscopic level and response to physical stresses at the macrostructural level of organization.

II. OBJECTIVES OF THE RESEARCH EFFORT

When bone matrix is disrupted, a transient cell population called osteoblasts appears and carries out the job of restoration. The osteoblasts arise from preexisting cells, the osteoprogenitors. The identity of the preosteoblasts or osteoprogenitors is a major unsolved question. The proposed solutions are a matter of controversy since several cellular types have been suggested as being the precursor cells.

There are therefore two basic objectives: firstly, to identify the precursor cells which give rise to the osteoblasts which manufacture bone matrix in an active bone modeling system; secondly, to determine in which component of bone the osteoblast precursors (osteoprogenitors) reside.

III. THE EXPERIMENTATION

EXPERIMENTAL DESIGN

A. Distribution of the animals : forty animal were divided into two groups, a treated group which received hydroxylurea, a control group which received a saline placebo. Both groups received label compound at selected times to be described below. Four long bones in each animals were be used for the study. Male Sprague-Dawley rats, 135 days old were used in the experiment (21b) .

B. Establishing a baseline label marker : all animals were dosed with tetracycline on day zero (D-0). The dosage was ten mg. per Kg. of body weight. This operation establishd the baseline label in the bones.

2) Day-6 : All animals were treated with the label compound, Xylenol orange, 10 mg per Kg of body weight, for one day (21b) .

3) Day-7 through Day-11 : dosing of the treated group with (HU) and the controls with saline, five days of treatment.

4) Day-12 : All animals were treated with Calcein at 10 mg per Kg (of body weight) .

5) Day-13 through Day-17 : repeated item ' 3)', above.

6) Day-18 :the animals were sacrificed. Carbon dioxide euthanasia was employed. Specimens were taken for histology, histomorphometry and electron microscopy.

C. Other experimental procedures .

After euthanasia, the long bones were removed and utilized in the following procedures:

1) histomorphometry to determine the amount of growth or inhibition of growth (18b), 2) histology and light microscopy to visualize the cells killed or injured by (HU), and to determine which cell populations participate in the recovery process; Hematoxylin stains and mallory's stain were used.

RESULTS

Because the rats were not available until the fifth week of the summer research period, the results obtained are incomplete and these conclusions are only tentative. The treatment protocol was completed and all of the specimens were collected. Currently only some of the histology specimens have been processed and studied. There will be no attempt to obtain quantitative data until all of the specimens have been processed. Currently, no histomorphometry data is available. The histological samples which were prepared at BB/BBD/AMRL during the last week of the project have been studied since returning to my home base. The following

conclusions are based on a small and incomplete sample and they will probably require revision if and when the experiment is completed. Since the histomorphometry was not done, there can be no conclusions about osteogenesis.

Five regions of bone seem to respond to the HU treatment; 1) chondrocytes in the epiphyseal plate, 2) cells in fibrocartilage, 3) cells in the cambial layer of the periosteum, 4) bone lining cells of the endosteum, 5) cells of the bone marrow. The most striking visual effects are seen in the bone marrow and the epiphyseal plate cartilage.

The target cell in the bone marrow seems to be cells of the reticular tissue. Inhibition of the reticular cells cause a depletion of the nucleated leucocytes, a transitory increase in red blood cells, followed by a decrease in red blood cells. When the HU treatment was discontinued, the bone marrow was restored. A tentative but potentially interesting conclusion is that the bone lining cells (BLC) of the endosteum are anatomically continuous with the reticular tissue of the bone marrow. The response of the endosteum is potentially the most significant effect observed up to this point. During the recovery period after the HU has been discontinued, the BLC transform from a flattened (squamous) contour to a cuboidal type cell, and in many regions the endosteum becomes a stratified cuboidal tissue which is continuous with the bone marrow reticulum. While the effect of the BLC is not visually spectacular, it could have profound implications if quantitation indicates that the effect is widespread.

Mitotic figures were detected in chondrocytes of epiphyseal cartilage and fibrocartilage from bone recovering from HU treatment. There was also

evidence of cellular changes in the basal layer of the periosteum in recovering bone.

There does not seem to be much evidence of cellular morphological damage. Rather certain cell types tend to become enriched during the recovery period and other cell types appear to be activated or transformed during the recovery period. It is ventured that some or all of these cells are the osteoprogenitors. These observations and conclusions must remain tentative until all of the data has been studied.

IV. RECOMMENDATIONS

The original research proposal submitted for the summer program anticipated about nine weeks for the actual experimentation to achieve the stated objectives. It was also suggested in that proposal that a statistical treatment of the quantitative data and scanning electron microscopy would add greatly to enhance the quality of the research, and it was proposed that the latter two modules be supported during the Mini Grant phase of the program.

Because of the delay in obtaining the rats only five week were available to carry out the experimentation. It is hoped that the experiment may be completed via a Mini Grant.

REFERENCES

1. Alberts, B., D. Bray, J. Lewis, M. Raff, K. Roberts, J. D. Watson, Molecular Biology of the cell, pp 611-668, 918-947, Garland Publishing Company, Inc. New York, 1983.
2. Anderson, Colin, Manual for the Examination of Bone, pp 1-109, Boca Raton, Fl, CRC Press, Inc., 1982.
3. Ashihara, E., et al. , "3H-thymidine Autoradiographic Studies in Electrically Stimulated Osteogenesis", in C. T. Brighton, J. Black and S. R. Pollack (eds): Electrical Properties of Bone and Cartilage, New York, Grune and Stratton, pp 401-425, 1979.
4. Farley, J. R., T Masuda, J.E. Wergedal and D. Baylink, Human Skeletal Growth Factor: Characterization of Mitogenic Effect on Bone Cells in vitro , Biochemistry, 21:3508 - 3513, 1982.
5. Frost, Harold, Tetracycline Based Histological Analysis of Bone Remodelling, Calc. Tiss. Res. 3: 211-237, 1969.
6. Goldstein, Avram, Biostatistics, pp51-92, New York, The MacMillan Company, 1969.
7. Huggins, C.B., The Formation of Bone Under the influence of Epithelium of the Urinary Tract, Archives of Surgery, 22: 377-407, 1931.

8. Huggins, C.B., Epithelium Osteogenesis- A Biological Chain Reaction, Proc. Amer. Philos. Soc. 113:458-463, 1969.

9. Huhmann, E.L., et al. , Innervation of Periosteum and Bone by Sympathetic Vasoactive Intestinal Peptide-containing Nerve Fibers, Science, 232:868-871, 1986.

10. Jankovich, J.P., The Effects of Mechanical Vibration on Bone Development in the Rat, J. Biomechanics, 5:241-250, 1972.

11. Landis, W.J., "Special Techniques for Problem Tissues, Bone and Collagen, in B> R> Jones (ed.) Electron Microscopy , 41 Exercises by 17 Scientists, Monroe, New York, Library Research Associates, Inc. pp328-339, 1985.

12. Linder, J.E., A Simple and Reliable Method for the Silver Impregnation of Nerves in Paraffin Sections of Soft and Mineralized Tissues, J. Anat., 127:543-551, 1978.

13. Menton, D.N., D.J. Simmons, S.L. Chang and B. Y. Orr, From Bone Lining Cell to Osteocyte - An Sem Study, Anat Rec., 209: 29-39, 1984.

14. Milch, R.A., D.P. Rall and J. E. Tobie, Basic Localization of the Tetracyclines, J. National Cancer Inst., 19: 87-93, 1957.

15. Smith, K.C., C.M. Olloff and L.E.Kazarian, AFAMRL-TR-81-122.

16. Timson, J., Hydroxyurea, Cancer Research, 32: 115-132, 1975.
17. Wlodarski, Krzysztof, Failure of Heterotropic Osteogenesis by Epithelial Mesenchymal Cell Interactions in Xenogenic Transplants in the Kidney, Calcif. Tiss. Res. 25: 7-11, 1978.
18. Wronski, T.J. and E. R. Morey, Inhibition of Cortical and Trabecular Bone Formation in Long Bones of Immobilized Monkeys. NASA Technical Memorandum
19. Unist, M. A., and K.H. Ibsen, The Chemical Reactivity of Mineralized Tissue with Oxytetracycline, Arch. Pathol. 76: 484-496, 1963.
- 20 Yagiela, J. A., and D. Woodbury, Osteoblast Isolation from Fetal Rat Calvaria, Anat. Rec., 188:287-307, 1977.
21. Aerospace Medical Association, 58th Annual Scientific Meeting, May 10-14, Las Vegas, NV, 1987, abstracts:
- 21a. Girtten, B., C. Oloff, L. Kazarian, S. Bloomfield, B. Smith, and R. Hamlin, Effects of Dobutamine on Suspension Hypokinesia/hypodynamia Deconditioning in Rats , #109, A19.
- 21b. Eveland, E. K. Smith, C. Oloff, K. Swenson, M. Souder, L. Kazarian, A Comparison of Bone Labeling Compounds: Tetracycline, Calcein, Xylenol Orange, and DCAF , #201, A34.

1987 USAF-UES SUMMER FACULTY RESEARCH PROGRAM

Sponsored by the

AIR FORCE OFFICE OS SCIENTIFIC RESEARCH

Conducted by the

Universal Energy Systems, Inc.

FINAL REPORT

Non-local Turbulance Theories

Prepared by:	Mayer Humi
Academic Rank:	Professor
Department and	Mathematical Sciences Department
University:	Worcester Polytechnic Institute
Research Location:	Air Force Geophysics Labs/LYP Hanscom Field, MA
USAF Researcher:	Don Chisholm
Date:	22 Aug 87
Contract No:	F49620-85-0013

Non - Local Turbulance Theories

by

MAYER HUMI

ABSTRACT

We show that nonlocal models for turbulence similar to transilient turbulence theory (T3) can be derived by the application of Leonard's filter to the appropriate flow equations. The numerical simulation of scalar dispersion in one dimension using this nonlocal formulation is carried out. Furthermore we examine the relationship between K-theory and T3 and obtain restrictions and relations between their parameters. The application of these models for the prediction of clear air turbulence and its effect on aircrafts is in progress.

Acknowledgements

I wish to thank the Air Force Systems command and AFOSR for sponsorship of this research. Universal Energy Systems and Mr. R. Darrah must be mentioned for their concern and help to me in all administrative and directional aspects of this program.

My experience at AFGL was rewarding and enriching because of many different influences. Dr. D. Chisholm and G. Modica provided me with support, encouragement and a truly enjoyable work atmosphere. The interaction with R. Banta, J. Morrissey, and V. Falcone was invaluable in motivating my work. Special thanks are also due to Ms. A. King of the AFGL Library for her patience and understanding.

I. Introduction.

The phenomena of turbulence in general and air turbulence in particular affect a wide range of Human activities. From the Air Force point of view turbulence might pose a hazard to aircraft and therefore the modeling and prediction of these phenomena is of interest and importance.

My research interest in the subject date to 1966 when as a research associate at the Institute of atmospheric science at Tel-Aviv University I tried to solve numerically Navier-Stokes equations and investigate the transition to turbulence. In the years since then I did not do active research in this area but kept my interest in it. In particular I was drawn to this field again with the new work about Chaos, Fractals, and Strange attractors. Last year my interests in the subject were stirred again due to work I carried about turbulence modeling of flows in engineering applications. This work and my background in the subject led to my assignment to the "prediction" section at AFGL to perform work related to the prediction of clear air turbulence.

II. Research objectives.

Before I started my work at AFGL I submitted a preliminary proposal regarding the research objectives of my work there. This preliminary proposal is attached hereby. In addition to carrying out the objectives listed there I was able to suggest an alternative method to derive nonlocal turbulence models. Furthermore I derived a parametrization for these models using basic physical principles.

A proposal for summer project on
"Transilient Turbulence Theory"

1. Relation to K-Theory.

Various phenomenological approaches to turbulence exist in the literature. Among these the mixing length theory of Prandtl and Kolmogorov are widely used in applications. Transilient turbulence theory falls within this class of theories and leads in the continuous space-time limit to the following equation for the dispersion of quantity S :

$$\frac{\partial S}{\partial t}(z,t) = \int_{a-z}^{b-z} [S(z+\zeta,t) - S(z,t)] \gamma(z,\zeta) d\zeta \quad (1)$$

where γ is the transilient rate coefficient. Thus while K-theory allows mixing between neighboring vertical boxes only transilient theory allows mixing between non-neighboring boxes.

However the basic dispersion equation in K-theory is

$$\frac{\partial S}{\partial t} = \frac{\partial}{\partial z} \left[K(t,z) \frac{\partial S}{\partial z} \right] \quad (2)$$

and there exist a "tight" relationship between (1) and (2) although this has not been observed by R. Stull.

Thus if we expand $S(z+\zeta,t)$ in a Taylor series around (z,t) we obtain

$$S(z+\zeta,t) = S(z,t) + \frac{\partial S}{\partial z}(z,t)\zeta + \frac{1}{2} \frac{\partial^2 S}{\partial z^2}(z,t)\zeta^2 + \dots \quad (3).$$

Substituting this expression in (1) we obtain

$$\begin{aligned} \frac{\partial S}{\partial t}(z,t) &= \frac{\partial S}{\partial z}(z,t) \int_{a-z}^{b-z} \zeta \gamma(z,\zeta) d\zeta + \\ &+ \frac{1}{2} \frac{\partial^2 S}{\partial z^2} \int_{a-z}^{b-z} \zeta^2 \gamma(z,\zeta) d\zeta + \dots \\ &= K_1(z,t) \frac{\partial S}{\partial z} + K_2(z,t) \frac{\partial^2 S}{\partial z^2} + \dots \end{aligned} \quad (4).$$

Hence there exists a direct link between the two theories which among other things establishes a connection between $K(z,t)$ in (2) and the moments of the transilient rate coefficient $\gamma(z,\zeta)$.

It is therefore our first objective in this project to compare and work out this relationship between the two theories from a theoretical and prediction wise point of view. In particular we shall examine in depth the relationships between the phenomenological coefficients which appear in these two theories.

II Non linear Transilient Turbulence Theory.

The basic relation for the dispersion in transilient theory is

$$[S_i] = [c_{ij}(\Delta t)] [S_j] \quad (5).$$

This establishes a linear relationship for this theory and leads to the linear eq. (1). However it is well known fact that turbulence is inherently nonlinear and it will be of interest therefore to replace (5) by

$$[S_i] = [c_{ij}(\Delta t)] f(S_j) \quad (6).$$

Our second objective in this project is therefore to develop the consequences such a nonlinear relationship and analyze appropriate data to determine the function f in eq. (6). and its continuous space time analog.

III Derivation of Transilient Theory from Basic Principles.

In recent years new ideas to explore Turbulence have been introduced. These are: Strange attractors (Bifurcation theory), fractals and renormalization group theory. It will be of interest to try and explore the possible link between transilient theory and these new ideas regarding turbulence. In particular an attempt should be made to find a way to derive this theory from basic physical principles rather than ad-hoc phenomenological assumptions.

III. Research.

The results of the research conducted by me at AFGL are summerized by the enclosed paper which will be submitted shortly for publication in a research Journal.

Derivation and parametrizations for
Transilient Turbulance theory

Mayer Humi*

Department of Mathematical Sciences
Worcester Polytechnic Institute
Worcester, Massachusetts

ABSTRACT

We show that nonlocal models for turbulence similar to transilient turbulence theory (T3) can be derived by the application of Leonard's filter to the appropriate flow equations. The numerical simulation of scalar dispersion in one dimension using this nonlocal formulation is carried out. Furthermore we examine the relationship between K-theory and T3 and obtain restrictions and relations between their parameters.

*Research sponsored by AFOSR/AFSC, United States Air Force, under contract F49G20-85-C-0013. The U.S. Government is authorized to reproduce and distribute reprints for governmental purposes notwithstanding any copyright notation hereon.

1. Introduction.

In a series of recent articles R. Stull [1-4] and others [5] discussed and applied transilient (nonlocal) theory of turbulence in one dimension. To derive the basic equations of this theory one considers the numerical simulation of a scalar conserved quantity. It is then rather obvious that in a finite time interval a box on a one dimensional (spatial) grid might receive (and make) contributions from all other boxes. Thus if S is the simulated quantity one is led to postulate the relation

$$S_i(t+\Delta t) = \sum_j c_{ij} S_j(t) \quad (1.1)$$

where $S_j(t) = S(z_j, t)$.

Taking the limits of this expression as $\Delta t \rightarrow 0$ and $\Delta x \rightarrow 0$ Stull [1] obtained the nonlocal expression

$$\frac{\partial S}{\partial t} = \int [S(z+\zeta, t) - S(z, t)] \gamma(z, \zeta, t) d\zeta \quad (1.2).$$

In its original version [1] transilient turbulence theory (T3) required the specification of $n^2 - n$ constants on n point grid (eq. (1.1)). To reduce this redundancy Stull suggested recently [4] a four parameter closure relation for the turbulent kinetic energy equation in the horizontal plane (assuming that turbulent mixing is taking place in the vertical z -direction)

$$\frac{\partial E}{\partial t} = - \overline{u'w'} \frac{\partial U}{\partial z} - \overline{v'w'} \frac{\partial V}{\partial z} + \frac{g}{\theta_v} \overline{w'\theta'_v} - \epsilon \quad (1.3)$$

and postulated that the c_{ij} are proportional to $\Delta_t E_{ij}/E_{ij}$ where $E_{ij} = E_j - E_i$ and U, V are the wind components in the x, y directions respectively. (It is obvious however that this last postulate cannot be true across large distances.)

In view of the heuristic nature of the arguments leading to (1.2) and the parametrization of the c_{ij} postulated above it seems worthwhile to attempt to derive a nonlocal theory of turbulence from basic physical principles. Such derivation might also shed some light on the proper choice of the transilient parameters c_{ij} . To accomplish these objectives we use in this paper Leonard's [6] subgrid filtering approach and show that it leads to a nonlocal theory of turbulence. At the same time we show that the limiting process which led to eq. (1.2) from (1.1) is not unique. Using the resulting model equations one can derive the transilient coefficients by well known and well established procedures (sec. 2). From another point of view T3 should be able to reproduce the results obtained using one dimensional K-theory [3,5] for turbulence in some limiting cases. In fact this correspondence has already been pursued by Stull [3]. However this relationship can be further explored to provide constraints and consistency relations on the coefficients in these theories and thus provide another means to parametrize the c_{ij} (sec. 3).

The plan of the paper is as follows: In sec. 2 we derive nonlocal turbulence theory using subgrid modelling. In section 3 we discuss the relationship that exists between K-theory (for turbulence diffusion) and T3 and in section 4 the results of some numerical simulations are presented. We end up in section 5 with some conclusions.

II. Nonlocal Turbulance Theory

One of the basic observations about turbulence is that it involves the interaction of eddies of various sizes. It follows then that while the larger size eddies can be simulated on a computer the smaller, subgrid size, will always present a problem in this regard. A way out of this dilemma has been suggested by Leonard's subgrid filter [6] which postulates that the smeared value of a given turbulent quantity f is given by

$$\bar{f}(\underline{x}, t) = \int_{\text{all space}} G(\underline{x} - \underline{x}') f(\underline{x}', t) d\underline{x}' \quad (2.1)$$

where G is some unspecified function (at the present).

For one dimensional turbulent flow the basic equation governing the evolution of a scalar quantity S is [7,8]

$$\frac{\partial S}{\partial t} + u \frac{\partial S}{\partial x} = k \frac{\partial^2 S}{\partial x^2} \quad (2.2)$$

(For clarity we consider here the one dimensional case only. The generalization of the following discussion to three dimensions is straightforward.)

Applying the filter operation to eq. (2.2) we obtain:

$$\frac{\partial \bar{S}}{\partial t} + \overline{u \frac{\partial S}{\partial x}} = k \frac{\partial^2 \bar{S}}{\partial x^2} \quad (2.3)$$

To rewrite the middle term in this equation using smeared quantities we introduce

$$u = \bar{u} + u' , \quad S = \bar{S} + S'$$

where u' , S' are the turbulent residuals. We then have

$$\overline{u \frac{\partial S}{\partial x}} = \overline{\bar{u} \frac{\partial \bar{S}}{\partial x}} + R_{Su} \quad (2.4)$$

where

$$R_{Su} = \overline{\bar{u} \frac{\partial S'}{\partial x}} + \overline{u' \frac{\partial \bar{S}}{\partial x}} + \overline{u' \frac{\partial S'}{\partial x}} \quad (2.5)$$

Several closure relations were suggested in the literature to model R_{Su} e.g., [7]

$$R_{Su} = -c \frac{\partial^2 \bar{S}}{\partial x^2} \quad (2.6)$$

which yields

$$\frac{\partial \bar{S}}{\partial t} + \overline{u \frac{\partial \bar{S}}{\partial x}} = (c+k) \frac{\partial^2 \bar{S}}{\partial x^2} \quad (2.7)$$

To write this equation explicitly we introduce $x' = x + \zeta$ and observe that

$$\begin{aligned} \overline{u \frac{\partial \bar{S}}{\partial x}} &= \int G(x-x') \bar{u}(x', t) \frac{\partial \bar{S}}{\partial x'}(x', t) dx' = \\ &= - \int \frac{\partial}{\partial x'} [G(x-x') \bar{u}(x', t)] \bar{S}(x', t) dx' = \\ &= - \int \frac{\partial}{\partial \zeta} [G(-\zeta) \bar{u}(x+\zeta, t)] \bar{S}(x+\zeta, t) d\zeta \\ &= - \int \gamma(x, \zeta, t) \bar{S}(x+\zeta, t) d\zeta \end{aligned}$$

Thus eq. (2.7) is equivalent to the integrodifferential equation

$$\frac{\partial \bar{S}}{\partial t} = (c+k) \frac{\partial^2 \bar{S}}{\partial x^2} + \int \gamma(x, \zeta, t) \bar{S}(x+\zeta, t) d\zeta \quad (2.8)$$

which is a nonlocal equation for the evolution of \bar{S} .

Eq. (2.8) demonstrates clearly that nonlocality is inherent to any theory of turbulence which smears out the effects of subgrid eddies on the flow. From a practical point of view eq. (2.8) has to be coupled with an equation for \bar{u} . Thus in one and three dimensions respectively, eq. (2.8) should be solved in conjunction with Burger's equation or Navier Stokes equations in their filtered form [7, 8] (furthermore in 3-d the proper generalization of (2.8) should be used). To see how this is done we consider Burger's equation

$$\frac{\partial u}{\partial t} + u \frac{\partial u}{\partial x} = \nu \frac{\partial^2 u}{\partial x^2} + F(x, t) \quad (2.9).$$

Applying the filter G to this equation yields

$$\frac{\partial \bar{u}}{\partial t} + \bar{u} \frac{\partial \bar{u}}{\partial x} = \nu \frac{\partial^2 \bar{u}}{\partial x^2} + \bar{F}(x, t) \quad (2.10).$$

Substituting $u = \bar{u} + u'$ in the second term of (2.5) we obtain

$$\overline{u \frac{\partial u}{\partial x}} = \overline{\bar{u} \frac{\partial \bar{u}}{\partial x}} + \overline{u' \frac{\partial \bar{u}}{\partial x}} + \overline{\bar{u} \frac{\partial u'}{\partial x}} + \overline{u' \frac{\partial u'}{\partial x}} = \overline{\bar{u} \frac{\partial \bar{u}}{\partial x}} + R_{uu} \quad (2.11).$$

A common closure relation for R_{uu} is [8]

$$R_{uu} = -\mu \frac{\partial^2 \bar{u}}{\partial x^2} \quad (2.12).$$

As to the first term on the right hand side of (2.6) we have

$$\begin{aligned}\overline{\bar{u} \frac{\partial \bar{u}}{\partial x}} &= \frac{1}{2} \int G(x-x') \frac{\partial}{\partial x} (\bar{u}^2)(x', t) dx' \\ &= \frac{1}{2} \int \frac{\partial G}{\partial \zeta} (-\zeta) \bar{u}^2(x+\zeta) d\zeta\end{aligned}\quad (2.13)$$

where $\zeta = x' - x$

We conclude therefore that the filtered form of Burger's equation is

$$\frac{\partial \bar{u}}{\partial t} = (v+\mu) \frac{\partial^2 \bar{u}}{\partial x^2} + \frac{1}{2} \int \frac{\partial G}{\partial \zeta} (-\zeta) \bar{u}^2(x+\zeta) d\zeta + \bar{F}(x, t) \quad (2.14)$$

Similar derivation can be carried out for the filtered form of Navier Stokes equation. We observe that the nonlocal form of eqs (2.2), (2.9) is new. In fact in the literature the normal procedure so far has been to approximate the second term in (2.5) by a higher (third) order derivative of \bar{u} . In the resulting numerical scheme to evaluate \bar{u} , \bar{S} the function γ is parameterized only in terms of basic physical constants and the choice of the filter G .

At first glance it might seem that eq. (1.2), which represents T3, and eq. (2.8) are quite different. However when we rewrite eq. (2.8) using finite differences on a one dimensional grid we obtain a relation which is exactly in the

form of eq. (1.1). This demonstrates that eq. (1.1) can result from different differential expressions if the constants c_{ij} are considered as parameters. Furthermore, eq. (2.8) demonstrates that a diffusion term should (most probably) be included in (1.2). Obviously, however, eq. (2.8) is somewhat superior to eq. (1.2) in that it does not require the heuristic relation with the turbulent kinetic energy equation which is needed to evaluate the c_{ij} in T3.

III. T3 and K-theory.

From its inception, T3 was closely related to K-theory for eddy diffusion which is governed (in one dimension) by

$$\frac{\partial S}{\partial t} = \frac{\partial}{\partial z} (K(z, t) \frac{\partial S}{\partial z}) \quad (3.1)$$

In fact Stull [3] has already explored the relationship between these two theories by comparing their predictions regarding the bulk dispersion rates of S (which are related to the second moment of S).

From another point of view, T3 can be considered as a "higher order" form of K-theory and therefore should match asymptotically with eq. (3.1). In fact if we make the Taylor expansion

$$S(z+\zeta, t) = S(z, t) + \frac{\partial S}{\partial z} \zeta + 1/2 \frac{\partial^2 S}{\partial z^2} \zeta^2 + \dots \quad (3.2)$$

and substitute in (1.2) we obtain

$$\frac{\partial S}{\partial t}(z, t) = \sum_{n=1}^{\infty} M_n(z, t) \frac{\partial^n S}{\partial z^n} \quad (3.3)$$

where

$$M_n(z, t) = \frac{1}{n!} \int_{-\infty}^{\infty} \zeta^n \gamma(z, \zeta, t) d\zeta \quad (3.4)$$

Thus K-theory can be considered as a truncated T3 where the infinite sum on the right hand side of (3.3) has been replaced by the first two leading terms with the additional constraint $\frac{\partial M_2}{\partial z} = M_1$. Our objective in this section is therefore to explore the correspondence between these two theories in order to find constraints and consistency relations between the general forms of K and γ . From a practical point of view such relations will enable us to obtain approximate expressions for the transilient coefficient and will thereby check the validity of the closure relation about these coefficients which was introduced by Stull through eq. (1.3).

To a certain extent, Stull [3] already made an attempt to explore this relationship between T3 and K-theory by expanding

both S and γ in (1.2) around $\zeta = 0$. This leads, however, to the erroneous expression

$$\frac{\partial S}{\partial t} = \frac{\partial S}{\partial z} \cdot \frac{\partial \gamma}{\partial \zeta}(z, 0, t) \int_{-\infty}^{\infty} \zeta^2 d\zeta + \frac{1}{2} \frac{\partial^2 S}{\partial z^2} \gamma(z, 0, t) \int_{-\infty}^{\infty} \zeta^2 d\zeta + \dots (3.5)$$

which is meaningless. To get out of this difficulty, Stull [3] suggests to introduce an arbitrary constant β and replace the infinite integral in (3.5) by an integral over $[-\beta, \beta]$. This then yields;

$$K = \frac{\beta^3}{3} \gamma(z, 0, t) \quad (3.6)$$

This equation can be used to find the functional dependence of γ on ζ only when γ is effectively a function of two variables e.g. $\gamma = \gamma(z-\zeta, t)$ which would imply that

$$\gamma(z-\zeta, t) = \frac{3K(z-\zeta, t)}{\beta^3} \quad (3.7).$$

In what follows we show that the results given above can be sharpened considerably by using an appropriate orthogonal expansion of γ . Moreover we shall demonstrate that the parameter β contains the nonlocal nature of T3.

We consider several cases:

(a) No apriori assumptions on the functional form of γ are made.

Since the integrals in (3.4) are over $[-\infty, \infty]$ it is natural to expand γ in terms of a complete set of orthonormal functions over this range. As is well known [9], such a set is given by $\{Y_n(\zeta)\}_0^\infty$ where

$$Y_n(\zeta) = \frac{1}{\sqrt{2^n \cdot n! \sqrt{\pi}}} e^{-\frac{1}{2} \zeta^2} H_n(\zeta) = \frac{1}{a_n} e^{-\zeta^2/2} H_n(\zeta) \quad (3.8)$$

where $H_n(\zeta)$ are Hermite polynomials.

Expanding γ using these functions

$$\gamma(z, \zeta, t) = \sum_{n=0}^{\infty} a_n(z, t) Y_n(\zeta) \quad (3.9)$$

and substituting in (3.3) we obtain

$$\frac{\partial S}{\partial t} = \frac{\partial S}{\partial z} \sum_{n=0}^{\infty} a_n(z, t) \int_{-\infty}^{\infty} \zeta Y_n(\zeta) d\zeta + \frac{1}{2} \frac{\partial^2 S}{\partial z^2} \sum_{n=0}^{\infty} \int_{-\infty}^{\infty} \zeta^2 Y_n(\zeta) d\zeta + \dots \quad (3.10)$$

The integrals

$$b_n = \int_{-\infty}^{\infty} \zeta Y_n(\zeta) d\zeta, \quad c_n = \int_{-\infty}^{\infty} \zeta^2 Y_n(\zeta) d\zeta$$

can be computed using basic identities of the Hermite

polynomials. It can be shown that, $b_n = 0$ when n is even and $c_n = 0$ when n is odd. Thus

$$\frac{\partial S}{\partial t} = \frac{\partial S}{\partial z} [b_1 a_1 + b_3 a_3 + \dots] + \frac{1}{2} \frac{\partial^2 S}{\partial z^2} [c_0 a_0 + c_2 a_2 + \dots] + \dots \quad (3.11)$$

Comparing (3.11) with (3.1) enables us to solve for a_0 , a_1 and we obtain a first approximation for γ in the form

$$\gamma(z, \zeta, t) = 2e^{-\zeta^2/2} \left[\frac{K(z, t)}{c_0} + \frac{\zeta}{\beta_1} \frac{\partial K}{\partial z}(z, t) \right] \quad (3.12)$$

(b) γ is symmetric in z and ζ i.e.

$$\gamma(z, \zeta, t) = \gamma(\zeta, z, t) \quad (3.13)$$

Writing

$$K(z, t) = \sum b_n(t) Y_n(z) \quad (3.14)$$

and

$$\gamma(z, \zeta, t) = \sum_{n=0}^{\infty} \sum_{m=0}^{\infty} a_{mn}(t) Y_n(z) Y_m(\zeta) \quad (3.15)$$

it follows from (3.13) that $a_{n,m} = a_{m,n}$. Comparing (3.1) and (3.3) using these expansions yield (after some algebra)

$$\sum_{n=1}^{\infty} b_n \left[\frac{n\alpha_{n-1}}{\alpha_n} Y_{n-1} - \frac{\alpha_{n+1}}{2\alpha_n} Y_{n+1} \right] =$$

$$= \sum_{n=0}^{\infty} \left(\sum_{m=0}^{\infty} a_{n,m} \beta_n \right) Y_n \quad (3.16)$$

Assuming that the b_n 's are known we can truncate eq. (3.16) and solve for $a_{n,m}$ of the resulting number of equations is equal to the number of unknowns. An easy calculation shows that this happens when $n = m = 3$. It follows then that under the present assumptions one can solve for the first six $a_{n,m}$ (actually nine due to symmetry) in (3.15).

$$(c) \quad \gamma = \gamma(z-\zeta, t)$$

Expanding γ as

$$\gamma = \sum_{n=0}^{\infty} a_n(t) Y_n(z-\zeta) \quad (3.17)$$

and substituting in (3.3) we obtain after evaluating M_1 , M_2 and comparing with (3.1) that K must be of the form

$$K(z, t) = [A(t)z^2 + B(t)z + C(t)]e^{-z^2/2} \quad (3.18)$$

Thus the ansatz $\gamma = \gamma(z-\zeta, t)$ is compatible with K-theory only if K is a second order polynomial in z for all t .

$$(d) \quad \gamma = \gamma(|z-\zeta|, t)$$

Since $|z-\zeta| \geq 0$ it is appropriate to use in this case an orthonormal basis of $L^2[0,\infty]$ to expand γ . Such a basis is given by [9]

$$\psi_K(\eta) = \frac{1}{a_K} e^{-\eta/2} L_K(\eta) \quad , \quad K = 0, 1, \dots \quad (3.19)$$

where

$$L_K(\eta) = e^{\eta} \frac{d^K}{d\eta^K} (\eta^K e^{-\eta}) \quad (3.20)$$

are the Leguerre polynomials and a_K are normalization constants. Letting

$$\gamma(\eta, t) = \sum_n a_n(t) \psi_n(\eta) \quad , \quad \eta = |z-\zeta| \quad (3.21)$$

and substituting in (3.3) we obtain after evaluating the appropriate integrals (and a long algebra) that

$$K = \sum_{n=0}^{\infty} a_n(t) \left[z^2 \int_0^{\infty} \psi_K(u) du + \int_0^{\infty} u^2 \psi_K(u) du \right] e^{-z/2} \quad (3.22)$$

Thus an expression for $K(z, t)$ is compatible with the present functional form of γ only if K is an even second order polynomial in z .

IV. Scalar dispersion in one dimension.

To simulate numerically scalar dispersion in one dimension using the nonlocal formulation derived in section II we use eqs (2.8) and (2.14). In these equations we approximate the partial derivatives using central finite differences and for G we use the Gaussian filter

$$G(x) = \frac{1}{\sqrt{\pi}\sigma} \exp(-x^2/\sigma^2) \quad (4.1)$$

where σ the standard deviation is considered as a parameter (σ essentially determines the nonlocality of the theory).

Introducing the notation $\bar{\mu}_i(t) = \bar{u}(x_i, t)$, $\bar{S}_i(t) = \bar{S}(x_i, t)$ and using the assumptions and approximations described above we obtain the following scheme for the evolution of u and S_i

$$\begin{aligned} \bar{\mu}_i(t+\Delta t) = & \mu_i(t) + \Delta t \left\{ \alpha \left[\frac{\bar{u}_{i+1} + \bar{u}_{i-1} - 2\bar{u}_i}{2\Delta x} (t) \right] + \right. \\ & \left. + \sum_{j=-K}^K G''(-\zeta_j) \bar{u}_{i+j}^2 \Delta x \right\} \end{aligned} \quad (4.2)$$

$$\begin{aligned} \bar{S}_i(t+\Delta t) = & \bar{S}_i(t) + \Delta t \left\{ \beta \left[\frac{\bar{S}_{i+1} \bar{S}_{i-1} - 2\bar{S}_i^2}{2\Delta x} (t) \right] \right. \\ & \left. + \sum_{j=-K}^K \gamma_i(\zeta_i, t) \bar{S}_{i+j} (t) \Delta x \right\} \end{aligned} \quad (4.3)$$

where α, β are the lumped diffusion coefficients, K a cutoff (integer) parameter and

$$\gamma_i(\zeta_j, t) = -G'(-\zeta_j)\bar{u}_{i+j}(t) + G(-\zeta_j) \left[\frac{\bar{u}_{i+j+1} - \bar{u}_{i+j-1}}{2\Delta x}(t) \right] \quad (4.4)$$

To gauge the effect of the filter G (and the nonlocal formulation) on the solution of eqs. (2.2), (2.9) we compared the numerical results for the evolution of \bar{S}, \bar{u} with the direct solution of these equations using central finite differences. However, to solve eq. (2.9) we first linearized it using the standard transformation

$$u = -2\nu \frac{\partial}{\partial x} \ln \varphi(x, t) \quad (4.5)$$

The results of these simulations for different values of ν and σ subject to the initial conditions

$$u(x, 0) = \sin(\pi x/100) \quad 0 \leq x \leq 100$$

$$s(x, 0) = \delta(x-50)$$

are summarized in tables 1,2.

V. Conclusions

We showed that nonlocal models of turbulence follow directly from Leonard's subgrid filtering. However the actual determination of this filter from basic physical principles remains an open problem.

While we have carried out some numerical simulation of these models in one dimension we have as yet to apply them to actual geophysical problems of interest. In particular it will be useful to simulate the turbulent boundary layer with this approach and compare the results with actual data. Work toward the resolution of this question is now in progress.

References

1. R. B. Stull - Transilient Turbulance theory I, J. Atmos. Sci. 41, p. 3351 (1984).
2. R. B. Stull - Transilient Turbulance theory II, J. Atmos. Sci. 41, p. 3368 (1984).
3. R. B. Stull - Transilient Turbulance theory III, J. Atmos. Sci. 43, p. 50 (1986).
4. R. B. Stull and A. G. M. Driedonks - Applications of the transilient trubulance parametrization to atmospheric boundary layer simulations, Boundary Layer Meteor. (1987) in press.
5. B. H. Fiedler and C. Moeng - A practical integral closure model for mean vertical transport of a scalar in a convective boundary layer, J. Atmos. Sci. 42, p. 359 (1985).
6. A. Leonard - Energy cascade in large eddy simulations of turbulent fluid flow, Adv. Geophys. 18A, p. 237 (1974).
7. M. A. Domis - Large eddy simulation of a passive scalar in isotropic turbulence, J. Fluid Mech. 104, p. 55 (1981).
8. M. D. Love - Subgrid modelling studies with Burger's equation, J. Fluid Mech. 100, p. 87 (1980).
9. B. Spain and M. G. Smith - Functions of Mathematical Physics, Van Nostrand Co., 1970 (New York).

IV. Recommendations.

The major points along which my research at AFGL should be continued are:

- (1) The modelling of Leonard's filter G from physical first principles.
- (2) Application of the resulting models to the prediction of clear air turbulence with and without Topography.
- (3) Apply the models to various practical situations. In particular we would like to create explicit "guide" to predict under what circumstances clear air turbulence is present and poses a hazard to aircrafts in the area.

In the proposal for a minigrant to be submitted shortly to AFOSR we expand on these research objective and suggest explicit techniques to resolve these issues.

1987 USAF-UES SUMMER FACULTY RESEARCH PROGRAM/

GRADUATE STUDENT SUMMER SUPPORT PROGRAM

Sponsored by the

AIR FORCE OFFICE OF SCIENTIFIC RESEARCH

Conducted by the

Universal Energy Systems, Inc.

FINAL REPORT

LEACHING AND HYDROLYSIS OF SOME CHLORINATED SOLVENTS

Prepared by: Peter M. Jeffers, Ph. D.

Academic Rank: Professor and Chairman

Department and Chemistry Department

University: SUNY - Cortland

Research Location: HQAFESC

Tyndall AFB

Panama City, Fl. 32601

USAF Researcher Dr. Tom Stauffer

Date: 8/28/87

Contract No: F49620-85-C-0013

LEACHING AND HYDROLYSIS
OF SOME
CHLORINATED SOLVENTS

by

PETER M. JEFFERS

ABSTRACT

Rapid Runway Repair material, PERCOL S-100, was evaluated to determine if its use and/or disposal poses any significant environmental hazard. Perchloroethylene does leach from PERCOL S-100 into water to a potentially alarming extent.

High temperature hydrolysis measurements were performed with carbon tetrachloride, trichloroethylene, and perchloroethylene from pH 2 - 12 and 100° C - 170° C. Under these conditions perchloroethylene remains essentially inert while TCE is reactive under basic conditions, and CCl₄ reacts regardless of pH. The data allow extrapolation to neutral, room temperature conditions with predicted half lives of 2.6 years for CCl₄ and 4.4 x 10⁵ years for TCE.

Acknowledgements

Sincere thanks to HQAFESC, the Air Force Systems Command, and the Air Force Office of Scientific Research for sponsoring this research. Universal Energy Systems effectively administered the program.

Dr. Tom Stauffer suggested directions and provided help where and when it was needed. Mr. Don Wickman was always willing to assist with equipment operation. Ms. Kim Buggs was a willing assistant in performing many of these experiments. TSgt. Jim Whitcomb provided invaluable legwork during the research period.

I. INTRODUCTION

PERCOL S-100 is a rapid runway repair material formulated for Air Force use. Many tons of the polymer material have been produced. One of the two components of the S-100 (which are mixed 1:1) is supplied in 70% by weight C_2Cl_4 solution. The first objective of this particular research effort was to determine the extent to which S-100 might be a hazardous (waste) material because of its PCE content. An investigation of the rate of PCE loss both into a vacuum and into water was made.

There is a closely related but more general problem. Once any halogenated solvent is introduced to the ground water system, it will migrate with the aquifer flow, retarded by adsorption, and possibly will be consumed either by soil microbes or by abiotic hydrolysis reactions. Few reports are in the literature on the rate of hydrolysis of halogenated solvents, yet such processes may be significant sinks for contaminants, especially in light of the very long residence times of ground water in aquifers. Some knowledge of hydrolysis loss rate is required to do valid modelling calculations which often are the basis of clean-up actions which can be very costly.

A major resource on the chemistry of various contaminants is the EPA publication "Water Related Environmental Fate of 129 Priority Pollutants" (Callahan, 1979). This volume gives a half life for CCl_4 of between 7 years and 7000 years at pH 7 and 25°C with the reaction listed as pH sensitive. Dilling (1975) reports the TCE is hydrolyzed/oxidized with a half life of about 10.7 months at 25°C, but says

nothing about pH dependence of the reaction. The EPA states (Kover, 1975) that TCE is not hydrolyzed by water under normal conditions. Finally, Dilling (1975) found a half life of about 8.8 months for PCE at room temperature. Enough uncertainty exists in all these reports that additional study of the hydrolysis reactions appeared a valuable contribution.

II. EXPERIMENTAL APPROACHES AND RESULTS

A. PERCOL S-100

A Varian gas chromatograph, model 3700 with flame ionization detector and SPD-5 Supelco .75mm x 30 m column was used for all analyses.

Air samples taken near a freshly broken surface of PERCOL S-100 did contain PCE. This escape of PCE into the air was measured more quantitatively by placing several fresh chips of S-100 in a 40 ml glass vial with teflon lined septum cap for 30 min. A sample of the air from the vial contained PCE at over one half the vapor pressure of pure liquid PCE. The actual partial pressure was 8.4 torr (vapor pressure of PCE is 14 torr).

Fresh chips of S-100 were placed in distilled water, 0.1 M NaOH, and 0.1 M HCl in 40 ml septum vials for 24 hours. All three of these solutions leached PCE to the same extent, within experimental error, which was about 200 mg/l or essentially the saturation value for PCE/water.

A further check on PCE loss from PERCOL S-100 was a measurement of weight loss of a 1.8 g sample of the polymer as it was continuously pumped on a vacuum system. Figure 1 shows the weight loss - time curve for 100 hours. After an initial rapid weight loss, further loss was slower but nearly linear. The 100 hour weight loss was about 2%

of the total weight. After 200 hours under vacuum, the chips looked chalky green-white rather than their initial sea green color. When these chips were cut into smaller chunks, the "white" layer appeared much less than 1 mm thick. An additional 45 hours pumping led to a further 0.5% weight loss which corresponds very nearly to the linear rate observed between 20 and 100 hours. The material pumped off was trapped in a liquid nitrogen trap and was identified as PCE.

B. HYDROLYSIS STUDIES - METHODS

Since all indications are that hydrolysis for most halogenated solvents is slow, high temperature studies appeared the only feasible approach to determining rates for these reactions. Careful rate measurements over a range of temperatures allows evaluation of the Arrhenius parameters and thus valid extrapolation to temperature conditions outside the range of the experiments. The general procedure was to prepare aqueous solutions of a mixture of CCl_4 , TCE, and PCE in the concentration range 10 - 100 mg/l at pH adjusted to 2 - 12, and seal the solutions in pyrex bulbs, about 250 microliter in volume. These bulbs were placed in the oven of a HP 5710A gas chromatograph and were removed at appropriate time intervals, opened, and analyzed for decrease of reactant concentration. Several bulbs were kept at room temperature to serve as standards. The temperature range was $100^\circ - 170^\circ \text{C}$.

The Pyrex bulbs were either drawn from standard wall 6 mm tubing or blown from 7mm o.d. x 2mm i.d. capillary tubing. In either case it was essential to leave about 30 μl of a 250 μl bulb unfilled with liquid to avoid explosion of the bulbs upon heating.

The water used was distilled water which was purged with a stream

of nitrogen for 30 minutes. Solvents were reagent grade, used as supplied. Solutions were prepared in two ways. Usually the solvents were dissolved, by weight, in methanol and a carefully measured volume of the CH_3OH solution was added to water with stirring. Some reaction mixtures were prepared by diluting water shaken with a mixture of the pure halogenated solvents to get nearly saturated solutions free of methanol or other solvents. Results from either method of sample preparation were comparable. Desired values of pH were attained by adding .1 M NaOH or .1 M HCl to the de-aerated water, monitoring pH with an Orion Research model digital pH meter. Immediately after pH adjustment, the chlorinated solvents were added and the solution was poured into a 25 ml beaker containing the sample bulbs so they would fill completely and simultaneously. The bulbs were all sealed within three minutes of filling. This procedure was necessary to assure all starting concentrations were equal since vaporization loss is very rapid with these materials.

Concentrations were determined by measuring peak areas, using computer data acquisition and the HP Lab Automation System. The base line was determined individually for each peak, since in many instances the peak of interest was on the tail of some other component. A sample chromatograph is shown in Figure 2 with the base lines drawn in and the computer measured areas printed near the peaks.

Preliminary hydrolysis measurements were planned for PCE because of its potential introduction into groundwater from PERCOL S-100, and for TCE which is a common groundwater contaminant and has been spilled on Air Force installations. The inclusion of CCL_4 in the reaction mixture was planned as an internal standard since a comment by Vogel (1985) implied ~ 1000 years half life for CCL_4 in aqueous solutions.

Since hydrolysis reactions may be either acid or base catalyzed, a wide pH range was planned to see if reactive conditions could be spotted.

The first experiments were at 135 - 150°C, in .1 M HCl, .1 M NaOH, or neutral water solution, and were allowed to react for one to three days. Further early studies utilized nominal pH's of 2, 4, 7, 10, and 12, with sampling at 2 hr - 95 hr. These experiments were hampered by frequent explosions of the Pyrex bulbs which eventually led to the realization that a small air space in the sealed bulb was essential. The explosions were not due to the increase in water vapor pressure but rather to the water thermal expansion and the inherent incompressibility of any liquid. However, the air space was kept as small as possible, since calculations with the Henry's law constants for these solvents show that there will be significant escape to the gas phase.

Early positive observations were that TCE hydrolyzed in basic solution with a significant activation energy. CCl_4 was found to react rapidly at 100° at all pH values. The reaction rates were such that nearly all the CCl_4 and TCE had disappeared within the initial 2 hour check period, indicating that lower temperatures and shorter time intervals should yield reasonable kinetics results. The PCE was stable at all pH values and temperatures, for up to the 95 hours of the longest test. Thus PCE was chosen as the internal standard for all further kinetics experiments.

C. KINETICS RESULTS

All rate experiments were analyzed as (pseudo) first order processes:



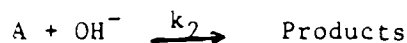
$$-dA/dt = k_1 A$$

or, in integrated form:

$$\ln A_0/A_t = k_1 t.$$

Thus a plot of $\ln (A_0/A_t)$ vs time gives the rate constant as the slope, where A_0 is the initial reactant concentration and A_t is the concentration at time t . Since the ratio is calculated, absolute concentrations need not be determined.

For a base catalyzed hydrolysis, the rate law frequently found is:



$$-dA/dt = k_2 (OH^-)(A)$$

$$= k_1 (A)$$

where $k_1 = k_2 \times (OH^-)$ is the pseudo first order rate constant, which obviously now depends on base concentration. The value for k_1 can be found as above. This treatment is valid if the OH^- concentration is significantly larger than the reactant concentration, so OH^- concentration remains essentially constant as the reaction proceeds. The concentrations of TCE and CCl_4 were in the range $1 - 2 \times 10^{-4}$ mole/l, while pH = 12 has OH^- at 10^{-2} mole/l, so the assumption of pseudo first order conditions is valid for the pH 11 - 12 range where base catalysis was observed for the TCE reaction.

A further check of the validity of the first order or pseudo first order assumption is the shape of the $\ln (C_0/C)$ vs. time plot. If the curve is linear, the assumption is reasonable. Mabey and Mill (1978) refer to Fells (1959), asserting that CCl_4 hydrolyzes by a second order rate law.

Figures 3 and 4 show experimental results for CCl_4 disappearance

at 160°C for two initial concentrations, different by a factor of 7. Both plots show the points calculated for both first order decay ($\ln C_0/C$) and second order reaction ($1/C$). Both sets of data fit the same linear $\ln C_0/C$ relation, and the 2nd order data treatment is clearly a poor representation of the reaction. All further experiments for both TCE and CCl_4 were analyzed as 1st order reactions with reasonably linear results substantiating the 1st order assumption.

Dilling's (1975) experiments imply that at least some of the reactant loss, especially of TCE, may be due to oxidation or may be oxygen accelerated. This possible effect of oxygen was tested by preparing two sets of samples: one set utilized water equilibrated with air, and the sample bulbs contained the usual 30 μ l of air. The second set was prepared from water which had been de-aerated by bubbling a stream of nitrogen through it for 30 min. and the solvent addition and bulb filling and sealing were accomplished under a nitrogen blanket to exclude all oxygen. Figure 5 shows that for both CCl_4 and TCE the presence or absence of O_2 makes no change in the rate of reactant loss, although a calculation shows that the amount of O_2 in the 30 μ l air space is about a 3 fold molar excess, compared to the amount of reactant in the solution. Further experiments were executed with no attempt to exclude O_2 .

The EPA summary (Callahan, 1979) reports CCl_4 hydrolysis at pH 7 and makes no mention of pH with TCE hydrolysis. Figures 6 and 7 show results of hydrolysis experiments for CCl_4 and TCE with pH varied from 4 to 12. Figure 6 indicates that the reaction of CCl_4 is pH insensitive. The same line is a reasonable representation of the

results at pH 4, 11.4, or 12.0. Early experiments over the entire range pH 2 - 12 were consistent with the conclusion that CCl_4 decomposes at the same rate at all pH. Figure 7, on the other hand, shows the strong influence of pH on the TCE reaction. The pH 12.0 and pH 11.4 runs were done simultaneously, and the slopes of the rate curves differ by a factor of 4, within experimental error. A run at pH 4 showed essentially no reaction at over 2 hours. These results are consistent with a base catalyzed hydrolysis, 1st order in OH^- . The uncatalyzed or acid catalyzed reaction proceeds at a negligible rate. One other set of runs at pH 12 and pH 11 gave rates different by a factor of ten, as expected, while numerous runs at pH 5 - 7 and early experiments at pH 2 showed no reaction of TCE over times up to 60 hours.

Reaction rates were determined over a series of temperatures from 100°C to 170°C , with results shown by Figures 8 and 9. The TCE runs were all at pH 12.0. Slopes of these curves give the rate constants at each temperature and the Arrhenius plots of these results are shown in Figure 10 from which activation energies and pre-exponential factors were determined. The rate expressions found are:

$$k_1(\text{CCl}_4) = 4.79 \times 10^9 e^{-21,790\text{cal}/RT} \text{ min}^{-1}$$

$$k_1(\text{TCE}) = 7.51 \times 10^{13} e^{-27,820\text{cal}/RT} \text{ min}^{-1}.$$

The expression for TCE is a pseudo 1st order rate constant, for pH 12. For any other value of pH, the corrected rate constant would be multiplied by a factor of $(\text{OH}^-)/10^{-2}$. Specifically, at pH 7,

$$k_1(\text{TCE}) = 7.51 \times 10^8 e^{-27,820\text{cal}/RT} \text{ min}^{-1}.$$

at 25°C , $k_1(\text{CCl}_4) = 4.99 \times 10^{-7} \text{ min}^{-1}$ and

$k_1(\text{TCE}) = 2.97 \times 10^{-12} \text{ min}^{-1}$. For a first order process, the half life is found by $\tau_{1/2} = 0.693/k$ which gives

$$\tau_{1/2}(\text{CCl}_4) = 2.64 \text{ years}$$

$$\tau_{1/2}(\text{TCE}) = 4.4 \times 10^5 \text{ years.}$$

These results mean that there can be significant reactive loss of CCl_4 in aquifers, in view of the very long residence times common for groundwater flow. However, since groundwater systems would never approach strongly basic conditions, it is likely that abiotic loss of TCE by hydrolysis is a process which can legitimately be ignored.

III. RECOMENDATIONS.

a. Rapid Runway Repair material PERCOL S-100 may be a toxic waste. It does contain large amounts of PCE which will leach into ground water at significant concentrations and rates. Total loss of PCE will be very slow, certainly a time period of very many years. The rate of loss will increase with surface area, so if the solid PERCOL S-100 is ground, crushed, or otherwise broken into small pieces, it represents more of a hazard. Once leached into groundwater, PCE is a very long lived material.

b. Hydrolysis experiments at 100 - 170°C allowed extrapolation of reaction rates to room temperature conditions. Measurements on PCE, TCE, and CCl_4 show that both PCE and TCE should be very stable and long lived in aquifers. However, CCl_4 has a half life of about 2.6 years, so significant loss can occur by hydrolysis in aquifers and in the ocean. The loss of CCl_4 was found to be 1st order in contrast to the previous literature report of a 2nd order reaction.

REFERENCES

Callahan, M. A., et.al, "Water Related Environmental Fate of 129 Priority Pollutants", EPA-440-79-029b, Vol. 2, (1979).

Dilling, W. L., N. B. Tefertiller, and G. J. Kallos, Environ. Sci. Technol. 9(9), 833, (1975).

Fells, I. and E. A. Moelwyn-Hughes, J. Chem. Soc., 398, (1959).

Kover, F. D., "Prelim. Study of Selected Environ. Contaminants", EPA 560-2-75-002, (1975).

Mabey, W. and T. Mill, J. Phys. Chem. Ref. Data 7, 383, (1978).

Vogel, T. M., and M. Reinhard, "Hydrolysis and Dehydrobromination of Simple Bromoalkanes", preprint, (1985).

PERCOL S-100

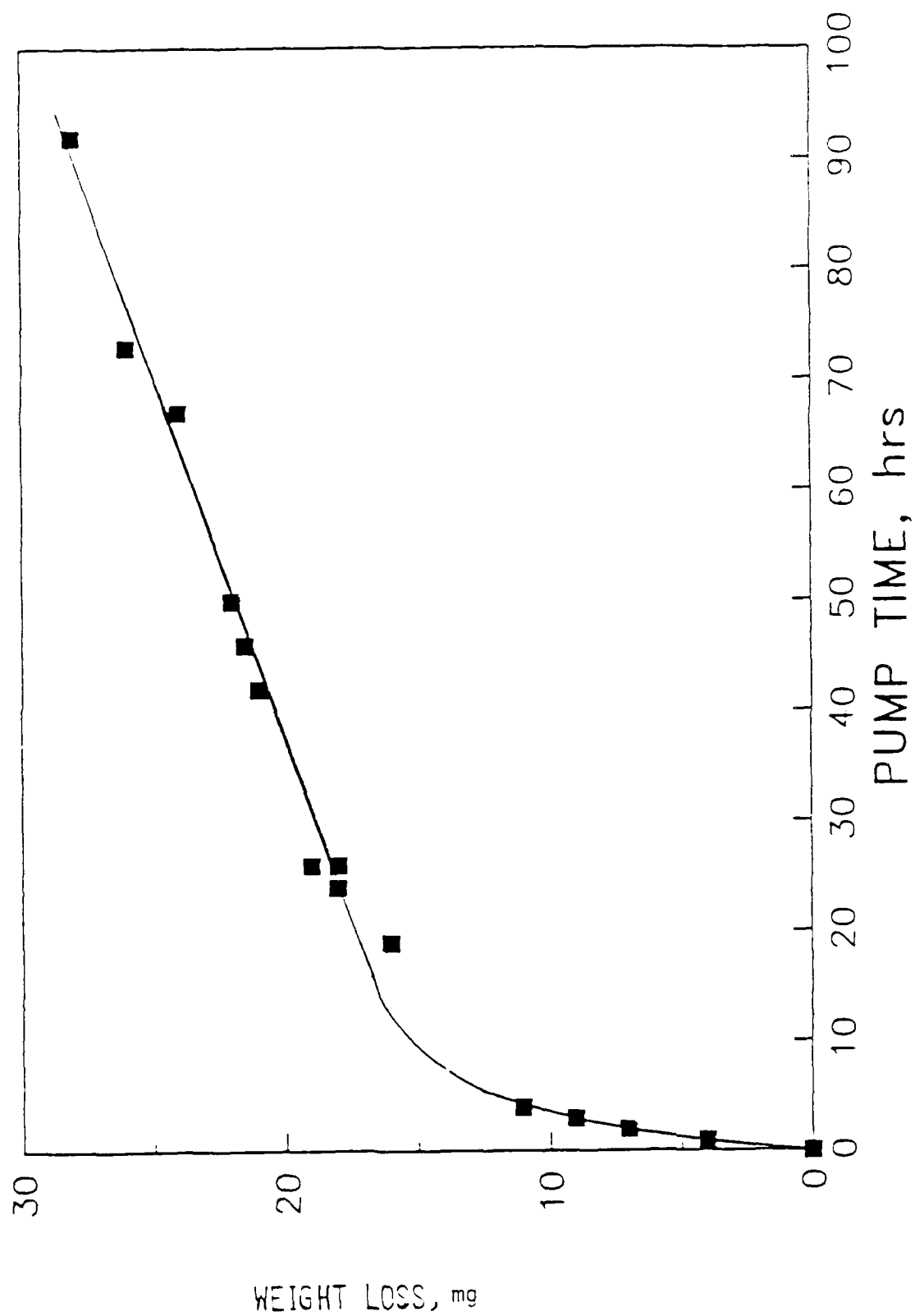
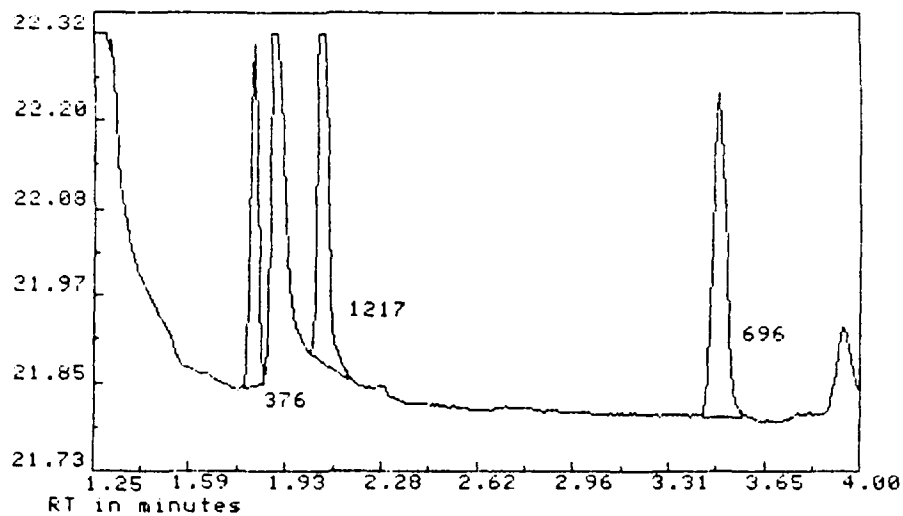


Figure 1

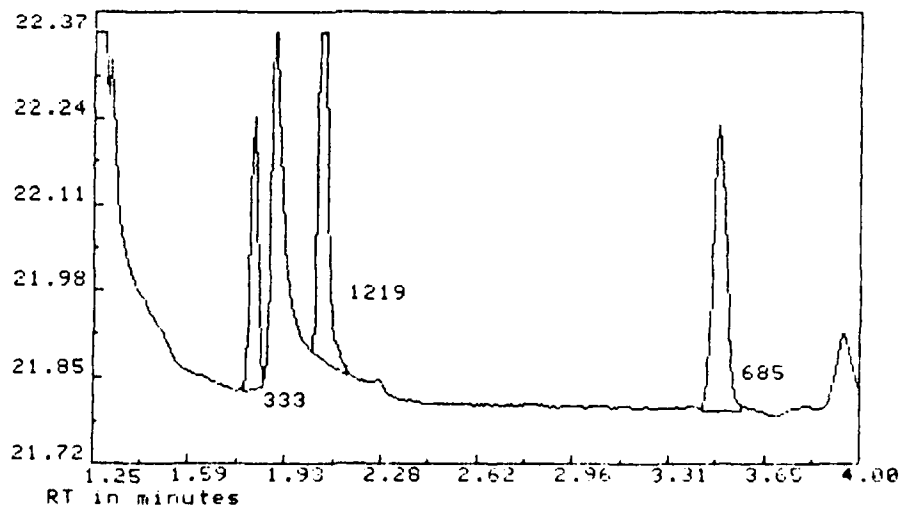
AMPLITUDE/1000 (Enlarged x 100.0)



SAMPLE: PCE
Meth: PJMETH

INJECTED AT 15:15:46 ON AUG 13, 1987
Raw: R02335 Proc: P02335

AMPLITUDE/1000 (Enlarged x 100.0)



SAMPLE: PCE
Meth: PJMETH

INJECTED AT 15:20:38 ON AUG 13, 1987
Raw: R02336 Proc: P02336

Figure 2

LOW CCl_4

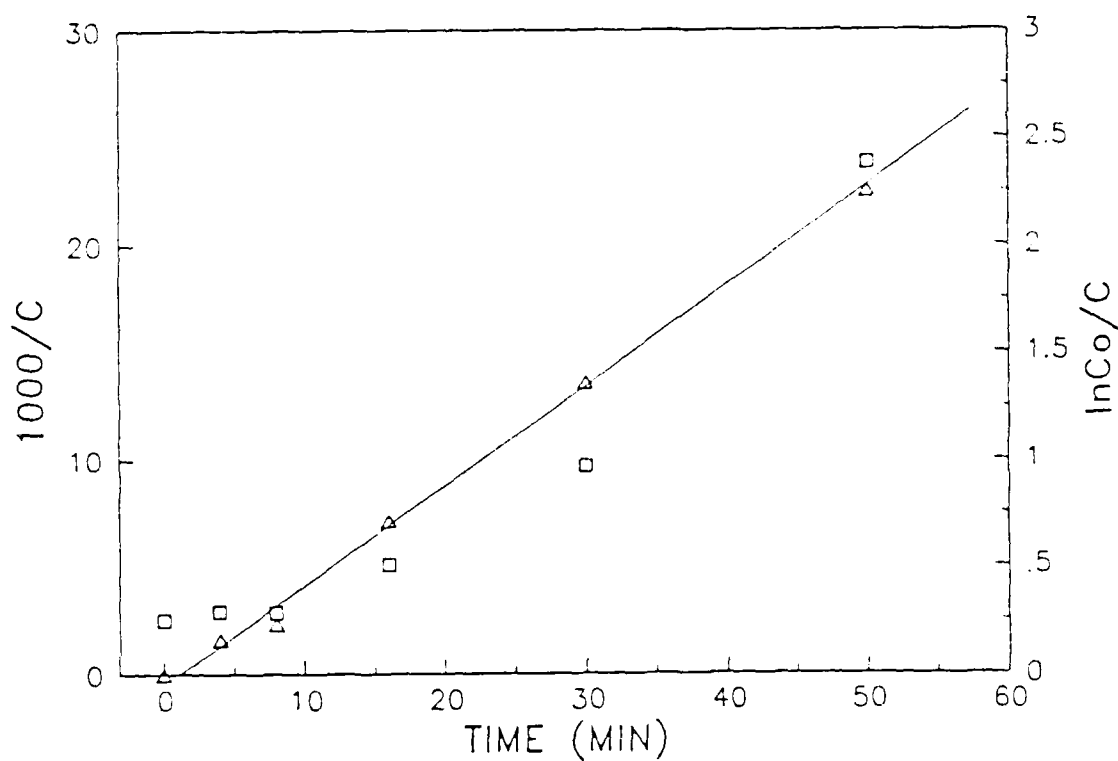


Figure 3

HIGH CCl_4

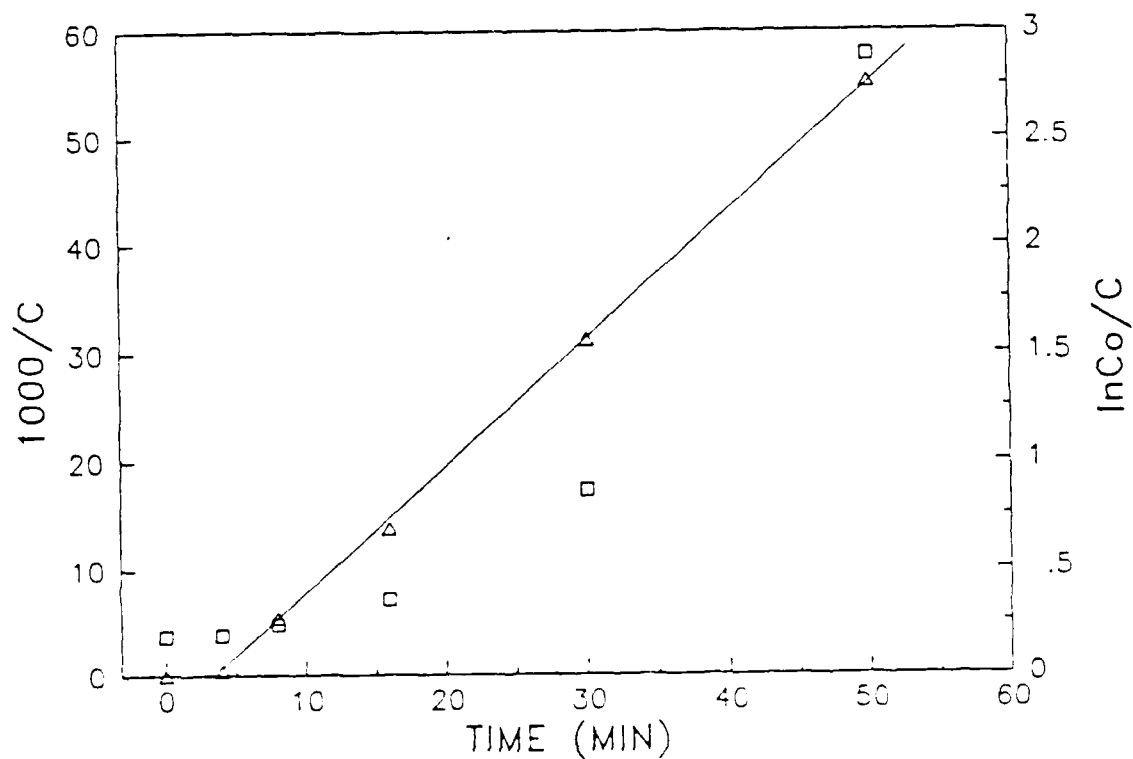


Figure 4
72-16

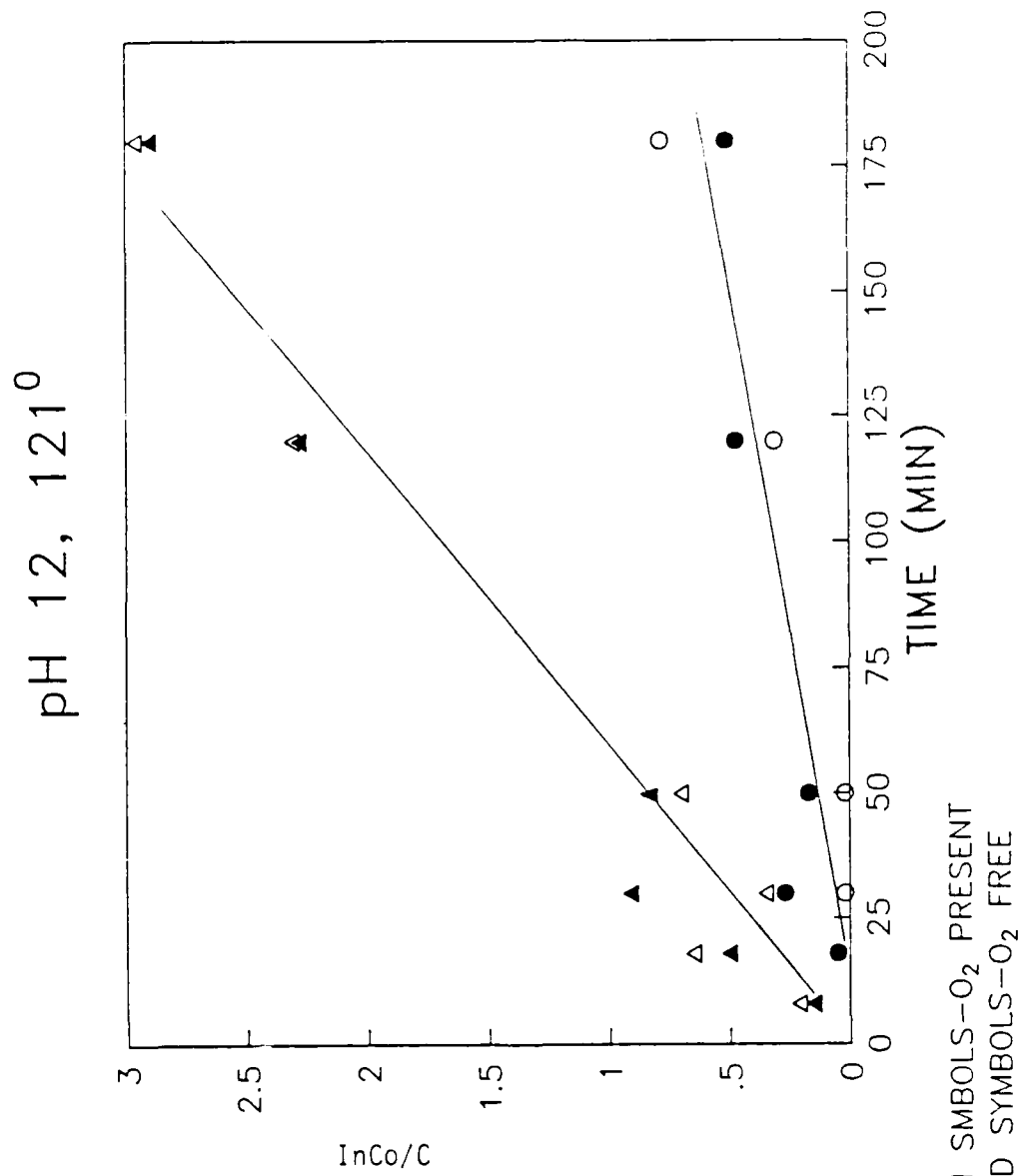


Figure 5

CCl₄ pH EFFECT

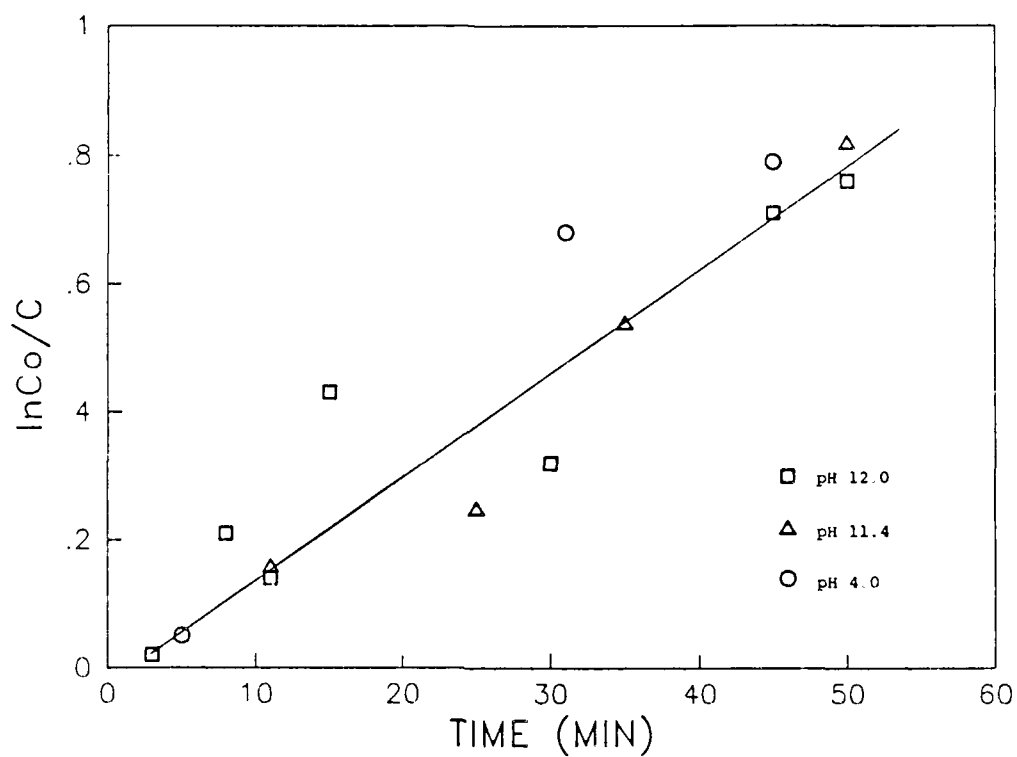


Figure 6

TCE pH EFFECT

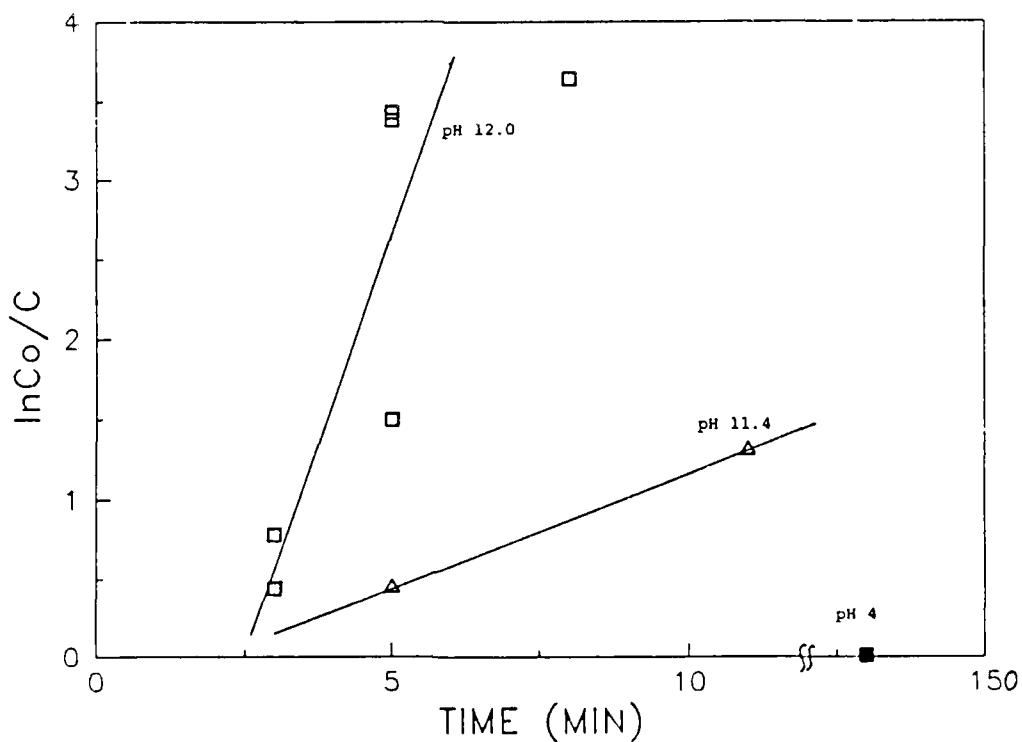


Figure 7

CCl_4 1ST ORDER PLOTS

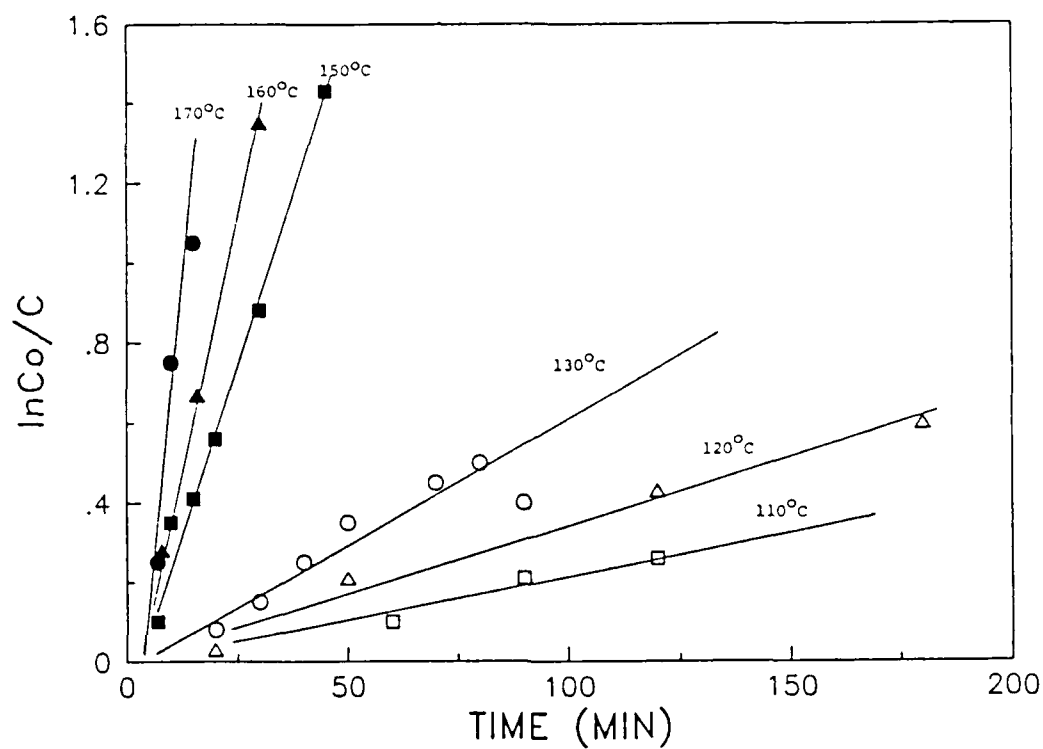


Figure 8

TCE 1ST ORDER PLOTS

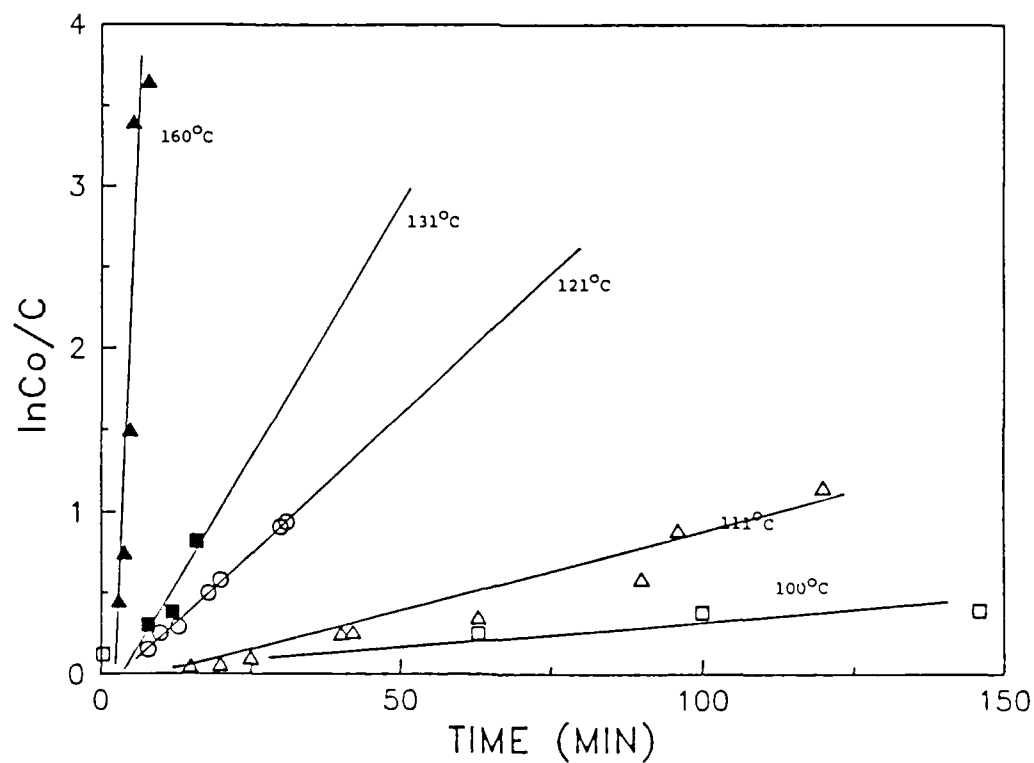


Figure 9

ARRHENIUS PLOTS

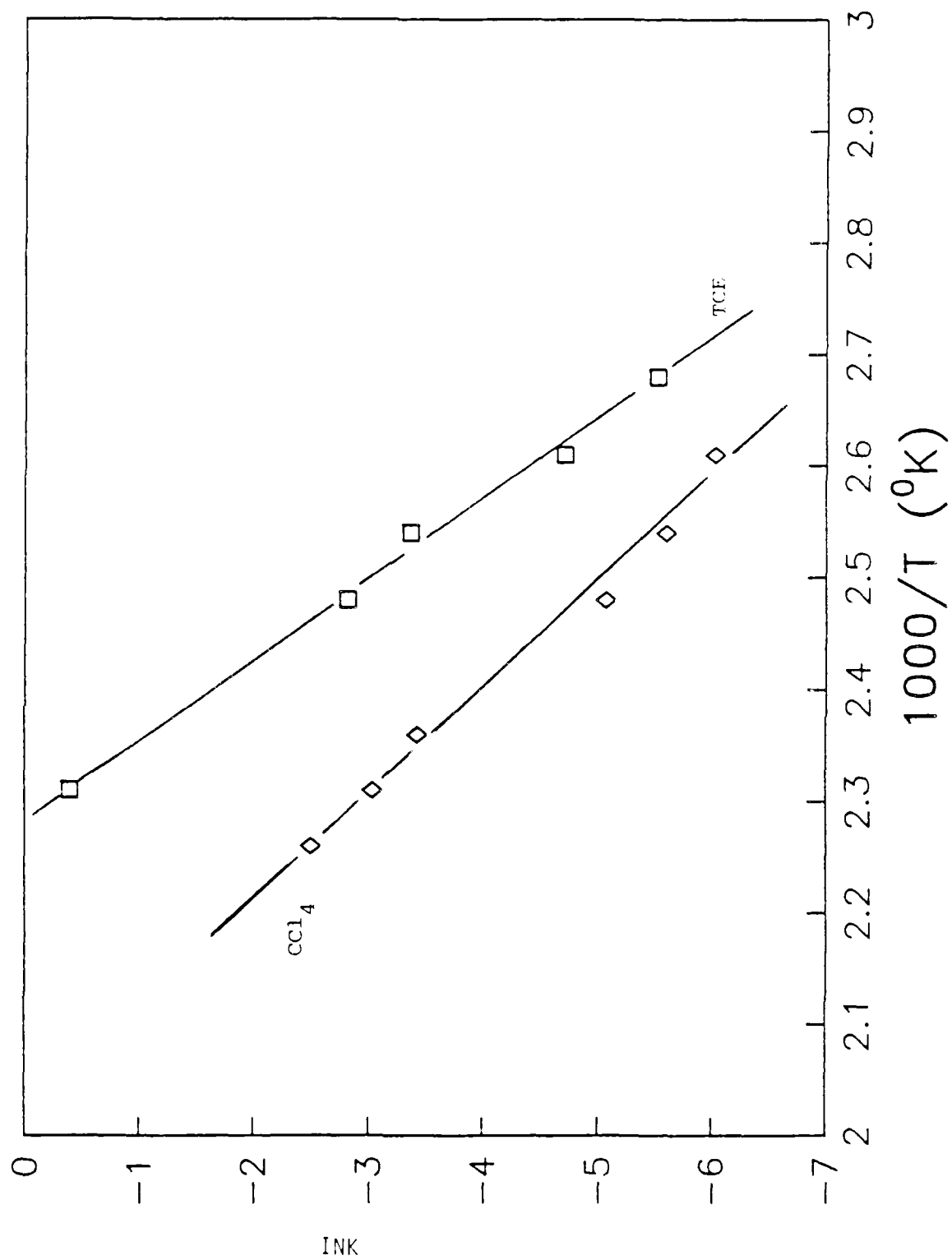


Figure 10

1987 USAF-UES SUMMER FACULTY RESEARCH PROGRAM/
GRADUATE STUDENT SUMMER SUPPORT PROGRAM

Sponsored by the
AIR FORCE OFFICE OF SCIENTIFIC RESEARCH

Conducted by the
Universal Energy Systems, Inc.

FINAL REPORT

CHOLESTERIC LIQUID CRYSTALS OF BIOMOLECULES
FOR USE AS OPTICAL FILTERS

Prepared by:	Gordon O. Johnson, Ph.D.
Academic Rank:	Professor
Department and	Physics Department
University:	Walla Walla College
Research Location:	AFWAL/MLPJ Wright-Patterson AFB Dayton, OH 45433
USAF Researcher:	Ray Linville
Date:	September 10, 1987
Contract No:	F49620-85-C-0013

CHOLESTERIC LIQUID CRYSTALS OF BIOMOLECULES

FOR USE AS OPTICAL FILTERS

by

Gordon O. Johnson

ABSTRACT

The biomolecule poly- γ -benzyl-L-glutamate (PBLG), a long chain polymer with a helical backbone, forms cholesteric liquid crystals above certain minimum concentration levels in various solvents at room temperature. Solutions of 10%-40% PBLG (by weight) in dioxane were studied using a polarizing microscope in the visible spectrum and an infrared spectrophotometer. The presence of the cholesteric phase was verified by observation of the characteristic Grandjean structure in these solutions, and the helical period of the cholesteric structure was determined. This period decreased as the concentration of PBLG increased, essentially varying as the inverse square of the concentration. For most optical filter applications the PBLG molecules should lie in planes parallel to the substrate. Lightly etching glass substrates in hydrofluoric acid is found to enhance this alignment. Theoretically when light is normally incident on a layer of such a cholesteric liquid crystal structure, a strong reflection will occur when the wavelength in the material is equal to the period of the cholesteric helix. No such reflection has been seen with the spectrophotometer indicating that better alignment of the molecules must be achieved.

ACKNOWLEDGMENTS

I would like to thank Professor Herbert Klei and Zbigniew Takarski for many helpful discussions during the course of this work. For making my stay pleasant and profitable I want to thank Bob Crane and Ray Linville.

Of course my participation in the Summer Faculty Research Program has only been possible because of the sponsorship of the Air Force Systems Command, the Air Force Office of Scientific Research, and the Materials Laboratory of the Air Force Wright Aeronautical Laboratory. The administrative support of United Energy Systems has also been much appreciated.

NO-A191 284

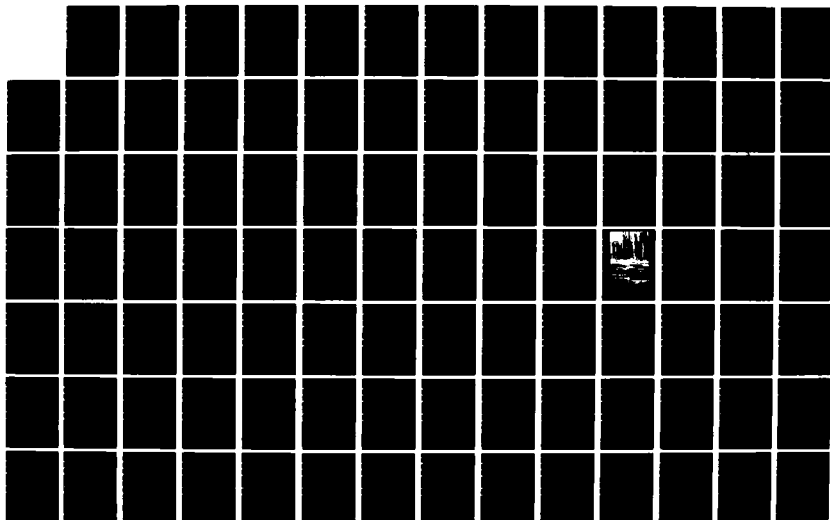
UNITED STATES AIR FORCE SUMMER FACULTY RESEARCH PROGRAM
(1987) PROGRAM TE. (U) UNIVERSAL ENERGY SYSTEMS INC
DAYTON OH R C DARRAH ET AL. DEC 87 AFOSR-TR-88-0213

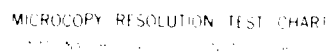
5/11

UNCLASSIFIED

F/G 5/1

NL





I. INTRODUCTION:

The use of biomolecules for laser filters holds promise due to considerations of speed and versatility. Response times of femtoseconds and the possibility of tailoring the optical characteristics of the filters has attracted the attention of the Air Force and makes these materials good candidates for laser hardening applications. In particular the molecules in liquid crystal materials are aligned in various ways depending on the particular phase which is present. Such alignment can be utilized for optical filtering, thus the present study focused on the use of liquid crystal materials.

In studying the optical properties of these materials it is important to understand the interaction of radiation and matter in order to predict the behavior of the material when exposed to light. Also for many applications it is desired that a thin, uniform coating of these materials can be made, thus a knowledge of thin films and various coating procedures can prove valuable.

My background in optics, electric and magnetic fields, and thin films contributed to my selection as a participant in this particular research program of the Laser Hardened Materials Branch of the Materials Laboratory.

II. OBJECTIVES OF THE RESEARCH EFFORT:

Two techniques for filtering laser light were to be pursued by the group; 1) reflection of a specific wavelength of light and 2) absorption of the laser light energy by generation of higher harmonics, an effect to be greatly enhanced by adding so-called guest molecules in the liquid crystal structure. My work as a participant in the 1987 Summer Faculty Research Program (SFRP) centered primarily on producing

a liquid crystal film that would selectively reflect light.

The polypeptide molecule, poly- γ -benzyl-L-glutamate (PBLG), was chosen because its molecular structure is conducive to interactions with guest molecules and its liquid crystal properties have been well characterized in the literature.[1-9] The PBLG molecule has a helical backbone with various molecular residues attached and can be polymerized into various molecular weights. In the present study the molecular weights were approximately 260,000. Since this area of biotechnology was begun at the Materials Laboratory of the Air Force Wright Aeronautical Laboratory in January, 1987, a number of preliminary studies needed to be made in order to insure that our materials were behaving in a known way and in agreement with findings reported in the literature. The cholesteric liquid crystal structure was desired so appropriate concentrations of PBLG in dioxane were used. It was necessary to verify that indeed the cholesteric structure was present. Then films of the material were to be made and the selective reflection was to be observed. The last phase was to control the wavelength of the reflection in a reproducible way.

III. PRELIMINARY WORK

Cholesteric liquid crystals are characterized by stacked planes of aligned molecules with the direction of the molecules in adjacent planes rotated slightly with respect to each other.[8] Thus the planes are twisted to form a planar helical structure. The period of the helix so formed can be determined optically, because the index of refraction for light polarized perpendicular to the molecules is less than the index for light polarized parallel to the molecules. Light which is polarized parallel to the planes of molecules and traveling parallel to

these planes will be deflected toward the regions with a higher index of refraction, that is, regions where the polarization is parallel to the molecules. Thus contrast differences are produced with a periodicity equal to half of the period of the helix. The striped structure that results is known as the Grandjean structure and is characteristic of the cholesteric phase.

In order to verify the presence of the cholesteric phase in our solutions capillary tubes were filled with 10%, 15%, 20%, 30%, and 40% by weight of PBLG in dioxane. The Grandjean structure was observed in each of the above concentrations indicating that indeed the cholesteric phase was present, and the periods of the helices were thus determined. The results are summarized in Table I. It is easily seen that the period decreases with increasing concentrations of PBLG. In fact converting the weight percents to volume percents, using densities of 1.283 g/ml for PBLG and 1.034 g/ml for dioxane, the period varies nearly as the inverse square of the concentration by volume. These results are in good agreement with previous work.[2] Extrapolation would seem to indicate that increasing the concentration toward 100% PBLG would easily result in helical periods in the same range as visible light wavelengths. Phase diagrams show that the cholesteric phase should still be observed at room temperature up to virtually 100% PBLG. Unfortunately solutions with 50% or greater concentration by weight of PBLG are very viscous, take weeks to dissolve, and appear somewhat opaque in visible light, consequently some practical limitations are imposed.

A striped pattern is also observed with a microscope when polarized light is passed through a film of PBLG solution which has been smeared unidirectionally on a glass microscope slide forming a thin layer and allowed to dry. Preliminary thinking on our part interpreted

this stripe pattern as the Grandjean structure of interest. Some reports in the literature indicated that the layers of molecules in the cholesteric phase formed parallel to the surface of the glass. Since the solutions are quite viscous, smearing the solution was thought to tip the planes sideways so that the edges could be seen and the spacing determined. When attempts were made to reproduce results by this method, it was found that the speed with which the solution was smeared changed the observed spacing of the lines. If the stripes were really the desired Grandjean structure, they should be constant for a particular concentration of PBLG. Further investigation revealed that the stripes were due to a regular zig-zag pattern of the PBLG molecules in the plane of the film in agreement with the results reported by Horio et al.[3] Although our initial thinking was incorrect, the solution to this problem led to a much better understanding of our material and sharpened our techniques for interpreting the structure of the films using a polarizing microscope. At this point the decision to look for the Grandjean structures in the liquid solutions was made with the results as described above.

IV. MAKING FILTERS

The characteristic reflection for light propagating in a direction normal to the molecular planes of a liquid crystal in the cholesteric phase occurs when the wavelength of the light in the material is equal to the period of the planar helix.[8] Since the Grandjean spacing, and thus the period, was measured for liquids, the first attempts to make filters were also made with thin liquid layers with known helical periods. Although the wavelengths for our concentrations of PBLG are all in the infrared, the availability of an infrared spectrometer (2-50 micron range) made it possible to search for the desired reflection.

Dioxane is relatively volatile and thus the solvent in a thin liquid layer will evaporate quite rapidly leaving behind a PBLG film. Assuming that the periodicity of the dried film is the same as the liquid solution would seem unlikely. To overcome this difficulty thin liquid layers from 40-240 microns (1-6 mils) were sandwiched between glass microscope slides or salt windows (alkali halide crystals necessary for passing the long infrared wavelengths). Spacers of aluminum foil or thin cover glass were used to achieve the desired thicknesses.

Twenty percent solutions of PBLG were initially used. Helical periods of this concentration are approximately 18 microns, requiring a wavelength of light in the medium of 18 microns for reflection to take place. With the index of refraction of the PBLG solutions equalling about 1.5 this implied that the incident wavelength in air be 27 microns, well within the range of the spectrophotometer. An immediate difficulty was sealing the sandwiched liquid well enough to prevent evaporation of the solvent, at least for a period of several days. Using a spacer with a hole cut out for the liquid and allowing excess solution squeezing out the edges of the spacer to form a rather tight seal usually inhibited evaporation sufficiently. Using this technique sandwiches made between two glass slides or between a glass slide and a potassium bromide (KBr) window appeared to be very similar using the polarizing microscope. With the microscope the depth of field was small enough that the interior structure of the liquid layer could be differentiated from the structure at the upper and lower interfaces. At the glass-liquid or KBr-liquid interfaces the polarized light illumination revealed a "worm-like" structure reminiscent of worms tightly packed on a flat surface while in the interior of the layer the structure appeared to be twisted patterns of Grandjean stripes. In

order to be the most efficient reflector the planes of the PBLG molecules should be parallel to the thin dimension of the layer. If this were totally the case, then no Grandjean stripes should be visible looking at normal incidence to the layer. Not too surprisingly no characteristic reflection was observed with the spectrophotometer.

Various authors have reported that the PBLG molecules should preferentially align themselves parallel to the glass surface, thus it was felt that reducing the liquid layer thickness from 240 microns to 40 microns should make a visible difference, since the interface alignment would more readily affect the molecules in the bulk of the film for the thinner layer. No dramatic differences were observed. More literature searching revealed that the molecular alignment of various liquid crystals can be controlled by proper surface treatment of the glass.[10-12] Techniques tried were as follows: 1) rubbing the glass surface unidirectionally with a cotton swab, 2) polishing the glass surface unidirectionally using 0.3 micron alumina grit on a cotton swab, 3) polishing the glass surface unidirectionally using 0.3 micron alumina grit against another glass surface, and 4) etching the glass for 30-60 seconds in dilute (2-5%) hydrofluoric acid (HF). Glass-liquid-glass sandwiches were made in each case for viewing under the polarizing microscope. Only the last method with a 40 micron thick liquid layer revealed essentially no Grandjean structure and no wormlike patterns at the interfaces. Unfortunately the interface with the KBr cannot be treated in similar fashion. Also 40 microns represents only about 2 periods of the helical structure for 20% PBLG solutions. In a rugate filter structure such a small number of periods will result in a very small reflection coefficient. A thicker liquid layer (240 microns) between etched glass slides was made but the parallel alignment of the molecules to the interfaces did not seem to

be preserved in the interior of the film as evidenced by the presence of Grandjean stripes.

V. SUMMARY

The presence of the cholesteric phase has been observed in solutions of PBLG in dioxane ranging from 10-40 wt.% PBLG. The period of the cholesteric helix has been measured for these solutions with the aid of a polarizing microscope and found to correspond with wavelengths of light in the infrared. Thin layers of 20% and 30% PBLG solutions have been made in sandwich configurations in order to demonstrate optical filtering properties. Although these attempts have been unsuccessful so far, methods of achieving the desired molecular alignment are being perfected.

VI. RECOMMENDATIONS

This research effort has shown sufficient promise to warrant further study in the following areas:

- 1) Continue working with PBLG to achieve better alignment of the molecules; in this case parallel to the substrate. At a free surface of the liquid the molecules will be parallel to the surface. Thin layers of the liquid should be formed in a solvent atmosphere in order to prevent evaporation of the solvent. After the molecules have become aligned, the solvent can be evaporated thus forming a solid film. The effects of the drying process on the period of the cholesteric helix can then be determined.
- 2) Use dimethyl formamide (DMF) as a solvent since it is reported that submicron periods are found for weight percentages of PBLG of about 40% or greater.[1] The use of DMF will

necessitate a careful procedure to prevent contamination by absorbed water in the solvent.

- 3) Use poly- γ -ethyl-L-glutamate (PELG) instead of PBLG because helical periods in the visible range have been reported for 30-40 wt.% PELG in the solvent ethyl acetate.[2]

TABLE I

The periods of the cholesteric helices are shown for various solutions of PBLG in dioxane as determined from photographs taken through a polarizing microscope.

<u>Weight % of PBLG</u>	<u>Cholesteric Period (microns)</u>
10	80
15	39
20	18
30	10
40	8.5

REFERENCES

1. Miller, W. G., Russo, P. S., and S. Chakrabarti, "Composition, Phase Behavior, and Morphology in Poly(amino acid)s Forming Lyotropic Liquid Crystals," Journal of Applied Polymer Science: Applied Polymer Symposium, Vol. 41, 1985, pp. 49-63.
2. Robinson, C., "The Cholesteric Phase in Polypeptide Solutions and Biological Structures," Molecular Crystals, Vol. 1, 1966, pp. 467-494.
3. Horio, M., Ishikawa, S., and K. Oda, "Fine Structures of Fibers and Films Made from Lyotropic Liquid Crystals of Polymers," Journal of Applied Polymer Science: Applied Polymer Symposium, Vol. 41, 1985, pp. 269-292.
4. Watanabe, J., Imai, K., Gehani, R., and I. Uematsu, "Structural Differences Between Two Crystal Modifications of Poly(γ -benzyl-L-glutamate)," Journal of Polymer Science: Polymer Physics Edition, Vol. 19, 1981, pp. 653-665.
5. Watanabe, J. and I. Uematsu, "Anomalous Properties of Poly(γ -benzyl-L-glutamate) Film Composed of Unusual 7/2 Helices," Polymer, Vol. 25, December, 1984, pp. 1711-1717.
6. Samulski, E. and A. Tobolsky, "Cholesteric and Nematic Structures of Poly- γ -benzyl-L-glutamate," Liquid Crystals and Ordered Fluids, edited by J. Johnson and R. Porter, Plenum, 1970.

7. Johnson, J. and R. Porter (editors), Liquid Crystals and Ordered Films, Vol. 2, Plenum, 1973, pp. 237-242.
8. Saeva, F. (editor), Liquid Crystals, Marcel Dekker, 1977.
9. Robinson, C., Ward, J., and R. Beevers, "Liquid Crystalline Structure in Polypeptide Solutions, Part 2," Discussions Faraday Society, Vol. 25, 1958, pp. 29-42.
10. Berreman, D., "Alignment of Liquid Crystals by Grooved Surfaces," Molecular Crystals and Liquid Crystals, Vol. 23, 1973, pp. 215-231.
11. Creagh, L. and A. Kmetz, "Mechanism of Surface Alignment in Nematic Liquid Crystals," Molecular Crystals and Liquid Crystals, Vol. 24, 1973, pp. 59-68.
12. Cognard, J., Molecular Crystals and Liquid Crystals Supplement 1: Alignment of Nematic Liquid Crystals and Their Mixtures, Gordon and Breach, 1982.

1987 USAF-UES SUMMER FACULTY RESEARCH PROGRAM

Sponsored by the
AIR FORCE OFFICE OF SCIENTIFIC RESEARCH

Conducted by the
Universal Energy Systems, Inc.

FINAL REPORT

Contribution of the Value Assignment Problem to the

Complexity of Test Generation in Combinational

Logic Circuits

and

Power Line Testing of CMOS Digital Logic Circuits

Prepared by:	Dr. Louis G. Johnson
Academic Rank:	Associate Professor
Department and	Electrical and Computer Engineering
University:	Oklahoma State University
Research Location:	Rome Air Development Center
	Microelectronics Reliability Division
	Reliability Physics Branch
USAF Researcher:	Dr. Mark W. Levi
Date:	21 September 1987
Contract No.:	F49620-85-C-0013

Contribution of the Value Assignment Problem to the
Complexity of Test Generation in Combinational
Logic Circuits

and

Power Line Testing of CMOS Digital Logic Circuits

by

Dr. Louis G. Johnson

ABSTRACT

The effects of reconvergent fanout loops in combinational logic networks were determined for the value assignment problem which underlies most test generation methods. Simple rules were derived for the implication constraints imposed by reconvergent fanout loops to give the complete implications of any single value assignment in a general combinational logic circuit with an arbitrarily complex interconnect of fanout loops. The results show that the complexity of the value assignment problem is proportional to the number of reconvergent fanout loops in the circuit which can be exponential in the number of circuit nodes.

An exploration was conducted into the feasibility of testing digital CMOS integrated circuits through the use of excess leakage current in the power line inputs. A circuit design technique with multiple power inputs was discovered that allows power line testing to be used for dynamic CMOS circuits.

Acknowledgments

I wish to thank the Air Force Systems Command and the Air Force Office of Scientific Research for sponsorship of this research. Universal Energy Systems also provided valuable assistance in administrative aspects of this program.

Special thanks go to Dan Burns for encouraging my participation in the program and for supplying a warm family atmosphere. Dr. Mark Levi has provided many hours of stimulating conversation and technical guidance that has made the summer productive and helped to show the way toward further progress. The help of Marty Walter and Mark Pronobis with the computer is appreciated. All of the members of the Reliability Physics Branch were friendly and helpful.

I. INTRODUCTION:

With the increasing number of circuit elements inside a single integrated circuit provided by modern technology, it has become increasingly difficult to thoroughly test electronic components. There is a well developed set of algorithms[1-4] for test generation in digital logic circuits that attempt to take advantage of knowledge of circuit structure to insure adequate test coverage. An important step in these algorithms is to insure that value assignments made during the test generation process are mutually consistent. In principle, if the complete implications of every single value assignment were known, it should be possible to always make logically consistent value assignments with no conflicting values. Unfortunately, in circuits with reconvergent fanout, existing algorithms do not find all of the implications of single assignments before making additional assignments. This can lead to conflicting value assignments later on in the test generation process which make it difficult to find tests for all parts of the circuit. Furthermore, if more than one fault occurs simultaneously, the existing methods of algorithmic test generation are not always effective.

The Microelectronics Reliability Division at the Rome Air Development Center is concerned with testing and reliability measures for electronic circuit components. They are interested in new methods that may make it possible to more adequately test complex microelectronic circuits and in characterizing failure modes for different classes of circuits. Therefore, a better solution to the test generation problem is of vital interest.

For several years, I have been investigating the effects of reconvergent fanout on the test generation process. I have taught a graduate level course on testing techniques and the design of digital integrated circuits. Thus, I have a thorough understanding of the testing issues and the electronic circuit properties necessary to attempt an improvement to the solution of the test generation problem.

II. OBJECTIVES OF THE RESEARCH EFFORT:

The first objective was to explore the properties of combinational logic circuits that give rise to the computational complexity of generating logically consistent value assignments for combinational logic circuits. This would be a culmination of my earlier research and have publishable results[5]. The results should serve as a foundation for further research into improved test generation algorithms and testability measures.

A second objective was to investigate the practicality of power line testing for general CMOS digital logic circuits. This would be an extension to earlier work done by Dr. Levi[6]. Dr. Levi showed that static CMOS logic circuits can be tested for multiple open and short faults by monitoring the current on the power line input to a CMOS digital integrated circuit. More work was needed in the following two areas a) a test generation algorithm was needed to insure coverage of as many multiple faults as possible and/or reasonable, and b) a way to extend the technique to dynamic circuit designs was needed.

III. VALUE ASSIGNMENT PROBLEM:

a. Approach

To simplify the problem, we only considered the value assignment problem for combinational logic circuits although the results should apply to sequential circuits also. Combinational logic circuits have no internal feedback and physical signals flow unidirectionally from external inputs to external outputs. Test generation algorithms do not necessarily follow the direction of physical signal flow when making value assignments to the circuit. It may be desirable to have an internal node somewhere in the circuit set to some value. This value assignment has implications for logically consistent value assignments at circuit nodes backward toward circuit inputs as well as forward toward circuit outputs in the direction of normal physical signal flow. Since a value assignment can propagate in two directions, any loop in the circuit can be a possible source of conflicting logical consistency requirements. Since combinational logic circuits have no feedback, the only possible loops are reconvergent fanout loops.

It has long been recognized that certain circuit topologies are more easily testable than others. Many have realized that the amount of reconvergent fanout is a critical factor in determining realistic measures of the difficulty of generating tests[4,7-9]. Thus, we examined the value assignment problem for circuits with increasing reconvergent fanout complexity. In my work before arriving at RADC, single isolated reconvergent fanout loops were studied. At RADC, the results for single loops were generalized to explain the effects of connected reconvergent fanout loops on the value assignment problem.

b. Results

A complete description of the solution derived for the value assignment problem in digital logic circuits is given in the paper that has been submitted for publication[5]. A summary of the results is as follows.

To successfully predict the extra value assignment constraints imposed by isolated reconvergent fanout loops, we determined all the ways that it is possible for a loop to cause a gate to have to simultaneously satisfy more than one consistency requirement. Examination of the parts of a reconvergent fanout loop show that there are only a limited number of ways for a loop to impose the extra relationships and that they fall into one of the following two cases.

Case 1: In isolated loops where the number of inverters plus the number of reconvergent gates is odd, if all of the reconvergent gates in the loop are sensitized and the branches are appropriately sensitized, then one or more nodes in the loop are constrained to have values consistent with the reconvergent gate outputs if and only if both of the following conditions are met.

1. The constrained loop nodes are between two adjacent reconvergent gates of the same type.
2. No other adjacent reconvergent gates in the loop are the same type.

All other value assignment constraints are included in the single gate implication relationships.

Case 2: In isolated loops where the number of inverters plus the number of reconvergent gates is even, if all of the reconvergent gates on the

loop are sensitized except one and the branches are appropriately sensitized, then the remaining reconvergent gate must be sensitized if and only if both of the following conditions are met.

1. The type of reconvergent gates in the loop on either side of the reconvergent gate with the constraint must be the same type as the reconvergent gate with the constraint.

2. No other adjacent reconvergent gates in the loop are the same type.

All other value assignment constraints are included in the single gate implication relationships.

Reconvergent gate sensitization is defined as assigning a value to the reconvergent gate output such that a value assignment on one input of the reconvergent gate implies a value assignment on the other input. Gates are defined as the same type if they are both AND's or OR's after all intervening inverters have been transformed away using De Morgan's laws. Reconvergent gates are defined to be adjacent when there are no other intervening reconvergent gates while propagating an implication around a loop.

Application of cases 1 and 2 gives the constraint locations shown in figure 1 by the darkened lines. Not all of the possible loops have implication constraints beyond those of individual gates as shown by the loops in figure 1 that do not have any darkened line. De Morgan's laws have been used so that the constrained value is always 1.

When loops occur with any branches in common, we no longer have isolated loops as assumed previously, but more complex structures. The only case not covered already is when connected loops are simultaneously sensitized. In this case, the same rules (cases 1 and 2) should apply as

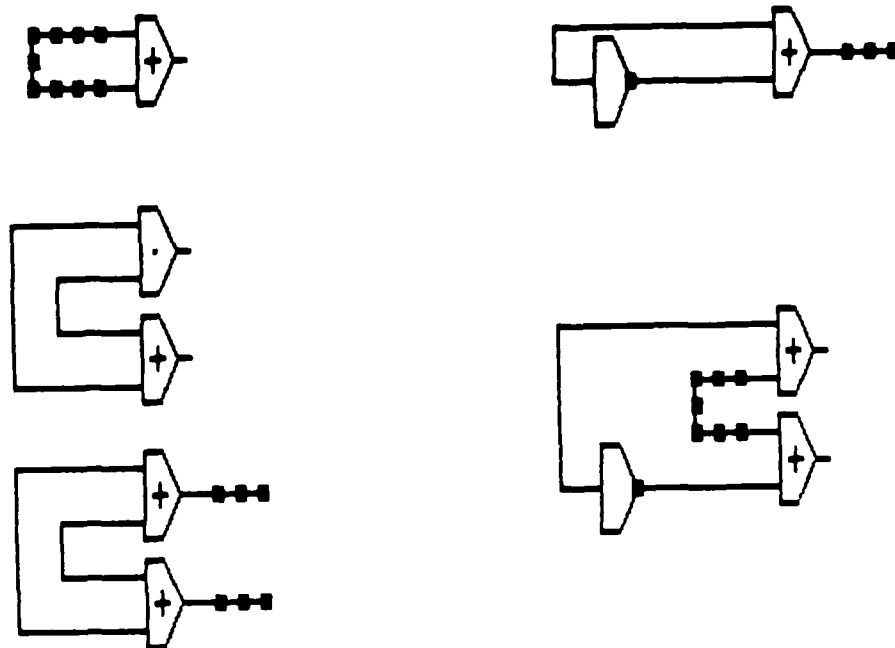


Fig. 1

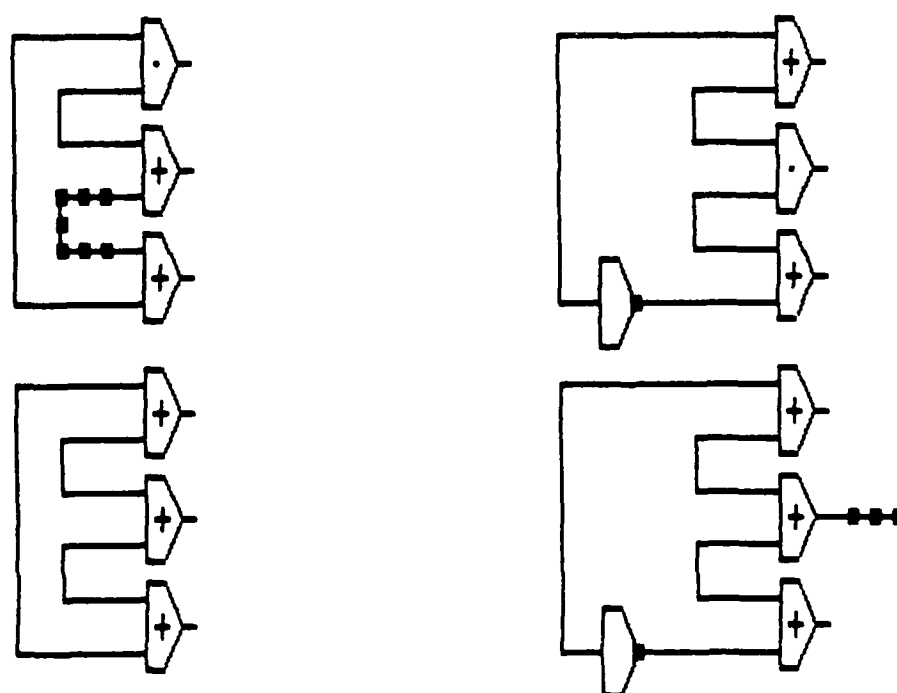


Fig. 1 (cont)
74-9

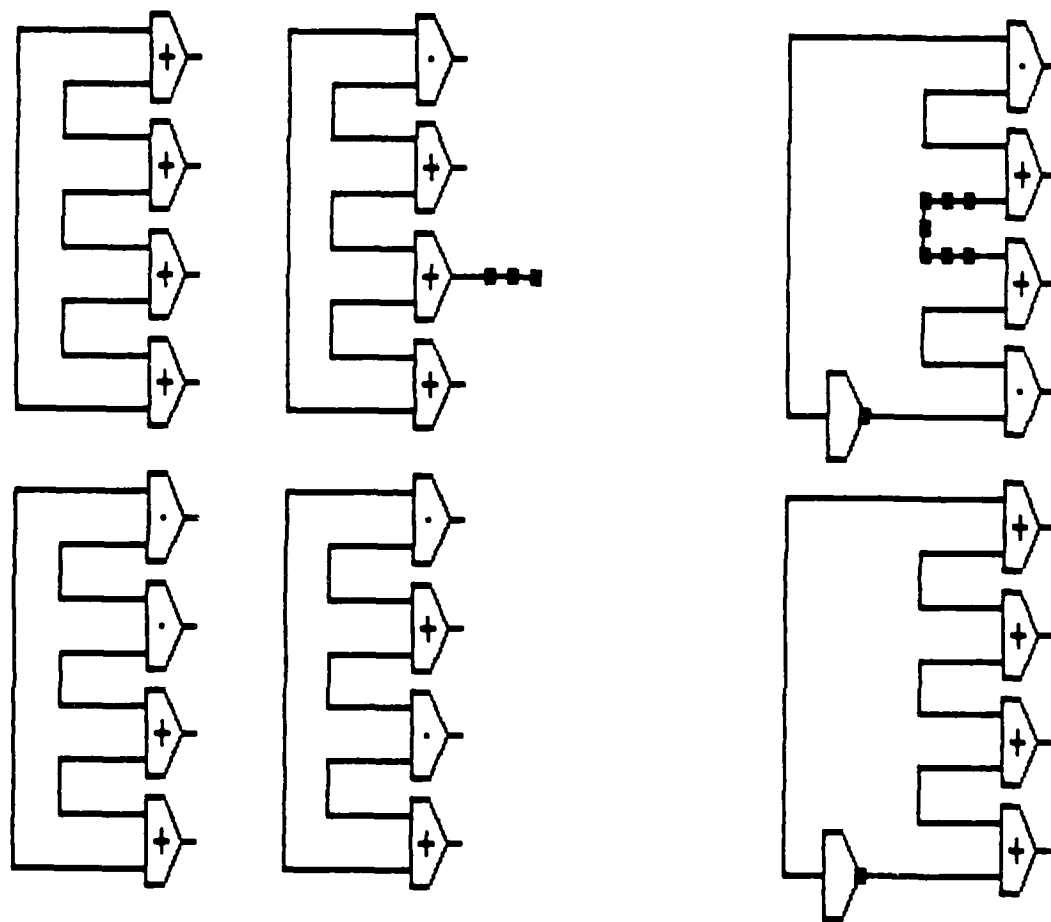


Fig. 1. All possible single reconvergent fanout loops that are not equivalent by De Morgan's laws. The constraint locations, if any are indicated by the darkened lines. The branch gates are not shown explicitly for clarity.

those for unconnected loops since these rules were derived from conditions necessary for the implication constraints to propagate around any single loop. The only difference is at internal reconvergent gates. An internal reconvergent gate is a reconvergent gate for one loop and a branch gate for another loop in a connected loop structure. The equations for the activation of the connected loop implication constraints must take into account properly that the internal reconvergent gates need not be completely sensitized when one loop provides the proper sensitization for another loop at the internal reconvergent gate. This provides extra ways to sensitize the loop for a given implication constraint, but it does not change the location or the value of the single loop constraint found using cases 1 and 2 around all possible single loops in the connected loop structure.

We must now find assignments consistent with the constraints imposed by all loops simultaneously. We found it possible to prove that if two single loop implication constraints require the same or the opposite sensitization of a common branch or reconvergent gate, then it must be possible to simultaneously satisfy both constraints with consistent assignments. Since no new conflicting value assignments are possible, it follows that in well formed combinational logic circuits, all implication constraints may be found by simultaneously enforcing all single gate implications and all possible single loop implication constraints in the circuit.

IV. POWER LINE TESTING OF CMOS:

a. Approach.

It was decided to concentrate on developing a power line testable dynamic CMOS logic design methodology during my time at RADC. Further research would be conducted during the academic year on new test generation algorithms using power line testing for multiple short and open faults. In Dr. Levi's earlier work[6], he has shown that the small leakage currents in fault free CMOS circuits allow the direct observation of the current of a single gate in a large integrated circuit by monitoring the current on the power line.

The detection of short circuits is straightforward; if the gates driving the two shorted circuit nodes have opposite output values (one high, the other low), then large currents will flow from power to ground through the two drivers. Open circuits may also be detected, as shown in figure 2, if the floating input to the inverter can be driven to a mid-range voltage where both the pull up and pull down transistors are on, causing large currents to flow once again. Dr. Levi has suggested taking advantage of the capacitive coupling between the power line and the floating open node, as shown in figure 2b, to apply a modulating voltage to the power line that will drive the floating node to the desired mid-range value. Note that in the absence of an open fault, static CMOS designs do not have any floating nodes so that any observed power line current beyond leakage or switching transients must come from open faults.

In dynamic CMOS designs, the circuit designer takes advantage of the charge storage capability of MOSFET gates and may intentionally leave some gate inputs open circuited for short periods of time. If the

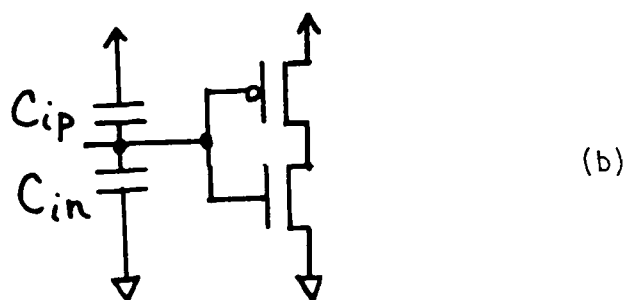
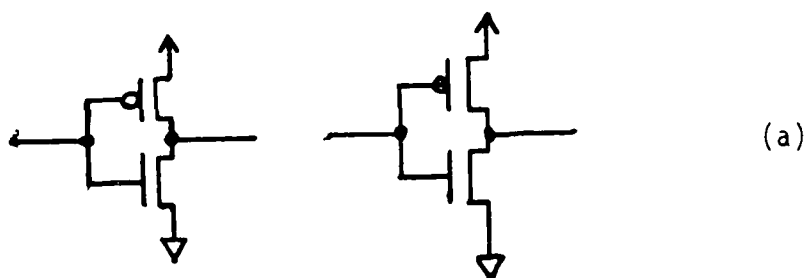


Fig. 2. An open circuit in a CMOS digital circuit. (a) A logic gate left with an open input. (b) The equivalent circuit for the input.

power line testing method is used, then it would be impossible to tell the difference between a real open fault and one of the intentionally open nodes. A possible solution is to have multiple power line inputs to the chip and impose a circuit design methodology to insure that no nodes are intentionally left floating on one of the power inputs at a certain time. Then, excessive current on that particular power lead at that particular time indicates the presence of an open fault. These ideas were tried out on a SPICE simulation of a simple psuedo-two phase clocking scheme for a CMOS shift register.

b. Results.

The first step was to establish the amount of asymmetry in the capacitive coupling to a floating node that could be tolerated with the assurance that the node voltage would be brought into the mid-range region. If the magnitude of the modulation of the power line voltage, $V_{ph} - V_{pl}$, satisfies the following inequality, then the floating node will settle at a mid-range value that will cause detectable current to flow.

$$V_{ph} - V_{pl} > \max \{ (1 + C_{in}/C_{ip}) * V_{tn}, (1 + C_{ip}/C_{in}) * V_{tp} \}$$

The quantities V_{tn} and V_{tp} are the switching thresholds of the n-channel and p-channel FET's respectively, and C_{in} and C_{ip} are the coupling capacitances from figure 2b. In principle, any capacitance ratio could be detected by using a large enough power modulation, but in practice, the maximum power voltage must be kept below the break down voltage of the FET's. Thus, for any given fabrication process, there will be a maximum tolerable capacitance ratio beyond which it will be impossible

to detect open faults. This maximum tolerable ratio is probably near to 10 for most processes.

The application of power line testing to the CMOS shift register shown in figure 3 was then examined. The transmission gates are controlled by the clock signals such that no two are on at the same time. When the transmission gate is off, the input to the following inverter is floating. Thus, at least one of the inverter inputs is intentionally left floating during normal clocking operation of the circuit. For testing purposes, one could consider artificially turning on at the same time all clock driven transmission gates, but this would risk the possibility of circuit oscillations. For example, if the output of the shift register was connected back to the input with an odd number of inverters in the loop, the circuit would oscillate when all the transmission gates were on which would cause switching current to flow in fault free circuits as well as faulty circuits. There seems to be no way to test the circuit as originally designed with the power line technique.

If two independent power sources are provided and wired to alternating clocked stages inside the circuit as shown in figure 3, SPICE simulations of the circuit verify that it is possible to use the power line testing technique even though the circuit retains its dynamic design characteristics. When Φ_{11} is high, the input of the inverter powered by V_{dd2} is connected through the on transmission gate to the preceding inverter. The only intentionally open nodes will be on inputs to inverters powered by V_{dd1} . Thus if we modulate the power supplies during Φ_{11} and look only at the current out of V_{dd2} , a non-zero steady state current is indicative of an open fault. To test the

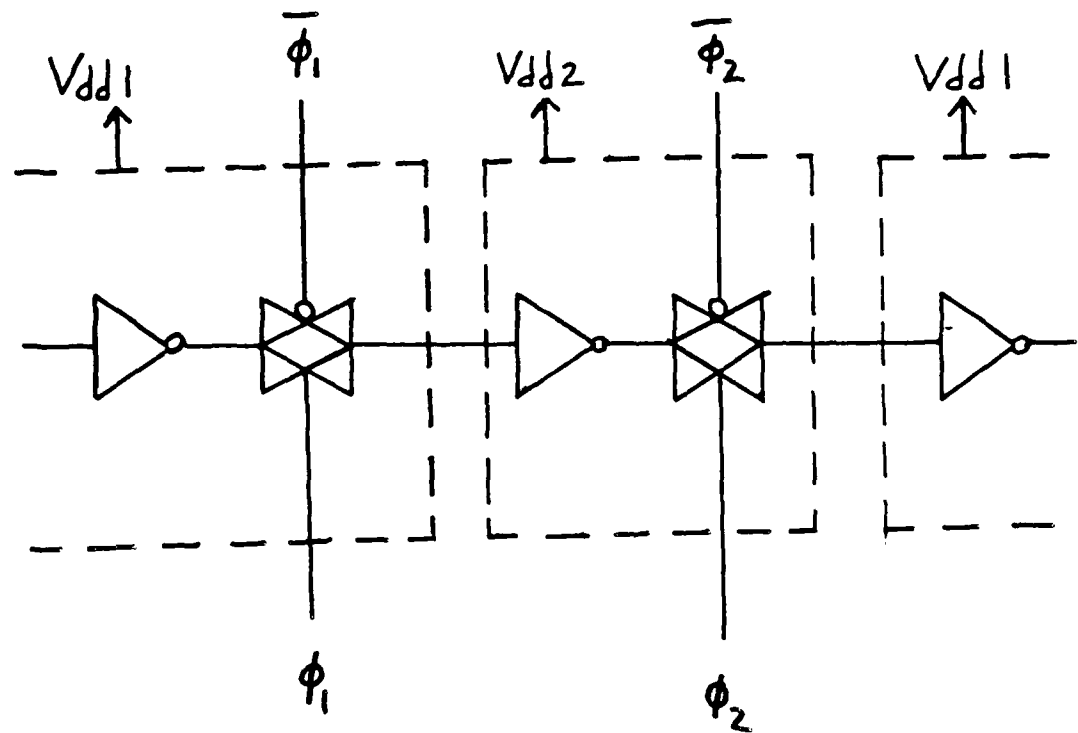


Fig. 3. A dynamic CMOS shift register with two power inputs.

other half of the circuit, modulate during Φ_2 and monitor the current out of V_{dd1} . It is important that the substrates for the transmission gates be wired to the power supplies as shown in order for the correct capacitive coupling to be provided to an open fault between the two inverters.

V. RECOMMENDATIONS:

a. Implementation.

In combinational circuits, we have shown that the complete implications of any independent value assignment may be found by the single gate implications directly between the gate inputs and outputs combined with extra implication constraints imposed by all possible reconvergent fanout loops. Previous work on this problem[10] did not clearly relate the implications to circuit structure nor was the possibility of sensitization of secondary loops taken into account. We also found that not all reconvergent fanout loops produce implications beyond those for single gates and in these cases, the reconvergent fanout is relatively harmless.

Unfortunately, the number of reconvergent fanout loops in an arbitrarily complex circuit can be exponential in the number of circuit nodes. The general value assignment problem for combinational logic is thus exponentially difficult. This is in agreement with previous work that indicate the value assignment problem to be polynomially complete[11], i.e. equivalent to other known difficult problems such as the traveling salesman problem. It has been shown[12] that the test generation problem has at least as much complexity as the value assignment problem in that the existence of a polynomial algorithm for

test generation would imply that a polynomial algorithm for value assignment exists. Any attempts to speed up the test generation process[4,8,9] and still use the circuit structure must account for the computational complexity of the underlying value assignment problem. In addition, test generation must make faults observable by sensitizing a path from a fault location to an observable output. Since path sensitization requires many independent value assignments any of which could inadvertently desensitize the path due to an unforeseen loop constraint, it is possible that test generation may be even more complex than value assignment.

As applied to testability analysis, our results demonstrate that the number of reconvergent fanout loops in a circuit is a much more accurate measure of the difficulty of testing a given circuit than the current methods used[7,13]. Also, one new testability measure recently proposed[14] does not take into account the full complexity of reconvergent fanout as we have shown it to be. It should be obvious that modularizing the circuit into parts that have no common reconvergent fanout loops should rapidly increase the testability because of the exponential fall off in the number of fanout loops in a smaller module. It may be very difficult in practice to achieve a complete modularization. The simple rules found may prove useful in that some common reconvergent fanout between modules may be left without adversely effecting the testability.

Applying traditional testing methods to CMOS has been a problem because of the occurrence of charge storage at internal circuit nodes with open faults. The power line testing method actually takes advantage of the internal charge storage to make the open faults

detectable. Traditional testing methods do not work well with multiple faults because it is difficult to be sure that the faulty circuit will have a different output than the fault free circuit. With the power line testing technique, the presence of multiple short and open faults causes the monitored power current to increase in most cases. The only exception is when the gates in the faulty circuit are left with no outputs tied together and no floating inputs. The probability of this happening for random faults is very low, but it does point out the necessity for monitoring the circuit outputs for correct functional output in parallel with monitoring the power line current.

The power line testing technique in its simplest form does not give any information about where the fault is. In many cases, it is not important to know where a fault is inside an integrated circuit; it is important to know only that the integrated circuit is faulty. If more information is desirable, the idea of multiple power inputs can be extended to provide separate power inputs to additional blocks of internal circuitry. Alternatively, one could use more exotic techniques such as infra-red scanning of the circuit to find the location of high current flow.

b. Further Research

The work on the value assignment problem completed at RADC has laid the foundation for further advances in at least two areas, test generation algorithm development and development of better measures of testability. The Critical Path Method of test generation is a very popular technique, but suffers from not deriving tests for all testable faults. One can easily show that the complete description of the value assignment constraints provided by the current work would allow the

critical path method to find all testable faults. More work is needed to demonstrate the practicality of integrating the reconvergent fanout loop constraints into the Critical Path Method. Counting the number of reconvergent fanout loops that have extra value assignment constraints would be a good measure of test generation complexity. More work is needed to find a simple and fast algorithm to find all the loops in arbitrary networks.

The work on power line testing is very promising, but it has only just begun. Tests need to be run on integrated circuits fabricated with modern processing techniques to verify that a single fault may be detected over the leakage background current on the power input. The question of the maximum tolerable capacitance ratio must be addressed. It may be necessary to impose some constraints on circuit layout to insure that the parasitic capacitances remain as balanced as possible between power and ground. The details of using the power line testing methods on other dynamic design styles have yet to be worked out. For example, pre-charged logic and domino logic are so different from the psuedo-two phase clocking scheme that it is not obvious how to apply the multiple power input testing idea. Finally, a test generation algorithm is necessary to exercise the circuit inputs so that single and multiple short and open faults will cause measurable current to flow in the power input(s).

References

- [1] J. P. Roth, "Diagnosis of automata failure: A calculus and a method," IBM J. Res. Devel., vol 10, pp. 278-291, Jul 1966.
- [2] J. J. Thomas, "Automated diagnostic test program for digital networks," Comput. Des., pp. 63-67, Aug 1971.
- [3] P. Goel, "An implicit enumeration algorithm to generate tests for combinational logic circuits," IEEE Trans. Comp., vol. C-30, pp. 215-222, Mar 1981.
- [4] H. Fujiwara and T. Shimono, "On the acceleration of test generation algorithms," IEEE Trans. Comp., vol. C-32, pp. 1137-1144, Dec 1983.
- [5] L. G. Johnson and B. Karimi, "Value Assignment Implication Constraints in Combinational Logic Circuits," submitted to IEEE Trans. Comp.
- [6] M. W. Levi, "CMOS is Most Testable," Proc. of 1981 Intl. Test Conf., pp. 217-220, Oct 1981.
- [7] R. G. Bennetts, C. M. Maunder and G. D. Robinson, "CAMELOT: a computer aided measure for logic testability," IEE Proc., vol. 128-E, pp. 177-189, Sep 1981.
- [8] M. Abramovici, J. J. Kulikowski, P. R. Menon and D. T. Miller, Test generation in LAMP2: concepts and algorithms," Proc. 16th Intl. Test Conf., pp. 49-56, Nov 1985.
- [9] K. S. Hwang and M. R. Mercer, "Derivation and Refinement of fan-out constraints to generate tests in combinational logic circuits," IEEE Trans. Comput.-Aided Des., vol. CAD-5, no. 4, pp. 564-572, Oct 1986.
- [10] S. D. Butland, "Determining the mutual consistency of internal linestates within a network," Comput. & Elect. Eng., vol. 6, pp. 69-78, 1979.
- [11] S. A. Cook, "The complexity of theorem proving procedures," Conf. Rec. 3rd ACM Symp. Theory of Comput., pp. 151-158, 1971.
- [12] O. H. Ibarra and S. K. Sahni, "Polynomially complete fault detection problems," IEEE Trans. Comp., C-24, no. 3, pp. 242-249, 1975.
- [13] L. H. Goldstein and E. L. Thigen, "SCOAP: Sandia controllability/observability analysis program," Proc. 17th IEEE Design Automation Conf., pp. 190-196, Jun 1980.

- [14] W. Jian-Chao and W. Dao-Zheng, "A new testability measure for digital circuits," Proc. 17th Intl. Test Conf., pp. 506-512, Nov 1986.

1987 USAF-UES SUMMER FACULTY RESEARCH PROGRAM/
GRADUATE STUDENT SUMMER SUPPORT PROGRAM

Sponsored by the
AIR FORCE OFFICE OF SCIENTIFIC RESEARCH

Conducted by the
Universal Energy Systems, Inc.

FINAL REPORT

Effect of Stacking Sequence Upon
Delamination Fracture Toughness

Prepared by:	Dr. William M. Jordan
Academic Rank:	Assistant Professor
Department and University:	Mechanical and Industrial Engineering Department Louisiana Tech University Ruston, LA 71272
Research Location:	AFWAL/MLBM Wright -Patterson Air Force Base, Ohio
USAF Researcher:	Dr. Stephen Tsai
Date:	August 14, 1987
Contract No.:	F49620-85-C-0013

Effect of Stacking Sequence Upon
Delamination Fracture Toughness

by

Dr. William M. Jordan

ABSTRACT

The effect of stacking sequence upon delamination fracture toughness was examined for the relatively brittle AS4/3501-6 graphite/epoxy and for the relatively ductile AS4/APC2 (peek) graphite/thermoplastic. For both systems quasi-isotropic laminates were examined. The difference in stacking sequence related to the degree of slicing that occurred. A different number of plies of the same angle were grouped together in each layup. (Grouping either 1, 2, 3, 4, or 6 plies of the same orientation together). The most spliced system (no grouping of same orientation plies together) had the largest mode I and mode II delamination fracture toughness.

In a second phase of the project, the effect of voids on the delamination fracture toughness of AS4/3501-6 was examined. The voids were introduced during curing and occurred at the ply interfaces. Up to 6% voids were found to increase both the mode I and mode II delamination fracture toughness.

In the third phase of the project the effect of prior loading history on delamination fracture toughness was examined for both the AS4/3501-6 and AS4/APC2 systems. Previous mode II crack extension was found to increase the subsequent mode I delamination fracture toughness. Previous mode I crack extension increased the subsequent mode II fracture toughness.

ACKNOWLEDGEMENTS

I wish to thank the Air Force Office of Scientific Research, the Air Force Systems Command, and the Materials Laboratory for the sponsorship of this research. Personnel at Universal Energy Systems, Inc., are thanked for their work in the administrative details of this project. Particular thanks go to the technicians under the direction of Tim Hartness who helped with fabrication, curing and testing of the composite laminates.

This work could not have been done without the love and encouragement of my wife, Gail, and my sons Robbie and Steven. Without their willingness to move for the summer this never would have been possible.

I. INTRODUCTION

Avoiding delamination failure of composite materials is one of the major goals of the designer. This has been approached from several directions. One approach has been to resist delamination through the development of tougher resin systems, so that delamination is less likely to occur under the designed loads. Changing to a different material system is not always an option, so the Air Force is interested in attempting to improve toughness by other methods. One possibility is that a change in stacking sequence may improve the toughness of the laminate.

A quasi-isotropic layup is a common composite stacking sequence in aerospace applications. A frequent method of accomplishing this is for the composite to be symmetric with respect to its midplane and have equal numbers of 0, +45, -45, and 90 degree plies. The question to be dealt with in this project is to determine if either of the following options will improve toughness: grouping plies of the same orientation together or splicing them (separating layers of the same orientation).

My research interests are in the area of failure of composite materials, and how failure can be avoided. My particular research has dealt with delamination failure of composite materials. My Ph.D. dissertation examined the effect of elastomer additions on the delamination fracture behavior of graphite/epoxy laminates. This use of a tougher resin system was the first approach to avoiding delamination mentioned above. This project examines a second approach to avoiding delamination, namely the careful choice of the stacking sequence within the laminate.

My previous work included mode I and mode II delamination fracture testing. The mode I tests were conducted here in the same manner as was done in my dissertation. The mode II delamination tests conducted during this project involved different fixturing than was used in my dissertation.

II. OBJECTIVES OF THE RESEARCH EFFORT

The main objective of this project was to determine if the stacking sequence of quasi-isotropic laminates affected their mode I and mode II delamination fracture toughness. Two different resin systems were to be examined: (1) AS4/3501-6, a relatively brittle graphite/epoxy and (2) AS4/APC2 (peek), a very ductile graphite/thermoplastic system.

Much delamination fracture toughness work has been done on unidirectional systems, for a variety of reasons. Unidirectional systems are easier to fabricate. They are stiffer than quasi-isotropic systems, frequently making data analysis simpler as well. However, quasi-isotropic systems, while more common in structural applications, have less frequently been examined.

Four laminates of each system were to be tested. All of them are quasi-isotropic (for specific layups see Table I). The difference between the layups was how many plies of each orientation were stacked together. For the AS4/3501-6 system groups of 4, 3, 2, or 1 ply of each orientation were grouped together. That resulted in three laminates of 32 plies and one of 24 plies. For the AS4/APC2 system groups of 6, 3, 2, or 1 ply of each orientation were grouped together (all four laminates had 48 plies).

Several minor objectives were also examined during this project. The first one was the effect of voids upon delamination fracture toughness. A series of four AS4/3501-6 laminates were cured with three different void contents. The question of whether voids would improve or lower delamination fracture toughness is not initially obvious. For example, one of the suggested explanations for how rubber particles toughen epoxy resins is that they allow local voiding, which changes the nature of the state of stress at the crack tip (Jordan, 1985).

The second minor objective was to examine the effect of loading history on delamination fracture toughness. Specimens that had been tested under mode II conditions were later tested in mode I conditions. Some preliminary work by Cohen (1982) appears to indicate that the history of previous loading can have a significant affect upon mode I delamination fracture toughness.

The third minor objective was to complete a few experiments that would allow two refereed publications to be completed based largely on previous experimental work. This

involved several types of tests that could not be performed at my home university (such as rheological tests).

III. EXPERIMENTAL PROCEDURE

The AS4/3501-6 panels were layed up according to the specified orientations in 25 square centimeter panels (See Table I for details). A strip of teflon was placed at the midplane about 4 cm into one edge of the laminate to provide a starter crack. This would provide a starter crack that would grow in the 90 degree direction (parallel to the fibers at the center plane). The AS4/APC2 was layed up in 10 by 15 cm laminates with an aluminum insert to provide a starter crack at the midplane. The starter cracks went into the laminate a distance of approximately 4 cm.

The choice of layups was made to allow the effect of splicing on delamination fracture toughness to be examined. One difficulty in designing the choice of stacking sequence relates to the problem of twisting occurring during testing. During mode I testing, only one half of each laminate is actually being bent. To eliminate coupling between twisting and bending each half laminate has to be symmetric. However, during mode II testing, the entire laminate is bending and to eliminate coupling between bending and twisting an overall symmetric layup is required. The choice made during this project was to use a symmetric stacking sequence, knowing there will be some slight twisting during mode I testing. (A calculation of the laminate stiffness showed that for the systems used in this study, the values of the [B] matrix are small with respect to that of the [A] matrix, indicating twisting should not be a large problem).

The laminates were cured in an autoclave according to standard practices for such materials. The cured laminates were C-scanned and X-rayed to establish that there were no internal defects other than the cracks caused by the edge inserts.

The mode I double cantilevered beam (DCB) test specimens were cut to be approximately 2 to 2.5 cm wide and up to 20 cm long. The mode II end notch flexure specimens were cut to be approximately 2 to 2.5 cm wide and about 18 cm long.

The mode I tests were performed on a screw driven Instron tensile test machine operating in displacement control. The crosshead rate used was .05 in/min. The load and displacement were continually recorded on a strip chart. The side of the specimen was coated with a brittle white coating to aid in determining the growth of the crack. The crack length was monitored at discrete intervals (every .5 inch of crack growth) and this length was marked on the load-displacement chart. The crack was grown from its original length

to a length of 4.5 inches on each specimen. At one point during the crack growth period, the specimen was unloaded so that the shape of the unload/load curve could be determined.

The mode II tests were performed on a screw driven Instron tensile test machine operating in displacement control and with a crosshead displacement rate of .05 in/minute. The test fixture used for this is a three point bend geometry. The span of the two bottom supports was four inches, with the load being applied at the center of the specimen. For most of the tests, the crack tip was placed one-half way between one of the lower supports and the applied center load (this provided a starter crack of 1 inch). The load was slowly applied until the crack began to grow. Crack growth was usually unstable, with the crack growing in one step to the center loaded region. One of the advantages of this test geometry is that once the crack has grown, the specimen can be slid over so that a crack length of 1 inch is again obtained, and another test can be performed on the same specimen. This is why the mode II specimens were cut considerably longer than the span of the three point test fixture.

Metallographic specimens were cut from the uncracked portion of the laminates and examined within a metallograph. This was used to help verify the nature and amount of the voids in the panels where voids were deliberately obtained.

IV. EXPERIMENTAL ANALYSIS AND RESULTS

Mode I Analysis

Mode I tests using Double Cantilevered Beam test specimens have been done by a number of investigators, including this one (Jordan, 1985). The most common analysis has been one using linear beam theory (Jordan, 1985). Devitt, et al, (1980) allowed for non-linear elastic behavior but not for permanent damage in the composite caused by crack growth. The results in this study were all in the linear elastic region as defined by Devitt. However the layups so marked in Table I had significant permanent deformation as a result of crack growth. (This permanent deformation is in the form of a permanent opening displacement.) The results for those layups were calculated using linear elastic beam theory and labelled as upper bound limits to G_{IC} . The remaining layups did not have significant permanent deformation and the fracture toughness results reported can be considered to be accurate.

Mode I Results

Mode I test results are reported in Table I. The fracture toughness values reported in this study are for steady state crack growth. In each system, there was a smaller value of an apparent initiation fracture toughness. There was then a region where the value of G_{IC}

did not change with respect to crack length. This is the value of G_{Ic} reported in this study. For long crack lengths (on the order of 9-10 cm) there was then an increase in fracture toughness. This may be related to permanent damage occurring within the laminate as the crack grows.

For the AS4/3501-6 system the first two layups listed had significant permanent deformation after the cracks had grown to a length of 11.4 cm. For the AS4/APC2 system only the first layup listed had significant permanent deformation after the crack growth. These results are reported as upper bound limits to G_{Ic} . The remaining layups all had small amounts of permanent deformation and valid G_{Ic} results. The systems that had a large permanent deformation also had some twisting. This was not considered large enough to effect the mode I results.

For the AS4/3501-6 system, there was an increase in fracture toughness as the number of splices increased. Grouping plies of the same orientation together increased the amount of permanent deformation as well as decreasing the fracture toughness. Splicing increased the fracture toughness by at least 15%. (The increase may be larger than that for there is only an upper bound limit to the toughness for the system where 4 plies of each orientation were grouped together).

For the AS4/APC2 system, there was an increase in fracture toughness as the number of splices increased. The increase may be more than 75% (again it may be larger because of the uncertainty in the toughness for the unspliced system). Both the AS4/3501-6 and AS4/APC2 systems had the biggest increase in toughness when the first round of splicing began. Grouping only 2 plies together was significantly tougher than grouping 4 or 6 plies together, but further splicing did not have a significant effect upon fracture toughness (Compare the last two layups with each system with the first two layups for each system).

Mode II Analysis

Two common methods of performing mode II delamination fracture toughness tests are the end notch flexure test (E.N.F.) and the end-loaded split laminate. The end-loaded split laminate method was used in my dissertation (Jordan, 1985). In a recent conference presentation Corleto and Bradley (1987) reported a comparison of these two test methods for use with a brittle and a ductile resin system. Their conclusion was that these two methods give similar results. Since the E.N.F. test method uses simpler fixtures (a three point bend test geometry) that is the method that was used in this study. There were nonlinearities in the load/unload curve for some of the systems. To deal with this issue, I followed the example of Corleto and Bradley (1987) and calculated G_{IIc} using the area

within the load/unload curve as the energy required to grow the crack. This was divided by the specimen width and the length of crack extension to get a value for G_{IIc} .

Mode II Results

Mode II results are shown in Table I. For three of the layups indicated in the table, there was significant permanent deformation and the mode II fracture toughnesses reported are upper bound limits to G_{IIc} . There was a small permanent opening displacement for these systems as well as a permanent bending of the laminate. In addition, for these systems the outside layers (that were in tension) delaminated in a few locations prior to extension of the main crack.

When comparing the layups where a legitimate G_{IIc} could be obtained, splicing increased the fracture toughness of the system. In contrast to the mode I results, continuing to splice the laminate (after the first time) continued to increase the fracture toughness. For both of the mode I and mode II tests, increased splicing had a bigger effect on the toughness of the more ductile AS4/3501-6 system than it did on the more brittle AS4/3501-6 system.

Effects of Voids Upon Delamination Fracture Toughness

Voids were deliberately put into two AS4/3501-6 laminates with different stacking sequences in an attempt to determine their impact upon delamination fracture toughness. Following the example of Harper, et al (1987) this was accomplished by varying the time and amount of pressure applied to the laminate during curing. The standard temperature and vacuum cycle was applied to these laminates.

The effect of voids upon fracture toughness is shown in Table II. The addition of voids increased both the mode I and mode II delamination fracture toughness for both layups. This result is what was expected. Harper et al (1987) and Tang et al (1987) both reported that the presence of voids decreased the strength and transverse modulus of graphite/epoxy systems. Frequently whatever will decrease strength and modulus will increase toughness. This turned out to be correct in this case as well. The laminates with voids had a lower bending modulus and a higher toughness.

The voids typically occurred at the interfaces of the original plies. This is shown in the photomicrographs in Figure I. Volume percentage of voids were calculated from the difference in specific gravity and are reported in Table II.

Effect of Loading History on Delamination Fracture Toughness

Preliminary work by Cohen (1982) indicated that the loading history may have an affect upon mode I delamination fracture toughness. In this project some specimens were delaminated under mode I conditions (crack grown to about 11 cm length) and then

delaminated under mode II conditions. Other specimens were delaminated under mode II conditions and then delaminated under mode I conditions.

Test results for this trial are shown in Table III. To avoid having to deal with the problem of a large degree of permanent deformation obscuring the results, the layups used in this portion of the project were the heavily spliced ones that had no significant permanent deformation.

Previous delamination increased both the mode I and mode II fracture toughness. The effect of prior mixed mode delamination on mode I toughness had been reported by Cohen (1982). In both cases, the subsequent mode I delamination fracture toughness was increased. This may be related to internal damage caused by the mode II loading. The mode I crack is now growing through damaged material instead of virgin material.

More surprising was the result that prior mode I delamination crack growth increased subsequent mode II toughness. Apparently mode I crack growth also somehow damages the laminate, resulting in the mode II crack growing through a damaged region.

V. DISCUSSION OF RESULTS

Effect of Splicing on Delamination Fracture Toughness

The nature of the effect of splicing on delamination fracture toughness is not surprising. If there was to be any effect at all, it would be expected that increased splicing would increase the delamination fracture toughness. When the laminate is cured, there will always be some residual stresses left within the laminate. These residual stresses result from the different thermal properties of the resin and the fibers. If the laminate is heavily spliced then the tendency of one ply to cause the laminate to bend in one direction will be countered by its adjacent plies which may want the laminate to bend in a different direction. However, if plies of the same direction are grouped together then different portions of the laminate will have very different residual stresses. These stresses will make it easier to delaminate the laminate, for there are now significant stresses present acting to pull the laminate apart at its weakest link (the ply interface).

It is interesting to note that splicing had a larger effect upon the more ductile AS4/APC2 system. This may be related to the poor interfacial bonding between plies in the AS4/3501-6 system. Previous work on this system indicates that delamination typically occurs at the resin/fiber interface rather than within the resin itself (Cohen, 1982). This poor bonding may result in delamination occurring in the spliced layups before the intrinsic resin toughness could be obtained. The total increased toughness expected in the unspliced system could not be obtained because of the fiber/resin interfacial failure.

Effect of Voids on Delamination Fracture Toughness

The presence of voids (in the amounts indicated in Table II) increased both the mode I and mode II delamination fracture toughness. This is not surprising when the effect of voids on other mechanical properties is examined. The presence of voids decreases transverse strength and modulus as was previously noted. Typically a material that has lower modulus and strength is also tougher, and that was the situation in this case.

There are several possible explanations for this voids' effect upon toughness. The first one might simply be that the presence of the voids decreases the modulus and increases the inherent toughness of the resin system. A more ductile system is typically a more tough system, and this just may be an illustration of that.

A second possibility is that the presence of the voids may change the state of stress near the crack tip, thus postponing the time when crack propagation will begin. A variation of this has been suggested for the reason why rubber particles toughen epoxy resins. It has been suggested that there are small voids near the vicinity of the rubber particles that relax the stresses and make the system more ductile (and therefore tougher) (Jordan, 1985). However, it must be noted that any voids occurring near rubber particle additions are several orders of magnitude smaller than these voids.

A third possibility is that the presence of the voids changes what is occurring near the crack tip. A system without voids would tend to have a very sharp crack tip (with a high stress concentration at that location). With large numbers of voids, the crack may grow from void to void, always keeping a relatively blunt crack tip (the edge of the void is now the crack tip). This blunt crack tip now has a low stress concentration and a higher stress must be applied before a critical value of stress is reached at the crack tip that will allow continued crack extension.

The designer must be cautioned, in that I am not recommending that voids be deliberately added to a resin system in order to improve toughness. This study only dealt with a very specific type of void (at the ply interface) and only with a void content up to 6% by volume. A different type of void or an increase in void content above 6% may have very different results.

The results of this study on voids has two positive benefits for the designer. The first one is that the mere presence of interfacial voids may not mean that a composite part must be rejected. A few voids may not hurt the toughness of the composite and may indeed increase the composite toughness. (The presence of the voids may however lower the stiffness of the composite laminate below acceptable levels). The second positive benefit is that if the designer uses a void free laminate toughness for design, his design will

always be conservative, for a part with voids will be at least as tough as the void free laminate he used for design purposes.

Effect of Loading History on Delamination Fracture Toughness

Prior loading of the laminate increased the fracture toughness. This was true irrespective of whether the mode I delamination crack extension was done before or after the mode II delamination crack extension. This is in accord with the results of Cohen (1982). He delaminated some specimens at about 35% mode II conditions and then found that the subsequent mode I delamination fracture toughness was larger than before. In this study laminates layups were chosen so that there would be no significant permanent deformation resulting in the specimens after crack extension had occurred. This was verified by the fact that all of the mode II unload curves reached a zero load at the same time they reached a zero extension. This does not mean that there was not permanent damage within the laminate. The prior loading effect on toughness appears to indicate that there was permanent damage in the laminates before the second set of tests were begun.

These results raise again the question of whether the reported fracture toughness results are the intrinsic fracture toughness or merely reflect the far field damage that was caused by the initial test. It was not possible to definitely tell the difference from the current test results. However, if a system is loaded more than one time, it may be damaged before the second loading has begun. Then these fracture toughnesses may reflect what is actually occurring in the laminate, even though it might not be the toughness in a virgin, undamaged laminate.

These results indicate a potential problem with some mode II delamination fracture toughness results reported previously by other investigators. When using E.N.F. test specimens a starter crack is typically made through the use of some type of insert into the edge of the laminate at the midplane. This results in a resin pocket at the end of the insert. Many investigators typically grow a mode I crack through this resin pocket before the mode II test is begun. This study indicates that investigators should not grow the mode I crack too long or the laminate may become damaged and the resulting mode II toughness may become larger than it intrinsically should be. A standard short mode I starter crack grown through the resin pocket should be employed.

One positive aspect of the history effect is that prior loading will provide a laminate that will be tougher than one that had not been loaded or tested before. This means that if a designer uses results from a test on an virgin laminate he will be using a conservative value of the fracture toughness.

VI. CONCLUSIONS AND SIGNIFICANCE

Several significant results have been obtained in this research program:

(1) Increased splicing will increase the delamination fracture toughness under both mode I and mode II loading conditions. This is useful to the designer who frequently may be limited to quasi-isotropic laminate layups, but would like to improve the fracture toughness. This shows that fracture toughness can be improved by a proper choice of stacking sequence. It must be noted that this improvement is not as great as might be obtained if the material system could be changed. (There is a greater difference between the AS4/3501-6 and the AS4/APC2 toughness than there is between the spliced and unspliced layups within each laminate system.)

(2) The presence of voids at the ply interface may in some situations actually increase the mode I and mode II fracture toughness. This is useful in that the manufacturer does not necessarily have to remove all voids from the laminate for it to be successfully used in a real world application. Designing from void free laminate test results will provide a conservative estimate of fracture toughness.

(3) Prior loading (particularly with prior crack growth) tends to increase the fracture toughness of the composite. This is probably related to some type of permanent damage that has been created within the laminate. This is useful to the designer in that a previously damaged laminate may still be usable in many applications where toughness is the controlling parameter. Designing from previously unloaded laminate test results will provide a conservative estimate of fracture toughness.

Conclusions (2) and (3) above must be tempered with the fact that this increased toughness may be accompanied by a decreased stiffness that may make a laminate unusable for that reason (even though the toughness is still acceptable).

VII. RECOMMENDATIONS

I have four major recommendations for continuing work in this area. The first one is make detailed fractographic examinations in a scanning electron microscope on the fractured surfaces of the systems studied in this program. This might enable a determination to be made as to whether the different layups fractured by the same micro-

mechanisms or not. This could help in determining the reasons behind the stacking sequence effect seen in the macroscopic test results.

The second major recommendation is for samples of these same materials to be fractured within a scanning electron microscope and the microscopic nature of the fracture process recorded. Some of the layups produced much more permanent, measurable damage than did the others. This would help to determine if the difference in fracture toughness resulted from changes that occurred near the crack tip or whether the results merely reflected differences in far field damage.

The third major recommendation is for a study to be undertaken to look at the effect of spiralling upon delamination fracture toughness. This involves studying the effects of trying to minimize the differences in fiber orientation between adjacent plies. This is another type of stacking sequence effect, but it is different from the issue discussed in this study (which involved grouping of common orientations together).

The fourth major recommendation is based on the fact that it is not always possible to analyze delamination fracture within quasi-isotropic laminates by linear elastic beam theory methods. Precise fracture toughness numbers could not be obtained for some of the systems studied in this project because there was no good way to separate the effects of far field damage from what was occurring in the vicinity of the crack tip. Some approach similar to the J-integral approach suggested by Schapery and Jordan (1986) needs to be developed to allow for analysis of these systems.

All four of the above recommendations are incorporated into my Research Initiation Program proposal that follows from this summer's project. All of the above suggestions could be performed during this follow-up project with the exception of mode II fracture within the scanning electron microscope. That project does not have a large enough budget to allow for the new fixtures needed for in-situ mode II delamination.

REFERENCES:

- Cohen, R.N., "Effect of Resin Toughness on Fracture Behavior of Graphite/Epoxy Composites", M.S. Thesis, Texas A & M University, December 1982.
- Corleto, C.R., and Bradley, W.L., "Mode II Delamination Fracture Toughness of Unidirectional Graphite/Epoxy Composites", presented at an A.S.T.M. Symposium, Cincinnati, Ohio, April 1987.
- Devitt, D.F., Schapery, R. A., and Bradley, W.L., "A Method for Determining the Mode I Delamination Fracture Toughness of Elastic and Viscoelastic Composite Materials", Journal of Composite Materials, Vol. 14, October 1980, pp. 270-285.
- Harper, B.D., Staab, G.H., and Chen, R.S., "A Note on the Effects of Voids Upon the Hygral and Mechanical Properties of AS4/3502 Graphite/Epoxy", Journal of Composite Materials, Vol. 21, March 1987, pp. 280-289.
- Jordan, W.M., "The Effect of Resin Toughness on the Delamination Fracture Behavior of Graphite/Epoxy Composites", Ph.D. Dissertation, Texas A & M University, December 1985.
- Schapery, R.A., Jordan, W.M., and Goetz, D.P., "Delamination Analysis of Composites with Distributed Damage using a Work Potential and J-integral", presented at International Symposium on Composite Materials and Structures, Beijing, China, June 10-13, 1986. In Proceedings, pp. 543-548.
- Tang, J., Lee, W.I., and Springer, G.S., "Effects of Cure Pressure on Resin Flow, Voids, and Mechanical Properties", Journal of Composite Materials, Vol. 21, May 1987, pp. 421-440.

Table I

Mode I and Mode II Delamination Fracture Toughness

Material	Layup *	Number Plies	G _{Ic} (J/m ²)	Permanent Opening Displacement (mm) **	G _{IIc} (J/m ²)	Upper Bound Limit to G _{IIc} (J/m ²)
AS4/3501-6						
	[-45(4)/0(4)/45(4)/90(4)] S	32	133 ***	22.2		853
	[-45(3)/0(3)/45(3)/90(3)] S	24	154 ***	30.2		483
	[-45(2)/0(2)/45(2)/90(2)] 2S	32	158	6.4	434	
	[-45/0/45/90] 4S	32	152	2.4	564	
AS4/APC2						
	[-45(6)/0(6)/45(6)/90(6)] S	48	877 ***	27.8		2422
	[-45(3)/0(3)/45(3)/90(3)] 2S	48	1454	7.1	1687	
	[-45(2)/45(2)/45(2)/90(2)] 3S	48	1523	5.6	1692	
	[-45/0/45/90] 6S	48	1509	4.0	2077	

* Systems delaminated at midplane in 90 degree direction.

** Permanent displacement after completion of mode I tests (with final crack length of 11.4 cm).

*** Upper bound estimate because of large degree of permanent deformation.

Table II
Effect of Voids on the Delamination
Fracture Toughness of AS4/3501-6

Layup *	Percent Voids	G_{Ic} (J/m ²)	Modulus E_{90} From Mode I Test (GPa)	G_{IIc} (J/m ²)
[-45(4)/0(4)/45(4)/90(4)] S	0	133 **	40.1	853 **
	6.0	316	38.4	1325
[-45/0/45/90] 4S	0	152	55.4	564
	3.6	281	50.7	785

* Systems delaminated at midplane in 90 degree direction.

** Upper bound estimate because of large degree of permanent deformation.

Table III
Effect of Loading History on
Delamination Fracture Toughness

Material	Layup *	G_{Ic} (J/m ²)	G_{Ic} (J/m ²) After Mode II Crack Growth	G_{IIc} (J/m ²)	G_{IIc} (J/m ²) After Mode I Crack Growth
AS4/3501-6					
	[-45(2)/0(2)/45(2)/90(2)] 2S	158	190	434	904
	[-45/0/45/90] 4 S	152	140	564	742
AS4/APC2					
	[-45(2)/0(2)/45(2)/90(2)] 3 S	1523	1864		
	[-45/0/45/90] 6 S	1509	2084		

* Systems delaminated at midplane in 90 degree direction.

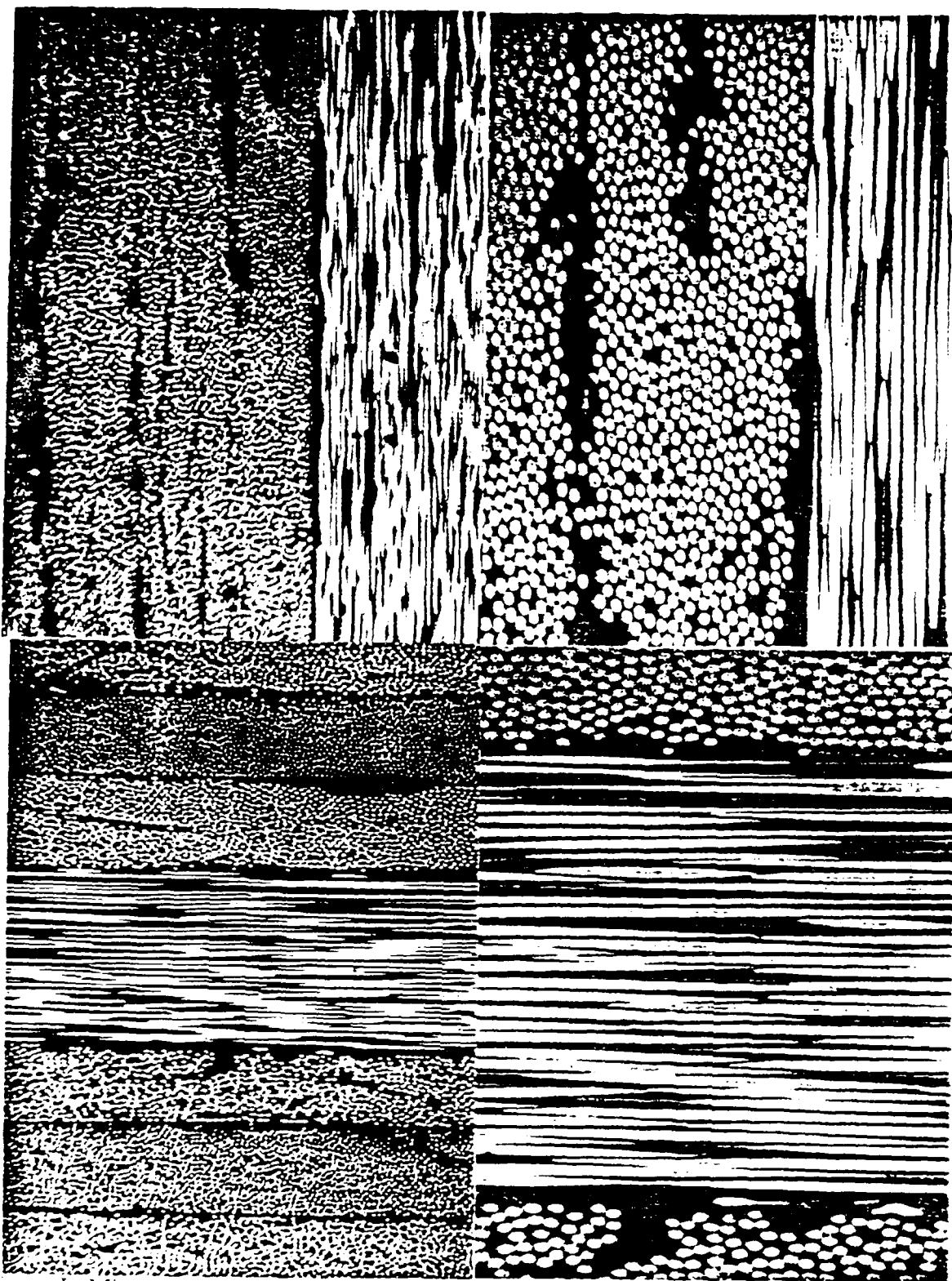


Figure 1. Microstructure of panels with intentional voids. Upper photomicrographs show AS4/3501-6 panel with $[-45(4)/0(4)/45(4)/90(4)]$ S layup and lower photomicrographs show AS4/3501-6 panel with $[-45/0/45/90]$ 4 S layup. Left photomicrographs are at 100 x and right photomicrographs are at 250 x.

1987 USAF-UES SUMMER FACULTY RESEARCH PROGRAM/
GRADUATE STUDENT SUMMER SUPPORT PROGRAM

Sponsored by the
AIR FORCE OFFICE OF SCIENTIFIC RESEARCH

Conducted by the
Universal Energy Systems, Inc.

FINAL REPORT

"GENERIC" CREDIT CARD FEASIBILITY STUDY

Prepared by:	William F. Kauder, Jr., Ph.D.
Academic Rank:	Assistant Professor
Department and	Accounting Department
University:	Winston-Salem State University
Research Location:	AFLMC/LGC Gunter AFS Gunter AFS, AL 36114
USAF Researcher:	Captain Chuck Coffin
Date:	11 Sept 87
Contract No:	F49620-85-C-0013

"GENERIC" CREDIT CARD FEASIBILITY STUDY

by

William F. Kauder, Jr., Ph.D.

ABSTRACT

This study documents the results and findings of a project concerning the availability of a "generic" credit card for the United States Air Force to use in simplifying and reducing the cost of procedures used in making small local purchases. It involved contracting a sample of ten banks and lending institutions to request their cooperation in providing this type of card. A "generic" credit card is one issued to a specific organization rather than in the name of an individual. The use of a "generic" credit card to obtain "Wash Post Items" could effect a great savings in Air Force expenditures if procedures could be changed for its incorporation. Some obstacles are evident but are not insurmountable roadblocks inasmuch as five banks and lending institutions have agreed to participate further in achieving this objective.

The author recommends an in-depth study of Time and Methods to determine an accurate estimate of cost saving from the improved procedures. If cost justified, a Model Installations Program test, using the five positive respondents from this "generic" study, should be carried out at Maxwell Air Force Base or at other selected sites in the southeastern United States.

ACKNOWLEDGEMENTS

I wish to thank the Air Force Systems Command and the Air Force Office of Scientific Research for sponsorship of this research. Universal Energy Systems, who conducted this study, must be mentioned for their concern and help to me in all administrative and directional aspects of this program. I also wish to thank the Commander and all the Staff of the Air Force Logistics Management Center at Gunter AFS, AL for their cooperation and willing assistance in this project.

I enjoyed this experience and believe it to have been rewarding and enriching because of the many contacts that I made and the exposure to the vast research materials that were available through the Air Force Libraries. These experiences were enhanced by many different influences.

Lt. Col. Thomas G. Jones, Capt. Chuck Coffin, and Capt. Dan Daley provided me with support, encouragement, and an enjoyable working atmosphere. The help of Sgt. Chuck Swartz, Sgt. David Pearson, and Sgt. Bo Hill were invaluable to me in overcoming many technical problems. The assistance of Ms. Sally (Powell) Kendal and Mr. Harold I. Newhouse, Jr. are greatly appreciated.

Acknowledgements and thanks are also extended to Capt. Peter Hart POC HQPAF/LGC, Capt. Jim Pena POC HQTAC/LGC, and Ms. Thelma Shelton POC AFAFC/XSPBS. The Library Staffs at Gunter AFS and at Maxwell AFB were very helpful and cooperative in assisting me in this project. Special thanks are also extended to Ms. Kay Booth for her help in proof reading many of my rough drafts.

WFK

I. INTRODUCTION:

The results of three Air Force Logistic Management Center (AFLMC) Reports published in 1983 and 1984 indicated that the Air Force had experienced serious problems involving the high cost and frequent delays in making small local purchases. These purchases were for amounts of less than \$1,000.00, and comprised approximately eighty five (85) percent of all small purchase transactions, as stated in Reference No. 4. Many of these transactions were of a repetitive nature. One method recommended in two (2) of these studies (References No. 2 and 3) was to use credit cards to reduce the cost and improve the efficiency of making small local purchases. The Air Force desired to locate local banks or lending institutions that would be willing to issue it "generic" credit cards (cards in the name of the Air Force or of an Air Force organization rather than in the name of an individual). This type of card would allow small local purchases to be made in an efficient and timely manner.

The Contracting Section of the AFLMC at Gunter Air Force Station, AL is particularly concerned with reductions in the cost and improvements in the efficiency of making small local purchases. Special attention has been directed to using modern means of financing these purchases. These changes would reduce the number of steps that Base Contracting and Base Supply would have to make to carry out these transactions. Prior efforts to obtain credit cards that would satisfy the Air Force's requirement were unsuccessful. Therefore, locating banks or lending institutions that would issue "generic" credit cards to the Air Force was an essential step in revising procedures for making small local purchases.

Managerial Accounting and Cost Control has been my major area of research interest. I have had experience carrying out literature searches, conducting surveys, analyzing results, and preparing technical reports of the results. I used these methods in the preparation of a dissertation to complete my Ph.D. in Accounting. This experience contributed to my assignment to the Contracts Section of the Air Force Logistic Management Center.

II. OBJECTIVES OF THE RESEARCH EFFORT:

The Air Force met with a major obstacle when they attempted to incorporate the use of credit cards to make small local purchases at two (2) bases (Hickam AFB and Langley AFB). To efficiently carry out improved, low cost, and rapid small local purchase procedures, the Air Force needed a "generic" credit card. This would allow the individual who needed to make the purchase to visit Base Supply, have the request approved, withdraw a "generic" credit card, make the purchase from the vendor (charging it on the credit card), return with purchase to Base Supply for its approval, and to return the credit card used for the purchase. By using this procedure, considerably less cost and time would be involved than with the present procedure which requires Base Contracting to prepare and issue a purchase order.

My assignment as a participant in the 1987 Summer Faculty Research Program (SFRP) was to locate banks and (or) lending institutions in the southeastern United States that would be willing and able to provide the Air Force with a "Generic" credit card (one issued in the name of the Air Force or a unit of the Air Force and not in the name of a private individual) that could be used in future Air Force tests. These tests would be to determine if credit cards can be effectively used to reduce the cost and increase the speed of making the purchases described above.

III. APPROACHES:

The author made a comprehensive literature search of past projects at the AFLMC, of projects from other sections of the Department of Defense, and of other literature sources concerning credit cards and their use by the Air Force at the Gunter AFS and Maxwell AFB libraries.

The Point of Contact (POC) at Hickam AFB, HI (Capt. Peter Hart, LGCP), at Langley AFB, VA (Capt. Jim Pena, LGCP), and at Lowry AFB, CO (Ms. Thelma Shelton, a systems accountant at the AF Accounting and Finance Center) were contacted to determine the status of credit card projects at these bases. Each POC sent back written responses outlining the status of their projects and the procedures they used or planned to use in carrying them out.

A stratified sample of ten (10) banks and lending institutions was made by the author. This sample was composed of seven (7) banks, one (1) savings and loan association, one (1) credit union, and The American Express Company. These firms and representatives of VISA and MasterCard were contacted to determine if they would be willing to establish a "generic" credit card account for the USAF to use in making small local purchases. The initial contact with the sample institutions was made by telecon. The author contacted the vice president in charge of credit cards for their firms to inform them of the problem and ask if their firm was interested in providing a generic credit card. They were requested to initiate a written response of either their desire to participate further in the project or to give their reasons if they did not so desire to participate. The respondents that were considering further participation in the project received a letter confirming the telecon and included a sample copy of Terms of Commercial Agreement (TOCA) based on those presently in existence between the USAF & The First Hawaiian Bank at Hickam AFB, HI (copies of which are included as Attachment 1.). The TOCA was included to assist the banks and lending institutions in the evaluation of feasibility of cooperating further in this project.

IV. RESULTS:

Small local purchases, which are referred to as "Wash Post Items" by Base Supply, must meet the following four (4) criteria: a) be base procured expendable supplies, b) be one-time requirements and not expected to recur within 180 days, c) must cost less than \$1,000.00, and d) must not be equipment items, stocklisted items or local L or P number items.

AFLMC Report LC840116 (Reference No. 2) contained finding that small local purchases consisted of the following items: administrative supplies, camera supplies, chemicals, clothing, electrical components, floor coverings, hand tools, hardware, kitchen supplies, lighting hardware, navigational flight supplies, paints, and miscellaneous. Therefore, this category of military purchases contains a large number of various small line items to be purchased from many different types of vendors and is quite costly under present procedures.

AFLMC Report LS830205 (Reference No. 4) described the magnitude of small local purchases. It was determined that Base Contracting processed over 4.6 million purchasing actions in FY83. The report also estimated the extent to which these actions would increase in the future, and estimated that by 1995 they would reach 6.25 million actions. The report indicated that eighty-five (85) percent of all actions were less than \$1,000.00 per individual purchase, and therefore classified as small purchases.

AFLMC Report LS840120 (Reference No. 3) described present procedures used to make small local purchases and innovative changes in procedures that were proposed to improve efficiency, timeliness, and customers' attitudes. One recommendation concerned an investigation regarding the feasibility of allowing customers to make their own "Wash Post" purchases and to use credit cards as a means of securing and financing the transactions. This recommendation was also made in AFLMC Report LC840116 (Reference No. 2).

AFISC Report PN85-615 (Reference No. 1) described the proposal initiated by Hickam AFB, HI under the Model Installations Program (MIP) to authorize the controlled base wide use of commercial credit cards. The report indicated that initiating this proposal would reduce the number of contracting procedures required to make a local purchase from forty (40) separate task steps [which presently require a minimum of three (3) working days] to five (5) task steps [requiring only one (1) hour to complete]. This would yield a major reduction in the Contracting workload and would lead to major cost savings in making small local purchases. However, Hickam AFB LGC was unable to reap these potential savings because they were unable to locate a bank that would issue a "generic" credit card which would allow this proposal to be implemented. Lt. Col. Kent R. Carlson USAF Acting Director of Contracting and Deputy Chief of Staff, Logistics at Hickam AFB indicated in his letter of June 25, 1986 that use of credit cards in support of the Commander's Contingency Fund continues to be well accepted by all parties involved, and that although a MIP proposal had been approved for use by the entire base, this had not been implemented due to their inability to resolve the problem of "generic" accounts (Reference No. 5). Confirmation on 6/25/87,

Major Donald J. McCarthy, USAF Acting Director of Contracting Deputy Chief of Staff, Logistics at Hickam AFB, stated their use of credit cards continued to be well accepted by all parties involved and provided them with a convenient alternative to the standard small-dollar purchase methods. It was their feeling that the expansion of credit card use as an acquisition method would result in much improved customer support (Reference No. 6).

AFISC PN85-615 "The TIG Report" (Reference No. 1), concluded that a significant reduction in administrative costs and improved customer support could be realized through the effective use of all simplified small purchase procedures. It recommended that HQ USAF/RDC (now SAF/ACQ) should task MAJCOMs to reduce cost by decentralizing contracting authority throughout the Air Force, and reemphasized to commanders the importance of their active involvement in the contracting process.

The response from the POC at Hickam AFB, HI confirmed that currently Hickam is continuing to use credit cards that are not "generic" in support of the Commander's Contingency Fund and are very satisfied with this arrangement. They would like to expand the use of the card base wide if a "generic" card could be obtained.

Col. Robert P. Lansell, Director of Contracting at Langley AFB, VA, reported that they attempted to use credit cards to make small purchases of less than \$500.00; however when their proposed bank card agreement was submitted to the bank, the bank would not issue credit cards with only "US Air Force, Langley AFB, VA" on the card. The bank insisted on having an individual's name on the card in addition to the above information. Since this would not permit the degree of flexibility necessary for the incorporation of the most efficient method of making small purchases, the placing of an individual's name on the card was determined by Langley LGC to be an unacceptable option. This caused the use of credit cards to make small local purchases to be dropped at Langley (Reference No. 7).

Ms. Thelma Shelton POC AFAFC/XSPBS, Denver, CO notified the author by letter on July 29, 1987 that the AF Accounting and Finance Center at Lowry AFB is controlling a Test Program at eleven (11) test locations. This test involves an agreement with Citicorp Diners Club, Inc. to issue charge cards to Federal travelers for official travel expenses of lodgings, meals, and vehicle rental. It provides travelers with check cashing

privileges, guaranteed reservations, and protection against loss of cash. The use of this card has helped to improve Government cash management by delaying some travel disbursements. The test, begun January 1, 1986 and extended through September 1988, is still in progress, and its overall evaluation is incomplete (Reference No. 8).

Response letters from the ten (10) banks and/or lending institutions in the sample were divided into two groups. The first (affirmative) group consisted of those respondents [three (3) banks, one (1) savings and loan association, and one (1) credit union] that agreed to participate further in the study. The second (negative) group consisted of respondents [four (4) banks, and The American Express Company] that did not agree. For more detailed information regarding the banks and lending institutions involved such as their names, addresses, persons contacted, phone numbers, and comments, see Attachment 2. in this report.

Many firms claimed that their policies prevented them from issuing a "generic" credit card. Three (3) of the four (4) banks in the negative group and one (1) bank in the affirmative group mentioned that they would not be able to offer a card unless a charge could be paid by the Air Force which was greater than what was stated in the Terms of Commercial Agreement in existence between the Hickam AFB, HI and The First Hawaiian Bank. In recontacting the POC at Hickam AFB by telecon on August 6, 1987, the author discovered that had their project for credit card use been expanded base wide, The First Hawaiian Bank would have charged an additional amount for that service. This charge would have depended upon the amount of use given to the additional cards. Three (3) of the banks and The American Express Company (in the negative group) stated that if they issued a card their firms would be exposed to greater liability and therefore should receive compensation for this additional risk.

V. CONCLUSIONS:

Based upon the results of the library research, the Air Force appears to have serious problems with the cost, effectiveness, and the negative customer attitudes caused by their small local purchasing procedures.

The items are referred to as "Wash Post Items", and major savings in cost and time of completion of the purchase process could be achieved if improved purchase procedures utilizing credit cards could be incorporated. Since this category of military purchases involves many different types of purchases from a diverse group of vendors, the credit card that the Air Force selects must have wide acceptance if it is to be used effectively. The communications with POCs at Hickam AFB, Langley AFB, and Lowry AFB revealed the following facts. First, that credit cards with individuals' names on them (not "generic" cards) were presently being used at Hickam AFB in charging costs to the Commander's Contingency Fund, and second, that charge cards are being used at eleven (11) AF installations throughout CONUS for Federal travel purposes where their test use is under the control of Lowry AFB. Hickam AFB, LGC was definitely pleased with the use of the cards and wished to expand their use. The eleven (11) bases under Lowry's control are still undergoing test and have not completed an analysis of the results as the test period is to run through September 1988. It appears to the author that they view the benefits of the card's use very favorably. Therefore, the author believes that credit cards can be used effectively by the AF to make small local purchases. Third, at Hickam AFB and Langley AFB, efforts were made to obtain "generic" credit cards to use for base wide tests, however, the banks in their local areas were not willing to offer the bases these essential "generic" credit cards.

The sample of ten (10) banks and lending institutions revealed that there are three (3) banks, one (1) savings and loan association, and one (1) credit union in the southeastern United States that have expressed a desire to cooperate with the Air Force and would, under certain conditions, issue "generic" credit cards to use in a future test at Maxwell AFB, if the test could be arranged. The author concluded that the availability of "generic" credit cards did not appear to be a "roadblock" to this test.

The major reasons the banks and The American Express Company gave for not cooperating in this project involved their basic policies against issuing "generic" credit cards, and insisting upon having an individual's name on the card. A general concern was expressed by the banks and The American Express Company that a fee would have to be charged to the Air Force for use of the cards. Also, they were concerned that they would

be adding additional liability to their firms, caused by the added risk from any unauthorized use of the credit cards which might occur after notification had been made by the Air Force.

The author concluded that the Air Force should address these concerns of the lending institutions in the procedures which they may eventually set up for use of the "generic" cards. This might increase participation of lending institutions if this change was to be adopted by the Air Force.

VI. RECOMMENDATIONS:

Local purchases for small dollar amounts represent a very large percentage of the transactions handled by Air Force Base Contracting, although they involve only a small percentage of the total contracting dollars. The present purchasing procedures are long, involved, and time consuming. Therefore, deliveries are frequently not able to be made in a timely manner and this has led to user illwill. To reduce the cost, and improve the efficiency and timeliness of the Air Force's small purchases procedures, recommendations have been made in several recent studies to use "generic" credit cards to secure and finance small local purchases. However, problems arose in obtaining these cards because the banks and lending institutions were concerned regarding the possible liabilities they would incur if the "generic" credit card was lost or stolen. To reduce these doubts and remunerate the banks and lending institutions for assisting the Air Force in achieving its objective, I recommend a further in-depth Time and Methods study to determine accurately the cost savings from adopting the new purchase procedures. These results could then be used to determine what, if any, fair price the Air Force should offer to compensate lending institutions for assuming these additional risks. Every "for profit" business is geared toward that end and should be compensated a fair and reasonable amount for their services rendered provided they fulfill the requirements and needs of their customers. To acquire the best services, operate more efficiently and effectively, and at the greatest cost-savings, methods should be of prime concern in achieving these goals. The major amount of cost involved in Base Contracting would be considerably reduced by changing the present

procedures and processes for small local purchases to procurement of same through "generic" credit card use by the Air Force Bases. The overall savings now and in the future could far outweigh the costs.

After the study has been made, the Air Force should initiate a Model Installations Program (MIP) at Maxwell AFB (or at another selected installation) to incorporate the use of credit cards in making small local purchases. The Air Force should then recontact the affirmative respondents of the sample [three (3) banks, one (1) savings and loan association, and the MAX credit union] and negotiate a contract for the number of cards and the credit limits the Air Force desires.

The Air Force should give careful attention to the procedures used in safeguarding the "generic" credit cards so that the banks and lending institutions might develop greater confidence in how the cards would be controlled. This should reduce their fears regarding the risk of losses which might result from a lost or stolen credit card.

The author assumed that if banks and lending institutions in the southeastern United States would be willing to issue credit cards with only "United States Air Force (USAF)" on them, then banks and lending institutions in other parts of the CONUS would also be willing to issue these cards. This assumption may not hold true in Hawaii or Virginia where problems have already been experienced at Hickam AFB and Langley AFB. It should also be considered that although the banks and lending institutions may agree to participate in the project at this time, they may change their minds when and if the tests are actually initiated.

As a final recommendation, I would suggest that the Air Force closely coordinate with the banks and lending institutions the formulation of the "generic" credit card procedures, uses, and Terms of Commercial Agreement in order to reduce or eliminate these possible problems.



DEPARTMENT OF THE AIR FORCE
AIR FORCE LOGISTICS MANAGEMENT CENTER
GUNTER AIR FORCE STATION, AL 36114-6693

ATTACHMENT 1.

2 July 1987

Mr. John Doe, Vice President
XYZ Bank
Credit Card Center
P. O. Box 12345
ABC, AL 00000

Reference: Telephone conversation of June 24, 1987 concerning a research study involving the feasibility of issuance of an Air Force Credit Card.

Dear Mr. Doe:

This letter is to confirm our telephone conversation referenced above. My summer Research Project is with the USAF Logistic Management Center at Gunter AFS in Montgomery, AL. The subject of the study concerns the feasibility of USAF using a credit card to simplify their methods of making local purchases of items costing less than \$2,500.00. These represent at least 85% of all USAF transactions.

I am contacting the large banks that operate in the Montgomery, AL area to determine if any of the banks would be willing to issue a generic credit card (one issued to an Air Force organization rather than a specific person). Many of the vendors with whom the Air Force make local purchases presently accept VISA and (or) MasterCard. Therefore, these are the two types of cards in which the Air Force is most interested. You indicated in our conversation that (your bank) would be interested in investigating further the feasibility of issuing a credit card that would meet the needs of the Air Force.

In order to assist (your bank) in evaluating the feasibility of cooperating further in this research study, I have included for informational purposes only, a copy of the terms that presently exists between the United States Air Force and First Hawaiian Bank. The names of the organizations have been removed. This does not imply that these would be the terms that the Air Force would wish to negotiate in any future agreement concerning credit card issuance with your bank or any other lender.

Thank you for your cooperation in this research effort. I hope to be communicating with you in the near future. Please send your letter to AFLMC/LGC, Gunter AFS, AL 36114 or call (205) - 279-3535(or3355).

Sincerely

William F. Kauder Jr.
William F. Kauder Jr.

1 Atch
Terms of Commercial Agreement

Terms of Commercial Agreement

General

This agreement would be between (The United States Air Force, Responsible Organization, Organzaton No., Initials, & Location) and (Participating Bank and Location) for the use by contracting of (Number) of banks VISA cards or MasterCard.

This agreement will be binding upon the (Air Force Orgaization) from the first time any of its authorized officers use the account.

Use

The cards may be used only for purchases of goods or services from participating merchants up to the credit limits. They may be used only by persons (The Air Force Organization) authorizes and identifies to (The Participating Bank).

Credit Limits

(The Participating Bank) will notify (The Air Force Organization, Organization's Telephone number) and (The Air Force Organization's) Accounting and Finance Office (ACF) of its overall credit limit. Total unpaid purchases may not exceed the overall credit limit. (The Participating Bank) may decrease the credit limit by providing 30 days written notice to (The Air Force Organization). (The Air Force Organization) shall designate a credit limit for each individual credit card holder within the overall credit limit. Total unpaid purchases by an individual credit card holder may not exceed this credit limit. If the credit limit is exceeded, the excess amount must be repaid immediately.

Waiver of Annual Membership Fees

(The Participating Bank) agrees to waive membership fees and all other charges for VISA cards or MasterCards issued to or used by (The Air Force Organizations).

No Waiver of Rights

If (The Participating Bank) chooses to give (The Air Force Organization) a break, such as by not declaring the entire balance due when the minimum monthly payment has not been made on time, it does not mean that (The Participating Bank) has waived, or given up, their right to exercise any of their rights or remedies under this agreement in the future. (The Participating Bank) is not required to use any particular kind of demand or notice in order to collect amounts due under this agreement.

Waiver of Certain Rights by Contract Office Base

(The Air Force Organization) agrees that they will be liable for repayment of everything owed under this agreement even if (The Participating Bank) does not follow all "legal procedures" such as diligence, demand, presentment and notice and protest of dishonor which the participating bank might be required to follow if it were not for this waiver.

Entire Balance Due

(The Participating Bank) may declare the entire balance due and payable at once with or without notice or demand if one of these events happen:

1. If (The Air Force Organization) fails to make payment under this agreement.
2. If (The Air Force Organization) violates any terms of this agreement.
3. If any representation or warranty made by (The Air Force Organization) to (The Participating Bank) is false.
4. If (The Air Force Organization) becomes insolvent or bankrupt.

Changing Agreement Terms

Either party to the agreement may at anytime request the other to make changes to the terms of this agreement. All such changes must be agreed to by both parties and be in writing.

Cancelling This Agreement

(The Participating Bank) reserves the right to cancel this agreement providing 30-days advance written notice is given to (The Air Force Organization) and Air Force Accounting and Finance may also cancel this agreement at anytime providing 30-day advance written notice is given to (The Participating Bank). If this agreement is cancelled, (The Air Force Organization) agrees to repay amounts it already owes to the participating bank under the terms and conditions of this agreement. The cards issued under this agreement remain the property of (The Participating Bank) and must be returned in the event that this agreement is cancelled or when any authorization for credit card use is revoked or terminated.

Unauthorized Use

(The Air Force Organization) may be liable for the unauthorized use of any card issued under this agreement. (The Air Force Organization) will not be liable for unauthorized use of the card which occurs after it notifies (The Participating Bank) orally at (The Participating Bank's phone number) or in writing at The Participating Bank's VISA card or MasterCard section address, of loss, theft, or possible unauthorized use. (The Air Force Organization's)

liability for unauthorized use of the card will not exceed \$50.00. However, a card in the possession and control of an (Air Force Organization's) authorized credit card holder, even after his or her authority to use the card has been revoked by the (Air Force Organization) is not considered lost or stolen, and its use by such individual is not unauthorized (The Air Force Organization) must recover the card from the individual.

Signature of Agreement

By signing this agreement, (The Air Force Organization) and (The Participating Bank) agree to all terms and conditions contained herein.

Date & Signature

ATTACHMENT 2.

First or Affirmative Group of
Respondent Banks or Lending Institutions

<u>Banks or Lending Institutions</u>	<u>Bank Officer/ Position/Phone No.</u>	<u>Comments</u>
<u>AMSOUTH</u> Bank Card Service Ctr. P. O. Box 216 Birmingham, AL 35201	Wm. E. Horton Vice President (205) 326-5700	Interested in developing this concept further to determine feasibility of implementing such a program for the AF.
<u>CENTRAL BANK OF THE SOUTH</u> P. O. Box 2210 Decatur, AL 35699	John L. Jackson Vice President (205) 834-7400	Central Bank of the South would consider conducting a test in the credit card area.
<u>COLONIAL BANK</u> P. O. Box 1108 Montgomery, AL 36192	Diane Caldwell Marketing Officer (205) 240-5216	We are interested in pursuing further the possibility of issuing a credit card (VISA/MasterCard) to the Air Force.
<u>FIRST FEDERAL SAVINGS AND LOAN ASSOCIATION OF CHATTANOOGA</u> 601 Market Center Chattanooga, TN 37402-4892	Ann Sherrill For John P. Reddan Vice President (615) 756-4600	This study of the possible use of credit cards for local purchases by the Air Force may be beneficial to both the AF and First Federal. We will let you know as soon as we have a proposed agreement for you to examine.
<u>MAX FEDERAL CREDIT UNION</u> 400 Eastdale P. O. Box 17930 Montgomery, AL 36193-2501	Robert J. McCormick Sr. Vice President Tech./Services/Credit (205) 279-7550	This credit union would like to have its name placed on your list of "interested" financial institutions concerning the "Air Force Organization Credit Card" Program.

Second or Negative Group of
Respondent Banks or Lending Institutions

<u>AMERICAN EXPRESS</u> Travel Related Services Travel Mgmt. Services 302 Perimeter Ctr., N. Suite 400 Atlanta, GA 30346	Joyce K. Whitley Corporate Sales Mgr. (404) 391-9080	We must have an individual's name listed on each and every card we issue. Only in this way can we have a legal framework of liability.
<u>C & S THE CITIZENS AND SOUTHERN CORP.</u> P. O. Box 4899 Atlanta, GA 30302-4899	O. T. Moody Vice President Bk. Card Services (404) 581-4262	Based on what you told me, this bank would not be interested in a "general issue" card based on 1) A lack of ability to control usage (cards issued to individuals & even company cards are the responsibility of the employee), and 2) Special billing with insufficient revenue potential.

(Second or Negative Group - continued)

<u>Banks or Lending Institutions</u>	<u>Bank Officer/ Position/Phone No.</u>	<u>Comments</u>
<u>FIRST ALABAMA BANK</u> First AL Services, Inc. P. O. Box 4899 Montgomery, AL 36101-4899	Len Parker Vice President (205) 832-8500	First AL would have to assess some form of annual fee to compensate for our liability in issuing plastic for the purposes you've outlined. Parker stated in Telecon that he was reluctant to issue a "generic" credit card.
<u>SOUTH TRUST BANK</u> <u>CARD CENTER</u> P. O. Box 122 Birmingham, AL 35201	Elbert L. Williams Credit Officer (202) 592-4921	There are three areas of concern which would not enable us to sign the agreement. 1) We issue cards in the name of the organization and the individual designated by the organization. Regulations require the name on the card and the signature panel be available for the merchant as signature comparison of the card panel signature and sale draft signature. 2) We are unable to provide our services without income which would ordinarily come as annual card holder fees and finance charges. 3) The liability for unauthorized use of the credit card after notification could result in a financial loss to the bank.
<u>UNION BANK</u> Union Bank & Trust Co. P. O. Box 2191 Montgomery, AL 36197-5401	Mark C. Jenkins Bank Card Representative (205) 265-8201	It is unfortunate that at this time we do not offer an account which would accommodate your specific needs.

REFERENCES

1. AFISC report "Functional Management Inspection of Effectiveness of Base-Level Small Purchases of Material and Services (TIG)", 10 March - 26 November 1985. (AFISC Report PN85-615.)
2. AFLMC report S M Sgt Chapman, John C., and Powell, Sally, "Copper Small Purchase Initiatives", November 1984. (AFLMC Report LS840116.)
3. AFLMC report Powell, Sally; Major Blazer, Douglas; Faulkner, Wayne; and S M Sgt Chapman, John C., "Streamlining Local Purchase Procedures", October 1984. (AFLMC Report LS840120.)
4. AFLMC report M Sgt Urey, Jr., Robert S., "Small Purchase Threshold Study", July 1983. (AFLMC Report LS830205.)
5. Lt Col Kent R. Carlson, USAF Acting Director of Contracting Deputy Chief of Staff, Logistics, Hickam AFB, HI. Letter to HQ USAF/RDCL AFLMC/LGC, HQ PACAF/ACFAG/LGC, 15 ABW/LGC, 6/25/1986. Subject: Status of Credit Card Account for Commander's Contingency Fund.
6. Major Donald J. McCarthy, USAF Acting Director of Contracting Deputy Chief of Staff, Logistics, Hickam AFB, HI. Letter to AFLMC/LGC, 6/25/87. Subject: Credit Card for Commander's Contingency Fund.
7. Colonel Robert P. Lansell, USAF Director of Contracting, HQTAC, Langley AFB, VA. Letter to AFLMC/LGC (Dr. William F. Kauder, Jr.), Gunter AFS, AL, 7/6/87. Subject: Credit Card Usage.
8. Thelma Shelton, AFAFC/XSPB, Denver, CO. Letter to AFLMC/LGC, Gunter AFS, AL, Attn: William F. Kauder. Subject: Point Paper on Air Force Test of Diners Club Charge Cards, 7/28/1987.

1987 USAF-UES SUMMER FACULTY RESEARCH PROGRAM/
GRADUATE STUDENT SUMMER SUPPORT PROGRAM

Sponsored by the
AIR FORCE OFFICE OF SCIENTIFIC RESEARCH

Conducted by the
Universal Energy Systems, Inc.

FINAL REPORT

HIGH ENERGY METASTABLE SPECIES IN CRYOGENIC MATRICES:
PREPARATION, PHOTOPHYSICS, AND PHOTOCHEMISTRY

Prepared by:	Dr. John W. Kenney, III
Academic Rank:	Assistant Professor of Chemistry
Department and	Department of Physical Sciences--Chemistry
University:	Eastern New Mexico University
Research Location:	AFAL/CX Edwards Air Force Base, California 93523
USAF Researcher:	Dr. Stephen L. Rodgers
Date:	August 5, 1987
Contract No:	F49620-85-C-0013

HIGH ENERGY METASTABLE SPECIES IN CRYOGENIC MATRICES:
PREPARATION, PHOTOPHYSICS, AND PHOTOCHEMISTRY

by

John W. Kenney, III

ABSTRACT

A spectrophotometer system based upon an optical multichannel analyzer was set up to monitor the kinetics of cryogenic matrix formation and monitor the kinetic behavior of active metals deposited in both noble gas and reactive matrices. A matrix cell was constructed to perform these experiments and successfully tested. Preliminary matrix formation studies were carried out using xenon and ammonia as the matrix gases. A xenon-sulfur matrix was also prepared and subjected to spectroscopic study.

ACKNOWLEDGMENTS

It is a pleasure to acknowledge the entire AFAL/CX group--especially Dr. Stephen L. Rodgers and Lt. Walter Lauderdale, directors of the HEDM Program--at the Air Force Astronautics Laboratory, Edwards Air Force Base, CA, for providing a stimulating project and an atmosphere that *encouraged initiative*. It is also a pleasure to acknowledge Dr. E. Miller Layton, Jr., of the University of Dayton Research Institute, for sharing his spectroscopic facilities at AFAL and for assisting me to acquire crucial supplies and equipment for this project. Maj. Gerald Nordley deserves special thanks for vaulting me over numerous administrative barriers and for opening my perspective to the possibilities in antimatter rocket propulsion systems. Many people at AFAL contributed important details necessary for the implementation of my research program. Special mention goes to Mr. Mel Abrego and Ms. Ronnette Griggs for helping me with a multitude of technical problems. Dr. Jeff Gilman graciously loaned me his computer system for word processing tasks. Ms. Jolaine Lamb did an exemplary job on literature searches and library materials. Finally, I would like to thank Dr. Allan Burkett, a fellow UES summer faculty member at AFAL/CX, for lively scientific dialog. Grateful acknowledgement is made to the Air Force Systems Command, the Air Force Office of Scientific Research, and Universal Energy Systems for my participation in this research program.

I. INTRODUCTION:

The high energy density materials (HEDM) research program at the Air Force Astronautics Laboratory (AFAL), Edwards Air Force Base, California, is spearheading a new research effort aimed at identifying, characterizing, and ultimately implementing novel new classes of high energy rocket fuels whose performance significantly exceeds that of existing rocket propulsion systems. The HEDM program is designed to simultaneously approach problems in high energy density materials by experimentation and by computer modeling. The newly initiated experimental component of the HEDM program has as its focus the production and spectroscopic analysis of high energy atomic and molecular species.

One area of particular emphasis at HEDM is the study of dispersed high energy metals in cryogenic solutions and matrices. This area closely overlaps with my research program at Eastern New Mexico University devoted to the synthesis of complexes containing two or more metal atoms and to the development of cryogenic optical spectroscopic probes of weak metal-metal interactions in these systems.

II. OBJECTIVES OF THE RESEARCH EFFORT:

My assignment was to initiate a program of cryogenic matrix isolation spectroscopy on the light alkali metals with the objective of increasing the alkali metal concentration in the matrix. The idea was to disperse

the metal atoms in a weakly bound metastable matrix to avoid the large enthalpy of vaporization penalty resulting from the injection of the solid metal into the rocket combustion chamber (1). Specific research objectives included (a) designing and constructing an optically transparent cryogenic cell with appropriate gas and metal deposition apparatus to carry out matrix studies (b) setting up and calibrating a newly acquired spectrophotometer based upon a computer controlled optical multichannel analyzer (OMA) to be used as the detection unit (c) designing light sources and optical trains to implement optical absorption studies on samples deposited in the matrix cell (d) developing spectroscopically based procedures for measuring matrix deposition rates, substrate deposition rates, and photochemically induced substrate reaction rates.

III. MATRIX CELL DESIGN:

A matrix isolation cell, suitable for immersion in a liquid nitrogen filled optical dewar, was fabricated from quartz tubing in the glassblowing shops of the Jet Propulsion Laboratory (see Fig. 1). Square 22.2 mm (0.875 in.) quartz tubing with a 1.60 mm (0.0625 in.) wall was used in the region of the cell where matrices were to be deposited and optical access was desired. The top of the cell was fitted with a head equipped with three teflon O-ring type vacuum feed-through ports set into S/T 14/20 ground glass joints: a central port for the 6 mm (0.25 in.) stainless steel matrix gas delivery tube and two side ports for the

power wires to the Knudsen cavity resistance heater. A vacuum side port, fitted with a teflon/glass needle valve, was attached near the top of the cell.

The Knudsen cavity for vaporizing the sample was fabricated from a small length of suitably bent 3.2 mm (0.125 in.) stainless steel tubing. The end of the tubing was tapped with 4-40 threads to accept a small 4-40 stainless steel set screw through which a #60 nozzle hole (1.02 mm, 0.040 in.) was drilled. Heat was delivered to the Knudsen cavity via a coaxially wound length of nichrome wire electrically insulated from the stainless steel cavity by a piece of ceramic tubing. Preliminary experiments indicated that it was necessary to wrap the nichrome heating coil with asbestos tape to facilitate more efficient heat transfer from the coils to the cavity and to shield the deposited matrix against damaging infrared radiation. Two 0-120 V variable transformers were employed in series to achieve low, easily adjustable AC voltages suitable for the nichrome heater. Knudsen cavity temperature control was achieved by adjusting the transformers to a precise voltage output and comparing the output to previously determined temperature vs. voltage calibration data (Table I). The Knudsen cavity was based upon a standard matrix gas-sample vapor pre-mix design (2). The matrix gas is injected into the back of the cavity; a mixture of matrix gas and vaporized sample is then sprayed through the nozzle onto the cryogenically cooled quartz wall. The Knudsen cavity and nozzle assembly may be rotated in the cell a full 360° and translated

vertically ± 25 mm (1 in.) to allow spectroscopic access to any area of a deposited matrix or to deposit multiple matrices on different areas of the quartz cell.

A matrix gas delivery manifold--featuring stainless steel needle valves, a measured gas storage volume, and a sensitive mechanical pressure gauge--was constructed to precisely regulate the flow of matrix gas into the cell (see Fig. 2). The manifold was incorporated into the design to allow vacuum/pressure purge cycles to be performed on the system to eliminate unwanted gaseous contaminants. This gas delivery system may be calibrated for absolute flow rates ($\mu\text{mol}/\text{min}$) by measuring the temperature of the standard gas storage volume and carrying out simple ideal gas law calculations.

IV. SPECTROSCOPIC MEASUREMENTS:

All spectroscopic measurements in the ultraviolet-visible-near infrared (UV-VIS-NIR) were performed using an E.G.&G. PARC model 1460 computer controlled OMA. Spectral dispersion to the OMA was achieved by a Jarrell-Ash Monospec 27 polychromator equipped with a $25\ \mu\text{m}$ entrance slit and a $150\ \text{gr}/\text{mm}$ grating to give broad spectral coverage. The gratings and wavelength counter were aligned with respect to the $632.8\ \text{nm}$ He/Ne laser line. A low pressure Penray Hg/Ar lamp was used as the wavelength calibration source. Calibration spectra were acquired during the lamp warm-up period ($t < 1\ \text{min}$) to assure roughly equal Hg

and Ar emission line intensities (see Fig. 3). Cubic fits of calibration data on four widely spaced reference emission lines from this lamp gave excellent results. A 1000 W FEL type standard quartz-halogen lamp (#ES-8224) with a wavelength dependent spectral intensity profile traceable to the National Bureau of Standards was used to calibrate the intensity response of the OMA/polychromator system. The standard lamp was placed 1.25 m from the entrance slit to put the entire spectrum on scale.

Standard lamp values were entered into the computer program without correction for the intensity difference between the recommended 0.50 m lamp placement distance and the 1.25 m distance since an absolute intensity correction was not needed. The correction software takes the ratio between the reported standard lamp intensity and the standard lamp intensity as measured by the OMA/polychromator to generate a correction file (see Figs. 4-6)

$$C = I_{\text{std. (reported)}}/I_{\text{std. (measured)}}.$$

Subsequent spectra are corrected by taking the product of the correction file with the spectral data file of interest:

$$I_{\text{sample (corrected)}} = C \times I_{\text{sample (measured)}}.$$

These corrections allowed transmission spectra of deposited matrices to be recorded in a single shot. Absorbance spectra of very high quality were obtained by measuring sample and reference spectra under identical optical conditions and calculating

$$A = \log (I_{\text{ref}}/I_{\text{sample}}).$$

Neither the sample nor the reference spectrum needed to be calibrated with respect to the standard lamp in this mode. Special software modes exist for automatically carrying out these calculations. Alternatively, they may be implemented in the "Curve Calculations" section of the OMA's software.

The OMA/polychromator was set up for matrix absorption and transmission measurements using a 150 W Xe arc lamp as the light source. The arc image was focused through an array of quartz lenses and the quartz window of a liquid nitrogen filled optical dewar to a 1.5 x 3 mm oval at the quartz cell window upon which the matrix was deposited. Another quartz lens was employed to collect light transmitted through the matrix and focus it on the OMA/polychromator entrance slit (see Fig. 1).

V. SPECTROSCOPIC RESULTS

It was desired to monitor matrix formation rates by spectroscopy to provide a time baseline for subsequent kinetic and photochemical studies of deposited matrix material. The OMA/polychromator was set to do repetitive shots of transmitted light intensity while the matrix was being deposited. The matrix deposition rate was measurable spectroscopically with much greater precision than that measurable by pressure changes in the matrix gas delivery system (see Fig. 7).

Matrix deposition rates were monitored spectroscopically for both noble gas matrices (Xe) and reactive gas matrices (NH₃). Laboratory interest in the metastable species xenon sulfide, XeS, prompted an experiment using Xe as the matrix gas passing over molten S in the Knudsen cavity to produce a co-deposited xenon-sulfur matrix at 77 K (see Fig. 8). This study served to test the co-deposition technique with a system less subject to contamination and pre-reaction than the alkali metals.

VI. RECOMMENDATIONS:

- a. Matrix isolation studies should be performed on the alkali metals in both noble gas and reactive matrices with special emphasis on spectroscopically monitored kinetic processes as related to matrix formation, matrix substrate photochemistry, and time dependent metal-metal interaction as a function of metal concentration, temperature, and matrix.
- b. The matrix cell design developed for this project effectively passed all preliminary tests. The cell could be improved substantially by including a second matrix gas delivery manifold for simultaneous deposition of two matrix gases. Twin Knudsen cells that can be heated at different rates to match the vapor pressure/temperature characteristics of different metals/solids would allow matrix studies of metal-metal interactions between different species. Internal thermocouples should be fitted to each Knudsen cavity for more precise temperature

regulation. A variable slit capability on the OMA/polychromator would give the instrument a much wider dynamic range than it now has. This capability is particularly important if the instrument is to be used to detect weak luminescence signals from deposited matrices.

c. A literature review and preliminary calculations (3) on alkali metal ammonia solutions indicate that these cryogenic solutions have considerable promise as high energy rocket fuels or rocket fuel additives. I plan to initiate a program of synthetic and spectroscopic studies on these systems emphasizing time resolved spectroscopy as a follow up on my summer project.

VII. REFERENCES

1. Herm, R.R. "Metastable Metal in Matrix Materials"; Research Proposal; The Aerospace Corporation: Los Angeles, 1986.
2. Meyer, B. Low Temperature Spectroscopy, Elsevier: New York, 1971.
3. Rodgers, S.L.; Lauderdale, W., Air Force Astronautics Laboratory, Edwards AFB, CA, unpublished results.

TABLE I. CHROMEL-ALUMEL THERMOCOUPLE IN KNUDSEN
CAVITY IN AIR

Voltage	$^{\circ}\text{C}$	K	min	s
0	18	291	0	0
0.25	17	290	55	44
0.50	16	289	49	47
0.75	27	300	45	27
1.00	69	342	40	19
1.25	87	360	35	15
1.50	119	392	30	31
1.75	147	420	25	22
2.00	172	445	20	33
2.25	209	482	15	37

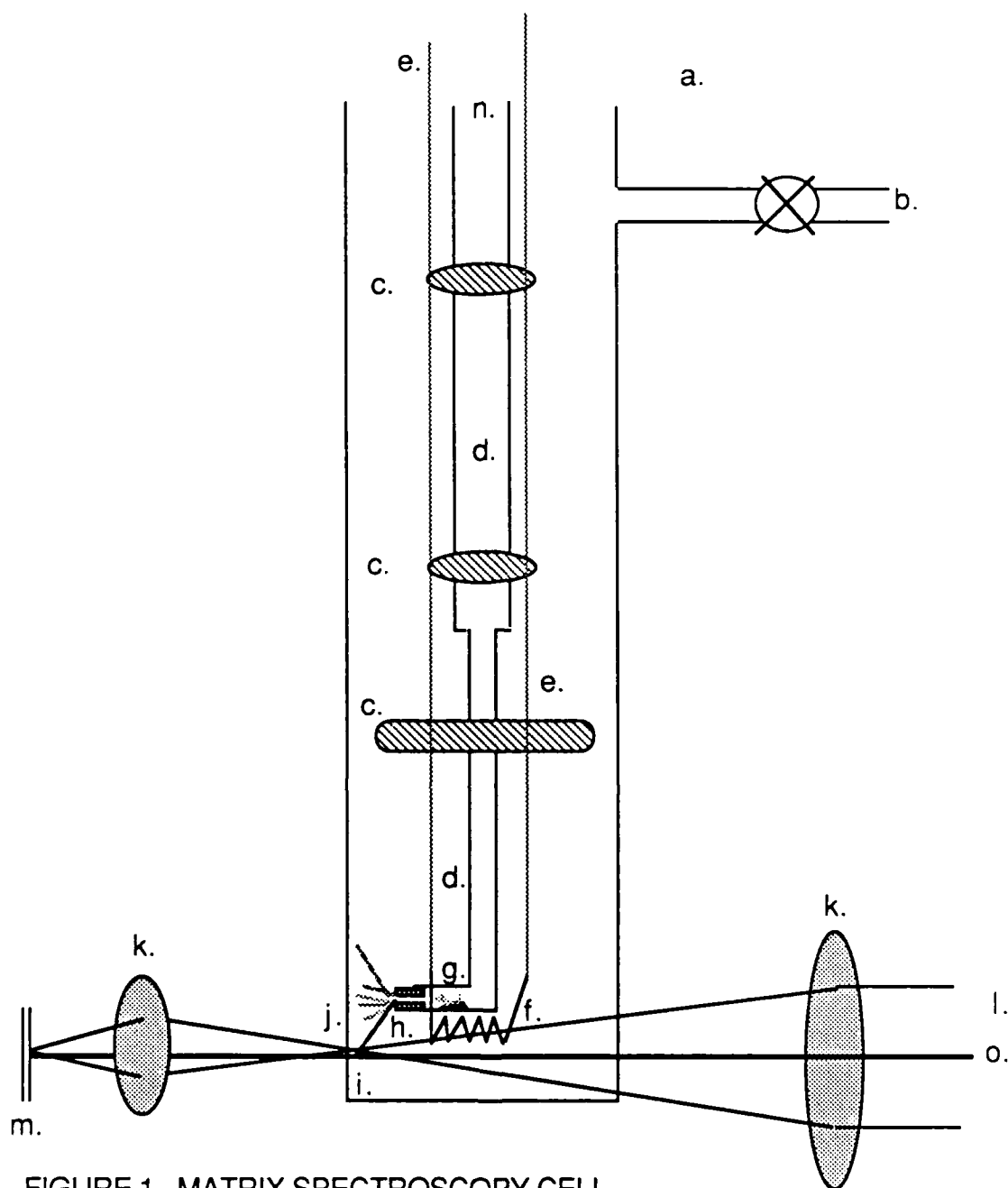


FIGURE 1. MATRIX SPECTROSCOPY CELL

- | | |
|---|--------------------------------|
| a. vacuum feed through head (not shown) | c. teflon spacer |
| b. to vacuum line | e. heater power wires |
| d. stainless steel tubing | g. solid sample |
| f. nichrome heater coil | i. matrix |
| h. knudsen cavity nozzle | k. quartz lenses |
| j. quartz wall | m. OMA entrance slit |
| l. Xe arc | o. optical center (adjustable) |
| n. matrix gas inlet | |

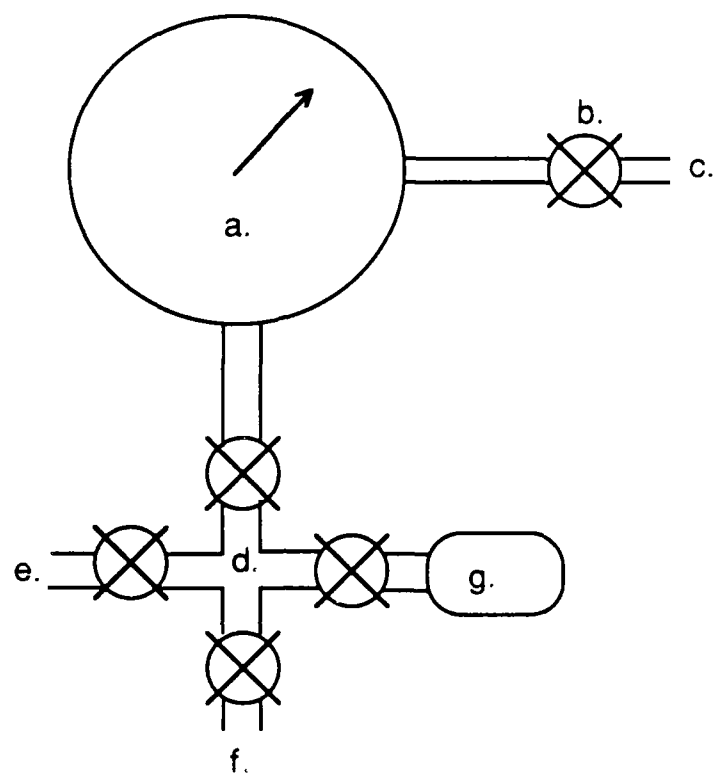


FIGURE 2. MATRIX GAS DELIVERY MANIFOLD

- a. 0-760 mm Hg gauge or 0-110 mm Hg gauge
- b. gas bleed valve
- c. gas outlet (to matrix cell)
- d. gas manifold and valves
- e. gas inlet (from storage tank)
- f. vacuum outlet (to vacuum line)
- g. measured storage volume (10 mL)

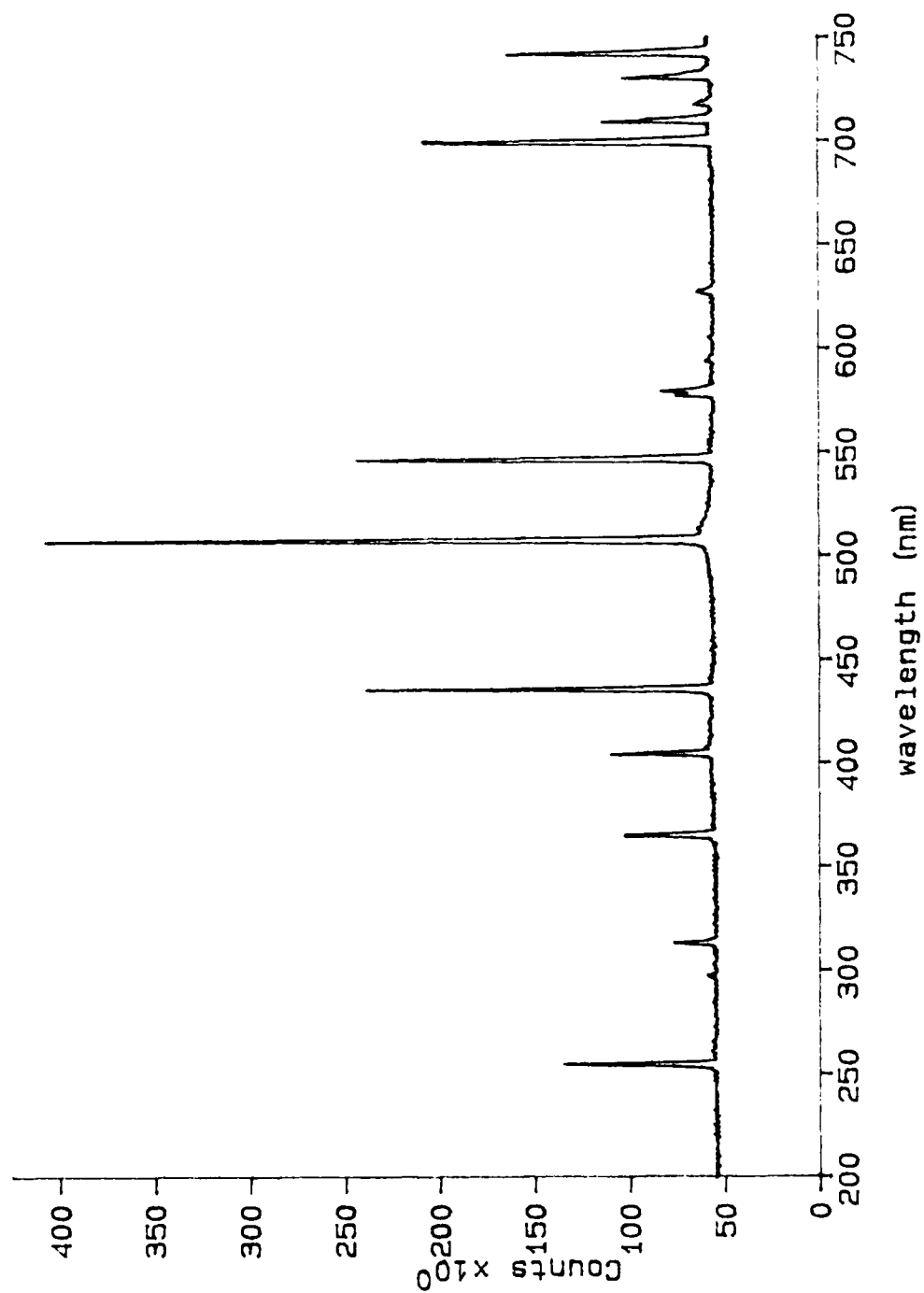


FIGURE 3. Hg/Ar PENRAY WAVELENGTH CALIBRATION SPECTRUM

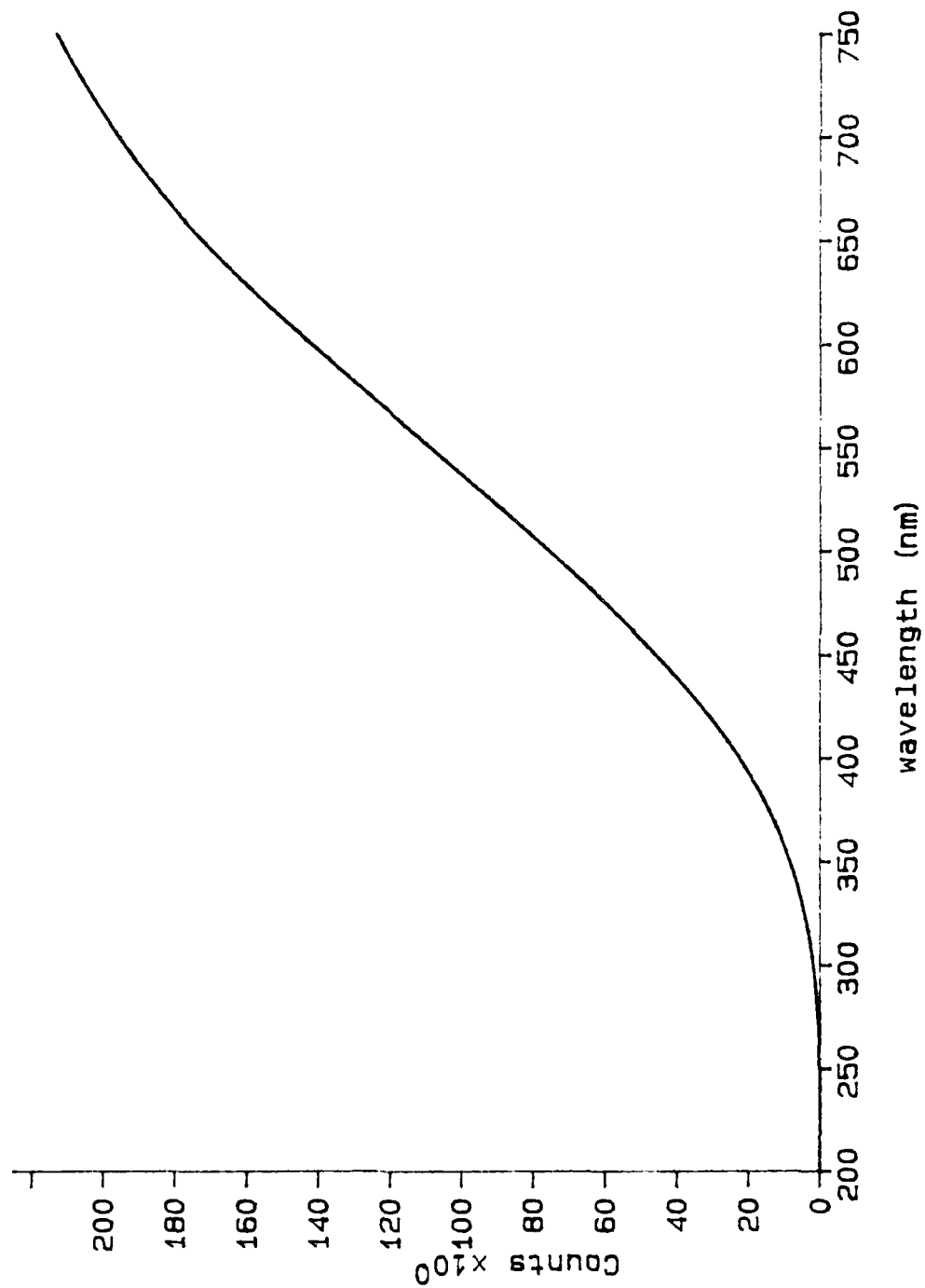


FIGURE 4. STANDARD LAMP CALIBRATION CURVE--
COMPUTER GENERATED

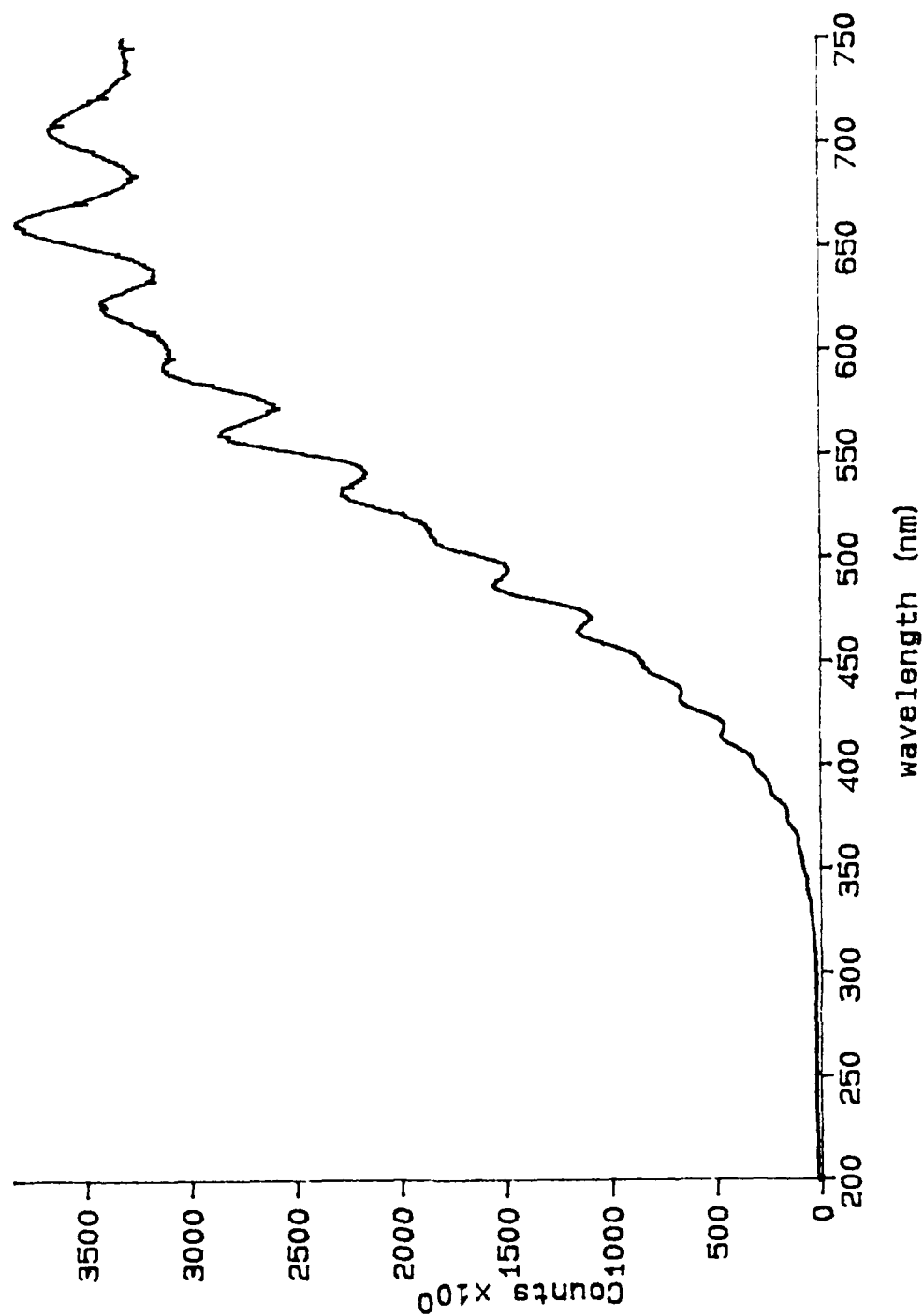


FIGURE 5. STANDARD LAMP CALIBRATION--MEASURED

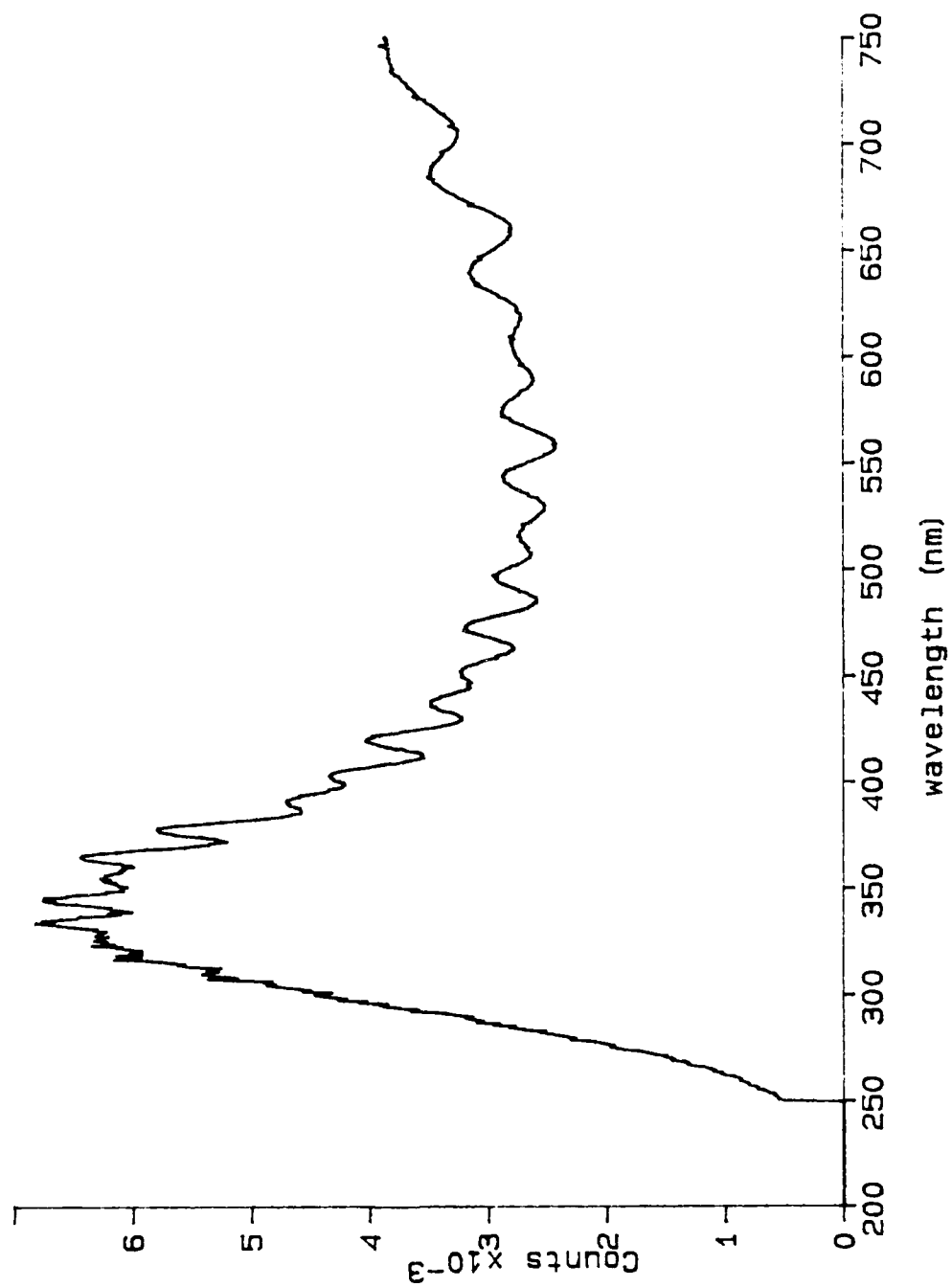


FIGURE 6. OMA/POLYCHROMATOR CORRECTION CURVE

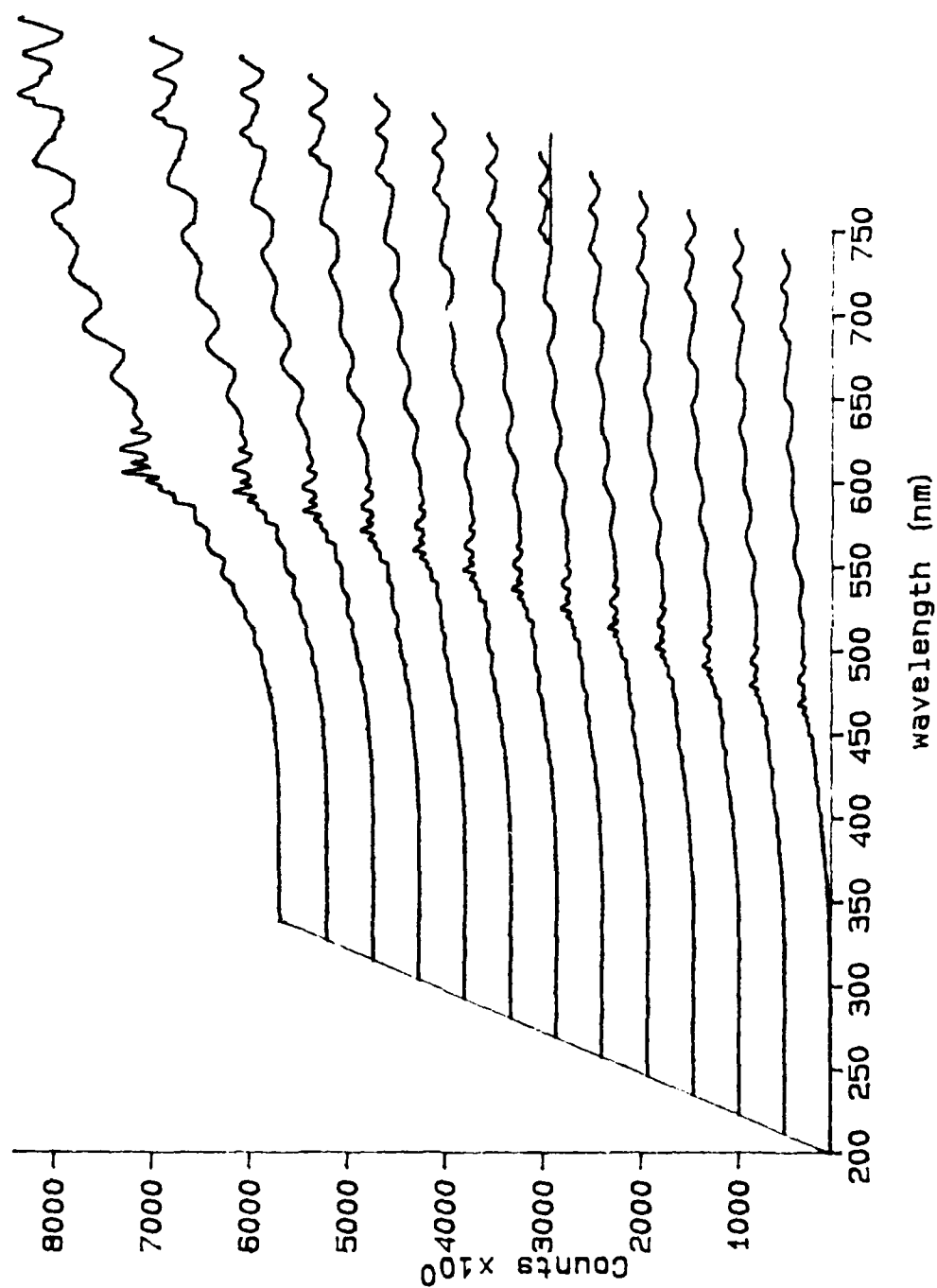


FIGURE 7. XENON MATRIX DEPOSITION PROFILE

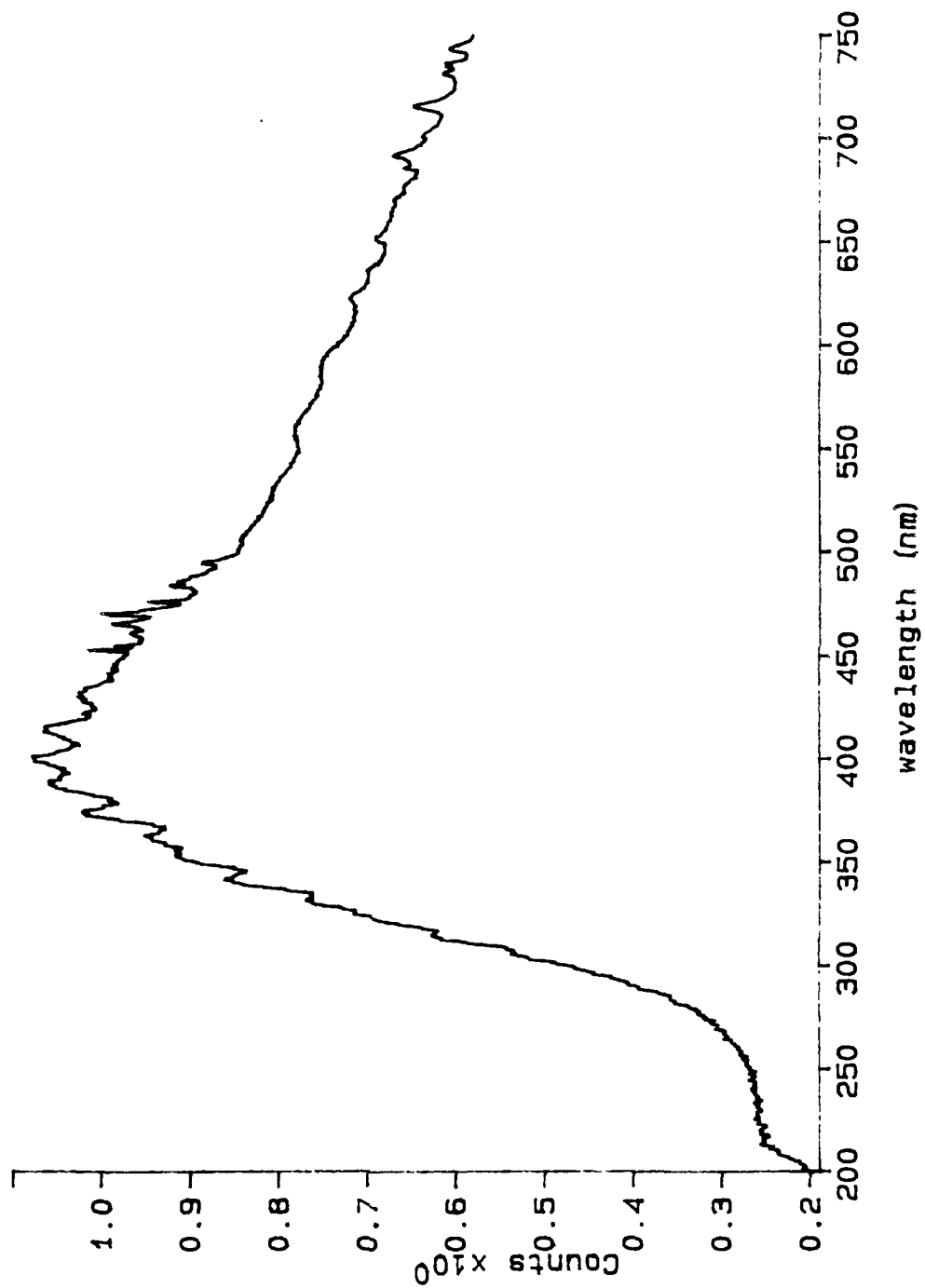


FIGURE 8. ABSORPTION--SULFUR IN XENON MATRIX AT 77 K

1987 USAF-UES SUMMER FACULTY RESEARCH PROGRAM/

GRADUATE STUDENT SUMMER SUPPORT PROGRAM

Sponsored by the

AIR FORCE OFFICE OF SCIENTIFIC RESEARCH

Conducted by the

UNIVERSAL ENERGY SYSTEMS, INC.

FINAL REPORT

DEVELOPMENT OF A GEOTECHNICAL CENTRIFUGE

FACILITY AT TYNDALL AIR FORCE BASE

Prepared by:	Dr. Yong S. Kim
Academic Rank:	Assistant Professor
Department and University:	Department of Civil Engineering The Catholic University of America
Research Location:	Air Force Engineering and Services Center, Engineering Research Division, Facility System and Analysis Branch
USAF Research:	Dr. Paul Y. Thompson
Date:	September 25, 1987
Contract No.:	F49620-85-C-0013

DEVELOPMENT OF A GEOTECHNICAL CENTRIFUGE
FACILITY AT TYNDALL AIR FORCE BASE

by

Yong S. Kim

ABSTRACT

A medium size centrifuge for geotechnical studies was installed in the Air Force Engineering and Services Center (AFESC) at Tyndall Air Force Base. It has been operational since April, 1987. This report describes details of the testing facility, ongoing research projects and scope of future centrifuge model studies.

ACKNOWLEDGEMENT

The author would like to thank the Air Force Systems Command, the Air Force Office of Scientific Research and the Universal Energy Systems, Inc. for providing him with the opportunity to spend a very worthwhile and interesting summer at the Air Force Engineering and Services Center, Tyndall AFB, Florida. He would like to acknowledge the Center, in particular the Facility Systems and Analysis Branch and the Operations Support Branch for their hospitalities and excellent working conditions.

Also, he would like to thank Dr. Paul Y. Thompson, Mr. Stan Strickland and Major Bob Majka for suggesting this area of research and for their collaborations and technical supports. Finally, he would like to thank Mr. R. Domingo, a graduate student from The Catholic University of America, for his help in carrying out 1-g and high-g model tests, and Ms. T. Taylor, a graduate student from the Washington State University at Pullman, for her help in setting up the projectile launching system.

DEVELOPMENT OF A GEOTECHNICAL CENTRIFUGE
FACILITY AT TYNDALL AIR FORCE BASE

1. INTRODUCTION

1.1. General

The author is an Assistant Professor of Civil Engineering at The Catholic University of America. He received his B.S., M.S. and Ph.D. degrees in Civil Engineering from the University of California at Davis. During his graduate study, the author worked as a research civil engineer at the California State Department of Transportation. His research interest has primarily focused on static and dynamic soil-structure interactions of buried structures and foundations. His published articles include centrifuge model studies and numerical analyses of reinforced earth support systems, oil storage tank foundations on soft ground, rigid box culverts under shallow embankments, and rigid and flexible circular culverts under deep embankments with different bedding and backpacking compactions.

With this background, the author was invited for research at the Facility Systems and Analysis Branch, Engineering Research Division in the Air Force Engineering and Services Center at Tyndall Air Force Base. During his stay at the Center, the author learned that one of the Center's major missions is to develop new innovative and advanced high technologies for military facilities to withstand various conventional weapons attacks. Specifically, one of the Branch's upcoming research projects is a small-scale model study to investigate the behavior of buried structures under dynamic (impact and blast) loadings. This report describes development of a new model technology (centrifuge model

technology) and ongoing research projects at AFESC, that would demonstrate potential savings and enhance insight into soil-structure interactions.

II. AFESC GEOTECHNICAL CENTRIFUGE FACILITY

II.1. Description of the Centrifuge

The centrifuge installed at Tyndall Air Force Base (AFB) was originally built for testing of electronic and mechanical packages under G-loadings that simulate those experienced in actual flight. It was initially installed at Kirtland AFB, New Mexico. The machine was modified for geotechnical studies in 1981 and moved to the Air Force Engineering and Services Center (AFESC) at Tyndall AFB in 1986. The centrifuge was assembled and housed in a 7-foot high, 16-foot diameter, 9-inch thick reinforced concrete retaining structure (Figure 1).

The Center's centrifuge is a medium size rotary accelerator designed by Genisco Inc. of California (Model E185). The machine is capable of applying controlled centrifugal accelerations up to 100 g's and a limit of 17,000 g-lbs with a swing-up platform (or 30,000 g-lbs with a fixed platform) at a nominal radius of 72 inches. The payload of the test package can be as heavy as 500 pounds. The machine includes a variable-speed hydraulic drive system, timing belt drive, RPM pick-up, rotating arm assembly, terminal box for control and test connections.

The hydraulic drive system consists of an electric drive motor coupled to a variable-displacement pump, a constant-displacement fluid motor coupled to the rotor drive shaft, and two pressure-relief valves. A 4-way solenoid-operated spring-loaded control valve provides rotational stability, maximum hunting, and constant torque

characteristics. The hydraulic power unit is enclosed in the console, and the fluid motor is installed at the bottom of the rotor assembly (Figure 2). Maximum pressure of the hydraulic system has been set at approximately 2200 psi.

The boom consists of two symmetrical cantilever arms, and an adjustable 30-inch square cradle-type mounting platform carried on aircraft-type roller bearings. The platform is held by two arms attached to the spokes by two pivots. It can be locked into horizontal, 45, 90, 135 or 180 degree positions. This permits the soil surface to remain perpendicular to the vector sum of the centrifuge acceleration and the acceleration due to gravity.

One of unique features of the machine is the automatic dynamic balancing system. Dynamic balance is accomplished automatically by vertical displacement of the two arms of the boom until the center of gravity of the opposing mass lies in the same horizontal plane. It requires approximately 20 seconds for full compensation. If compensation cannot be accomplished within the 12-inch travel limitations, the balance motor is automatically shut down by limit switches. Corrective measures are indicated by the relative attitudes of the mounting platforms after shut down.

Hydraulic and electrical services are available to the model in flight. The hydraulic lines may be used to conduct compressed air or fluids from the outside control area to the model. Hydraulic services are transmitted through rotary joints. Electrical signals are transmitted to the centrifuge rotor and then to the model in flight through a stack of slip rings. A total of 40 slip rings (electrical channels) are provided on the machine, of which 24 are available for

AD-A191 284

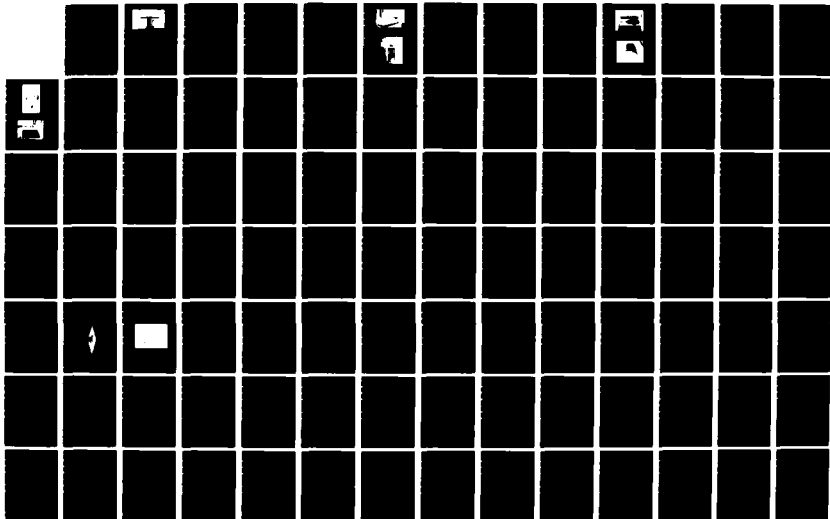
UNITED STATES AIR FORCE SUMMER FACULTY RESEARCH PROGRAM
(1987) PROGRAM TE (U) UNIVERSAL ENERGY SYSTEMS INC
DAYTON OH R C DARRAH ET AL DEC 87 AFOSR-TR-88-8213
F49628-85-C-8813

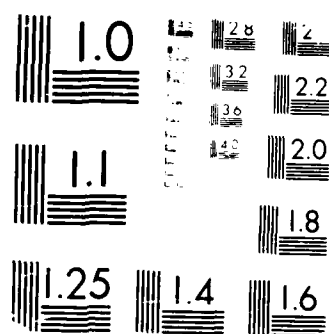
6/11

UNCLASSIFIED

F/G 5/1

NL





MICROCOPY RESOLUTION TEST CHART
 NATIONAL BUREAU OF STANDARDS-1963-A

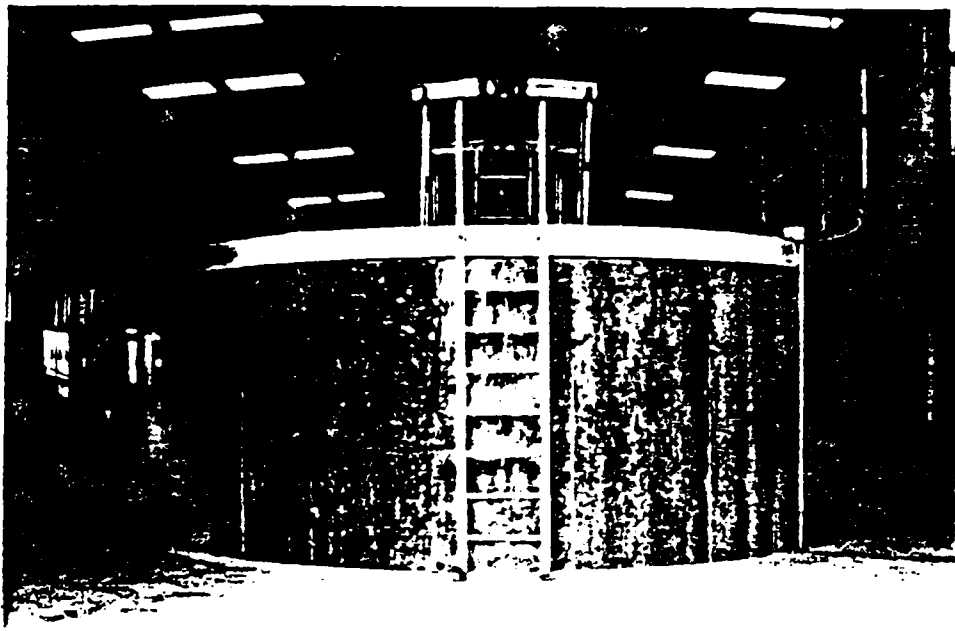


Figure 1. Reinforced Concrete Structure

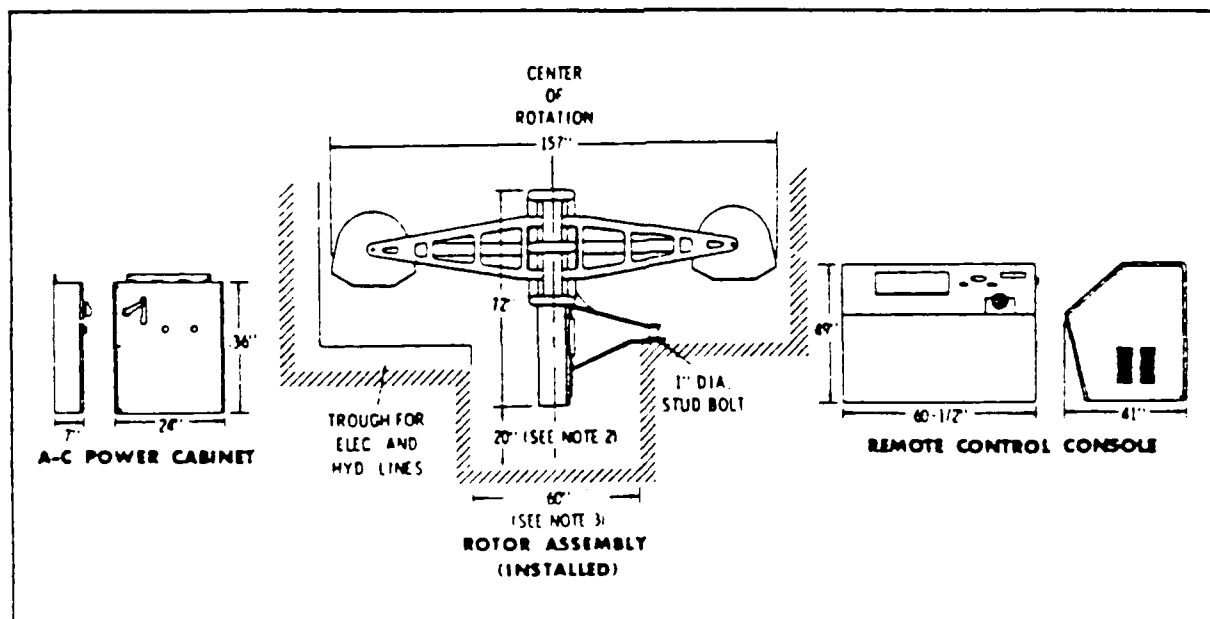


Figure 2. Rotary Accelerator (Model E-185) - Outline Drawing (Reference 4)

sending power and receiving signals from transducers which monitor behavior of the model. These 28 slip rings include 12 instrumentation slip rings (shielded-conductor) designed for 1-amp, low resistance and low noise, and 16 power slip rings (shielded-conductor) of 5-amp current rating. The twelve slip rings not used for test purposes are part of the static and dynamic balancing motor and control circuitry for televsion. A summary of major specifications is listed in Table 1.

TABLE 1. Major Specification

Maximum Centrifugal Capacity:	
(i) with fixed plstform	30,000 G-lbs.
(ii) with swing-up platform	17,000 G-lbs.
Maximum Acceleration	100 G
Maximum Payload	500 lbs.
Maximum Effective Radius	72 inches
Maximum Number of Rotation	220 rpm
Electric Slip Rings	40
Space of Swinging Platform	30 in. X 30 in.

II.2. Photographic and Video Recording Systems

A still photographic system is available to permanently record selected periods of the centrifuge model tests. A camera can be mounted near the hub of the centrifuge. Thus still photographs can be taken with an on-board camera-flash unit by remote control during the tests. The photographs may be used later for analyses.

Video camera and recording device are also available as part of the monitoring system. This video camera is mounted near the hub of the centrifuge. This system provides a continuous and instantaneous monitor of the test while in progress, and a permanent, replayable record of model tests.

II.3. Microcomputer Based Data Acquisition Systems

Digital oscilloscopes (Nicolet Models 4094 and 3034) are available for collecting sensor signals from model structures on dynamic soil-structure interaction studies. The Model 4094 digital oscilloscope with multi-channel plugs is capable of performing acquisition with 12 bit resolution at a rate of 2 million sample/sec (16 bits samples). The system allows zero time to be set anywhere in the displaying area and enables two-channel measurements with each channel set at an independent pre- or post- trigger delay. It displays these two functions as well as a combination of them. Also, the system is able to save and recall data on floppy or hard disk. The IBM PC/AT interfaced with the oscilloscope is available to create hard copy records with plotter and/or printer.

Figure 3 shows a data acquisition system used for the summer research project.

II.4. Insrumentation

Commercial linear variable differential transducers (i.e., Hewlett Packard LVDT), strain gages (i.e., Micro Measurement Group, Inc. gages) and accelerometers (i.e. Endevco pizeoelectric and pizoresistive accelerometers) are available to measure deformations, strains and accelerations of the structure, respectively. No major difficulties have been met so far in use of the gages for the centrifuge model study. Yet, unlike these gages, stress gages to measure the soil pressure around the structure have not been successfully used for model study, especially under dynamic loading conditions. Soil pressure gages are being developed to measure reliable soil pressures.

II.5. Soil Pluviator

A pluviator was designed by the author based on work done by Eid (1987). The method adopted is simple and inexpensive, and is the most efficient way to produce repeatable sand samples in the laboratory. A typical pluviator works simply by dispersing sand jets from a hopper into "rain" by letting it fall through a set of sieves and into the model box. Through the pluvial deposition method, it was possible to produce sand specimens repeatedly that were uniform and homogeneous with a wide range of relative densities. Figure 4 shows the pluviator.

III. ONGOING RESEARCH PROJECTS

During the last five years, AFESC has sponsored several centrifuge research projects on: (1) simulation of blast parameters (Nielson, 1983), (2) effects of blast loading on tunnels (Kutter, 1985), (3) advection and dispersion process during pollutant travel in soil

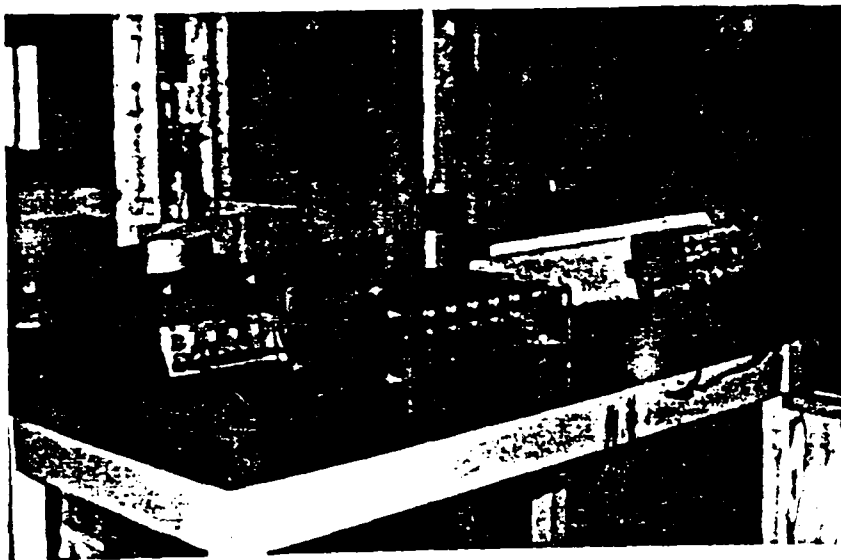


Figure 3. A View of Data Acquisition System



Figure 4. A View of Soil Pluviator

(Arulanandan, 1985 and Townsend, 1986), (4) a static response of buried concrete box culvert (Kim, 1986), (5) subterranean structure subjected to blast loading (Townsend, 1985), and (6) feasibility study on rock mechanics (Einstein, 1987). All of these efforts were carried out by research groups in universities and nonprofit research and development organizations at their institutions. Currently, AFESC is sponsoring three research projects which are being carried out using the centrifuge facility at Tyndall AFB. The three research projects are briefly described.

III.1. Projectile Penetration Study

A research group from Washington State University at Pullman is working on a projectile penetration project. The main objective of this study is to determine the penetration depth for sand using the centrifuge model technique and to compare results with existing penetration equations.

The initial series of tests investigated vertical impact into dry Ottawa silica sands. The soil samples were prepared in a 45.7 cm diameter, 45 cm deep aluminum model box using a sand rainer. The projectile launching system, consisting of a commercially available pistol with interchangeable barrels was developed and mounted along the rotor arm platform. Projectiles manufactured from nylon, polyvinylchloride, aluminum and brass were launched at different velocities into sand soils. Penetration depths were measured using a profilometer after each test. The results will be published by the research group in the near future.

III.2. Large Concrete Structure with Varying Backfill Parameters

A research group from The Catholic University of America in Washington, D.C. is working on this project. The main objective of this study is to investigate the behavior of a large reinforced concrete structure (i.e., 50-foot diameter) under different backfill conditions and different types of soil installations.

During the past decade, research on soil-structure interaction of small structures (i.e., less than 10-foot diameter) under embankments was performed by numerous research groups. Empirical data on soil pressure distributions and structural stresses and deflections has been collected for shallow to moderate depth installations. As a result, the soil-structure interaction problems of small structures embedded in embankments have been better understood, and new design and analysis procedures are being proposed. However, research on large structures has been very limited, and the behavior of these structures is not well understood. Due to an increased interest in protective and buried structures, a better understanding of soil-structure interaction and more accurate calculation of soil pressure distributions and concrete section behavior is required.

In recognition of further research needed in these areas, a comprehensive research program has been initiated to study the behavior of a large concrete structure under static and dynamic loadings. A preliminary small scale (1/60) model test has been planned with emphasis on: (1) development of an experimental technique to make a small-scale reinforced concrete, (2) the influence of installation and soil types, and (3) a comparison study between results of centrifuge and numerical models (finite element method) for structural responses.

The small-scale structure was made of gypsum molding plaster, Ottawa silica sand and water, with gypsum-sand-water ratio of 1.0:0.8:0.8 by weight. The model was a reinforced arch structure with the exterior dimension of 16 inches (length) by 10 inches (width) by 5 inches (height). Thickness of the structure was 0.3 inch. Figure 5 shows an arrangement of reinforcement with a mold before pouring a mixture and Figure 6 shows a completed reinforced arch structure.

Commercial strain gages made by Measurements Group, Inc. was used to measure the strains of the structure. The gages were placed at the mid-section of the structure. Figures 7 and 8 show dimensions of the model structure and location of the gages, respectively, while Figures 9 and 10 show measured strains for bending moment and thrust under 30-g conditions.

The computer code, CANDE (Culvert ANalysis and DEsign) (Katona, 1978), is being used for the analysis. Details on experimental and numerical techniques and analysis on experimental results, numerical predictions and a comparison study will be published in the near future.

III.3 Dynamic Response of Buried Structure under Impact Loadings

Currently, the author is investigating the particle size and gravitational effects on structural response under impact loadings. The loading mechanism for this study is penetrating projectiles. The main objective of this study is to answer the following questions: (1) are there gravity effects under impact loadings by penetrating projectiles?, (2) if there are effects, how significant are they on structural response and penetration depth, and are the centrifuge scaling laws

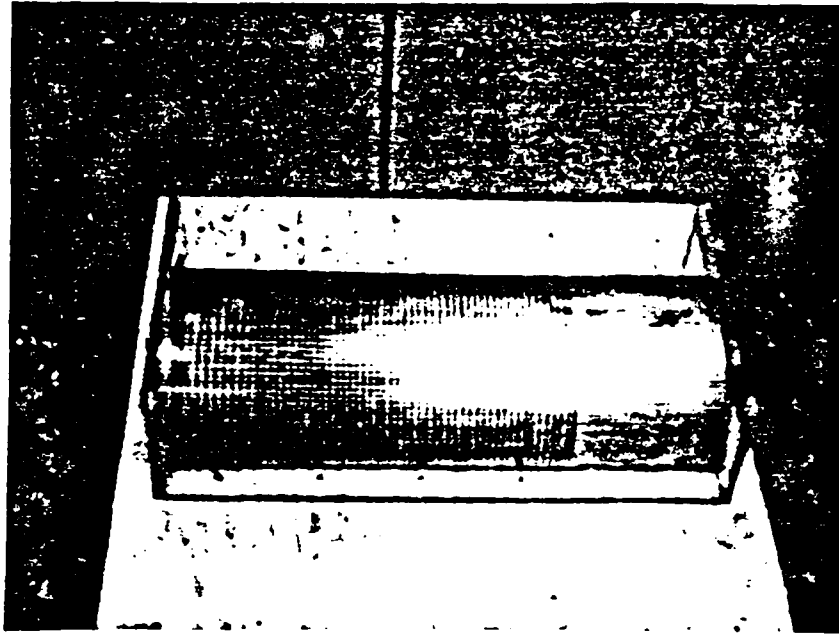


Figure 5. Reinforcement in a Mold

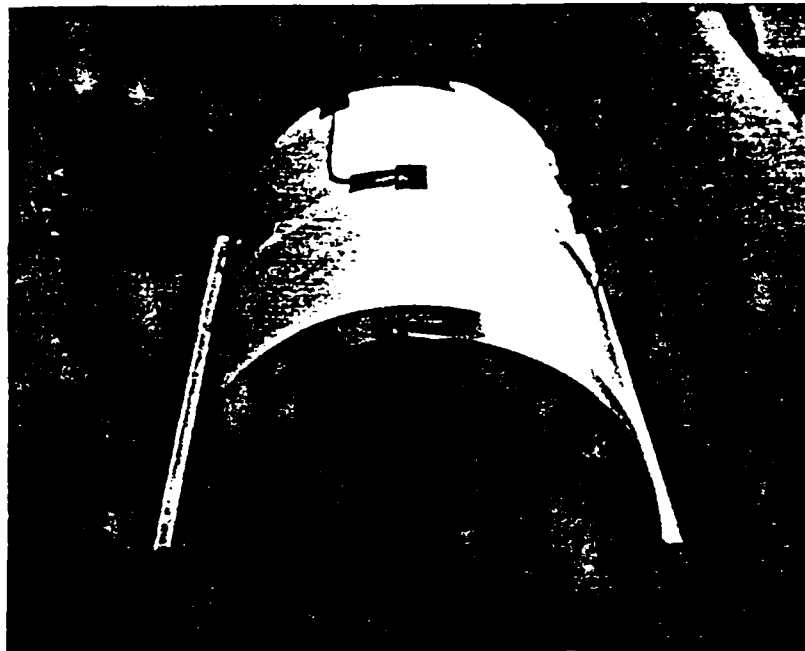


Figure 6. Completed Model Structure

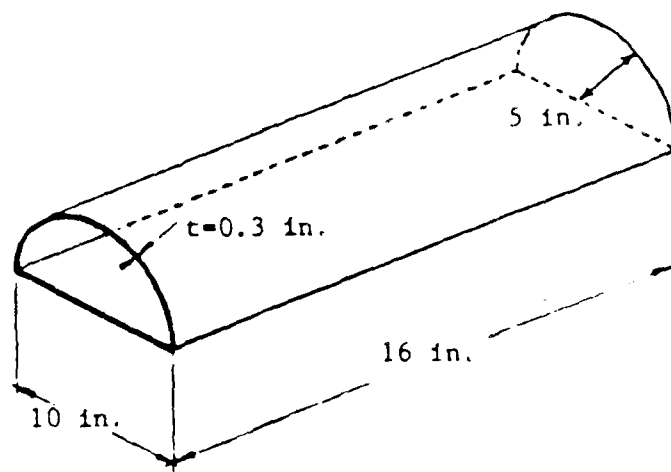


Figure 7. Dimension of the Model Structure

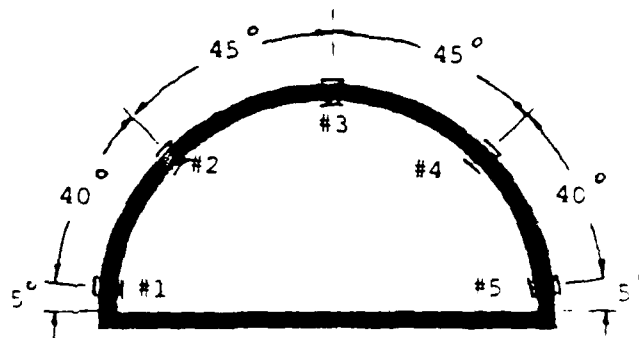


Figure 8. Location of Strain Gages

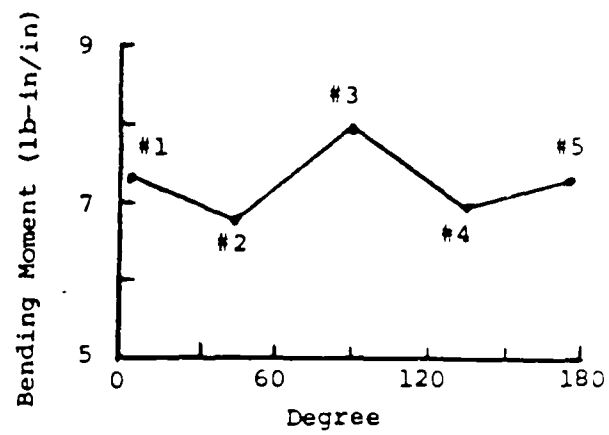


Figure 9. Bending Moment of Structure at 30 g

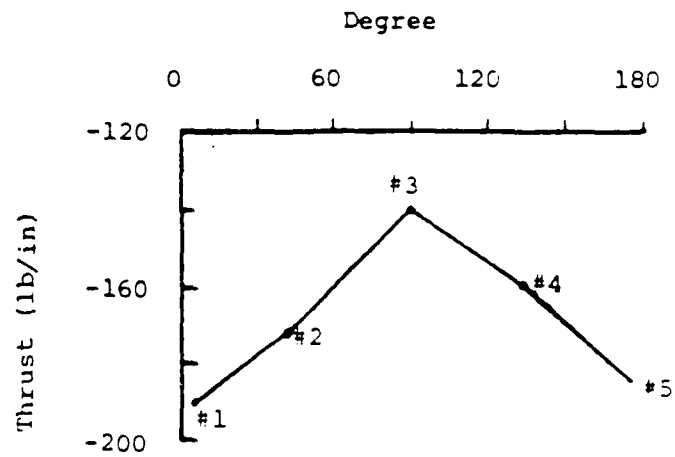


Figure 10. Thrust of Structure at 30 g

valid? and (3) how do different particle sizes (e.g., rock/rubble, gravel, sand or burster slab) affect mechanics of the projectile, soil and structure, and can the physical characteristics be quantified?

Three approaches were adopted: 1-g tests, high-g (centrifuge) tests and numerical analysis. For the experimental studies, the reinforced concrete structure developed in section III.2 and a launching projectile system shown in Figure 11 were used. Strain gages were attached on the surface of the structure and an accelerometer (Endevco 7264) was attached under the crown of the structure. The impact velocity of the projectile was set at 1000 ft/sec and a 6-mm diameter sphere brass projectile was used. Figure 12 shows a model after penetration test.

For the numerical analysis, a computer code, DYNA3D (a vectorized explicit three-dimensional finite element code for analyzing the large deformation dynamic response of inelastic solids under shock waves) was used. The DYNA3D analysis was carried out on a supercomputer (CRAY X-MP/48) at the San Diego Supercomputer Center in California. Figure 13 shows the acceleration of the structure in Ottawa sand due to projectile impact, while Figure 14 shows the corresponding acceleration calculated using the computer code.

IV. POSSIBLE FUTURE RESEARCH TOPICS

Followings are possible research topics using the centrifuge modeling technique: (1) civil engineering applications, (2) weapons effects and (3) hazardous waste pollutant transport. The study includes basic research such as particle size and boundary effects, time conflicts in scaling laws and liquefaction phenomena, and exploratory and advanced engineering developments.

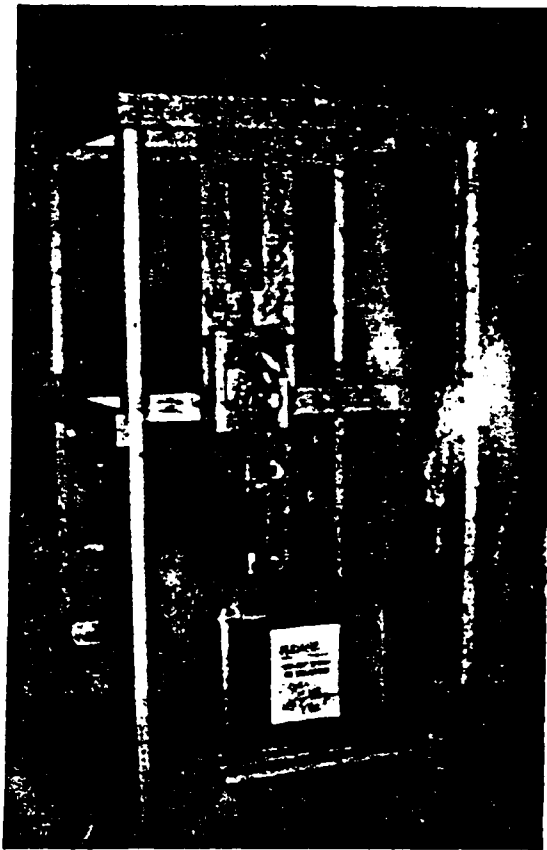


Figure 11. A View of Launching Projectile System

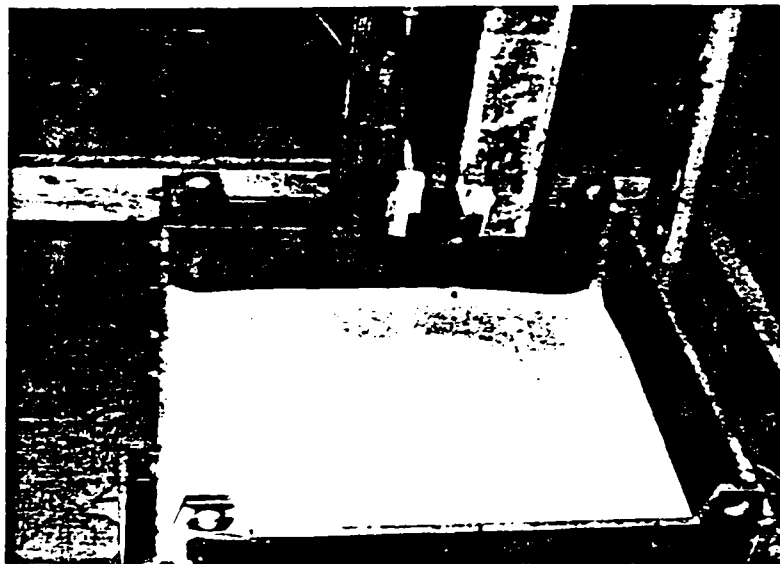


Figure 12. A View of Crater after Model Test

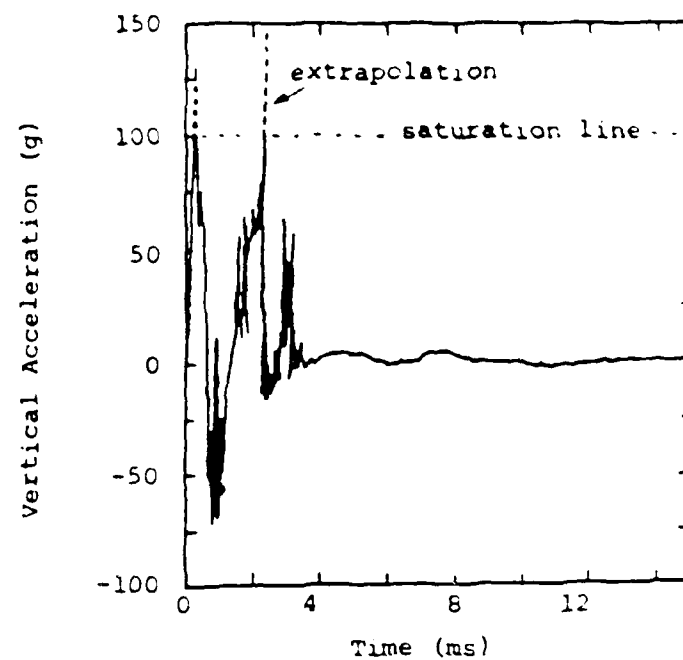


Figure 13. Vertical Acceleration of the Crown
at 1 g (Experimental Study)

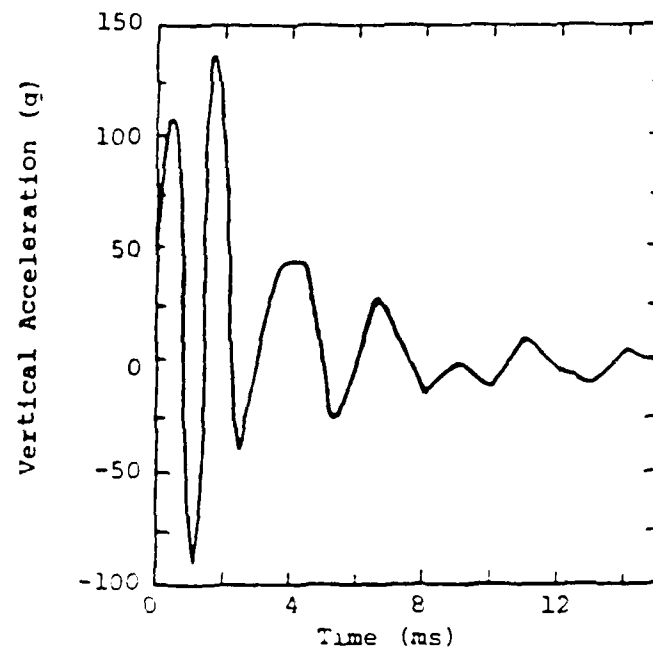


Figure 14. Vertical Acceleration of the Crown
at 1 g (Numerical Study)

Currently, the author is planning to study the behavior of protected arch structures under blast loadings using the centrifuge modeling technique.

V. SUMMARY

A medium size centrifuge installed in the Air Force Engineering and Services Center (AFESC) at Tyndall Air Force Base for geotechnical studies is described. In addition, ongoing research projects are introduced, and some of preliminary results at 1-g and high-g conditions are presented. Finally, possible research topics using the centrifuge modeling technique is mentioned. It is anticipated that the use of centrifuge small-scale model technique and numerical analysis would result in a better understanding of soil-structure interaction and should be of benefit to structural designers.

REFERENCES

1. Arulanandan, K., Thompson, P.Y., Meegoda, N.J., Kutter, B.L. and Krone, R.B. 1985. Centrifuge modeling of advection and dispersion process during pollutant travel in soil. Proceedings of Second Symposium on the Interaction of Non-Nuclear Munitions with Structures, Panama City Beach, Florida, USA: 418-423.
2. Eid, W.K. 1987. Scaling effect in cone penetration testing in sand. Ph.D. thesis, Virginia Polytechnic Institute and State University, Virginia, USA.
3. Einstein, H.H., Joseph, P.G. and Whitman, R.V. 1987. A literature review of geotechnical centrifuge modeling with particular emphasis on rock mechanics. A report submitted to Tyndall AFB, Florida, USA.
4. Genisco Incorporated. 1956. Handbook of instructions for G-Accelerator Model E-185.
5. Hallquist, J.O. 1983. Theoretical manual for DYNA3D. Report No. UCID-19401, University of California, Lawrence Livermore National Laboratory, California, USA.
6. Katona, M.G., Smith, J.M., Odello, R.J., and Allgood, J.R. 1976. CANDE-A modern approach for the structural design and analysis of buried culverts. Report No. FHWA/RD-77/5, Federal Highway Administration, Washington, D.C., USA.
7. Kim, Y.S. and Thompson, P.Y. 1986. A buried rigid concrete box culvert in embankment. Presentation of Third International Conference on Computational Methods and Experimental Measurements, Porto Carras, Greece.
8. Kutter, B.L., O'Leary, L.M. and Thompson, P.Y. 1985. Centrifugal modeling of the effect of blast loading. Presentation of Second Symposium on the Interaction of Non-Nuclear Munitions with Structures, Panama City Beach, Florida, USA.
9. New Mexico Engineering Research Institute. 1982. Modified handbook of instructions for G-Accelerator Model E-185.
10. Nielson, J.P. 1983. The centrifuge simulation of blast parameters. Report No. TR-83-12, Air Force Engineering and Services Center, Tyndall AFB, Florida, USA.
11. Shen, C.K., Li, X.S. and Kim, Y.S. 1984. Microcomputer based data acquisition systems for centrifuge modeling. ASTM Geotechnical Testing Journal, Vol. 7, Number 4: 200-204.
12. Townsend, F.C., McVay, M.C., Bradley, D.M., Cunningham, C.H. and Yovaish, D.J. 1985. Numerical and centrifugal modelling of buried structure response to near blast. Proceedings of Second Symposium on the Interaction of Non-Nuclear Munitions with Structures, Panama City Beach, Florida, USA: 482-487.

13. Townsend, F.C. 1986. Pollution study. A final report submitted to Air Force Engineering and Services Center, Tyndall AFB, Florida.

1987 USAF-UES SUMMER FACULTY RESEARCH PROGRAM
GRADUATE STUDENT SUMMER SUPPORT PROGRAM

Sponsored by the
AIR FORCE OFFICE OF SCIENTIFIC RESEARCH
Conducted by the
Universal Energy Systems, Inc.

FINAL REPORT

Emergent Leadership and Team Effectiveness
on a Team Resource Allocation Task

Prepared by:	Charles E. Kimble, Ph.D.
Academic Rank:	Professor
Department and University:	Psychology Department University of Dayton
Research Location:	AAMRL/HED Wright-Patterson AFB Dayton, OH 45433
USAF Researcher:	Michael D. McNeese
Date:	21 Aug 87
Contract No:	F49620-85-C-0013

Emergent Leadership and Team Effectiveness on a Team Resource Allocation Task

by

Charles E. Kimble

ABSTRACT

Team communication patterns on the Team Resource Allocation Problem (TRAP) were evaluated to determine characteristics of leaders and elements of effective team performance. Talking frequencies and durations and types of verbalizations (commands, suggestions, etc.) of team members during TRAP performances were used as indices of leadership. Individual background information and task and setting features were assessed to see how they related to leadership behavior. Team characteristics and communication patterns were related to team performance scores under high and low time pressure to evaluate team effectiveness. Results indicated that teams with computer-experienced members and teams which were given strategies for doing the task performed better. Also, teams with equal verbal participation rather than having one person who dominated talking performed better. Older people, people with computer experience, and men assumed leadership roles by giving suggestions and issuing commands more than others did.

ACKNOWLEDGMENTS

I am grateful to the Air Force Systems Command, Air Force Office of Scientific Research, and the Human Engineering Division of Armstrong Aerospace Medical Research Laboratories for sponsorship of my research efforts this summer and to Universal Energy Systems for administering the program. I also appreciate Michael McNeese's encouragement, helpful guidance, and sponsorship in starting and sustaining this project. Many others, Donald Monk, Major Bill Marshak, Walt Summers, Dr. Ron Katsuyama, Dr. Rod Wellens, and Capt. Dan Snyder have been friendly and helpful coworkers. I am indebted to Maj. D. J. McBride for allowing me to use the data she has been collecting for her dissertation in this project. Curtis Mayrand, Greg Bothe, and especially Chuck Goodyear of SRL have been extremely helpful in conducting this research. Tracy Vogler was very efficient in organizing the data for analysis and in organizing and executing the coding of audiotape information. He and Rob Lindner, Greg Peyton, and Skip Shattuck of SRL deserve special thanks for their long hours of coding data. All of these people, and others, have made this a very fruitful and enjoyable experience.

I INTRODUCTION

I became aware that studies on group performance were being conducted at this AMRL lab through Cliff Brown of Wittenberg University and Michael McNeese, a staff member of this unit and sponsor of my efforts this summer. Being a social psychologist involved in research on small group interactions, I was interested and excited about this research opportunity. I visited the lab last summer, met with Cliff Brown and Mike McNeese, and went through the TRAP task which Dr. Brown had developed. I also met Dr. Rod Wellens, a social psychologist from the University of Miami who was a summer faculty appointee last summer, at that time. Within a week, I wrote a letter to Mike McNeese relating my interests and suggestions about studying communication factors in team problem solving.

When I received the Summer Faculty Research brochure, I indicated a desire to work in the C(3) Operator Performance Engineering (COPE) facility of the Human Engineering Division of AMRL. I was informed in late May that I had received an appointment into the program.

II. OBJECTIVES OF THE RESEARCH EFFORT

Here I will present a paraphrased and revised version of the research goals and objectives which I wrote at the beginning of

the program.

My primary objectives were to assess the most effective team communication patterns on the Team Resource Allocation Problem (TRAP) task and to determine which individual, role, and task factors affect the emergence of leaders. To examine effective communication, it was necessary to measure what behaviors occurred on trials with good team performance scores and those that occurred on less successful trials. Computer-recorded talking frequencies and durations for each individual on each trial in two TRAP studies were examined. Audiotapes from one study were coded according to the incidence of certain behaviors and the incidence of these behaviors were compared to the team performance score on each trial.

To evaluate factors in emergent leadership, available background information on each individual such as sex, age, seat position, subjective workload judgments (SWAT profiles), and computer and video game experience was obtained and compared with their influential or leaderly behaviors.

The ultimate goal was to be able to maximize team performance through structuring tasks and through assignment of capable individuals to appropriate roles on the team or crew.

III. BACKGROUND INFORMATION

The Team Resource Allocation Problem (TRAP), the task used in both studies that we analyzed, was developed by Cliff Brown (Brown & Leupp, 1985). It is a task which requires that team members coordinate their efforts to maximize their team score. In the graphic display mode, targets appear on the screen and move from left to right. There are eleven rows on the screen and, at a particular time, there are targets on most of the rows. Some targets require all three team members to use their cursors to be to the same row simultaneously. Others require two team members and others, one. The way the targets are staggered across the screen, it is impossible to respond to all targets during the time they are on the screen. As you can see in the table below from Wilson, McNeese, and Brown (1987), targets on the screen which require all three members to respond are worth more than two-person targets and one-person targets.

Table 1 Target Values

One Person Targets	Point Value
Blue triangle	1
Red triangle	3
Blue circle	3
Red circle	5
Two Person Targets	
Blue triangle	4
Blue circle	4
Red triangle	8
Red circle	8
Three Person Targets	

Blue circle	3
Red circle	9
Blue triangle	9
Red triangle	15

The task is to accumulate as many points as possible on a trial. Figure 1 from Wilson, McNeese, and Brown (1987) illustrates how the screen could look at one time on a trial. There are other variations of the task which were used in the two studies from which we analyzed data. One variation in the study by Wilson, McNeese, and Brown (1987) was to present 11 labels such as "blue triangle" with a clock ticking off the time rather than having targets moving across the screen. The McBride (in preparation) study used the original graphic display and three other moving target displays: 1) letter targets, 2) color targets, and 3) letter/ color targets.

An important addition to all displays in the McBride study was black rectangular, "uncertain value" targets. To find out an uncertain target's potential value, all three members had to cursor to the row and press "start". After a time, the potential points and the probability of getting the points appeared on the rectangle; for example, L84 meant that there was a low probability (20%) of getting 84 points. At that point, the team could abandon that target for other opportunities or press "start" to

ROW	A	B	C	TARGET	TIME	STATUS
1				RED CIRCLE	24	WORK
2				BLUE TRIANGLE	18	
3						
4				RED CIRCLE	7	
5				RED TRIANGLE	2	
6				BLUE TRIANGLE	15	
7				BLUE TRIANGLE	5	WORK
8				BLUE TRIANGLE	25	
9				RED TRIANGLE	20	
10				BLUE CIRCLE	13	
11				RED CIRCLE	29	
A B C						
				FREE	ACCUMULATED POINTS 35	
				WAIT		
	9	9	3	WORK		

ROW	A	B	C	OPPORTUNITY WINDOW
1				
2				
3				
4				
5				
6				
7				
8				
9				
10				
11				
A B C				
				FREE
				WAIT
	9	9	3	WORK
				ACCUMULATED POINTS 35

Figure 1: Alphanumeric Display (Top);
Graphic Display (Bottom)
79-8

commit to that target. The net effect of adding these targets was to make the task simpler because most valuable targets required all three members to work together so the other targets should be ignored most of the time.

IV METHOD

We analyzed computerized data from the Wilson, McNeese, and Brown (1987) study, and computerized and audiotaped information from the McBride (in preparation) study. The primary independent variables of the Wilson et al study were: 1) display speed (fast & slow); 2) setting (large screen display and small screen with isolated team members) and 3) display format (alphanumeric and graphic). The effects of these variables on team performance is presented in that paper. The primary independent variables of the McBride study were: 1) display speed (fast and slow); 2) display format (original graphic, color, letter, & letter/color); and 3) heuristics (possible strategies presented or not). It should also be noted that uncertain targets were a constant in the McBride study, while they did not appear at all in the Wilson et al study. The effects of these variables on team performance will be presented elsewhere.

Subjects

Sixteen three-person teams participated in the Wilson et al

study, and 32 three-person teams participated in the McBride study. The sex composition of the teams varied from all male to all female. All individual background information available was used in the analysis. This included computer and video game experience from self-reports and subjective workload (SWAT) preferences.

Procedure

Information on experimental conditions, talking duration per individual per trial, talking frequency per individual per trial, and team performance score per trial was derived from computer records for the two experiments. Other individual information and sex composition of the team were combined with that data from both experiments.

We also analyzed audiotape information from the McBride study. Coders listened to one or two channels of the audiotapes in a single pass corresponding to utterances of one or two team members during the trials of the first and last sessions. For each utterance, the coder recorded the person speaking (A, B, C) and classified the verbal content as 1)a command, 2)a suggestion, 3)a question, 4)a statement, 5) an agreeing response, or 6)a disagreeing response. From this raw data, we derived the number of each type of verbalization by each person on each trial. This

information and the talking frequencies and durations were used to assess the amount of influential or leaderly behavior by each individual.

Subjective estimates of the influence of each team member were also obtained from each subject.

V RESULTS AND DISCUSSION

Wilson, McNeese & Brown Results

At the team level, trial speed (involving time pressure) had some interesting effects on behavior. Teams talked more times per minute on the fast trials, $F(1, 15) = 9.17$, $p < .01$, and they talked in shorter utterances on the fast trials, $F(1, 15) = 12.13$, $p < .005$. Also, a talking leader emerged most on the fast trials with graphic displays, $F(1, 15) = 3.88$, $p < .07$, and the variation in talking frequency among team members was greatest on the fast trials, $F(1, 15) = 6.28$, $p < .05$. As for team performance, teams scored better on the slow trials than on the fast trials, $F(1, 15) = 188.19$, $p < .0001$; and they scored better with graphic displays than with alphanumeric displays, $F(1, 15) = 23.35$, $p < .0002$. The group versus isolated setting did not affect performance or behavior. Nor did the sex composition of the teams affect behavior or performance of the team as a whole.

When behavior at the team level was correlated with team

performance, an interesting pattern appeared. The teams who had more dominant talking leaders scored worse, $r(16) = -.50$, $p < .05$ between MAXFREQ and SCORE. When the experimental conditions were ignored, the correlation between team talking duration and team performance was significant, $r(128) = .22$, $p < .02$, indicating that teams which talked in longer utterances scored better.

In this study, we only had three individual factors to examine to see which kinds of people exhibited the most leaderly behavior. Those three factors were sex of the individual (within particular sex composition teams), individual SWAT preferences, and individual seat position. The overall Fs of sex composition did not approach significance for any of the measures. But according to pairwise comparisons, the solitary women in majority male teams talked more than women in majority female teams ($p < .06$) in terms of individual talking frequencies; and in terms of standardized frequencies (ZFREQ) and durations, they talked more and in longer utterances than men in those majority male teams ($p < .07$ for both measures). For the SWAT preference types, we only used the data from the four teams who had a team member of each SWAT type for analysis; and the overall ANOVA results were not significant, $F(2,9) = 2.63$, $p < .13$. However, pairwise comparisons showed that subjects who focused on

cognitive effort in their subjective workload judgments talked more than team members who emphasized psychological stress in their workload judgments ($p < .05$). Seat position did not affect the amount of leaderly behavior displayed.

The McBride Computerized Data Results

The effects of trial speed on team performance and behavior in this study were very consistent with the results in the Wilson et al. study. Again, teams talked more times per minute on the fast trials, $F(1,24) = 61.70$, $p < .0001$; and they talked in shorter utterances on the fast trials, $F(1,24) = 24.24$, $p < .0001$. Also as in the Wilson et al. study, teams scored better on the slow trials than on the fast trials, $F(1,24) = 470.53$, $p < .0001$. As in the earlier study, variation in talking frequency was greater on the fast trials, $F(1,24) = 10.11$, $p < .005$.

The sex composition of the teams did not affect behavior or performance according to the overall F 's, but pairwise comparisons suggested that variances in talking frequency ($STDFREQ$ $p < .07$) and duration ($STDDUR$ $p < .05$) were greater in majority male teams than in majority female teams. Also, among teams which were not given heuristics, all male and majority male teams performed better than majority female teams, $F(2,13) = 3.75$, $p < .052$.

Other factors present only in the McBride study affected team performance and behavior. Teams that received heuristics about the task performed better than teams who did not, $F(1,24) = 13.67$, $p < .005$, with the best scores being achieved by teams with heuristics on the fast trials, Interaction $F(1,24) = 8.28$, $p < .01$. Teams given heuristics also talked in longer utterances, $F(1,24) = 6.42$, $p < .02$; and on the fast trials, these teams with heuristics spoke more than teams in the other three conditions, Interaction $F(1,24) = 7.01$, $p < .02$. In addition, variability in talking frequency was greatest among teams given heuristics on fast trials, STDFREQ Interaction $F(1,24) = 12.84$, $p < .005$.

The statistics on sessions revealed some interesting patterns of behavior as the teams became more experienced at the task. Teams scored better in the final two sessions than in the first one, $F(3,72) = 10.11$, $p < .0001$; and they talked less, $F(3,72) = 4.26$, $p < .01$. Also, leaderly talking behavior increased from the early sessions to the later ones; MAXFREQ $F(3,72) = 3.99$, $p < .01$ and MAXDUR $F(3,72) = 3.69$, $p < .02$; and the variability in talking frequency and duration increased from the early sessions to the later ones, STDFREQ $F(3,72) = 9.79$, $p < .0001$ and STDDUR $F(3,72) = 9.26$, $p < .0001$.

When behavior at the team level was correlated with team

performance, the negative correlation between dominance of the talking leader on the team and score was not significant, $r(32) = -.15$, $p = .41$; unlike in the previous study. Results indicated that overall team computer use experience was related to team performance, $r(32) = .54$, $p < .002$.

At the team level, partial correlations between behavioral measures and score (adjusted for teams, meaning that teams' intercepts were equated) at different levels of heuristics, sessions, and trial speeds were calculated. Most significant correlations occurred in the first session on fast trials with the teams which were given heuristics. Under those conditions, teams which talked less scored better, $r(64) = -.30$, $p < .05$, and teams with more dominant talking leaders and greater variability in team members' talking scored better, r 's between score and MAXFREQ, MAXDUR, STDFREQ, and STDDUR ranged from .30 to .35, p 's $< .05$. By the last session and for the slow trials throughout, these correlations disappeared for the teams with heuristics. The only significant partial correlation for the teams which were not given heuristics occurred in the first session on the slow trials. This result indicated that teams which talked in longer utterances under these conditions scored better, $r(64) = .31$, $p < .05$. No other partial correlations with team performance were

significant

On the individual level, we evaluated the relationships of academic class, age, sex (in particular sex composition groups), computer experience, and video game experience to talking leadership measures (frequency, standardized frequency, and average talking duration) and rated influence on the team's decisions. Among the individual background variables, males had more video game experience, $F(1,94) = 14.20$, $p < .001$; as did lower academic classification subjects, $r(96) = -.20$, $p < .053$. Males also had slightly more computer experience, $F(1,94) = 3.77$, $p < .06$. There were no differences in computer experience between subjects based on age or classification.

On the individual level, some interesting patterns emerged in the data on rated influence of the individuals. Recent video game players were rated as more influential than those who had not played recently, $r(48) = .28$, $p < .054$. Also, those who talked less, according to ZFREQ, were rated as more influential, $r(48) = -.27$, $p < .07$. Video game players talked less than non-players, $r(96) = -.21$, $p < .05$. To examine this pattern more closely, we broke rated influence down into rated influence on fast and slow trials, and we examined the correlations at different levels of heuristics and trial speed. It occurred that the strongest

correlations with rated influence (on fast trials) appeared for the members of teams given heuristics on the fast trials. Under these conditions, persons who talked (ZFREQ) less were rated as more influential, $r(27) = -.36$, $p < .07$, and experienced video game players were rated as more influential, $r(27) = .39$, $p < .05$.

Sex of the individual did affect talking behavior in different sex composition teams. Pairwise comparisons on the frequency measure indicated that females in majority female teams ($M=9.91$) talked more than females ($M=4.19$, $p < .052$) or males ($M=5.86$, $p < .02$) did in majority male teams. The average duration data revealed that females in a majority ($M=4.41$ sec) talked more than males in a majority ($M=3.30$ sec, $p < .03$). Also on the duration measure, males in all male teams ($M=4.47$) talked in longer utterances than males in majority male teams ($M=3.30$, $p < .005$).

Types of Verbalizations Analysis

Four coders recorded the six types of verbalizations spoken by the three members of the 32 teams during their first and last (fourth) sessions of eight trials. Because each team's sessions required two or three hours to code, each coder did approximately one-fourth of the coding of comments. All coders did one session of one team in order to check on the reliability of the coders.

The pairwise reliability coefficients among three of the coders were .97, .93, and .94. However, partly because he coded what the other three coders had recorded as suggestions as commands, the correlations between the fourth coder's observations and those of the other three coders were .10, .08, and .29. The data from the teams he coded were eliminated from the analysis. In addition, data from nine teams which talked very infrequently were eliminated because we judged that their data would distort some of the percentage-wise or proportional results. Consequently, data from only 18 of the 32 teams were used in the analysis.

First, we examined the effects of heuristics session, and trial speed on the team's verbalizations. As in the previous analyses, trial speed had powerful effects on team verbal behavior. Fast trials elicited more comments per time unit made by the whole team in the verbal categories of commands, $F(1,16) = 20.47$, $p < .001$; suggestions, $F(1,16) = 80.28$, $p < .0001$; agreeing responses, $F(1,16) = 4.45$, $p < .051$; and disagreeing responses, $F(1,16) = 7.50$, $p < .02$, than slow trials did. As would be expected, fast trials elicited more total team communications than slow ones did, $F(1,16) = 69.93$, $p < .0001$.

Trial speed had different effects on how much one member

dominated in giving suggestions and on how much one person disagreed more than the others. On slow trials, one person dominated in giving suggestions more than on fast trials, $F(1,16) = 10.43$, $p < .01$. However, more domination by one person in disagreeing occurred on the fast trials than on slow ones, $F(1,16) = 6.58$, $p < .05$.

Teams consistently made more commands, $F(1,16) = 7.21$, $p < .02$; more task-related statements, $F(1,16) = 4.14$, $p < .06$; and more agreeing responses, $F(1,16) = 10.86$, $p < .005$; during the first session than during the last session. Total team communications followed the same pattern, $F(1,16) = 7.78$, $p < .02$. There was an Heuristic X Session interaction on MAXNO, the leadership measure for disagreeing responses, $F(1,16) = 4.25$, $p < .056$, indicating that dominance in disagreement decreased from the first to the last session on teams without heuristics but increased for teams given heuristics.

There were no significant correlations between team scores and the team amount or leadership measures for any of the verbal categories overall. It is interesting to note, however, that team members did fit into different roles. That is, the person who emitted the most of each type of verbalization gave significantly more than 33.3% of those responses. The foremost

contributors of commands gave 68.1% of the team's commands, suggestions, 52.6%, questions, 64.8%, task-relevant statements, 52.1%, questions, 64.8%, agreements, 62.6%, and disagreements, 71.3%. But those who gave the most commands, suggestions, and disagreements to direct or redirect actions must not have been the most talented at the game because leadership on these categories was uncorrelated with team scores. Suggestions were the most common type of verbalization ($n=16.0$ per team per 4 minutes of trial time), disagreeing responses were the most uncommon ($n=1.2$).

On an individual level, correlational analyses indicated that several verbal categories were related to the rated influence of the individual on the team's decisions. Relative to others on their teams, those who issued more commands, $r(30) = .40$, $p < .05$; those who made more suggestions, $r(30) = .61$, $p < .001$; those who made more disagreeing responses, $r(30) = .52$, $p < .005$; and those who made more total comments, $r(30) = .75$, $p < .0001$, were rated more influential. Making suggestions was most strongly related to influence.

Some individual characteristics were related to the number and types of comments made. Older people made more suggestions, $r(30) = .42$, $p < .02$, made more agreeing, $r(30) = .61$, $p < .001$, and

disagreeing responses, $r(30) = .45$, $p < .02$; and made more total task-related comments, $r(30) = .50$, $p < .005$, than younger people did. Also, individuals who had more computer experience made more suggestions than computer-inexperienced people did, $r(54) = .33$, $p < .02$. A similar pattern appeared for video game players, $r(54) = .26$, $p < .061$.

When we examined the verbalizations of men and women, we found that women asked more questions than men did, $F(1,52) = 7.39$, $p < .01$. Relative to other team members, men made more task-relevant statements than women did, $F(1,28) = 18.67$, $p < .001$; and men made more suggestions than women did, $F(1,28) = 5.85$, $p < .05$. When the verbalizations of men and women were considered in the context of different sex composition teams, similar results were obtained. For instance, women in female majority teams asked more questions than people in any of the other teams did, $F(4,49) = 2.70$, $p < .05$. Relative to other team members, men in majority male and majority female teams made more task-relevant statements than women in majority male and majority female teams did, $F(3,26) = 7.05$, $p < .005$. Also, although the overall F test was not significant, pairwise comparisons showed that men in majority male teams made more suggestions than women in the same teams; male ZCOUNT $M = .46$, female ZCOUNT $M = -.92$, $p < .05$. On the other

verbal categories, no sex differences occurred

Conclusions

Older people, people with computer experience, and men emerged as leaders on this task. The teams which performed best were those whose members were computer-experienced and teams who had been given information on strategies for executing the task. Performance seemed to be hindered if a dominant talking leader emerged on this particular task

VI. RECOMMENDATIONS

a. This research was conducted to examine the group decision making process on a dynamic task akin to the types of tasks found at command and control centers. Specifically, we wanted to see how leaders emerge, and what team communication patterns are related to optimizing performance. Results which occurred in a consistent pattern should be applicable to similar dynamic tasks in small team settings.

b. In order to understand how small teams and crews operate in C(3) environments better, it will be necessary to get more information about the background and traits of the team members. It will also be necessary to create a task setting that does not restrict, or make unnecessary, communication among team members. Heretofore, the emphasis has been on what task or setting fea-

tures affect team performance without examining the patterns of team communication or the effects of members' traits or their relationships on team performance. It is important that we understand that C(3) systems are not man-machine systems, but they are teams-machines systems. We must seek to understand the coordination among persons as well as person with machine.

REFERENCES

1. Brown, C. E. & Leupp, D. G. (1985). Team performance with large and small screen displays. AAMRL-TR-85-033, Harry G. Armstrong Aerospace Medical Research Laboratory, Wright Patterson Air Force Base, Ohio.
2. McBride, D. J. (In preparation). An exploration of team information processing in a dynamic group choice task involving uncertainty. Ph D dissertation, University of Minnesota.
3. Wilson, D. L., McNeese, M. D., & Brown, C. (1987). Team performance of a dynamic resource allocation task: Comparison of shared versus isolated work setting. Proceedings of the Human Factors Society, 31st annual meeting, New York City.

1986 USAF-UES SUMMER FACULTY RESEARCH PROGRAM/

GRADUATE STUDENT SUMMER SUPPORT PROGRAM

Sponsored by the

AIR FORCE OFFICE OF SCIENTIFIC RESEARCH

Conducted by the

Universal Energy Systems, Inc.

FINAL REPORT

EXPERIMENTAL TESTING OF IMAGING CORRELOGRAPHY

Prepared by:

Jerome Knopp

Associate Professor

and

Brian K. Spielbusch

Graduate Student

Department and

Department of Electrical and Computer Engineering

University:

University of Missouri - Columbia

Research Location:

Air Force Weapons Laboratory

Kirtland AFB, NM 87117-6008

Group ARBB

USAF Researcher:

Captain Paul S. Idell

Date:

19 August 1987

Contract No:

F49620-85-C-0013

EXPERIMENTAL TESTING OF IMAGING CORRELOGRAPHY

by

Jerome Knopp

and

Brian K. Spielbusch

ABSTRACT

An experimental verification of imaging correlography was completed. A laboratory testbed was set up using a CCD camera to collect speckle data from a diffuse object. The collected data was averaged and processed to estimate the Fourier modulus (FM). The FM was then used to estimate the image of the diffuse object using phase retrieval algorithms. A high quality image was recovered using approximately 1200 frames of speckle data.

Acknowledgements

The authors would like to express their appreciation for the summer support and the research opportunities provided for us under the sponsorship of the Air Force Systems Command, the Air Force Office of Scientific Research and the Air Force Weapons Laboratory. Our experiences at the Laboratory have given us a unique opportunity to participate in forefront research in imaging technology.

We would like to thank Captain Paul Idell for his guidance and for making the decisions needed to expedite a significant piece of research in only ten weeks. We also wish to acknowledge the important and crucial team effort that was the key in sorting out problem areas. Besides Paul Idell, John Gonglewski and David Voelz made significant contributions to the results reported here.

We also wish to thank Ray Lagarde for getting us the little things we needed to get by day to day such as office keys and passes.

Finally, we wish to express our deepest gratitude to Nena Bui, who typed our report (somehow) despite being immensely overloaded with work. She is presently trying to handle the reports and typing for over 30 professional level staff members.

I. Introduction

Imaging Correlography

Imaging correlography [1] refers to a technique for image synthesis that is similar to holography in that it records an interference pattern from a coherently illuminated object. This pattern is the speckle pattern one normally observes when coherent light is reflected from a diffuse object [2]. The speckle represents the coherent interference of many point scatterers on the surface of the object. Unlike conventional holography where a reference wave is used to form a hologram, the object to be imaged is in a sense its own reference. However, because the object and hence the reference wave are both unknown, special processing techniques are used to recover the image.

Image synthesis using imaging correlography (IC) is based on the fact that the autocorrelation function of the illuminated object's brightness distribution can be obtained from the average energy spectrum of a laser speckle pattern [3] (The brightness distribution is essentially the object's irradiance distribution had the object been illuminated with an incoherent light source). Since the inverse Fourier transform of the autocorrelation of the object's brightness function is equal to the squared-modulus of the Fourier transform of the brightness function [4], an image of the object can be obtained if the phase associated with this Fourier transform can be determined. To obtain this phase we use a Fourier modulus (FM) estimated from

the speckle data together with an iterative transform algorithm of the type previously demonstrated by Fienup [5-7]. Once the phase associated with the Fourier modulus is determined, the image is recovered by inverse transforming the synthesized Fourier plane data. Because the image is recovered from an estimate of the energy spectrum of the object's brightness distribution, we find that the recovered image is unspeckled, even though the data for imaging correlography was obtained from measurements of speckle intensity.

One of the primary motivation for using IC in Air Force applications, as opposed to conventional imaging, is the potentially low cost of imaging hardware with large effective apertures. IC represents a synthetic aperture technique that allows one to replace a large telescope with a relatively inexpensive, lightweight array of detectors. IC may also have an aberration correcting capability similar to that of conventional holography [8] which is useful in seeing images through an aberrating media (eg. a turbulent atmosphere).

Background of the Authors

Jerome Knopp is presently an Associate Professor of Electrical and Computer Engineering with the University of Missouri - Columbia. He teaches and conducts research at the Kansas City engineering branch. He has a strong background in both theoretical and experimental optics, especially in holography and image processing. His background in the latter areas resulted in his selection for the Air Force summer research program at the Air Force

Weapon's Laboratory to pursue research in imaging. Besides teaching optics at the University of Missouri he has over twelve years of related experiences that include high energy laser research at M.I.T. Lincoln Lab, phase conjugation research at Rome Air Development Center and industrial research in holography with Hallmark Cards in Kansas City.

Brian K. Spielbusch is presently a graduate student at the University of Missouri - Kansas City working under Dr. Knopp on his Master's thesis in Electrical and Computer Engineering. His current research interests are in image processing.

II. Objectives of the Research

Computer simulations demonstrating the theoretical feasibility of correlography have been under way at the AFWL in the ARBB group under the direction of Captain Paul Idell. When Dr. Knopp visited the laboratory during April of 1987, on a presummer visit, it was agreed that he and his graduate student would participate in an experimental verification of the imaging correlography technique. Their primary goals were to set up a testbed that would gather speckle patterns from coherently illuminated targets.

Specifically they were to:

- i) Design an experimental system to collect speckle data
- ii) Characterize the system.

As this work progressed two new goals were added:

iii) Validation of the data

iv) Reconstruction of a target image using the Fienup phase retrieval algorithms.

III. Design of the experimental system

The laboratory experiments for correlography involve the digitized recording of large numbers speckle patterns from test targets. A large number of patterns (on the order of hundreds) are required for averaging to produce an acceptable estimate of the FM of the target image. This requires an automated testbed to produce and record patterns in a reliable and timely manner.

Figure 1 shows a design for the lab experiments. The target is mounted on a rotating table. A digital controller is used to rotate the target in fixed increments via signals to a stepper motor. Small rotations of the target are used to change in the speckle pattern observed on a charge coupled device (CCD) array camera. Each angular position of the target represents an independent speckle pattern on the camera. Each speckle pattern from the camera is digitized by a frame grabber and stored as a two dimensional array of intensity values in a computer. The computer estimates the average FM of the target image using an array processor.

The key design elements in setting up the system shown in Figure 1 are the scaling of the speckle pattern size to the sampling array in the CCD camera and the allowable target rotation. These constraints define the geometry for the experimental set-up and will be discussed in more detail.

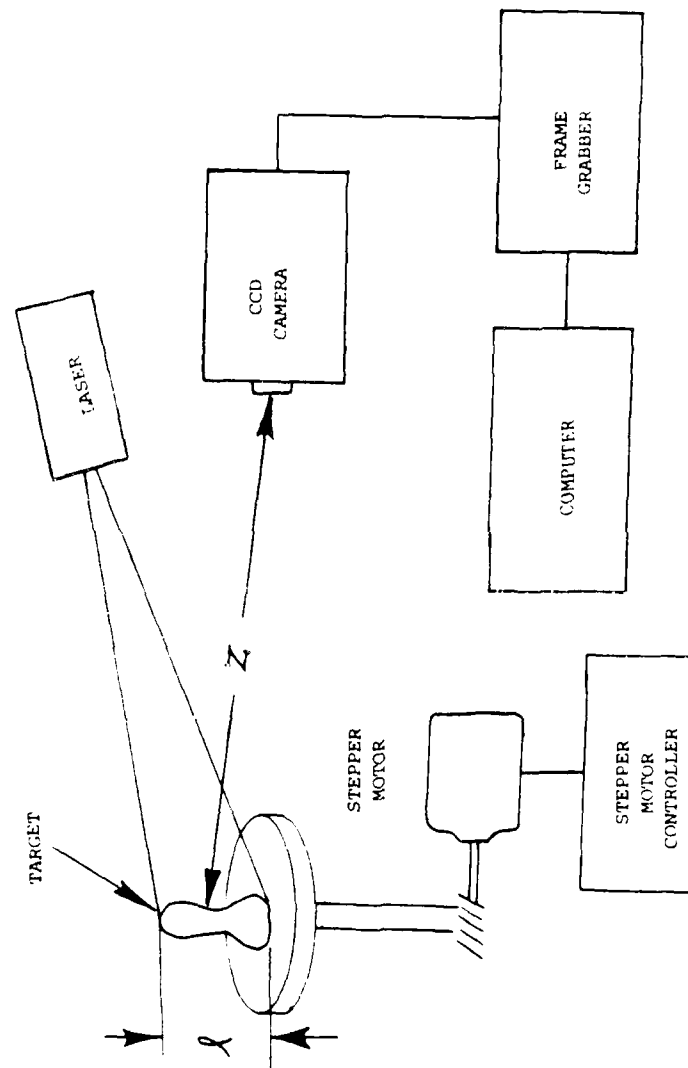


FIGURE 1. THE EXPERIMENTAL ARRANGEMENT

Scaling of the Speckle Pattern

If a target of size ℓ is positioned a distance Z from the CCD camera the highest spatial frequency associated with the field is determined by the largest separation of points on the target, obviously ℓ . For two points in the same plane the field amplitude fringe frequency is

$$f_n = \frac{\ell}{\lambda Z} \quad (1)$$

where λ is the laser wavelength. The camera records the intensity of the scattered speckle. Since the intensity is proportional to the field squared, the observed fringe frequency f_o is doubled, i.e.

$$f_o = \frac{2 \ell}{\lambda Z} \quad (2)$$

The CCD camera must sample this fringe at least at the Nyquist rate. If the spatial frequency of the camera detector elements is f_e then

$$f_e \geq \frac{4 \ell}{\lambda Z} \quad (3)$$

Allowable Target Rotation

The rotation of the target is the simplest technique for producing independent speckle patterns; however, the rotation must not significantly effect the target image. Since the target aspect angle is changed by rotation, the apparent width of the target is altered. If the apparent change is limited to one resolution element then the change will not be apparent in the image eventually produced by correlography. The number of resolution elements is determined by the camera array. If the array is assumed to have

n_p elements on a side then the target aspect angle θ_A is determined by

$$\theta_A = \cos^{-1} \left(\frac{n_p - 1}{n_p} \right) \quad (4)$$

If $n_p \gg 1$ then using small angle approximations

$$\theta_A = \sqrt{2/n_p} \quad (5)$$

Layout Constraints

The requirements for at least 1000 frames of independent speckle patterns requires the target rotation increments $\Delta\theta$ must satisfy

$$\frac{\theta_A}{\Delta\theta} \geq 1000 \quad (6)$$

For a CCD array of size S , a shift of one speckle frame requires

$$\Delta\theta = \frac{S}{2Z} \quad (7)$$

for small angles. This implies the speckle field rotates at twice the rate of the target. Combining equations (5) and (6) and (7) gives

$$2.83 \frac{Z}{S\sqrt{n_p}} \geq 1000 \quad (8)$$

Assuming equation (3) is satisfied then

$$f_e = \frac{n_p}{S} \geq \frac{4 \ell}{\lambda Z} \quad (9)$$

Inequalities (8) and (9) determine layout geometry constraints.

IV. Experimental Set-Up and Characterization

The test arrangement that was finally used was identical to the one shown in Figure 1. An Argon ion laser was used as a coherent source to illuminate the target. The targets were various shapes cut from Scotchlite. Scotchlite is a beaded reflector sold in flat sheets and used commercially to make reflective signs. It has a surface coated with a large number (on the order of $10^4/\text{in}^2$) of retro-reflecting microspheres averaging about 50 microns in diameter. The scatter from the Scotchlite doesn't dipolarize significantly, thus it makes a nearly ideal target. About 12% of the laser light is returned within a narrow cone angle under 20° . These targets provided strong speckle patterns that were observed with a Fairchild 3000 CCD camera at distances up to 5 meters with approximately 100 milliwatts of laser power on target.

The targets were glued on a glass flat that was attached to a rotation stage driven by a stepper motor. The key items to be characterized in this set-up were the laser coherence and the modulation function (MTF) of the CCD camera.

A Michelson interferometer was used to measure the longitudinal coherence. The coherence was found to be on the order of meters below about 75 milliwatts. Above this level the coherence dropped sharply to a few centimeters (This was probably due to multiple modes in the laser cavity). As long as the coherence length is twice the target depth the experimental arrangement would work. Since the targets used were flat this didn't pose a problem. The lateral coherence was measured in a separate experiment (by other researchers) and found to be acceptable over about one third of the beam diameter. For typical beam diameters used (on the order of 10 cm) this

limited the target sizes to about 3 centimeters.

The camera MTF was measured using the same Michaelson interferometer to generate sinusoidal fringe patterns that were projected onto the camera CCD array. Both horizontal and vertical fringe patterns were used to measure the MTF in the vertical and horizontal directions. The contrast was measured using the computer to grab fringe pattern frames and calculate the ratio of the standard deviation of the intensity to its mean. A separate comparative technique, using eye measurements of plotted fringe profiles, was also used along the horizontal axis. The data collected is shown in Figure 2. Note the contrast on the horizontal axis dropped significantly at less than 10 cycles/mm, (below the theoretical Nyquist frequency for this camera). About 8 cycles/mm was used experimentally as the upper limit on the frequency permitted in the speckle field.

Once the experimental system was characterized, the system was ready for test data.

V. Validation of the Data

The most difficult part of the experiment was validation of the data collected from the CCD camera. Speckle Frames were collected and stored on a VAX RA81 450 Megabyte disk using a Recognition Concepts Inc. Trapix Frame grabber. Data frames were processed using micro-VAX II equipped with a Sky Inc. Warrior array processor. The validation data was collected using a square target. A total of 50 camera frames of speckle data were collected

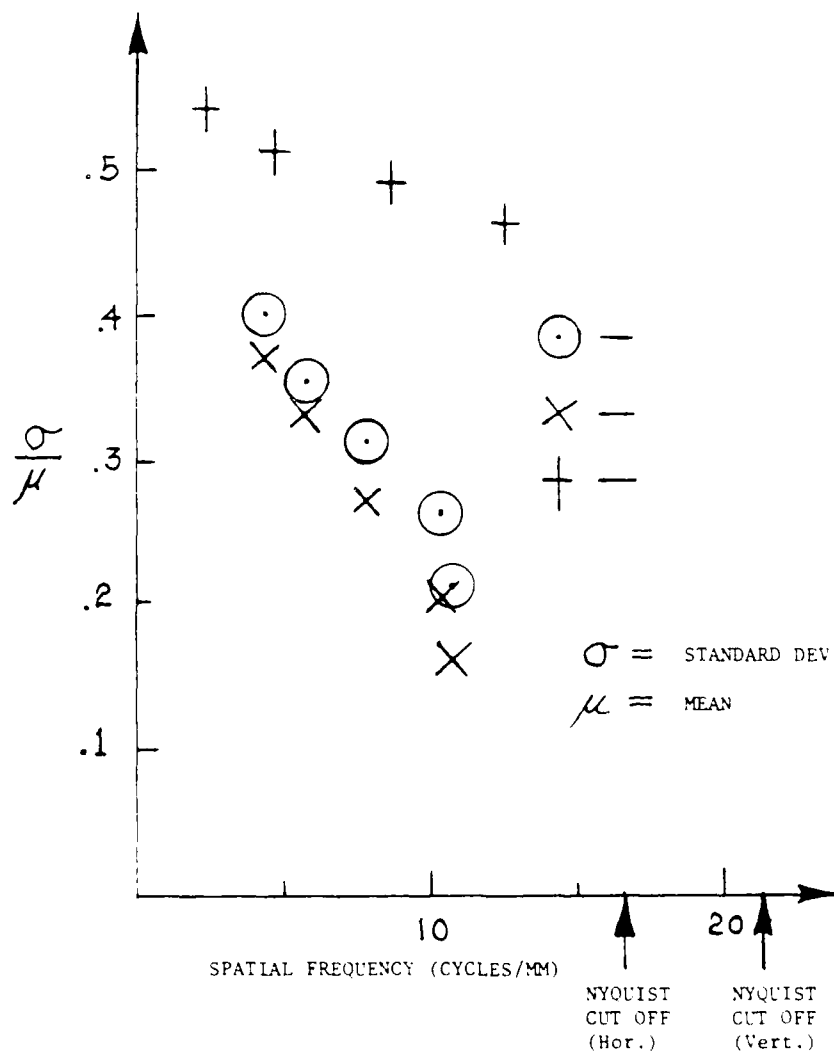


Figure 2. Raw MTF Data For The Fairchild 3000 Camera

from the target. Each camera frame provided 512×488 pixels of speckle data that frame was subdivided in twelve 128×128 subframes. These subframes were averaged to produce an estimate of the FM of a square aperture. First attempts to match the expected FM failed due to programming bugs. Once these were corrected the FM shown in Fig. 3 was obtained. It shows reasonably good agreement with the expected sinc function except for a low frequency "hump", that causes it to be slightly raised. Also there is a lack of amplitude symmetry due to the differences in the MTF associated with the two axes. Although they aren't easily seen in Fig. 3, significant noise and camera artifacts were observed along crosssections taken along the axes. The artifacts could possibly contribute to the low frequency hump, this is expected theoretically to be associated with any spurious terms near zero frequency. Effects of the noise were partially mitigated using Wiener filtering.

VI. Image Reconstruction

Once a reasonable approximation to the FM was obtained for the square, it was expected that a reasonable estimate of the target image could be recovered using phase retrieval algorithms. However, a more complex object than the square was needed to provide evidence that the IC approach was working. Fig. 4 shows a more convincing case. The target selected is shown Fig 4(a), it is asymmetric, consisting of a triangle and a circular disk with a "bite" out of it. (The asymmetry and the separated support normally resulted in good reconstructions during the previous simulations). Fig. 4(b) shows the FM

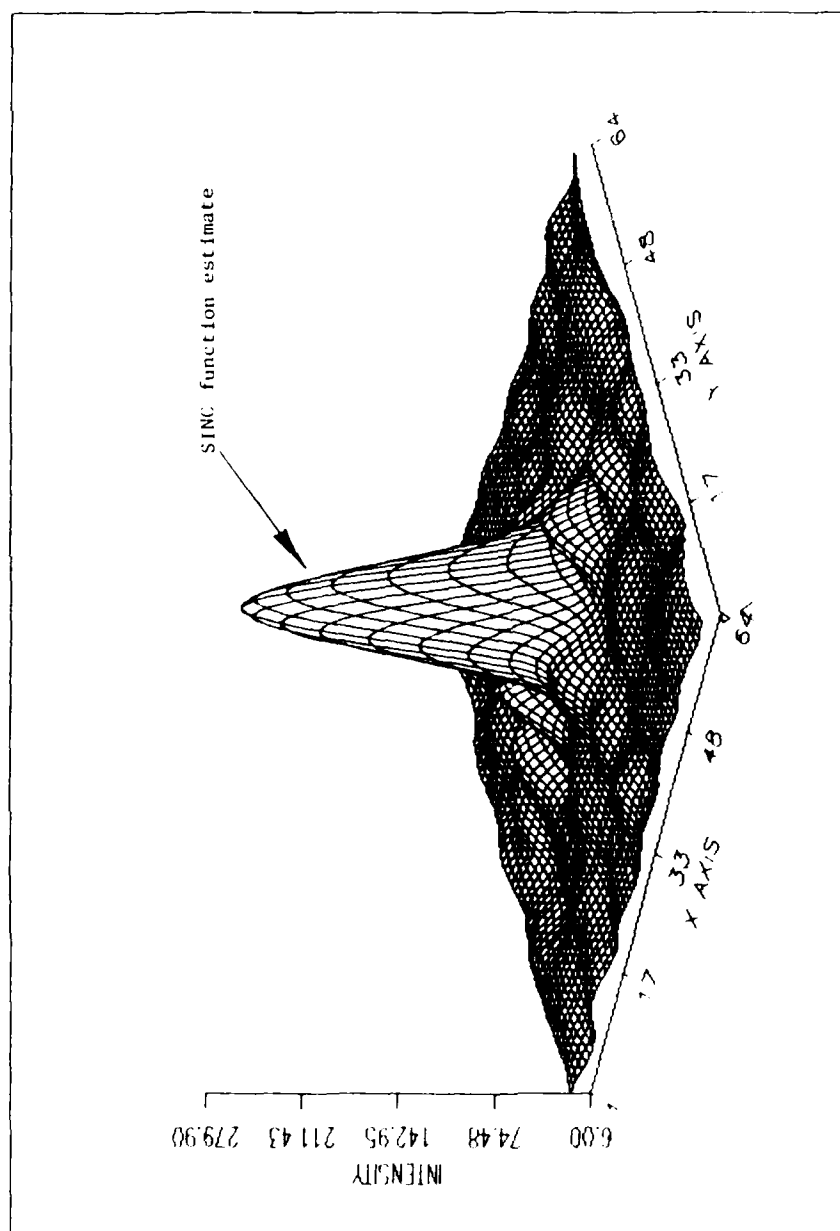


Figure 3. Estimate of the SINC function. Note the function is raised and sitting on a low frequency "hump".

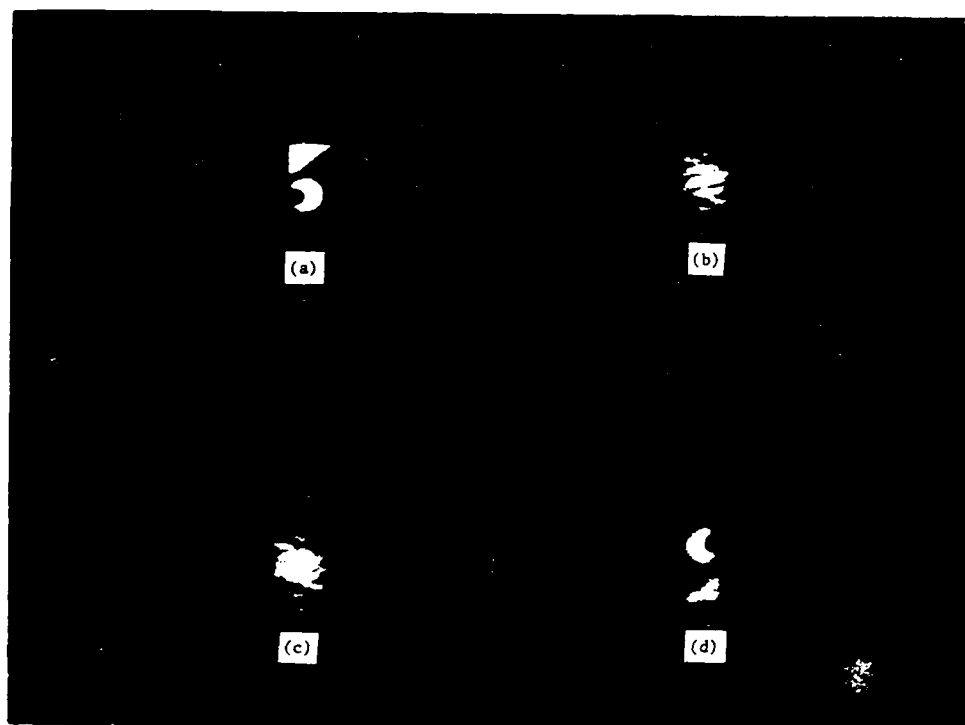


Figure 4. (a) Original test object, (b) the estimated Fourier modulus, (c) the Fourier modulus after Wiener filtering and (d) the reconstructed object estimated from phase retrieval algorithms.

modulus, 4(c) shows the FM modulus with its noise reduced by a Weiner Filter and Fig. 4(d) shows the estimated image. Approximately 1200 subframes were used to obtain this quality of reconstruction. A detailed look at the edge response of the recovered image suggests a resolution spot size that is about twice diffraction limited.

VII. Conclusions and Recommendations

It can be concluded that IC works well on targets that do not significantly depolarize the beam. However, more experimental research is needed. Suggestions for future research include:

- i) More practical target surfaces need to be tested especially targets that depolarize the beam
- ii) Experiments need to be designed to test the aberration correcting potential of correlography.
- iii) Successful laboratory testing indicates that small scale field test planning should begin as soon as possible to integrate smoothly from laboratory to large scale testing.
- iv) Other camera types should be investigated especially cameras equipped with the image intensifiers needed in practical applications
- v) More testing of phase retrieval algorithms is needed; especially experiments that make good use of additional image information such that might also provide phase estimates of the Fourier transform, such additional information might be available in blurred images.

v1) Design of optimal filters that used improved noise estimates would appear to be quite helpful. The parameters used in the Weiner filtering in the experiments were based on poor estimates yet the image quality improvement was quite significant.

References

1. Idell P.S. and J. R. Fienup, "Image Synthesis From Nonimaged Laser Light", submitted for publication in Opt. Let., May 1987.
2. Dainty J.C. (ed.), Laser Speckle and Related Phenomena, 2nd edition, Topics in Applied Physics, Vol. 9, Springer, Berlin, 1982.
3. Gold Fischer, L.I., "Autocorrelation Function and Power Spectral Density of Laser-Produced Speckle Patterns", J. Opt. Soc. Am., Vol 55, P. 247-253, 1965.
4. Bracewell, R.N., The Fourier Transform and its Applications, McGraw Hill (San Francisco), P. 115, 1978.
5. Fienup J.R., "Reconstruction of an Object From the modulus of its Fourier Transform", Opt. Let., Vol 3, P. 27-29, 1978.
6. Fienup J.R., "Phase Retrieval Algorithms: A Comparison", Appl. Opt., Vol 21, P. 2758-2769, 1982.
7. Fienup J.R., and W.C. Wackerman, "Phase Retrieval Stagnation Problems and Solutions", J. Opt. Soc. Am. A, Vol 3, P. 1897-1907, 1986.
8. Goodman J. W. et al, "Wavefront - Reconstruction Imaging through Random Media, App. Phy. Let., Vol. 8, P. 311, 1966.

1987 USAF-UES SUMMER FACULTY RESEARCH PROGRAM/
GRADUATE STUDENT SUMMER SUPPORT PROGRAM

Sponsored by the
AIR FORCE OFFICE OF SCIENTIFIC RESEARCH

Conducted by the
Universal Energy Systems, Inc.

FINAL REPORT

A Study of the Electrochemical Behavior of Trihalide Ions
Containing Bromine and Chlorine in Melts Composed of
Aluminum Chloride and 1-Methyl-3-Ethylimidazolium Chloride

Prepared by:	Lawrence F. Koons
Academic Rank:	Professor
Department and	Chemistry
University:	Tuskegee Institute
Research Location:	Frank J. Seiler Research Laboratory United States Air Force Academy Colorado Springs CO 80840
USAF Research:	Dr. John S. Wilkes
Date:	21 August 1987
Contract No.:	F49620-85-C-0013

A STUDY OF THE ELECTROCHEMICAL BEHAVIOR OF TRIHALIDE IONS
CONTAINING BROMINE AND CHLORINE IN MELTS COMPOSED OF
ALUMINUM CHLORIDE AND 1-METHYL-3-ETHYLIMIDAZOLIUM CHLORIDE

by

Lawrence F. Koons

ABSTRACT

Cyclic voltammetry was used to study the properties of trihalide ions in the title system. The formation constant of the tribromide ion was estimated to be of the order of 1000. The chloride ion exchanges with bromide ion on the tribromide ion to form the dibromomonochloride ion. The tribromide ion is oxidized at a potential more positive than is bromine ion; it is reduced at a potential more negative than is bromine. The reduction of the tribromide ion at tungsten electrodes may occur through an intermediate with a lifetime of the order of seconds. The tribromide ion and Br_2Cl^- are oxidized at approximately the same potential and they are reduced at approximately the same potential. The Cl_2Br^- ion is oxidized at approximately the same potential as is the chloride ion. It is reduced at a potential 0.2 V more positive than is the Br_3^- ion.

ACKNOWLEDGEMENTS

The author wishes to acknowledge the support and assistance of the Air Force Systems Command, the Air Force Office of Scientific Research, United Energy Systems and, in particular, the personnel of the Frank J. Seiler Research Laboratory of the United States Air Force Academy.

I. INTRODUCTION

Systems composed of aluminum chloride and 1-methyl-3-ethylimidazolium chloride (MEIC) are important members of a general class of mixtures of aluminum halides and nitrogen-containing organic salts that have freezing points below normal room temperature. One of their several possible potential applications is their use as electrolytes in batteries.(1) Among the types of information required for that application is knowledge of the behavior of practically useful electrode systems in these melts. A likely such system for the cathode is the bromine/bromide couple at an inert electrode.

For this reason workers at the Seiler Laboratory are in the process of determining the properties of bromine and the bromide ion in the indicated salt system by a variety of modern techniques, including electrochemical ones. Most of the research that I have done and supervised has involved electrochemistry, in particular the study of electrode processes by means of polarography and related potential-sweep methods. When I served as a Summer Faculty Research Participant at Seiler Laboratory in 1985 I studied the bromine/bromide couple, primarily by means of cyclic voltammetry. The results of the study showed that the trihalide ions are intimately involved in the electrode processes in which bromine and bromide take part. There were features that consistently appeared on the current-voltage curves obtained then, but for which unambiguous interpretations were not obtained. The work done this summer was a systematic extension of the previous work, done in an attempt to resolve the ambiguities.

II. OBJECTIVES OF THE RESEARCH EFFORT

Cyclic voltammetry had been used previously to study the electrochemical behavior of the bromine/bromide couple in the melts.(2) In general there were several cathodic and several anodic waves that appeared on the cyclic voltammograms obtained with these systems. The assignment of these features to various electrode reactions was done largely on the basis of indirect evidence but there remained some ambiguity and even certain inconsistencies. The prior results were obtained on systems to which various combinations of bromine, bromide and chloride had been added in controlled amounts. Although the possibilities of this approach had not been exhausted, the fact that stable salts of the trihalide ions exist offered the possibility of doing potentially more definitive experiments. That is studying by cyclic voltammetry the electrochemistry of these ions after their addition as such to the melts. This would result in there being fewer variables to take into consideration in the interpretation of the results. Thus in the experimental sense, the objective of the research was to obtain cyclic voltammograms on melts to which salts of the tribromide, dibromochloride and monobromodichloride ions would be added, alone or in combination with bromide or chloride ions or bromine. The ultimate objective was to be able to infer from the results of these experiments, plus those of previous experiments, to what reactions the features on the voltammograms correspond, and thus in what form bromine exists in the melts.

III. STUDY OF THE INTERACTION OF BROMINE WITH BROMIDE AND CHLORIDE IONS IN MEIC/ AlCl_3 MELTS

Methods were found in the literature for the synthesis of tetra-alkylammonium salts of the Br_3^- , Br_2Cl^- and BrCl_2^- ions (3). The synthesis of tetramethylammonium tribromide was straightforward. That of tetramethylammonium monobromodichloride required some empirical modification of the procedure, but posed no real problem. The synthesis of tetraethylammonium dibromochloride was not achieved in a practical sense. The given procedure called for simply exposing tetraethylammonium chloride to an excess of bromine vapor whereupon $\text{Et}_4\text{NBr}_6\text{Cl}$ would be formed. This compound was reported to lose bromine on storage to form the desired compound. In fact one batch of a few milligrams of $\text{Et}_4\text{NBr}_2\text{Cl}$ was obtained. All other attempts to prepare it, including several variations on the given procedure, led to the formation of a substance that appeared homogeneous but which melted over a range of several degrees that was between the reported melting point of the desired product and that of its precursor. Nevertheless insight on the Cl_2/Br^- system was obtained from data from experiments on melts to which bromine and chloride salts were added and their comparison with those of systems for which the salts of the trihalide ions were obtained.

Many apparent ambiguities in the results of previous experiments were resolved by a series of cyclic-voltammetry experiments in which a trihalide salt, halide salts or bromine were added in various combina-

tions to neutral melts. A neutral melt is one that contains equivalent amounts of chloride ions and aluminum chloride.

It is essential that neither of these be in excess of the other by amounts comparable to or greater than the amount (in moles) of the substances to be added. Precise neutrality can be achieved by the addition, in small portions, of aluminum chloride to a slightly basic (excess chloride ion) melt until the waves corresponding to the oxidation of Cl^- and the reduction on the reverse sweep of the resultant chlorine are just suppressed. The results of these experiments are now summarized.

Tribromide Ion. When a salt of the tribromide ion is added to a neutral melt at low concentrations (approximately one millimolar) two anodic and two cathodic waves are seen on the CV scans. The first oxidation wave appears as a very gradual increase in anodic current that merges into the prominent second wave. For both oxidation and reduction the magnitude of the second wave relative to that of the first increases with increasing formal Br_3^- concentration. The peak heights of the second waves are proportional to formal Br_3^- concentrations at values thereof greater than a few millimolar. The interpretation of these facts is that the second anodic wave corresponds to the oxidation of Br_3^- to Br_2 and the second cathodic wave corresponds to the reduction of Br_2 formed by the dissociation of Br_3^- and the first anodic wave corresponds to the oxidation of the corresponding Br^- . Additional evidence is provided for this by the fact that the first wave is augmented if there has been a prior sweep in the opposite

direction. If only bromine is added to a neutral melt, both the first and second cathodic waves appear. The first, of course, corresponds to the reduction of bromine. The second corresponds to the reduction of the tribromide ion formed by the reaction between bromine and the bromide ion that results from the first reduction. The appearance of two anodic waves if bromide ion is added to a neutral melt is explained by an exactly analogous argument. Several other lines of evidence support this interpretation. The addition of bromine to a melt containing excess bromide diminishes the first anodic wave and augments the other three waves. When the bromine concentration exceeds the bromide concentration the first oxidation wave is suppressed, the peak height of the first reduction wave increases with increasing bromine concentration and the second waves are only slightly affected. The analogous effect takes place when bromide ion is added to a melt containing bromine. If one assumes that peak heights are proportional to the concentrations of the species reacting at the electrodes it is possible to obtain an estimate of the formation constant of Br_3^- , namely 10^3 .

There is some uncertainty about the nature of the first oxidation wave. On a sweep in the positive direction, following a sweep in the negative direction during which reduction has occurred, this wave is stretched out and shows evidence of being two poorly separated waves. If so the reduction of the bromine or tribromide ion could have produced some species in addition to Br^- , such as Br_2^- . Alternatively there could be two oxidation processes involving Br^- . This seems the

more likely since the first cathodic wave appears to be complex even on the first sweep in the negative direction when only Br^- is present.

Dibromomonochloride ion. Information concerning this species was obtained from experiments in which various combinations of chloride salts and bromine were added to neutral melts. If chloride is added to a melt containing bromine the first reduction wave diminishes as chloride is added and is suppressed when added chloride is equivalent in amount to bromine. The slight shift in the potential of the second reduction wave as chloride is added, but the observation that there is little other evident change, imply that Br_3^- and Br_2Cl^- are reduced at potentials too close together for the corresponding waves to be distinguished, one from the other. The slight appearance of the apparent bromide-oxidation wave on the reverse sweep is evidence for the formation of Br^- upon the reduction of Br_2Cl^- . As more chloride is added there appears an oxidation wave that gets larger with increasing amount of added chloride until chloride is in excess. This apparently corresponds to the oxidation of Br_2Cl^- . When the amount of added chloride approaches equivalence to the amount of bromine, an anodic wave that increases with increasing amount of chloride appears at a more positive potential. It must result from the oxidation of chloride ion.

The addition of bromine to a melt containing chloride causes the appearance of the cathodic wave attributed to the reduction of Br_2Cl^- . Its peak height increases with increasing amount of bromine until the bromine is in excess, at which time the cathodic wave corresponding to

the reduction of bromine appears. Also as bromine is added the peak height of the aforementioned wave attributed to the oxidation of Br_2Cl^- increases and that of the peak corresponding to the oxidation of chloride diminishes. If again it is assumed that peak height is a measure of concentration it may be estimated that the formation constant of Br_2Cl^- is approximately 800. Experiments in which chloride, then bromine were added to a melt originally containing added tribromide ion yield results that adhere to the same pattern as those just discussed.

Dichloromonobromide ion. When Cl_2Br^- is added to a neutral melt there appears a single anodic wave on an initial sweep in the positive direction. As more Cl_2Br^- is added the peak potential of that wave does not change and its peak height increases proportionally to Cl_2Br^- concentration. The wave must correspond to the oxidation of Cl_2Br^- . It is followed on the reverse sweep by a cathodic wave that is of the same form and at the same potential as the cathodic wave that appears subsequently on reverse cathodic sweeps when an excess of bromide is added. This wave is attributed to the reduction of bromine. If the initial sweep is in the negative direction there is a cathodic wave that shifts to more negative potentials as more Cl_2Br^- is added. Its peak height is proportional to the formal Cl_2Br^- concentration. It must correspond to the reduction of Cl_2Br^- . On the reverse sweep following the appearance of this wave there is a wave that very much resembles the wave attributed to the oxidation of Br_3^- . An additional small wave that appears on the negative side of the described cathodic wave is

tentatively ascribed to the reduction of Br_2Cl^- . Its size is augmented by the addition of Br^- . The addition of a large excess of Br^- also increases the size of the wave attributed to the reduction of Br_3^- or Br_2Cl^- at the expense of the size of the one attributed to the reduction of BrCl_2^- .

Basic Melts. A simple experiment done with basic (excess chloride) melts indicates strongly that bromine exists in basic melts as Br_2Cl^- . When Br_3^- was added in small increments to a melt in which the mole fraction of AlCl_3 was 0.45 there was a single cathodic peak, the height of which was proportional to the formal Br_3^- concentration. Then when bromine was added in an amount equivalent to the amount of Br_3^- present, the height of the peak doubled without there being a change in the peak potential or the height of the peak.

One last experiment that provides information about the relative stabilities of Br_3^- and Br_2Cl^- was done. A typical set of scans was obtained with a neutral melt to which Br^- had been added at a concentration of 0.0086 m. When bromine was added at essentially the same concentration the height of the first anodic wave corresponding to the oxidation of bromide fell by 85%. (An estimate of the formation constant of Br_3^- can be obtained from this information. The resultant value is 4×10^3 . A comparison of this with the value of 10^3 given previously provides an indication of the uncertainty.) Then the addition of chloride at the same concentration restored that wave to a peak height of approximately 90% of what it had been before the addition of bromide. The inference is that the chloride replaced the

bromide on the tribromide ion, converting it to Br_2Cl^- . The addition of the chloride also had the effect of shifting the peak of the wave attributed to the reduction of the trihalide ion in the positive direction by 0.15 V. Incidentally these results seem to imply that the formation constants of Br_3^- and Br_2Cl^- are of comparable magnitude, but that of Br_2Cl^- is the larger.

Miscellaneous. Prior to the undertaking of the experiments with the trihalide ions some CV scans were obtained on melts containing bromide ion at relatively high concentrations. (Imidazolium bromide at mole fractions up to 0.10) Their simple configurations are readily explainable in view of the information obtained from the subsequent experiments. If the positive sweep is reversed before chloride starts to be oxidized there are often two sections on the steep cathodic wave, which never actually reaches a peak. The first corresponds to the oxidation of bromide and the second to the oxidation of Br_2Cl^- . On the reverse sweep there is a single cathodic wave that corresponds to the reduction of the Br_2Cl^- formed on the positive sweep.

The results obtained initially in the studies on the trihalide ions were often neither reproducible nor explainable by obvious hypotheses. An examination of several of the scans showed that the problem apparently was a result of the fact that the melts were not rigorously neutral, but contained an excess of aluminum chloride. For example, when trihalide ions were added to the melt there was no anodic wave until the concentration of the trihalide was of the order of several millimolar. Apparently in the titration of the melts to neutral, too

much attention had been paid to the disappearance of the cathodic wave on the return sweep and not enough to the disappearance of the anodic wave corresponding to the oxidation of the chloride ion. Once this was realized the generally consistent results described in the foregoing were obtained.

IV. RECOMMENDATIONS:

Although "generally consistent," the obtained results are essentially qualitative. There is also the fact that no meaningful data were obtained on the basis of the addition of Br_2Cl^- to a neutral melt. Logically an immediate extension of the work could concentrate on the preparation of an authentic sample of a tetraalkylammonium salt of the dibromomonochloride ion. This should not be difficult. Systematic variation of the conditions of debromination of the precursor, accompanied perhaps by analyses of the intermediates, should lead to the obtaining of the desired product without serious complications. (Moreover, although most researchers who have worked with trihalide ions in the past sixty years list the cited article as the source of their methods of synthesis, alternative procedures appear in the literature, e.g. 4,5)

The resolution of the uncertainties and the obtaining of quantitative information appear to be obtainable from modifications under controlled conditions of the described experiments. The measuring of the height of the anodic wave corresponding to the oxidation of bromide ion as bromine is added to a melt containing an

excess of bromide would allow the calculation of the formation constant of the tribromide ion over a range of concentrations. If the values were consistent then one could have some confidence in presenting a value for the constant. If they varied with concentration the nature of the variation would provide information concerning the reasonableness of the presented interpretation of the results presented thus far. An independent determination of the association constant by spectrophotometric methods would appear to be straightforward.

A first step in the resolving of the uncertainty concerning the wave(s) attributed to the oxidation of the bromide ion would be the determination of the effect thereon of successive small changes in the limiting potential of the negative sweep prior to its (their) appearance. Probably the simplest approach to the testing of the hypothesis concerning the nature of the reduction waves obtained when the BrCl_2^- ion is added to neutral melts would be to determine the properties of the waves obtained when both Br_2Cl^- and BrCl_2^- ions are added to melts as the ratio of the amount of one to the other is varied continuously. It is also possible that information on both of these matters could be obtained from investigating the effect of scan rate on the CV features. If the possible dual nature of the anodic wave ascribed to the oxidation of bromide is caused by an unstable intermediate the relative importance of the contribution of each step should vary with scan rate. In the case of the Cl_2Br^- , if the anodic wave at the most negative potential is due to the reduction of ClBr_2^- and the latter exists as the result of the replacement of Cl^- by Br^-

generated in the prior reduction, there might be achievably large scan rates at which the wave following the generation of Br^- would be relatively less important.

REFERENCES

1. Floreani, D., D. Stech, J. Wilkes, J. Williams, B. Piersma, L. King and R. Vaughn, "A New Class of Molten Salts for Room-Temperature Battery Applications," Proc. 30th Power Source Symp., June 1982, The Electrochemical Society.
2. Koons, L., "A Study of the Electrochemical Behavior of the Bromine/Bromide Couple in Melts Composed of Aluminum Chloride and 1-Methyl-3-Ethylimidazolium Chloride " Final Report 1985 USAF-UES Summer Faculty Research Program.
3. Chattaway, F. D. and G. Hoyle, "Perhalides of Quaternary Ammonium Salts," J. Chem. Soc., 1923, 123, 654.
4. Rozinov, V. G., "The Reduction of Phosphorus Pentachloride by Tetraalkylammonium Halides and Tetraorganylphosphonium Halides," Zh. Obshch. Khim., 1986, 50 (6), 1414.
5. Buckles, R. E., A. I. Popov, W. F. Zelzny, and R. J. Smith, "A Spectrophotometric Study of Tetrabutylammonium Tribromide," J. Am. Chem. Soc., 1951, 73, 4525.

1987 USAF-UES SUMMER FACULTY RESEARCH PROGRAM,
GRADUATE STUDENT SUMMER SUPPORT PROGRAM

Sponsored by the
AIR FORCE OFFICE OF SCIENTIFIC RESEARCH

Conducted by the
Universal Energy Systems, Inc.

FINAL REPORT

SEMIEMPIRICAL CALCULATION OF NON-LINEAR OPTICAL PROPERTIES

Prepared by:	Dr. Henry A. Kurtz
Academic Rank:	Assistant Professor
Department and	Department of Chemistry
University:	Memphis State University
Research Location:	FJSRL/NC USAF Academy Colorado Springs, CO
USAF Researcher:	Major Kenneth Dieter
Date:	August 25, 1987
Contract No:	F49620-85-C-0013

SEMIEMPIRICAL CALCULATIONS OF NON-LINEAR OPTICAL PROPERTIES

by

Dr. Henry A. Kurtz

ABSTRACT

The MOPAC semiempirical electronic structure program was modified to calculate the polarizability and first and second hyperpolarizabilities for molecules. A finite field approach was used based on both energy and induced dipole expansion. Test calculations were done on a series of mono- and di-substituted benzenes.

ACKNOWLEDGEMENTS

I wish to thank the Air Force Systems Command and the Air Force Office of Scientific Research for sponsorship of this research and Universal Energy Systems for administrating and directing the SFRP program. I also would like to express my thanks to all the members of the F. J. Seiler Research Laboratory for making my stay so pleasant.

I. INTRODUCTION:

The polarization, P , induced in a medium by an external electric field F is given by

$$P = P_0 + \chi^{(1)} \cdot F + \chi^{(2)} \cdot F \cdot F + \chi^{(3)} \cdot F \cdot F \cdot F + \dots \quad (1)$$

where $\chi^{(n)}$ is the n^{th} order susceptibility tensor of the bulk medium. The bulk susceptibilities can be expressed in terms of the molecular induced dipole. The dipole moment of a system interacting with an electric field can be written

$$\mu_i = \mu_i^0 + \alpha_{ij} F_j + (1/2) \beta_{ijk} F_j F_k + (1/6) \gamma_{ijkl} F_j F_k F_l + \dots \quad (2)$$

where μ^0 is the permanent dipole moment and α_{ij} , β_{ijk} , and γ_{ijkl} are tensor elements of the linear polarizability and the first and second hyperpolarizabilities, respectively, of the molecule. The second order term gives rise to sum and difference frequency mixing (including second harmonic generation) and optical rectification. The third order term is responsible for third harmonic generation and two-photon resonances. Typical applications where these nonlinear effects are important include amplification, high-resolution spectroscopy, picosecond pulse generation, infrared image conversion, image transmission through optical fibers, optical processing, and information transfer in general.

II. OBJECTIVE OF THE RESEARCH EFFORT:

My assignment as a participant in the 1987 Summer Faculty Research Program (SFRP) was to develop the computer software to calculate first and second hyperpolarizabilities for molecules. This software was to be incorporated into the MOPAC program for performing semiempirical electronic structure calculations. This

program was written by Dr. James J. P. Stewart of the F. J. Seiler Laboratory at the USAF Academy.

III. THEORY FOR CALCULATING POLARIZABILITIES:

The energy of a system in an electric field is given by

$$E(F) = E(0) - \mu_i F_i - (1/2!) \alpha_{ij} F_i F_j - (1/3!) \beta_{ijk} F_i F_j F_k - (1/4!) \gamma_{ijkl} F_i F_j F_k F_l - \dots \quad (3)$$

The above equation contains implied sums over repeated indices and $E(0)$ is the energy with no field present.

If the molecule is considered to be in a uniform electric field aligned along one of the axis of the system, F_i (i.e., $[F_x, 0, 0]$ or $[0, F_y, 0]$), the values of the polarizabilities along that axis (μ_i , α_{ii} , β_{iii} , and γ_{iiii}) can be obtained. For this case the energy expression reduces to

$$E(F_i) = E(0) - \mu_i F_i - (1/2) \alpha_{ii} F_i^2 - (1/6) \beta_{iii} F_i^3 - (1/24) \gamma_{iiii} F_i^4 - \dots \quad (4)$$

By truncating this expression after the F^4 term and evaluating the energy at four field strengths ($\pm F_i, \pm 2F_i$), there are four equations in four unknowns. These unknowns can be solved for explicitly and the results are

$$\mu_i F_i = -(2/3)[E(F_i) - E(-F_i)] + (1/12)[E(2F_i) - E(-2F_i)] \quad (5.1)$$

$$\alpha_{ii} F_i^2 = (5/2)E(0) - (4/3)[E(F_i) + E(-F_i)] + (1/12)[E(2F_i) + E(-2F_i)] \quad (5.2)$$

$$\beta_{iii} F_i^3 = [E(F_i) - E(-F_i)] - (1/2)[E(2F_i) - E(-2F_i)] \quad (5.3)$$

$$\gamma_{iiii} F_i^4 = -6E(0) + 4[E(F_i) + E(-F_i)] - [E(2F_i) + E(-2F_i)] \quad (5.4)$$

These are the same equations as found in the paper of Bartlett and Purvis (1979) with several errors corrected.

To try to improve the accuracy, terms through F^6 in the energy expansion can be kept. If fields of $\pm F_i$, $\pm 2F_i$, and $\pm 3F_i$ are used the following expressions are obtained

$$\mu_i F_i = -(3/4)[E(F_i) - E(-F_i)] + (3/20)[E(2F_i) - E(-2F_i)] - (1/60)[E(3F_i) - E(-3F_i)] \quad (6.1)$$

$$\alpha_{iii} F_i^2 = (49/18)E(0) - (3/2)[E(F_i) + E(-F_i)] \\ + (3/20)[E(2F_i) + E(-2F_i)] - (1/90)[E(3F_i) + E(-3F_i)] \quad (6.2)$$

$$\beta_{iii} F_i^3 = (13/8)[E(F_i) - E(-F_i)] - [E(2F_i) - E(-2F_i)] + (1/8)[E(3F_i) - E(-3F_i)] \quad (6.3)$$

$$\gamma_{iiii} F_i^4 = -(28/3)E(0) + (13/2)[E(F_i) + E(-F_i)] \\ - 2[E(2F_i) + E(-2F_i)] + (1/6)[E(3F_i) + E(-3F_i)] \quad (6.4)$$

The other components of the polarizabilities are also important. It is necessary to calculate the values of α_{ij} to verify rotational invariance and to find the principal "optical" axes. The values of β_{ijj} and γ_{ijj} are needed for a comparison with experimental quantities. To obtain these "off-diagonal" components with only two different indices (i and j) electric fields are applied in the ij plane along a 45° line between axis i and axis j. In this case the energy expression is

$$E(F_i, F_j) = E(0) - \mu_i F_i - \mu_j F_j - (1/2)\alpha_{iii} F_i^2 - (1/2)\alpha_{jjj} F_j^2 - \alpha_{ij} F_i F_j \\ - (1/6)\beta_{iii} F_i^3 - (1/6)\beta_{jjj} F_j^3 - (1/2)\beta_{ijj} F_i F_j^2 - (1/2)\beta_{jii} F_j F_i^2 \\ - (1/24)\gamma_{iiii} F_i^4 - (1/24)\gamma_{jjjj} F_j^4 \\ - (1/6)\gamma_{ijjj} F_i F_j^3 - (1/6)\gamma_{jiii} F_j F_i^3 - (1/4)\gamma_{iijj} F_i^2 F_j^2 \quad (7)$$

If the "diagonal" calculations have already been done, then there are only 6 unknowns in this expression. By using the results of energy calculations at (F_i, F_j) , $(F_i, -F_j)$,

$(-F_i, F_j)$, $(-F_i, -F_j)$, it is possible to solve for 4 of the unknowns. The results of the manipulations of the energy expressions are

$$\begin{aligned} \alpha_{ij} F_i F_j = & (1/48)[E(2F_i, 2F_j) - E(2F_i, -2F_j) - E(-2F_i, 2F_j) + E(-2F_i, -2F_j)] \\ & - (1/3)[E(F_i, F_j) - E(F_i, -F_j) - E(-F_i, F_j) + E(-F_i, -F_j)] \end{aligned} \quad (8.1)$$

$$\begin{aligned} \beta_{ijj} F_i F_j^2 = & (1/2)[E(-F_i, -F_j) - E(F_i, F_j) + E(-F_i, F_j) - E(F_i, -F_j)] \\ & + [E(F_i) - E(-F_i)] \end{aligned} \quad (8.2)$$

$$\begin{aligned} \gamma_{ijj} F_i^2 F_j^2 = & -4E(0) - [E(F_i, F_j) + E(-F_i, -F_j) + E(F_i, -F_j) + E(-F_i, F_j)] \\ & + 2[E(F_i) + E(-F_i)] + 2[E(F_j) + E(-F_j)] \end{aligned} \quad (8.3)$$

Further calculations must be done to solve for γ_{ijjj} and γ_{jjjj} .

The above equations for the polarizabilities and hyperpolarizabilities are all given in terms of the total energy of the system (with various fields). It is important to note that all the expressions are unchanged by addition of a constant to the energy. For this reason the heats of formation provided by the MOPAC program can be used instead of total energies and still obtain the correct results.

An alternate method for obtaining the polarizability and hyperpolarizabilities is to use the equation for the induced dipole moment instead of the energy. By using the value of the dipole at various field strengths the following equations can be derived.

$$\mu_i = (2/3)[\mu_i(F_i) + \mu_i(-F_i)] - (1/6)[\mu_i(2F_i) + \mu_i(-2F_i)] \quad (9.1)$$

$$\alpha_{ii} F_i = (2/3)[\mu_i(F_i) - \mu_i(-F_i)] - (1/12)[\mu_i(2F_i) - \mu_i(-2F_i)] \quad (9.2)$$

$$\alpha_{ij} F_j = (2/3)[\mu_i(F_j) - \mu_i(-F_j)] - (1/12)[\mu_i(2F_j) - \mu_i(-2F_j)] \quad (9.3)$$

$$\beta_{iii} F_i^2 = (1/3)[\mu_i(2F_i) + \mu_i(-2F_i) - \mu_i(F_i) - \mu_i(-F_i)] \quad (9.4)$$

$$\beta_{ijj} F_j^2 = (1/3)[\mu_i(2F_j) + \mu_i(-2F_j) - \mu_i(F_j) - \mu_i(-F_j)] \quad (9.5)$$

$$\gamma_{iiii} F_i^3 = (1/2)[\mu_i(2F_i) - \mu_i(-2F_i)] - [\mu_i(F_i) - \mu_i(-F_i)] \quad (9.6)$$

$$\gamma_{iijj} F_i F_j^2 = (1/2)[\mu_i(F_i, F_j) - \mu_i(-F_i, F_j) + \mu_i(F_i, -F_j) - \mu_i(-F_i, -F_j)] \\ - [\mu_i(F_i) - \mu_i(-F_i)] \quad (9)$$

These expressions are similar to those recently published by Williams (1987).

All three methods (the F^4 energy expansion, the F^6 energy expansion and the F^3 dipole expansion) have been implemented in the MOPAC program. For the F^3 dipole method, the γ_{iijj} terms are currently left out but are being added. In the early part of this study, a comparison of the results provided a check on the equations derived. All methods give essentially the same results and because of the larger number of calculations needed for the F^6 energy method, it is probably not cost effective for routine calculations. Only the axial components are currently computed with the F^6 energy method.

IV. RESULTS

Once all the components of the hyperpolarizabilities have been obtained it is necessary to convert them into "experimental" quantities. For the second hyperpolarizability, the quantity of interest is the mean value given by

$$\gamma = 1/5 \{ \gamma_{xxxx} + \gamma_{yyyy} + \gamma_{zzzz} + 2[\gamma_{xxyy} + \gamma_{xxzz} + \gamma_{yyzz}] \} \quad (10)$$

For the first hyperpolarizability, β , the vector component along the dipole moment is important. If the principle symmetry axis (and dipole moment) lie along the x axis, the hyperpolarizability is given by

$$\beta_x = 3/5 \{ \beta_{xxx} + \beta_{xyy} + \beta_{xzz} \} \quad (11)$$

If the dipole moment does not lie along one of the computational axes, the quantity of interest is

$$\beta_{\mu} = (3/5)(\beta \cdot \mu) / \|\mu\| \quad (12)$$

where $\beta \cdot \mu = \beta_x \mu_x + \beta_y \mu_y + \beta_z \mu_z$.

Test calculations were performed on substituted benzenes. Initially, results for benzene were obtained for reference. These are shown in Table I. All the first hyperpolarizability components are zero as the molecule has a center of symmetry. Next, calculations were performed on a series of mono-substituted benzenes and the results are summarized in Tables II, III, and IV. The molecular geometries used were chosen by the program such that the moments of inertia were aligned along the x, y, and z directions. All calculations were done with the MNDO Hamiltonian at the MNDO optimized geometries, except nitrobenzene. The geometry used for nitrobenzene was an AM1 optimized geometry.

For these singly substituted systems, the sign of the second hyperpolarizability is indicative of whether the group is electron withdrawing or donating. The electron withdrawing groups (CN and NO₂) have positive β while the electron donating groups (F, OH, NH₂) have negative β .

Further test calculations were done for a system with both an electron withdrawing and a donating group: nitroaniline. These results are shown in TABLE IV. This is a good test case because the nonlinear effects are quite large and there is experimental data with which to compare. It is clear that for systems like these where charge transfer is important, a better description of the molecule is needed such as a CI treatment.

V. POLYMER APPLICATIONS

Using the methodology developed in this work the only way to treat polymers is by studying oligmers of increasing size. The convergence of any properties of interest with oligmer size can be monitored. The infinite system methods within the MOPAC program are not applicable because the addition of the electric field along the polymer direction destroys the periodic boundary conditions. If the field is held perpendicular to the direction of a 1-D polymer, then the perpendicular components of the various polarizabilities can be calculated. However, these are not usually the ones of interest. Shown in TABLE VI are some very preliminary results on the polarizabilities of idealized all trans forms of polyacetylene and polydiacetylene. As these molecules all possess a center of symmetry it was not possible to study the first hyperpolarizability.

VI. RECOMMENDATIONS

The first recommendation is that the subroutines for the calculation of the hyperpolarizabilities become a part of the new release of the MOPAC program. This program can be used to calculate reasonably accurate static polarizabilities and first hyperpolarizabilities (β). Applications to molecules of Air Force interest should be carried out. For example, the program can be used to assess the magnitude of the nonlinear effects in poly(benzobisoxazole) [PBO] and poly(benzobisthiazole) [PBT].

Further research is needed in a couple of areas. For polymers, a methodology is needed that will allow the calculation of the hyperpolarizabilities in conjunction with the polymer capabilities of the MOPAC program. A potential solution to this problem lies in using a sum-over-states method. This method can be implemented in the MOPAC method using the configuration interaction capabilities already a part of the program. Another method, and potentially more general procedure, would be to use a polarization propagator method (Oddershede 1986).

The other important development is to calculate the frequency dependent hyperpolarizabilities. This is most easily done using a sum-over-states methods, mentioned in the above section. In calculating frequency dependent second hyperpolarizabilities, $\gamma(-\omega_0; \omega_1, \omega_2, \omega_3)$, the importance of the vibrational contributions depends on the process envisioned. For example, for third harmonic generation (THG), the vibrational contribution to $\gamma(-3\omega; \omega, \omega, \omega)$ is quite small but for electric-field-induced second harmonic generation (ESHG) the vibrational part of $\gamma(-2\omega; \omega, \omega, 0)$ may be large (Lu and Sheldon, 1987).

Further work also needs to be done with regard to the static second hyperpolarizability (γ). The electronic contribution to the hyperpolarizability can be broken down into two contributions - an atomic contribution and a bond contribution. Dewar and Stewart (1984) showed that the MNDO method could be made to give quite accurate polarizabilities by computing an atomic correction factor. This same approach should be applicable to γ . The main effort here is a thorough literature search to find a set of accurate experimental data.

TABLE I
Benzene Results

Polarizability		Second Hyperpolarizability	
xx	89.06	xxxx	1835.7
yy	89.06	yyyy	1835.7
zz	28.17	zzzz	16.7
		xxyy	612.0
α (a.u.)	68.43	xxzz	532.4
$\alpha(\text{\AA}^3)$	10.14	yyzz	532.3
		γ (a.u.)	1408.3
		$\gamma(10^{-36}\text{esu})$	0.71
Exp ^a	10.33	Exp ^b	2.06

^aDewar and Stewart 1984 ^bWilliams 1987

TABLE II
Mono-substituted Benzenes

	F	CN	OH	NO ₂	NH ₂
Dipole Moments					
x	0.7695	-1.3151	0.1017	-2.0407	-0.0616
y	0.0	0.0	0.4468	0.0	0.0025
z	0.0	0.0	-0.0009	-0.0002	0.5727
μ_{tot} (au)	0.7695	1.3151	0.4582	2.0407	0.5760
(D)	1.9557	3.3424	1.1645	5.1866	1.4640
Polarizability					
xx	92.80	130.37	103.26	119.919	112.545
yy	89.19	93.58	93.30	112.209	97.925
zz	28.07	33.50	30.05	33.801	33.968
xy	0.0	0.0	-1.94	0.0	-0.001
xz	0.0	0.0	0.01	-0.004	-1.885
yz	0.0	0.0	0.0	-0.024	-0.017
α_{iso} (au)	70.02	85.82	75.54	88.64	81.48
(\AA^3)	10.38	12.72	11.19	13.14	12.07

TABLE II
First Hyperpolarizabilities (β)

	F	CN	OH	NO ₂	NH ₂
xxx	-135.166	-116.483	-274.088	-165.222	-378.541
xyy	8.411	22.166	21.771	90.322	23.689
xzz	1.773	12.280	-1.363	1.232	-5.718
yyy	0.0	0.0	-5.841	0.0	-0.116
yxx	0.0	0.0	-12.103	0.0	-0.186
yyz	0.0	0.0	-2.427	0.0	0.042
zzz	0.0	0.0	0.004	0.0	-2.390
zxx	0.0	0.0	0.058	0.0	-66.247
zyy	0.0	0.0	0.010	0.0	6.440
β_x	-47.989	-49.222	-252.208	-44.201	-360.570
β_y		-20.371		-0.260	
β_z					-75.077
β_μ (a)	-74.989	49.222	-53.644	44.201	-113.205
(b)	-0.65	0.43	-0.46	0.38	-0.98
β_{exp} (b,c)	0.53	0.48	0.17	2.3	1.23
(b,d)	0.44			2.0	0.89

(a) atomic units (b) 10^{-30} esu (c) Zyss (1979) (d) Levine and Bethea (1975)

TABLE III
Second Hyperpolarizabilities (γ)

	F	CN	OH	NO ₂	NH ₂
xxxx	5666.3	23769.3	10752.6	32026.3	21368.3
yyyy	2110.0	1874.4	1808.1	310.1	1855.7
zzzz	17.9	12.2	19.7	17.8	29.2
xyyy	-102.9	-407.2	-523.3	-1252.1	-644.5
xxzz	581.6	565.1	709.3	574.1	1006.8
yyzz	561.6	511.1	561.4	539.4	535.0

γ (a) 1975.0 5398.8 2815.0 6415.4 5009.6
(b) 1.00 2.73 1.42 3.24 2.53

(a) atomic units (b) 10^{-36} esu

TABLE IV
Nitroaniline Results

		Para	Meta	Ortho
Beta ($\times 10^{30}$ esu)				
MNDO	SCF	5.82	1.85	1.14
AMI	SCF	5.42	1.59	0.80
Exp (a)		21.1	4.2	6.4
Gamma ($\times 10^{36}$ esu)				
MNDO	SCF	9.14	5.25	4.42
AMI	SCF	8.52	4.81	4.07

(a) Levine (1976)

TABLE V
Oligomer Polarizabilities

number of units	ΔH_f^a	$\Delta H_f/\text{unit}^a$	α^b	α/unit^b
Polyacetylene				
3	42.562	-	90.736	-
4	56.115	13.553	131.877	41.142
5	69.666	13.551	177.183	45.306
Polydiacetylene				
2	130.439	-	155.916	-
3	187.952	57.513	240.713	84.797
4	245.474	57.522	330.169	89.456

^akcal/mole ^batomic units

REFERENCES

- Bartlett, R. J. and Purvis, G. D., "Molecular Hyperpolarizabilities. I. Theoretical Calculations Including Correlation", Phys. Rev. A Vol 20, 1979 pp 1313-1322.
- Dewar, M. J. S. and Stewart, J. J. P., "A New Procedure for Calculating Molecular Polarizabilities: Applications Using MNDO", Chem. Phys. Lett. Vol 111, 1984 pp 416-420.
- Levine, B. F. "Donor-Acceptor Charge Transfer Contributions to the Second Order Hyperpolarizability", Chem. Phys. Lett., Vol. 37, 1976 pp 516-520.
- Levine, B. F. and Bethea, C. G., "Second and Third Order Hyperpolarizabilities of Organic Molecules", J. Chem. Phys., Vol. 63, 1975 pp 2666-2682.
- Liu, Z. and Shelton, D. P., "Vibrational Contributions to the Second Hyperpolarizability of CH₄", J. Chem. Phys., Vol. 87, 1987 pp 1967-1976.
- Oddershede, J., "Propagator Methods", Adv. Chem. Phys. vol 69, 1986 pp 201-239.
- Williams, G. R. J., "Finite Field Calculations of Molecular Polarizability and Hyperpolarizabilities for Organic π -Electron Systems", J. Molec. Struct. (Theochem) Vol 151, 1987 pp 215-222.
- Zyss, J., "Hyperpolarizabilities of Substituted Conjugated Molecules. I. Perturbated INDO Approach to Monosubstituted Benzene", J. Chem. Phys., Vol. 70, 1979, pp 3333-3340.

1987 USAF-UES SUMMER FACULTY RESEARCH PROGRAM/
GRADUATE STUDENT SUMMER SUPPORT PROGRAM

Sponsored by the
AIR FORCE OFFICE OF SCIENTIFIC RESEARCH

Conducted by the
Universal Energy Systems, Inc.

FINAL REPORT

Mathematical Removal of Low Frequency Fluctuations
From Experimental LDV Data

Prepared by: Thomas R. Lalk
Academic Rank : Associate Professor
Department and Department of Mechanical Engineering
University: Texas A&M University
Research Location: AFWAL, Aero Propulsion Laboratory, Advanced Propulsion
Division, Experimental Research Branch (POPT)
Wright- Patterson Air Force Base,
Dayton, Ohio 45433
USAF Researcher: Dr. A.S. Nejad
Date: September 27, 1987
Contract No.: F49620-85-C-0013

Mathematical Removal of Low Frequency Fluctuations

From Experimental LDV Data

by

Thomas R. Lalk

ABSTRACT

A computer software technique for identifying and removing low frequency fluctuating components from LDV velocity measurements was developed and verified. The velocity realizations from the LDV measurement of turbulent flow velocities in an experimental model of a dump combustor were stored on magnetic tape and constant time interval sampled to provide a secondary data set for Fourier analysis. A fast Fourier transform algorithm was used to transform the data set to the frequency domain where identification and removal of dominant frequencies was accomplished. The remaining data was inverse transformed to the time domain resulting in a data set devoid of the removed frequencies. The technique was tested by analyzing functions of known frequency content and actual LDV data for which the frequency content had been determined with an electronic analyzer. It was determined that the software technique functioned as intended.

Acknowledgements

I want to express my thanks to the Air Force Systems Command and the Air Force Office of Scientific Research for their sponsorship of this summer research program. I also wish to thank Universal Energy Systems for their competent, flexible and thoughtful administration of this program. Their efforts made it a pleasant experience by "cutting the red tape" and going out of their way to be helpful. Special thanks are due Lou and Dan Danishek who were always helpful and friendly in their dealings with me.

I truly enjoyed my research experience due to the challenge of learning applications of many aspects of engineering I had not dealt with in some time, but also in large measure to the people I was fortunate enough to work with. I found them all, from the Branch Chief and Division Head to the Branch secretary to be enthusiastic, competent and friendly. Many thanks to Abdi, Ken, Shane, and Doug for all the stimulating conversations and provocative questions, and friendship you extended. I also wish to thank Rick, Jorge, Ragu Craig, Tim, John C. and Virginia for making my summer that more enjoyable by creating an atmosphere that is truly one of friendly cooperation. Finally I wish to thank John for his outlook that encourages those that work with him to strive for their best.

1. INTRODUCTION

The objectives of the Experimental Branch (POPT) of the Advanced Propulsion Division of the Aero Propulsion Laboratory, as defined in a Technical Area Definition report, are to develop: new and improved combustor computational models, fundamental understanding of turbulence, and experimental data for computational model development and validation. One on-going effort of the Branch toward satisfying these objectives is the measurement of velocities and turbulent flow parameters in an experimental model of a ram jet combustor. Figure 1 is a drawing of the dump combustor used for these experiments which are described in reference 1. A swirler was installed at the dump plane to impart a tangential swirl to the flow as it entered the sudden expansion section of the duct. Data was obtained with a two-component laser doppler velocimeter (LDV). The measurements were compared with the results of a $k-\epsilon$ turbulent flow computer model.

Agreement between the computer model predictions and the experimental results has not been good. Figure 2 shows comparisons of the experimental and computational mean velocities and turbulent kinetic energy radial profile results at various positions downstream of the dump plane. As can be seen from these profiles, at positions far downstream ($x/H > 8.0$) the predicted axial and tangential mean velocities results differed considerably from the measured. Predicted values of the turbulent kinetic energy were also substantially lower than those measured at axial positions downstream. The conclusion drawn in reference 1 was that "the $k-\epsilon$ model needs further modifications and improvements before it can successfully be used to predict swirling flows." The particular numerical model used for this investigation

is relatively easy to use and can be run on an enhanced microcomputer. Therefore it would be desirable to be able to identify reasons for the lack of agreement with experimental results and possibly define modifications and improvements that would result in a more accurate predictive code.

As illustrated in Figure 3, the major portion of the turbulent energy is contained in the large scale turbulent structures (large eddies) and transfers down the "cascade" to the smaller eddies where dissipation occurs. Figure 4 indicates that the energy is greatest for low frequency oscillations that are associated with the large scale structures. Frequency measurements that were made of the turbulent flow in the model combustor with swirl (reference 1) indicated the presence of low frequency oscillations. This, considered with the fact that numerical predictions of the turbulent kinetic energy were lower than the measurements, suggests that possibly the $k-\epsilon$ predictive model is not able to account for the large scales of turbulence, that is, those corresponding to the low frequency oscillations. This, in turn, suggests that if the low frequency components (or their effect) could somehow be removed from the experimental data or suppressed, the numerical model may more closely agree with the experimental results. If this were determined to be the case, it could result in identification of ways in which the model could be modified for improved modeling of the actual flow. My summer assignment was to investigate this approach.

My interests and experience fit in well with this research effort. In two industrial positions, I conducted experimental research in gas dynamics and gained experience with instrumentation, the methodology for fluid dynamics diagnostics, and data acquisition and analysis. My experience and interest since entering academia have been with experimental research in combustion and

ND-A191 284

UNITED STATES AIR FORCE SUMMER FACULTY RESEARCH PROGRAM
(1987) PROGRAM TE (U) UNIVERSAL ENERGY SYSTEMS INC
DAYTON OH R C DARRAH ET AL DEC 87 AFOSR-TR-88-8213

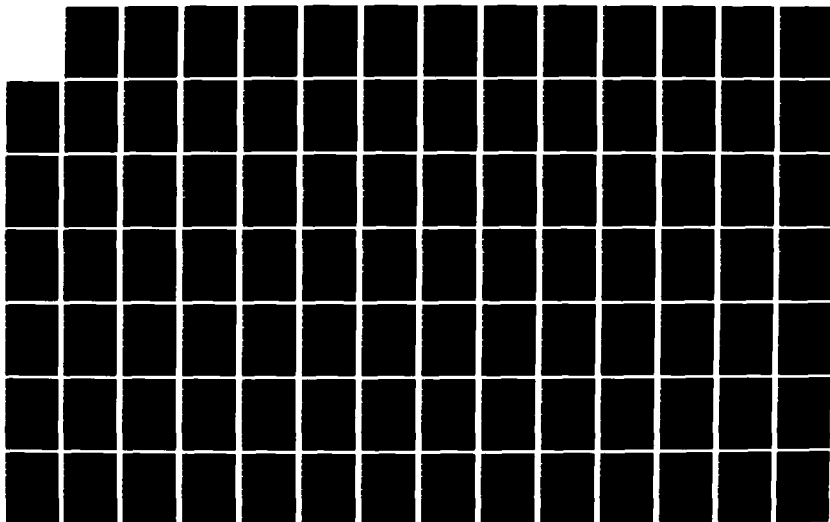
7/11

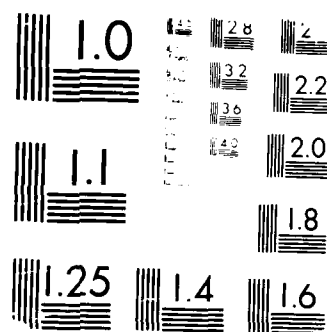
UNCLASSIFIED

F49620-85-C-0013

F/G 5/1

NL





MICROCOPY RESOLUTION TEST CHART

1. $\chi^2 = 1.0$, $df = 1$, $p = 0.32$

teaching in combustion, gas dynamics and experimentation. I have also had experience in numerical simulation of compressible fluid flow.

11. OBJECTIVES OF THE RESEARCH EFFORT

The forgoing discussion leads to the basic question, would the $k-\epsilon$ numerical model more realistically model the turbulent flow in the combustor if the large scales of turbulence (low frequency components) were not present? This suggests the additional question, what would the experimental results be if the low frequency fluctuations had not been present or were suppressed? This second question must be answered before the first can be addressed. Thus the objectives of the investigation were to : (1) develop and verify a method for identifying and suppressing the effect of the dominant low frequency components from the velocity measurements and create a new data set; and (2) determine whether the numerical model more accurately models the new data set.

The second objective could only be satisfied by analyzing a complete set of data including all radial and axial locations within the flow field. That is, at each location at which velocity measurements had been made the low frequency components would have to be identified and removed to create a new set of data. The numerical model results would then have to be compared to this new set of results to determine if there was better agreement. This would require analysis of data for each of approximately thirty points across the duct diameter at each of several axial locations. Therefore, as a consequence of time constraints it was decided that only the first of the objectives be addressed during the ten week Summer Faculty Research Program. In the course of developing the software to satisfy the first objective, a routine for

storing velocity data on magnetic tape was developed and found to operate satisfactorily. Thus data can be stored for later analysis so that the second objective could be pursued at a later date and at a site other than where the measurements are taken.

The basic approach to the problem was to:

1. Fourier transform the laser doppler velocimeter (LDV) measurements for a particular location in the flow field, consisting of velocity-time pairs (u_i, t_i) , from the time domain to the frequency domain.
2. Identify and remove the dominant low frequency components from the data set and finally,
3. Inverse transform the remaining components back to the time domain to create a new set of velocity-time pairs that could be analyzed to determine the statistical moments at the particular location. This would result in recalculation of the turbulence intensity and turbulent kinetic energy.

III. PROCEDURE

Considering the objectives of the investigation the initial task was to develop a means for using computer software to identify dominant low frequency components in the otherwise random data, remove these components in the frequency domain and then transform the remaining data back to the time domain to create a new data set devoid of the low frequency components.

The first step in the procedure was to store the LDV data on magnetic tape so that it could be analyzed separately from the actual velocity data taking

process. This was required because of the extremely large number of velocity measurements (27,000 or greater) at each location and the limited memory capacity of the data acquisition computer. The LDV data acquisition procedure required that the data from a particular flow location be discarded before taking data at the next location in the flow field.

The FFT computation required that the points be equally spaced, that is, at constant time intervals. As the LDV velocity measurements were random in time (corresponding to the arrival times of the seed particles at the measurement location) the data from the tape had to be sampled at constant time intervals. This also resulted in the removal of velocity bias from the data (ref. 4). The constant time interval sampling resulted in a secondary set of velocity measurements (realizations). This set contained fewer members, the number depending on the sampling frequency. Usually the secondary set contained approximately ten percent as many points as the original depending upon the size of the time interval selected. The sampling frequency was restricted to a value at least twice the highest frequency that we wished to identify. This was a consequence of the sampling theorem (ref. 3, p. 123) and was necessary to avoid aliasing -- the folding over of higher frequencies into the lower frequency range resulting in false detection of low frequencies.

The next step was to create a data set for actual Fourier analysis. This was done by sampling the constant time interval data set. The number of members in this data set had to be a power of two so that the FFT algorithm could be implemented. The number of points desired and the sampling rate were specified and sampling continued until the specified number was obtained. The sampling rate again had to be at least twice the highest frequency it was desired to

detect in order to avoid aliasing errors.

The data was then transformed to the frequency domain by applying the FFT algorithm. An amplitude spectrum was obtained in the frequency domain by performing the complex multiplication of each $X(n)$ with its complex conjugate before plotting the amplitude-frequency spectrum. This spectrum was observed on a CRT display and the dominant low frequency component(s) was (were) identified by noting the presence of a peak in the spectrum. It should be noted that the fluctuations in the magnitude of the velocity corresponded to fluctuations about a mean value so that the amplitude spectrum in the frequency domain represented the amplitudes of these fluctuations that occurred at various frequencies. If an amplitude was small that signified that there was little or no fluctuations at that frequency. As only the fluctuations were of importance in identifying frequencies, the mean value could be subtracted off before transformation to the frequency domain. The individual $[X(f)]^2$ can be interpreted as the amplitude of sine waves with the various frequencies. Then the overall function is composed of the sum of all these sine waves. Another interpretation is that these spectra, in the frequency domain, are the squared coefficients of a sine series representing the fluctuating portion of the function, and when this series is added to the mean (non-fluctuating portion) the total function is represented.

The identified frequency component was removed by using an interactive CRT display to mark the frequency range that was to be eliminated by setting the associated $X(f)$'s equal to zero. Although the removal process was implemented by observing and identifying the frequency peak on a plot it could have done by examining the set of complex coefficients, $X(f)$ in the frequency domain. The number of coefficients in this set is exactly equal to the number of

members in the time domain sequence $x(m)$. However, as can be seen by observing the small example set of complex $X(f)$'s shown in Figure 5, the set of complex coefficients is hermitian. That is, there is a symmetry about the point at which the imaginary part of the number is zero such that the real parts are the same on either side and the imaginary parts are complex conjugates. Thus for practical purposes the useful range of the FT is only one-half the total range. The frequencies associated with each of these coefficients would depend upon the constant time interval between members of the time domain sequence. For the illustrative example of Figure 5 that interval was assumed to be 1/64 sec. with $N = 32$. The value of Δt would be the value specified for the constant time sampling of the time domain sequence from the tape. Thus, the frequencies are given by :

$$f_n = \frac{n}{N \Delta t} \quad , \quad n = 0, 1, 2, \dots, (N/2)-1 \quad (1)$$

For this example the largest value of $[X(f)]^2$ occurs at a frequency of 6 Hz. and this component would be set equal to zero before inverse transformation. In actual practice the frequency interval would be much smaller as there would be many more points sampled and the Δt would be much smaller. This would allow a much more accurate identification of frequencies. The hermitian nature of the $X(f)$ data set resulted from the fact that the input values to the DFT were real rather than complex. Due to the symmetry of this set we initially set one-half of the set equal to zero and removed the peak value from only the remaining half of the set before transforming back to the time domain. This resulted in incorrect values for the amplitudes in the time domain. Thus we discovered that the peak value had to be removed from both halves of the set of complex coefficients before transformation back to the time domain.

Once the computer software had been developed to implement the steps as outlined above, it remained to be determined whether it could be used to accomplish the desired task of identification and removal of selected frequency components from the LDV data. This was done by first applying it to known functions such as sine waves with known frequency content. The analysis software was then applied to actual LDV data stored on tape. The results of this analysis were compared to the frequency spectra obtained with a commercial electronic FFT analyzer while the LDV data was actually being taken. Once frequencies had been removed and inverse transformed back to the time domain the new data set was again transformed to the frequency domain as a check to see if the desired frequencies had actually been removed. The statistical moments were recalculated and compared to the original. Other tests that were run were to investigate the effect on the moments of removing more than one frequency component and the effect of removing frequency components from the axial velocity data set as well as that for the radial velocity.

IV. RESULTS AND DISCUSSION

The results of the verification tests of the Fourier analysis software are presented in Figures 6 through 14.

Several tests were conducted where a known function was analyzed to determine if the frequency analysis program was operating properly. After numerous modifications to the program it could be used to accurately identify the frequencies present and to remove selected frequency components. Figure 6 shows the result of the analysis of a triple sine wave, a function composed of the sum of three sine waves of different frequencies. Figure 6a is a plot of

the function and Figure 6b the frequency domain representation of the function which was the summation of sine waves of frequencies 4.2, 8.4 and 16.8 Hz. The frequency domain exhibited peaks at the correct frequencies. Figure 6c is a plot of the function in the time domain after inverse transformation following removal of the lowest frequency peak, showing that the lowest frequency was removed from the time domain. Thus the analysis software appeared to be operating as intended.

Following verification of the analysis program when applied to known functions it was applied to actual LDV velocity data. Figure 7 is a plot of the power density spectrum obtained with an electronic FFT analyzer simultaneously with the actual velocity measurements. Figures 8 and 9 are amplitude spectra obtained by analyzing the data from the same measurements used for Figure 7 except the data was stored on tape and sampled. Figure 8 shows that the dominant frequency identified with the software analysis routine agreed with that of the electronic analyzer. Figure 9 shows the frequency spectrum after the removal of the lowest frequency. Note that there is a "hole" in the spectrum where the frequency component was removed. Finally, Fig. 10 shows the various moments of the data for the original data, the data with the dominant frequency removed from the axial velocity data and the data with the dominant frequencies removed from both the axial and radial data. These results show that the mean velocity did not change at all when the frequencies were removed. Mathematically, this is as it should be, because all that is being removed are the fluctuations about the mean which should not affect the non-fluctuating part of the function. Physically, however, this presents a problem because the removal of a fluctuating component would result in the removal of some of the turbulent energy. This is verified by the lower values

for the turbulence (USIG on the printouts of Figure 10) when the frequency component is removed. A great deal of discussion revolved around this question. It was decided that the energy had to be added back into the flow somehow, but there are at least two ways of viewing just how it should be redistributed. One viewpoint is that as the mean flow is the source of the turbulent energy in the first place, the turbulent energy "removed" when a frequency is removed should be added to the mean flow. This approach would view the situation as if the low frequency fluctuations (large scale structures) had never been formed. Another view of the same situation is that the large scale structures with which the low frequency fluctuations are associated could break up immediately upon their formation such that the energy associated with them would be distributed among the smaller scale, higher frequency components in the flow. The problem with this approach is that some means of how to distribute the energy over the smaller scales would have to be decided upon and in addition all the scales (frequencies) present and their relative strengths would have to be first identified. At any rate an examination of the moments after the removal of the low frequency components shows that the turbulence and higher moments (UV , U^2V , UV^2) decreased after the low frequency component was removed.

Additional data from other locations in the flow field were analyzed with the same basic result as discussed above. At a flow location further downstream the electronic FFT analyzer indicated the presence of two dominant frequencies and the software accurately identified the same two frequencies. Removal of each frequency resulted in a decrease in the turbulence level and the higher moments. Removal of the radial velocity lowest frequency component seemed to have little effect on the moments, but this is something that must be investigated further at many more locations in the flow field.

V. CONCLUSIONS

- The software Fourier analysis technique can be used to identify and remove selected frequencies from LDV data sets.
- Questions remain as to which and how large of frequency range(s) to remove and exactly what, from a physical sense, is being removed.
- Question remains as to how to redistribute the removed turbulent energy.
- The removal of a particular frequency from the LDV velocity data will result in the decrease of the turbulence, but questions remain about the effect throughout the flow field and the agreement with the numerical model.

VI. RECOMMENDATIONS

1. Before the objective of determining whether the numerical model agrees more closely with a modified data set a method for automating the frequency identification and removal should be developed. This would require the development of software to replace the interactive technique being used. This would greatly expedite the data analysis procedure.
2. The most important recommendation is that a full set of LDV data be analyzed to determine whether the technique is worth pursuing. If the numerical model shows no better agreement with the experimental data after removal of the frequency components from all the measurement locations then possibly other types of models should be evaluated. Data sets at higher levels of swirl should also be analyzed and compared to the numerical model.

3. If the numerical model shows better agreement with the modified data than with the original then reasons for the original disagreement and modifications to the model should be identified.

4. If the technique proves to be a promising one other modifications to the software should be implemented. For example, a technique for computing the full discrete Fourier transform which does not require that the time intervals be equal should be added and compared to the FFT method. Other detailed modifications to the software can be added to determine the effect on the frequency removal procedure. For example, other window functions can be investigated, a spectral density function computation routine can be added to more precisely identify frequencies, and a technique for identifying the energy associated with the turbulence removed can be added such that it could be added back into either the mean flow or smaller scale structures.

5. Cross correlation routines should be added to the analysis software so that the relationships among various scales of turbulence can be investigated.

REFERENCES

1. Samimy, M., A. S. Nejad, C.A. Langenfeld, R. R. Craig and S.P. Vanka, "Isothermal Swirling Flow in a Dump Combustor," Proc. AIAA 19th Fluid Dynamics, Plasma Dynamics and Lasers Conference, Honolulu Hawaii, June 1987.
2. Bendat, J. S. and A. G. Piersol, Random Data-Analysis and Measurement Procedures, second edition, Wiley-Interscience, New York, N. Y..
3. Ahmed, N. and T. Natarajan, Discrete - Time Signals and Systems, Reston Publishing Company, Reston Virginia.
4. Nejad, A. S. and D. L. Davis, "Velocity Bias in Two Component Individual Realization Laser Doppler Velocimeter," available from Aero Propulsion Lab (POPT), Wright-Patterson AFB, Dayton Ohio.

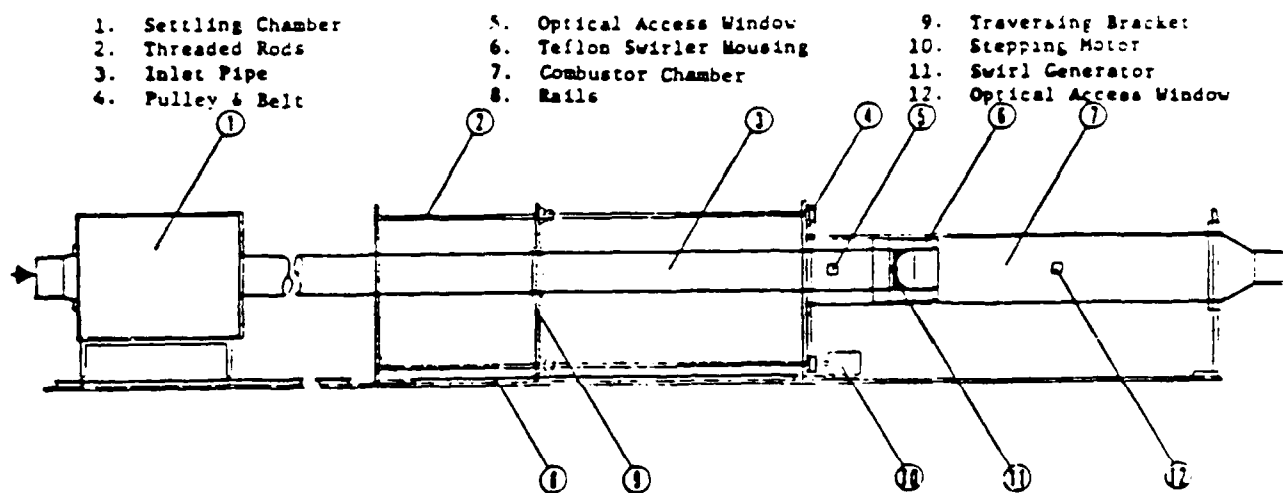


Figure 1. Schematic of the experimental dump combustor

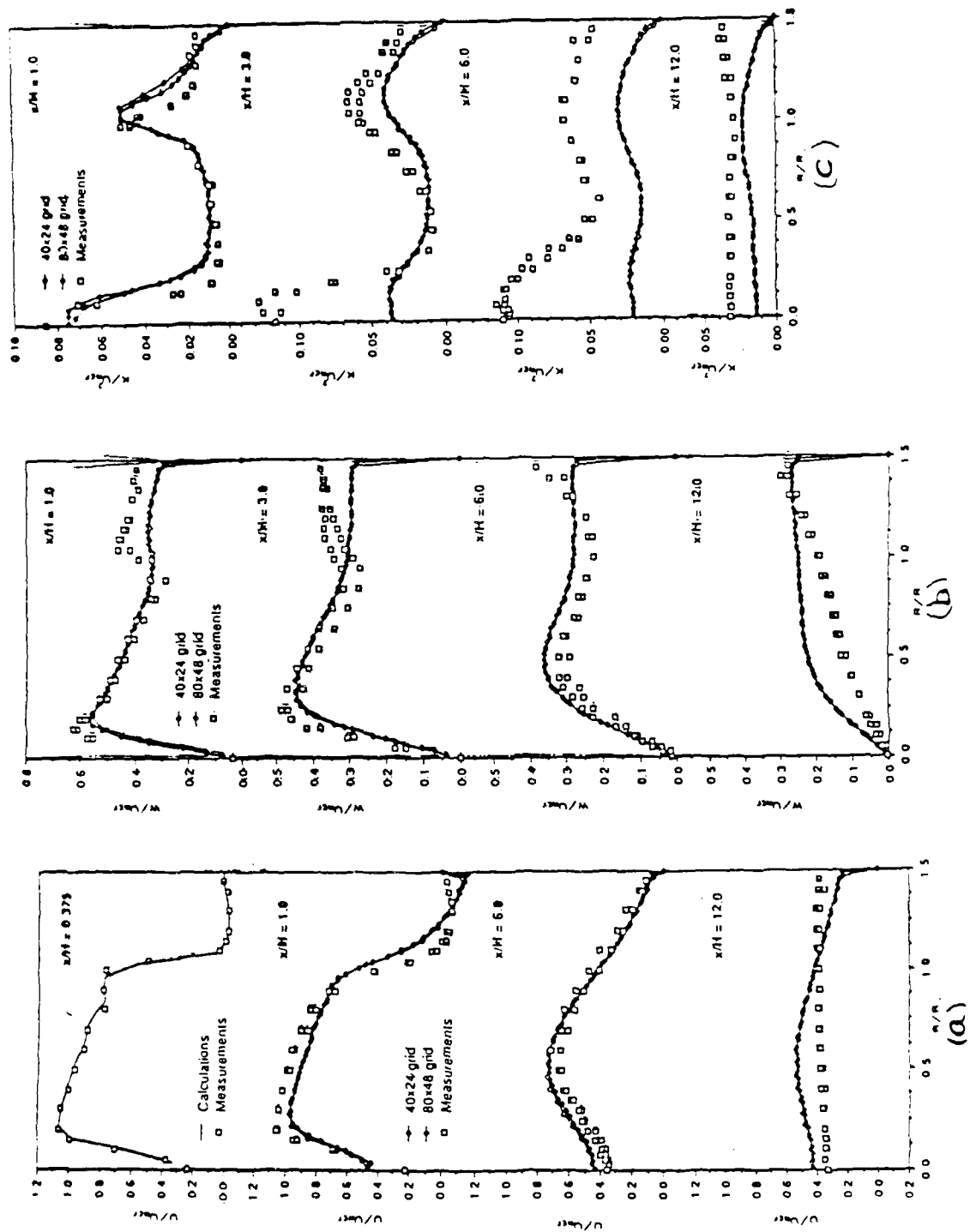


Figure 2. Comparison of experimental and computed axial velocity (a) tangential velocity (b) tangential mean velocity and (c) tangential velocity.

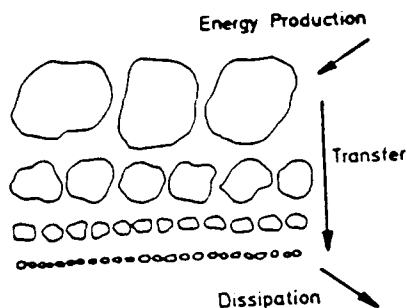


Figure 3. Turbulent energy cascade (Large eddies break up into smaller and smaller ones and are finally dissipated)

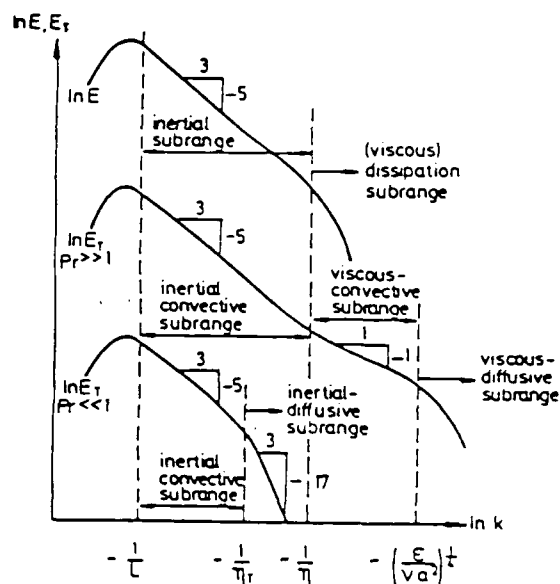
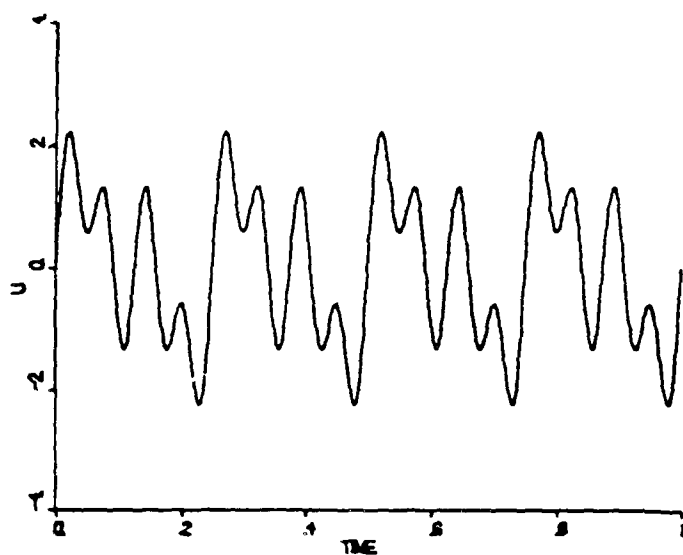


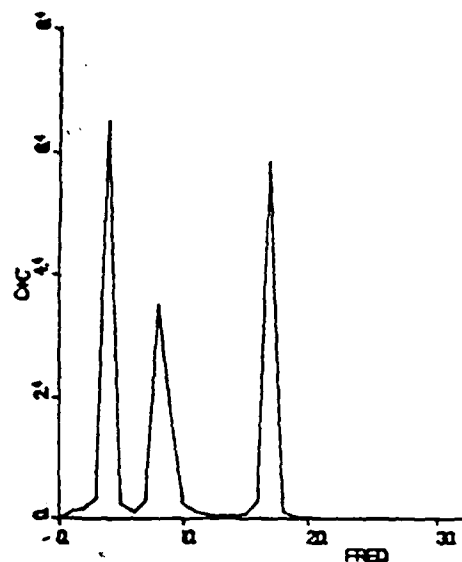
Figure 4. Turbulent energy and temperature spectra (Wave no. k proportional to frequency)

frequency (Hz)	REAL	IMAG
0	7.39383	0.00000
2	8.23938	-3.98435
4	14.03937	-15.50320
6	-17.23565	37.68157
8	-1.91366	10.42849
10	0.16443	6.27709
12	0.94395	4.47994
14	1.33523	3.42614
16	1.56250	2.70633
18	1.70614	2.16632
20	1.80193	1.73406
22	1.86781	1.37063
24	1.91366	1.05349
26	1.94517	0.76707
28	1.96576	0.5011
30	1.97774	0.24759
	1.98117	0
	1.97774	-0.24759
	1.96576	-0.5011
	1.94517	-0.76707
	1.91366	-1.05349
	1.86781	-1.37063
	1.80193	-1.73406
	1.70614	-2.16632
	1.56250	-2.70633
	1.33523	-3.42614
	0.94395	-4.47994
	0.16443	-6.27709
	-1.91366	-10.42849
	-17.23565	-37.68157
	-14.03937	15.50320
	8.23938	3.98435

Figure 5. Illustrative example of a set of complex coefficients $X(f)$ in the frequency domain

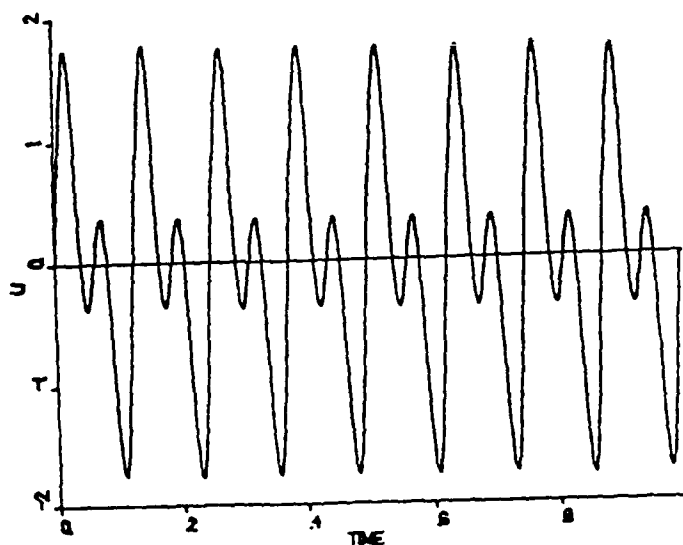


(a)



(b)

Figure 6. Triple sine wave test function: (a) original function with frequencies of 4.2, 8.4, and 16.8 Hz.; (b) frequency spectrum of triple sine wave; (c) time domain function after removal of lowest frequency component



(c)

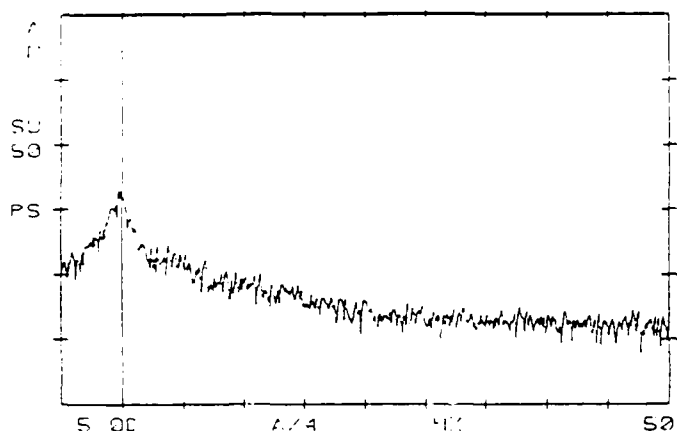


Figure 7. Power density spectrum obtained with electronic FFT analyzer (swirl no. of 0.3 at $x=3''$, $r=0.4''$)

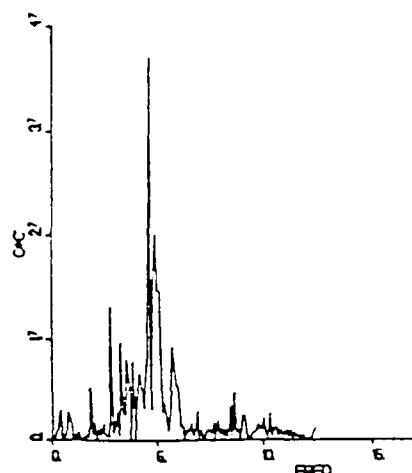


Figure 8. Amplitude spectrum obtained with software. (swirl no. of 0.3 at $x=3''$, $r=0.4''$)

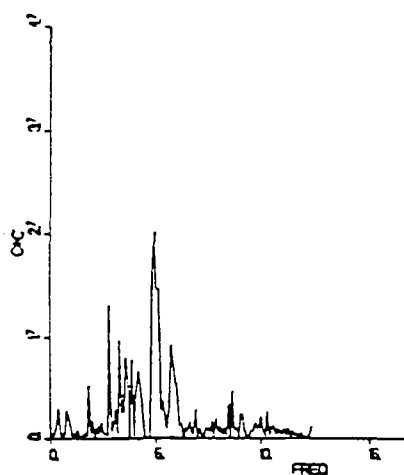


Figure 9. Amplitude spectrum after removal of lowest frequency peak. (swirl no. of 0.3 at $x=3''$, $r=0.4''$)

TIME-15:02:26.53 DATE-08/10/87 MODE-3 RATE-200
 UMEAN- 47.19 UMEAN- -0.98 URMS- 50.00 URMS- 13.62
 USIG- 16.53 USIG- 13.58 USKEU- -0.91 USKEU- 0.39
 UV- -73.47 UV- 1163.02 UV2- -901.94

(a)

TIME-15:02:26.53 DATE-08/10/87 MODE-3 RATE-200
 UMEAN- 47.19 UMEAN- -0.98 URMS- 49.74 URMS- 13.62
 USIG- 15.72 USIG- 13.58 USKEU- -0.82 USKEU- 0.39
 UV- -63.41 UV- 971.39 UV2- -794.12

(b)

TIME-15:02:26.53 DATE-08/10/87 MODE-3 RATE-200
 UMEAN- 47.19 UMEAN- -0.98 URMS- 49.74 URMS- 13.07
 USIG- 15.72 USIG- 13.04 USKEU- -0.82 USKEU- 0.35
 UV- -63.41 UV- 869.56 UV2- -719.09

(c)

Figure 10. Moments of velocity set
 (a) original data;
 (b) after removal of low f peak from axial velocity data
 (c) after removal of low f peak from axial and radial data (swirl no. of 0.3 at $x=3''$, $r=0.4''$)

1987 USAF-UES SUMMER RESEARCH PROGRAM
SUMMER FACULTY RESEARCH PROGRAM
GRADUATE STUDENT SUMMER SUPPORT PROGRAM

Sponsored by the
AIR FORCE OFFICE OF SCIENTIFIC RESEARCH

Conducted by the
Universal Energy Systems, Inc.

FINAL REPORT

CONSTRUCTION AND PRELIMINARY VALIDATION
OF AN EQUAL OPPORTUNITY CLIMATE ASSESSMENT INSTRUMENT

Prepared by:	Dan Landis, Ph.D Gloria Fisher, M.Ed., M.S.
Academic Rank:	Professor (Landis) Graduate Student (Fisher)
Department and	Psychology Department
University:	University of Mississippi
Research Location:	DEOMI Patrick Air Force Base, FL
USAF Researcher:	Lt Col Mickey Dansby
Date:	21 Aug 87
Contract No:	F49620-85-C-0013

CONSTRUCTION AND PRELIMINARY VALIDATION
OF AN EQUAL OPPORTUNITY CLIMATE ASSESSMENT INSTRUMENT

by

Dan Landis, Ph.D.
and
Gloria Fisher, M.Ed., M.S.

ABSTRACT

Construction and preliminary validation of an instrument to assess equal opportunity climate in the military was begun. The research was conducted at the Defense Equal Opportunity Management Institute (DEOMI) at Patrick Air Force Base, FL. Students who are undergoing equal opportunity training at the institute served as subjects. A definition of equal opportunity climate is provided. A model linking equal opportunity climate to other organizational variables is also presented. Preliminary results in the development of the assessment instrument indicate that it is reliable and has some measure of construct validity. Further laboratory research and field validation among a random selection of military bases are recommended.

Acknowledgments

We wish to thank the Air Force Office of Scientific Research for sponsorship of the research. Additionally, we acknowledge the assistance of Universal Energy Systems in administrative matters.

The staff at the Defense Equal Opportunity Management Institute have been extremely helpful and cooperative in all stages of this research. It has been both a pleasure and a learning experience to be able to work with them. We particularly wish to thank Lt Col Mickey Dansby for his encouragement and guidance on this project. Col. E. E. Wiggins, Commandant of DEOMI, was most helpful and placed the resources of the Institute at our disposal.

I. INTRODUCTION

Considerable research has been conducted on the climate of organizations (Forehand & Gilmer, 1964; Litwin & Stringer, 1968; Taguiri, 1968) and on aspects of equal opportunity (Fahey & Pati, 1975; Faley, 1982). However, no previous research has attempted to combine the concepts and determine what constitutes equal opportunity climate. Nor has any previous study attempted to determine what relationships, if any, exist between equal opportunity climate and other organizational variables, such as satisfaction, commitment, or effectiveness.

It seems particularly appropriate to investigate these relationships in the context of military organizations in view of the large number of minorities and women that they employ. Concern with equal opportunity and treatment for minorities and women in the military has provided the impetus for the creation of the Defense Equal Opportunity Management Institute (DEOMI), formerly the Defense Race Relations Institute (DRRI). DRRI was created by the Department of Defense in 1971, in part as a response to racial incidents and violence both in the military and without. The Institute was given a mandate to develop and implement a program of classes in race relations designed to prevent racial unrest,

tension, or conflict from impairing combat readiness and efficiency (Day, 1983; Lovejoy, 1977). This institute has been known as the Defense Equal Opportunity Management Institute (DEOMI) since 1979. The current name reflects a change of focus to include equal opportunity for women in the military and to emphasize a shift toward a management oriented approach to equal opportunity. With the change to DEOMI came a change in emphasis toward examining institutional discrimination, as opposed to personal racism or sexism, and an emphasis on organizational management approaches. DEOMI training, a 16 week curriculum, is similar for all branches of the service, with special service-specific programs that are in addition to the core program. Our research interests have, in the past, focused on equal opportunity employment, organizational climate, and cross cultural training and research. These interests led to our assignment to the Defense Equal Opportunity Management Institute at Patrick Air Force Base.

II. OBJECTIVES OF THE RESEARCH EFFORT

Although previous research on climate in military organizations has not focused on the construct of Equal Opportunity Climate, several researchers have attempted to assess both organizational climate and race relations climate in the military.

Bowers (1975) measured organizational climate variables in the Navy by using the Survey of Organizations (SOO). In general he found that "on all measures of organizational climate . . . Navy respondents were lower than nearly three-fourths of civilian respondents." The findings revealed more felt discrimination among minorities and particularly blacks, and at the same time showed a negative relationship between felt discrimination and climate (i.e. the better the climate, the less the felt discrimination).

Parker (1974) found almost no difference between perceptions of organizational climate by race, also using Navy personnel as respondents. Results indicated that racial composition of the work group was a critical moderator variable of the relationship between experienced practices and felt discrimination. Research by Pecorella (1975) indicated that organizational climate measures presented patterns of (if anything) perceived reverse discrimination; although objective data, such as advancement and training opportunities did not. Pecorella also noted that felt personal discrimination seems to be closely tied to one's immediate work environment (particularly to advancement opportunities and friendly relations with one's peers). This research suggests that much of the perception that one is discriminated against stems from job characteristics (e.g. promotions), and from relations with one's co-workers.

In surveys by the Army Research Institute (Brown, Nordlie, and Thomas, 1977) there was a notable difference in how the "race problem" was seen by whites and blacks in the Army. Whites in the Army tended to accept the proposition that the Army is free from racial discrimination. Blacks saw the Army as highly discriminatory. This difference also correlated with grade. Officers and higher enlisted saw the race problem as less serious than did the lower enlisted grades. The 1972 results were virtually replicated in 1974, in spite of the existence of an all-volunteer Army and an increase in black enlisted individuals. In 1978, Hiett and Nordlie concluded, in their study on unit race relations program in the Army, that despite the relative absence of overt interracial violence, race-related tensions persist.

It is notable that most of the research on climate and race relations in the military has focused solely on differences between blacks and whites. That focus has now been expanded to include sexual discrimination and harassment, as well as discrimination against other racial minorities. In one of the few research efforts in the military regarding sexual harassment, a survey of 104 Navy women (Reilly, 1980), almost all had experienced sexual harassment in their careers; lower grade enlisted women were harassed the most. The data indicated that sexual harassment negatively affected the attitude of the female service member, as well as her desire

and intent to remain.

It is apparent that the military could benefit by a reliable and valid measure of equal opportunity climate. This instrument could be used by the command, along with other data such as objective management indices, to effectively assess how command units "stand" in relation to equal opportunity climate.

The objectives of this research then were to 1) provide a definition of equal opportunity climate, 2) begin construction and preliminary validation of an instrument to measure equal opportunity climate that can be used by all branches of the military, and 3) hypothesize a model which relates equal opportunity climate to other organizational variables.

III. DEFINITIONS AND MODEL

a. Equal Opportunity Climate was defined as

the expectation by individuals that opportunities, responsibilities, and rewards will be accorded on the basis of a person's abilities, efforts, and contributions; and not on race, color, sex, religion, or national origin. It is to be emphasized that this definition involves the individual's perceptions and may or may not be based on the actual witnessing of behavior.

b. Model of Equal Opportunity Climate.

The model (see Figure 1) developed in this project is an expansion of the definition given above. While it is beyond the scope of this report to give a full explication of the

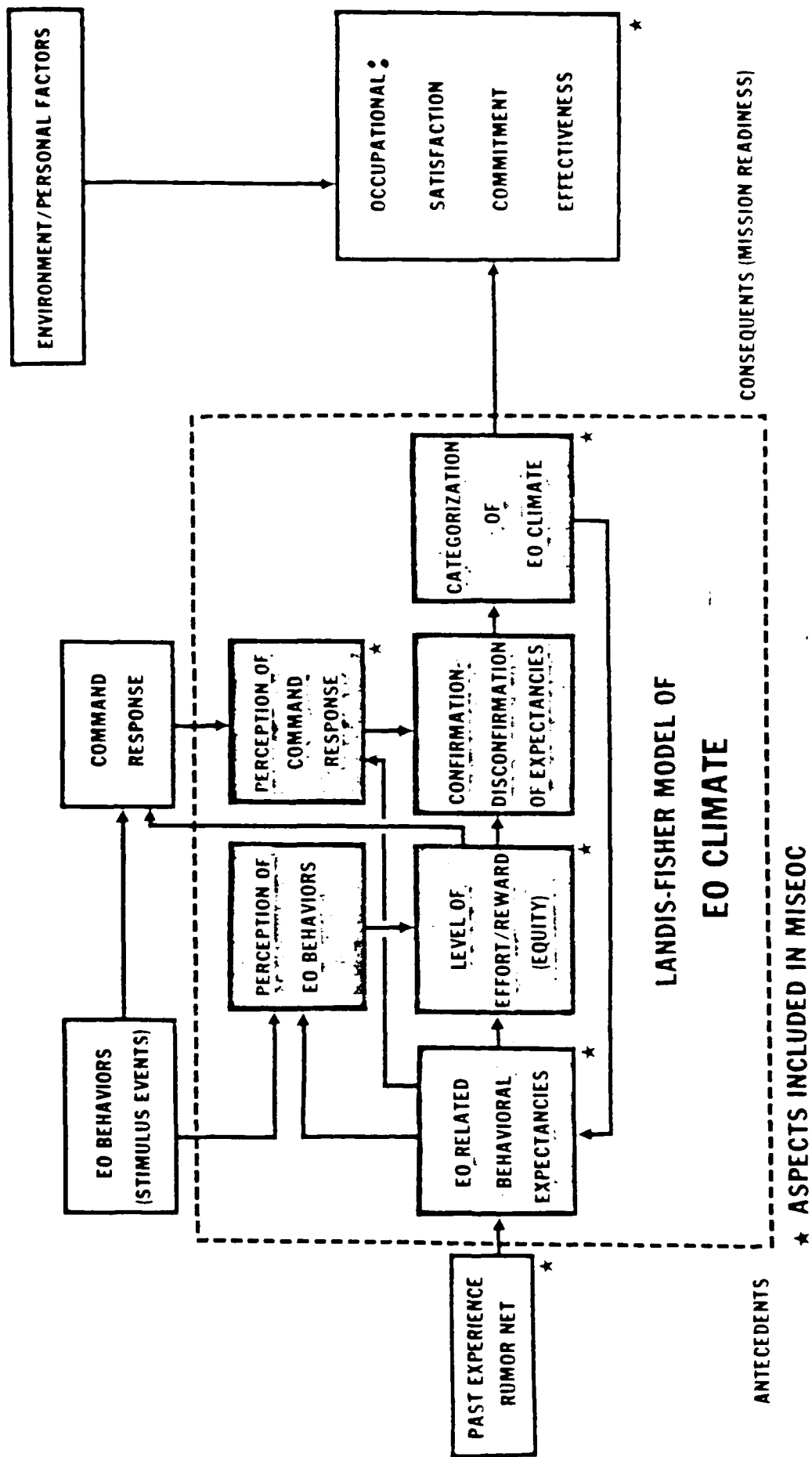


Figure 1. Model of Equal Opportunity Climate

proposed model, some comments are in order.

EO climate is visualized as the result of several cognitive operations, which in turn have antecedents both in the person's past history and in events in the outside world. At the same time, EO climate has impacts on a number of cognitive and motivational processes which are part of what may be called "readiness."

Briefly, the individual comes to the situation with a set of expectancies which are the result of past experiences and information provided about the locale. These expectancies involve the types of behaviors that will likely occur in the situation. The expectancies result in set of perceptual screens which act on the actual behaviors. Perceptions of equal opportunity behaviors are related to the level of effort that the individual expends in order to obtain some kind of reward. The actual behaviors, both from others and from the individuals, meanwhile engender some kind of response from the command (it may be no response, of course). This response is perceived by the individual (conditioned of course by his/her expectancies), and the expectancies confirmed or disconfirmed (e.g. that a particular EO behavior is common or rare in a given locale). Finally, the locale is categorized as, at the very least, a "good" or "poor" EO site. The categorization acts to change the expectancies and the process begins again.

The important aspect here to note is that EO climate is essentially an internal process which is only tangentially under the control of environmental events. As such, the model suggests that command's responses must be timely and vigorous in order to change negative or reinforce positive expectations by personnel.

IV. METHODS AND PROCEDURES

a. Sample: The respondents were the members of DEOMI class 87-2 (51 Men, 11 Women; 6 Officers, 57 Enlisted Personnel; 42 Army, 5 Air Force, 14 Navy, 2 Undefined. The total is less than the number used for analysis due to failure of 11 respondents to provide identifying information).

b. Questionnaire Design:

1. Elicitation of Behaviors: The training and facilitator staff of DEOMI (n=20) were asked to list "Five specific behaviors that would be indicative of 'poor equal opportunity climate.'" An example of a "specific" behavior was provided. The emphasis here was on a definable unit of behavior, not a series of events spread out over time. Over 100 behaviors were provided and examined for 1) specificity and 2) redundancy. The analysis reduced the list to 78.

2. Importance Ranking: A separate group of personnel from the reserves (n=50) taking a DEOMI short course was asked to assign a rating of 1-10 to each behavior. The lower

end of the scale represented "No importance," while the high end was anchored at "Of critical importance." After examining the items and the ratings, the number of items was further reduced to 71.

3. Design of Response Dimensions: The response category was designed around a five-point scale. This was done for two reasons: 1) There is ample evidence that in asking for probability estimates, 20% interval width is about optimal for most people and 2) DEOMI has structured most of its evaluation forms around such a format. By adopting this format, we were able to use already existing response forms and reduce possible confusion on the part of the respondents. Thus, for the Equal Opportunity Behaviors part of MISEOC, the responses were cast as follows:

1=There is almost no chance that the behavior occurred.

2=There is a small chance that the behavior occurred.

3=There is a moderate chance that the behavior occurred.

4=There is a reasonably high chance that the behavior occurred.

5=There is a very high chance that the behavior occurred.

4. Selection of Items for Measuring Work-group Effectiveness and Organizational Commitment: Items for these two sections were taken from two sources--1) Work-group effectiveness: Fifteen items from the United States Air Force Organizational Assessment Package (Short 1985) were selected.

These items had high loadings on a factor labeled "Work Group Effectiveness" and "General Organizational Climate." For a description of the standardization process used in the OAP, see Short, 1985. 2) Organizational Commitment: Fifteen items from the questionnaire designed by Mowday, Steers, and Porter (1979) were selected and rewritten to conform to a military situation.

5. Development of Situational Scenarios: In order to test the MISEOC format for discriminant validity, two hypothetical locales were devised. Information was provided on each locale along six dimensions which were taken from the management indices used by the United States Air Force to assess the level of human relations climate (Air Force Pamphlet AFP 30-13, issued 21 January, 1985). The locales were described on each dimension as having "an above average rate" or "a significant change from the previous year" for the "poor equal opportunity climate locale." For the "good" locale, the descriptors were "a below average rate" or "a significant reduction from the previous year" on each dimension. The six dimensions used were

- a. There is (filled in) percentage of Articles 15 for minorities and for whites.
- b. There is (filled in) percentage of involuntary separations for minorities and for whites.
- c. There is (filled in) percentage of courts-martial for

minorities and for whites.

d. Sexual discrimination complaints filed and confirmed are (filled in)

e. Sexual harassment complaints filed and confirmed are (filled in).

f. There have been (filled in) hate group (like Ku Klux Klan) activities in this locale.

c. Experimental Design: Variations of the questionnaires were administered twice to the members of DEOMI class 87-2. The purpose of each administration is indicated below.

1. Administration 1: The 71 equal opportunity climate behaviors were given to 74 members of the class. The instructions were to judge the "chances that the behavior occurred in the non-DEOMI portion of Patrick Air Force Base during the past 30 days." The purpose of this administration was to explore the factorial structure of each part of MISEOC and to assess the reliability of each factor as well as the total survey.

2. Administration 2: This was seven days after the first survey was taken. Again, the target of Patrick Air Force Base was used; however, the order of the behaviors was randomly mixed from the first testing. In addition, half of each group was asked to rate the "good" locale and half the "poor" locale on each of the 71 behaviors. A manipulation

check was added by asking at the end of group of the 71 behaviors how "most people at this locale would rate the equal opportunity climate". The response was made on a 1-5 scale from "very poor" to "very good."

The purpose of this second administration was to assess the test-retest reliability as well as probe the discriminant validity of MISEOC.

d. Analyses of Data:

1. Structure of MISEOC. Principal Component Factor Analyses of the 71 equal opportunity behaviors was performed. Separate analyses were done for each administration of the "Patrick" and the "good" and "poor" versions. The analyses used unity in the diagonals and Varimax rotation (oblique rotation failed to converge in 25 iterations).

2. Reliability Analysis. This analysis used the two administrations of the "Patrick" questionnaire. Cronbach alphas were computed for the total and for factors of each administration. In addition, scores were computed for the total and for factors for each administration. These were then correlated over all subjects for an estimate of the test-retest reliability.

3. Manipulation Check: An Analysis of Variance was used with form number (1 or 2, corresponding to the type of scenario provided) as the grouping variable and global equal opportunity climate as the dependent variable.

4. Effect of Situation on MISEOC Factors: From the data obtained on the second administration, factor scores were computed for each subject within each scenario condition. This gave six scores for each respondent. A Multivariate Analysis of Variance was performed using the six factors as the dependent variables and scenario ("good" or "poor") to group the subjects.

V. RESULTS

a. Structure of Equal Opportunity Behaviors: Six factors were retained from the Principal Components Analysis. These factors together accounted for 65% of the total variance with eigenvalues of 33.68 (47.4%), 3.67 (5.2%), 2.77 (3.9%), 2.16 (3.0%), 2.01 (2.8%) and 1.83 (2.6%), respectively. These six were selected using a scree line approach. There is not enough space here to present the rotated factor table; however, the names assigned to the dimensions are

Factor I: Overall Concern with Equal Opportunity Issues.

Items here deal with both race and sex discrimination as well as administrative reactions to sexual harassment. The focus is on-base behavior.

Factor II: Differential Behavior by Commanders. All of the items here deal with commanders' treating minorities differently than majority persons.

Factor III: Stereotypes. These items deal with minorities and women being treated in stereotypic fashion (e.g. females

being mistaken for secretaries).

Factor IV: Sexual Role Definition. These items imply that the military is a man's job.

Factor V: Overt Sexual Harassment. Here the items deal with superiors' using their positions to demand sexual favors from subordinates.

Factor VI: Covert Sexual Harassment. These items suggest that a woman's role is to be subordinate to a man as well as being decorative.

b. Reliability of MISEOC: MISEOC exhibits a high degree of internal consistency. The Cronbach alpha over all items is .98 and for two random halves .96 and .97, respectively. The six scales were also highly reliable (alpha of .95, .93, .91, .87, .86, .88, respectively). The correlation between the two halves is .88. All of the above analyses were based on a n of 74. On the second administration, the reliability of the six scales continued to show a satisfactory level of reliability (.92, .93, .86, .84, .89, .87, respectively). When the target was changed to the constructed locales, the reliability of the scales remained quite good (.94, .93, .91, .82, .85, and .76 respectively).

c. Manipulation Check. The "good" and "bad" scenarios produced the desired effects. The global judgment means for the two scenarios were significantly different ($F=63.07$, $df=1,59$, $p<.00001$) and in the expected direction. (Mean

(good)= 3.46, Mean (bad)=2.62).

d. Effect of External Conditions on Equal Opportunity Climate. The MANOVA used type of "locale" as the independent variable and the six scales as criteria. The Multivariate F was highly significant (Mult F=3.46, df=12,104, p <.0001) as were the univariate tests for five of the six scales. The "Overt Sexual Harassment" (Scale V) was non-significant. The means were all in the expected direction (see Figure 2).

The results summarized above indicate that MISEOC has both a high reliability and construct validity. It appears to be sensitive to changes in the external world, the exact range of which will need to be investigated.

VI. RECOMMENDATIONS

The beginning stages of construction and validation of an instrument to assess equal opportunity climate have been completed. Initial indications are that MISEOC is reliable and has some construct validity. We have every reason to believe that the technique will prove to be both reliable and valid when tested in the field. The next phase of validation will require both more piloting at DEOMI as well as testing pilot versions in the field. Further reliability checks should be undertaken, as well as cross validation of the factor structure of the measurement technique. After these steps have been completed and the instrument revised

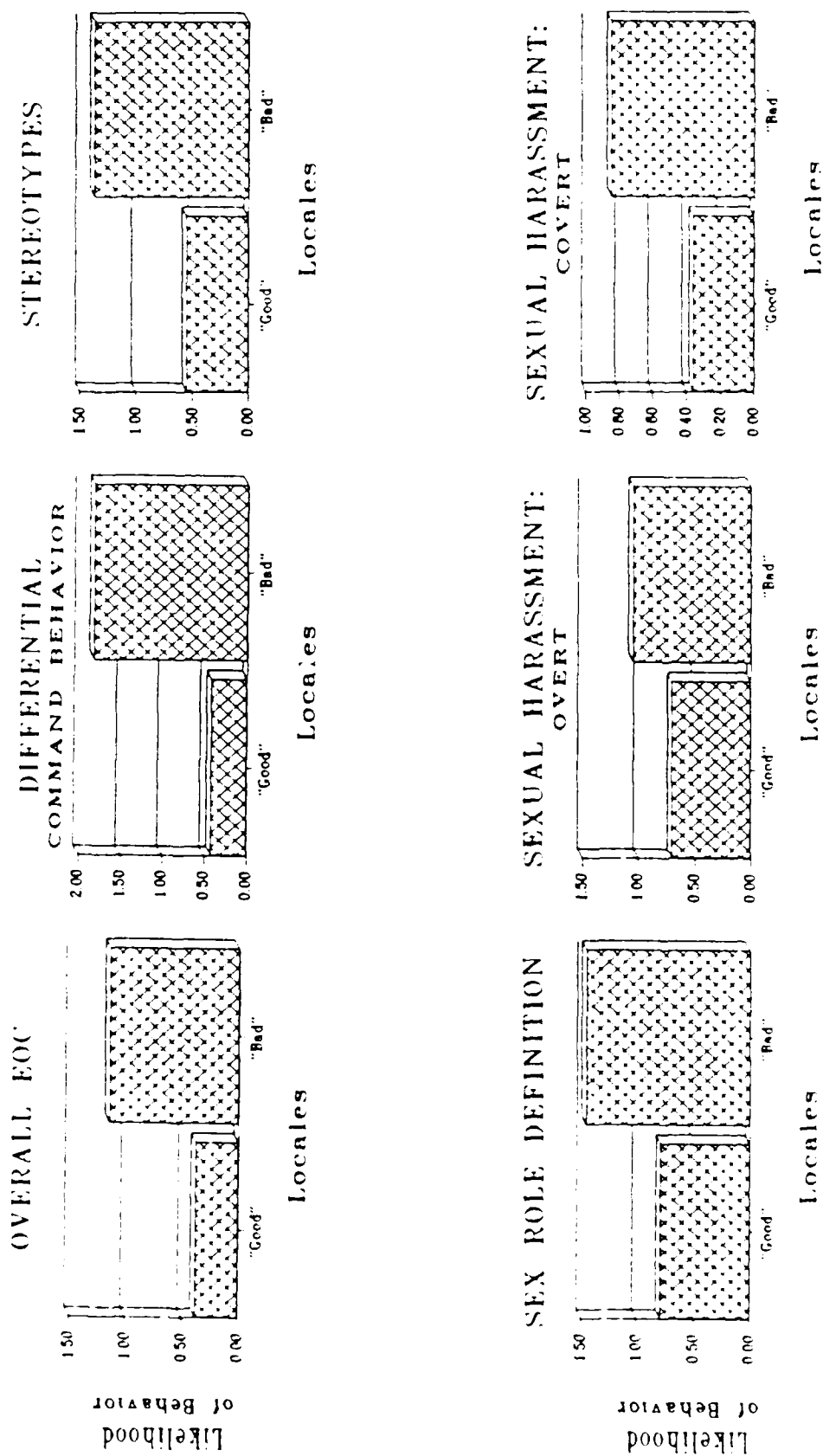


Figure 2. Effect of Situations on Equal Opportunity Climate Scales

accordingly, field validation can begin. The full field validation should use at least 20 military sites (four from each service, two in CONUS and two outside of CONUS). The instrument should be administered to a large number of subjects and convergent validation checks made using objective management indices.

REFERENCES

- Brown, D. K., Nordlie, P. G. & Thomas J. A. (1977). Changes in black and white perceptions of the Army's race relations/equal opportunity programs--1972 to 1974. Technical Report & Tr-77-B3. U.S. Army Research Institute, Alexandria, VA.
- Bowers, D. G. (1975). Navy manpower: Values, practices, and human resources requirements. University of Michigan, Institute for Social Research.
- Day, H. R. (1983). Race relations training in the military. In D. Landis and R. W. Brislin (Eds.) Handbook of intercultural training. Vol.II. New York: Pergamon.
- Department of the Air Force. (1985) Air Force Human Relations climate assessment. Air Force Pamphlet 30-13.
- Fahey, P. E. and Pati, G. C. (1975). Trying to be equable about equal employment. The Conference Board Record, 12, 37-40.
- Faley, R. H. (1982). Sexual harassment: Critical review of legal cases with general principles and preventive measures. Personnel Psychology, 35, 583-600.
- Forehand, G. A. & Gilmer, B. (1964). Environmental variation in studies of organizational behavior. Psychological Bulletin, 62, 361-381.

- Hiett, R. L. & Nordlie, P. G. (1978) An analysis of the unit race relations training program in the U. S. Army. Alexandria, VA.: U. S. Army Research Institute.
- Litwin, G. H. & Stringer, R. A. (1968). Motivation and organizational climate. Boston: Harvard University Graduate School of Business Administration.
- Lovejoy, J. E. (1978). A history of: The Defense Race Relations Institute (DRRI). Vol. I. DRRI historical file, Patrick Air Force Base, FL.
- Mowday, R. T., Steers, R. M., & Porter, L. W. (1979). The measurement of organizational commitment. Journal of Vocational Behavior, 14, 224-247.
- Parker, W. S. (1974). Differences in organizational practices and preferences in the Navy by race. University of Michigan, Institute for Social Research.
- Pecorella, P. A. (1975). Predictors of race discrimination in the Navy. University of Michigan, Institute for Social Research.
- Reilly, P. J. (1980). Sexual Harassment in the Navy. Thesis, Naval Postgraduate School, Monterey, CA.
- Short, L. O. (1985). The United States Air Force Organizational Assessment Package. Leadership and Management Development Center Air University, Maxwell Air Force Base, AL.

Tagiuri, R. (1968). The concept of organizational climate.
In R. Tagiuri and G. H. Litwin (Eds.) Organizational
Climate: Explorations of a concept. Boston: Harvard
Graduate School of Business Administration.

1987 USAF-UES SUMMER FACULTY RESEARCH PROGRAM/
GRADUATE STUDENT SUMMER SUPPORT PROGRAM

Sponsored by the
AIR FORCE OFFICE OF SCIENTIFIC RESEARCH

Conducted by the
Universal Energy Systems, Inc.

FINAL REPORT

A HYPERBOLIC INTERPOLATION ALGORITHM FOR
MODELLING RADIANCE DATA AND EXPONENTIAL INVERSION

Prepared by:	Steven J. Leon
Academic Rank:	Professor
Department and University:	Mathematics Department Southeastern Massachusetts University
Research Location:	Air Force Geophysics Lab, Atmospheric Sciences Division, Hanscom Air Force Base
USAF Researcher:	Jean I. F. King
Date:	August 10, 1987
Contract No.:	F49620-85-C-0013

A Hyperbolic Interpolation Algorithm for
Modelling Radiance Data and Exponential Inversion

by

Steven J Leon

ABSTRACT

Transfer theory relates the upwelling intensity to the integral transform of the Planck intensity $B(t)$. Radiance values can be obtained by remote sensing from satellites. In order to recover the Planck intensity from the data one must solve an integral equation of the first kind. Such equations are notoriously ill-posed and consequently difficult to solve in a numerically stable manner. If one assumes an exponential model for $B(t)$, then it follows that the radiance data should be represented as a rational function. Jean I. F. King has proposed an algorithm for a rational interpolation of the radiance data at $2n$ points. The Planck intensity can then be reconstructed analytically using the coefficients and weights of the interpolating function. In this paper we develop and test the interpolating algorithm. We also develop software for reconstructing the Planck intensity and discuss the stability of the inversion. Significant errors in the data will cause one of the components of the interpolating function to have a positive pole. The algorithm has been designed to detect this situation and then locate and correct those points which are in error. Thus the algorithm can be used to detect and compensate for a faulty sensing channel.

Acknowledgements

I wish to express my gratitude to the Air Force Systems Command and the Air Force Office of Scientific Research for sponsorship of this project. Universal Energy Systems should also be acknowledged for their help in administrative aspects of this program.

Above all I would like to express my appreciation to Jean I. F. King for his guidance and supervision in this research. It has been both an honor and a privilege to have been able to spend a summer working with him. Thanks also to Bob McClatchey and others in the Atmospheric Sciences Division for providing such a congenial atmosphere and work environment. Thanks to Chris Johnson for helping me get the necessary software transferred to the VAX and to A. S. Jursa for his efforts in coordinating the summer faculty research program at the Geophysics Lab.

The summer faculty research program has been a rewarding and enriching experience. In a short period of time I have been able to accomplish a significant amount of research. This research has important applications which should prove most valuable to the Air Force. I would not hesitate to recommend this program to my colleagues at Southeastern Massachusetts University.

I. INTRODUCTION

The Atmospheric Sciences Division of the Geophysics Laboratory at Hanscom Air Force Base does a considerable amount of work with radiance data obtained by remote sensing from satellites. According to transfer theory the upwelling intensity is the integral transform of the Planck intensity. One can obtain valuable information about the structure of the atmosphere by applying an inversion method to the data to recapture the Planck intensity. Unfortunately this entails solving an integral equation of the first kind. This type of integral equation is ill posed in that the solution does not depend continuously on the data. This makes it extremely difficult to obtain meaningful solutions in the presence of noise.

As an applied mathematician specializing in numerical analysis and linear algebra, I am particularly intrigued with the challenge offered by this type of integral equation. I have experience with some of the techniques for solving these equations and in 1986 I gave a lecture on this subject at the Royal Institute of Technology in Stockholm. It is because of this expertise that I felt I could contribute to the projects of the Atmospheric Sciences Division at the Geophysics Lab.

II. OBJECTIVES OF THE RESEARCH EFFORT

The major objective of this research project was to develop an algorithm for modelling radiance data by a special form of rational function. We initially assumed that the radiance data could be modelled by a function of the form

$$a(s) = \sum_{j=1}^n \frac{w_j}{s - k_j} \quad (1)$$

and later modified our model to include a linear component. Thus (1) was replaced by

$$a(u) = w_1 + w_2 u + \sum_{j=3}^{n+1} \frac{w_j}{1 + c_j u} \quad (2)$$

Ideally the hyperbolic components of the function should have poles k_i that either lie on the negative real axis or appear as complex conjugate pairs. However, if there are significant errors in one or more of the data points, then in order to achieve a hyperbolic fit one would expect a term with a positive pole. If such

turns out to be the case, the location of the pole could be used to determine which point is in error. If the algorithm produces a positive pole with a relatively small weight w_i , then that term could be eliminated from the model (2) and the resulting curve should give a close fit to the data. The point in error would be the point with the largest deviation to the modified curve. In this way the model could be used to detect a faulty or incorrectly calibrated sensing channel.

Thus our primary objectives were to design an algorithm to interpolate the radiance data by a function of the form (1) or (2) and to use the computed coefficients to detect faulty sensing channels. To realize these objectives it was necessary to develop software for implementing the algorithm and displaying graphically the resulting curves. This software was then tested on simulated and actual radiance data.

The upwelling intensity is the integral transform of the Planck intensity. The Planck intensity can be recovered from the radiance data by solving an integral equation of the first kind. Such equations are difficult to solve in a numerically stable manner. If radiance data can be represented by a function of the form (1) or (2), then the inversion can be performed analytically. The Planck intensity $B(t)$ can be constructed from the coefficients in (1) or (2). Thus another objective of our research was to use our algorithm to reconstruct the Planck intensity.

Because of the sensitivity of this problem, it is desirable to perform tests on simulated data in order to determine the effect that small perturbations in the data would have on the calculation of the inverse. This perturbation analysis should provide useful guidance in the choice of an appropriate value for n in (1) or (2). It should also provide valuable information as to how many digits of accuracy in the data are necessary in order to avoid significant perturbations in the computed inverse.

III. THE INTERPOLATION ALGORITHMS

Initially we assumed that the Planck intensity could be represented as a linear combination of n exponential functions

$$B(t) = \sum_{j=1}^n w_j \exp(k_j t). \quad (3)$$

According to transfer theory the upwelling intensity $a(s)$ is the integral transform of the Planck function. For our model we represented $a(s)$ as the Laplace transform of $B(t)$

$$a(s) = \int_0^{\infty} B(t)e^{-st}dt = \sum_{j=1}^n \frac{w_j}{s - k_j}.$$

Given values of the upwelling intensities $a_i = a(s_i)$ sampled at $2n$ arbitrary nadir secant directions s_i , we wish to determine a function of the form (1) that interpolates the data, i.e.,

$$a_i = \sum_{j=1}^n \frac{w_j}{s_i - k_j}.$$

This is accomplished via the following algorithm.

Hyperbolic Interpolation Algorithm (J. I. F. King)

1. Compute

$$R_{ik} = \left[\prod_{\substack{l=i \\ l \neq k}}^{i+n} (s_k - s_l) \right]^{-1}$$

for $i = 0, 1, \dots, n-1$; $k = i, i+1, \dots, i+n$.

2. For $i = 0, 1, \dots, n-1$; $j = 0, 1, \dots, n$ set

$$\gamma_{ij} = \sum_{k=i}^{i+n} R_{ik} \alpha_k s_k^j.$$

3. Solve the linear system

$$\sum_{j=0}^{n-1} \gamma_{ij} c_j + \gamma_{in} = 0, \quad i = 0, 1, \dots, n-1$$

for c_0, c_1, \dots, c_{n-1} .

4. Set

$$p(x) = x^n + \sum_{j=0}^{n-1} c_j x^j$$

and solve the characteristic equation $p(x) = 0$ for the roots k_1, k_2, \dots, k_n .

5. Solve the linear system

$$\sum_{j=1}^n \frac{w_j}{s_i - k_j} = a_i, \quad i = 0, 1, \dots, n-1.$$

If some of the roots k_i turn out to be multiple real roots or complex conjugate pairs of roots the appropriate modifications must be made in step 5 of the algorithm and to the equation (3) for the inverse. A positive root k_i would indicate that one of

the data points is in error. Indeed this proved to be the case when the algorithm was tested on simulated data.

Testing on Simulated Data

Data was simulated by constructing functions of the form (1) and adding low level noise. The interpolation algorithm proved to be stable if n were not too large. The cases $n = 2$ and $n = 4$ were studied to determine the effect that a significant perturbation in one of the data points (s_i, a_i) would have on the computed roots of the characteristic equation. It was found that a perturbation significantly above low noise levels would cause one of the roots k_j to be positive. Furthermore the perturbation in a_i causes the positive pole k_j to be close to s_i . Thus by taking the closest value of s to k_j from the data points, one can determine which data point is in error.

Testing on Actual Radiance Data

During the ninth week of the project we were able to test the algorithm on actual radiance data. The data used was taken from McClatchey [5]. The actual data appeared to differ from the simulated data by a linear component. Consequently the algorithm was not successful in interpolating all of the data points. It was necessary then to add a linear component in order to successfully interpolate the radiance data.

The Modified Algorithm

In the modified algorithm it is assumed that the interpolating function is of the form (2). Because the actual data consisted of sets of 6 points and because of time constraints, we choose to develop the algorithm only for the case $n = 3$. In this case the interpolating function will be of the form

$$a(u) = w_1 u + w_2 + \frac{w_3}{1 + c_1 u} + \frac{w_4}{1 + c_2 u}. \quad (4)$$

The values of the upwelling intensity a_i are sampled in the nadir cosine directions u_i , $i = 1, \dots, 6$. Our previous algorithm is then modified to incorporate the linear component. The new algorithm is summarized as follows:

Hyperbolic Interpolation Algorithm 2

1. For $i = 1, \dots, 6$ set

$$\beta_{i1} = a_i / \prod_{j=1, j \neq i}^6 (u_i - u_j).$$

2. For $j = 2, 3, 4$ set

$$\beta_{ij} = \beta_{i1} u_i^{j-1}, \quad i = 1, \dots, 6.$$

3. For $j = 1, 2, 3, 4$ set

$$M_j = \sum_{i=1}^6 \beta_{ij}.$$

4. Solve the system

$$M_1 c + M_2 b = -M_3$$

$$M_2 c + M_3 b = -M_4$$

for c and b .

5. Find the roots r_1 and r_2 to the quadratic equation

$$x^2 + bx + c = 0.$$

6. For $i = 1, \dots, 6$ set

$$a_{i1} = u_i, \quad a_{i2} = 1, \quad a_{i3} = -r_1/(u_i - r_1)$$

$$a_{i4} = -r_2/(u_i - r_2).$$

7. Solve the linear system

$$Aw = a$$

for w .

8. Set $c_1 = -1/r_1$ and $c_2 = -1/r_2$.

The interpolating function is then of the form given in (4).

Test Results

Algorithm 2 was tested on 18 sets of radiance data. In each case the interpolating function fitted the data very accurately and in each case one of the poles turned out to be positive. The weight w_i corresponding to the positive pole was always small compared to the other weights. Thus if that w_i were set to 0, the resulting function would still come close to interpolating the data. The 18 data sets

were all determined from sensing channels using nadir cosine directions u_i of 0.017, 0.066, 0.170, 0.400, 0.750, 0.920. For each set of radiance values the algorithm was applied and the weight corresponding to the positive pole was set to zero. We will refer to the resulting function f as the zero-weight approximating function. In 17 of the 18 data sets the radiance value a_4 was slightly higher than $f(u_4)$ and in all 18 of the data sets the value of a_5 was slightly smaller than $f(u_5)$. In thirteen of the eighteen sets the maximum deviation occurred at u_4 and the remaining five data sets had maximum deviations at u_5 . This provides a strong indication that something is wrong with data obtained from the fourth sensing channel and perhaps the fifth channel as well. Figures 1 and 2 show the graphs of $a(u)$ and $f(u)$ for a typical data set.

Correcting the Data

The algorithm not only spots errors in the data but also corrects them. The algorithm checks each data point to determine which point gives the maximum deviation from the zero-weight approximating function. The a_i value at that point is then replaced by the value of $f(u_i)$. For the data set in Figures 1 and 2 the maximum deviation occurs at $u_4 = 0.400$. Here the radiance value a_4 was 64.3 and $f(u_4)$ turns out to be 58.2971. We can replace a_4 by this new value and rerun the algorithm. The new interpolating function will be referred to as the corrected interpolating function. The graph of this function is shown in Figure 3. The maximum deviation for the corrected data is 2.8×10^{-14} . This was typical for the majority of the data sets. For twelve of the eighteen data sets the maximum deviation was on the order of 10^{-14} after one correction. Four of the data sets required two or three corrections to achieve this accuracy. The corrections failed to bring about improvements in only two cases. In one of these cases the corrections resulted in an additional positive pole very close to 0. The algorithm then sets both hyperbolic weights equal to zero. The resulting linear function did not give a good fit to the nonlinear data. We were, however, able to get a good fit in this case by making a small adjustment to the algorithm. A summary of the corrections for all 18 data sets is given in Table 1.

IV. THE INVERSION PROBLEM

Initially it was assumed that the Planck intensity could be modelled by a function $B(t)$ of the form given in equation (3) and that the upwelling intensity could be represented as the Laplace Transform of $B(t)$. Thus if $a(s)$ is a rational

interpolating function of the form (1), then the coefficients and weights in equation (1) can be used to reconstruct $B(t)$. Software was developed to implement this reconstruction. The software was tested on simulated data. A perturbation analysis was carried out to determine the effects of perturbations in the data on the calculated inverse.

The analysis showed that the inversion was stable in the case that $n = 2$, however, the inversion becomes increasingly unstable as n increases in size. For $n = 2$ the loss of accuracy was at most one digit. Thus if the radiance data were accurate to three digits, one would expect the computed inverse to agree with the inverse predicted by the model to either two or three digits. In the case $n = 3$ there was generally a loss of three digits. Thus four digit accuracy in the data would result in one digit accuracy in the inverse. Less than four digits of accuracy could give a wide range of computed inverses. In the case $n = 4$ we observed generally a four digit loss of accuracy. For $n = 5$ there was a six digit loss of accuracy and for $n = 6$ the loss of accuracy was at least seven digits.

Inversion of the Revised Model

For the revised model we assumed that the radiance data could be represented by a function $a(u)$ of the form (4). Using the H-function inversion theory of J. L. F. King [4] the corresponding form for the Planck intensity will be

$$B(t) = w_1 + w_2 t + w_3 \exp(-c_1 t) + w_4 \exp(-c_2 t) \quad (5)$$

To construct $B(t)$ we apply Algorithm 2 to the radiance data. If there are errors in the data the appropriate corrections are made using the techniques described in the previous section. Algorithm 2 is then reapplied to give a corrected interpolating function whose coefficients and weights are used to determine $B(t)$. This process was carried out on all 18 sets of radiance data. The graph of a typical computed Planck intensity is given in Figure 4. The data set used in Figure 4 is the same one that was used in Figures 1, 2, and 3.

The interpolation here requires a linear function and two hyperbolas. Thus $n = 3$ and there are 6 degrees of freedom. The characteristic polynomial is degree 2 and the weights are determined by solving a 4×4 system of linear equations. Although time constraints did not permit a perturbation analysis for the inversion of the revised model, the computations here are comparable to the $n = 2$ case in the original model. Thus, we expect that the inversion algorithm should be stable when $n = 3$.

V. RECOMMENDATIONS

The revised algorithms are currently in a form where they can be applied to any data set consisting of six points. If the data set contains a larger number of points, then a subset of six points must be strategically chosen. Included in this report are MATLAB programs for carrying out the interpolation, the corrections, and the inversion. MATLAB is an interactive program for scientific and engineering numeric computations and graphics. Versions of MATLAB are available for Macintosh and IBM compatible personal computers as well as for larger machines like Sun Workstations and VAX computers.

While much has been accomplished there remains a great deal of follow-up research that still must be carried out. The following is a list of further research efforts that are necessary to complete this study.

1. The algorithms have not yet been tested on normalized data. This is an important step in evaluating the effectiveness of the inversion. It should not be difficult to build the normalization process into the algorithm itself.

2. The original algorithm allowed for complex conjugate and multiple roots of the characteristic equation. We need to incorporate these same features into the algorithms for the revised model.

3. The current algorithms are designed for data sets consisting of six points. They should be generalized to handle sets of $2n$ points. The interpolation should be stable for values of n greater than 3. The error correction and detection should also work for larger values of n .

4. Further study needs to be done on the correction part of the algorithm. How accurate are the corrections? Can the corrections be improved? Is the corrected interpolating polynomial really better than the zero-weight approximating function? Is there a better correction method?

5. A stability study should be carried out for the inversion algorithm based on the revised model. This study should be similar to the one conducted on the inversion algorithm for the earlier model. It will allow us to determine the values of n for which the algorithm is stable.

6. The results of the inversion algorithm need to be treated against known results and against results obtained by other methods. Once the algorithms have been tested on normalized data, it should be possible to compare predicted temperatures to observed temperatures.

7. A lesson learned from polynomial interpolation is that local fitting by low degree polynomials generally gives a much truer description of the data than global fitting by a single higher degree polynomial. A similar situation holds here. For

large data sets where n is much greater than 3, the inversion algorithm is not likely to be stable. Even if it were numerically stable, we would probably get a truer representation of the data by doing local hyperbolic fitting with $n = 2$ or 3 than by doing global fitting with larger n . This suggests that it would be desirable to develop an algorithm for piecewise hyperbolic interpolation.

8. J. I. F. King has proposed a generalization of the models discussed in this paper. The new model would involve generalized exponential weight functions defined in terms of a parameter k . For each value of k we could invert our interpolating function to obtain a Planck intensity depending on k . For a given radiance profile we can then obtain a family of Planck intensity curves. By comparing these curves to actual observed temperatures, it should be possible to choose the appropriate value of the parameter k . This seems like a natural way to generalize our current work. The extra degree of freedom should give us a much more accurate model.

In summation, the algorithms that have been developed for modelling radiance data and solving transfer equations have shown impressive results, however, there is still much to be done. The algorithms need to be tested further, improved and generalized. Our initial successes would indicate much promise for these lines of research. The results of a complete study should prove to be of great value to the Air Force. Fortunately, the AFOSR Research Initiation Program provides a mechanism for follow-up research. I strongly urge taking advantage of this mechanism to see that the research is continued.

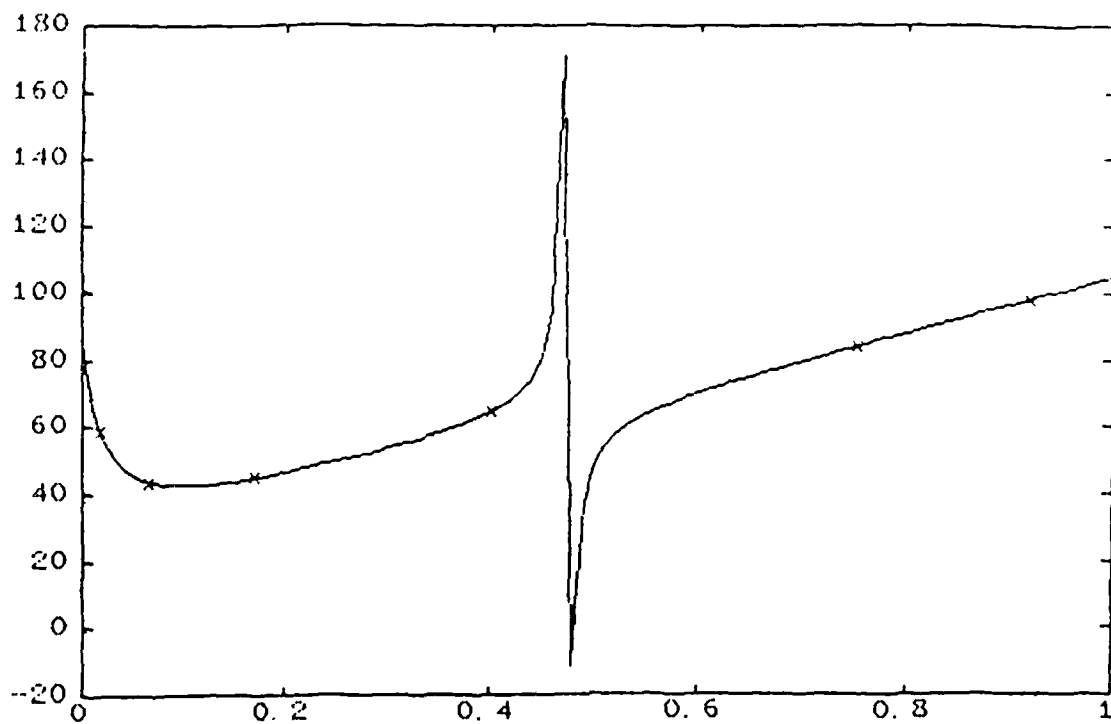


Figure 1 Hyperbolic Interpolation of Radiance Data

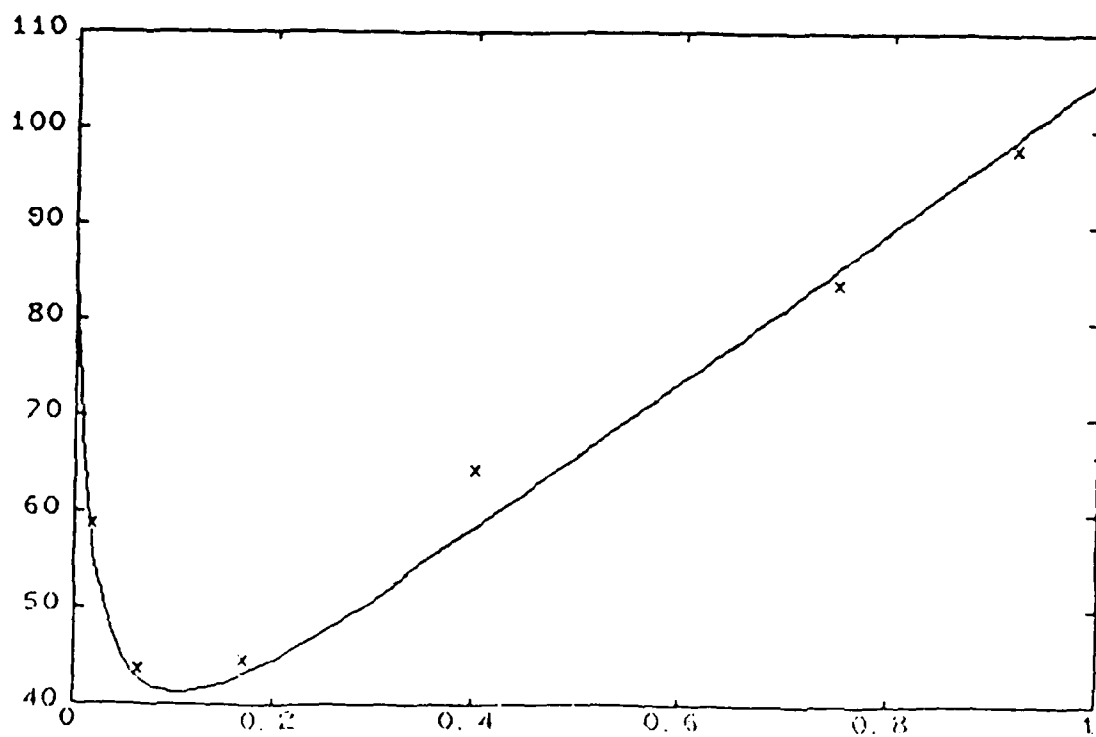


Figure 2 Zero-Weight Approximating Function

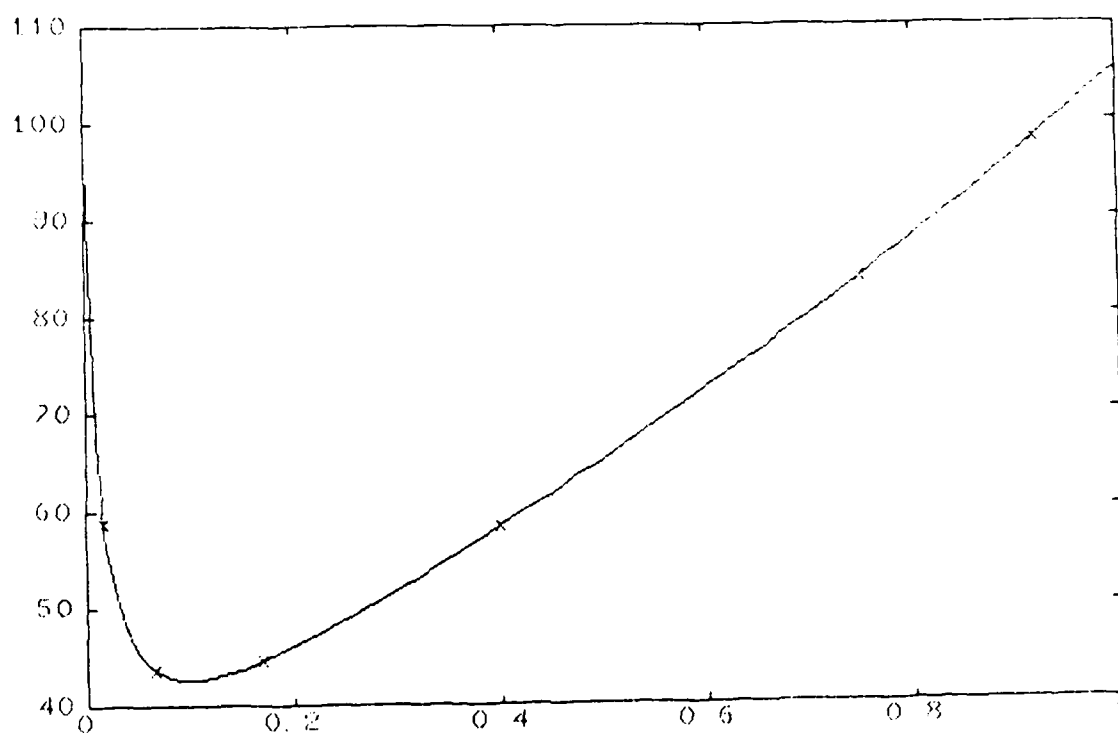


Figure 3 Interpolation of Corrected Data

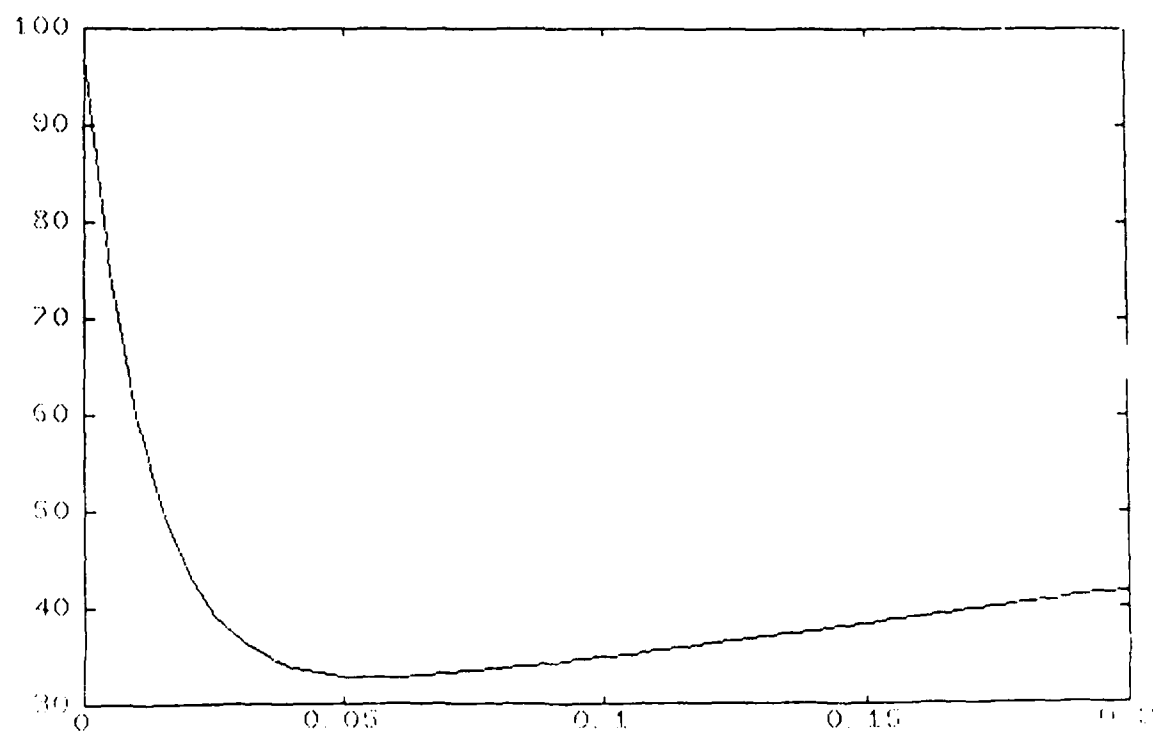


Figure 4 Graph of the Planck Intensity

data set	u(i)	m dev	pt1	m dev	pt2	m dev	pt3	m dev
1	0.400	5.10	0.920	5.03	0.750	0.86	0.066	0.00
2	0.400	3.07	0.920	0.00				
3	0.750	3.61	0.017	0.00				
4	0.750	2.13	0.066	0.00				
5	0.400	6.38	0.017	23.21*				
6	0.400	3.88	0.750	0.00				
7	0.400	6.00	0.066	0.00				
8	0.400	5.98	0.017	0.00				
9	0.400	4.16	0.920	3.87	0.750	0.05	0.920	0.00
10	0.400	5.26	0.017	0.00				
11	0.750	3.96	0.170	2.60	0.017	23.07*		
12	0.750	3.97	0.170	1.82	0.400	0.21	0.017	0.00
13	0.750	4.01	0.170	2.01	0.017	0.00		
14	0.400	3.18	0.920	0.00				
15	0.400	6.17	0.017	0.00				
16	0.400	7.69	0.750	0.00				
17	0.400	6.19	0.750	0.00				
18	0.400	4.40	0.017	0.00				

Table 1 (* correction fails)

```

% RATIONAL INTERPOLATION OF RADIANCE DATA AND GRAPH
for iter=1:2
    ALPHA=AA(JJ,:),ALPHA=ALPHA';
    [C,W]=INVT(U,ALPHA),PAUSE
    T=0:0.01:1;
    OT=ONES(T);ou=ones(u);
    Y=W(1)*T+W(2)*OT+(W(3)*OT)./(OT+C(1)*T)+(W(4)*OT)./(OT+C(2)*T);
    PLOT(U,ALPHA,'X',T,Y)
    title('Hyperbolic Interpolation of Radiance Data'),pause
    if c(1)<=-1
        w(3)=0.0
    end
    if c(2)<=-1
        w(4)=0.0
    end
    y=w(1)*t+w(2)*ot+(w(3)*ot)./(ot+c(1)*t)+(w(4)*ot)./(ot+c(2)*t);
    plot(u,alpha,'x',t,y)
    if iter==1
        title('Zero-Weight Approximating Function'),pause
    else
        title('Corrected Hyperbolic Interpolation'),pause
    end
    yy=w(1)*u+w(2)*ou+(w(3)*ou)./(ou+c(1)*u)+(w(4)*ou)./(ou+c(2)*u);
    [mdev,kk]=max(abs(yy-alpha'))
    aa(jj,kk)=w(1)*u(kk)+w(2)+w(3)/(1+c(1)*u(kk))+w(4)/(1+c(2)*u(kk));
end

FUNCTION [C,W]=INVT(U,ALPHA)
N=LENGTH(U);
FOR I=1:N
    XX=U(I)*ONES(U)-U; XX(I)=1.;
    BETA(I,1)=PROD(XX);
END
U=U';
BETA(:,1)=ALPHA./BETA(:,1);
FOR J=1:3
    BETA(:,J+1)=BETA(:,J).*U;
END
EM=ONES(1,N)*BETA;
G(1,:)=EM(1:2); G(2,:)=EM(2:3);B=-EM(3:4)';
B=G\B;BB=[1. B(2) B(1)];
Z=ROOTS(BB)
C=-ONES(2,1)./Z;
ONS=ONES(6,1); A(:,1)=U; A(:,2)=ONS;
A(:,3)=-Z(1)*ONS./(U-Z(1)*ONS);A(:,4)=-Z(2)*ONS./(U-Z(2)*ONS);
W=A\ALPHA;

% EVALUATION OF COMPUTED PLANCK INTENSITY FUNCTION AND GRAPH
t=-0.00:0.005:0.20;
ot=ones(t);
pl=w(1)*t+w(2)*ot+w(3)*exp(-c(1)*t)+w(4)*exp(-c(2)*t);
plot(t,pl)
title('Graph of Planck Intensity'),pause

```

REFERENCES

1. Chandrasekhar, S., Radiative Transfer, London, Oxford University Press, 1950.
2. King, Jean I. F., "Theory and Application of Differential Inversion to Remote Temperature Sensing" in Advances in Remote Sensing Retrieval Methods, edited by A. Deepak, et al., A. Deepak Publishing, Hampton, Virginia, 1985.
3. King, Jean I. F., "Nonlinear Exponential Inversion for Arbitrary Viewing", AFGL Notes, Hanscom AFB, undated.
4. King, Jean I. F., "H-Function Inversion", AFGL Notes, Hanscom AFB, undated.
5. McClatchey, Robert A., "Satellite Temperature Sounding of the Atmosphere: Ground Truth Analysis", AFGL Technical Report 76-0279, Hanscom AFB, 1979.

1986 USAF-UES SUMMER FACULTY RESEARCH PROGRAM
GRADUATE STUDENT SUMMER SUPPORT PROGRAM

Sponsored by the
AIR FORCE OFFICE OF SCIENTIFIC RESEARCH

Conducted by the
Universal Energy Systems, Inc.

FINAL REPORT

Experimental Protocols for Investigating the Physiology
of Orthostatic Intolerance in Humans

Prepared by:	David A. Ludwig, Ph.D
Academic Rank:	Assistant Professor
Department and	Mathematics Department
University:	University of North Carolina at Greensboro
Research Location:	USAFSAM/VN Brooks AFB San Antonio TX 78235
USAF Researcher:	Russell R. Burton Larry P. Krock
Date:	21 Aug 87
Contract No.	F49620-85-C-0013

Experimental Protocols for Investigating the Physiology
of Orthostatic Intolerance in Humans

by

David A. Ludwig

ABSTRACT

Orthostatic intolerance is associated with the inability of cardiovascular reflexes to maintain arterial pressure and can be manifested by the onset of presyncopal symptoms or syncope during exposure to hydrostatic stress in the head:foot (+G_z) direction. Two experimental protocols are presented to further study the physiology of this condition. It is hoped that the data from these two investigations will allow for a more complete understanding of orthostatic intolerance in humans. At this point, the relative contribution of venous compliance and arterial pressure have not been demonstrated.

Acknowledgements

I wish to thank the Air Force Systems Command and the Air Force Office of Scientific Research for sponsorship of this research. Universal Energy Systems must be mentioned for their concern and help tome in all administrative and directional aspects of this program.

I also wish to thank all of the researchers in acceleration effects especially Russell Burton and Larry Krock.

I. Introduction and Objectives

Venous Compliance Determinations Using the USAFSAM Human-Use Centrifuge

A positive correlation between orthostatic tolerance and G tolerance among individual subjects have never been determined to be statistically significant in several studies designed to measure this relationship (Voloshin et al, 1974; Dlunkaya and Khomenko, 1985; Klein et al 1969). This absence of direct relationship between these 2 tolerances is difficult to imagine since one would think that someone with a good orthostatic tolerance would have a good increased G tolerance. The reason for this poor relationship is probably because increased G tolerance is based on an arterial pressure function and orthostatic tolerance is a venous compliance determination (Newberry and Bryan, 1967). This study is designed to develop an increased G tolerance measurement with a venous compliance basis.

All relaxed $+G_z$ human tolerance measurements are based on an arterial pressure deficiency resulting in a rapid loss of vision called peripheral and central light loss (PLL; CLL). The standard exposure duration for this type of determination is either 15 sec for rapid onset run (ROR) G tolerance (1G/sec onset rates) or a continuous slow increase in G at 0.1 G/sec onset rates until PLL or CLL occurs immediately at which time the exposure is terminated--called gradual onset run (GOR).

This study will measure relaxed G tolerance using a deficiency in venous return as the basis for PLL or CLL; i.e. a test of the compliance of the venous vascular system below the level of the heart. This test will be conducted with $+G_z$ exposures at lower G levels than required for immediate PLL but exposing subject to this level of G until PLL occurs because of a change in the functional blood volume thereby limiting VR. This reduction in functional blood volume will be caused by some loss of blood fluid components extravascularly (reduction in total blood volume) and venomotor fatigue--a test of venous compliance.

Each subject will have a series of "compliance" G tolerance measurements conducted as different percentages of their GOR tolerance (i.e. 97.5%, 95%, 92.5%, and 90%). These measurements, which will be durations of G exposures, should give a regression for each subject as related to % of GOR. These individuals with smaller slopes of that equation have the least compliant venous system and should have the best orthostatic tolerances.

This study will be conducted to determine if a regression, as hypothesized, exists and if these regressions are characteristic for individual subjects. The orthostatic tolerance of these same subjects will be conducted at a later date lower body negative pressure (LBNP) apparatus for testing orthostatic tolerance under another human-use experimental protocol to be submitted to ACHE at a later date. LBNP is considered to be an excellent test for orthostatic tolerance (Hyatt, et al, 1975).

Establishing this ability to measure G tolerance with a compliance basis will broaden the testing capability of the human-use centrifuge; i.e. the creation of another measure of G tolerance. Once this is established and with the follow on study with LBNP, the centrifuge will be capable of measuring both tolerances as well as having the capacity of maintaining these tolerances in a space (weightless) environment. This study is critical in determining the physiologic relationship between orthostatic tolerance and increased G tolerance.

II. Experimental Plan and Recommendations

a. List of Equipment and Facilities: USAFSAM Human-use Centrifuge and all related equipment.

b. Subjects to be used: Ten subjects will be used from the USAFSAM acceleration subject panel.

c. Duration of the Study: Ten weeks.

d. Experimental Procedures: A GOR tolerance evaluation will be conducted on all of the subjects involving 4 runs at .10G/sec. Each subject will be evaluated on two separate days (two tests per day) to establish a reliable baseline and also determine how much variability to expect when subjects report for the experimental phase of centrifugation. This variability is quite small (Whinnery and Jackson, 1979). Once this baseline G tolerance has been established, subjects will be subjected to compliance tolerance runs of 97.5%, 95%, 92.5%, and 90% of their baseline G tolerance. The order in which the subjects receive the sub-maximal compliance G runs will be established at random and each run will be conducted on four separate days to eliminate carry over effects from run to run. Prior to testing of the submaximal stresses, each subject will be given a GOR tolerance run which will be compared to the results of the four previous (baseline) G tolerance evaluation runs. If the subject is not within two standard deviations of these initial GOR tolerance runs he will not be tested on that day. This criterion will insure that the subject has not altered his G tolerance during the course of the experiment. It will also insure that the submaximal percentages are accurate G proportions of the subjects maximal G tolerance.

Fluid shifts into the lower body will be measured using an impedance plethysmograph developed for use on the USAFSAM centrifuge (Montgomery et al 1987). To insure that the subjects are relaxed during these exposures EMG measurements will be made on the thigh muscle.

The statistical analysis will involve individual subject curve fitting across the four submaximal G runs. This will be accomplished through orthogonal polynomials within the framework of a repeated measures analysis of variance.

REFERENCES

1. Dlusskaya I.G. and M.N. Khomenko. Responses of subjects differing in tolerance of $+G_z$ to tilt tests and water loading tests.

Kosm. Biol. i Avia. Med. 19:22-27, 1985.

2. Hyatt, K.H., L.B. Jacobson, and V.S. Schneider. Comparison of 70° tilt, LBNP, and passive standing as measures of orthostatic tolerance. Avia. Space Environ. Med. 46:801-808, 1975.

3. Klein, K.E., H. Bruner, D. Jovy, L. Vogt, and H.M. Wegmann. Influence of stature and physical fitness on tilt-table and acceleration tolerance. Aerosp. Med. 40:293-297, 1969.

4. Montgomery, L.D., H.M. Hanish, and J.W. Burns. Lower body volume changes during rapid onset high G acceleration. Aerosp. Med. Ann. Meeting Abstract No. 96, 1987.

5. Newberry, P.D. and A.C. Bryan. Effect of venous compliance and peripheral vascular resistance of headward (+G_z) acceleration. J. Appl. Physiol. 23:150-156, 1987.

6. Voloshin, V.G., P.M. Suvorov, A.R. Kotovskaya and R.A. Vartbaronov. Predicting resistance to G-forces by the aid of a decomparison functional test. Voenno-Med. Zhur. 5:56-59, 1974. (NASA TT F-15, 823).

7. Whinnery, J.E. and W.G. Jackson, Jr. Reproducibility of +G_z tolerance testing. Avia. Space Environ. Med. 50:825-828, 1979.

IA. Introduction and Objectives

Tolerance to Lower Body Negative Pressure in Individuals With Varied Tolerances to Positive Gravitational Acceleration

The present protocol is the second part of a research effort seeking to assess the relationship between tolerance to lower body negative pressure (LBNP) and tolerance to positive gravitational acceleration stress ($+G_z$). This relationship, while never experimentally demonstrated, has achieved wide spread acceptance (Lategola and Trent, 1979; Dlusskaya and Khomenko, 1985; Vettes and Viellefond, 1983; Voloshire et al. 1974).

Intuitively the relationship is constructed upon a common end effect of excessive exposure to either of the two stresses--syncope; $+G_z$ syncope resulting from the inability of the arterial pressure system to provide adequate brain perfusion, while an LBNP syncopal event is due, in whole or part, to a compliant venous system sequestering blood within the lower extremities (Luft et al., 1976; Newberry and Bryan, 1967).

Since different cardiovascular mechanisms are responsible for the syncopal event to either stress, it is possible to suggest that a sample of the population may tolerate one of the two stresses better than the other. It is the global objective of this research effort to explore the relationship between tolerances to $+G_z$ and LBNP stress.

The first part of this effort sought to develop a $+G_z$ stress tolerance measurement with a venous compliance component (Proposal submitted by Drs. Burton, Krock and Ludwig and approved by ACHE in May, 1987) employing the human-use centrifuge as the device. The data gathered thus far appears to support the proposed hypothesis. During the first phase the subjects experienced four different onset rates ranging from rapid to very gradual. Subjects responded in two different ways: they tolerated the rapid onset rates better than the gradual ones or they responded in the opposite manner.

The second part, the present proposal will employ LBNP, the traditional device, to examine the venous compliance response of the participants. Lower body negative pressure has been successfully employed since the early 1960's as a mechanism of simulating orthostatic stress (Hoffler et al., 1974; Stevens and Lamb, 1965). Redistribution of blood volume is the primary effect with a secondary response being a reduction in venous return to the thorax consequently decreasing cardiac output and stroke volume (Stevens and Lamb, 1965). Studies show that the range of individual LBNP tolerance extends from approximately -40 mm Hg to -110 mm Hg with respect to ambient atmospheric pressure.

The net result of this research will be to provide an answer to whether or not tolerance to LBNP is related to a variety of $+G_z$ tolerances--Is there a direct correlation between LBNP and $+G_z$ tolerances designed for orthostasis? Having established a relationship between the two, a broader capability will be available to a human-use centrifuge, that is, measuring and maintaining orthostatic and $+G_z$ tolerances in a zero-gravitational (space) environment. Completion of this study is critical to understanding the cardiovascular relationship between tolerance to positive gravitational acceleration and lower body negative pressure.

IIA. Experimental Plan and Recommendations

a. List of Equipment and Facilities: USAFSAM lower body negative pressure device and all related equipment.

b. Subjects to be used: The same subjects employed during the sustained $+G_z$ tolerance phase of the study will be employed during this LBNP phase.

c. Duration of the Study: Individual experimental sessions are anticipated to last less than one and one-half hour total. The exposure to negative pressure should be less than 30 minutes. Data gathering should be complete within three months from the onset of the study; however, scheduling and equipment performance will be the rate

limiting factors.

d. Experimental Procedures: A stepwise incremental protocol will be employed to determine individual pre-syncopal tolerance to lower body negative pressure.

The subject will report to the laboratory on the morning of the test rested and non-fasted; a two-hour, post-prandial interval is requested. The subject will be instrumented (12-lead electrocardiogram, impedance plethysmograph, 3-lead electromyograph, and a blood pressure cuff) then assisted into the supine position of LBNP chamber. A foam-padded stabilization saddle will be adjusted to subject comfort and an air-tight seal secured at the subject's waist. [USAF/SAM/VN protocol - Dr. David H. Glaister (RAF), September, 1985]. The participant will rest quietly for a minimum of 10 minutes. During the final minute of the base line period, physiologic measurements will be taken to assure participant readiness for LBNP. Pressure within the chamber will then be reduced by 25 mm Hg from atmospheric and remain at that level for three minutes. Additional 15 mm Hg pressure reductions will occur at three-minute intervals until one of the following test terminating criteria is achieved: (1) The subject chooses to end the LBNP exposure (2) Completion of three minutes at a relative pressure of -100 mm Hg (3) Onset of pre-syncopal symptoms such as an abrupt decrease in blood pressure and/or a precipitous decrease in heart rate--(15 bpm) from the previous recording, (4) A progressive decline in systolic blood pressure to less than 80 mm Hg (5) The medical monitor and/or investigator deems it in the interest of subject safety.

Electrocardiographic, electromyographic and impedance plethysmographic information will be monitored throughout the experimental session. Blood pressure will be monitored at the end of the early stages, then at one minute intervals following stage two.

Linear regression and correlation analyses will be used to study the statistical relationships between tolerance to LBNP and tolerance

to various onset rates of gravitational acceleration.

REFERENCES

1. Burton, R.R., L.P. Krock and D.A. Ludwig. Venous compliance determination using the USAFSAM human-use centrifuge, approved ACHE protocol, May, 1987.
2. Dlusskaya I.G. and M.N. Khomenko. Responses of subjects differing in tolerance of $+G_z$ to tilt tests and water loading tests. Kosm. Biol. Avia. Med. 19:22-27, 1985.
3. Glaister, D.H., N.L. Lewis, J.W. Burns, K.K. Gillingham, S.G. Schiflett and J.E. Whinnery. Evaluation of psychomotor performance during application of lower body negative pressure (LBNP) in relation to cerebral tissue oxygen status. Approved ACHE protocol, October, 1985.
4. Hoffler, G.W., R.A. Wolthius and R.L. Johnson. Apollo space crew cardiovascular evaluations. Aerosp. Med. 45: 807-820, 1974.
5. Lategola, M.T. and C.C. Trent. Lower body negative pressure box for $+G_z$ simulation in the upright seated position. Avia. Space Environ. Med. 50: 1182-1184, 1979.
6. Luft, V.C., L.G. Myhre, J.A. Ledpsky and M.D. Vettters. A study of factors affecting tolerance of gravitational stress simulated by lower body negative pressure in specialized physiological studies in support of manned spaceflight. Contract NASA 9-14472, Albuquerque, Lovelace Foundation, 2-60, 1976.
7. Newberry, P.D. and A.C. Bryan. Effects on venous compliance and peripheral vascular resistance of headward ($+G_z$) acceleration. J. Appl. Physiol. 23: 150-156, 1967.
8. Stevens, P.M. and L.E. Lamb. Effects of lower body negative

pressure on the cardiovascular system. Amer. J. Card., 16: 506-515, 1965.

9. Vettes, B. and H. Viellefond. Value of the lower body negative pressure test in Aerospace Medicine. In AGARD Non-invasive Methods of Cardiovascular Exploration in Aerospace Medicine. p.189-192, 1983.

10. Volshine, V.G., P.G. Suvorov, A.R. Kotouskaya and R.A. Vartbaronov. Predicting resistance to G-forces by the aid of a decompression functional test. Volenno-Med Zhur. 5:56-59, 1974 (NASA TT F-15, 823).

1987 USAF-UES SUMMER FACULTY RESEARCH PROGRAM
GRADUATE STUDENT SUMMER SUPPORT PROGRAM

Sponsored by the
AIR FORCE OFFICE OF SCIENTIFIC RESEARCH

Conducted by the
Universal Energy Systems, Inc.

FINAL REPORT

Effect of Repeated Low Dose Soman On Acetylcholinesterase Activity

Prepared by:	Mohammed A. Maleque, Ph.D.
Academic Rank:	Associate Professor
Department:	Pharmacology
University:	Meharry Medical College Nashville, Tennessee
Participants:	Antoinne C. Able Otis Cosby
Research Location:	USAFSAM/RZB Brooks AFB San Antonio, TX 78235
USAF Researcher:	Lt. Col. Stan L. Hartgraves
Date:	28 August 87
Contract No:	F49620-85-C-0013

EFFECT OF REPEATED LOW DOSE SOMAN ON ACETYLCHOLINESTERASE ACTIVITY

By

MOHAMMED A. MALEQUE, PH.D.
Antoinne Able, Otis Cosby, Jr.

ABSTRACT

Acetylcholinesterase activity was measured in rodents during repeated low dose soman exposure and following the cessation of exposure by spectrophotometric and radioisotopic methods. A repeated single dose of soman (39.0 ug/kg., s.c.) inhibited the acetylcholinesterase activity both in rat blood serum and brain hippocampus and amygdala. However, the degree of inhibition varied from one tissue to another. Similarly to the differential inhibition, recovery of the enzyme activity was also observed following the cessation of soman exposure over a 5 day period. This research was conducted as part of a larger study which is attempting to measure the effect of repeated soman on biochemistry, neurohistology, and performance in either the same subjects or in subjects matched for soman poisoning. The study will provide a unique opportunity to obtain neurochemical information concurrently with information on neurohistological changes and performance.

ACKNOWLEDGEMENTS

I wish to thank the Air Force Systems Command and the Air Force Office of Scientific Research for sponsorship of this research. Universal Energy Systems must be mentioned for their concern and help to me in all administrative and directional aspects of this program.

My experience was rewarding and enriching because of many different influences. I met many Air Force Scientists and learned a lot about the needs and goals of various Air Force Research Projects. Lt. Col. S. Hartgrave's interest in every phase of this research truly served as a constant source of stimulation. He provided us with support, encouragement, and a truly enjoyable working atmosphere. The help of Dr. M. Murphy was invaluable in overcoming many roadblocks. The help of Dr. M. Murphy, Lt. S. Kerenyi, SSGt. D. Evans, AlC L. Albano, Ms. S. Miller, and Ms. H. O'Neil was greatly appreciated. The administrative support and kindly treatment of Dr. J. Wolfe is certainly praiseworthy. Finally, I must thank Ms. M. Lopez for typing this report.

I. INTRODUCTION

Much of what we know about acetylcholinesterase (AChE) and neuropathy target esterase come from studies involving irreversible inhibitors such as organophosphorous esters and carbamates. The physiological function of AChE in nervous tissue is well known: it hydrolytically inactivates the cholinergic neurotransmitter, acetylcholine (ACh), thereby terminating the chemical signal. Irreversible inhibition of AChE in vivo by a variety of inhibitors such as diisopropylfluorophosphate (DEP) and pinacolyl methylphosphonofluoride (soman) produce an identical effect, namely accumulation of unhydrolyzed ACh with well known pharmacological and acutely toxic effects. The duration of effects depends on the degree of inhibition and the persistence thereof. Although numerous studies on acute soman toxicity have been conducted, a well planned, simultaneous study on low dose soman effects on biochemistry, behavior, and neurohistology is lacking.

The Radiation Biology Branch, Radiation Sciences Division of the USAF School of Aerospace Medicine at Brooks Air Force Base is particularly interested in the bioeffects of repeated low dose soman on lethality, clinical symptoms, brain and blood chemistry, neural degeneration and performance. Recently, operational planners have directed a greater attention to the battlefield scenario in which personnel may be exposed to repeated low doses of nerve agent over a period of many days. To address this issue, scientists at Brooks AFB-SAM/RZB have proposed a project titled, "Effects of Soman on Rodent Performance, Physiology, and Tissue Cholinesterase Levels".

My research interest have been in the area of neurotransmission,

particularly cholinergic neurotransmission. I have applied biochemical and electrophysiological techniques in the investigation of synthesis, release and activation of receptors by ACh and its interaction with agonists and antagonists. My previous biochemical work includes choline uptake, ACh synthesis and release processes in the invertebrate CNS. Electrophysiological work includes elucidation of the mechanism(s) of action of cholinergic agonists (including anticholinesterases) and antagonists on ACh receptor-ion channel complexes. My research experience in the cholinergic system and previous work with nerve gases (e.g. soman, sarin, tabun and VX) contributed to my assignment to this project. Antoine Able and Otis Cosby were chosen because they have studied biochemistry, physiology and pharmacology in their Medical Sciences course, have previous research experience, and have shown keen interest in the cholinergic system.

II. OBJECTIVES OF THE RESEARCH EFFORT

The overall goal of the main project includes studies on:

1. biochemistry; 2. neurohistology and; 3. performance during repeated exposure to soman and following the cessation of soman exposure. The objectives of the biochemical study include measurement of AChE activity, choline uptake, choline acetyltransferase (CAT) enzyme activity, and glutamate uptake. Since it is a vast project and will require a long period of time for completion, we were assigned to do a part of the biochemical study.

My assignment as a participant in the 1987 Summer Faculty Research Program (SFRP) was to measure the AChE activity during the

repeated exposure to low dose soman and following the cessation of soman exposure. Antoine Able and Otis Cosby, as participants in the 1987 Graduate Student Summer Support Program (GSSSP), also worked with me on this project.

Neurochemical analysis is very important to this project since the phenomena of behavior, tolerance, withdrawal, recovery, and neurohistological changes are expected to be reflected in changes in brain neurochemistry. Although blood AChE levels may grossly correlate with effects of soman on performance, such changes in the body periphery do not necessarily reflect changes in the CNS. The primary interest of the RZB chemical defense research program is to obtain neurochemical information concurrently with information on peripheral biochemistry, neurohistology and performance. To achieve that goal, a simultaneous study was conducted to measure the effect of repeated soman on blood and brain AChE activity, performance and neurohistological changes in either the same subjects or in subjects matched for soman dosing. Results of this study to date have provided very important positive information and certainly warrant continuation of this project.

III. STUDY PLAN

The plan for the proposed biochemical study to measure of AChE levels is presented in Table 1. The data in the cells of Table 1 indicate the number of rats sacrificed under each condition for each day. This plan was repeated once, doubling the total number of animals used. The LD₅₀ estimates were determined first, with the acute LD₅₀ dose for soman being 125ug/kg, and the 5 day chronic LD₅₀

being 48ug/kg. The soman dose chosen for biochemical studies was 39ug/kg. This matches the lower dose that will be used in performance and neurohistological studies. The measurement of AChE levels was carried out in whole blood, serum and brain amygdala and hippocampus.

Possible relationships between blood AChE measures and brain AChE measures were tested by the Pearson Product-moment correlation coefficient, r . Possible relationships between symptom ratings and brain AChE were examined by means of the Spearman rank correlation coefficient, r_s .

Radioisotopic Assays of AChE: The assay used to determine brain AChE levels was radioisotopic modification of the technique of Siakotos et al, 1969, as described by Michalek and Stavinoha, 1978. The activity of brain AChE was measured by the enzymatic conversion of acetyl-1-¹⁴C-choline iodide. Radiolabelled substrate (50uCi, S.A.3mCi/mmol) was added to a reaction mixture and diluted brain homogenate. The reaction was ended after 5 minutes by adding resin in dioxane to remove unhydrolyzed substrate. After centrifugation for 10 minutes at 2000 rpm, an aliquot of supernatant (5ml) was diluted to 20ml with Bray's cocktail and was analyzed by liquid scintillation counting. Data is reported as nmol/mg tissue/hr.

Spectrophotometric Assays of AChE: Acetylcholinesterase (whole blood) and butyrylcholinesterase (serum) activities were measured as described by Ellman et al., 1961 with a spectrophotometer. The final concentration of the reagents was 48.0 mM phosphate buffer, pH 7.2, 5.0 mM ACh iodide, and 0.24 mM, 5, 5-1 dithiolobis (2 nitrobenzoic acid), DTNB. The reaction mixture was composed of 3.0 mM of buffer containing DTNB; 0.10 ml of ACh iodide solution and routinely 0.02ml

of serum of hemolyzed whole blood. The serum samples were centrifuged for 10 minutes at 4000 rpm at 4⁰C. The spectrophotometer was set at a wavelength of 405 nm. The absorbance (A/min) was calculated to yield an enzyme activity expressed at mU/ml.

b. Results: A single dose (39 ug/kg, s.c.) of soman decreased the serum AChE activity by about 90% in 1 hour. However, there was a partial recovery 24 hours after the first injection. When the same dose was repeated, similar inhibition followed by recovery occurred during the 5 day repeated soman protocol (Table 1). These results generally agree with those reported earlier on monkeys receiving 0.97 ug/kg soman for 5 consecutive days (Blick et. al., 1987). Following cessation of repeated soman administration in rats, recovery reached approximately 75% of control in a 5 day period. A similar pattern but less consistent effect of soman was observed in the whole blood AChE levels.

Measurement of AChE Activity in the brain hippocampus from the same soman-treated rats revealed an inhibition of the enzyme activity in 1 hour following 5 days chronic treatment. The inhibition and recovery of AChE activity fluctuated in a regular pattern in the 5 day period of repeated soman injections. AChE activity in the hippocampus 5 day after the last soman injection showed slight recovery. In the amygdala, the AChE activity was less suppressed and the reading less consistent.

The significance and importance of this finding can be summarized as follows:

a. In the presence of the same dose of soman, AChE activity in the serum appeared to be much more suppressed compared to that of the

hippocampus.

- b. AChE activity in the serum showed a trend of recovery after the last soman injection while the AChE activity in the hippocampus showed relatively slow recovery.
- c. This study made a comparison between AChE activities in the periphery and brain tissues, and will ultimately correlate these measures with performance and neurohistological changes. While changes in ChE activity, especially in periphery, do not correlate well with behavioral changes, it is hoped regional changes within the brain may suggest more appropriate behavior tests. Correlations between degree of brain ChE inhibition and the neurohistological damage are also possible.

IV. RECOMMENDATIONS

- a. Results of this summer research clearly demonstrate biochemical effects in the hippocampus and amygdala of the rodent brain and in blood serum following repeated low level exposure to soman. Since some animals died during this low level exposure and the recovery of the AChE activity was not complete following the cessation of soman exposure, further study should be conducted with several low doses and longer recovery periods.
- b. As several other brain regions also showed neurohistological abnormalities following soman exposure, more brain regions should be included for the measurement of biochemical parameters.
- c. Finding of a good correlation between biochemical and neurohistological change would suggest that more biochemical parameters such as CAT activity, glutamate uptake, etc., as proposed by the main proposal should be carried out.

- d. It is entirely possible that the detection of early biochemical changes may be used as diagnostic tool for the treatment and/or prevention of brain damage and performance decrement.
- e. Determination of biochemical changes following low dose soman is very important. As this piece of research has provided very important findings, I would like to continue this project in collaboration with RZB researchers. As a UES Summer Faculty Research Fellow I would like to submit a Mini Grant Proposal. Lt. Col. Hartgraves, my technical focal point, shown keen interest in this project.

REFERENCES

- Ellman, G.L., Courtney, K.D., Andres, V. Jr. and Featherstone R.M. (1961). A new rapid colorimetric determination of acetylcholinesterase activity.
- Siakotos, A.N., Filbert, M., and Hester, R. (1969). A specific radioisotopic assay for acetylcholinesterase and pseudocholinesterase in brain and plasma. *Biochem. Med.* 3. 1-12.
- Michalek, H., and Stavinoha, W.B. (1978). Effect of chlorpromazine pre-treatment of the inhibition of total cholinesterase and butyrylcholinesterase in brain of rats posioned by physostigmine or dicholorvos. *Toxicol.* 9. 205-218.
- Blick, D.W., M.R. Murphy, G.C. Brown, M.G. Yochmowitz, and S.L. Hartgraves (1987). Primate equilibrium performance following soman exposure: Effects of Repeated daily exposures to low soman doses. *Proc. 6th Med. Chem. Def. Biosc. Rev. Aug.* 4-6, 317 p.

TABLE 1: Biochemistry Plan

Experimental Day	Repeated Soman					Post Soman						
	1 *B A	2 B A	3 B A	4 B A	5 B A	6	7	8	9	10	11	12
Control (N = 60)	** 4 4	4 4	4 4	4 4	4 4			4	4	4	4	4
Soman*** (N = 75)	5 5	5 5	5 5	5 5	5 5			5	5	5	5	5

*B = Before daily injection; A = After daily injection.
 **Number of subjects.

1987 USAF-UES SUMMER FACULTY RESEARCH PROGRAM

GRADUATE STUDENT SUMMER SUPPORT PROGRAM

Sponsored by the

AIR FORCE OFFICE OF SCIENTIFIC RESEARCH

Conducted by the

Universal Energy Systems, Inc.

FINAL REPORT

DISPOSAL OF CHEMOTHERAPEUTIC WASTES

Prepared by:	Robert E. Masingale, Sr., Ph.D. and Donna N. Edwards, graduate assistant
Academic Rank:	Professor of Chemistry
Department and University	Division of Science and Mathematics Jarvis Christian College
Research Location:	USAF OEHLE/ECQ Brooks AFB TX 78235-5501
USAF Researcher:	Elliot K. Ng, Maj, USAF, BSC
Date:	4 August 1987
Contract No:	F49620-85-C0013

DISPOSAL OF CHEMOTHERAPEUTIC WASTES

by

Robert E. Masingale, Sr.

ABSTRACT

Air Force medical facilities are generating chemotherapeutic wastes from care and treatment of oncologic cases. Proper disposal of these wastes are dependent upon guidelines that are currently insufficient or nonexistent. A survey reveals that the majority of Air Force medical facilities generated a small quantity of chemotherapeutic waste and that less than 5% of Air Force medical facilities were responsible for the majority of the chemotherapeutic wastes. Many facilities are disposing their chemotherapeutic waste in pathological incinerators. This study focused on exploring chemical deactivation and incineration as disposal methods. Chemical deactivation was explored as an alternate means for facilities with limited access to cost-effective disposal systems. Incineration was also investigated because it was stated to be the disposal method of choice.

ACKNOWLEDGEMENTS

I wish to thank the Air Force Systems Command, the Air Force Office of Scientific Research and the USAF Occupational and Environmental Health Laboratory for sponsorship of this research. Universal Energy Systems must be mentioned for their concern and help to me in all administrative and directional aspects of this program.

My experience was rewarding, enriching and especially educational. Maj Elliot K. Ng provided me with support, encouragement, and a truly enjoyable working atmosphere. MSgt Horace L. Burbage helped in supplying all administrative needs. Special thanks to my graduate assistant Donna Norris-Edwards whose loyalty and dedication made this effort possible.

I. INTRODUCTION

A problem facing Air Force medical facilities is the ultimate disposal of chemotherapeutic waste generated in care and treatment of oncogenic cases. Although the occupational hazards of chemotherapeutic agents are well documented,¹⁻⁴ documented research on environmental consequences from disposal of chemotherapeutic agents is still virtually nonexistent.

The USAF Occupational and Environmental Health Laboratory, Consultant Services Division, Environmental Quality Branch, is concerned with disposal of chemotherapeutic waste, because there are insufficient guidelines available to Air Force medical facilities.

My main research interest has been with metabolic antagonists. In this area, inhibitors of enzymes may be used to suppress growth of pathogens, tumors or viruses. Work with the synthesis and study of structure - activity relationships of potential antineoplastic substances - probably contributed to selection and assignment with the Consultant Services Division, USAF Occupational and Environmental Health Laboratory.

An excellent academic record in undergraduate and graduate school, as well as her knowledge of medicinal chemistry was of particular importance for the selection of my graduate assistant for this research effort.

II. OBJECTIVES OF THE RESEARCH EFFORT

Currently, there are no known state or federal guidelines available to the Air Force for disposal of chemotherapeutic waste. Such waste may be in the form of unused antineoplastic agents, used needles, syringes, vials, ampuls, gloves, gowns and other protective devices used in care

of oncogenic patients. Due to the potential environmental hazards of such materials, it is necessary to formulate precise safe disposal practices.

My assignment as a participant in the 1987 Summer Faculty Research Program (SFRP) was to explore the problem of disposal of chemotherapeutic waste generated in Air Force medical facilities.

To obtain a better understanding of the chemotherapeutic waste disposal problem in general, it was deemed necessary to consult other institutions outside the Air Force. Facilities consulted included: national research institutions, state environmental agencies, hospitals, Army medical facilities, disposal services and pharmaceutical laboratories (Appendix A).

Due to factors such as variability of facility size, availability of drug and treatment alternatives, and budgetary constraints, the elements of a waste disposal program differed among facilities. Disposal practices commonly employed were: pathological or hazardous waste incinerators, municipal or hazardous waste landfills, and sanitary sewers (after chemical deactivation).

Incineration was considered the method of choice because afterwards the agent was considered completely destroyed and/or the inert residue was easily disposed of.⁵

The majority of the institutions contacted suggested a minimum temperature of 1000 °C was necessary to completely destroy chemotherapeutic waste. Unfortunately, there is very little documented research to determine whether the minimum suggested temperature of 1000 °C is sufficient to completely destroy chemotherapeutic waste without formation of other undesirable by-products.

Listed below are some of the advantages and disadvantages of commonly employed disposal options extracted from an article in the Canadian Journal of Hospital Pharmacy:⁶

Sanitary Sewer (after chemical deactivation)

Advantages

1. Easily accessible to all hospital pharmacists.
2. With a dilution factor involved, trace contaminated amounts of pharmaceuticals into the sewer and the natural excretion of drugs and their metabolites in urine and feces should not present a hazard.

Disadvantages

1. Bulk contaminated amounts and indiscriminate disposal of pharmaceuticals, may result in contamination of water supply and disruption of sewage treatment process.
2. Antibiotics (etc.) can upset the bacterial flora.

Landfills

Advantages

1. Specialized landfills do exist in which leaching by groundwater will not contaminate aquifers.

Disadvantages

1. If not a specialized landfill, water supplies may be contaminated by groundwater flowing through and solubilizing the drug.
2. Antibiotics and antiseptics may upset the bacterial flora used in the compost process.
3. Precautions are necessary during transporting of hazardous agents to site, to prevent accidental exposure of handlers to dangerous medicinals.

Incineration

Advantages

1. Best method of disposal as it results in the destruction of drugs.

Disadvantages

1. Many hospitals do not have on-site EPA permitted hazardous waste incinerators.
2. Transportation precautions must be taken for off-site incineration, and its costs.
3. Some incinerator operators do not allow noncombustible products to be incinerated (i.e., injectables in glass containers).
4. Emissions from the incinerator can present another type of environmental problem.

III. AIR FORCE SURVEY RESULTS

To assess the magnitude of the chemotherapeutic waste disposal problems within Air Force medical facilities a survey was initiated. This survey was designed to determine the types, amounts and methods of managing chemotherapeutic waste.

The seventy-six agents selected for the survey were taken from a previous USAFOEHL Report.⁷ This list of chemotherapeutic agents included the best inventory available of agents used within the Air Force. All agents on the list were classified as either carcinogenic, mutagenic or teratogenic. Thirty-two are antineoplastic, and twenty-three are classified as hazardous waste by the Environmental Protection Agency, i.e., U - Coded (Appendix B).

Results of the survey revealed that less than 5% of the Air Force facilities that responded had ongoing oncology programs. These medical

facilities were therefore responsible for a very large percentage of antineoplastic waste generated in the Air Force. The amounts and methods of disposal of chemotherapeutic waste from these medical facilities are shown in Table 1.

Table 1. Waste Amounts and Disposal Methods of Selected USAF Hospitals

AF Facilities	Command	No. of Beds	Waste/Year*	Disposal** Method
Lackland AFB TX	ATC	1000	24	HC
Homestead AFB FL	TAC	70	4	HC
Keesler AFB MI	ATC	305	20	PI
Scott AFB IL	MAC	250	48	HC
Sheppard AFB TX	ATC	250	4	PI

* 55-gallon drums

** HC = Hazardous Waste Contractor

PI = Pathological Incinerator

An overall summary of types of waste, amounts and disposal practices by command from those USAF medical facilities which responded is given in Table 2 (Exclusive of those in Table 1).

Table 2. Waste Types and Management of USAF Hospital Response

Command	No. of Facilities	No. of Beds	Type* Waste	Disposal** Method
USAFE	37	0-20	MT, X items, AW	PI = 11.0% NP = 74.0% HC = 15.0%
	2	21-40	X items, AW	PI = 50.0% NP = 50.0% HC = 0.0%
	4	41-80	MT, X items, X solns	PI = 0.0% NP = 75.0% HC = 25.0%
	1	81-up	MT, X items,	PI = 0.0% NP = 100.0% HC = 0.0%
TAC	5	0-25	MT, X items, AW	PI = 20.0% NP = 60.0% HC = 20.0%
	6	26-50	X items, MT	PI = 17.0% NP = 50.0% HC = 33.0%

Table 2, continued

Command	No. of Facilities	No. of Beds	Type* Waste	Disposal** Method
TAC cont'd	2	51-75	MT, X items, AW	PI = 0.0% NP = 50.0% HC = 50.0%
SAC	10	0-25	MT, X items,	PI = 50.0% NP = 30.0% HC = 20.0%
	9	26-50	MT, X items, AW	PI = 44.0% NP = 56.0% HC = 0.0%
	4	51-up	MT, X items, AW	PI = 50.0% NP = 25.0% HC = 25.0%
MAC	5	0-25	MT, X items, X solns, AW	PI = 20.0% NP = 40.0% HC = 40.0%
	3	26-50	AW	PI = 0.0% NP = 100.0% HC = 0.0%
ATC	6	0-25	MT, X items, X solns, AW	PI = 33.0% NP = 67.0% HC = 0.0%
	2	26-50	MT, X items, X solns, AW	PI = 50.0% NP = 0.0% HC = 50.0%
AFSC	1	0-100	No waste	PI = 0.0% NP = 0.0% HC = 0.0%
	1	101-up	MT, AW	PI = 100.0% NP = 0.0% HC = 0.0%
AAC	1	0-100	AW	PI = 0.0% NP = 100.0% HC = 0.0%
AFLC	2	0-100	MT, X items, X solns	PI = 100.0% NP = 0.0% HC = 0.0%
	1	101-up	AW	PI = 0.0% NP = 0.0% HC = 100.0%

*MT = empty containers

X items = expired items up to 2 Kg

X solns = reconstituted unused i.v solutions, up to 16 Qts.

AW = less than one 55-gallon drum/yr of antineoplastic waste, e.g., vials, needles, syringes, gowns, gloves, masks, bags and tubing.

**HC = Hazardous Waste Contractor

PI = Pathological Incineration.

NP = Non-specified; includes trash, sewer, landfills, incineration, or no plan.

IV. CHEMICAL DEACTIVATION

From the survey results it was apparent that the majority of Air Force medical facilities generate small quantities of chemotherapeutic waste. Consequently, there is a necessity for methods to manage small amounts of chemotherapeutic agents, without the cost associated with contractual disposal at an approved hazardous waste disposal site.

Therefore, this search has led to chemical deactivation as an alternative: (a) where meager quantities of chemotherapeutics are being generated; (b) for small facilities; and (c) where cost of contractual disposal is prohibited.

Few reports of research on chemical deactivation are available, however, pharmaceutical laboratories (Appendix B) have supplied material safety data sheets for their drugs. In this effort these were used, as well as other reports from the literature.⁸⁻⁹

The seventy-six chemotherapeutic agents chosen for this study have been characterized into alkylating agents, antimetabolites, natural products, hormones and antagonists, miscellaneous agents and laboratory chemicals (Appendix B). Each category was subdivided for similarity in reactivity and deactivation.

Since most of the non-antineoplastic agents were infrequently used, we only focused our search for chemical deactivation methods on the antineoplastic agents.

These chemical destruction and deactivation methods listed in Appendix C are not intended to substitute for any other methods, but to provide an alternative for facilities with limited access to cost-effective disposal systems.

V. INCINERATION

Since approximately 30% of the agents chosen for this study has an EPA U-Coding, they must be disposed of in a RCRA (The Resource Conservation and Recovery Act) permitted hazardous waste incinerator or landfill.¹¹ At the present there are no regulations issued by the Environmental Protection Agency requiring a minimum incineration temperature for chemotherapeutic agents. However, a recent letter from the Hazardous Materials Technical Center (HMTTC) states that the director of the Incinerator Permit Assistance Branch of EPA recommends a minimum incineration temperature range of approximately 982-1093 °C. In addition, HMTTC recommends that cytotoxic drugs that are either listed or characteristic hazardous waste be incinerated in facilities that are RCRA approved, to include even small quantities (Appendix D).

The National Institute of Health's preliminary studies on thermal destruction of cytotoxic drugs states that 982 °C might be sufficient for destruction of drugs under ideal conditions. After further studies taking into consideration the variables (retention time, temperature, mixing turbulence and oxygen content) they recommended a minimum temperature of 1000 °C and closely monitoring stack emissions (Appendix D).

At the Research Institute, University of Dayton, a carefully controlled study was carried out using cyclophosphamide (a listed RCRA hazardous waste with the EPA hazardous number U-058) a widely used chemotherapeutic agent. Under pyrolytic conditions (100% N₂) at temperatures greater than 1000 °C, and a retention time of two seconds, the agent was not completely destroyed, and other toxic thermal reaction by-products were observed. However, destruction of the compound was complete under oxidative conditions (air) at 800 °C and retention time

of two seconds with only trace amounts of thermal reaction detected in emission gases. Increased effectiveness of thermal destruction of this agent appears to be due to the excess oxygen.¹²

Chem Waste Management Company of Memphis, Tennessee is a disposal service with experience in the incineration of cytotoxic drugs. Their EPA permit for incineration of these drugs requires a minimum incineration temperature of 982 °C. According to the manager of government contracts, secondary burners and scrubbers, either wet or dry are required for complete destruction of drugs at this temperature (Appendix D).

The Environmental Protection Agency has concluded that 1000 °C does destroy organics. Their analysis was done at industrial settings. A few publications have also stated that 1000 °C is sufficient to destroy chemotherapeutic waste.¹³⁻¹⁴ This may be the reason that many of the institutions contacted, have stated and/or practiced, 1000 °C for destruction of chemotherapeutic waste. Unfortunately, there is still a serious lack of documented research to support the minimum required temperature for complete thermal destruction.

VI. RECOMMENDATIONS

1. Since much of the waste generated in Air Force medical facilities results from expired items in pharmaceutical inventories, stock levels should be kept to an absolute minimum, and items should be returned to the vendor before the expiration date.

2. Preparing and administering antineoplastic agents can result in small amounts of residues absorbed on barrier clothing, in needles, syringes, ampuls and vials. Permeation of the chemotherapeutic drugs

may be minimized by using protective clothing made of Saranex-laminated Tyvek material.¹⁵

3. Syringes, vials and ampuls could be rinsed with a volatile solvent such as methanol, and the rinse placed in an evaporating dish and allowed to evaporate in a ventilation hood to dryness. The drug residue could then be disposed of by chemical or thermal destruction.

4. Further investigations of chemical deactivation methods for antineoplastic drugs should be undertaken because the cost-effectiveness might rival or exceed that of incineration of small amounts of waste as encountered in Air Force medical facilities. For example, in a given class such as alkylating agents, mechlorethamine was recommended for deactivation with 10% sodium thiosulfate and 10% sodium carbonate. The reactive center common to this class of reagents is the chloroethylamine function. A proposed future research problem would be to find if a single reagent system could be used to deactivate this entire class of drugs, i.e., a separate reagent system for each class of drug.

5. Another method for chemical destruction of organic compounds which might be worth considering, is the Kjeldahl Method.¹⁶ Using this method, organic compounds are completely destroyed in concentrated sulfuric acid with a catalyst. In the original process, the organic substance is digested in concentrated sulfuric acid with a catalyst such as mercury, copper or selenium. When digestion is complete, the digest is neutralized with sodium hydroxide. This method could easily be modified for chemical destruction of antineoplastic drugs, or other chemical agents.

6. Since a majority of Air Force medical facilities have pathological incinerators available, modification might be practicable

and prove to be the most cost-effective method to dispose of chemotherapeutic waste, by incineration. This modification would most likely include a secondary chamber and burner, and the use of a catalyst such as aluminum coated with noble metals (e.g., platinum, palladium and rhodium) and other materials (e.g., copper chromate, copper oxide, chromium and manganese) to lower the temperature to 260-480 °C, and to decrease retention time.¹⁶ A disadvantage with this approach may be the eventual requirement to permit this modified incineration as a hazardous waste treatment unit.¹⁷

REFERENCES

1. Selevan, S.G., et. al., "A Study of Occupational Exposure to Antineoplastic Drugs and Fetal Loss in Nurses," The New England J. of Medicine, 1985, Vol. (19) 313, pp 1173-1178.
2. Taylor, T.A., and Wade, A.E., "Chemical Carcinogenicity and the Antineoplastic Agents," Amer J. of Hospital Pharmacy, 1984, Vol. 41, pp. 1844-1845.
3. Yodiaken, R.E., and Bennett, D., "OSHA Work Practice Guidelines for Personnel Dealing with Cytotoxic (Antineoplastic) Drugs," Amer J. of Hospital Pharmacy, 1986, Vol. 43, pp. 1193-1204.
4. Vaughn, M.C., and Christensen, W.D., "Occupational Exposure to Cancer Chemotherapeutic Drugs," USAFOEHL Report 84-273EH111GGA.
5. Bacovsky, R., "Disposal of Hazardous Pharmaceuticals," The Canadian J. of Hospital Pharmacy, Jan-Feb 1981, Vol. XXXIV, No. 1, pp. 12-13.
6. *ibid*
7. Artiglia, E.W., and Elves, R.G., "Handling, Storage and Disposal of Chemotherapeutic Agent Residues and Wastes," USAFOEHL Report, 85-085EQ111EHH.
8. Wilson, S.J., "Safe Disposal of Some Commonly Used Injectable Antineoplastic Drugs," J. of Clinical and Hospital Pharmacy, 1983, Vol. 8, pp. 295-299.
9. Castegnaro, M., Adams, J., Armour, M.A., Barek, J., Benvenuto, J., Confalonieri, C., Goff, U., Ludeman, S., Reed, D., Sansone, E.B., and Telling, G., "Laboratory Decontamination and Destruction of Carcinogens in Laboratory Wastes: Some Antineoplastic Agents, 1985, IARC Scientific Publications, No. 73.

10. Hazardous Materials Technical Center, "Bibliographic Data Base Search on the Disposal of U-Listed Chemotherapeutic Drugs," 1986.
11. RCRA 1987 Handbook Update, Title 40, Code of Federal Regulations (CFR), Part 216.33.
12. Hall, D.L., Tiney, D.A., Dellinger, B., "Thermal Destruction of Antineoplastic Agents," 1985, University of Dayton Research Institute Environmental Sciences Group.
13. Stolar, M.H., Power, L.A., and Viele, C.S., "Recommendation for Handling Cytotoxic Drugs in Hospitals," Amer J. of Hospital Pharmacy, 1983, Vol. 40, pp. 1163-1171.
14. Rogers, R.W., "Management of Cytotoxic Agents." J. of Hospital Supply, Processing and Distribution, Jul-Aug 1985, Vol. 3, No. 4.
15. Laidlaw, J.L., Connor, T.H., Theiss, J.C., Anderson, R.W., and Matney, T.S., "Permeability of Four Disposable Protective Clothing Materials to Seven Antineoplastic Drugs," Amer J. of Hospital Pharmacy, Nov 1985, Vol. 42, pp. 2449-2454.
16. Steyermark, Al, Quantitative Organic Microanalysis, The Blakiston Co., 1951, pp. 134-155.
17. EPA Handbook, Permit Writer's Guide to Test Burn Data Hazardous Waste Incineration, EPA/625/6-86/012, Sep 1986, PEI Associates Inc., and JACA Corp., pp. 2-7.
18. Appendices A-D are in the possession of Maj Elliot K. Ng, USAF Occupational and Environmental Health Laboratory/EOQ, Brooks AFB TX, to satisfy the maximum number of pages to this report.

UNITED STATES AIR FORCE SUMNER FACULTY RESEARCH PROGRAM
(1987) PROGRAM TE (U) UNIVERSAL ENERGY SYSTEMS INC
DAYTON OH R C DARRAH ET AL DEC 87 AFOSR-TR-88-0213
F49620-85-C-0013 F/G 5/1

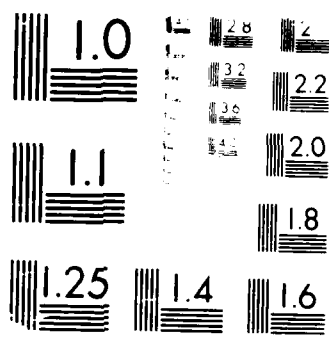
218

UNCLASSIFIED

DAYTON OH R C DARRAH ET AL DEC 87 AFOSR-TR-88-0213
F49620-85-C-0013 F/G 5/1

F/G 5/1

ML



MICROCOPY RESOLUTION TEST CHART
1000-10

1987 USAF-UES SUMMER FACULTY RESEARCH PROGRAM

GRADUATE STUDENT SUMMER SUPPORT PROGRAM

Sponsored by the

AIR FORCE OFFICE OF SCIENTIFIC RESEARCH

Conducted by the

Universal Energy Systems, Inc.

FINAL REPORT

Prepared by: Michael D. Matthews, Ph.D.

Academic Rank: Assistant Professor

Department: Behavioral Sciences Department

University: Drury College

Research Location: USAFAFHRL/MOM

Brooks AFB

San Antonio TX 78235

USAF Researcher: Timothy M. Bergquist

Date: 3 AUG 87

Contract No: F49620-85-C-0013

Assessing Costs and Benefits of Personnel Research:
Application of Utility Concepts to Military Programs

by

Michael D. Matthews

ABSTRACT

A major problem in the manpower and personnel research community is the transfer of technology from the laboratory to operational settings. One solution to this problem involves translating arcane statistical findings into economically meaningful statements. Utility analysis is one way of accomplishing this translation. The purpose of the current report is to critically review recent developments in utility analysis and to assess how applicable these developments are to military manpower and personnel research programs. Illustrative examples of the application of utility models to ongoing Air Force personnel research projects are given. Recommendations are made for what variables are and are not critical in applying utility analysis to military research programs.

ACKNOWLEDGMENTS

I express my appreciation to the Air Force Systems Command and the Air Force Office of Scientific Research for sponsorship of this research. Also, Universal Energy Systems personnel were extremely helpful and supportive of this effort, and their valuable assistance is recognized. During the first six weeks of my fellowship, I had the opportunity to have Michael Timothy Sewell assist in reviewing and interpreting the economics literature pertaining to utility analysis. Tim is a senior at the U.S. Air Force Academy, and was at AFHRL for a summer research program. His contribution to the project was substantial. I also thank Major Timothy Bergquist and Mr Larry Looper for setting the occasion for productive scholarly work. 2Lt John McGarrity and Mr Winston Bennett engaged me in stimulating conversations concerning the project. Dr William Alley provided a great deal of insight and perspective on the project. Walter Albert's assistance in interpreting the utility models is greatly appreciated. Finally, I would like to thank Dr Charles N. Weaver for his assistance in all phases of the project.

I. INTRODUCTION

A major problem faced by researchers in the military manpower and personnel domain is transferring technology from the laboratory to operational settings. Like their counterparts in the civilian sector, military psychologists often meet with considerable resistance from management personnel when attempting to make this transfer. One reason that such resistance is encountered is that scientists and managers often communicate in a different language. As Hunter and Schmidt (1983), pointed out, "to assess the practical impact of findings, one must translate such arcane psychological jargon as ' $p < .01$ ' into economically meaningful statements such as 'a 10% increase in output' or 'a reduction of \$100 million in labor costs'".

The most actively researched method of dealing with this problem in the past 10 years has been a decision-theoretic approach known as "utility analysis" (Hunter & Schmidt, 1983). This method uses information concerning the validity of a selection test or other organizational intervention, the selectivity of the test, estimates of job performance in dollars and cents terms, and costs incurred with the selection test or intervention. Until recently, estimating certain parameters in these equations was so cumbersome as to severely limit the practical application of utility analysis to the evaluation of research. Recently, however, improved ways of providing these estimates have been advanced.

II. OBJECTIVES OF THE RESEARCH EFFORT

The first objective of the current effort is to critically review recent developments in the domain of utility analysis. This review focuses on developments occurring in the past decade, although some attention is given to earlier advances in the field. In addition to reviewing these developments, their applicability to the evaluation of

manpower and personnel research in large non-profit organizations, such as the Air Force, is questioned. A conceptual framework for conducting utility analysis in military organizations is also a major objective of the effort. Because military organizations are unlike the civilian organizations on which many developments in utility analysis have been based, the model most appropriate for military use may differ from those most appropriate for civilian organizations. A basic model is proposed, and areas where further conceptual developments are needed are pointed out. Finally, the application of the proposed utility model to an ongoing Air Force research program is illustrated. Although certain assumptions must be made in conducting such an illustration, it is hoped that such an exercise will underscore the potential value of utility analysis to the evaluation of military personnel research programs.

Many of the issues inherent in this problem are complex and a full treatment of them is beyond the scope of this paper. However, Matthews and Sewell (1987) report a more thorough and detailed discussion of the topics and issues introduced in this paper. Copies may be obtained through AFHRL. In addition, Roach (1984) provides a comprehensive historical review of various approaches to this topic.

III. RECENT DEVELOPMENTS IN UTILITY ANALYSIS

The objective of utility analysis is to allow researchers to translate sometimes esoteric research findings into practical terms. Said another way, utility analysis is one method of evaluating the costs versus the benefits of a given selection test or post-selection organizational intervention. The rapid development in this area of inquiry has yielded many elaborations to the basic utility models and concepts first espoused by Taylor and Russell (1939), Brogden, (1949) and Cronbach and Gleser (1965). Because the majority of these elaborations are based on the application of utility models to

profit-making organizations, their relevance to large non-profit organizations like the military must be examined.

The very basis of utility analysis involves viewing utility as a function of returns and costs. Cronshaw and Alexander (1985) express the model as

$$\text{Utility (U)} = \text{Returns (R)} - \text{Costs (C)}$$

Cronbach and Gleser's (1965) utility model estimated R by the quantity

$$R = N_s SD_y r_{xy} Z_x$$

where SD_y refers to the standard deviation of job performance expressed in dollars, r_{xy} is the correlation between a selection test and work performance, and Z_x is the mean standard score for selectees. C was simply

$$C = N_s C$$

or the number (N) of individuals given the selection test times the cost (C) of each administration. Modifications to the basic conceptual model that have been made over the past decade have focused on expanding the R vector. What follows is a brief review of each of these modifications in terms of their applicability to the evaluation of military manpower and personnel research.

The major parameter that has posed difficulties for researchers in utility analysis is the SD_y . Until recently, only costly and cumbersome cost-accounting procedures were available in estimating this value. Schmidt, Hunter, McKenzie, and Muldrow (1979), however, proposed a method for estimating the value of SD_y that involves obtaining expert judgments of the dollar value of workers at the 50th, 15th, and 85th percentile of work performance. By making the appropriate subtractions, estimates of SD_y are thus obtained.

A lot of additional work has been done which examines the validity of this approach (e.g., Bobko, Karren, & Parkington, 1983; Weekly, Frank, O'Connor, & Peters, 1985). While some problems do exist, derived estimates compare favorably to those obtained using other

methods (Hunter & Schmidt, 1983). Moreover, Eaton, Wing, and Mitchell (1985) describe two variations in Schmidt's procedure that make the technique more suitable for application to military organizations. More specifically, they note that it may be more meaningful and easier for military supervisors to quantify performance in terms of the number of workers needed to accomplish a job, rather than assigning a dollar value to various levels of performance. Their procedures then allow information of this sort to be translated into estimates of SD_y . Additional research is needed to further examine the psychometric characteristics of these methods for estimating SD_y but at the current time they hold promise for application to military utility analysis efforts.

Economic variables have also been incorporated into the Cronbach-Gleser utility formula. Boudreau (1983a) examined three such variables - variable costs, discounting, and taxes-and developed terms to account for their impact on assessing utility. Military assets are not taxed, and since most military products are more dependent on human resources than on natural resources, variable costs are not relevant in this context. Only the vector for discounting seems appropriate for inclusion into a military utility analysis model. The issues in this area are complex, and are addressed in more detail by Matthews and Sewell (1987).

Early utility models assumed a more or less stable workforce. Obviously, however, the gains expected from a given selection test or other intervention will be affected by the flow of employees into and out of the organization. For example, suppose a training program was administered to a given work organization consisting of 100 workers. If the average turnover rate is 25 employees per year, then after one year only 75 workers would remain who had received the treatment, after 2 years only 50 would remain, and so on. Boudreau (1983b)

traced the development of utility theory and thoroughly developed equations to take into account the flow of employees into and out of an organization. Note, however, that this development was based on the application of utility models to for-profit industries.

At a glance, the role of employee flow into and out of an organization would seem particularly relevant to military research. The average tenure for most assignments in the Air Force does not exceed four years, and many are substantially less. Thus, even given the best case of a four year tour, an organization will show substantial gains and losses of personnel in any given year. So, if a training program is given once at time X in a unit, then by $X + 1$ year, only 75 percent of the personnel in the unit will have received the treatment, and by $X + 4$ years, none will remain who received the treatment. Thus, returns resulting from the treatment will decline rapidly, or repeated treatments may be necessary. Also, when treated workers move to other organizations, the receiving organization may experience benefits, even if they have not directly experienced the intervention.

The important question is, to what extent does this parameter apply in military settings? It may may not be of critical importance for several reasons. First, many military human resources programs are ongoing, thus all subjects in the workforce will be treated. For example, all accessions take the ASVAB. Second, and most importantly, while military organizations do experience substantial employee flow, as discussed above, many of the accessions into a given unit will have had a very similar or identical job at another duty assignment. So, employees flowing into the organization are not as naive, as a group, as employees entering a typical civilian work organization. If turnover is to be included in military utility analysis, the turnover parameter should be modified to account for the consideration discussed above. Such an extension of this parameter is beyond the scope of the current effort. At present, it is suggested that the

turnover parameter not be included in the utility model adapted for application to military organizations pending further development of the turnover vector.

Another recent major advance in utility analysis involves the expansion of the basic utility model from selection tests to allow for the evaluation of post-selection organizational interventions, such as training programs or the introduction of job performance feedback systems. This is an important extension from the perspective of military applications, because many military manpower and personnel research programs focus on post-selection interventions.

Landy, Farr, and Jacobs (1982) and Schmidt, Hunter, and Pearlman (1982) suggested very similar ways of expanding utility formulas to account for post-selection interventions. Both suggest substituting a term that expresses the difference in performance between an experimental group (that is, the one receiving the treatment) with a control group (which does not receive the treatment). A drawback to the use of these two methods is that the researcher must know the magnitude of difference between treated and non-treated groups. Consequently, in some cases an experiment must be performed to estimate the magnitude of this difference before the utility analysis may proceed. However, this may not pose a problem for researchers in the R & D environment, who (presumably) will have performed several studies on an intervention prior to reaching the stage of applying a utility analysis to the procedure in question.

Two other modifications to utility models have been suggested. Boudreau and Rynes (1985) argued that recruitment practices may alter the pool of applicants and to the extent this is true, affect the expected utility of a given selection test or organizational intervention. While this may be an important consideration in smaller organizations its relevance to the military situation is

questionable. The Air Force's recruitment methods aim at the general population of 18 - 21 year old citizens. Barring massive changes in recruitment or selection policies, the sample of applicants to the Air Force should remain representative of the population as a whole. Thus, the incorporation of this parameter appears unnecessary.

Murphy (1986) discusses the effect of top applicants turning down offers on the accuracy of utility estimates. Most utility models assume that the selection of applicants from the pool of those qualified for the job is random. This is often not the case. For example, applicants to graduate school often apply to more than one institution. The most highly qualified applicants are accepted by several programs. If half of a graduate school's first choices for admission turn them down, then potential selections remaining in the pool are not representative of the original pool. Their selection test scores will be lower because of the non-random attrition of more highly qualified applicants. To the extent this is true, expected utility should decrease. Murphy offers modifications to the basic utility model to account for this. Additional thought needs to be given to this issue in the military context. An analysis of recruiting records should reveal whether rejected offers are substantially altering the profile of selectees. Until this research and conceptualization is accomplished, it is recommended that the role of rejected offers not be considered essential to utility models as applied in military settings.

The objective of Section III was to review recent developments in utility analysis and evaluate their applicability to the assessment of human resource research programs in military settings. Methods for estimating SD_y were examined as were modifications to formulas for application to post-selection interventions. Eaton et al.'s (1985) thoughts were viewed as being of particular importance in this context. Both Landy et al.'s (1982) and Schmidt et al.'s (1982)

extensions to post-selection interventions appear of great potential use to military research personnel. Of the other modifications considered, only the parameter for discounting seems relevant in the context being considered. Variable costs, taxes, recruitment and rejected offers all appear irrelevant for various reasons. Thus, the formula suggested for application to military research is

$$U = N_s r_{xy} SD_y Z_x [1/(1 + i)^t] N_c C$$

where i is the discount rate, t is the time period in which the net benefits occur, and the other variables are defined as they were previously.

IV. ILLUSTRATIVE EXAMPLE

In this section the application of utility concepts to an ongoing AFHRL research project is illustrated. It focuses on the Vocational Interest Career Examination (VOICE). The VOICE is an interest battery designed to assess interests among recruits for blue-collar jobs typical of Air Force enlisted occupations. The basic interest scales have been validated against job satisfaction (Alley, Wilbourne, & Berberich, 1976). Predicted job satisfaction (PJS) scores based on the basic interest scale scores have been validated against attrition (Matthews, 1982), technical school attrition (Matthews & Ballentine, 1983), and rated work performance (Berry & Matthews, 1982). A thorough description of the VOICE, its development, and its psychometric characteristics is provided by Alley and Matthews (1982). The intended use of the VOICE is in the classification of recruits to first - term Air Force assignments. It would be used to help place recruits into jobs that they would be likely to enjoy and be successful at. Unlike the ASVAB, it would not be used to exclude a recruit from a given career field. Rather, it would be used more as a classification tool to help the recruit make an informed choice regarding a selection of a job among those available.

The first assumption that is required is that the VOICE will be administered to all Air Force enlisted accessions, which averages about 55,000 per year. For the purposes of the model, we will assume a discount rate of 10 percent. SD_y may be estimated by using the observation that its value is usually between 40 and 70 percent of the mean annual salary of the target workers (Hunter & Schmidt, 1983). In this case, the target sample is first term airmen, whose average annual salary including benefits and allowances for food, housing, and clothing is approximately 15,000 dollars per year. Using the most conservative value (i.e., 40%) as the basis for estimating SD_y , it may be estimated to be 6000 dollars. For r_{xy} , a value may be obtained from data published by Berry and Matthews (1982). They showed that the VOICE correlates with supervisor's ratings of incumbent job performance at a significant ($p < .01$) but low value of .053. This value may be taken as a conservative estimate of the true value of r_{xy} , because many low performers in the Berry and Matthews study had attrited from the Air Force prior to information on their job performance being obtained.

It is also assumed that the average Z_x score for each applicant is .8. Naturally, the estimated dollar savings resulting from implementation of any selection test will depend on how selective the test is, but this value would seem to be a reasonable one. Finally, it is estimated that the cost for administering and scoring the VOICE is 20 dollars per selectee. The VOICE may be administered in the field at MEPS stations, where the cost could be a little higher due to the one-on-one nature of testing in those environments. It may also be administered during BMT, where the costs would be somewhat lower, due to the possibility of testing large numbers of subjects at a time.

Using the the utility formula defined earlier, U may be estimated by substituting in for the missing values. In this case it turns out

that $U = \$11,619,999$. This savings value does not even include that which might result from decreased attrition resulting from VOICE implementation. Additionally, this illustration is conservative. If any of these parameter values (SD_y , r_{xy} , Z_x) were larger, U would be much larger.

It is also interesting to note that the actual increase in utility per individual is rather small. In the example given above, the value of U for each individual is \$231.27, or less than two percent of the worker's annual salary. Such increments in performance are so small as to be nearly inconsequential in the case of an individual, but spread over large numbers of workers, the returns can be substantial.

V. RECOMMENDATIONS

Utility analysis seems very well suited for evaluating the return on projects and programs central to industrial and organizational psychological research. Such programs range from selection tests to a variety of other organizational interventions including training, feedback, and goal setting. In this sense, utility analysis is more appropriate than other methods of assessing costs and benefits, which often neglect the impact of personnel variables.

A large number of variations and modifications have been added to the basic utility concepts first proposed by Taylor and Russell (1939), Brogden (1949), and Cronbach and Gleser (1965). The developments in the area of estimating SD_y , notably Eaton's (Eaton et al., 1985) methods, seem of particular importance. Much of Boudreau's and his associates work in expanding basic utility concepts to include economic and related factors is also of great potential value, although not all of these developments are germane to utility applications in non-profit organizations like the military.

Despite these and other advances discussed in this paper, caution may be in order in applying utility analysis to the evaluation of research programs. The first major problem is that utility formulas require that job performance be measureable in some reasonably accurate manner. r_{xy} involves direct measurements of performance. While such measures may be attainable in organizations with explicit products, such as many factories, the assessment of performance in less explicit circumstances is a problem that has long plagued psychologists. This criterion problem manifests itself in virtually every phase of industrial/organizational psychology, and in utility analysis it may lead to difficulties in obtaining valid estimates of important parameters. Some advances have been made in this area recently (see Hunter Hunter, 1984 for a discussion) but to the extent that measures of performance are invalid, then utility analysis based on them is suspect. It should be noted also that AFHRL is currently addressing this performance measurement problem in two large scale studies.

Another problem is the concept of SD_y . While Schmidt et al. (1979) and others have developed ways of estimating this parameter, there are certain problems associated with those measures as reviewed above. Also, it may be questioned whether job performance is indeed a normally distributed phenomenon, and/or if the optimal metric is currently being used to estimate performance in dollars and cents terms. At the current time, SD_y estimates should be viewed cautiously.

More development needs to be done in the area of tailoring utility models to non-profit organizations and/or situations where there is not a tangible product. Extension of terms, like turnover, to military organizations is needed. For example, the impact of turnover in the military is probably different from that in civilian jobs. While some members do leave the Air Force, many simply move on to

highly similar jobs in different units. Thus, an experienced aircraft jet engine mechanic added to a maintenance shop at one air base will not be as costly to the receiving organization in terms of training as is the addition of an inexperienced mechanic.

Because of the considerations just discussed, it may be prudent at this point to be conservative in interpreting the results of utility analysis. Utility analysis can be very useful in evaluating alternatives. For example, it could help a manager select among two or more alternative selection tests under consideration for use in selecting or classifying workers. Utility analysis would rank order, at the very minimum, which tests should show the greatest return. However, it would be an error to interpret the dollar estimates obtained in a utility analysis too literally. Because of the concerns already voiced, these figures probably do not serve as a highly valid dollar estimate of returns accruing from a given course of action.

In summary, utility analysis provides a potentially useful means of quantifying the impact of manpower and personnel research programs in practical terms. Many advances have been made in this technology, but more work needs to be done to adapt this technology to military settings. At the current time, utility analysis provides a good means of evaluating in a general way alternatives, but too literal interpretations of the results of utility analysis is cautioned against.

References

- Alley, W. E., & Matthews, M.D. (1982). The Vocational Interest Career Examination: A description of the instrument and possible applications. Journal of Psychology, 112, 169-193.
- Alley, W. E., Wilbourn, J. M., & Berberich, G. L. (1976) Relationships between performance on the Vocational Interest Career Examination and reported job satisfaction. AFHRL-TR 76-89, AD-A040 754. Lackland Air Force Base, Texas: Air Force Human Resources Laboratory, December 1976.
- Berry, G. A., & Matthews, M. D. (1982). Predicting job satisfaction and job performance. Proceedings of the 24th Annual Conference of the Military Testing Association. San Antonio, Texas: Air Force Human Resources Laboratory.
- Bobko, P., Karren, R., & Parkington, J. J. (1983). Estimation of standard deviations in utility analysis: An empirical test. Journal of Applied Psychology, 68, 170-176.
- Boudreau, J. W. (1983a). Economic considerations in estimating the utility of human resource productivity improvement programs. Personnel Psychology, 36, 551-576.
- Boudreau, J. W. (1983b). Effects of employee flows on utility analysis of human resource productivity improvement programs. Journal of Applied Psychology, 68, 396-406.
- Boudreau, J. W., & Rynes, S. L. (1985). Role of recruitment in staffing utility analysis. Journal of Applied Psychology, 70, 354-366.
- Cronbach, L. J., & Gleser, G. C. (1965). Psychological tests and personnel decisions (2nd ed.). Champaign, IL: University of Illinois Press.
- Cronshaw, S. F., & Alexander, R. A. (1985). One answer to the demand for accountability: Selection utility as a investment decision. Organizational Behavior and Human Decision Processes, 35, 102-118.
- Eaton, N. K., Wing, H., & Mitchell, K. J. (1985). Alternative methods of estimating dollar value of performance. Personnel Psychology, 38, 27-40.
- Hunter, J. E., & Hunter, R. F. (1984). Validity and utility of alternative predictors of job performance. Psychological Bulletin, 96, 72-98.

- Hunter, J. E., & Schmidt, F. L. (1983). Quantifying the effects of psychological interventions on employee job performance and work-force productivity. American Psychologist, 38, 473-479.
- Landy, F. J., Farr, J. L., & Jacobs, R. R. (1982). Utility concepts in performance measurement. Organizational Behavior and Human Performance, 30, 15-40.
- Matthews, M.D. (1982). Vocational interests, job satisfaction, and turnover among Air Force enlistees. Proceedings, Fourth International Learning Technology Congress and Exposition. Orlando, Florida: Society for Learning Technology.
- Matthews, M. D., & Ballentine, R. D. (1983). Predicted job satisfaction and attrition from Air Force technical schools. Proceedings, 25th Annual Meeting of the Military Testing Association. Gulf Shores, Alabama: U.S. Navy.
- Matthews, M. D., & Sewell, M. T. (1987). Application of utility models to the evaluation of military manpower and personnel research programs: A critical review and illustrations. Brooks AFB, TX: Air Force Human Resources Laboratory, in press.
- Murphy, K. R. (1986). When your top choice turns you down: Effect of rejected offers on the utility of selection tests. Psychological Bulletin, 99, 133-138.
- Roach, B.W. (1984). Decision-theoretical approach to personnel selection: a review. AFHRL TP-84-19, AD A143 388. Brooks AFB, TX: Air Force Human Resources Laboratory.
- Schmidt, F. L., Hunter, J. E., McKenzie, R. C., & Muldrow, T. W. (1979). Impact of valid selection procedures on work-force productivity. Journal of Applied Psychology, 64, 609-626.
- Schmidt, F. L., Hunter, J. E., & Pearlman, K. (1982). Assessing the economic impact of personnel programs on work force productivity. Personnel Psychology, 35, 333-347.
- Taylor, H. C., & Russell, J. T. (1939). The relationship of validity coefficients to the practical effectiveness of tests in selection: Discussion and tables. Journal of Applied Psychology, 13, 565-578.
- Weekley, J. A., Frank, B., O'Connor, E. J., & Peters, L. H. (1985). A comparison of three methods of estimating the standard deviation of performance in dollars. Journal of Applied Psychology, 70, 122-126.

1987 USAF-UES SUMMER FACULTY RESEARCH PROGRAM/
GRADUATE STUDENT SUMMER SUPPORT PROGRAM

Sponsored by the
AIR FORCE OFFICE OF SCIENTIFIC RESEARCH

Conducted by the
Universal Energy Systems, Inc.

FINAL REPORT

Investigation of new luminescent rebroadcasting devices for optical information processing

Prepared by:	Alastair D. McAulay PhD
Academic Rank:	Professor
Department and	Department of Computer Science
University:	Wright State University
Research Location:	AFWAL/AADO-2, WPAFB, Dayton, Ohio
USAF Researcher:	Joseph E. Brandelik
Date:	1 Sept. 1987
Contract No.:	F49620-85-C-0013

Investigation of new luminescent rebroadcasting devcies for optical information processing

by

Dr. Alastair D. McAulay

ABSTRACT

Preliminary experiments were performed to characterize thick and thin film samples of a new luminescent rebroadcasting device. Results are limited by the equipment used and show resolutions to 50 line pairs per inch, read speeds to 5 kHz, and write speeds to 0.3 kHz. Clearing the device takes longer. Methods of performing basic processing functions were developed including analog addition and multiplication and the 16 Boolean logic operations. Some results are presented. Optical information processing schemes most suitable for the new devices are discussed including: analog matrix-vector multiplication for probabilistic expert systems and neural networks, symbolic substitution, interconnection networks, and analog to digital conversion.

Acknowledgements

I wish to thank the Avionics Laboratory at Wright Patterson Air Force Base and the Air Force Office of Scientific Research for sponsorship of this research. Also I wish to thank Universal Energy Systems for administering this program. I wish to thank the technical focal point, Joseph E. Brandelik, for his interest, valuable discussions and feedback. I appreciated the laboratory support, and technical interest of the technical staff of AADO-2: Lt. Pete Collins, and Dale Stevens. Technical support from other members of AADO is also appreciated: Richard Lane and Dr. Ken Schepler. Finally I appreciated the support of the management at AFWAL/AADO: Richard Remski and Capt. Mike Prairie.

I INTRODUCTION:

WPAFB/AFWAL/AADO is supporting the development of new photonic devices that could permit optical information processing systems that are noticeably superior to those using other technologies. One of these devices uses II-VI semiconductor materials to provide 2-D luminescent rebroadcasting (LR) [1]. Electrons are trapped in a spatially varying distribution on illuminating the device. The electrons may be released by exposure to light of a second wavelength resulting in release of light at a third wavelength. The device differs from conventional spatial light modulators (SLMs) for which the transmittance or reflectance varies spatially. Also, the new approach should permit higher resolution and possibly higher speed than most presently available SLMs. The new devices could lead to new and effective optical information processing systems.

My assignment to AFWAL/AADO as a participant in the 1987 Summer Faculty Research Program was to perform preliminary research to (a) characterize devices composed of these materials, (b) investigate how the devices may be used in information processing, and (c) determine applications for which the devices are best suited. This task matches my experience in: investigating new devices for optical information processing for many years in the Corporate Research Laboratories at Texas Instruments and more recently at Wright State University (WSU), teaching graduate courses on Computer Architecture and Optical Computer Architecture in the Computer Science Department at WSU, teaching an annual SPIE Tutorial on Digital Optical Computing, and publishing over 40 papers on this subject in the past few years.

Section II summarizes the objectives. Sections III, IV, and V address the research approaches and results for device characterization, basic processing operations, and suitable applications. Section VI provides recommendations.

II OBJECTIVES OF THE RESEARCH EFFORT:

1. Perform preliminary characterization of 2-D devices made with new optical luminescent rebroadcasting (LR) materials; in particular resolution, speed, frequency response, and sensitivity.
2. Determine how the 16 Boolean logic operations between two variables may be computed using LR devices and demonstrate OR, AND, and inversion. Also demonstrate the method of performing analog addition and multiplication.
3. Investigate potential applications for which these devices are best suited, including: analog matrix-vector multiplication for probabilistic expert systems and neural networks; symbolic substitution; analog to digital conversion; and interconnection networks.

III PRELIMINARY DEVICE CHARACTERIZATION

Sample descriptions

Three types of luminescent rebroadcasting (LR) samples were available from Quantex. Sample A is 2 by 2 inch size thick film in a polymer encapsulation. Sample B is 0.85 by 0.85 inch thick film bonded to a sapphire window. Sample C is 0.85 by 0.85 inch thin film bonded to a sapphire window. Sizes refer to active surface area. Thick film is approximately 250 μm and thin film approximately 6 μm . The approach and results for experiments follow in categories of resolution, speed, and frequency response.

Resolution

The procedure was to illuminate the device with sufficient infrared (IR) energy at 930 nm. to read out all the stored energy. Light emitting diodes (LEDs) were used costing less then \$2. Clearing the thick film devices took up to 30 minutes due to the low power of the LEDs. A resolution chart was attached to the surface

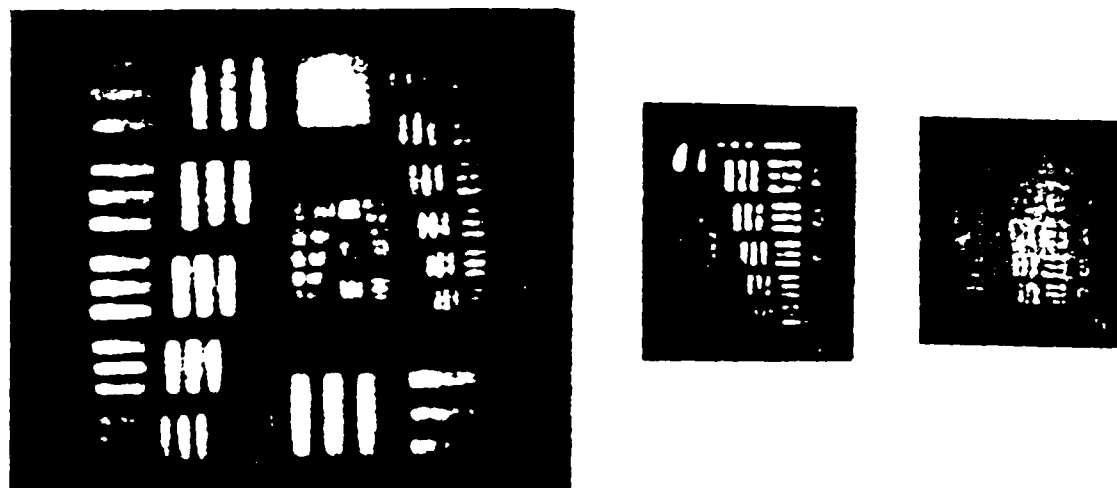


Figure 1: Resolution tests: (a) for thick film polymer encapsulated material (sample A), (b) for thick film on sapphire (Sample B), (c) for thin film on sapphire material (Sample C).

of the device. To reach saturation, sufficient energy from a blue Argon laser at 455 nm was used to write uniformly in space on the device. The chart was removed and IR at 930 nm was then used to cause luminescence. Samples A and C luminesce in orange, while sample B luminesces in green. A polaroid camera was used to photograph the luminescence.

Fig. 1(a) shows the result for the polymer encapsulated thick film, sample A. Magnification is 1.6. Based on the upper right of this chart the resolution is 20 line pairs per inch. This corresponds to distinguishing an array of at least 40 by 40 for sample A. Fig. 1(b) shows the result for the thick film on sapphire, sample B. Magnification is 1.3. The resolution is higher, at approximately 40 line pairs per inch. This would permit an array of 35 by 35 to be distinguished with the sample provided. However, the material is not uniform and black dots are clearly visible due to the imperfections.

Fig. 1(c) shows that the resolution of the thin film is higher still at over 50 line pairs per inch. The low contrast results from the low IR energy used to read the film, requiring 8 minute exposures, by which time most of the energy has been

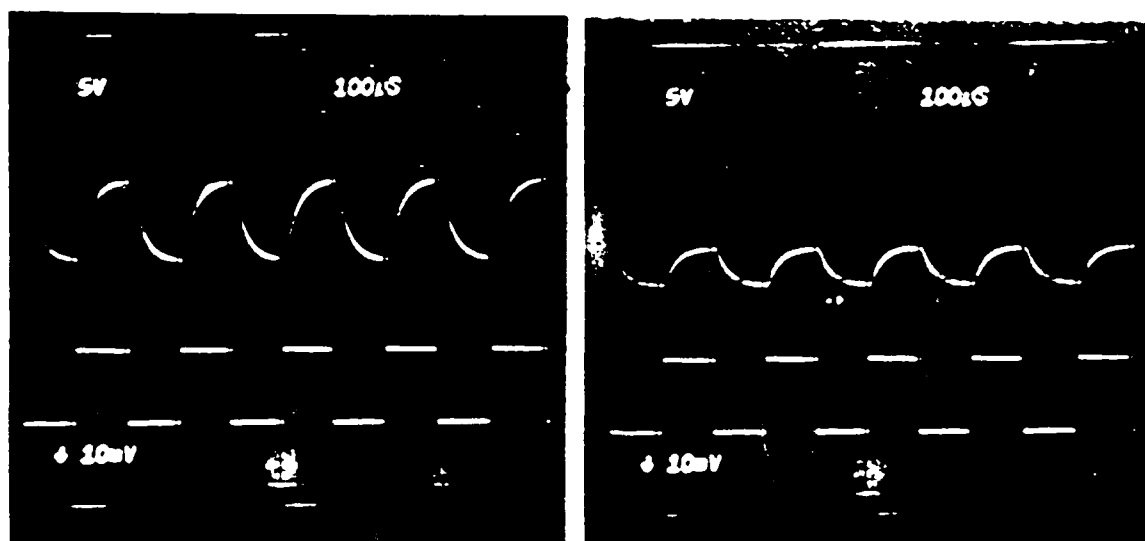


Figure 2: Detected luminescence with 5 kHz read out: (a) Immediately after writing. (b) After reading out for some minutes.

read out. Higher power IR is also needed to clear the film to produce a darker background. The material may also have degraded as it is an early sample without a protective coating. The resolution is supposed to be much higher than that measured. Improved measuring techniques are required to determine the attainable resolution.

Speed

Two experiments were performed, the first investigates reading speed, the second the speed of writing and reading. The reading speed was examined by pulsing the IR LED with a square wave and placing it close to the front surface of sample A. A silicon diode biased with 40 volts was placed behind sample A and covered with filters to attenuate IR and blue and to pass orange. The resulting bandpass filter has 3 dB points at 700 nm and 530 nm.

Fig 2-a) shows the results when pulsing the LED at 5kHz. The lower trace shows the drive voltage. The upper trace shows the detector output a few seconds after writing to the device. The upper trace in fig. 2(b) shows the output 30 minutes later. The time taken reflects the low IR power. After this time the trapped electrons have

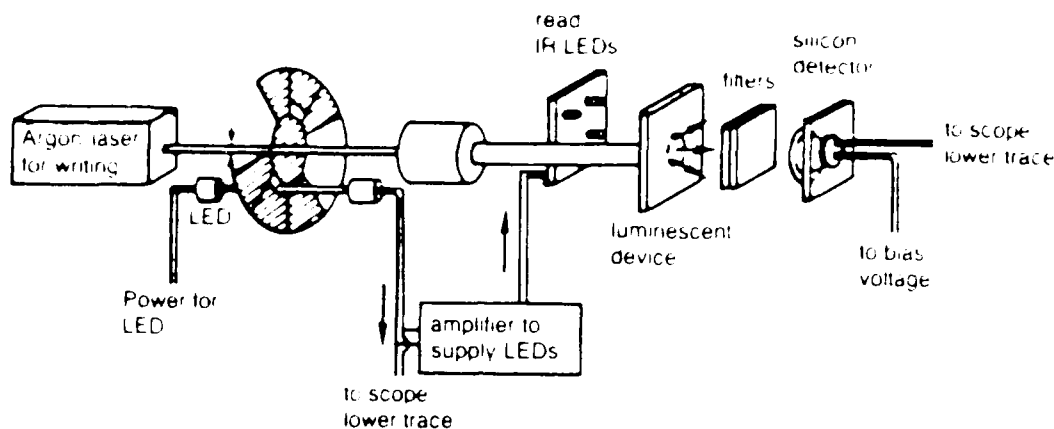


Figure 3: Experimental set up for cyclic write-read test.

been released and the remaining signal is that due to IR passing through the filters.

Fig. 3 shows an experiment to test both write and read speeds. A chopper was used to pulse the blue write beam twice per revolution of the chopper motor. A photodetector pair was used to provide a separate square pulse from the chopper at twice this frequency. This pulse is used to control the IR read source. Consequently, this is equivalent to writing one's and zeroes alternately and reading after each event.

Fig. 4 shows the result obtained from this experiment using the encapsulated thick film sample A. The upper trace shows the inverted read pulse at a rate of 312 Hz. Reading occurs when the pulse is low. The lower trace shows the inverted output of the photodiode detector. The signal is less than in Fig. 2 because the LEDs are approximately 3 inches away from the front surface of the sample to permit blue light to also reach the front surface of the sample. The write pulse occurs at alternate cycles and halfway through the time for which the read pulse is off. Therefore, the left shoulder of the head and shoulders pattern represents the detector output for writing in the absence of a read signal. Luminescent orange is generated while writing (even in the absence of reading) and this passes through the filters. The head represents the output for writing in the presence of a read

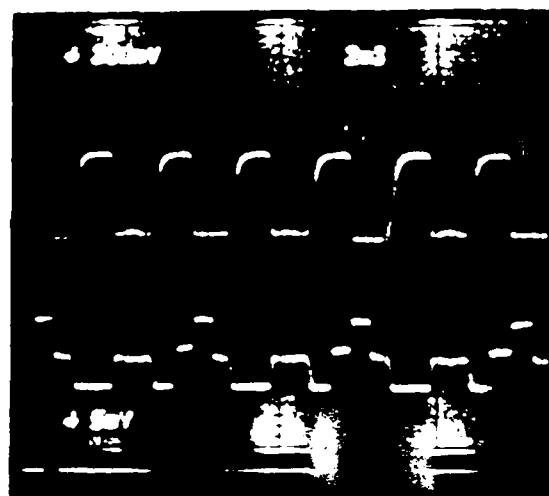


Figure 4: Results of cyclic write-read test.

pulse. Additional orange luminescence is generated when write and read occur together. The right shoulder represents the output signal for reading the device after writing has stopped. The IR source has insufficient power to read out much of the energy during one cycle from the thick sample which has a high density of trapped electrons. Consequently, there is no noticeable decrease in the detected levels for cycles without a write.

In order to ensure that the signal detected is luminescent orange and not purely IR the write beam was shut off, Fig. 5(a). After many minutes the output decayed as shown by comparing Fig. 5(a) and 5(b). This is the result of the stored electrons being removed. The remaining signal is attributed to the IR passing through the filters.

Similar tests were performed on the thin film, sample C. The lower density of electrons should permit much faster removal of the electrons. However, the luminescence generated is correspondingly less and is now small relative to the IR observed at the detector. Better filtering of the IR, and amplification of the detected signal are required to perform future tests.

Frequency response and sensitivity

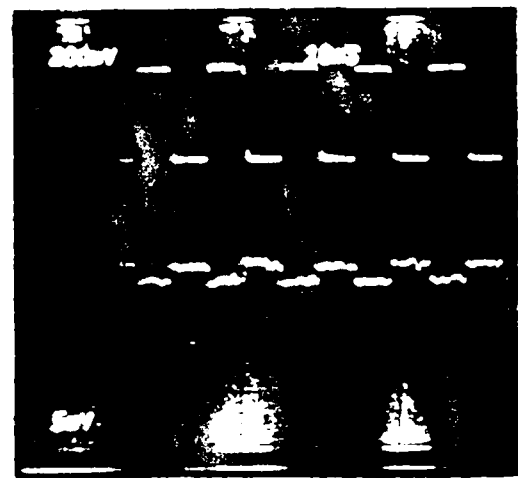
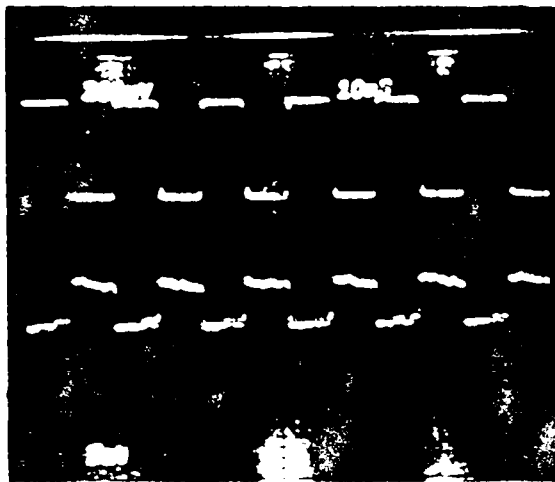


Fig. 1. Micrograph of thin film device. Horizontal lines of photoresist are used for alignment of the device on the substrate.

The device is mounted on a substrate of the type used in the experiment. The device is mounted on the substrate by using a thin layer of photoresist. The device is mounted on the substrate by using a thin layer of photoresist. The device is mounted on the substrate by using a thin layer of photoresist. The device is mounted on the substrate by using a thin layer of photoresist. The device is mounted on the substrate by using a thin layer of photoresist.

The device is mounted on the substrate by using a thin layer of photoresist. The device is mounted on the substrate by using a thin layer of photoresist. The device is mounted on the substrate by using a thin layer of photoresist. The device is mounted on the substrate by using a thin layer of photoresist.

EXPERIMENTAL RESULTS AND DISCUSSION

The

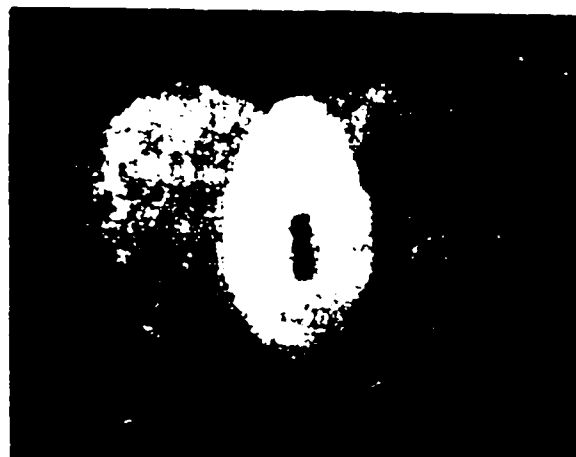


Figure 6: Illustrating analog addition with thick film polymer encapsulated sample (sample A).

be written:

$$S = A + B + C + \dots \quad (1)$$

On reading the device by flooding with IR, the intensity of the luminescence at a pixel is supposed to be the sum of the energies supplied to the pixel position by each of the images added, provided the operation remains in the linear range of the device.

Fig. 6 shows the result of exposure of the thick film, sample A, to a collimated beam at two different positions on the device for equal time. Stability and linearity of response with increasing write energy must be measured to verify analog addition and to determine the accuracy and range over which addition is possible.

Parallel multiplication of images A and B is performed by writing one image, say A, onto the device with spatially varying intensities representing one operand and then reading with IR having spatially varying intensities representing the second operand, B. The output luminescence at each pixel position is supposed to be proportional to the analog product of the read intensity at that pixel and the stored value at that pixel, i.e. $Out = A \cdot B$. Note that the energy that was not read out

remains for subsequent operations and equals

$$S = A - A \cdot B = A \cdot (1 - B). \quad (2)$$

Consequently, the device must be cleared before further multiplication.

Boolean logic

The device can perform a sequence of OR operations on a sequence of binary arrays by writing the arrays sequentially onto the device, equation (1). Addition is now interpreted as OR. The device can also perform a sequence of AND NOTs by successive reads with binary arrays B, C, D, etc. as indicated by equation (2) and assuming that A is all ones.

$$S = \overline{B} \cdot \overline{C} \cdot \overline{D} \cdot \dots \quad (3)$$

Multiplication is now interpreted as AND. As $\overline{B} \cdot \overline{C}$ is equivalent to $\overline{B + C}$ or NOR, the system is capable of performing a sequence of NORs, and hence performing any combinatorial or sequential logic system (provided cascading is possible).

In some cases, the ability to perform alternative logic operations leads to more efficient implementation than using a simpler complete set. Fig. 7 shows the 16 basic logic operations between two inputs. The lower part of the figure shows the sequence of incoherent writes and reads required to perform the corresponding logic operations with a single luminescent rebroadcasting device. Exceptions follow: exclusive OR (XOR) and its negation require coherent inputs out of phase by 180 degrees or two devices, and NAND requires two devices. 'All' refers to saturating the device all over. Note that all the basic logic functions may be performed in four or less time steps.

Every complete logic set involves inversion. This may be performed by flooding the device all over to saturation. The pattern whose inversion is sought is used to spatially modulate the IR in order to remove energy from the device where the

A	B	0	1	2	3	4	5	6	7	8	9	10	11	12	13	14	15
0	0	0	0	0	0	0	0	0	0	0	0	0	0	0	0	0	0
0	1	0	0	0	0	0	0	0	0	0	0	0	0	0	0	0	0
1	0	0	0	0	0	0	0	0	0	0	0	0	0	0	0	0	0
1	1	0	0	0	0	0	0	0	0	0	0	0	0	0	0	0	0
2	0	0	0	0	0	0	0	0	0	0	0	0	0	0	0	0	0
2	1	0	0	0	0	0	0	0	0	0	0	0	0	0	0	0	0
3	0	0	0	0	0	0	0	0	0	0	0	0	0	0	0	0	0
3	1	0	0	0	0	0	0	0	0	0	0	0	0	0	0	0	0
4	0	0	0	0	0	0	0	0	0	0	0	0	0	0	0	0	0
4	1	0	0	0	0	0	0	0	0	0	0	0	0	0	0	0	0
5	0	0	0	0	0	0	0	0	0	0	0	0	0	0	0	0	0
5	1	0	0	0	0	0	0	0	0	0	0	0	0	0	0	0	0
6	0	0	0	0	0	0	0	0	0	0	0	0	0	0	0	0	0
6	1	0	0	0	0	0	0	0	0	0	0	0	0	0	0	0	0
7	0	0	0	0	0	0	0	0	0	0	0	0	0	0	0	0	0
7	1	0	0	0	0	0	0	0	0	0	0	0	0	0	0	0	0
8	0	0	0	0	0	0	0	0	0	0	0	0	0	0	0	0	0
8	1	0	0	0	0	0	0	0	0	0	0	0	0	0	0	0	0
9	0	0	0	0	0	0	0	0	0	0	0	0	0	0	0	0	0
9	1	0	0	0	0	0	0	0	0	0	0	0	0	0	0	0	0
10	0	0	0	0	0	0	0	0	0	0	0	0	0	0	0	0	0
10	1	0	0	0	0	0	0	0	0	0	0	0	0	0	0	0	0
11	0	0	0	0	0	0	0	0	0	0	0	0	0	0	0	0	0
11	1	0	0	0	0	0	0	0	0	0	0	0	0	0	0	0	0
12	0	0	0	0	0	0	0	0	0	0	0	0	0	0	0	0	0
12	1	0	0	0	0	0	0	0	0	0	0	0	0	0	0	0	0
13	0	0	0	0	0	0	0	0	0	0	0	0	0	0	0	0	0
13	1	0	0	0	0	0	0	0	0	0	0	0	0	0	0	0	0
14	0	0	0	0	0	0	0	0	0	0	0	0	0	0	0	0	0
14	1	0	0	0	0	0	0	0	0	0	0	0	0	0	0	0	0
15	0	0	0	0	0	0	0	0	0	0	0	0	0	0	0	0	0
15	1	0	0	0	0	0	0	0	0	0	0	0	0	0	0	0	0

Figure 7: Computing 16 basic Boolean logic functions with luminescent rebroadcasting devices.

pattern is one. Those parts of the device not read out may now be read out with a uniform IR beam and represent the inverse of the pattern.

A test was performed with sample A in which a resolution chart was used to perform the modulation of the IR read beam. Fig. 8 shows the result obtained. The low power of the IR is considered responsible for poor resolution because the luminescence has ample time to bleed transversely during 8 minute exposures.

Logic must interface with other logic so that the zero and one levels must be restored after a logic operation is performed. This requires (a) thresholding so that small signals may be returned to zero, (b) gain so that large values may be restored to one, and (c) converting output frequencies to input frequencies. A second device, such as an image intensifier, may convert frequency and provide the threshold and gain required to reestablish zero and one respectively.

V SYSTEM APPLICATIONS WITH LR DEVICES

Factors affecting suitable applications

Open loop systems are considered first because they avoid the need for frequency conversion. The efficiency of conversion from input power (write or read) to output

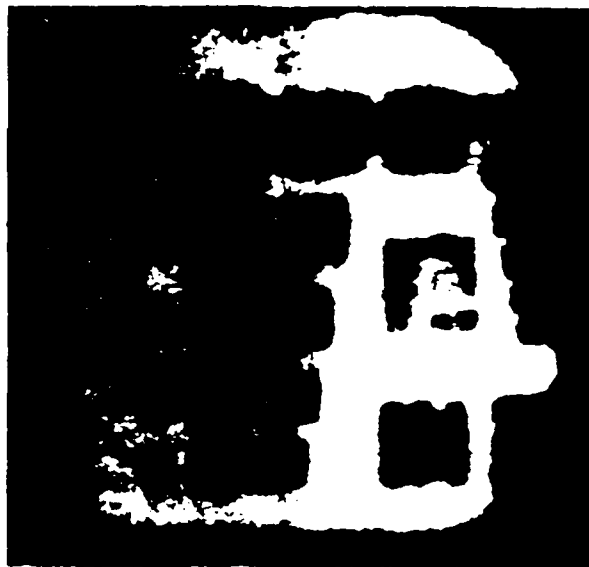


Figure 8: Illustrating inversion.

power (luminescence) appears low for the samples tested. Therefore, high IR energy seems to be required to clear the device (as distinct from only reading). Applications for which clearing occurs seldom should be faster. Applications that can directly use the analog range of the device are also of interest. The next section considers analog open loop systems and the subsequent sections closed loop systems.

Matrix-vector multiplication for probabilistic expert and neural network

A luminescent rebroadcasting (LR) device may be used for matrix-vector multiplication as shown in Fig. 9(a). The matrix elements are written to the device and stored. The intensity of the IR sources corresponds to the input vector elements. Each source illuminates a row of the device. The incoherent luminescence is observed via a lens system that images in a horizontal direction. A geometric correction is applied to the stored matrix values to compensate for the beam patterns and varying distances of vertically produced emitters on the luminescent device from the detector element observing them.

Many diagnostic expert systems [2],[3],[4] contain expertise in a database whose elements, $p(e_i|h_j)$, are analog values representing probabilities of sensor events e_i given hypotheses, h_j , e.g. a medical dictionary contains probabilities of symptoms

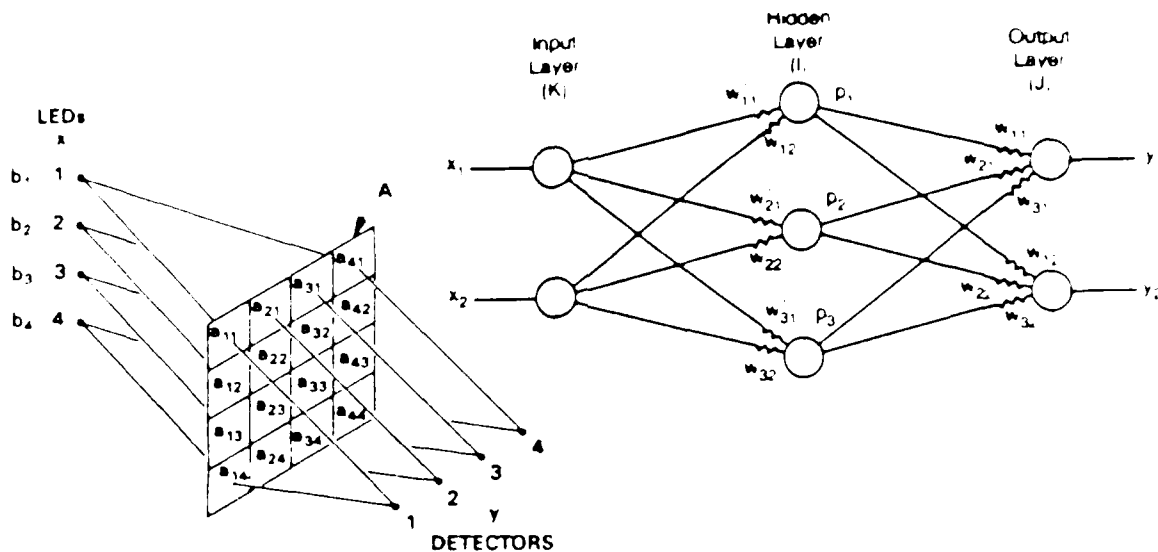


Figure 9: Artificial intelligence applications: (a) Matrix-vector multiplication, (b) Neural network.

given the illnesses. A diagnosis requires computation of a reverse expression, $p(h_j|\epsilon_1, \dots, \epsilon_M)$, the probabilities of hypotheses given M sensor events, e.g. the probabilities of each illness given a patient with a set of symptoms. This may be computed using Bayes theorem

$$p(h_j|\epsilon_1, \dots, \epsilon_M) = \prod_{i=1}^M \left[\frac{p(\epsilon_i|h_j)}{p(\epsilon_i|h_j) * p(h_j) + p(\epsilon_i|\bar{h}_j) * p(\bar{h}_j)} \right] * p(h_j). \quad (4)$$

Taking logs of both sides produces the matrix-vector equation [3] $\mathbf{f}^T = \mathbf{e}^T \mathbf{Q}$, where the matrix \mathbf{Q} is the stored database and the vector \mathbf{e} in the binary case has binary elements according to whether the event is true (one) or false (zero). The output vector \mathbf{f} has the probabilities for each hypothesis and may be computed using a matrix-vector multiplier as shown in Fig. 9(a).

Neural network schemes are aimed at providing more flexible analog processing by means of learning. The network can act as an associative memory, e.g. entering part of a persons name at the input can result in obtaining his full name and phone number at the output. A popular nonlinear network has multilayers, Fig. 9(b) [5].

The equations implemented by this network are

$$y_j = f \left[\sum_{i=1}^I w_{ij} f \left(\sum_{k=1}^K w'_{ki} x_k \right) \right], \quad f(q_j) = (1 + e^{-q_j})^{-1}. \quad (5)$$

The network may be implemented using LR devices, Fig. 9(a), by a sequence of analog matrix-vector multipliers. Nonlinearity is obtained from the natural saturation of the device. LR devices with matching output and input frequencies are required to provide more than one layer. The weights \mathbf{w} are changed incrementally and infrequently, avoiding the need to clear the LR devices fully.

Symbolic substitution for associative memory, logic programming, and numerical computation

Symbolic substitution normally uses a 2-D SLM to perform parallel logic between two input arrays. The output is fed back to the input of the SLM but displaced by one row or column. Repetitive cycles permit (a) parallel search for bit sequences, required in pattern searching, and (b) parallel substitution, required in unification, for AI logic programming [6], or numerical computation [7]. The shift during feedback is similar to a nearest neighbor connection. Other systems using nearest neighbor connections for analog operation have been proposed [8].

Associative memory provides a simple search example. Associated data is stored on a row of an LR device, unlike the neural network where learned information is distributed. Input data is located in parallel by symbolic substitution, and the whole line read out for every instance.

The LR device has a useful feature in comparison with SLMs for this application. It stores the current array for successive logic operations of the types discussed in equations (1) and (2). Consequently, bit sequences consisting of all ones or all zeroes are easy to find. However, whenever the bit sequence sought inverts, an inversion is required and this requires clearing the device. Also, gain and frequency conversion are required for the feedback.

Interconnection networks

Matrix-vector multiplication with SLMs using a binary matrix to represent crossbar switch settings has been shown to be a promising approach for computer interconnections because of the high throughput [9],[10],[11],[12],[13],[14]. Implementations of many algorithms have been considered on such an architecture [15],[16],[17],[18], including applications to many fields [19],[13].

The LR matrix-vector multiplier, Fig. 9(a), can act as a crossbar switch by performing AND operations between the IR sources and a blue binary array containing the switch setting information. The LR device throughput will be less than for an SLM because each piece of information passing through the switch requires a write-read cycle. However, the speed of reconfiguring the switch could be faster if rapid clearing is possible. The LR devices could be useful in the opto-electronic serial-parallel interface because of the buffering that is automatically provided in the write-read process. It should also be possible to write holograms onto the device for optical interconnections.

Analog to digital conversion (ADC)

Higher performance ADCs are required in the Air Force to permit the replacement of fixed analog circuits by more flexible digital circuits at the output to sensors such as radar and EW antennas. An optical ADC scheme was proposed and is described in [20]. The optical analog level input is broadcast to a 1-D array of comparators having increasing thresholds with position. Optical logic is used to convert the output step to a single pulse at a position corresponding to the analog level. This pulse illuminates the digital code in a look-up table. The parallel optical digital output is moved to a common location.

Fig. 10 shows the use of an image intensifier for the comparators, and a fluorescent rebroadcasting device for the optical logic. The logic operation performed is $A = \bar{A} + 1$ which was item 2 in Fig. 7.

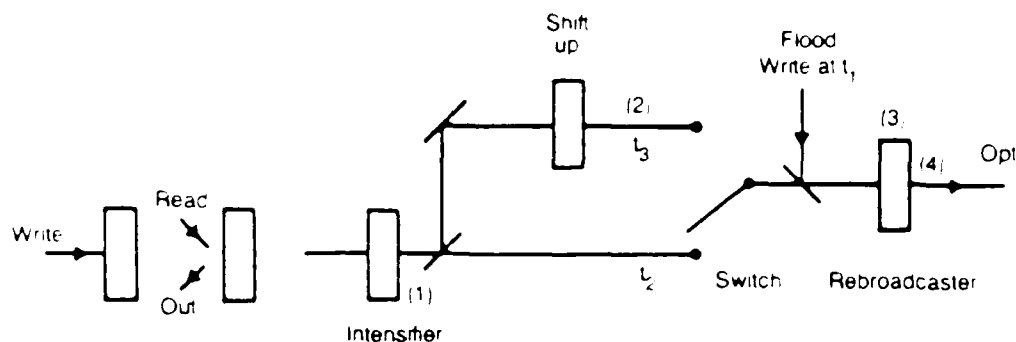


Figure 10: Illustrating logic for analog to digital conversion.

RECOMMENDATIONS

1. Improve experimental set up by having higher IR intensities for read out, better discrimination between IR and luminescence, and improved methods of testing resolution and speed.
2. Perform experiments to measure linearity and stability and hence verify analog addition and multiplication. For writing, reading, and clearing, measure time varying properties and spectral and power sensitivities. Improve device computer modeling to permit performance analysis of proposed systems.
3. Characterize image intensifiers to show both gain and thresholding may be accomplished for sequential logic and that frequencies may be converted for cascading of logic systems using LR devices.
4. Demonstrate correlation of patterns in a matched filter configuration. Demonstrate matrix-vector multiplication and corresponding systems such as a probabilistic expert system, or neural network.
5. Set up a loop having IR and image intensifiers to demonstrate symbolic substitution.

REFERENCES:

1. Gasiot J., and Brautlich P., "Nanosecond infrared laser stimulation of luminescence in rare-earth doped sulphides", Appl. Phys. Lett., **40** (5), 1982.
2. McAulay A.D., "Optical real time diagnostic expert system", Applied Optics, Vol. **26**, May 1987.
3. McAulay A.D., "Optical diagnostic processor for flight control", NAECON May 1987.
4. McAulay A.D., "Application of optical spatial light modulators to expert systems", Wright State University Fifth Internl. Conf. on Systems Eng., 1987.
5. McAulay A.D., "Engineering Design Neural Networks using Split Inversion Learning", IEEE First Internl. Conf. on Neural Networks, 1987.
6. McAulay A.D., "Optical Prolog computer using symbolic substitution", Digital Optical Computing Symposium, SPIE O-E LASE, Jan. 1988.
7. Brenner K.H., Huang A., Streibel N., "Digital Optical Computing with Symbolic Substitution," Applied Optics, Vol. **25**, Sep. 1986, pp 3054-3064.
8. McAulay A.D., "Deformable Mirror Nearest Neighbor Optical Computer", Optical Engineering, Vol. **25**, No. 1, 1986.
9. McAulay A.D., "Optical Interconnections for Real Time Symbolic and Numeric Processing", Invited Chapter in Book *Optical Computing: Digital and Symbolic*, Marcel Dekker, NY, 1988.
10. McAulay A.D., "Optical Crossbar Interconnected Signal Processor with Basic Algorithms", Optical Engineering, Vol. **25**, No. 1, 1986.

11. McAulay A.D., "Spatial light modulator interconnected computers", IEEE Computer, Oct. 1987.
12. McAulay A.D., "Parallel modular and optical supercomputer architectures for seismic modeling and inversion", Invited Chapter in Book, *Handbook of Geophysical Exploration*, 1988.
13. McAulay A.D., "Predictive Deconvolution of Seismic Array Data for Inversion", IEEE ICASSP, 180-183, 1985.
14. McAulay A.D., "An extendable optically interconnected parallel computer", IEEE-ACM Fall Joint Computer Conf., Proceedings, Vol. 1, (1986).
15. McAulay A.D., "Conjugate Gradients on Optical Crossbar Interconnected Multiprocessor", To appear in Journal of Parallel and Distributed Processing.
16. McAulay A.D. and Parsons E., "Performance of Schur's algorithm on an optically connected multiprocessor", IEEE ICASSP, 1987.
17. McAulay A.D., "Parallel AR Computation with a Reconfigurable Signal Processor", IEEE ICASSP, Vol. 2, 1986.
18. McAulay A.D., "Optimal Least Square Filtering with a Digital Optically Interconnected Processor", SPIE SE, Vol. 639, 1986.
19. McAulay A.D., "Speech recognition with an optical interconnected signal processor", SPIE Real Time Signal Processing, Vol. 698, (Aug. 1986).
20. McAulay A.D., "Optical A/D converters and application to digital multiplication by analog convolution", SPIE Real Time Signal Processing, Aug. 1987.

1987 USAF-UES SUMMER FACULTY RESEARCH PROGRAM/
GRADUATE STUDENT SUMMER SUPPORT PROGRAM

Sponsored by the
AIR FORCE OFFICE OF SCIENTIFIC RESEARCH

Conducted by the
Universal Energy Systems, Inc.

FINAL REPORT

Automated Extraction of Knowledge-Base Object Tuples
From Domain Documents

Prepared by:	Dr. Barry A. McConnell, CDP
Academic Rank:	Assistant Professor
Department and	Computer & Information Systems
University:	Florida A & M University
Research Location:	AFWL/SCR Kirtland AFB Albuquerque, NM 87117
USAF Researcher:	Captain Robert J. Millar
Date:	10 Jul 87
Contract No:	F49620-85-C-0013

Automated Extraction of Knowledge-Base Object Tuples
From Domain Documents

by

Dr. Barry A. McConnell, CDP

ABSTRACT

This study examined the use of automated semantic extraction of object-attribute-value (OAV) tuples from domain specific documents. Using techniques of natural language processing coupled with expert heuristics, the system is designed to identify objects of interest to a particular expert system domain and extract specific values for those objects by a semantic analysis of free-form text contained in domain documents. Attribute identification and value validation is accomplished with a worlds model database of potential OAVs developed for global concepts, and expanded with each application in a new domain. At present, this project has reached the stage of implementing a robust DCG which is functionally oriented towards object identification.

ACKNOWLEDGMENTS

I wish to thank the Air Force Systems Command and the Air Force Office of Scientific Research for sponsorship of this research. I would also like to thank Universal Energy Systems for their remarkably smooth and efficient handling of the administrative aspects of this program.

My introduction to this program and return to full-time research must be credited to Capt. Robert Millar. He has provided the much needed breath of air, intellectual stimulation and supportive encouragement to continue expanding my research efforts in the future.

I must also thank Mr. Paul Morrow and Dr. Larry Rapagnani for their logistical support of my efforts. Without their technical and administrative assistance, much of my work would have never been accomplished.

I also owe a debt of gratitude to Ms. Donna Cromer and Mrs. Virginia King of the AFWL Technical Library. Their ability to identify and locate often obscure references is truly phenomenal.

A most special thanks to Dr. Alex Pelin for his advice and friendship. Truly a scholar and a gentleman.

Thanks go to Capt. Jim Holten, Ph.D. for many hours of stimulating conversation, Mrs. Diane Wood for all the little things that keep the world turning smoothly, and to Ms. Lori Martinez, Ms. Denise Vodnick, and Mr. Hurst

Williams for their professional performance of tedious tasks, without which I could have never accomplished this project.

Finally, my deepest love and gratitude to my wife Nancy for her patience and support in my absence. And to my children, Alex and Karen, for understanding why I was away.

I. INTRODUCTION:

One of the most impeding aspects of expert systems development today is the knowledge acquisition 'bottleneck' (Cooke, N. & McDonald, J., 1986; Hayes-Roth, F. et al, 1983). Current research efforts to alleviate this problem include new techniques and structured methodologies for interviewing experts (Boose, J., 1986; Fox, J. et al, 1985), inductive learning of expert rules from raw data and case studies (Michalski, R., 1983; Michalski, R. & Chilausky, R., 1980; Nii, P. & Aiello, N., 1979; Thompson, B. & Thompson, W., 1986), and new tools and techniques for knowledge representation (Aikins, J., 1983; Guenther, F., Lehmann, H. & Schönfeld, W., 1986).

The Air Force Weapons Laboratory (AFWL) at Kirtland Air Force Base faces a problem common to many organizations, both military and industrial, in acquiring and using expert system technology. The shortage of trained knowledge engineers severely limits the ability of AFWL to develop expert systems that capture and distribute often-rare human expertise. A further complicating feature is the military custom of rotating it's personnel through different duty assignments approximately every three years, thus providing only a small window of access to their expertise. Consequently, development of tools which can aid in the process of knowledge engineering and

reduce the time demands for access to a domain expert would greatly enhance AFWL's abilities to develop and utilize expert systems technology.

My research interests have been in the development of expert systems on small-scale hardware (mini and microcomputers), machine learning, and tools development. My work in new approaches to inference engines is closely related to the knowledge acquisition and representation problems faced by AFWL. Further contributing to my assignment with AFWL was my background in learning psychology and human cognitive processes. The focus of these fields is on human extraction and use of information from various sources and is a pre-requisite to extracting knowledge from written documents via language understanding.

II. OBJECTIVES OF THE RESEARCH EFFORT:

The primary goal of this project was the development of a set of tools to aid in the knowledge acquisition task in implementing rule-based expert systems. Much of the base-line knowledge about a domain is contained in written form, e.g. textbooks, reports, regulations, etc., and consists largely of factual data, as opposed to operational rules. Since this data is available, an

automated system for extracting this information promises to be more cost-effective than current methods of knowledge engineering, requiring less of the domain expert's time.

Various subgoals were developed over the course of this project. The first is a sufficiently robust grammar parser to allow identification of functional, rather than simply syntactical, components of a sentence. Second is development of tools for building world knowledge databases, both globally independent, i.e. concepts of such a nature as to be independent of any particular application, and purely domain relevant, e.g. military or scuba diving concepts. The third goal is discovery of heuristics for mapping functional sentence components to world OAVs. A fourth goal is heuristics for identifying likely candidates for OAVs from overly ambiguous or syntactically indecipherable sentence structures.

Although not part of this project, a supplementary goal requiring additional research is the inductive learning of relational rules about the facts contained in the derived knowledge base.

III. TEXT ANALYSIS:

Although research has been conducted in extraction of data from verbal discourse (Ericsson, K. & Simon, H.,

1980), this approach still requires the physical presence of a domain expert. As noted above, often this access is restricted, and what time is available should not be used in eliciting fundamental, base-line knowledge. In fact, the expert is probably a poor choice for this type of information gathering (Johnson, P., 1983)! A better approach is to use automated text processing of basic domain documents (Hirschman, L. & Grishman, R., 1977).

The first step in such an approach is to parse the text. Parsing is the process of identifying the informational components of a sentence, and consists of two forms of analysis: syntactical and semantic. Syntactic analysis is concerned with the grammatical structure of a sentence and examines the "legality" of a sentence. Semantic analysis is concerned with the meaning of a sentence. The two are interrelated and need to be performed together.

Several approaches are currently used to parse sentences (Winograd, T., 1983), but for this project Definite Clause Grammar (DCG) was chosen. DCGs are an outgrowth of Colmerauer's (1977, 1975, 1970) work in context-free grammars and are very computationally efficient due to their close resemblance to Prolog and its underlying principles of logical resolution (Pereira, F. & Warren, D., 1980).

Due to the complex nature of naturally occurring text, it was decided to implement a DCG based on a restricted sublanguage. This approach has been documented to produce working systems (Schank, R. 1984; Kittredge, R. 1983) provided a sufficiently detailed structural analysis of the text as it normally appears in its domain has been performed. Analysis of military documents (specifically Air Force regulations) revealed a tendency to use syntactically unsound sentences, most commonly occurring as sentence fragments. A DCG (Appendix I) was designed that reflected a loosening of standard technical English grammar rules. This DCG was implemented in Prolog and used to parse a sample document (AFR 35-10). The parsing revealed that the sentence structures used in the document were too ambiguously constructed for a simple relaxation of standard English grammar (one sentence alone generated over 130 possible interpretations!). A new DCG (Appendix II & III) was then developed, based on a object/functional approach (Phillips, B., 1984) and coupled with the use of domain specific expert rules to aid in the proper interpretation of sentence structures (von Limbach, G. & Taylor, M., 1984). At the end of the project period, the DCG has not yet been implemented due to the need of a more semantically complex dictionary than could be developed in the time available. Initial work has also begun on identifying expert rules for semantic understanding, but

requires data from parsing analysis to finish.

IV. DOMAIN KNOWLEDGE:

In order to aid in the appropriate interpretation of ambiguous sentences, a domain-oriented database system was developed. This database will contain candidate OAVs that are relevant to the domain of the text being processed. The database is oriented in a worlds fashion, i.e. segmented into separate segments, each dealing with the OAVs for a single topic. One world is reserved for global concepts; those which are applicable in all areas. For example, a concept such as shoes would be global in nature, while combat boots would be contained in a military world. All domain worlds would have priority over the global world to allow for local re-definition of a concept, e.g. a boot means an article of footwear in a military world but is the bottom protector of scuba tanks in a diving world. Thus, in a diving domain the tank protector concept would be tried before looking for footwear.

The contents of the worlds are database relations stored in Prolog predicate format. Each OAV consists of a functor (`world_fact`) with an arity of three. The first argument is an atomic object (e.g. shoe). The second is

also atomic and specifies the attribute (some measurable quality) of the object (e.g. size). The final argument is a static list structure containing the set of possible values that this particular attribute can assume for this particular object.

These OAVs are used to help in interpreting the text. As each sentence is parsed, likely candidates for objects are the noun structures. When a candidate object has been isolated, it is compared against the database to see if it is an object that is of interest in this domain. When a match is found, the value lists (depending on how many attributes have been defined) can be used provide data on what to look for in the sentence for specific value references. If a matching value is found, a new predicate is asserted that contains the object, value, list of possible attributes, and an identifier of where it was located. For example, suppose the third sentence in the second chapter read "The Congressional Medal of Honor is worn at the left edge of the top row of ribbons.". The parser would identify the potential object 'medal' and scan the military world to see if medals are interesting. Assuming they are, the value lists are scanned to help identify what to look at as data. Under an attribute called 'placement' is found the values 'left', 'middle', 'right', 'first', 'second', 'third', 'fourth', 'fifth', 'top', and 'bottom'. Syntactic analysis reveals that

"Congressional" and "of Honor" are modifiers of 'medal' and are therefore relevant to this object. As can be seen, the appropriate data could be found in the sentence and a new fact asserted that looks like:
fact(congressional_medal_of_honor,location,[top,left]).

At present, the tools necessary to create and modify worlds of OAVs have been designed and implemented. The tools for using them as in the example above cannot be completed until the DCG parser is operational.

V. PROJECT STATUS:

The final two goals, developing heuristics for mapping OAVs and interpreting unrecognizable sentences could not be implemented due to the time frame of the project and unavailability of sufficient resources at AFWL.

VI. RECOMMENDATIONS

This project needs to be completed as it has the potential to significantly effect expert systems development in the future. As noted by Johnson (1983), simple factual data is difficult to extract from human domain experts and the resulting "twenty questions" so

common in current knowledge acquisition methodologies is a major source of frustration and expense. Furthermore, much of what an expert recalls and verbalizes may be erroneous due to the manner in which the information is requested (Ericsson, K. & Simon, H., 1980). Having a basic factual knowledge base can help guide the identification of causal and interactive effects and the ultimate development of heuristic rules which form the basis of expert or knowledge-based systems. Additional research into inductive rule learning is also needed; and the factual knowledge base generated by the tools from this project, coupled with statistically oriented data (such as frequency of occurrence), can serve as initial input to such learning systems.

Another potentially rewarding use of these fact-bases would be as input to systems similar to EURISKO (Lenat, D., 1983). EURISKO was designed to discover new scientific knowledge from generation of "interesting" concepts given an initial set of facts. The results so far have been staggering in their implication.

REFERENCES

- Aikins, J. "Prototypical Knowledge for Expert Systems". *Artificial Intelligence*, 20, 1983, 163-210.
- Boose, J. "ETS: A PCP-Based Program for Building Knowledge-Based Systems". Proceedings of WESTEX '86 (Anaheim), 1986, 19-26.
- Colmerauer, A. "Metamorphosis Grammars". in Bolc, L. (ed.) Natural Language Communication with Computers, Springer-Verlag: Berlin, May 1978.
- Colmerauer, A. "An Interesting Natural Language Subset". Groupe d'Intelligence Artificielle, Université de Marseille-Luminy, Oct 1977.
- Colmerauer, A. "Les Systèmes-Q ou un Formalisme pour Analyser et Synthétiser des Phrases sur Ordinateur". Internal publication No. 43, Département d'Informatique, Université de Montreal, Canada, Sep 1970.
- Cooke, N. & McDonald, J. "A Formal Methodology for Acquiring and Representing Expert Knowledge". *Proceedings of the IEEE*, 74 (10), Oct 1986, 1422-1430.
- Ericsson, K. & Simon, H. "Verbal Reports as Data". *Psychological Review*, 87 (3), May 1980, 215-251.
- Fox, J., Myers, C., Greaves, M. & Pegram, S. "Knowledge Acquisition for Expert Systems: Experience in Leukemia Diagnosis". *Meth. Inform. Med.*, 24 (2), 1985, 65-72.
- Guenther, F., Lehmann, H. & Schenfeld, W. "A Theory for the Representation of Knowledge". *IBM Journal of Research and Development*, 30 (1), Jan 1986, 39-56.
- Hayes-Roth, F., Waterman, D. & Lenat, D. Building Expert Systems. Addison-Wesley: Reading, MA 1983.
- Hirschman, L. & Grishman, R. ". Fact Retrieval from Natural Language Medical Records". *Proceedings 2nd World Conference Medical Informatics*, North-Holland: Amsterdam, 1977, 247-251.
- Johnson, P. "What Kind of Expert Should a System Be?". *Journal of Medical Philosophy*, 8, 1983, 77-97.

Kittredge, R. "Semantic Processing of Texts in Restricted Sublanguages". *Computer & Mathematics with Applications*, 9 (1), 1983, 45-58.

Lenat, D. "Eurisko: A program that learns new heuristics and domain concepts". *Artificial Intelligence*, 21, 1983

von Limbach, G. & Taylor, M. "Expert System Rules Read Natural Language". *Systems & Software*, 3 (8), Aug 1984, 119-125.

Michalski, R. "A Theory and Methodology of Inductive Learning". *Artificial Intelligence*, 20, 1983, 111-161.

Michalski, R. & Chilausky, R. "Learning by Being Told and Learning from Examples: An Experimental Comparison of Two Methods of Knowledge Acquisition in the Context of Developing an Expert System for Soybean Disease Diagnosis". *International Journal of Policy Analysis and Information Systems*, 4 (2), 1980, 125-161.

Nii, H. & Aiello, N. "AGE (Attempt to Generalize): A Knowledge-Based Program for Building Knowledge-Based Programs". *Proceedings of the 6th IJCAI (Tokyo)*, 1979, 645-655

Phillips, B. "An Object-Oriented Parser". in Bara, B. & Guida, G. (eds.) Computational Models of Natural Language Processing, Elsevier: New York, NY 1984.

Pereira, F. & Warren, D. "Definite Clause Grammars for Language Analysis - A Survey of the Formalism and a Comparison with Augmented Transition Networks". *Artificial Intelligence*, 13, 1980, 231-278.

Schank, R. The Cognitive Computer, Addison-Wesley: Reading, MA 1984.

Thompson, B. & Thompson, W. "Finding Rules in Data". *Byte*, 11 (12), Nov 1986, 149-158.

Winograd, T. Language as a Cognitive Process (vol. 1), Addison-Wesley: Reading, MA 1983.

Appendix I - Initial Definite Clause Grammar

Sentence ::= Noun Phrase Verb Phrase |
 <Conjunction> Noun Phrase Verb Phrase |
 <Adjective> Verb Phrase |
 <Preposition> <Verb> |
 <Pronoun> Verb Phrase |
 Sentence <Conjunction> Sentence

Noun Phrase ::= <Noun> |
 <Pronoun> |
 <Noun> Noun Phrase |
 <Pronoun> Noun Phrase |
 <Adjective> Noun Phrase |
 <Determiner> Noun Phrase |
 <Preposition> Noun Phrase |
 <Conjunction> Noun Phrase |
 <Noun> Verb Phrase |
 Noun Phrase Prepositional Phrase

Verb Phrase ::= <Verb> |
 <Adverb> |
 <Verb> Verb Phrase |
 <Adverb> Verb Phrase |
 <Verb> Noun Phrase |
 <Adverb> Noun Phrase |
 <Verb> Subject Complement |
 Verb Phrase Prepositional Phrase

Prepositional Phrase ::= <Preposition> Noun Phrase

Subject Complement ::= <Adjective> |
 <Adjective> <Conjunction>
 <Adjective>

Appendix II - Revised Definite Clause Grammar

Sentence ::= Subject Predicate
 Sentence <Subordinating Conjunction> |
 <,> Dependent Clause |
 Sentence <Coordinating Conjunction> |
 <;> Sentence

Predicate ::= <Intransitive Verb> |
 <Linking Verb> Subjective Compliment |
 <Transitive Verb> Direct Object |
 <Transitive Verb> Indirect Object
 Direct Object |
 <Transitive Verb> Direct Object
 Objective Compliment

[NOTE: Verbs may be in active or passive voice. To create passive, use the following rules:

1. Present form of be + past participle of verb
2. Past form of be + past participle of verb
3. Shall/will + present form of be + past participle of verb
4. Present form of have + past participle of be + past participle of verb
5. Past form of have + past participle of be + past participle of verb
6. Shall/will + past participle of be + past participle of verb
7. Linking verbs have no passive

Verbs may also be preceded by an auxiliary verb.]

Subject ::= <Noun> {nominative case} |
 <Pronoun> {nominative case} |
 Substantive Unit |
 Adjectival Noun

Substantive Unit ::= Dependent Clause |
 Gerundal Phrase |
 Modified Noun

Modified Noun ::= <Noun> {genitive case} <Noun> |
 <Adjective> <Noun> |
 Compound Adjective <Noun> |
 Dependent Clause <Noun>

Compound
 Adjective ::= <Adjective> <Noun> |
 <Adverb> <Verb> |
 <Noun> <Adjective> |
 <Noun> <Noun> |
 <Noun> <Verb> |
 <Preposition> <Verb> |
 <Verb> <Adverb> |
 <Verb> <Noun> |
 <Verb> <Preposition>

[NOTE: These are usually hyphenated, but not always.]

Subjective
 Compliment ::= <Predicate adjective> |
 <Adverb> {ending in -ly} |
 <Predicate noun> {nominative case} |
 Dependent Clause

Dependent
 Clause ::= <,> <Subordinating Conjunction> Subject
 Predicate |
 <Relative pronoun> Subject Predicate

Gerundal
 Phrase ::= <Gerund> |
 <Gerund> Object

Infinitive ::= <to> <Verb> {infinitive form}

Adjectival
 Noun ::= <Plural Adjective> |
 <Article> <Adjective>

Object ::= Dependent Clause |
 <Noun> |
 Substantive Unit

Direct
 Object ::= <Noun> {objective case} |
 <Pronoun> {objective case} |
 Gerundal Phrase |
 Infinitive |
 Dependent Clause |
 Adjectival Noun

Indirect
Object ::= <Noun> {objective case} |
 <Pronoun> {objective case} |
 Gerundal Phrase |
 Dependent Clause |
 Adjectival Noun

Objective
Compliment ::= <Noun> {objective case} |
 <Adjective> |
 <Adverb> |
 <Verb> {Past Participle} |
 Prepositional Phrase

Prepositional
Phrase ::= <Preposition> Object

Appendix III - Format of Dictionary for Revised DCG

Noun	= Number (Singular & Plural) Case (Nominative, Genitive & Objective)
Pronoun	= Person (First, Second & Third) Number (Singular & Plural) Case (Nominative, Genitive & Objective) Type (Personal, Intensive, Reflexive, Reciprocal, Indefinite, Relative, Interrogative, Demonstrative & Numerical)
Verb	= Infinitive Form Gerund Form Purpose (Transitive, Intransitive, Auxiliary & Linking) Number (Singular & Plural) Tense (Present, Past, Future, Present Participle, Past Participle, Future Participle)
Preposition	= Simple (One word) Compound (Adverb & Simple) Phrasal (Simple & Noun & Simple)
Conjunction	= Type (Coordinating & Subordinating)
Adverb	= Word Only
Adjective	= Word Only
Article	= Word Only

1987 USAF-UES SUMMER FACULTY RESEARCH PROGRAM/
GRADUATE STUDENT SUMMER SUPPORT PROGRAM

Sponsored by the
AIR FORCE OFFICE OF SCIENTIFIC RESEARCH

Conducted by the
Universal Energy Systems, Inc.

FINAL REPORT
AUTOMATED DESIGN OF LARGE-SCALED FRAME STRUCTURES
WITH MULTIPLE FREQUENCY CONSTRAINTS

Prepared by:	Oliver G. McGee, M.S.
Academic Rank:	Senior Research Associate
Department and University:	Civil Engineering Department The Ohio State University
Research Location:	AFWAL/FIBRA Wright Patterson AFB OH 45433
USAF Researcher:	Dr. V. B. Venkayya
Date:	30 Sep 87
Contract No:	F49620-85-C-0013

AUTOMATED DESIGN OF LARGE-SCALED FRAME STRUCTURES
WITH MULTIPLE FREQUENCY CONSTRAINTS

by_

Oliver G. McGee

ABSTRACT

Automated design of large-scaled frame structures for dynamic behavior using the optimality criteria (OC) method, typically involves structural members with rectangular or I-sections undergoing extensional plus flexural action. Since the response is primarily governed by a principal moment of inertia, it is considered as the primary design variable and crosssectional area as the secondary one. The thrust of this research effort was to formulate both design variable scaling procedures and member resizing relations. Developed formulae shows that the scaling procedure in conjunction with the finite element analysis of planar frame structures are both efficient and promising for future applications towards optimization of large-scaled frames using the OC method.

Acknowledgements

I wish to thank the Air Force Systems Command, the Air Force Office of Scientific Research (AFOSR), and the Air Force Wright Aeronautical Laboratory (AFWAL) for sponsorship of this research. Many thanks goes to the Universal Energy Systems officials for their efficient operation of the summer faculty research program.

My research experience at AFWAL/FIBRA was both rewarding and technically informative. Dr. V.B. Venkayya replenished me with a great deal technical insight and support both personally and through his many helpful published papers. Many thanks goes to Capt. Robert (Bob) Canfield, Raymond (Ray) Kalonay and Dr. R.V. Grandhi for affording me with many hours of consultation needed to overcome technical stumbling blocks and for providing a sincerely helpful working atmosphere.

I. INTRODUCTION:

The optimal design of large-scaled frame structures with multiple frequency constraints is extremely useful in controlling critical ranges of frequencies in narrow-band excitation problems. For aeroelastic applications, a typical frame can be design so that the bending and torsional frequencies are placed away from instability zones. In each case the ability to manipulate a given frequency value can significantly improve the behavior of the structure.

To automate the frame design for multiple frequency constraints, efficient optimization techniques are required, because of the large number of design variables present. Practical analyses typically involve frame finite elements with rectangular and I-sections capable of resisting extensional and flexural loads. Since the response is primarily governed by a principal moment of inertia, it is considered as the primary design variable and crossectional area as the secondary one.

Documented in the literature are numerous optimization procedures for structures with frequency constraints. A brief description of the previous research work is given in Grandhi and Venkayya (1986). Currently, these structures have been designed by using either a mathematical programming (MP) (Miura and Schmit (1978)) or an optimality criteria (OC) approach (Venkayya and Tischler (1983), Grandhi and Venkayya (1986), Fleury and Sander (1980)).

Both approaches are typically used in conjunction with the finite element technique of structural analysis. In the case of the OC method uniform Lagrangian energy densities exists in all of the elements at an optimum design. The formulae for this optimal condition consists of weight functions (Lagrangian multipliers) and gradients of the objective function (structural weight) and the constraints (frequencies).

In the work of Venkayya, etal (1983) and Grandhi, etal (1986) the OC method was applied to structures comprising of rod and membrane finite elements. According to these investigators the optimization technique involves three steps. "The first step is (a finite element) analysis of the structure followed by scaling and (element) resizing. Analysis gives the information about feasibility or nonfeasibility of the design." Scaling is for locating the desired frequency constraint. The finite elements are resized by enforcing the optimality condition.

For structures modelled with rod, pure flexure, and membrane finite elements, scaling and resizing is straightforward, since the structural matrices are linear functions of the primary design variable (i.e., area, principal moment of inertia, or thickness, respectively). In using the OC method for planar frames, both the scaling procedure and the resizing relations need development and verification on practical problems. Here, the structural matrices are nonlinear functions of the design variables and thus, the scale factors, in particular, are

obtained iteratively to reach the frequency constraint boundary.

II. OBJECTIVES OF THE RESEARCH EFFORT:

The purpose of the present study is to examine certain aspects of the problem of obtaining a minimum weight planar frame design satisfying multiple frequency constraints. As per work by Venkayya, et al (1983) and Grandhi, et al (1986), the OC method based on uniform Lagrangian energy densities for frame member resizing is used along with a scaling procedure to locate the desired frequency constraint boundaries. This report centrally focuses on formulae for the Lagrangian energy densities, resizing algorithm, and scaling procedures, as they apply to planar frame structural members undergoing extension plus flexure.

III. PROBLEM FORMULATION

The problem considered consists of minimizing structural weight of a planar frame while prescribing equality and inequality limits on the natural frequencies. In addition, side constraints are assigned to the design variables, which are taken as lower limits on the crosssectional areas of the frame members. Hence, the mathematical programming problem to be solved reads as follows:

$$\text{minimize} \quad W = \rho_i l_i a_i \quad (i=1,2,\dots,n) \quad (3.1)$$

subj. to

$$\begin{aligned} p_j - p_j^* &= 0 & (j=1,2,\dots,k) \\ p_j - p_j^* &\geq 0 & (j=k+1,\dots,m) \end{aligned} \quad (3.2)$$

side constraints

$$a_i > a_i^l \quad (i=1,2,\dots,n) \quad (3.3)$$

The natural frequencies, p , are obtained from the standard eigenproblem characterizing the structural modal analysis:

$$[K] \{q\} - p^2 [M] \{q\} = 0 \quad (3.4)$$

where in the above n equations $[K]$ and $[M]$ represent the global stiffness and mass arrays, respectively of the planar frame structure; and $\{q\}$ is the mode shape corresponding to the j th frequency. The global structural arrays are obtained by the conventional element assembly procedure of the finite element method (see Rao (1982)).

The optimality condition can be written as

$$e_{ij} \lambda_j = 1 \quad (i=1,2,\dots,n ; j=1,2,\dots,m) \quad (3.5)$$

where λ_j are the Lagrangian multipliers; and e_{ij} represents the ratio of j frequency constraints to objective function gradients with respect to the i design variables. An explicit expression is written as

$$e_{ij} = (q_j^T [k_i]_{,ai} q_j - p_j^2 q_j^T [m_i]_{,ai} q_j) / (\rho_i l_i) \quad (3.5a)$$

where $[k_i]_{,ai}$ and $[m_i]_{,ai}$ are gradients with respect to the design variables of the i th plane frame element stiffness and structural mass arrays, respectively in the global coordinate system. Structural matrices for a typical plane frame element are given in Rao (1982). Eigenvectors are assumed normalized with respect to the mass array (i.e., $q_j^T [M] q_j = 1$).

The resizing algorithm, as proposed by Venkayya, et al (1983),

remains the same:

$$a_i^{k+1} = a_i^k [C_j e_{ij}^k]^s , \quad (i=1,2,\dots,n; j=1,2,\dots,m) \quad (3.5b)$$

where the superscript s controls the iteration step size, C_j contains weight functions in terms of Lagrange multipliers, and superscripts k and $k+1$ denote iteration numbers.

Note that for bar and membrane finite elements, the gradients of the structural matrices, which appear in Eq. (3.5a), are proportional to $(1/a)$; However for plane frame elements undergoing both extension and flexure, these gradients are more complicated due to the relationship between the principal moment of inertia and the crosssectional area (to be discussed shortly).

The success of a scaling procedure depends on the mass distribution in the frame structure. In aerospace structures, a large amount of the mass distribution consists of non-structural mass. The effect of scaling is best investigated by examining Rayleigh's quotient for the j th structural frequency

$$p^2 = \{q\}^T [K] \{q\} / \{q\}^T [M] \{q\} \quad (3.4a)$$

where the total mass $[M] = [M_s] + [M_c]$ consists of structural mass plus non-structural mass.

The way to deal with structural optimization of planar frames with members capable of both extensional and flexural actions depends upon the relationship between the principal moment of inertia I and the crosssectional area a . The following general relation handles a wide variety of practical sections:

$$I = c a^x \quad (3.6)$$

where c is a crosssectional shape constant and x is a positive number (Fleury, etal (1980) and Kolonay (1987)). For the example cases when x is a positive integer we have the following: ($x=1$): thin-walled beams (Eq. 3.6 is linear); ($x=2$): I-sections (Eq. 3.6 is quadratic); ($x=3$): full (rectangular) sections (Eq. 3.6 is cubic).

A key to the success at reaching the desired frequency constraint boundary and hence, obtaining an approach towards a feasible design lies in the concept of scaling. If (a_o, I_o) are design variables representing a particular frame member's crosssectional area and principal moment of inertia at a current point in the design space, the scaling by a factor f yields design variables at a new point in the design space (a_n, I_n)

$$a_n = f a_o \quad I_n = f^x I_o \quad (3.7)$$

Consider storing the structural stiffness matrix as extensional plus flexural contributions as follows

$$[K] = [K_a] + [K_b] \quad (3.8)$$

It can be seen that the scaled global stiffness and structural mass arrays, respectively are given by:

$$\begin{aligned} [K]_n &= f [K_a]_o + f^x [K_b]_o \\ [M_s]_n &= f [M_s]_o \end{aligned} \quad (3.9)$$

Note that the non-structural mass array is independent of the design variables and is not affected by scaling.

To compute the scaling factor f , it is necessary to examine Rayleigh's quotient at the original (or unscaled) and new (or scaled) designs. The Rayleigh's quotient for a given frequency at the original design of the frame structure is written as

$$p_o^2 = \frac{\{q_a\}^T [K_a] \{q_a\} + \{q_b\}^T [K_b] \{q_b\}}{\{q\}^T [M_s] \{q\} + \{q\}^T [M_c] \{q\}} \quad (3.10a)$$

where p_o is the unscaled frequency and the subscript o attached to the matrices has been omitted for clarity. By scaling the design variables (and thus the structural matrices) by the factor f (according to Eq. 3.7 and 3.9), the scaled frequency, p_n is obtained. Rayleigh's quotient for the scaled frequency is

$$p_n^2 = \frac{f \{q_a\}^T [K_a] \{q_a\} + f^x \{q_b\}^T [K_b] \{q_b\}}{f \{q\}^T [M_s] \{q\} + \{q\}^T [M_c] \{q\}} \quad (3.10b)$$

Equations (3.10a-b) can be simplified by dividing the numerator and denominator thru by the generalized mass ($\{q\}^T [M] \{q\}$) and relating the scaled frequency, p_n with the unscaled frequency, p_o as

$$r^2 = (p_n^2/p_o^2) = \frac{f s_a + f^x s_b}{(s_a + s_b) (f m_1 + m_2)} \quad (3.11)$$

where s_a is the ratio of the axial modal stiffness to the generalized mass, s_b is the ratio of the bending modal stiffness to the generalized mass, m_1 is the ratio of the structural modal mass to the generalized mass, and m_2 is the ratio of the non-structural modal mass to the generalized mass. These quantities are formulated below:

$$s_a = \frac{\{q_a\}^T [K_a] \{q_a\}}{\{q\}^T [M] \{q\}}$$

$$s_b = \frac{\{q_b\}^T [K_b] \{q_b\}}{\{q\}^T [M] \{q\}}$$

$$m_1 = \frac{\{q\}^T [M_s] \{q\}}{\{q\}^T [M] \{q\}}$$

$$m_2 = \frac{\{q\}^T [M_c] \{q\}}{\{q\}^T [M] \{q\}}$$

$$s_a + s_b = p_o^2$$

$$m_1 + m_2 = 1 \quad (3.12)$$

An expression involving the scaling factor f is obtained from Eq. (3.11):

$$f^x s_b + f s_a - r^2 (s_a + s_b)(f m_1 + m_2) = 0 \quad (3.13)$$

It is interesting to look at specializations of Eq. (3.13) for the example cases of plane frame members with I-sections ($x=2$)

$$f^2 c_1 + f c_2 + c_3 = 0$$

$$f = \{-c_2 + (c_2^2 - 4c_1c_3)^{0.5}\} / 2c_1$$

$$c_1 = s_b$$

$$c_2 = s_a - (s_a + s_b)(m_1 r^2)$$

$$c_3 = (s_a + s_b)(m_2 r^2) \quad (3.14)$$

and plane frame members with rectangular sections ($x=3$)

$$f^3 c_1 + f c_2 + c_3 = 0$$

$$f = A + B$$

$$A = [-0.5c_2 + (0.25c_2^2 + 0.037c_1^3)^{1/2}]^{1/3}$$

$$B = [-0.5c_2 - (0.25c_2^2 + 0.037c_1^3)^{1/2}]^{1/3} \quad (3.15)$$

Eqs. (3.14) and (3.15) will yield positive and nonzero values for the scaling factor f provided that $(c_2^2 - 4c_1c_3) > 0$ in Eq. (3.14) and $(0.25c_2^2 + 0.037c_1^3) > 0$ in Eq. (3.15).

Alternatively, a nondimensional form of Eqs. (3.10a-b) is obtained by dividing the numerator and denominator thru by the generalized stiffness $\{q\}^T[K]\{q\}$ and relating the scaled frequency, p^n with the unscaled frequency, p_0 :

$$r^2 = \{ f s_1 + f^x s_2 \} / \{ f m_1 + m_2 \} \quad (3.16)$$

where s_1 is the ratio of the axial modal stiffness to the generalized stiffness and s_2 is the ratio of the bending modal stiffness to the generalized stiffness. As in Eq. (3.15), an expression involving the scaling factor, f becomes

$$f^x s_2 + f (s_1 - r^2 m_1) - (r^2 m_2) = 0 \quad (3.17)$$

A specialization of Eq. (3.17) for plane frame members with I-sections ($x=2$) is the following:

$$\begin{aligned} f^2 s_2 + f (s_1 - r^2 m_1) - (r^2 m_2) &= 0 \\ f &= \{-k_2 + (k_2^2 - 4k_1 k_3)^{0.5}\} / 2k_1 \\ k_1 &= s_2 \\ k_2 &= s_1 - r^2 m_1 \\ k_3 &= r^2 m_2 \end{aligned} \quad (3.18)$$

Similarly, a specialization of Eq. (3.17) for plane frame members with rectangular sections ($x=3$) leads to

$$\begin{aligned} f^3 s_2 + f (s_1 - r^2 m_1) - (r^2 m_2) &= 0 \\ f &= A + B \\ A &= [-0.5k_2 + (0.25k_2^2 + 0.037k_1^3)^{1/2}]^{1/3} \\ B &= [-0.5k_2 - (0.25k_2^2 + 0.037k_1^3)^{1/2}]^{1/3} \end{aligned} \quad (3.19)$$

Similarly, Eqs. (3.18) and (3.19) will yield positive and nonzero values for the scaling factor f provided that $(k_2^2 - 4k_1 k_3) > 0$ in Eq. (3.18) and $(0.25k_2^2 + 0.037k_1^3) > 0$ in Eq. (3.19).

Venkayya has recently proposed (in a private communique), what appears to be a general expression for the scaling factor, f , which has the added flexibility to handle structural plane frames comprising of members with different types of crosssectional shapes:

$$f = \{ s_5 + s_6 - 1 + m_2 r^2 \} / \{ s_5 + s_6 - m_1 r^2 \} \quad (3.20)$$

where two alternative modal parameters was obtained as

$$s_5 = \{q\}^T [K_a] \{q\} / \{q\}^T [K] \{q\}$$

$$s_6 = \{q\}^T [p_i \ k_{bi}] \{q\} / \{q\}^T [K] \{q\}$$

$$(i=1,2,3,\dots,\text{no. of members})$$

As in Grandhi, et al (1986), all of the above scaling procedures handle only one equality-type frequency constraint and the rest have to be inequality-type constraints. A scaling factor, f is calculated for each frequency constraint. The scaling factor corresponding the one equality-type frequency constraint is chosen above all other. For all inequality-type constraints, the scaling factor corresponding to the most violated constraint is chosen for the design cycle. In some design cycles iteration may be necessary to obtain an acceptable scaling factor. In addition, it may be possible that for some practical frame structures the proposed scaling procedures may fail.

IV. RECOMMENDATIONS:

The proposed scaling procedures and resizing algorithm appear to be sound on paper. However, no conclusions about the scaling

procedures can be made until they are tested on practical frame structures. The present writer has an efficient code that evaluates for a planar frame the structural matrices and their gradients and calculates a set of natural frequencies. Also, the proposed scaling procedure and resizing algorithm are currently being automated for any number of desired frequency constraints. A proposal for a AFOSR RIP mini grant is forthcoming. The main thrust of the proposed research is to extend the work reported herein by making available to researchers and engineers design information on the performance of the proposed scaling procedures for practical frame models. Intuitively, these conclusions can add to a computational understanding of optimum design techniques for large-scaled frames using the OC method in conjunction with a scaling procedure.

REFERENCES

Fleury, C., and Sander, G., "Generalized Optimality Criteria for Frequency Constraints, Buckling Constraints and Bending Elements" Tech. Rept., AFOSR-TR-80-107, 1980.

Grandhi, R.V. and Venkayya, V.B., "Structural Optimization with Frequency Constraints" SDM Conference Proceeding, 28th SDM Conference, Monterey, Calif., 1986.

Kolonay, R., "Structural Optimization of Large Scale Structures Under Multiple Loading Conditions Subjected to Stress and Displacement Constraints", M.S. Thesis, Ohio State University, 1987.

Miura, H. and Schmit, L.A., "Second Order Approximation of Natural Frequency Constraints in Structural Synthesis," Intl. J. for Numerical Methods in Eng., Vol. 13, p. 337-351, 1978.

Rao, S.S., "The Finite Element Method in Engineering", Pergamon Press, 1982.

Venkayya, V.B., and Tischler, V.A., "Optimization of Structures with Frequency Constraints", Computer Meth. for Nonlinear Solids and Structural Mech., ASME, AMD-54, p. 239-259, 1983.

1987 USAF - UES SUMMER FACULTY RESEARCH PROGRAM /

GRADUATE STUDENT SUMMER SUPPORT PROGRAM

Sponsored by the
AIR FORCE OFFICE OF SCIENTIFIC RESEARCH

Conducted by the
Universal Energy Systems, Inc.

FINAL REPORT

Statistical Methodology for Assessing Group Health Differences

Prepared by : Daniel Mihalko
Academic Rank : Associate Professor
Department and : Mathematics and Statistics
University : Western Michigan University
Research Location: USAFSAM/EKB
Brooks AFB, Texas 78235
USAF Researcher : Dr. Joel E. Michalek
DATE : September 10, 1987
Contract No. : F49620-85-C-0013

Statistical Methodology for Assessing Group Health Differences

by
Daniel Mihalko

ABSTRACT

Three major tasks were addressed: (1) Develop statistical methodology for analyzing mortality/morbidity data which involves periodic physical exam information; (2) Odds ratio estimation in the presence of three-factor interaction or confounding; (3) Estimation of half-life of blood dioxin level.

In task (1) we extended the survival/sacrifice literature by using a logistic model to adapt the estimation techniques of Dinse (1982) to include the comparison of two groups via relative risk. We also began investigating models which relate disease incidence, prevalence, mortality rates and survival experience.

In task (2) we developed and tested a method for estimating two factor association in the presence of a third factor. The resulting estimator uses statistical pretests to determine three-factor and two-factor interactions. A simulation study shows that this procedure reduces bias and mean square error over the crude collapsed estimator.

In task (3) we investigated introducing lab error with a specified coefficient of variance into the exponential decay model. We built likelihoods for two different such models in an attempt to estimate the half-life of the decay curve using only two points measured with error.

Acknowledgements

I wish to thank the Air Force Systems Command and the Air Force Office of Scientific Research for giving me the opportunity to do this work by sponsoring my research. I also thank Col. William Wolfe, chief of the Epidemiology Division of the School of Aerospace Medicine for providing the material and atmosphere required to do this work.

I am especially grateful to Dr. Joel E. Michalek, chief of the Biometrics Branch of the Epidemiology Division for his energetic partnership in this research project. Much of the computation work could not have been done without the expert help and advice of Mr. Thomas White. I cannot imagine an atmosphere and energy more conducive to good scientific work than that existing at the Biometrics Branch of the Epidemiology Division of the School of Aerospace Medicine.

I. INTRODUCTION

I have been developing statistical methodology for applications in Epidemiology for the past seven years. In particular I have developed methodology for determining differences in survival experience in matched case control studies. In Michalek and Mihalko (1983b, 1984) I helped develop an appropriate method for determining group differences in survival experience when cases and controls are matched on a vector of specific variables. This procedure replaced an incorrect procedure which had been published in the literature (see Michalek and Mihalko (1983a)). I helped to design and test the computer software needed to implement this methodology (see Michalek, Mihalko and White (1983)).

Since the Air Force Health Study on the Effects of Herbicide Exposure (Air Force Health Study) required monitoring of its matched cases and controls, I adapted the work of Michalek and Mihalko (1983b, 1984) to include repeated testing of the same subjects (see Mihalko (1987)).

Although all the work mentioned above has general application in clinical trials as well as Epidemiology, the main goal of my work was to develop Statistical methodology for analyzing the data being generated by the Air Force Health Study. In this context I helped develop methods for computing statistics for comparing groups on survival experience (Mehrotra, Michalek, Mihalko and White (1982) and Mehrotra, Michalek and Mihalko (1982)).

Statistical aspects of the Air Force Health Study are directed from the Biometrics branch of the Epidemiology Division of the USAF School of Aerospace Medicine by Dr. Joel E. Michalek. My assignment to this lab to work with Dr. Michalek is a direct result of the success Dr. Michalek and myself have enjoyed in working together to develop state-of-the-art statistical analysis for The Air Force Health Study.

II. OBJECTIVES OF THE RESEARCH EFFORT:

The general objective of this research effort was to continue developing statistical methodology for long term epidemiological studies involving matched subjects and periodic physical exams. We began or continued work on three separate tasks under this general objective.

Task 1: Develop Statistical Methodology for Analyzing Mortality/Morbidity Data Which Involves Periodic Physical Examination Information.

The goal of this effort is to develop statistical models and methodology for efficiently analyzing data generated by periodic physical examinations and death time information. The effort was two fold. Firstly, investigate adapting survival/sacrifice techniques to the situation of periodic physical examinations. Secondly, investigate mathematical models which relate disease incidence, prevalence, mortality rates and survival experience.

Task 2: Odds Ratio Estimation in the Presence of Three-factor Interaction or Confounding.

The goal of this work was to develop a method for estimating the association of two factors, say D and F , in the presence of a third factor, E . We intended to use the log-linear model for three factors, (see Bishop, Feinberg and Holland (1975)), to determine when collapsing over the strata of E produced an unbiased estimate of the FD association. In addition we intended to develop an estimation method to correctly estimate the FD association whether or not collapsing over E is appropriate.

Task 3: Estimation of Half-Life of Blood Dioxin Level.

The goal of this effort is to devise a statistical test for determining whether the level of dioxin in the human circulatory system has the same half-life in all human beings. The main problem is that this statistical method must be applicable to data which consists of only two measurements made five years apart on each of a sample of individuals.

III. TASK I INVESTIGATION DESCRIPTION:

Our survival/sacrifice extension work involved combining the work of Dinse (1982) with the works of Mitchell and Turnbull (1978, 1983) to provide a longitudinal statistical methodology for comparing disease incidence and prevalence between two groups of subjects (usually an exposed group versus a control group). We have been successful in partially solving this problem.

Dinse (1982) provides a nonparametric model for using survival/sacrifice data to estimate longitudinal incidence and prevalence in one group of subjects. The papers of Mitchell and Turnbull introduce a log-linear model to relate two groups of subjects. Unfortunately, their techniques do not apply to longitudinal studies.

In our first attempt at extending survival/sacrifice techniques to the periodic examination situation, we took the longitudinal model of Dinse and applied it to both groups individually. We then related the two groups' models by using a logistic model to relate disease state to group membership and survival time. That is, we used the logistic model to define the probability of an individual being in a particular disease state given his group membership and survival time. The estimation techniques of Dinse all apply to the individual groups. The final parameter, which is relative risk of disease of one group with respect to the other, can be estimated using the

standard technique of Mantel-Hanzenel for estimating a common odds ratio from several contingency tables.

We are now in the process of developing software to implement this methodology. When the software is built it will be applied to data from the Air Force Health Study on the effects of herbicide exposure. The results will then be written up and submitted for publication.

The second direction of our effort on this problem has been a review of medical screening literature to find mathematical models which relate disease prevalence and incidence, mortality rates and survival experience. This literature review has turned up several models; Zelen and Feinlieb (1969), Albert, et. al (1978a, 1978b), Louis, et. al. (1978), Melamed and Flehinger (1987) and Flehinger and Kimmell (1987).

The three papers by Albert et. al. and Louis et. al. are particularly promising. So, our first effort in this direction has been to begin a careful reading of these works. Our hope is to use these models to isolate the effect of periodic examinations on the progression of disease.

IV. TASK 2 INVESTIGATION DESCRIPTION

Using the three factor log-linear model (see Bishop, Fienberg and Holland (1975)) we expressed the simple odds ratio for two factors in terms of the three factor model. This produced the parameter which is actually being estimated when one collapses a 2x2x2 contingency cube over one of the factors. Using this expression we proceeded to demonstrate under what conditions the collapsed odds ratio is the appropriate measure of association for two out of three factors. We showed that the collapsed odds ratio is appropriate when there is no three factor interaction and when at least one of the two factor interactions with the collapsed factor is zero. In other

words one may collapse over a factor, E , if there is no three way interaction and if E is not confounded with both of the other factors, F and D . This result, in itself, is not new, however the analytical demonstration is new.

We continued studying this problem to determine what should be done if there is possibly a three-factor interaction or confounding by the collapsing variable. As a first and logical answer to this question we formed an estimate of the FD association using statistical pretests to determine three-factor interaction or confounding. More specifically, we estimate the two factor odds ratio according to the following rule:

- Step 1: Statistically test for three-factor, i.e. EFD , interaction. If there is evidence of three-factor interaction, do not collapse over E and use the odds ratios for each stratum of E to get separate estimates of the FD association. If there is no evidence of three-factor interaction then act as if there is a common DF odds ratio for all strata of E , and proceed to step 2.
- Step 2: Statistically test for DE and FE interactions. If one of these interactions is zero then collapse over E and use the odds ratio of the collapsed table. If both interactions are not zero then use the Mantel-Haenzel estimate of the common odds ratio.

Using a general indicator function for the possible outcomes of the statistical tests, we computed the asymptotic (sample size equals infinity) bias and mean square error of this procedure. We then computed these biases and mean square errors using a no apriori knowledge assumption and various values for the terms in the three factor log-linear model.

Firstly, our calculations showed that this pretesting procedure does reduce bias and the mean square error, over collapsing without pretesting.

However, the computations also showed that when there is no three-factor interaction, confounding must be quite strong before the bias of the collapsed odds ratio estimator becomes significant.

Secondly, our calculations demonstrated that bias is reduced as one accepts a greater amount of type I error in the pretests for three factor interaction and confounding.

The results of this work are being prepared for publication.

V. TASK 3 INVESTIGATION DESCRIPTION

Using the usual exponential model for decay of high levels of pollution in the blood we have attempted to mathematically model the variables which would affect the dioxin measurement. There is a belief among physicians working in this area that there is no individual variation in the dioxin decay curve when dioxin levels are very high. If this is true then the only source of variation is lab error in measuring dioxin level. So we have introduced lab error (as a normal deviate) into the exponential decay model. We have built two such models and have attempted to build likelihoods which would yield good estimates (maximum likelihood estimates) of the half-life of the decay curve.

This work is still in a very preliminary stage. We are currently trying to devise a way of modelling lab error with a known coefficient of variation into the exponential decay model in a realistic way.

VI. RECOMMENDATIONS TASK I:

I believe future research should be directed in the area of modelling the relationship between disease incidence, prevalence, mortality rates and survival experience. The models of Albert et. al. and Louis et. al. look very

promising. I will continue working with the School of Aerospace Medicine in this direction.

More explicitly, my future work will attempt to use the models of Albert et. al. and Louis et. al. with the hazard function techniques of McKnight and Crowley (1984). The effort here will be to build a likelihood function using hazard functions based on the incidence, prevalence, and duration models of Albert et. al. and Louis et. al. The likelihood would then explicitly contain the parameters of interest and use all available data. Standard likelihood methods might then apply to develop statistical estimates and tests for differences between groups on disease incidence, prevalence, mortality rates and survival time.

Despite the fact that the survival/sacrifice methodology developed under this contract does not directly apply to The Air Force Health Study, it still has a great deal of application in animal studies performed at the school of Aerospace Medicine. I recommend that the effort to develop computer software to implement these procedures be continued. I will be working with the Biometrics Branch of the Epidemiology Division at SAM to develop such software.

The results of the survival/sacrifice development will be prepared for publication as soon as the computer software is developed and applied to an example data set.

VII. RECOMMENDATIONS FOR TASK 2:

The results of our bias and mean square error calculations indicate that in assessing the effect of a treatment on disease susceptibility, an experimenter should investigate other variables via statistical pretests. Certainly whenever there is a third factor, such as smoking or drinking

involved in a study, this third factor should not be ignored without statistically testing it for confounding or multiway interaction.

VIII. RECOMMENDATIONS FOR TASK 3:

Since the half-life of the decay curve is a function of the ratio of the two measurements, modelling this ratio must continue to be investigated. Under the assumption (to be tested) that the only variability in measurements is due to lab error, this ratio is the only source of variability in the half-life formula. Furthermore, since the lab errors are known to be normal with a known coefficient of variation, this modelling attempt should be in the direction of a ratio of independent noncentral normal random variables. The problem that must be solved is the fact that the measurements cannot be negative. Thus we must somehow truncate our normal random variables to fit the physical situation. Perhaps this can be done by considering only observations that are above a certain threshold.

After the modelling problem is done to fit the actual physical situation, the resulting distribution will lead to a likelihood function. Maximum likelihood estimates for the half-life and nuisance parameters can then be found. The next step is then to investigate the distributional properties of a Kolmogorov-Smirnov type statistic using these estimators. Finally the sample of observations can be used to calculate a pseudo sample of half-lives. This sample of half-lives can be then used in the Kolmogorov-Smirnov test to see if they fit a decay curve generated by an exponential decay with lab error as the only source of variation.

This is a big job with many, many details to be ironed out. However, it is a problem which needs solving because it will have a big impact on building an exposure index for the Air Force Health Study.

5. REFERENCES

1. Albert, A., Gertman, P. M., and Louis, T. A. (1978a). "Screening for the Early Detection of Cancer-I. The Temporal Natural History of a Disease State." Mathematical Biosciences 40, 1-59.
2. Albert, A., Gertman, P. M., Louis, T. A., and Liu, S. I. (1978b). "Screening for the Early Detection of Cancer.-II The Impact of the Screening on the Natural History of the Disease " Mathematical Biosciences 40, 61-109.
3. Bishop, Y. M., Feinberg, S. E., and Holland, P. W. (1975). Discrete Multivariate Analysis; MIT Press, Cambridge, Mass.
4. Dinse, G. E. (1982). "Nonparametric Estimation for Partially-Complete Time and Type of Failure Date," Biometrics, 38, 417-431.
5. Flehinger, B. J. and Kimmel, M. (1987). "The Natural History of Lung Cancer in a Periodically Screened Population," Biometrics, 43, 127-144.
6. Louis, T. A., Albert, A., and Heghinian, S. (1978). "Screening for the Early Detection of Cancer-III. Estimation of Disease Natural History", Mathematical Biosciences, 40, 111-144.
7. Mehrotra, K. G., Michalek, J. E., and Mihalko, D. (1982). "A Relationship Between Two Forms of Linear Rank Procedures for Censored Data." Biometrika, 69, 674-676.

8. Mehrotra, K. G., Michalek, J. E., Mihalko, D., and White, T. (1982). "Score Computation for Linear Rank Procedures," Journal of Statistical Computation and Simulation, 16, 201-211.
9. McKnight, B. and Crowley, J. (1984). "Tests for Differences in Tumor Incidence Based on Animal Carcinogenesis Experiments," Journal of the American Statistical Association, 79, 639-648.
10. Melamed, M. R. and Flehinger, B. J. (1984). "Screening for Lung Cancer," Chest, 86, 2-3.
11. Michalek, J. E. and Mihalko, D. (1983a). "On the Use of Log-rank Scores in the Analysis of Litter-Matched Data on Time-to-Tumor Appearance." Statistics in Medicine, 2, 315-321.
12. Michalek, J. E. and Mihalko, D. (1983b). "Linear Rank Procedures for Matched Observations," USAFSAM-TR-83-16.
13. Michalek, J. E. and Mihalko, D. (1984). "Linear Rank Procedures on Litter-Matched Data," Biometrics, 40, 487-491.
14. Michalek, J. E., Mihalko, D., and White, T. (1983). "Matched Survival Analysis Package," USAFSAM-TR-83-15.
15. Mihalko, D. (1987). "Repeated Significance Testing in Survival Analysis Using a Litter-Matched Design," Biometrics, 43, 115-125.

16. Turnbull, B. W. and Mitchell, T. J. Exploratory Analysis of Disease Prevalence Data from Survival/Sacrifice Experiments." Biometrics, 34, 555-570.
17. Turnbull, B. W. and Mitchell, T. J. "Nonparametric Estimation of the Distribution of Time to Onset for Specific Diseases in Survival/Sacrifice Experiments," Union Carbide TR ORNL/CSD-111.
18. Zelen, M. and Feinleib, M. (1969). "On the Theory of Screening for Chronic Diseases," Biometrika, 56, 601-614.

1987 USAF-UES SUMMER FACULTY RESEARCH PROGRAM/
GRADUATE STUDENT SUMMER SUPPORT PROGRAM

Sponsored by the
AIR FORCE OFFICE OF SCIENTIFIC RESEARCH

Conducted by the
Universal Energy Systems, Inc.

FINAL REPORT

A COMPARISON OF TRACKING WITH ACTIVE STICK CONTROLLERS
WITH AN OPTIMAL CONTROL MODEL

Prepared by:	Augustus Morris, Jr.
Academic Rank:	Instructor
Department and	Natural Sciences Division
University:	Wilberforce University
Research Location:	Armstrong Aerospace Medical Research Laboratories, Biodynamics and Bioengineering Division, Acceleration Effects Branch
USAF Researcher:	Dr Daniel Repperger
Date:	August 10, 1987
Contract No:	F49620-85-C-0013

A Comparison of Tracking with Active Stick Controllers with
an Optimal Control Model.

Mr. Augustus Morris

Abstract

Active stick controllers are unique from traditional passive controllers by providing additional feedback to the human by means of an active force applied to the stick. A consistent empirical relationship has been found using an active controller, in previous studies, which allows greater tracking performance than tracking with passive controllers.

An optimal control model was developed to compare with a previous experiment in which a total of twelve conditions were tracked. It was found that the experimental results matched the optimal solutions when the product of the plant and active loop resembled Maki's crossover model. However, the best performance scores were found experimentally when the active loop had a crossover of 1.0. It was theoretically shown that when the active loop was 1.0, regardless of the plant, the system would still behave functionally as an optimal system.

involvement

...and in the Air Force... of
...research... of
...and the Armstrong Laboratory...
...laboratory... of
...and in the... of
...effects... of the... and...
...division of HAFEL.

It is known that the human body is not designed to withstand the high g-forces of a high speed aircraft. This leads to the possibility of a pilot being unable to perform the mission during the high speed portion of the mission. This is a serious problem for the military aircraft on the pilot and the mission. The research being done at the time of the writing of this report is on the pilot.

An obvious result of being subjected to high g-forces is loss of consciousness, and once again, this research is currently being conducted in this area. However, these same g-forces can alter the ability of the pilot to complete the tracking task. This alteration can be beneficial or detrimental to the actual performance of the mission. This led to research studying the tracking behavior of pilots performing in various complex g-fields. The culmination of this research was the design of an active motion tracking device which is able to produce forces on the pilot which are the opposite of the actual g-forces.

The active motion tracking device is a device which is able to produce forces on the pilot which are the opposite of the actual g-forces. This device is able to produce forces on the pilot which are the opposite of the actual g-forces. This device is able to produce forces on the pilot which are the opposite of the actual g-forces. This device is able to produce forces on the pilot which are the opposite of the actual g-forces.

dynamics were none (passive), 1.5, or 1/5.

The optimal closed loop system would be determined for each plant and compared with the experimental data for each particular plant. From these comparisons, along with the tracking score data, it was hoped to show that the active stick conditions that gave better performance also matched with the optimal model.

III. Development of an optimal closed loop system

This derivation is a slight modification of the model developed by Chang(2). In the basic regulator problem, the block diagram for the system is shown in Figure (1) where,

$R(S)$ = reference input=0

$H(S)$ = compensator

$U(S)$ = control signal

$D(S)$ = disturbance signal

$G(S)$ = plant

$C(S)$ = plant output

This block diagram can be redrawn as shown in Figure 2.

It is desired to choose a compensator, $H(S)$, such that the output, $C(S)$, is kept at the reference set point, $R(S)$, which equals zero. If we were to find an optimal

desired trajectory, and even though a cost function will be forced upon the system, the system designer will be able to choose the cost function to suit his needs. For example, if the system designer is concerned with the system's response to a step function, then the cost function should be chosen to reflect this. In this case, the cost function should be chosen to be the integral of the square of the error signal, which is the standard cost function for a step response. In this case, the cost function must be included in the cost function, and the cost function must be chosen to reflect the system's response to a step function.

Iterative cost functions have been used to optimize the control of a control-based system. The cost function is chosen to reflect the system's response to a step function. The cost function is chosen to be the integral of the square of the error signal, which is the standard cost function for a step response. Since, in man-machine systems, people tend to have greater control of the control rate, rather than just displacement position alone, $SU(S)$ rather than just $U(S)$ should be included in the cost function. In physical terms $U(S)$ would relate to the control stick position, while $SU(S)$ would relate to control stick velocity. In addition, typically there's a tradeoff between the amount of error that is allowed in a system and the amount of energy for control. That is, the cost function is chosen to reflect the system's response to a step function, and the cost function is chosen to reflect the system's response to a step function. This relationship needs to be brought out in the cost function.

Knowing the basic ingredients of a cost function, we can write down a cost function for a system.

$$J = \frac{1}{2\pi j} \int_{-\infty}^{+\infty} \left[k^2 E(s)E(-s) + (1-k^2) s U(s)(-s) U(-s) \right] ds \quad (1)$$

where $0 < k \leq 2$ and displays the weighting of the error in the functional. From this point on, in the derivation we denote $\bar{C} = C(s)$ and $\bar{D} = D(-s)$.

Following Chang's development, the optimal control law system for this system becomes:

$$M_{OK} = \frac{N_o}{D_o} - \frac{N_o}{D[k^2 N_o \bar{N}_o + (1-k^2) D_o \bar{D}_o S \bar{S}]} + \left[\frac{k^2 D G \bar{N}_o}{[k^2 N_o \bar{N}_o + (1-k^2) D_o \bar{D}_o S \bar{S}]} \right]_+$$

where $G = \frac{N_o}{D_o}$ (2)

Note that the disturbance input, D , in the above formulation represents a deterministic input. The actual disturbance input, in the simulation, is a randomly appearing sum of sine waves input which is still deterministic. However, the human operator injects randomness into the system. Nevertheless, the mean square error of a system with a deterministic input is the same as a random input if the Laplace transform of the deterministic input is identical to the spectral density of the random input (11).

In addition, it can be shown that if the disturbance input, D , contains only poles that are nonrepeating, the disturbance input cancels out of the optimal M_{OK} equation.

Therefore, the optimal closed-loop response is obtained by adjusting the controller parameters until the closed-loop system is having only a variation of the desired differential response and no overshoot. The optimal closed-loop response which is obtained by using the optimal filter with a loop gain of 4 is shown in Figure 4. The output error is and all as the system is adjusted.

4. Comparison with data

The theoretical optimal closed-loop response is compared with the experimental conditions and one very important result was seen. For each plant condition, an optimal response was found experimentally (in terms of reducing tracking error) when the plant loop product was 5. This is significant because it suggests that if the plant loop combination resembles McQuerry's crossover model, then all systems behaves optimal w. It is worth noting that the crossover model is optimal in all cases, even if ω_c is not 5; however, the validity of the model is not confirmed by the data and is not repeated.

Figures 4, 4A and 5 show the results of the comparison between the optimal closed-loop transfer function and the experimental response. The results show that the optimal closed-loop response is very close to the experimental response. The results also show that the optimal closed-loop response is very close to the experimental response. The results also show that the optimal closed-loop response is very close to the experimental response.

[illegible]

AD-A191 284

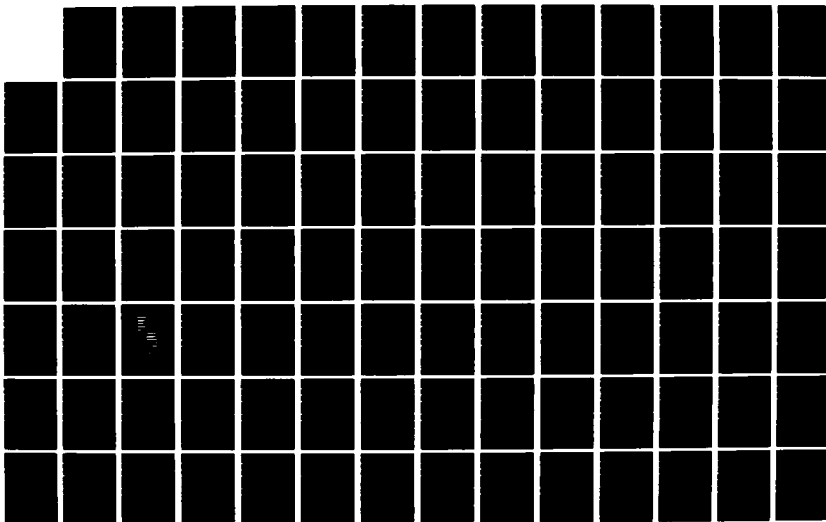
UNITED STATES AIR FORCE SUMMER FACULTY RESEARCH PROGRAM
(1987) PROGRAM TE (U) UNIVERSAL ENERGY SYSTEMS INC
DAYTON OH R C DARRAH ET AL DEC 87 AFOSR-TR-88-0213
F49620-83-C-0013

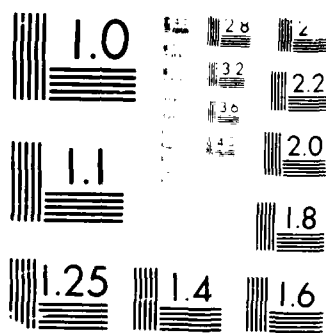
9711

UNCLASSIFIED

F/G 3/1

NL





MICROCOPY RESOLUTION TEST CHART
ANSI #2 - 1963

V. Explanation for the success of the S loop

It can be tentatively seen that human behavior in a near optimal manner when the active loop dynamics is $1/s$, regardless of the plant dynamics that were used in the study. This occurred because the S dynamics of the active loop compensate for the inherent $1/s^2$ phase lead requirement of the human operator in order to make the system to have indeed a gain of unity. It can be further argued that the conditions with the pilot loop product equal $1/s$ do not look structurally the same as the loops cases, but functionally the two conditions behave similarly.

VI. Recommendations

The conclusions from this study showed that active error controllers can allow improved tracking performance during simulated tracking tasks. This improvement occurs in a optimal fashion if the product of the plant and active loop dynamics is $1/s$, which is the basic form of a second order crossover model. More studies need to be done with more complex plants and active loops to see if the same relationship exists. Furthermore, a detailed crossover sensitivity analysis needs to be done on the effect of the track design on the $1/s$ result. This study did not include a detailed relationship between the $1/s$ result and the

active stick system and tracking performance.

These projects will be proposed in a RFP and grant soon to be submitted. What would be significant in conducting this research is the eventuality of having guidelines for designing active stick controllers for jet aircraft adaptable to changing environments and missions. This technology could lead to greater pilot control of future jet aircraft under higher performance level.

References

1. Anderson, J. L. Feedback Design of Control Systems. Significant Undergraduate Series. Prentice-Hall, Inc., Englewood Cliffs, New Jersey, 1982.
2. Chang, S. S. Synthesis of Optimum Control Systems. New York, McGraw Hill, 1961.
3. Kleinman, D. L., S. Baron, and W. J. Levinson, 'An Optimum Control Model of Human Response and Its Theory and Validation,' Automatica, 1970, 6:357-369.
4. McRuer, D. T., 'Human Dynamics in Man-Machine Systems,' Automatica, 1980, 16:237-253.
5. Repperger, D. W., J. W. Frasier, and R. E. van Patton, 'A Smart Stick Controller Design Based on a Static Equilibrium Model,' NAECON Proceedings, 1984.
6. Repperger, D. W., J. W. Frasier, and R. E. van Patton, 'Results from a Biomechanical Stick Study,' Aerospace Medical Association Conference, 1984.

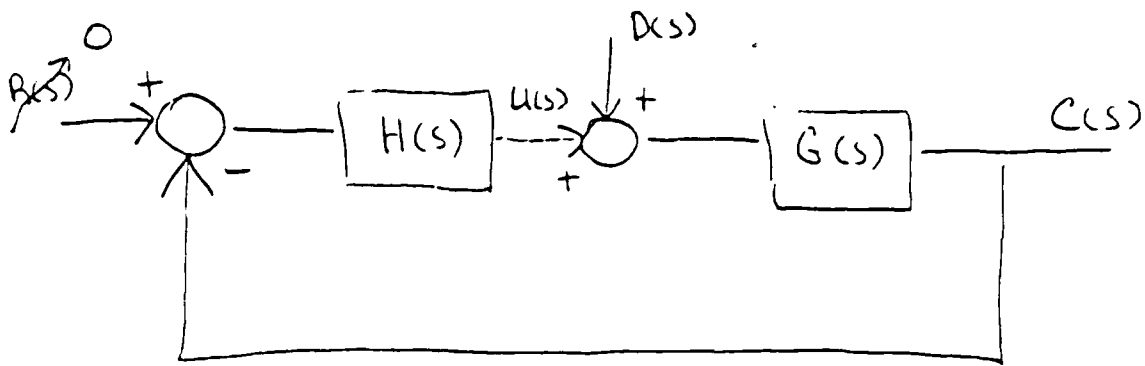


Figure 1 The basic regulator problem

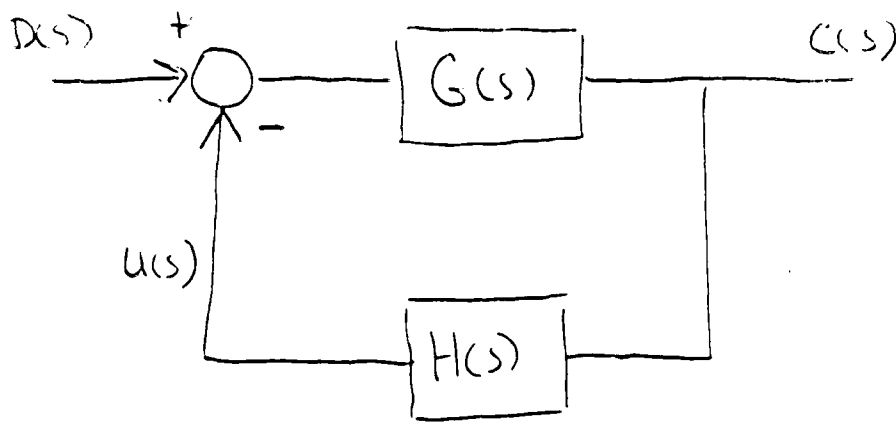


Figure 2 Regulator problem redrawn

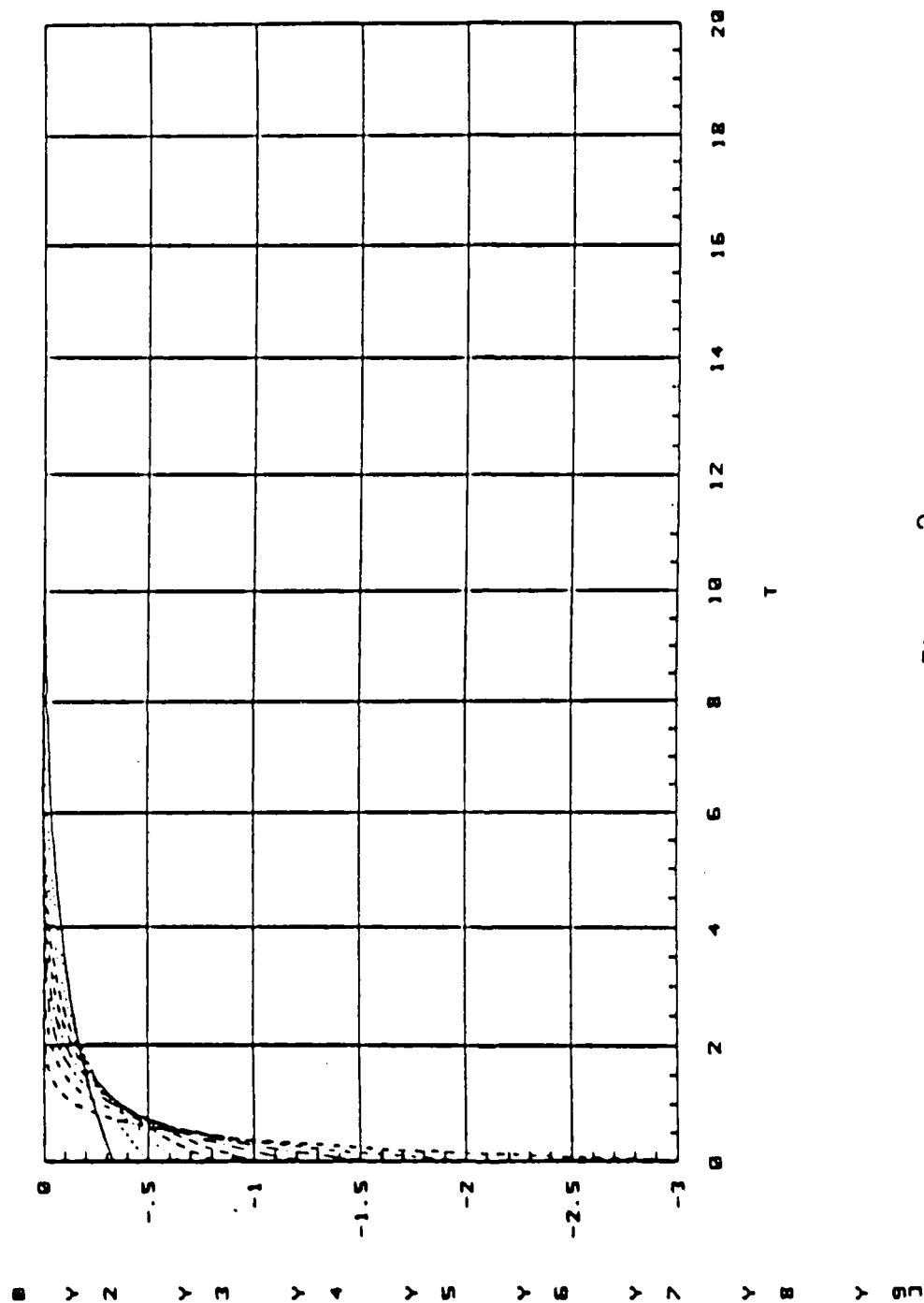


Figure 3
Impulse responses of optimal M_{0k} for plant 1 $0 \leq k' < 1$

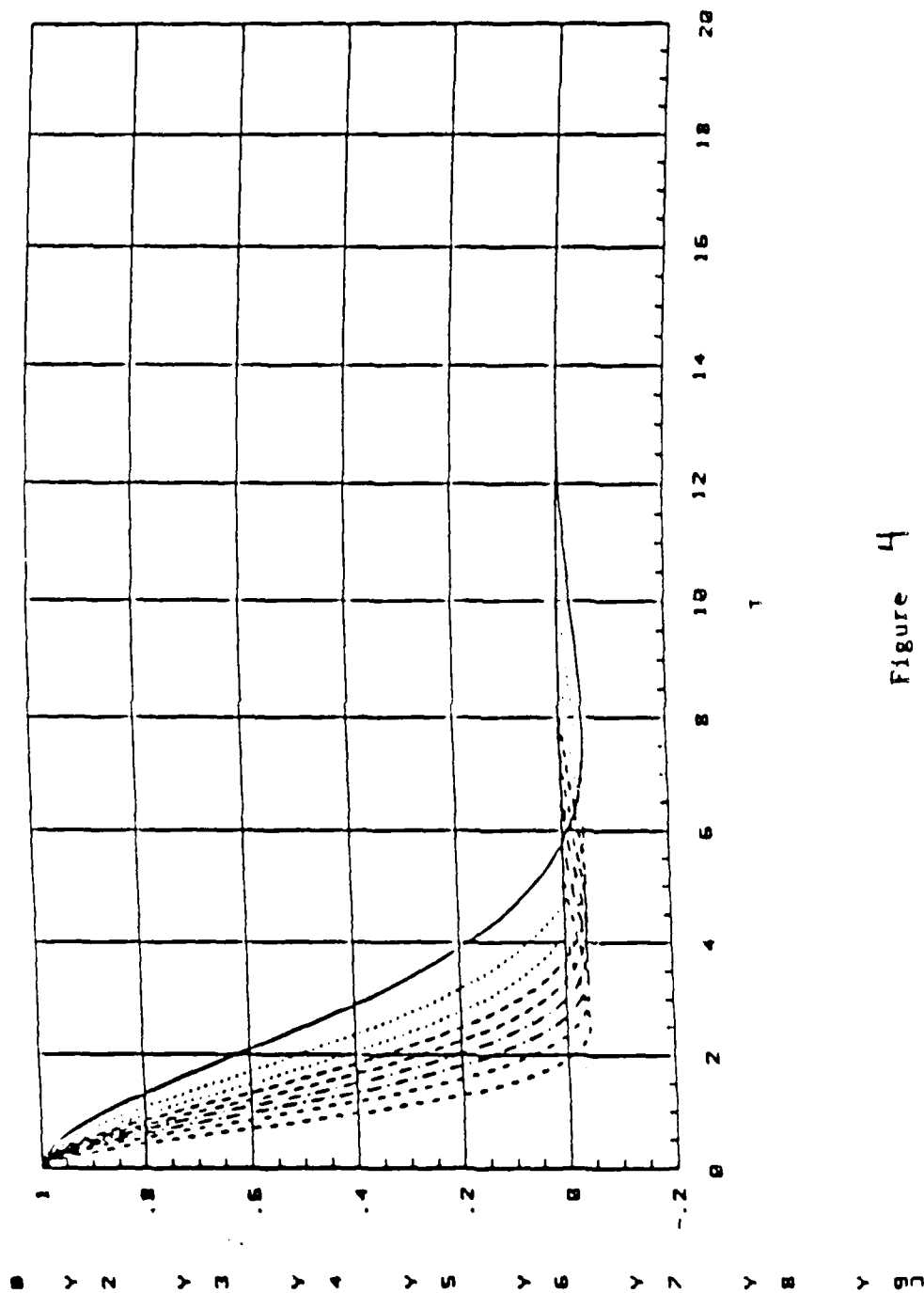


Figure 4
Impulse responses of optimal M_{0k} for plant $1/S$, $0 \leq k' < 1$

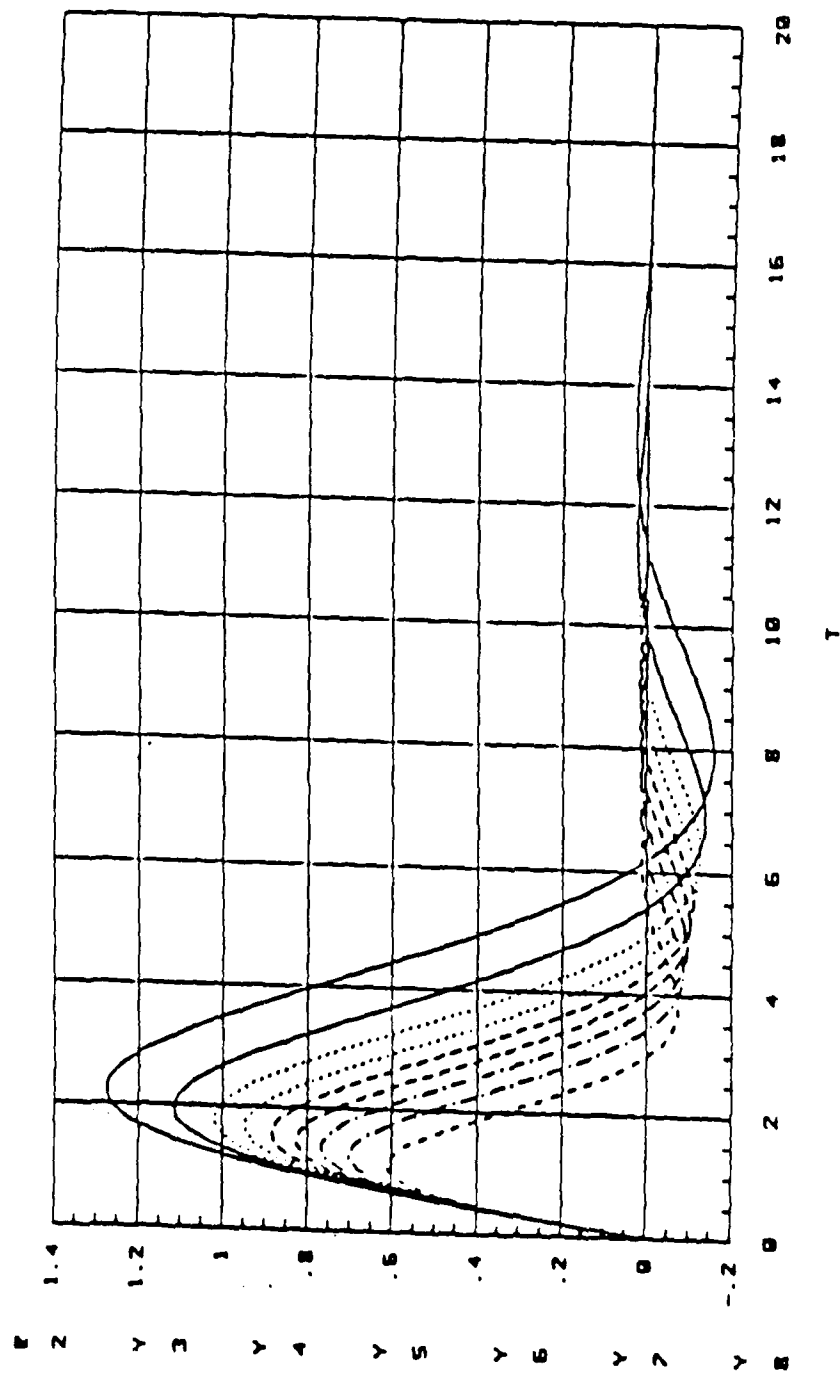


Figure 5
Impulse responses of optimal M_{0k} for plant $1/S$, $0 < k' < 1$

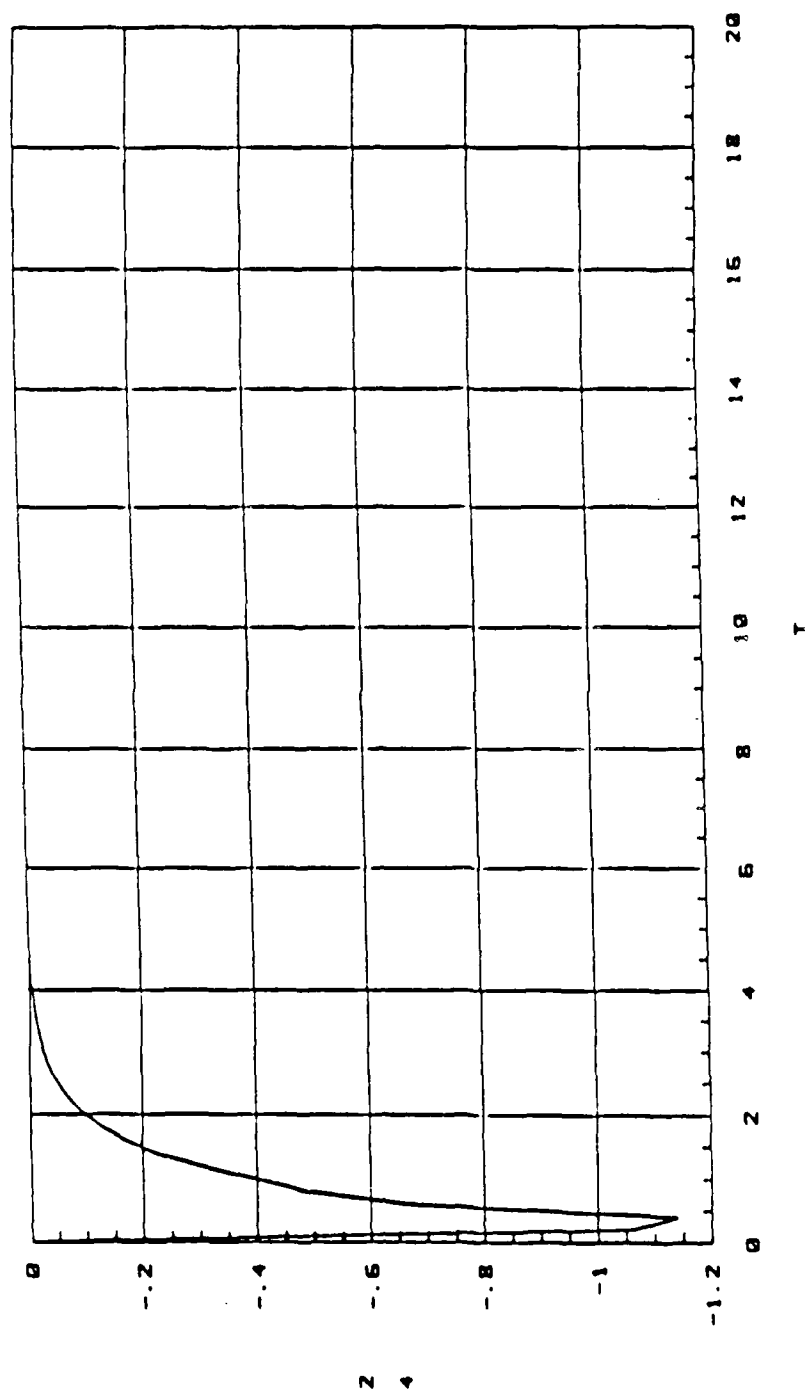


Figure 6

Impulse response of plant $1/S$
Based on experimental transfer function data

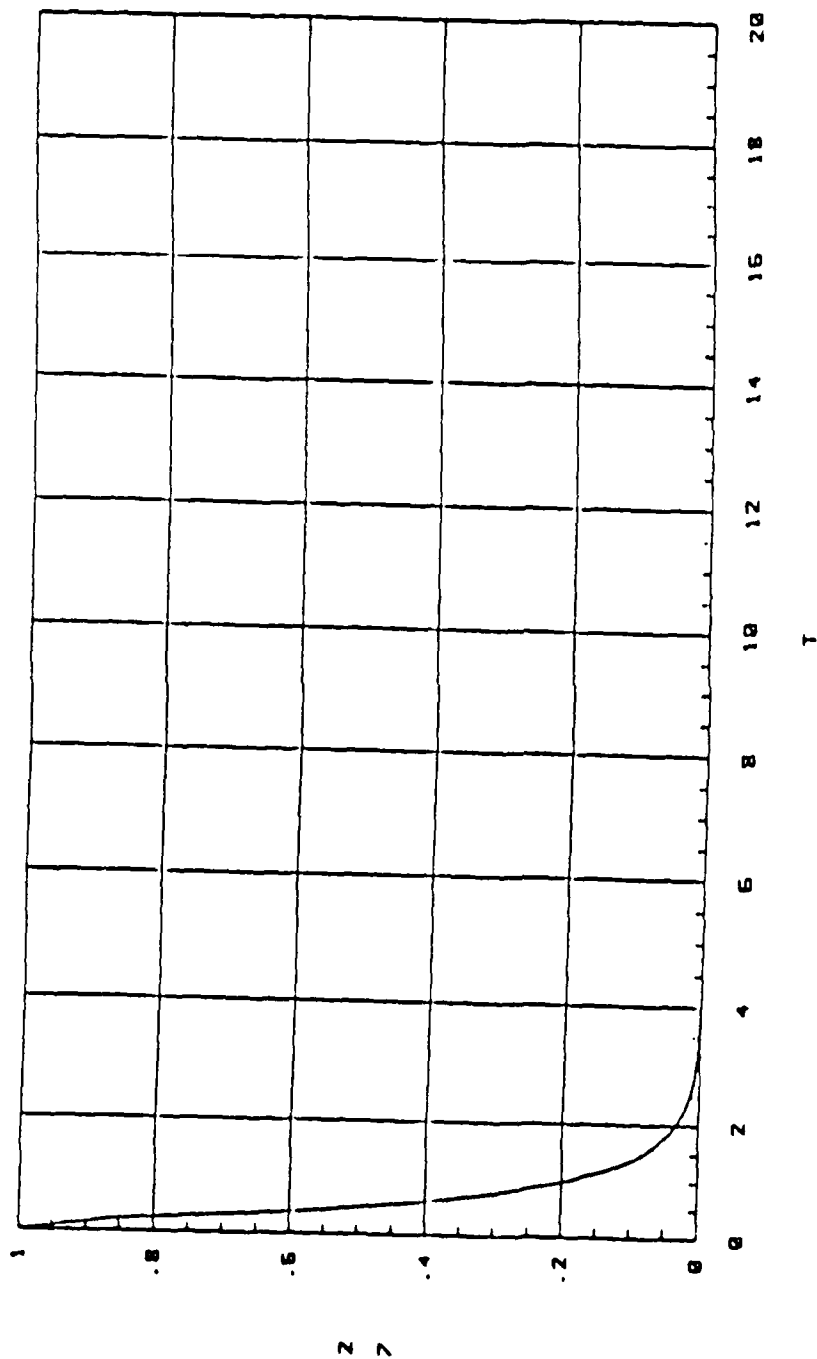


Figure 7
 Impulse response of plant 1/S loop 1
 Based on experimental transfer function data

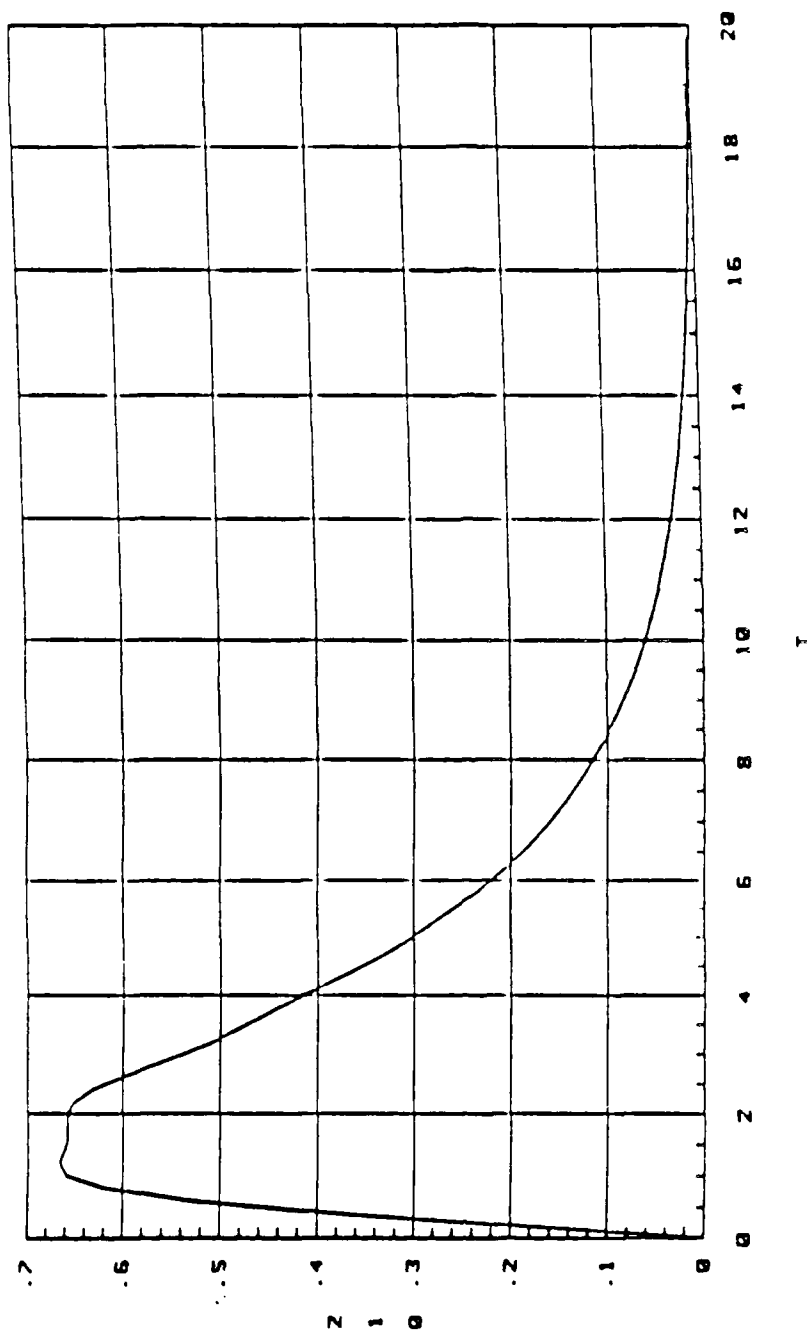


Figure 8
 Impulse response of plant $1/S'$ loop S
 Based on experimental transfer function data

1987 USAF-UES SUMMER FACULTY RESEARCH PROGRAM/
GRADUATE STUDENT SUMMER SUPPORT PROGRAM

Sponsored by the
AIR FORCE OFFICE OF SCIENTIFIC RESEARCH
Conducted by the
Universal Energy Systems, Inc.
FINAL REPORT

Examination of the Point Spread Function
in the RETINAL THERMAL MODEL

Prepared by:	Mary L. Morton-Gibson
Academic Rank:	Associate Professor
Department and University:	Department of Chemistry/Physics/Geosciences Lock Haven University of Pennsylvania
Research Location:	USAF School of Aerospace Medicine/RZV Brooks Air Force Base, TX
USAF Researchers:	Lt. Col. Robert M. Cartledge Dr. Ralph G. Allen
Date:	July 31, 1987
Contract No:	F49620-85-C-0013

Examination of the Point Spread Function
in the RETINAL THERMAL MODEL

by

Mary L. Morton-Gibson

ABSTRACT

The RETINAL THERMAL MODEL was originally developed for the Air Force in the early 1970's. It was designed to be used to predict retinal damage due to LASER assault. In the summer of 1986, the model was examined extensively. The basic equations and assumptions used in developing the model, the values of the constants used and the method of solution were determined (Morton-Gibson, 1986). At that time a number of recommendations were made for changes to the model. Two of those recommendations are addressed in this report.

1) Recently a limited set of experimental threshold data for multiple pulses became available (Zulich, unpublished results). The threshold prediction of the model was compared to those data. The model predictions and the experimental data show the same general form but the model predictions are consistently slightly lower than the experimental data.

2) The RETINAL THERMAL MODEL predicts an eccentric retinal irradiance profile for both uniform and Gaussian corneal profiles. The summation of the images of each of the points that constitute the incident beam should produce an approximately bell-shaped profile. A recently developed point-spread function was therefore examined. Polhamus, et al (1986) used double precision and a Gaussian quadrature scheme to perform the numerical integration. Their retinal profiles for a uniform incident beam do not show the off-center peak shown by the RETINAL THERMAL MODEL. Since their numerical solution appears to solve at least some of the problems inherent in the original model, that solution was incorporated into the RETINAL THERMAL MODEL.

ACKNOWLEDGEMENTS

I would like to express my appreciation to the Air Force School of Aerospace Medicine, the Air Force Office of Scientific Research, and Universal Energy Systems, Inc. for sponsoring my continued research at Brooks Air Force Base. I am particularly thankful for those who were responsible for providing a research opportunity that so closely matches both my experience and interests.

The professional and the support staff of the USAFSAM LASER Lab again made me feel welcome. The guidance of Lieutenant Colonel Robert Cartledge and Dr. Ralph Allen is very much appreciated. Stimulating discussions with Major Frank Cheney, Mr. Jack Labo and Captain Elmar Schmeisser contributed greatly to my work.

ACKNOWLEDGEMENTS

I would like to express my appreciation to the Air Force School of Aerospace Medicine, the Air Force Office of Scientific Research, and Universal Energy Systems, Inc. for sponsoring my continued research at Brooks Air Force Base. I am particularly thankful for those who were responsible for providing a research opportunity that so closely matches both my experience and interests.

The professional and the support staff of the USAFSAM LASER Lab again made me feel welcome. The guidance of Lieutenant Colonel Robert Cartledge and Dr. Ralph Allen is very much appreciated. Stimulating discussions with Major Frank Cheney, Mr. Jack Labo and Captain Elmar Schmeisser contributed greatly to my work.

I. INTRODUCTION

My formal educational background includes a Bachelor of Science in Mechanical Engineering and a Doctor of Philosophy in Physiology and Biophysics with a minor in Engineering, both from the University of Kentucky, Lexington, KY. Following the Ph.D., I was a post-doctoral trainee for three years in the Laboratory of Neurophysiology, University of Wisconsin-Madison. In addition, I also took graduate level courses in Mechanical Engineering and Gross Anatomy at the University of Wisconsin-Madison.

After the post-doctoral training I did neurophysiological research in the Departments of Ophthalmology and Neurophysiology and taught in the Department of Mechanical Engineering at the University of Wisconsin-Madison. Later I taught in the Department of Physics at The Citadel, The Military College of South Carolina, before moving to my present position. The results of the neurophysiological experiments were used to develop models of basilar membrane motion and neural coding in the visual and auditory systems. Most of my teaching responsibilities have been in mechanics and the thermal sciences. In particular, I taught the use of finite difference methods in the solution of both steady state and transient two and three dimensional thermal problems.

The unique combination of physiological, heat transfer and computer knowledge and experience led the USAFSAM LASER Laboratory to invite me to participate in the evaluation and revision of the RETINAL THERMAL MODEL.

II. OBJECTIVES OF THE RESEARCH EFFORT

The RETINAL THERMAL MODEL was originally developed for the Air Force in the early 1970's. It was designed to be used to predict retinal damage due to LASER assault. Since then considerable experimental data have been reported and new numerical analysis techniques have been developed. Until recently (Morton-Gibson, 1986) no changes had been made to the model to take advantage of these new findings.

Initially two goals were set for this project:

- 1) To compare the damage threshold predictions of the model with experimentally determined multiple-pulse damage thresholds. These comparisons should indicate areas of the model that require closer scrutiny.
- 2) To examine the point-spread function used in the model and to compare it to more recent formulations (Polhamus, et al, 1986).

III. BACKGROUND

In the 1970's a computer model to predict thermal injury to the eye following LASER exposure was developed under a United States Air Force contract (Takata, et al, 1974, Mertz, et al, 1976). Due to renewed interest the program was converted to run interactively in 1985. Unfortunately, no adequate documentation existed outlining the basic assumptions in the model, the values and meaning of the multitude of variables or even precisely what the model was designed to do. Furthermore, while attempting to predict eye temperature following multiple LASER assaults, Zuclich and his

colleagues (unpublished data) found significant errors in the predictions. There were also indications of discrepancies in the retinal irradiance profile (R. G. Allen, private communication). In the summer of 1986, the model was examined extensively. The basic equations and assumptions used in developing the model, the values of the constants used and the method of solution were determined (Morton-Gibson, 1986). The sources of some errors were identified and interim solutions implemented. At that time a number of recommendations were made for changes to the model. The recommended changes were of 3 types:

- 1) Changes in the way the user is required to interact with the computer. These revisions are entirely of a programming nature and do not require knowledge of the scientific basis of the model. They could best be implemented by a computer programmer not a scientist and will not be discussed further.

- 2) Examination of the modeling and solution techniques used and comparison with experimental results that have been published in the interim.

- 3) Expansion of the model to include additional LASER profiles.

The objectives for this research effort are a part of the type 2 recommendations.

IV. COMPARISON OF EXPERIMENTAL DATA AND MODEL PREDICTIONS

In order to be considered an accurate representation a model must be able to predict experimental results. For example, the RETINAL THERMAL

MODEL predictions should include, among other things: retinal irradiance, eye temperature distribution, retinal damage and threshold for damage. Accurate predictions support the validity of a model. On the other hand, inaccurate predictions indicate areas in which a model should be revised. To continue to be useful, a model must be periodically updated as new experimental evidence becomes available or new numerical solution techniques are developed.

The RETINAL THERMAL MODEL has been used in the past to make predictions of damage threshold for single pulses. Recently a limited set of experimental threshold data for multiple pulses became available (Zuclich, unpublished results). The threshold prediction of the model was compared to those experimental data. The parameter chosen for the comparison was the ratio of the threshold for one pulse to the threshold for multiple pulses as a function of the number of pulses. The stimulus parameters were: 647.1 nm wavelength, 100 msec pulses presented at the rate of 6.25 Hz. The beam profile was gaussian with a radius of 0.1cm at the cornea (width defined at the $1/e^2$ point). The experimental animals were rhesus monkeys. Experimental threshold was defined as the ED50/pulse for a minimal visible lesion. For the model predictions threshold was defined as the power required to produce a lesion of approximately 30 micrometers radius. Data for 3 experimental and 6 model predictions are shown in Table I. The same data are displayed graphically in Figure I.

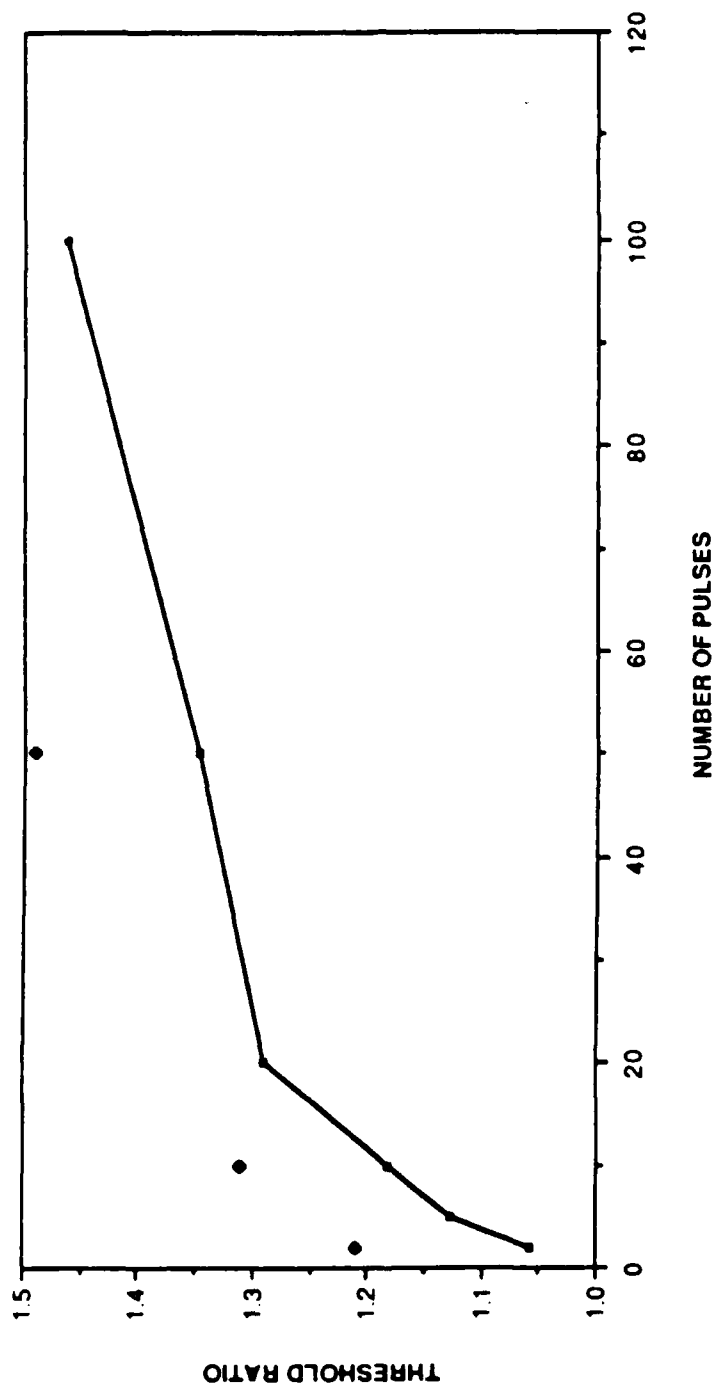


Figure 1: Ratio of threshold for one pulse to threshold for multiple pulses as a function of number of pulses. Comparison of experimental threshold (rhesus monkeys) to predicted threshold.

TABLE I. Ratio of single pulse threshold to multiple pulse threshold.

Comparison of model predictions with experimental data as a function of number of pulses.

<u>Single pulse threshold</u> <u>Multiple pulse threshold</u>		
# Pulses	Model Prediction	Experimental
2	1.0580	1.21
5	1.1260	
10	1.1826	1.31
20	1.2900	
50	1.3480	1.49
100	1.4627	

The model predictions and the experimental data show the same general form but the model predictions are consistently slightly lower than the experimental data. These results indicate that a retinal lesion would be produced before the level at which the model predicts damage. For example, the model predicts that two pulses must each have 95% of the single pulse power in order to produce a lesion. However, the experimental data indicate that a lesion will occur when each of the two pulses are at the 83% power level. The inaccurate predictions of the model could be the result of errors in:

- 1) The determination of the retinal irradiance.
- 2) The computation of ocular temperature as a function of time.

3) The way in which the ocular temperature is determined for multiple pulse exposures. The assumption made in the model is that the system is linear.

4) The assessment of damage as a function of the time-temperature history of the eye.

It is possible, of course, that more than one of these factors is involved. Furthermore, without additional comparisons, it is not possible to know which area of the model should be examined first. However, there had been some undocumented indications (R. G. Allen, private communication) that the retinal irradiance profile was inaccurate. Because of those indications the determination of the retinal irradiance profile was examined.

VI. RETINAL IRRADIANCE PROFILE: THEORETICAL

A point object will project a light distribution on the retina that is approximately bell-shaped in cross section. That distribution is termed the point-spread function (Westheimer, 1986). Conceptually, any object can be considered to consist of a collection of points. The retinal image of a LASER beam then consists of the superposition of the images of each of the points that make up the incident beam.

Expressed mathematically, the Fourier transform of the retinal image, $I(f_x, f_y)$, is the product of the Fourier transform of the incident beam, $O(f_x, f_y)$ and the Fourier transform of the impulse response (point-spread function), $H(f_x, f_y)$ of the eye.

$$I(f_x, f_y) = H(f_x, f_y) \cdot O(f_x, f_y) \quad (1)$$

The retinal image distribution can then be determined by taking the inverse transform of $I(f_x, f_y)$.

In the RETINAL THERMAL MODEL the normalized retinal irradiance is calculated using a cylindrically symmetric form of the Fresnel relation:

$$\frac{H(r)}{H(0)} = \left| \frac{1}{\lambda \cdot f'} \int_0^a \sqrt{P_p(\rho)} \cdot J_0 \left(\frac{2\pi r \cdot \rho}{\lambda \cdot f'} \right) \cdot F_1(\rho) \cdot F_2(\rho) \cdot \rho \, d\rho \right|^2 \quad (2)$$

Definitions of the parameters can be found in Table II.

The functions $F_1(\rho)$ and $F_2(\rho)$ account for chromatic and geometric defocusing and spherical aberration respectively. They are each a complex function with a magnitude of unity given by:

$$F_1(\rho) = \exp(i C_0 \rho^2) \quad (3)$$

$$F_2(\rho) = \exp(i C_2 \rho^4) \quad (4)$$

The constants are given by:

$$C_0 = \frac{2\pi n}{\lambda a^2} \left[-f' - \Delta z (1 - \cos \alpha) + (f'^2 - \Delta z^2 \sin^2 \alpha)^{\frac{1}{2}} \right] \quad (5)$$

$$C_2 = -3 \cdot 10^6 / \lambda \quad (6)$$

TABLE II. Nomenclature

λ	= wavelength
$P_p(\rho)$	= profile at the pupil plane
a	= pupil radius
f'	= $f_0 - p$
f_0	= second principal focal length at a reference wavelength, λ_0
p	= distance of pupil from second principal plane
ρ	= radial distance in the pupil plane
r	= radial distance in the retinal plane
J_0	= zero order Bessel function of the first kind
α	= angle between the refracted beam at the cornea and axis of the eye
n	= index of refraction at wavelength λ
z_0	= distance of pupil from waist of laser beam
f	= focal length at LASER wavelength
n_0	= index of refraction at reference wavelength, λ_0

The parameters α , Δz and f are related as follows:

$$f = \frac{f_o n(n_o - 1)}{n_o(n - 1)} \quad (7)$$

$$\tan \alpha = \frac{a}{(f' = \Delta z)} \quad (8)$$

$$\Delta z = \frac{n z_o (f/f_o)}{n(z_o/f_o) - (f/f_o)} - f_o \quad (9)$$

A derivation and a complete description of the variables is available (Takata, et al, 1974).

VII. RETINAL IRRADIANCE PROFILE: MODEL RESULTS

The RETINAL THERMAL MODEL will predict the normalized retinal irradiance profile for three different incident profiles:

- 1) Uniform at the cornea.
- 2) Gaussian distribution at the cornea with the beam radius specified at the $1/e^2$ point.
- 3) Any arbitrary corneal profile. This profile allows the investigator to simulate real-life LASER beams whose profile differs from the theoretical.

The predicted retinal irradiance was examined for a number of different beam radii and pupil diameters for each of the first two profiles. One example of the predicted retinal profile is shown in Figure 2. The wavelength was 647.1 nm. The beam was uniform with a radius of 1 cm.

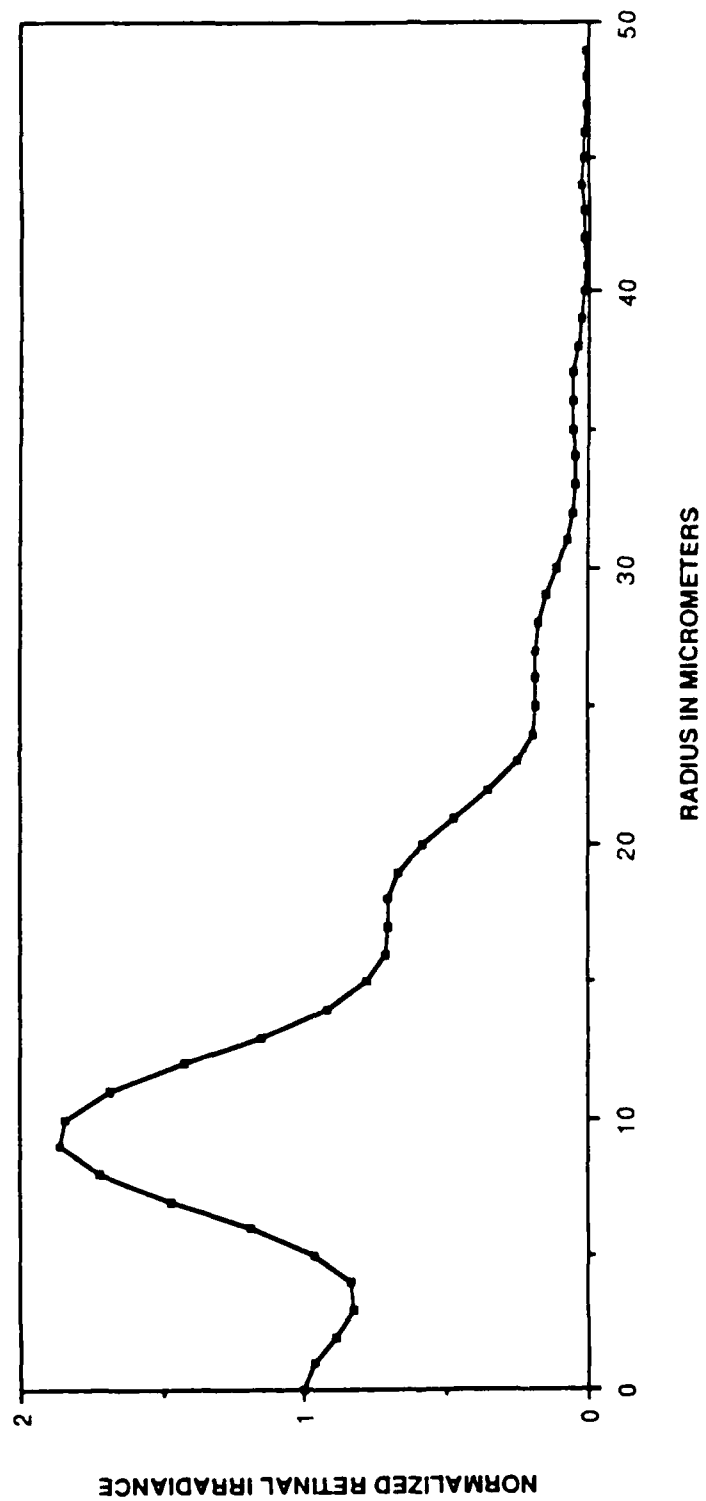


Figure 11: Normalized retinal irradiance used in the RETINAL THERMAL MODEL. Uniform beam, 647.1 nm wavelength.

This eccentric pattern is typical of the retinal irradiance profile predicted by the RETINAL THERMAL MODEL for both uniform and Gaussian corneal profiles. Recall that the expected profile is the superposition of a number of roughly bell-shaped profiles. That summation should produce an approximately bell-shaped profile. The low amplitude oscillations are caused by the diffraction (Goodman, 1968) associated with the circular aperture (the pupil). Because of their low amplitude they are of little consequence particularly when compared to the large unexpected off-center peak.

VIII. DISCUSSION

Irregularities in this model have been reported previously. In the Final Technical Report following the development of the model, Takata, et al (1974) reported discrepancies in lesion size predicted by the model when compared to experimental data, for small lesions. They were unable to identify the source of the discrepancy.

More recently, Polhamus, et al (1986) pointed out that the defocusing function $F_1(\rho)$, is highly oscillatory. The constant C_0 is the summation of two small negative quantities and one small positive quantity. To obtain a more accurate solution, they used double precision and a Gaussian quadrature scheme to perform the numerical integration. In addition, they made a slight revision to Equation 5. There was still a slight discrepancy between calculated and measured image size, which they attributed to measurement bias.

The retinal profiles determined by Polhamus and his colleagues do not show the off-center peak depicted in Figure II. Their numerical solution appears to solve at least some of the problems inherent in the original model. Therefore, that numerical solution for the retinal profile of a uniform beam was incorporated into the RETINAL THERMAL MODEL.

Time did not permit a systematic investigation of the retinal irradiance using the revised solution.

IX. RECOMMENDATIONS

A mathematical model of the point-spread function for a uniform beam has been developed (Polhamus, et al, 1986). That function has been added to the RETINAL THERMAL MODEL. The predicted retinal profile should be examined

Point-spread functions should be developed for Gaussian and irregular profiles and incorporated into the model. The Gaussian profile will be particularly useful for comparisons to laboratory data. The irregular profile will allow investigators to simulate real-life LASER beams whose profile differs from the theoretical.

Model predictions made with the revised point-spread functions should then be compared to the available experimental data. In addition to the data in Figure I, other experimental LASER exposure data is available (Stuck, et al, 1978).

If the model predictions still do not agree with the experimental data, other sections of the model should be examined. The assessment of damage as a function of the time-temperature history of the eye relies on experimental burn data for skin (Takata, 1974). That section should be examined next, with particular attention to any experimental data that has become available more recently.

The last recommendation is that the assumption of linearity in the addition of the effects of multiple pulses be examined.

REFERENCES

Goodman, J. W., "Introduction to Fourier Optics", p64, McGraw-Hill, NY, 1968.

Mertz, A. R., B. R. Anderson, E. L. Bell and D. E. Egbert, "Retinal Thermal Model of LASER-Induced Eye Damage: Computer Program Operator's Manual", Final Report for USAF School of Aerospace Medicine, Brooks AFB, TX, Report SAM-TR-76-33, 1976.

Morton-Gibson, M. L., "Evaluation of a Computer Program to Predict Thermal Retinal Damage from LASER Radiation", Final Report for Summer Faculty Research Program sponsored by Air Force Office of Scientific Research and Universal Energy Systems, Inc. Contract No. F49620-85-C-0013, 1986.

Polhamus, G. D., D. K. Cahoon and R. G. Allen, "Measurement and Prediction of the Point Spread Function in the Rhesus Monkey", Submitted for Publication, 1986.

Stuck, B. E., D. J. Lund and E. S. Beatrice, "Repetitive Pulse LASER data and Permissible Exposure Limits", Institute Report 58, Division of Non-Ionizing Radiation, Letterman Army Institute of Research, Presidio of San Francisco, CA, 94129, 1978.

Takata, N. A., L. Goldfinch, J. K. Hinds, L. P. Kuan, N. Thomopoulos and A. Weigandt, "Thermal Model of LASER-Induced Eye Damage", Final Report for USAF School of Aerospace Medicine, Brooks, AFB, TX, Report IITRI-J-TR-74-6324, contract F41609-74-C-0005, IIT Research Institute, Chicago, IL, 1974.

Westheimer, G., "The Eye as an Optical Instrument", Chapter 4 of Handbook of Perception and Human Performance, V1, Sensory Processes and Perception, K. R. Boff, L. Kaufman and J. P. Thomas, editors, New York, NY, John Wiley and Sons, 1986.

1986 USAF-UES FACULTY RESEARCH PROGRAM
GRADUATE STUDENT SUMMER SUPPORT PROGRAM

Sponsored by the
Universal Energy Systems, Inc.

FINAL REPORT

Prepared by:	Lena Wright Myers, Ph.D.
Academic Rank:	Professor
Department and	Department of Sociology
University:	Jackson State University
Research Location:	DEOMI/DE Patrick AFB, FL 32925
USAF Researcher:	Lt Col Mickey R. Dansby
Date:	23 July 87
Contract No:	F49620-85-C-0013

DEVELOPING MODELS FOR EMPIRICAL RESEARCH ON WOMEN IN THE MILITARY

by

Lena Wright Myers, Ph.D.

ABSTRACT

The primary objective of the research effort was to develop an empirical research design to examine role performance of women in the military. The researcher assumed that, theoretically, self-investment in work leads to commitment to the occupational role based on the relevance of work to self-esteem. The major variables identified for follow-on research were occupational and organizational commitments and self-esteem. The initial process by which the objectives for this project were achieved involved an in-depth search of literature with a similar focus. The process added impetus to the need for developing the research model titled: Occupational and Organizational Commitments of Women in the Military.

ACKNOWLEDGMENTS

The Researcher expresses her appreciation to the Air Force Systems Command, the Air Force Office of Scientific Research, and Universal Energy Systems for the sponsorship of this research effort.

She also expresses her gratefulness to the Commandant, Colonel E. E. Wiggins, and the Defense Equal Opportunity Management Institute (DEOMI) personnel for the professional experience.

She is expecially grateful to her USAF Research Colleague, Lieutenant Colonel Mickey R. Dansby, for the very professional leadership he provided to her overall research pursuit.

1. INTRODUCTION

Concerns and fears regarding the impact of increased utilization of women on the readiness and effectiveness of the Armed Forces have been voiced and these stimulated research on numerous issues. For example,

Can women adjust to military roles and males to the presence of women in these roles?

Do women perform well in all types of military roles?
and

Do performance levels of women affect military operations? (DeFleur and Warner, 1984)

It would be very unethical to attempt to concretely respond to those very important questions through personal generalizations. Those questions suggest the need for empirical research in an exploratory study to identify interesting relationships between certain variables relative to women in the military.

The Summer Faculty Researcher is not devoid of having research experiences with the military. During the summer of 1984, she developed a model for research on "Military Family Stress and Dual Career Families," with the School of Aerospace Medicine at Brooks Air Force Base, Texas (Myers, 1984). On July 31, 1985, she successfully completed research on "Military Family Stress and Job Performance" (Myers, 1985). Those experiences occurred during a period of eighteen years, to date, of research on civilian women with a primary focus on racism and sexism,

simultaneously; almost all of this research resulted in numerous publications. Having such a profound concern for disseminating information based on empirical data in addition to social psychological wisdom, she continued her research pursuit on "Occupational Role Performance Among Women in the Military." The researcher's prior knowledge that very little empirical research existed on such an issue compelled her to do an in-depth search of literature. This initial approach was necessary in order to clearly define the research problem to fulfill her proposed objectives. After having exhausted the literature, the effort of identifying certain measurable and testable variables for relationships between each was done.

After several sessions of open dialogue about the literature on the research prospectus with her Effort Focal Point, Lt Col Dansby, occupational role performance was confirmed as a primary variable to be operationalized. During a brief period of "self-brainstorming," the researcher included an added variable of organizational commitment.

II. OBJECTIVES OF THE RESEARCH EFFORT

An in-depth search of existing literature relative to the researcher's interest on women in the military was accomplished and complemented the prior assumed need for the proposed research objectives. They included:

1. To develop a strong quantitative research design relative to role performance of women in the armed forces;
2. To put Objective 1 into narrative form for implementation through the scientific method of social research; and
3. To produce a research model that can be used in explaining relationships between various social-policy issues relative to defense equal opportunity management.

III. THE APPROACHES TAKEN

The major approach in effecting the objectives was to carefully examine existing literature relative to the research problem. The first findings were from literature of a very general nature. They were mainly an historical overview of women in the military which suggested much redundancy. The researcher then secured a University Computer Search of the Literature that resulted in a limited number of sources available. After doing an annotative review of those sources, major variables were identified. Those were occupational role performance, organizational commitment, and level of self-esteem. A chronology of the approaches is given as follows:

1. Began review of literature from available sources (on base);
2. Secured University Computer Search of Literature;

3. Did annotated review of sources from the search, many of which confirmed the need for this research;
4. Identified variables to be tested;
5. Submitted first draft of research design to Effort Focal Point, June 29, 1987 (Objective II), and
6. Developed model to fit research design (Objective III).

IV. RELATIVE RESEARCH

Even though it was limited to men and women cadets at West Point, a study, in an attempt to define roles for women in the military, was furnished by Priest and Prince (1979). The primary objective of the symposium at which the research findings were presented was to raise questions about the role of women in the military "now that the traditional role has been abolished." The studies used by the authors focused on the performance of women in both enlisted and professional roles from all branches of the military. They suggested that it is not easy to satisfactorily define roles for women in the military, since using women in direct combat had been prohibited. Therefore, they provided a rational systems design clearly specifying the jobs to be held, followed by an analysis of necessary skills and training for effective job performance. Their research focused on performance correlates of perceptions of discriminatory treatment, satisfaction, and self-concept. The theoretical base was that one's self-concept is of primary importance in

predicting the level at which one adapts to a stressful environment, such as the first year at West Point. A second theoretical concern was that places and expectations for men and women relative to the life cycle events would be potentially different. The sample for the analysis included both men and women, 1,485 and 1,469 from classes of 1980 and 1981, respectively. The research report's focus was specifically on performance correlates of perceptions of discriminatory treatment, satisfaction, and self-concept. However, performance in training and academics, and leadership that led to attrition, were the subjects of several current theses. The research instruments used included: the Tennessee Self-Concept Scale (TSCS), Spence Attitude Toward Women Scale (AWS), a scale to measure rigidity vs. flexibility in one's approach to equality of treatment, measures of the subjective probability of remaining in the military, Military Career Commitment Gradient (MCCOG), the tactical officer (TAC) rating of "performance" and "potential," and the chain of command leadership (COC) scale.

The results of this study showed that although women cadets perform moderately well in cadet roles, certain aspects of their adjustment followed a different pattern of correlates than for men. The women's perceptions of discriminatory treatment were different from those of men. There was no difference in the women's leadership ratings pattern of correlates. However, when

the two were put together, women with the same performance level as men were given higher leadership ratings than men. The self-concept data showed a similar pattern of changes for both men and women. A general conclusion was, though men and women perform similar roles, they adapt in different ways to those roles.

V. LITERATURE AND RESEARCH COMPLEMENTING RESEARCH PROBLEM--
IN SUMMARY

Military service is a form of obligation citizens are supposed to owe their country on the grounds that the defense of citizens cannot occur unless they join in that defense. In past years, the government assumed the right to draft people into the service. However, traditionally women were excluded from the draft when it was in effect. Historically, in America, women had been barred from military service except in auxiliary capacities. Except for a few famous women such as "Molly Pitcher" who was a revolutionary fighter, women only participated in military action in the gender-prescribed roles of nurses, cooks, cleaners, etc. By World War I, an auxiliary corps of nurses were included. But, they were not at first given formal military status. Then came World War II where a few women served as pilots, but they were not given full military status and privileges either. In 1948, the United States Congress put a two percent ceiling on women in the military. Following the end of the draft in 1972, defense authorities were afraid there would not be enough to fill the

armed services. Thus, the ceiling was raised, and women were admitted to military academies. In 1980 and during the Carter administration, Congress reinstituted the draft registration, which was to include women. However, this provision met substantial resistance and was abandoned. As one writer puts it:

Because of the present volunteer nature of the U.S. Military Service, a decrease in the number of available males due to the lower birth rate, and competition from the civilian job market, the Armed Forces have had a difficult time filling the quotas with men. (Basow, 1986)

She states, "Thus they have been taking in more females but discriminatory regulations and practices abound."

Some writers even suggest that women in the military are often faced with an environment that is overtly hostile to them (Rustad, 1982; Shroeder, 1982; Yoder, 1984; and Cheatham, 1984).

Some of the related literature emphasizes the impact of women on the military, while other writers focus on the effects of the military on women. It is suggested that we must go beyond the issue of the former and concentrate on the latter. For a long time, supporters of women's rights have argued that military policies have not afforded women the same opportunities and privileges as other social institutions, and have taken an official monopoly on research data in support of their arguments (Binkin and Bach, 1977). "We need to re-examine this information and review recent research to provide insights into the effects

of military service on women" (DeFleur and Warner, 1984).

Greene and Wilson (1981) did a study to examine the effects of sex integration in the military on the attitudes and performance of male and female soldiers during basic training. A primary objective of their study seemed to have been to examine the consequences of female involvement in roles that were traditionally male. From a sample of 800 men and women, their findings revealed important differences among the integration alternatives. Therefore, to effect one mode of integration over another would affect the attitudes and performance of military personnel.

In June, 1977, a field experiment sponsored by the U. S. Army Research Institute for the Behavioral and Social Sciences was pursued. Data were collected for the MAX WAC project with the objective of assessing the effects on field performance of assigning women to non-combat U.S. Army companies. The research was undertaken with the concept of a gender-free role allocation as applied to soldiers in the Army. The general implication of the results is that gender is not a necessary criterion for the staffing of positions within combat-support and combat service-support companies in the Army (Schreiber and Woelfel, 1979).

Another contribution to the sociology of military life provided an historical overview of the association of women to the military and to war (Rustad, 1982). This study examines the

lives of women and of the men with whom they worked. The research, having taken place at an American military base in West Germany, first portrayed the community in which it occurred. It resulted in the recommendations of an increase in the number, improved quality, and better military effectiveness of both women and men, in addition to gender integration of the armed forces.

During a period of three years and nine months, data were secured on leadership and job satisfaction/career commitment of Air Force Personnel (Niebuhr and Dansby, 1986). Using the Air Force's Organizational Assessment Package (OAP) data base of almost 300,000 survey responses, the study reported a positive correlation between leadership behavior, job satisfaction, and career commitment intentions. Positive correlations were stronger for supportive leadership behaviors than for structured leadership behaviors.

It is stated that in all branches of the service, as in civilian life, women are restricted to the less prestigious, lower paying jobs. It is estimated that approximately 83% of enlisted women are in the four lowest pay grades, as compared to 68% of the men (Basow, 1986). There are even certain stereotypical explanations made about women who have assumed positions. They include:

- (1) Minorities and women who are given job opportunities are not as qualified as their white male counterparts.

(2) That these positions are gotten just to satisfy affirmative action requirements.

Conversely, minorities and women actively support affirmative action that will break the cycle of systematic discrimination they have experienced in the military (Hope, 1979).

According to one writer:

The study of women in the military is a valid and respected topic for research. It has roots in the social sciences and in the humanities. It has interest in the study of law. (Harrison, 1977)

He noted that recent academic interest in women in the military derived from the early 1970's when the Equal Rights Amendment gained momentum and women studies was accepted in academic institutions.

Although there are historical and descriptive accounts of female participation in the military, systematic empirical studies have been scarce, if not absent (Butler and Brewer, 1978).

VI. THEORETICAL PERSPECTIVE

Organizational and occupational commitments of persons in the military, either men or women, is a neglected area of study. The Summer Faculty Researcher's efforts during the past ten weeks have thoroughly confirmed the preceding statement, and have shown the need to develop a model for such research.

The model that she has developed proposes a study of the causes and consequences of the occupational and organizational commitments of a sample of women in the military. The theoretical perspective on occupational commitment to be used is "self-investment" in work (Faunce, 1975, 1982, 1984). Self-investment in work is defined as a commitment to the occupational role, based on the relevance of work to self-esteem. Research evidence indicates that occupational achievement is a major determinant of self-esteem to some people and has little effect upon the self-esteem of others. The researcher expects this variation to have an important impact on occupational role performance and organizational commitment. Figure 1 presents a graphic portrayal of the relationship between these variables and certain antecedent and outcome variables.

VII. RECOMMENDATION

The concept of employee commitment to organizations has received attention in the research literature recently as both managers and organizational analysts seek ways to increase employee retention and performance (Steers, 1977). Even though a number of studies have examined certain aspects of commitment, few studies have pursued empirical research on the concept. As a result of the limited amount of research, little information for guidance in model building is available. Therefore, the Summer Faculty Researcher has spent the past ten weeks developing such a model, and is strongly recommending that said research be

implemented in the future. Follow-on research from the model will be pursued in application for a mini-grant. The research model developed is consistent with and pertinent to this report.

RESEARCH MODEL

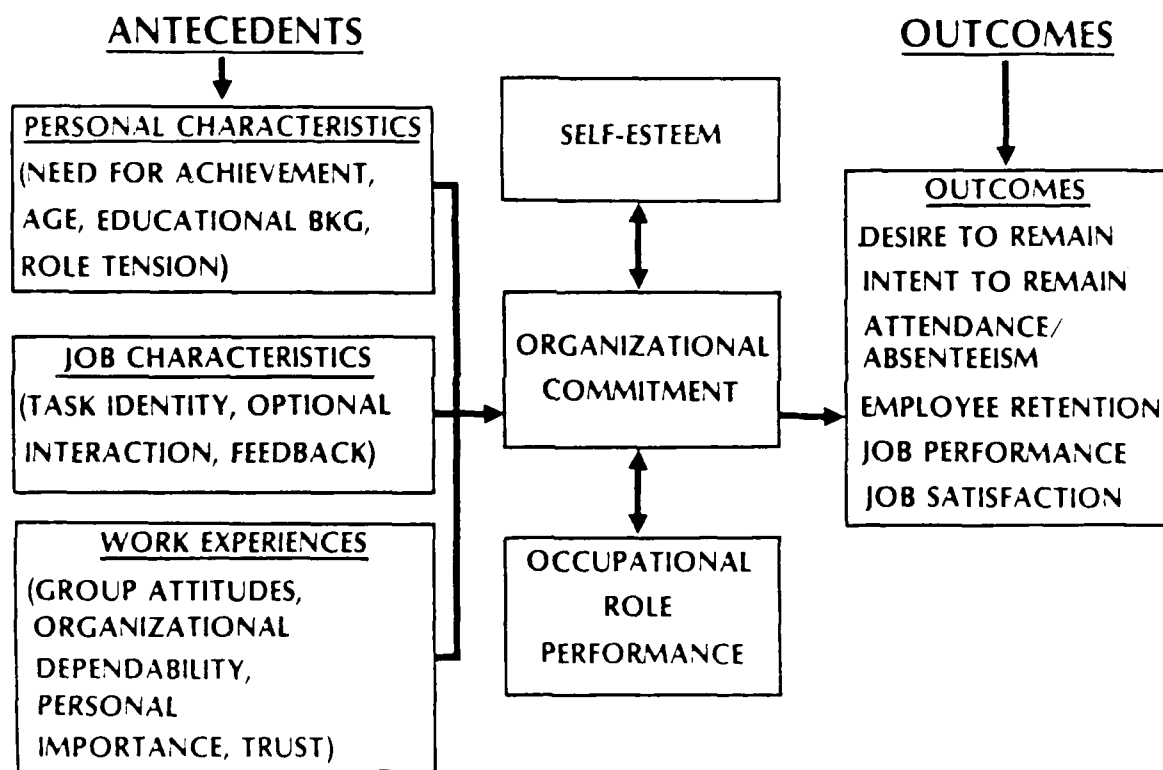


Figure 1. Research Model
(Initial focus, Indaco, Steers, 1977)

REFERENCES

Basow, Susan A., Gender Stereotypes: Traditions and Alternatives, Brook/Cole Publishing Company, Monterey, California: 1986, pp. 273-275.

Binkin, M., and S. J. Bach, Women and the Military (Washington, DC: The Brookings Institute, 1977).

Butler, J. S., and R. M. Brewer, "The Promotion of Enlisted Women in the Military: A Research Note," Armed Forces and Society, Vol. 4, No. 4 (August, 1978), pp. 679-688.

Cheatham, H. E., "Integration of Women into the U. S. Military," Sex Roles, Vol. 11, pp. 141-153.

DeFleur, L. E., and R. L. Warner, "The Impact of Military Service on Women's Status: A Neglected Area of Inquiry," in Nancy H. Loring, Women in the U. S. Armed Forces: Progress and Barriers in the 1980's, Inter-University Seminar on Armed Forces and Society, Chicago: 1984, pp. 1-13.

Faunce, W. A., Problems in Industrial Society, McGraw-Hill, New York: 1987, pp. 130-181.

_____, "The Relation of Status to Self-Esteem," Sociological Focus, Vol. 15, 1982, pp. 163-177.

Faunce, W. A., and R. Dubin, "Individual Investment in Working and Living," in The Quality of Working Life, Vol. 1, Free Press, New York: 1975, pp. 299-316.

Greene, B. D., and K. L. Wilson, "Women Warriors: Exploring the New Integration of Women into the Military," Journal of Political and Military Sociology, Vol. 9 (Fall), 1981, pp. 241-254.

Harrison, D. F., "Sources for the Study of Women in the Contemporary U. S. Military," (undated-direct quotation).

Hope, R. C., Racial Strife in the U. S. Military: Toward the Elimination of Discrimination, Praeger, New York: 1979.

Myers, Lena W., "Military Family Stress and Dual Career Families," Technical Report, United States Air Force Office of Scientific Research - SCREE, 1984, pp. 105-2--105-24.

_____, "Military Family Stress and Job Performance," Technical Report, United States Air Force Office of Scientific Research - SCREE, 1986.

_____, Black Women: Do They Cope Better?, Prentice-Hall, Inc., Englewood Cliffs, N. J.: 1980, pp. 19-23.

Niebuhr, R. E., and M. R. Dansby, "The Relationship Between Leadership and Job Satisfaction/Career Commitment of Air Force

Personnel," Psychology in the Department of Defense
(Proceedings), April, 1980, pp. 269-276.

Priest, R. F., and H. T. Prince, "Women at West Point: Their Performance and Adjustment," Report Number 79-0004, Office of the Director of Institutional Research, United States Military Academy, West Point, New York: 1979, pp. 1-28.

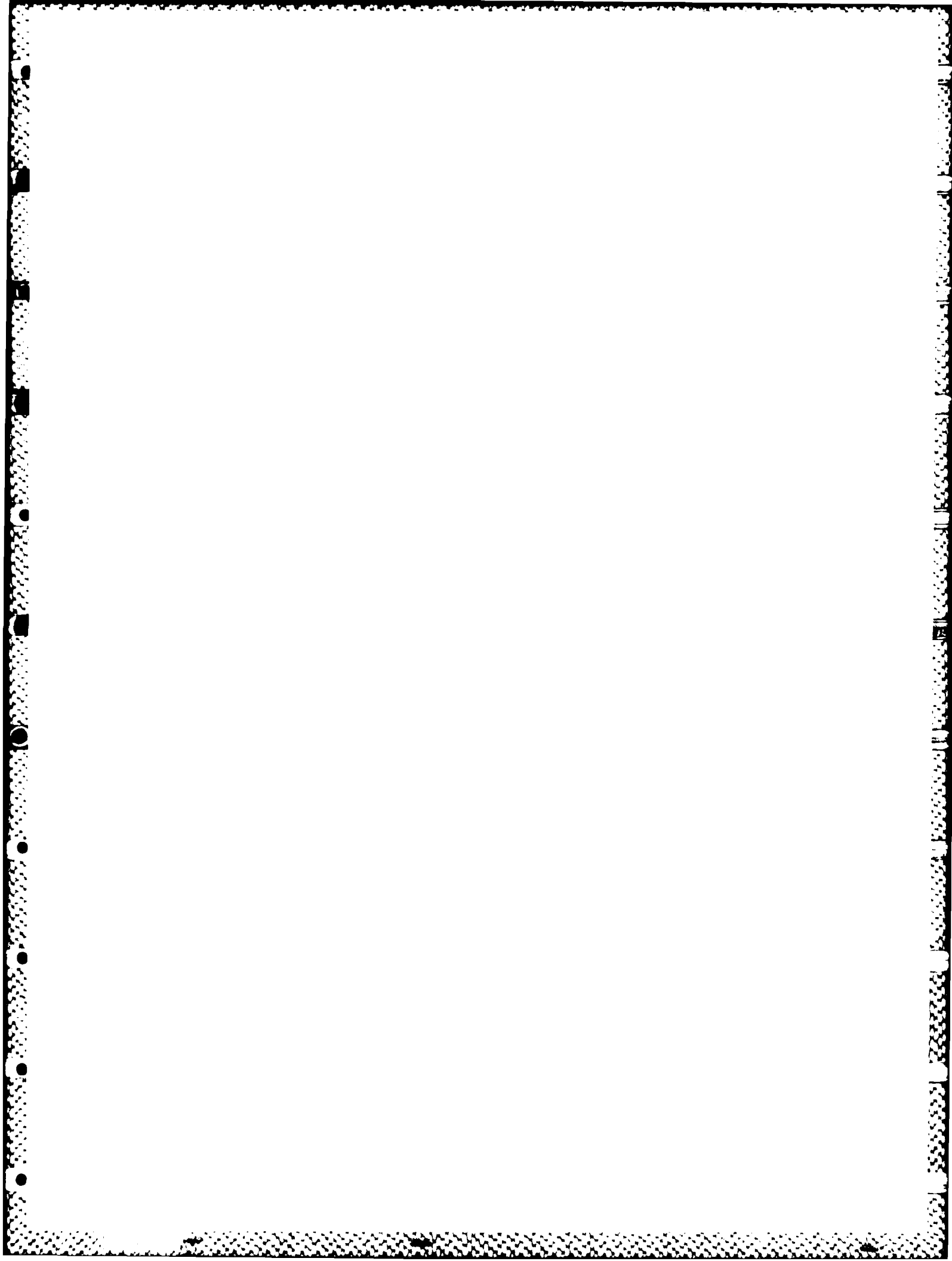
Rustad, M., Women in Khaki: The American Enlisted Woman, Praeger, New York: 1982.

Schreiber, E. M., and J. C. Woelfel, "Effects of Women on Group Performance in a Traditionally Male Occupation: The Case of U. S. Army," Journal of Political and Military Sociology, Vol. 7 (Spring), 1979, pp. 121-134.

Steers, R. M., "Antecedents and Outcomes of Organizational Commitments," Administrative Science Quarterly, Vol. 22, 1977, pp. 46-56.

Woelfel, J. C., "Women in the United States Army," Sex Roles, Vol. 7, No. 8, 1981, pp. 785-800.

Yoder, J. D., "Another Look at Women in the United States Army: A Comment on Woelfel's Article," Sex Roles, Vol. 9, pp. 219-234.



1987 USAF-UES SUMMER FACULTY RESEARCH PROGRAM/

GRADUATE STUDENT SUMMER SUPPORT PROGRAM

Sponsored by the

AIR FORCE OFFICE OF SCIENTIFIC RESEARCH

Conducted by the

Universal Energy Systems, Inc.

FINAL REPORT

MULTI-MODE SENSING IN AIR-TO-AIR MISSILES

Prepared by:	James Bert Nail, PhD.
Academic Rank:	Associate Professor
Department:	Electrical Engineering Department
University:	Mississippi State University
Research Location:	AFATL / ASR Eglin AFB, FL 32542-5434
USAF Researcher:	Dr. Steven F. Butler
Date:	10 Aug, 1987
Contract No:	F49620-85-C-0013

MULTI-MODE SENSING IN AIR-TO-AIR MISSILES

by

James Bert Nail

ABSTRACT

Multi-Mode guidance is the application of redundant sensors to improve missile specifications, enhance all-weather capability, and provide reliable operation despite countermeasures. The complexity of dual seekers can be self-defeating due to maintenance, reliability, and economics. This research attempts to define a sensor combination that is synergistic and feasible, then investigates the design constraints to extract specifications. The emphasis is on design for compatibility, reliability, and economy, mindful of the fact that most missiles are shot down by lack of funding. Recent advances in pyroelectric films are presented, and a simple pyroelectric sensor proposed.

ACKNOWLEDGEMENTS

I wish to thank the Air Force Systems Command and the Air Force Office of Scientific Research for sponsorship of this research, and Universal Energy Systems for able administration of the program. Thanks go also to Dr. Sam Lambert and Nell Ross for their special effort to introduce the summer researchers to the programs and people of Eglin Air Force Base.

The Armament Laboratory is to be commended for the capability and dedication of their personnel. It was my privilege to work with Dr. Steven F. Butler, who encouraged innovation and provided contacts, leads, and suggestions for exploration of any interesting avenue of research. Pat Coffield, Captain Larry Jones, Otto Martinez, Terry Sanks, Captain Chris Titus, and Rochelle Tyra were most helpful, volunteering their diverse expertise as they recognized my needs. Much of the educational aspect of my summer research is due to this group. They are a credit to their organization and profession.

Special thanks is due the contacts outside my immediate working group: Tom Noethan, who provided missile guidance and aerodynamics expertise; Robert Orgusaar, who brought me up-to-speed on piezo-film research; and "Mac" McCormick, who encouraged and helped perform initial steps toward a pyroelectric sensor.

I. INTRODUCTION

Multi-Mode refers to the inclusion of redundant sensors, primarily to improve accuracy and defeat the enemy countermeasures. There has been some scholarly work done on the topic, primarily dealing with Kalman Filtering aspects of accommodating the redundant measurements for maximum effect. Accordingly, I have chosen not to research in the same direction. My background encompasses the field of automatic control, and my specific interests include the sensing and hardware aspects of design. This "interface" area is a very challenging, but open, arena.

The sensors involved in air-to-air seekers are extremely sensitive, complicated, and thus expensive. Multi-mode guidance is a challenging topic, due to the difficulty of adding compatible sensing at reasonable cost.

II. OBJECTIVES

Previous Multi-Mode guidance research provided only cursory examination of the required sensors. The original objective of this research was to investigate techniques for weighting sensor technologies. This objective was revised to determination of feasible technology combinations for multi-mode guidance. This change resulted from concern over the cost / return for multiple sensor systems.

An added objective was a study of the application of pyroelectric film as a secondary sensor.

III. AIR-TO-AIR MISSILE PERFORMANCE ATTRIBUTES

The positive performance attributes of a missile are considered to be accuracy, speed, range, maneuverability, and payload. Negative attributes are weight, complexity, required support, detectability, and countermeasureability. Each attribute will be discussed comparatively, and a combined comparison provided in Figure 3.

ACCURACY Both RADAR and IR missiles are reasonably accurate, with single shot kill percentages (SSKP) of approximately 60%. Approximately equal ratios of the two seeker types are listed in Appendix A. Indeed, the philosophy of the Soviet Union is to fire one of each.⁶ The accuracy of an IR missile is maximum in a tail-chase trajectory, whereas the RADAR has the advantage head-on, and actually has more difficulty from "glints" in a tail-chase. Weather affects the two differently. RADAR is affected by fog, clouds, and rain with increasing severity, but remains operable.¹² IR is ill-suited to fog and clouds, but is less affected by rain.⁸ The analysis of elements affecting accuracy is strongly related to maneuverability, to be discussed later. For now, refer to Figure 1, which I believe to be a reasonably accurate portrayal.

Field-of-view bloom occurs at end-game, when the seeker sees nothing but target. A simple analysis (assuming 8° field-of-view, 10m target, and missile velocity three times that of the target) yields a miss distance of 23.8 meters. This calculation is conservative, since it gives the target maximum escape aspect and assumes that the field-of-view is obscured at maximum range. A good guidance law should negate the latter assumption.

Countermeasures are an evolving breed, and it is difficult to assess their value. Flares, flashing infrared, lasers, cooling (wavelength shift), chaff, decoys, and jamming signals are some of the most common.⁷ They are assumed to be about 30% effective.

Evasive maneuvers have high potential for escape with a head-on attack, but very slim chance for tail-chase. It is assumed that the usual scenario is a relatively head-on approach.

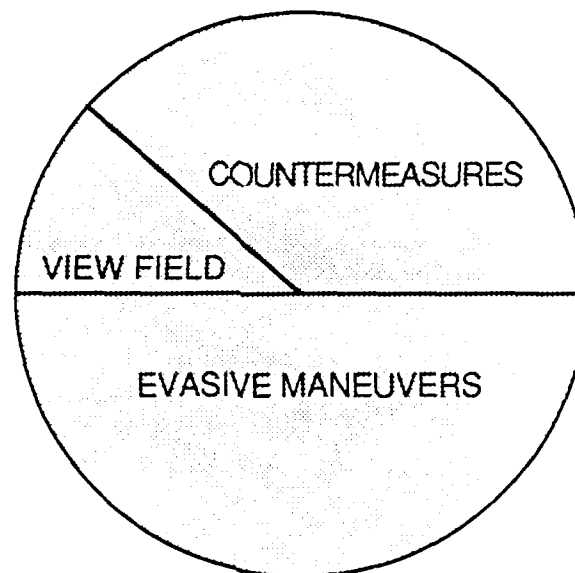


FIGURE 1. Factors contributing to Inaccuracy

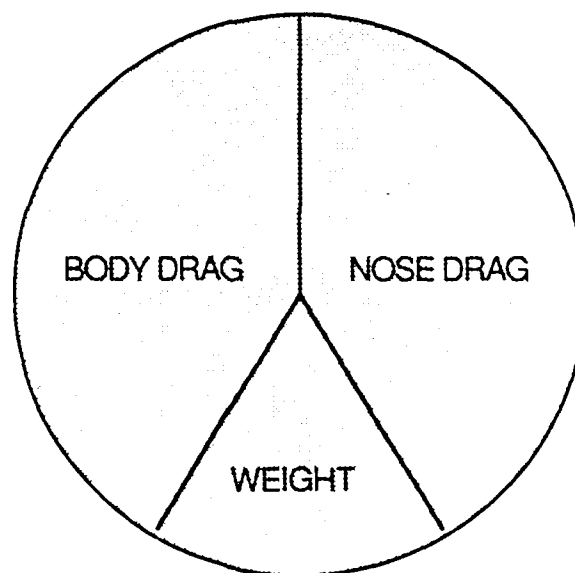


FIGURE 2. Factors Affecting Missile Velocity

SPEED The speed of comparable IR and RADAR missiles would be identical, except for the rounded IRDOME. The rounded dome affects only the nose drag contribution. Studies have shown that the drag coefficient for an IR window does not depart appreciably from that of an ogive, until the window diameter exceeds 20% of the missile diameter.³ If the diameter were 100% (hemispherical nose), the overall drag of a "clean" missile would double. A common design ratio is about 60%, which will contribute significantly to the nose drag, and thus to the overall drag coefficient. The overall contribution is probably 50% or less, which will not appreciably affect velocity, since the drag force is proportional to velocity squared. A 50% drag coefficient increase thus causes only an 18% decrease in velocity. The factors affecting speed are assumed to have the approximate proportions shown in Figure 2.

RANGE The range of a missile (for a given motor) depends primarily on the drag coefficient and the seeker capability. An approximately equal split between drag and seeker limitations is postulated, for the simple reason that this would indicate good engineering design. In other words, any effort to decrease drag for a missile that cannot "see" bears diminishing returns, and an effort to "see farther" for a missile that is drag-limited does also. If anything, the missile is probably more limited on average by the seeker, but a tail-chase aspect could be limited more by drag. A missile velocity much greater than that of the target is desirable, and it must at least exceed that of the target for a tail-chase encounter.

MANEUVERABILITY is an attribute of utmost importance, especially for a relatively head-on encounter. An extensive analysis is included in Appendix B. The major points are: (1) Proportional navigation assumes non-evasive action, (2) Evasive action can cause significant miss distances, and (3) Evasive action is extremely time critical. (4) A knowledge of time-to-go is essential, but (5) an automatic evasive system would be hard to hit. My interest in this topic, in retrospect, is hard to defend, since it is only slightly affected by choice of seeker type.

PAYLOAD and WEIGHT are attributes that are relatively unaffected by the seeker type, although the converse may not hold true, since the design payload would affect missile diameter, and thus affect the available seeker volume.

COMPLEXITY and SUPPORT Radar seekers require extensive processing and electronics, and may require additional support electronics. IR seekers are generally simpler as far as electronics and processing, but the optics and cryogenics make up for it.

DETECTABILITY All active seekers are detectable. Both Radar and IR seekers can be either passive or active. Radar is probably easier to detect, and it is more often deployed as an active seeker.

COUNTERMEASUREABILITY Every weapon modification will generate another countermeasure, but it will be less effective against diversity in measurement. This is the one attribute that can be positively affected by multi-mode sensing.

A comparison between Radar, IR, and Both is provided in figure 3. Positive attributes are left-adjusted and negative attributes are right-adjusted. This comparison assumes that the two seeker types are magically combined, and the characteristics of the hybrid are also magically provided. Note that the combined seeker is not desirable. At this point, enough is known to state a philosophy of multi-mode sensing development.

IV. MULTI-MODE DEVELOPMENT PHILOSOPHY

RISK should be minimized in any new development venture. The obvious way to do this is to retain one tried-and-proven technology. This means that a proven form of either RADAR or IR should be chosen, and then the augmented measurement can employ an untried technology, if desired.

CAPABILITY must not be compromised. Thus, any changes that might adversely affect the primary sensor must be disallowed. Once this is agreed upon, this relegates the secondary technology to retrofit status. Furthermore, the choice of the second technology should provide advantages that fill gaps in the primary seekers ability.

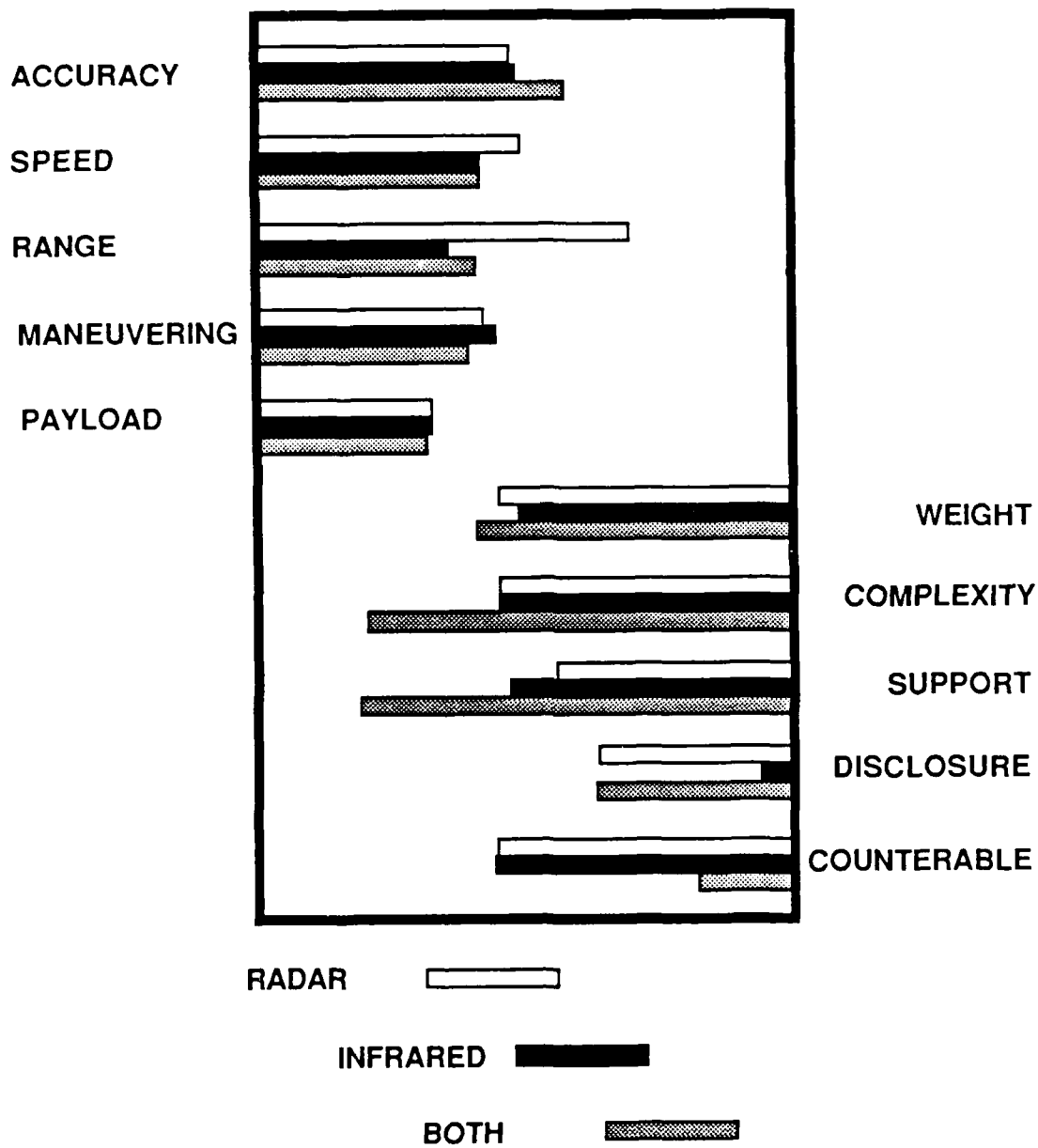


FIGURE 3. ATTRIBUTE COMPARISON AND EXTRAPOLATION

COST is the greatest danger to a multi-mode seeker. The normal approach is to maximize bang/buck. Another approach is to determine the bang decreed by the capability gaps of the primary seeker, then minimize buck/bang.

MAJIC is desirable, because there are a lot of conventional approaches that have been tried before and proven marginal. The probability of exceeding the historical base is minute, unless a "new" piece of technology surfaces. New technology usually follows the development of new materials.

V. EXAMPLE: EXTRACTION OF DESIGN SPECIFICATIONS

Suppose, for example, that a proven form of RADAR is chosen as the primary seeker. All other things being equal, this weapon will possess adequate range but will be more susceptible to detection. As a result, countermeasures are more likely with this initial choice. The secondary sensor should emphasize discrimination against countermeasures, conform to available space, and be economical. Exceptional range will not be required for the secondary sensor.

Discrimination against countermeasures is a tough requirement. One possibility is to image the scene and provide target recognition algorithms that work in real time. Another possibility is to directionally "listen" to the target area, and use the target noise signature for discrimination. At supersonic speeds, sound is not a reliable indicator. There are, however, listening systems that eliminate sonic delay. One example is a laser interferometry technique that allows a spy to detect conversation within a closed room, if it has a window on which to train the laser.

The noise generated by a jet engine will be found to consist of a deterministic component emanating from vanes, rotation, etc., and a random component, which comes primarily from the individual "packets" of burning fuel. It is reasonable to assume that the infrared or visible emission will also exhibit the same components as the audible noise. Thus, it should be possible to "listen" to a target by "looking" at it. The reticle seeker is such an obviously superior

approach that this possibility may have received little research.

The countermeasure discrimination alternatives considered both lead to an optical detector scheme. The expense of conventional optical seekers dictates a very nonconventional approach. Range may be traded off in the process, if required.

VI. POLYVINYLENE FLUORIDE (PVDF) PIEZO-FILM

Pyroelectric detectors have existed long enough to develop a reputation of fragility and poor detectivity. Pyroelectric films such as Polyvinylidene Fluoride (PVDF) are helping to change this reputation, and the potential for even better characteristics is being developed. The application of this material appears plausible because:

- * It can conform to practically any shape.
- * Pyroelectric response is in the audio range at least.
- * The material has a wide, adjustable optical span.
- * The overrange capacity of the film is exceptional.
- * The temperature limit is 100°C.
- * Several similar films are under development.
- * Microelectronics fabrication techniques apply.

This interesting material was developed in 1971 at BELL Labs, and results from proper stretching and quenching of the original plastic material. A resulting crystalline structure is formed in the plastic that is found to be piezoelectric, with response to approximately 10 Ghz, and additional passband above 40 Ghz.² The usual configuration is to provide a thin metallic coating to both sides, which makes the contact for the sensor. Pressure and acceleration transducers are obvious applications, and the film also serves as a large-area audio transducer (both ways). The film is relatively inexpensive, and is now employed under carpet to detect illegal entry.

The interesting aspect is that it is also a pyroelectric detector. Unfortunately, the passband is limited, and in early research, the material was discarded for applications requiring fast response. Recent research has been applied to a 30nm. film that is much more encouraging.⁴ The film was pulsed with a laser, and exhibited a response from excitation to peak much less than 1 millisecond. Pennwalt produces the KINAR film, which set new records for speed of response reported in the literature. Douglas Kerhung (215-337-6710), Applications Engineer at Pennwalt, mentioned picosecond pyroelectric response in some advanced research¹. At this point, I became convinced that piezo-films have significant application potential for the military. The ensuing discussion is a focused analysis on the pyroelectric application to seekers.

VII. PYROELECTRIC MEASUREMENT

Pyroelectric devices are deceptive. Pyroelectrics would appear to have a very slow response, due to thermal time constants. Surprisingly, this is not the case. Figure 4 is a common model for thermal response analysis¹, where C_T is the thermal capacity, G_T is the thermal conductivity, T is the film temperature, ϵ is the emissivity of the surface, and $P(t)$ is the incident power. A straightforward analysis yields:

$$\begin{aligned} C_T \dot{T} + G_T T &= \epsilon P(t) , \\ C_T s T(s) + G_T T(s) &= \epsilon P(s) , \\ T(s) &= \epsilon P(s) / (s C_T + G_T) . \end{aligned} \quad (1)$$

The thermal response to a step input is obviously slow, as expected. But the pyroelectric response is related to temperature change:

$$i(t) = p A \dot{T} ,$$

where $i(t)$ is the current produced, p is the pyroelectric coefficient,

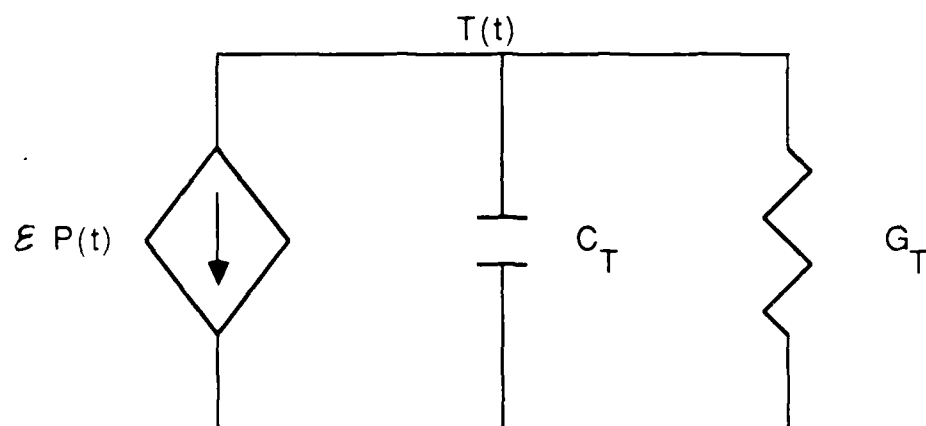


FIGURE 4. THERMAL MODEL FOR FILM ANALYSIS

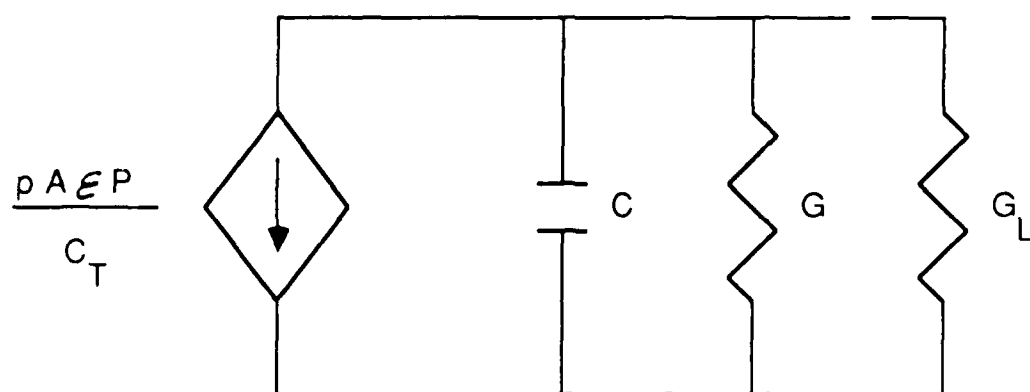


FIGURE 5. MODEL DEMONSTRATING ELECTRICAL RESPONSE PROBLEM

and A is the detection area. Thus,

$$I(s) = p A s T(s) ,$$

$$I(s) = p A \epsilon s P(s) / (s C_T + G_T) . \quad (2)$$

The time constant, C_T / G_T , is thus seen to limit the low frequency response, which we don't need anyway. Above this frequency,

$$I = p A \epsilon P / C_T . \quad (3)$$

Although the time constant is of little consequence (provided we can work at higher frequencies), it is obviously desirable to decrease the heat capacity.

A simple analysis on the bulk material is informative. The thermal conductivity is

$$G_T = .13 A / t \quad (W / ^\circ K) , \quad (4)$$

where A is the detector area and t is the thickness. The heat capacity is

$$C_T = 2.314 \times 10^6 A t \quad (J / ^\circ K) , \quad (5)$$

The thermal break frequency then occurs at

$$f_T = 8.94 \times 10^{-9} / t^2 . \quad (6)$$

Interface circuitry must operate above this frequency (110 Hz, for 9 μ m film). Mounting techniques can affect this frequency significantly. Substituting equation (5) into equation (3) yields

$$I(t) = p A \epsilon P / 2.314 \times 10^6 A t . \quad (7)$$

Before cancelling terms, recall that optic elements may be used to concentrate incident infrared to the order of pixel size, A . Thus,

$$P = P_i A_o / A ,$$

$$I = -10.8 \times 10^{-12} \epsilon P_i A_o / A t . \quad (8)$$

It is now evident that response is increased by decreasing detector area or thickness, but the thermal break frequency can move out of range, and is very sensitive to thickness. Remember, however, that the bulk material is sandwiched between conductive material. As dimensions shrink, conductor and spatial effects become dominant, and this analysis is no longer valid. It does explain the effort to achieve very thin piezo-films.

The electrical properties are more severe and less controllable. The resistance is

$$R = 10^{13} \ t / A \quad (\text{ohms}) , \quad (9)$$

and the capacitance is

$$C = 116.76 \ A / t \quad (\text{pF}) . \quad (10)$$

The electrical break frequency then occurs at 1.4×10^{-4} Hertz, and we have no control over it! Interface circuitry must defeat this problem.

Surprisingly, the electrical parameters are more unforgiving than the thermal. The model shown in figure 5 is simple, but foreboding. The usual logic is as follows:

- * The time constant, C / G , is large.
- * To decrease the time constant, make G_L large.
- * For good signal transfer, $G_L = G$ (small).
- * Conflict, end of analysis --- usually.

VIII. A PROPOSED PYROELECTRIC SENSOR

An array of 100 pixels is shown in figure 6, etched in 9 um Kinar film. Each pixel is a square, .040 inches on a side, with .020 inches between pixels. This choice is not necessarily optimum, but approaches the limits of printed circuit etching capability. A procedure is proposed that allows a detecting circuit to work with any

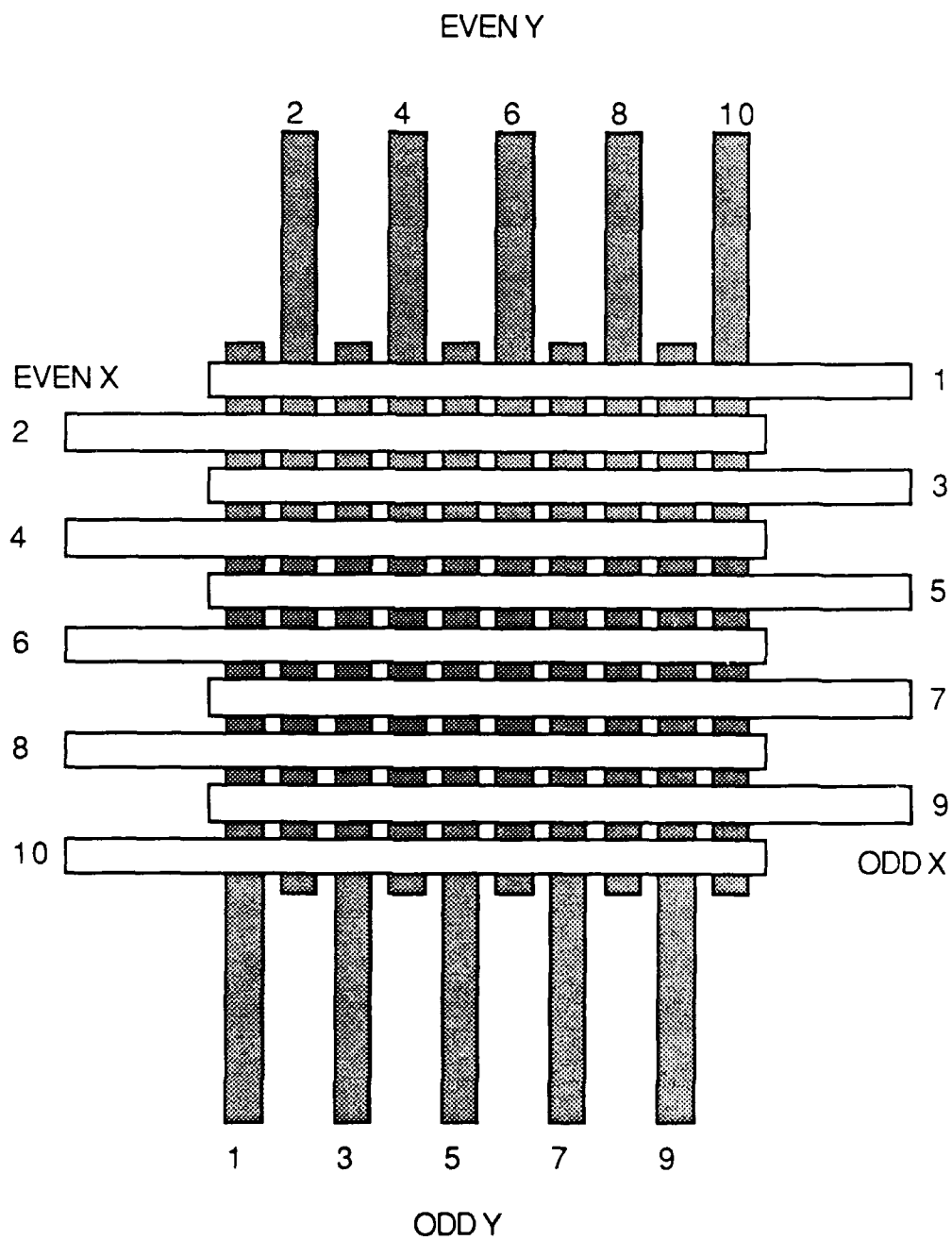


FIGURE 6. ETCH PATTERN FOR PYROELECTRIC SENSOR

combination of pixels, from 1 all the way to 100. It is obvious that the electrical interface must operate above 110 Hertz, and it must have exceptionally high input impedance, on the order of 10^{14} ohms.

The sensor array could be located slightly off focal, and mounted on a vibrating beam. The vibration would be driven at the passband of the analog interface, and this would be chosen to avoid modal frequencies of the missile. An amplitude and center position control would be required, and this could best be implemented digitally. Industrial sensors already incorporate this technology (Corialis Flowmeters). The amplitude should be on the order of one pixel width, and in a direction at 45° to the etched lines. Sub-pixel resolution is possible by comparing relative magnitudes of both input configurations, and phase comparison with a boresight sync signal.

It should be mentioned that this design is approached from the wrong direction, due to prototyping limitations. Since the material is compatible with vacuum sputtering techniques used in microelectronics fabrication, it is possible to fabricate the integrated circuit that performs the multiplexing, then attach the film and process after completing all oxide growth steps.

IX. CONCLUSION

Due to restricted space, the report body contains general information that presents the scope of research, with specific detail relegated to Appendices, to reside with Dr. Steven F. Butler. Appendix C continues the logic to develop a novel sensor concept using PVDF film to provide a pseudo-image. The combination of thermal and electrical time-constants are found to be the major hindrance to use of this film, demanding careful attention. Appendix D contains vendor literature and a discussion of concurrent research that may apply. The advances underway in this field are eroding the limits to the detectivity of piezo-film, and ultimately opening new avenues for application.

X. RECOMMENDATIONS

Piezoelectric films currently provide mediocre, but improving, detectivity. Major improvements are expected to result from film thickness, surface deposition, and spatial pattern. Taken together, the detectivity may increase to a level commensurate with the requirements for a secondary sensor. The materials are already capable of operation in ambient temperatures, a critical requisite for economy. Working with available films, a proof-of-concept and scaling analysis would be timely.

The focus of interest in air-to-air missiles is usually at the "blood-and-feathers" end of the trajectory, but "leaving the nest" is a very transient affair that can significantly detract from missile capability. Pre-launch missile control to maintain specified pylon attachment forces and moments could provide a much more predictable, and thus controllable, launch transient phase. This is another excellent application for piezoelectric film as the sensor element.

REFERENCES

1. Boyd, Robert W., Radiometry and the Detection of Optical Radiation, John Wiley and Sons, 1983.
2. Carlisle, Ben H., "Piezoelectric Plastics Promise New Sensors", Machine Design, Oct. 23, 1986, pp 105-110.
3. Chin, S. S., Missile Configuration Design, McGraw Hill, 1961.
4. Coufal, H., "Highly Time-Resolved Calorimetry Using Pyroelectric Thin-Film Electrets", IEEE Transactions on Electrical Insulation, vol. EI-21 No. 3, June 1986, pp 495-500.
5. Day, G. W., Hamilton, C. A., Gruzensky, P. M., and Phelan, R. J., Jr., "Performance and Characteristics of Polyvinylidene Fluoride Pyroelectric Detectors", Ferroelectrics, vol.10, pp 99-102, 1976.
6. Gunston, Bill, Modern Airborne Missiles, Prentice Hall Press, New York, NY, 1986.
7. Heaston, R. J., and Smoots, C. W., Precision Guided Munitions, GACIAC HB-83-01, Vol. 1: tutorial, May, 1983.
8. Hudson, Richard D., Jr., Infrared System Engineering, John Wiley and Sons, 1969.
9. Jane's Weapon Systems, Jane's Publishing Co. Ltd., 238 City Road, London, UK, 1986-1987.
10. Korn, U., Rav-Noy, Z., and Shtrikman, S., "Pyroelectric PVF₂ Infrared Detector Arrays", Applied Optics, vol. 20, No. 11, June 1, 1981.
11. Ravich, Leonard E., "Pyroelectric Infrared Detectors", Sensors, June, 1984, pp. 66-72.
12. Stimson, George W., Introduction to Airborne Radar, Hughes Aircraft Company, El Segundo, CA, 1983.

1987 USAF-UES SUMMER FACULTY RESEARCH PROGRAM/
GRADUATE STUDENT SUMMER SUPPORT PROGRAM

Sponsored by the
AIR FORCE OFFICE OF SCIENTIFIC RESEARCH

Conducted by the
Universal Energy Systems, Inc.

FINAL REPORT

NIGHT-TIME CO₂(001) VIBRATIONAL TEMPERATURES
AND LIMB-VIEW INTEGRATED RADIANCES
IN THE 50 TO 150 KM ALTITUDE RANGE

Prepared by:	Dr. Henry Nebel
Academic Rank:	Associate Professor
Department and	Physics Department
University:	Alfred University
Research Location:	Air Force Geophysics Laboratory, Infrared Technology Division, Infrared Backgrounds Branch.
USAF Researcher:	Dr. Ramesh D. Sharma
Date:	14 August 1987
Contract No.:	F49620-85-C-0013

NIGHT-TIME CO₂(001) VIBRATIONAL TEMPERATURES
AND LIMB-VIEW INTEGRATED RADIANCES
IN THE 50 TO 150 KM ALTITUDE RANGE

by

Henry Nebel

ABSTRACT

Night-time vibrational temperature profiles as functions of altitude have been obtained for the (001) state of carbon dioxide using a line-by-line infrared radiance code developed at the Air Force Geophysics Laboratory (AFGL). The calculation assumes absorption of earthshine and airglow, collisional interaction with N₂, O₂, and O, and spontaneous emission. Results are presented for the principal isotopic form ¹²C¹⁶O₂ as well as for the less abundant forms ¹³C¹⁶O₂, ¹⁶O¹²C¹⁷O, and ¹⁶O¹²C¹⁸O. The resulting profiles are used to calculate infrared radiance from the 4.3 micron (ν_3) band of CO₂ through the atmosphere in a limb-viewing geometry. This has been done for the four isotopic forms indicated above in the fundamental band and also for selected higher order transitions. The resulting radiance is compared with data from the Spectral Infrared Rocket Experiment (Stair, et. al., 1985). Recommendations are made for resolving the discrepancies observed.

ACKNOWLEDGEMENTS

I wish to thank the Air Force Systems Command and the Air Force Office of Scientific Research for sponsorship of this research. I thank Dr. Ramesh D. Sharma of the Air Force Geophysics Laboratory for making it possible for me to spend ten weeks in residence at AFGL and for continued guidance during the course of the work. I thank Universal Energy Systems, Inc. for administration of the Summer Faculty Research Program.

I also thank Dr. Peter Wintersteiner of Arcon Corporation for many useful discussions and for assistance in implementing the infrared radiance code. This research would not have been possible without his assistance.

I. INTRODUCTION: This research is a continuation of work initiated last summer (1986) when I also participated in the Summer Faculty Research Program. The research involves the theoretical consideration of infrared radiation under non-equilibrium conditions in the atmosphere. Under these conditions, local thermodynamic equilibrium may not be assumed to apply, i.e. collisions among molecules are not frequent enough to bring a parcel of air into equilibrium before radiative deexcitation occurs. This is generally the situation in the earth's upper atmosphere (above 60 km altitude). An infrared radiance computer code has been developed at the Air Force Geophysics Laboratory (AFGL) by Dr. Ramesh D. Sharma of AFGL and Dr. Peter Wintersteiner of Arcon Corporation. This code treats absorption, emission, and transmission of infrared radiation in the atmosphere under non-equilibrium conditions. I began working with this code briefly while a NASA Summer Fellow at Langley Research Center in Hampton, Virginia in 1985. During the summer of 1986 at AFGL I made a preliminary study of the application of the infrared radiance code to the asymmetric stretch (ν_3) mode of excitation of carbon dioxide (4.3 micron band) (Nebel, 1986). This report describes a continuation and refinement of that effort.

II. OBJECTIVES: My objectives were as follows:

1. Calculation of the night-time vibrational temperature profile of the asymmetric stretch (ν_3) mode of excitation of

carbon dioxide (4.3 micron band) in the upper atmosphere using the AFGL infrared radiance code. This was to be done for the most abundant isotopic form of carbon dioxide ($^{12}\text{C}^{16}\text{O}_2$) labeled 626, as well as for the three most important minor isotopic forms ($^{13}\text{C}^{16}\text{O}_2$, $^{16}\text{O}^{12}\text{C}^{17}\text{O}$, $^{16}\text{O}^{12}\text{C}^{18}\text{O}$) labeled 636, 627, and 628 respectively. "Vibrational temperature" is an indication of the population density of the molecular excited state in question.

2. Calculation of total infrared radiance for the 4.3 micron band in a limb view for various tangent heights (see Fig. 1). This was to be done for the fundamental band (first excited state to ground state) for the four isotopic forms considered, and also for the most important "hot" bands (higher order transitions) for the 626 and 636 isotopic forms.

3. Comparison of total calculated radiance with experimental data from the Spectral Infrared Rocket Experiment, or SPIRE (Stair, et. al., 1985), which measured infrared radiance in a limb view for several spectral regions including the 4.3 micron band of CO_2 .

III. APPROACH: To achieve my first objective (calculation of vibrational temperature profiles), I used a component of the infrared radiance code called RAD. This program calculates population densities of excited states, assuming various mechanisms of excitation and deexcitation, and assuming the population densities are constant in time. The kinetic equations required are given in my final report from last summer (Nebel, 1986) and will not be repeated here. Excited state densities are calcul-

ated for the (001) state of CO₂ (4.3 micron vibrational state) and for the first vibrational state of the N₂ molecule which has very similar energy (see Fig. 2), causing a rapid interchange of vibrational quanta between the two states. Vibrational temperatures are then calculated by means of the formulas

$$[\text{CO}_2(001)]/[\text{CO}_2(000)] = \exp(-h\nu/kT_{001})$$

and

$$[\text{N}_2(1)]/[\text{N}_2(0)] = \exp(-h\nu/kT_{N2})$$

where [] represents a population density, T₀₀₁ and T_{N2} are the vibrational temperatures of the CO₂(001) state and the N₂(1) state respectively, and ν is the frequency associated with the transition in each case.

The computer program requires as input for the calculation an "initial guess" vibrational temperature profile. An iterative technique is then used to approach the final profile for the CO₂(001) state. Convergence is achieved when successive iterations produce no further change in the vibrational temperature profile. Also required as input for the calculation are line parameters for the various spectral lines within the band. These were obtained from the AFGL line tape (Rothman, et.al., 1983).

To achieve my second objective (calculation of total infrared radiance in a limb view), I used a component of the infrared radiance code called NLTE (Wintersteiner & Sharma, 1985). This

calculates integrated radiance in a limb view for each spectral line within the band for selected tangent heights. The program then sums the results to obtain total band radiance for each selected tangent height. Required as input are the vibrational temperature profile calculated in RAD (indicating excited state population densities) as well as line parameters for the various spectral lines, which were again obtained from the AFGL line tape (see above). The calculation was done for the fundamental band using the four most important isotopic forms of CO_2 , and also for the most important "hot" bands using the 626 and 636 isotopic forms.

To achieve my third objective (comparison with SPIRE data), results for all isotopic forms and the selected hot bands were added for each tangent height. A direct comparison could then be made with the SPIRE data (Stair, et. al., 1985, Fig. 20).

In the course of this work, all recommendations made in last year's final report (Nebel, 1986) have been carried out. Input profiles were extended to 150 km. Full band calculations were made with as many iterations as were required to achieve convergence of the vibrational temperature profile (this varied with isotopic form). Rate constants were taken from a paper by López-Puertas, et. al. (1986). The most important hot bands have been included. The first excited vibrational state of O_2 has been considered as an unknown population density, with the result that this state is in local thermodynamic equilibrium

for the set of kinetic equations used. The isotopic forms 627 and 628 have been included in addition to 626 and 636. Other isotopic forms have very low line strengths and were therefore neglected.

IV. RESULTS: Night-time vibrational temperature profiles for the (001) vibrational state of CO₂ as calculated from the AFGL infrared radiance code are shown in Fig. 3 for the four most important isotopic forms. For the principal form (626), 100 iterations were required to achieve adequate convergence of the vibrational temperature profile. For the minor forms, 12 iterations were sufficient since the corresponding bands are much weaker. Ideally, the final vibrational temperature profile should be the same regardless of the initial guess profile used. Two widely different initial guess profiles were used, resulting in the same vibrational temperature profile in both cases. This identity of final profiles was achieved with far fewer iterations for the weaker isotopes than for the 626 isotope.

As can be seen in Fig. 3, the temperatures for the minor isotopes (636, 628, 627) are higher than that of the major isotope (626) above about 60 km, indicating greater enhancement of excited state population densities over equilibrium values than is the case for the 626 isotope. Since the minor isotopes correspond to weaker bands, the molecules at a given altitude are receiving photons from much farther above and below that altitude than is the case for the principal (626) isotope.

Since kinetic temperature peaks at about 50 km and increases without limit above 100 km (see Fig. 3), molecules between 60 and 100 km are receiving photons from warmer regions for the minor isotopes than for the principal isotope. This explains the higher vibrational temperatures for the minor isotopes in the middle atmosphere (60-100 km). The curves are in excellent agreement with those of López-Puertas, et. al. (1986) which were obtained from a band model (see Fig. 4 of their paper).

Total calculated band radiance in a limb view as a function of tangent height is shown in Fig. 4. Also shown in this figure are the locations of experimental integrated radiance values from the SPIRE mission (shaded region). These were obtained from Stair, et. al. (1985), Fig. 20. As can be seen in Fig. 4, the calculated radiance values are smaller than the experimental values above 60 km. They are about an order of magnitude too small from 100-120 km. Thus the present model does not explain the "night-time" experimental data from the SPIRE mission.

V. DISCUSSION: The view paths used in the SPIRE mission to obtain "night-time" radiance were not actually in total darkness. The rocket itself was in sunlight at the time of the measurements, and a portion of each view path was also in sunlight (Stair, et. al., 1985, Fig. 2). Solar pumping will increase the number of CO₂ molecules in excited states, thereby increasing the measured radiance in a limb view. It is believed that this is the reason the results of the present calculations do not

agree with the data labeled "night-time 4.3 micron radiance" by the SPIRE mission (Stair, et. al., 1985, Fig. 20). A preliminary calculation assuming the entire view path is sunlit with a very low sun angle produces too much radiance compared to the "night-time" SPIRE data. Thus it is reasonable to expect better agreement with these data if the view paths are considered as being partly sunlit and partly in darkness.

VI. RECOMMENDATIONS: In light of the above discussion, the principal recommendations of this report are as follows:

1. Determine what portions of the various view paths used for the "night-time" SPIRE data are sunlit.
2. Try to model these "composite" situations (part sunlit, part darkness) in terms of vibrational temperatures.
3. Calculate total band radiance in a limb view using this "composite" model.
4. Compare with "night-time" experimental data from the SPIRE mission.

REFERENCES

- López-Puertas, M., R. Rodrigo, J. J. López-Moreno, and F. W. Taylor, "A non-LTE radiative transfer model for infrared bands in the middle atmosphere. II. CO₂(2.7 and 4.3 μ m) and water vapor (6.3 μ m) bands and N₂(1) and O₂(1) vibrational levels", J. Atmos. Terr. Phys. 48, 749 (1986).
- Nebel, H., "CO₂(001) Vibrational Temperatures in the 50 to 150 km Altitude Range", Final Report/ 1986 USAF-UES Summer Faculty Research Program (1986).
- Rothman, L. S., R. R. Gamache, A. Barbe, A. Goldman, J. R. Gillis, L. R. Brown, R. A. Toth, J.-M. Flaud, and C. Camy-Peyret, "AFGL Atmospheric Absorption Line Parameters Compilation: 1982 Edition", Appl. Opt. 22, 2247 (1983).
- Stair, A. T., R. D. Sharma, R. M. Nadile, D. J. Baker, and W. F. Grieder, "Observations of Limb Radiance With Cryogenic Spectral Infrared Rocket Experiment", J. Geophys. Res. 90, 9763 (1985).
- Wintersteiner, P. P., and R. D. Sharma, "Update of an Efficient Computer Code (NLTE) to Calculate Emission and Transmission of Radiation Through Non-Equilibrium Atmospheres", AFGL-TR-85-0240 (1985).

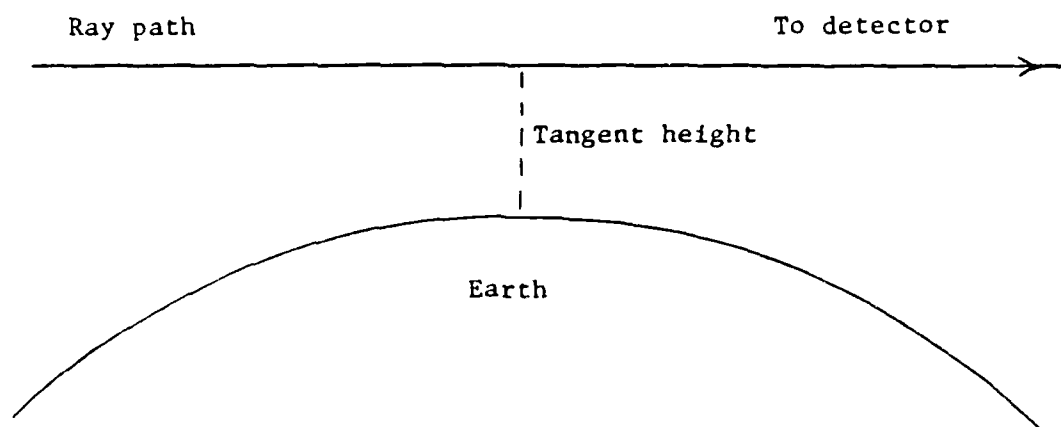


Fig. 1. Limb-viewing geometry. The tangent height is the shortest distance between the ray path and the earth.

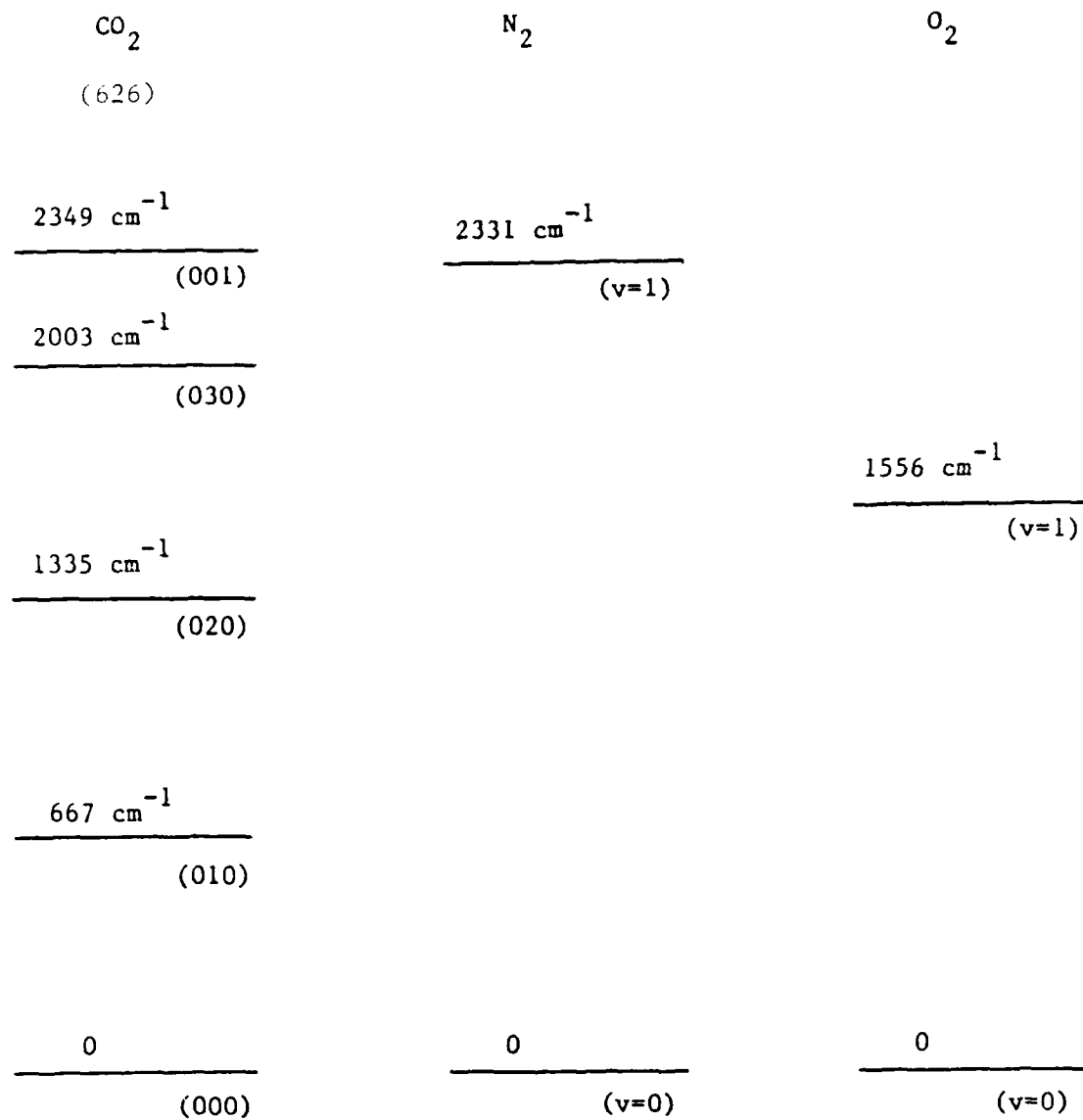


Fig. 2. Low-lying vibrational levels of CO_2 , N_2 , and O_2 .

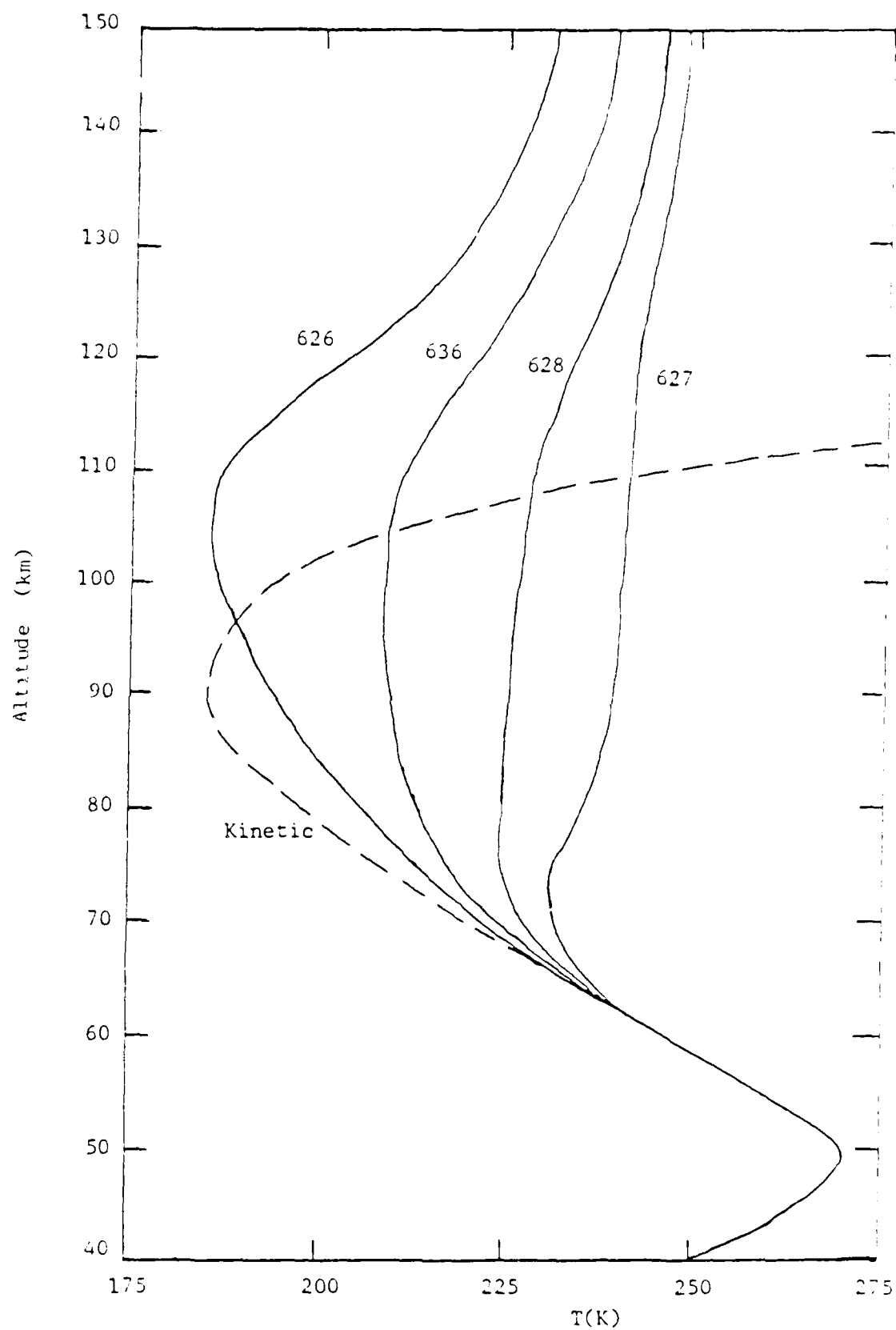


Fig. 3. Night-Time CO2(001) Vibrational Temperatures

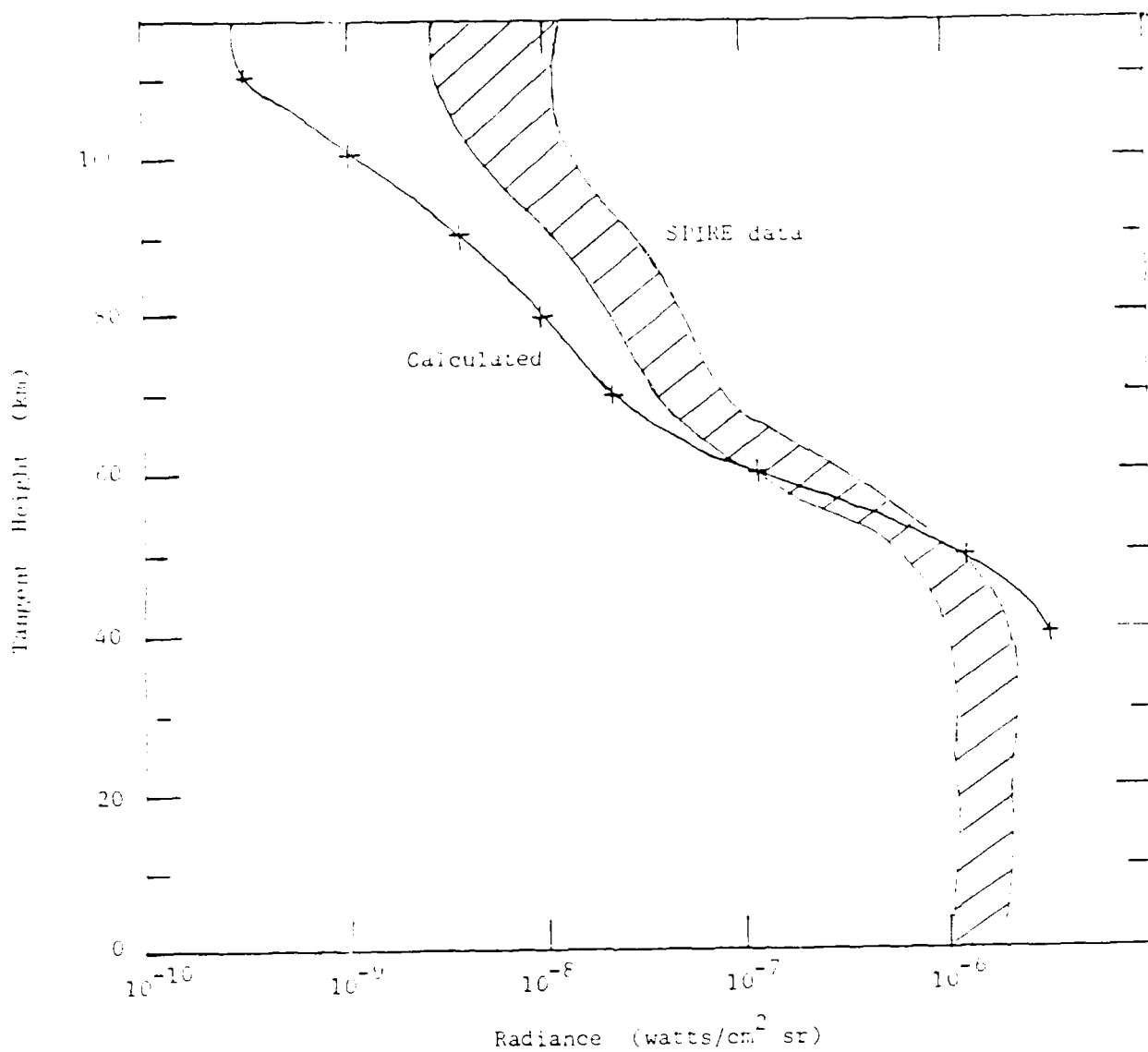


Fig. 4. Total Night-Time Band Radiance in a Limb View

1987 USAF-UES SUMMER FACULTY RESEARCH PROGRAM/
GRADUATE STUDENT SUMMER SUPPORT PROGRAM

Sponsored by the
AIR FORCE OFFICE OF SCIENTIFIC RESEARCH
Conducted by the
UNIVERSAL ENERGY SYSTEMS, INC.

FINAL REPORT
A KINETIC STUDY OF THERMAL DECOMPOSITION OF TNT
BY HIGH PERFORMANCE LIQUID CHROMATOGRAPHY

Prepared by:	Maurice C. Neveu
Academic Rank:	Associate Professor
Department and University:	Chemistry Department State University of New York, College at Fredonia
Research Location:	Frank J. Seiler Research Laboratory (AFSC) USAF Academy, Colorado Springs, CO 80840
USAF Research Colleague:	Jon T. Swanson
Date:	12 August 1987
Contract No:	F49620-85-C-0013

A Kinetic Study of Thermal Decomposition of TNT by
High Performance Liquid Chromatography

by

Maurice C. Neveu

Abstract

Thermal decomposition of TNT was carried out at 240°C. The amount of unreacted TNT as a function of time was measured isocratically in 70% methanol/water by high performance liquid. A plot of percent reaction against time resulted in a sigmoid type of curve in which the extent of reaction increased slowly up to 120 minutes and then increased rapidly. This indicates autocatalysis whereby product formed during the reaction catalyzes further reaction.

I. Introduction

The kinetics and mechanism of TNT decomposition have been studied by various techniques including differential scanning calorimetry (DSC) 1,2 and electron paramagnetic resonance spectrometry (EPR) 3,4. The DSC studies measured energy changes occurring during thermal decomposition of TNT over the range 245-269°C. From the interpretation of the resulting data rate constants, order, activation energies, enthalpies, and entropies of activation were calculated for TNT and TNT-d₃ (with three deuterio atoms on the methyl carbon atom). A k_H/k_D value of 1.35 was obtained indicating that the breaking of a C-H bond in the methyl group was involved in the transition state of the rate determining step. The EPR experiments involved the observation of EPR Spectra of free radicals formed in the decomposition of TNT from which kinetic information and structural information about the intermediate free radicals could be obtained. These are indirect methods, and it was felt that a direct measurement of disappearance of TNT would supplement these methods.

It was decided to carry out the measurements utilizing high-performance liquid chromatography (HPLC). The author of this report had some experience on a previous minigrant studying thermal decomposition of 1,4-butanediammonium dinitrate (BDD) with a Waters Modular HPLC instrument.

II. Objective of the Research Project

The decomposition of TNT will be monitored as a function of time

by measuring the amount of TNT remaining in a neat sample after heating at the decomposition temperature for various time intervals. From these data a reaction curve showing extent of reaction as a function of time will be constructed. The characteristics of this curve may have some mechanistic implications.

III. Approach

Components of a solution can be separated and quantitatively assayed by high-performance liquid chromatography (HPLC). Each component appears as a peak occurring at a specific time, known as the retention time, after introduction of the solution, as the component makes its way through the column to the detector. The area of the peak is proportional to the amount of component. Thus, the amount of remaining TNT corresponding to a particular reaction time can be assayed. At the same time decomposition products can also be detected.

IV. Procedure

Weighed samples of chromatographically pure TNT (100 mg) in 5 x 260mm pyrex tubes were heated for various time intervals at 240°C in a temperature controlled techam SBL-1 fluidized sand bath reaction was quenched by placing the tube in an ice bath. The reaction mixture was then dissolved by introducing acetone into the tube with a 300mm syringe needle. Several washings were made for each mixture and the resulting solutions drawn up with the syringe and transferred to a 5ml volumetric flask. A 100 microliter aliquot was added to a 2ml

volumetric flask and the solution made up to volume with methanol. Particulate matter was removed with a millex-SR 0.5 micron filter unit (Millipore Corp.)

The resulting solution was separated and analyzed isocratically at 70% methanol/water utilizing a Hewlett Packard 1090 High Performance Liquid Chromatograph equipped with a Diode Array Detector. The column used was of a reverse phase type, specifically, ultrasphere ODS Micron 4.6mm x 25cm (Beckman). The sampling loop had a 5 microliter capacity. Flow rate was 1ml/min. and column pressure 285 bars. Chromatographic data and peak spectra were stored on disk.

V. Results

Calibration solutions were made up in the following manner: A stock solution consisting of 104.33 mg of TNT per 5.00 ml in acetone was made up. A series of solutions were made up by diluting 50, 100, 150, and 200 microliters of the stock acetone solution to 2.00 ml in methanol.

Samples of the methanol solutions were then analyzed by HPLC. Four trials were made for each calibration solution. The chromatographs showed acetone and TNT peaks with retention times of 3.079 and 5.563 minutes respectively.

Chromatographic data is tabulated below (Table I).

Table I

MICROLITERS STOCK ACETONE SOLUTION OF TNT	AVE TNT PEAK AREA (MAUS)	STD. DEV.	AVE. ACETONE PEAK AREA (MAUS)	STD. DEV.	PEAK HEIGHT (MAU)
50	4969	50	780	8	762
100	9281	307	1495	47	1381
150	14492	183	2371	21	2111
200	18609	159	3065	14	2529

Standard deviations indicate good reproducibility. A peak height of 1381 milliabsorbance units for the 100 microliter solution suggests that at this level reliable absorbance readings would be obtained. This prompted the decision to use 100 microliters of acetone stock solution for the HPLC analyses of the decomposed TNT samples. From this table a calibration curve (Figure 1) of TNT peak area showing good linearity, was construed (correlation coefficient = 0.999).

The acetone peak areas given in Table I are linear (correlation coefficient = 0.999) with respect to volume. A value of 15.40 maus per microliter of acetone can be calculated or obtained graphically. Therefore, for a 100 microliter aliquot of acetone solution, an area of 1540 maus would be expected. This value could be applied using acetone as an internal standard in decomposition mixture measurements. This value can be used in the following expression to

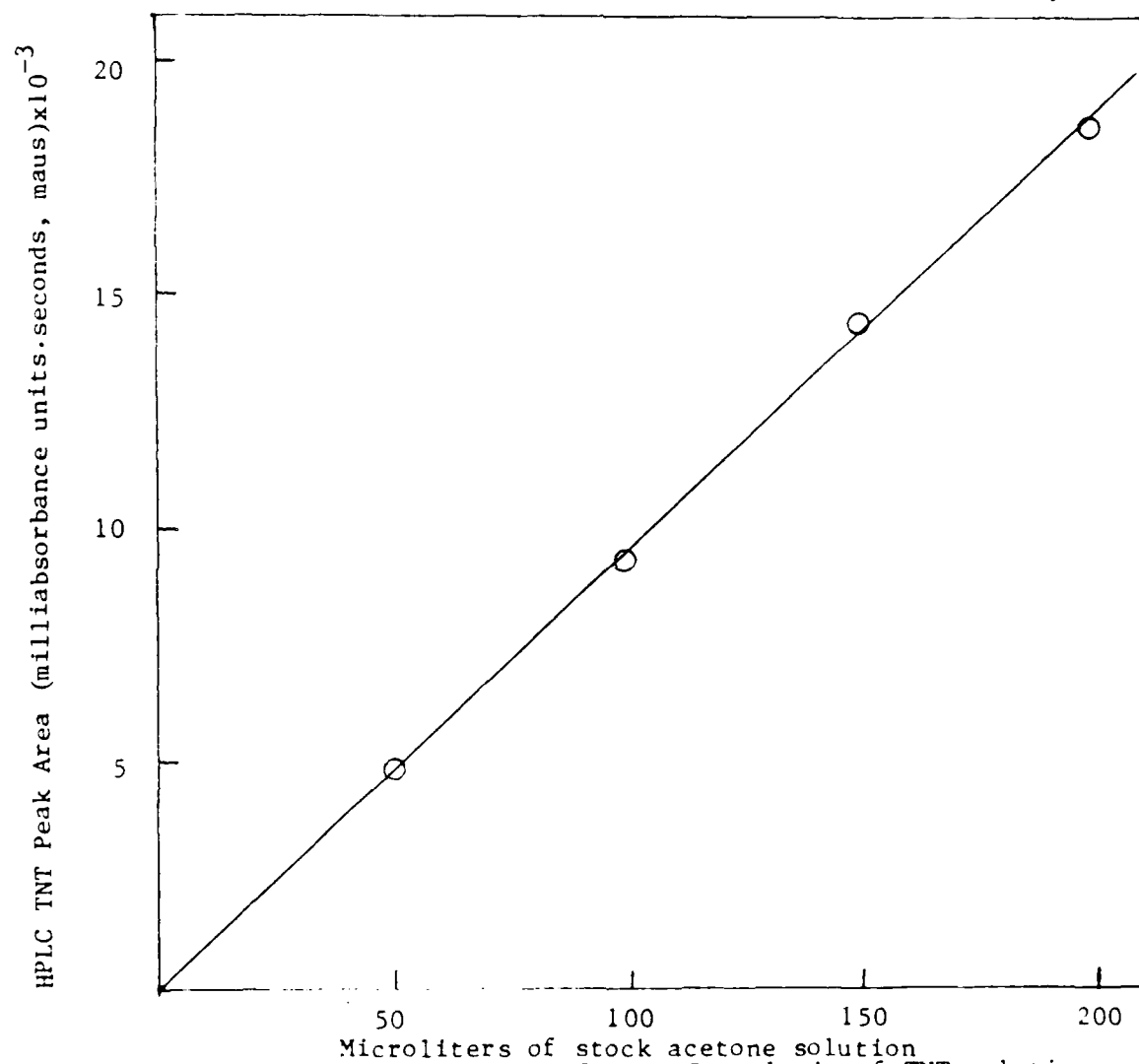


Figure 1. Calibration plot for HPLC analysis of TNT solutions

obtain a TNT peak area normalized to 100 microliters of acetone as well as the 104.33 g TNT used in the calibration.

$$\text{OBS. TNT Peak Area} \times \frac{1540}{\text{OBS. Acetone Peak Area}} \times \frac{104.33}{\text{WT. TNT Sample}}$$

Percent reaction can be obtained by dividing the normalized TNT peak area by 9600, the peak area corresponding to 100 microliters of acetone solution used in the calibration.

Table II summarizes the decomposition data obtained.

Table II

REACTION TIME (MINUTES)	TNT SAMPLE WEIGHT (mg)	OBS. ACETONE AREA (maus)	OBS. TNT AREA (maus)	NORMALIZED TNT AREA (maus)	PERCENT REACTION
29.7	96.10	1462	8322	9544	0.68
59.8	98.62	1545	8599	9094	5.27
91.3	95.79	922	4907	8954	6.73
106.4	98.63	1373	7231	8796	8.37
111.5	95.74	996	2040	3294	65.68
125.5	97.76	811	3714	7548	21.37
128.0	95.44	986	1595	2726	71.60
135.0	96.18	981	2658*	4539	52.71
142.4	96.19	1013	830	1370	85.73
156.1	97.02	984	835	1409	85.32
174.0	95.71	1001	1036	1743	81.85
190.0	95.79	1051	515	824	91.41

*Adjusted for twice normal dilution.

A plot of percent reaction against time, shown in Figure 2, has a sigmoid shape characteristic of an autocatalytic reaction. A slow increase in percent reaction is followed by a rapid increase. This behavior is expected when product formed in the initial phase catalyzes further reaction.

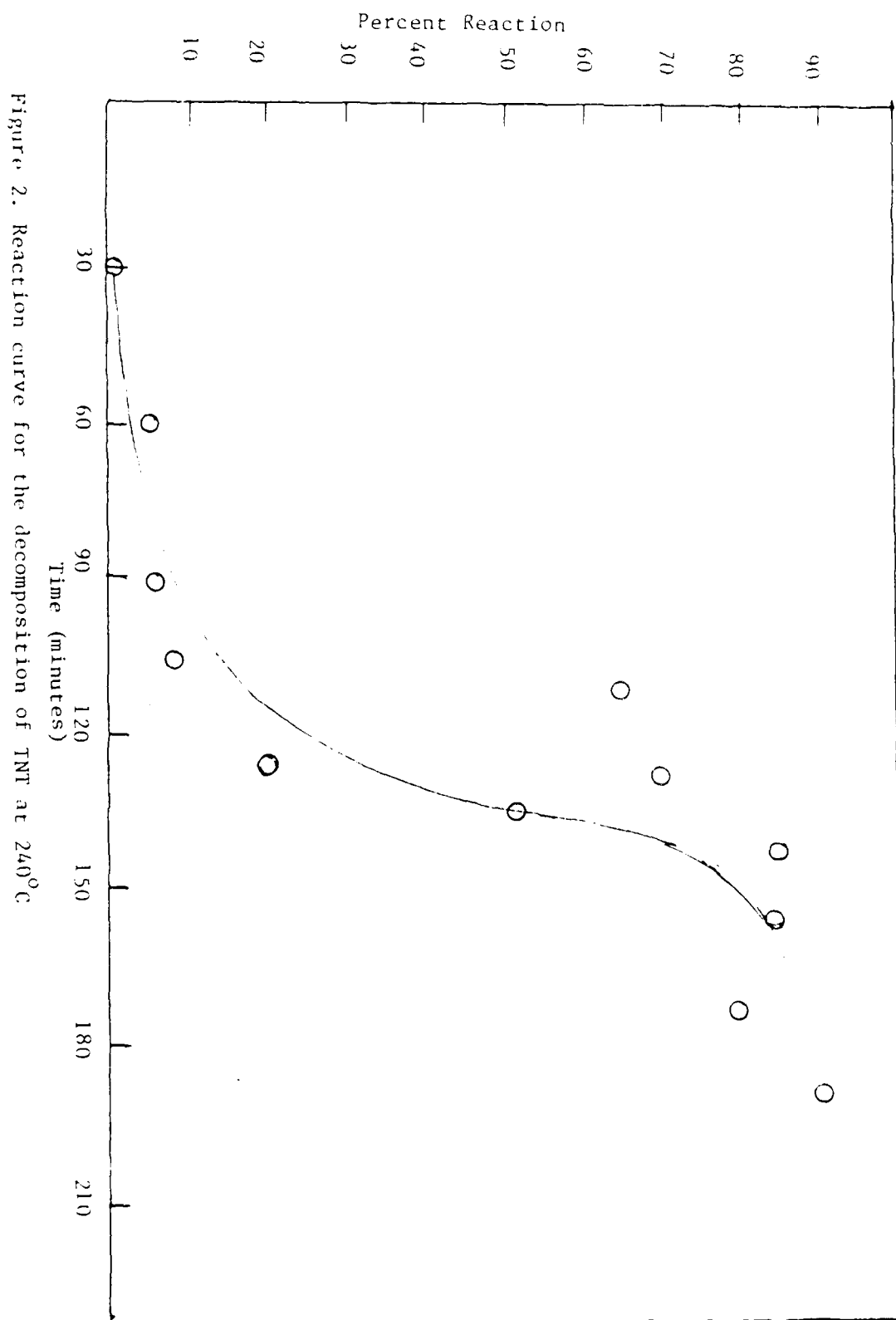


Figure 2. Reaction curve for the decomposition of TNT at 240°C

VI. Recommendations

More work would be needed to improve the reproducibility of the thermal decomposition data. Inaccuracies are introduced by the sublimation of TNT to a higher level in the tube resulting an excess unreacted TNT. Also, decomposition products may be lost by distillation. Sealing the tubes before heating could be tried.

It would then be necessary to identify the decomposition products, particularly the catalyzing species. Its concentration would have to be measured as a function of time and the data incorporated into an autocatalytic rate law to obtain the specific rate constant.

Finally, the same experiment could be repeated with TNT with a deuterated methyl group to determine an isotope effect which would give valuable mechanistic information.

Acknowledgements

The author would like to thank the Air Force Systems Command, the Air Force Office of Scientific Research and the Frank J. Seiler Research Laboratory for sponsorship of this research project. He also wishes to thank the personnel at Seiler for their helpfulness, particularly Lisa Cooke and Norm Heimer for aid in overcoming the vagaries of the HPLC, Fred Kibler for sharing his skill in glass-blowing, and Missy Landess for her efficient typing. Thanks are due to Jon Swanson for suggesting this challenging project.

References

1. Shackelford, S. A., J. W. Beckmann, and J. S. Wilkes, "Deuterium Isotope Effects in the Thermochemical Decomposition of Liquid 2,4,6-Trinitrotoluene: Application to Mechanistic Studies Using Isothermal Differential Scanning Calorimetry Analysis," Journal of Organic Chemistry, Vol. 42, No. 26, 1977, pp. 4201-4206.
2. Beckmann, J. W., J. S. Wilkes, and R. R. McGuire, "2,4,6-Trinitrotoluene Thermal Decomposition: Kinetic Parameters Determined by the Isothermal Differential Scanning Calorimetry Technique," Thermochemical Acta, Vol 19, 1977, pp. 111-118.
3. Swanson, J. T., L. P. Davis, R. C. Dorey, and W. R. Carper, "An EPR Study of the Thermal Decomposition of Molten 2,4,6-Trinitrotoluene and its Isotopic Analogs," Magnetic Resonance in Chemistry, Vol. 24, 1986, pp. 762-767.
4. Guidry, R. M. and L. P. Davis, "Thermochemical Decomposition of Explosives. I. TNT Kinetic Parameters Determined from ESR Investigations," Thermochemical Acta, Vol. 32, 1979, pp. 1-18.

1987 USAF-UES SUMMER FACULTY RESEARCH PROGRAM

Sponsored by the
AIR FORCE OFFICE OF SCIENTIFIC RESEARCH
Conducted by the
Universal Energy Systems, Inc.
FINAL REPORT

EVALUATING EXPERT SYSTEMS

Prepared by:	James L. Noyes
Academic Rank:	Associate Professor
Department and	Mathematics and Computer Science Department
University:	Wittenberg University
Research Location:	AFWAL/AAI
	Wright-Patterson AFB
	Dayton, OH 45433
USAF Researcher:	Maj. Stephen A. Cross
Date:	28 August 87
Contract No:	F49620-85-C-0013

Evaluating Expert Systems

by

James L. Noyes

ABSTRACT

The evaluation of artificial intelligence (AI) expert systems involves additional considerations over that of conventional software evaluation. Some of these relate to the evaluation of the knowledge base with respect to consistency, completeness and quality of information that is provided by the experts. Other considerations relate to the expert system software itself. This report addresses the traditional software engineering aspects, but focuses upon the issues that relate to expert systems in particular. These issues are identified and discussed. An expert system evaluation strategy is presented to begin with the identification of the software to be evaluated, and to aid in the evaluation.

AD-A191 284

UNITED STATES AIR FORCE SUMMER FACULTY RESEARCH PROGRAM

10/77

(1987) PROGRAM TE (U) UNIVERSAL ENERGY SYSTEMS INC

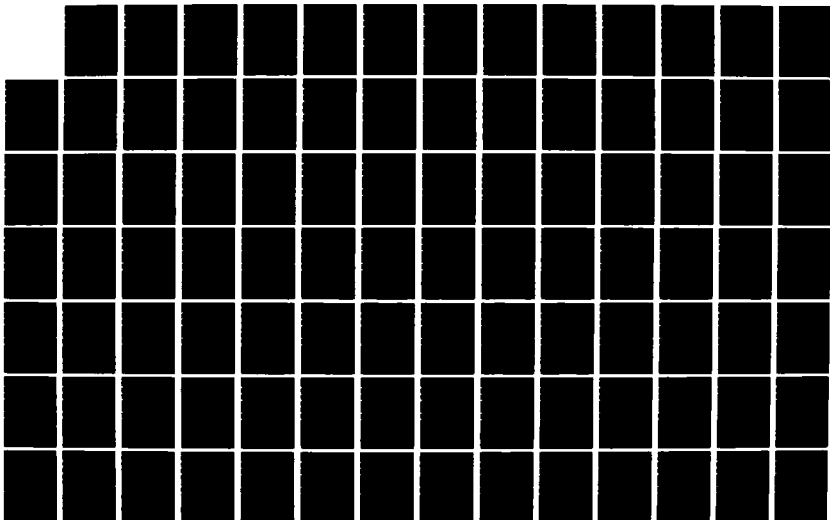
DAYTON OH R C DARRAH ET AL DEC 87 AFOSR-TR-88-0213

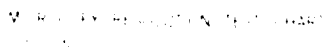
UNCLASSIFIED

F49620-85-C-0013

F/G 5/1

ML





ACKNOWLEDGMENTS

I wish to thank the Air Force Systems Command and the Air Force Office of Scientific Research for their sponsorship of this research. I would also like to thank the Air Force Wright Aeronautical Laboratories (AFWAL) for inviting me as a Summer Research Fellow. The personnel at Universal Energy Systems were also very helpful with all administrative aspects of this program.

Mr. David Kaiser and Maj. Stephen Cross of the Artificial Intelligence Applications Office in the Avionics Laboratory of AFWAL defined the areas for research and provided support and encouragement. Maj. Cross was also instrumental in identifying some specific sources that greatly aided in this research. Cpt. Dale Childs and Lt. James Wilson were very helpful in facilitating the use of the required computing resources. The entire staff of the AFWAL Avionics Laboratory has provided a very enjoyable working atmosphere for these last ten weeks.

I. INTRODUCTION:

This author's research interests are in the area of artificial intelligence (AI) and expert systems. Specifically, recent work has been done in the area that addresses the integration of symbolic and numerical mathematics. This includes the application of AI methodologies, such as those for expert systems, toward the solution of mathematical optimization (mathematical programming) problems as well as the evaluation of those methodologies.

The evaluation of expert system (ES) software used for AI applications is a major issue and is frequently not addressed. While there are some similarities between the evaluation of conventional software and expert systems software, there are several additional issues that must be treated.

Conventional software code is usually written in an imperative language such as Fortran, Pascal, C or Ada. Usually a programmer writes code to perform a specific overall task according to a given set of specifications. The program typically provides many functions that are invoked by a user according to a predictable set of inputs. The outputs are also predictable and in many cases verifiable. One does not normally expect a conventional program to change the way it handles inputs over a period of time. One also does not expect a change in the results for the same input unless a data base is also used and periodic updates are made. While a great number of branch-points may exist, these can be identified in advance by careful examination of the code. These properties all facilitate what is known as a "white-box" testing process when the source code is available. Overall, software verification and validation (V&V) are key issues that are fairly well understood (although not always followed).

Expert systems software code is often written in a non-imperative language such as LISP or Prolog. Sometimes, in order to improve

efficiency or to meet certain language requirements, it is written (or rewritten) in a language such as C or Ada. Alternately the expert system may be developed by using expert systems tools which provide specialized ES language constructs and utilize a pre-written "shell" consisting of everything necessary but the knowledge base. The ES developer supplies this knowledge based upon information derived from the experts in a particular problem domain. Conventional applications start on a much firmer ground and their algorithms in many cases are provable. This is not true of heuristics which may be valid for a variety of cases, but untried for others. These heuristics may be based upon practice, but are seldom subject to rigorous examination. Formal and fixed specifications that are often associated with conventional software do not, in practice, readily apply to AI problems. The conventional problem description is not the same as an intrinsically ill-defined and dynamic problem description associated with many AI applications. Hence for AI systems in general, and expert systems in particular, additional evaluation activities are necessary.

II. OBJECTIVES OF THE RESEARCH EFFORT:

Little is readily available in the way of a total ES evaluation methodology to help the ES developer or end-user in evaluating an expert system. The well-known works on conventional software evaluation methods do not address expert systems. The ES related papers seldom mention evaluation at all and those that do, usually fail to address it with the appropriate emphasis. Even the conventional evaluation procedures are often not rigorously followed (if followed at all). The objectives of this research consisted of the following: (1) To determine what has been done to date in the separate areas of expert systems and software engineering that could aid in the evaluation process. (2) To combine and apply any relevant methodologies toward the development of expert systems evaluation strategies. (3) To

apply some of these strategies toward the evaluation of the NASA developed CLIPS (C Language Intelligent Production System) software. (4) To produce a report summarizing this information, including a generic evaluation plan. The citation to this full report [Noye87], which contains additional details together with a complete set of references and a glossary may be found at the end of this final report.

III. DIFFICULTIES IN EVALUATING EXPERT SYSTEMS:

Expert systems knowledge is made up of facts, assumptions and heuristic relationships (usually in the form of rules). The assumptions upon which facts and rules are based must closely model the realities associated with the domain area. This human expertise can include specialized knowledge, complex skills, expert common sense and intuition. There must be some external method of verifying the reliability of this knowledge.

An inference engine relates the knowledge base to the problem situation entered by the ES end-user. The manner in which these facts and rules are related tries to emulate human intelligence. This is a critical factor. The program must perform the same tasks as are performed by a human expert who listens while a human describes a problem and then uses unique expertise to arrive at a recommended solution.

The user interface displays, prints, plots or transmits the recommended solution in a manner that can be understood by the end-user or can be used by another program. The ES end-users do not have to be knowledge or domain experts, but they must be capable of understanding the recommended solution.

Conventional software malfunctions are usually relatively easy to detect unless the system is extremely large or complex. On the other hand, even small expert systems may produce plausible but

logically invalid conclusions. Even if the conclusions might follow logically, the rules may be improperly selected and hence the conclusion may actually be invalid. To identify these difficulties, something like "bottom-up" testing is required in order to guarantee that certain rules (or relationships) are tested. With conventional programs, one can remove a certain subprogram and write a special "driver" program to test its code. For expert systems, another approach is needed since the knowledge is separated from the code. In fact, rules in the knowledge base may be viewed as external code. Hence the process of ES evaluation is usually considered to have two distinct parts: checking that the knowledge base is correct and insuring that the inference engine can apply this information correctly.

It may be impossible to establish the accuracy of judgments by results alone. A system may be judged to be very poor when measured against reality, but these same judgments may be very good when measured against the conclusions by leading experts in the field using the same information. A lot depends upon how the expert system is to be used.

Overall, for an expert system to function properly, five things are necessary: (1) accurate facts, (2) "good" rules, (3) a correctly operating inference engine, (4) clearly stated recommendations and justifications, (5) efficient execution.

Nearly all the literature that discusses the evaluation of ES software states that it should begin with the system requirements specifications. It should, just as with any conventional software development. However, just as with conventional software, users often acquire it "after the fact." These users may have an even greater need to evaluate it since they may have little or no idea of the underlying philosophy, let alone the implementation methods. Hence their specifications may be written after the fact and even modified, based upon the results of the evaluation. The next section addresses these issues.

IV. REQUIREMENTS SPECIFICATIONS:

A set of ES specifications is needed before evaluation can formally begin. These can be grouped into four categories.

Specifications for the Inference Engine: The specific ES application may dictate the type of control mechanism that is the most effective (such as forward chaining, backward chaining or a combined strategy). For a system to be realistic, certainty factors may be necessary for both facts and rules. Rule processing priorities may be used to govern the order of their firing. There are many other issues here relating to what data structures are used for the information to be effectively (and efficiently) stored and accessed.

Specifications for the Knowledge Base: Researchers in expert systems agree that the emphasis should be on knowledge itself rather than on formal reasoning methods. Knowledge base specifications relate to the required knowledge domain and while it is very difficult to specify exactly all the facts and rules that must be present, it is easier to specify that they be individually verified. Actually, individual facts and rules are normally easier to verify than typical segments of code. However, in combination, the problem becomes far more complex due to gaps and inconsistencies that are more likely to arise in a large knowledge base. It would be very beneficial for the new knowledge to be somehow compared to the current knowledge before it was actually added to the system [Nguy87]. It is important to note, however, that in theory the results obtained when the given facts are applied to the knowledge base can be confirmed independently of the inference engine.

Specifications for the Explanation Subsystem: For any user to have confidence in an ES, it is essential that the user be able to "trace" the reasoning that resulted in a specific conclusion. This is obviously also necessary during any ES evaluation. This

subsystem must correctly report how a conclusion was reached and this must be in agreement with the original logic that the inference engine actually used. This is also necessary for the maintenance process.

Specifications for the User Interface: The specifications for an ES user interface are not much different than for conventional software. The main difference is a higher reliance upon English-like symbolic information to be input and output. The user-friendly interaction is more important for ES applications in the same way that a user-friendly human expert is better to deal with than someone who is not.

V. EVALUATION CRITERIA:

The following seven items constitute basic criteria that can be used to evaluate an expert system [Sell85], [Buch84], [Gasc83]:

1. Consistency. This criterion requires the system to produce similar answers to similar questions. There are no guaranteed tests to do this, only tests that can increase confidence. This type of test is capable only of locating inconsistencies, not of proving consistency. In effect one is trying to ensure that no two rules produce opposing conclusions from the same premises.
2. Completeness. This criterion requires a total coverage of the domain (or a specified subset) by the knowledge base. When this holds, everything derivable from the given data will be derived. Hence, the knowledge base must be sufficiently wide in its coverage to allow the system to address any problem within its domain. There must be a reasonable number and variety of tests to cover the area in a fairly uniform way. Ideally, if one can list all of the input classes and output classes, then one can even automate the test.

3. Soundness. This criterion requires that everything derivable is "true" (in agreement with the expert's judgment). One method to test this is to have the expert(s) who helped build the system prepare a set of test cases and an expected conclusion from each.

4. Precision. This criterion is specific to systems that produce qualified judgments and may be considered as an extension of the requirement for soundness. That is, the certainty factor of the result must be appropriate to the information used. While some use the term precision, accuracy might be a better term (i.e., its not the number of digits in the factor, but rather how close it is to the "true" factor). This in turn is related not only to the heuristic used in the fact and rule combination, but also to the sensitivity of the final result in terms of the data used to conclude it. Sensitivity analysis is used to relate the variability of the conclusions to the variability of the data.

5. Usability. This criterion is the expert systems counterpart to the criterion "user friendly" used in conventional programs. The so-called user interface is a key item here. This can include the ease of use, ability to communicate with other systems or data bases and inclusion of a natural language facility. It includes the ability to allow the end-user to have easy access to explanations for its decisions and to have them customized appropriately. It also includes the ability of the ES to give advice and to educate the user in an appropriate fashion whenever help is required.

6. Efficiency. This criterion may be the most critical, especially if the expert system is embedded within another system or must be used in real-time. A system that requires an excessive time commitment by the users or requires too much time to produce a result, may fail to be accepted even if it ranks high in the other areas. In addition, one must be sure to measure the execution efficiency using a knowledge base of an appropriate size. It is necessary to have a computer which is

large enough and fast enough to solve the actual real-world problem, not just a small prototype.

7. Cost-Effectiveness. This may be the most difficult criterion to achieve since there is still much research going on in the field of expert systems. Even the off-the-shelf systems will likely need to be tailored to specific applications thereby adding an additional cost to the overall system.

It should be noticed from these items that different types of evaluation are implied because different viewpoints are reflected. The end-user is most interested in consultation validity and ease of use. The knowledge engineer is concerned with the knowledge representation facilities and ease of building and checking the knowledge base. The programmer is interested in efficiency and code maintenance issues. Finally, the manager who is responsible for acquiring this system is interested in cost-effectiveness. This implies that a team of individuals from the representative areas should participate in the evaluation if at all possible.

VI. ANALYSIS:

The analysis is designed to indicate how well the aforementioned specifications and associated ES criteria are being met.

Criticality of Output: This deals with the overall impact of failure of the expert system and is a function of the combined knowledge base and ES software complexity. Hence it becomes important to estimate this complexity. Metrics can be used to do this. Further, a distinction can be made between the types of failure, these will be called Type I and II Errors. One involves producing the wrong answer and the other is associated with not providing the right answer.

METRICS. The notion of software metrics (measures) has been utilized in software engineering for a long time. These same metrics can be directly used to aid in the evaluation of ES code implemented in an imperative language. They are harder to apply if a functional or logic-oriented language is used. These metrics have been discussed in several references [Cont86], [Beiz84], [Myer77], [McCa76]. In addition, metrics may also be developed for the evaluation of a knowledge base independent of the inference engine. The purpose of these metrics is to obtain a quantitative complexity measurement. Since the amount of testing is directly related to complexity, these metrics are usually employed to indicate the amount of testing that is needed. They do not by themselves indicate which test cases should be chosen. For that, something else is needed. Several metrics may be directly applied to measure ES code and may be modified to also measure the complexity of a rule base. In the following, only the McCabe metric will be discussed (others are covered in [Noye87]).

The McCabe Cyclomatic Complexity metric $V(G)$ is based upon Graph Theory and is related to the number of decision statements of a conventional program [Cont86], [McCa83], [McCa76]. (Hetzl calls testing related to this metric "basis testing" [Hetz84].) This metric will allow one to determine how many tests are required to obtain a complete structural coverage of a program where every statement is executed at least once and every decision is exercised over all possible outcomes. Note that this is not the same as an exhaustive test sequence which is usually impractical.

The McCabe metric can also be adapted for measuring the complexity of a rule base independently of the ES software. This may be done by examining the antecedents (simple or compound) in each rule and representing them by a corresponding graph. The complexity of the resulting graph is given by: $V(G) = e - n + 2$ where e is the number of directed edges and n is the number of nodes for a given graph G . By examining the complexity of each

rule, one can then determine the number of test cases (fact combinations) that are needed to guarantee that each path is checked at least once. One can also augment this process by writing a program to examine an entire rule base for a given ES in order to determine the following for each fact pattern found in the rules:

- * The total number of times it appears as an antecedent
- * The total number of times it appears as a consequent
- * The total number of rules in which it appears
- * The identifiers for the rules in which it appears

This information, combined with the complexity number of each rule will aid in the selection of the appropriate test cases. The reason for this is that basis testing is a pure white-box method and hence is independent of the functional specification. By examining the above output augmented with a fact-rule matrix presentation or network rule (goal tree) diagrams together with the ES rule specifications, one can determine which test cases are the most important. Notice that this method is independent of the inference engine so it may be used to evaluate any rule base. However, because of this independence, it does not specifically evaluate the inference engine.

TYPE I AND II ERRORS. The notion of Type I and Type II errors comes from hypothesis testing in statistics. Hypothesis testing addresses the question of how to choose among alternative propositions while controlling or minimizing the risks of making the wrong decisions. The essence of this notion can also be applied to expert systems as there is a different "penalty" for each type of error. These are analogous to advising someone not to cross a railroad track when a train is not coming vs. advising them to cross when it is. The first error may cause a delay, but the second error causes a disaster! To prevent these errors, the meaning of the information must be understood.

Interaction Analysis: Some researchers (such as Green and Keyes [Gree87]) describe interaction analysis as assessing the ability of the interacting components of the ES to produce the desired results. Here the components consist of the rules or objects of the knowledge base together with the inference engine. By the nature of this interaction, the processing sequence and results are not easy to predict. To facilitate this prediction, one may use the results obtained from an independent analysis of the knowledge base (without the ES inference engine).

Rule Verification: Because of the complex pattern-matching performed, some researchers believe that exhaustive testing of every possible combination of patterns is the only way to perform a complete V&V of the system. For a rule base of any size and complexity, this approach may not be practical. Hence, a method that utilizes an approach based upon the McCabe metric would be one possible alternative. Another alternative would be to develop or modify a program such as CHECK described by Nguyen [Nguy87]. Here an independent program is used to check the rules associated with either a forward chaining or backward chaining ES control mechanism. This program is reported to check for circular rules, conflicting rules, redundant rules, subsumed rules and more. As a by-product it produces a rule-dependency table so that the interaction of the various rules may be better depicted. Certainty factors may also be accommodated. Some expert systems such as TEIRESIAS and ONCOCIN have a more system dependent rule checking capability [Suwa84]. Also, special tools such as ARC (the ART Rule Checker) are being developed [Nguy87a]. Other more specialized programs are oriented towards evaluating typical application situations. For example, Scambos describes a scenario-based tool called FCCBMP-FRESH to evaluate a specific Force Requirements Expert System for the Pacific Fleet [Scam86].

Fact Verification: Facts are usually easier to verify than rules since they are less subjective than rules and more widely available in published data. The verification largely consists

of checking the facts in the knowledge base against this data or having them evaluated by an independent expert.

Uncertainty Analysis: Both rule and fact verification become more difficult if the expert system utilizes certainty factors. Certainty factors are valuable because they provide a convenient way to express a degree of belief associated with a given fact or rule. In this case, a mechanism is used to combine these factors in a reasonable way. Here one must check for such things as: monotonicity, commutativity, associativity and threshold values. This can be done by applying the standard software engineering precept and constructing special facts and rules to test the mechanism at its "boundary conditions." In addition, whatever type of certainty measure is used, rule combination techniques must also be evaluated in a similar manner. Uncertainty analysis addresses issues of this nature.

Sensitivity Analysis: This may be considered as a variation of numerical analysis applied to expert systems. The question is just how sensitive are the algorithms and heuristics to changes in the data? Is the particular method stable? That is, do small changes in the data (e.g., certainty factors) produce large changes in the resulting recommendations? This isn't as straightforward as dealing with continuously varying real functions defined over a real domain. If certainty factors are used with threshold values, then the results are analogous to those produced by discontinuous functions. If certainty factors are not used at all, then these results are discrete. One way to do this is to execute some representative and important cases without any perturbations in the fact or certainty factors and observe the resulting recommendations. Follow this by various perturbations singly and in combination and observe these results also. This process can be time-consuming, and again points out the need for prioritizing the test cases.

Software Efficiency: Efficiency in conventional software is usually measured in terms of execution time and storage requirements for primary and secondary memory. For expert systems, this can be further refined for measurement purposes. If ES development is involved, then there is an additional evaluation phase involving the efficiency of the ES creation. The most important part, assuming the ES software will be frequently used, is the consultation efficiency. This measurement is the most critical when real-time requirements are to be met. (Note that the number of rules/second processed may not be a good measure since one system may be coded to actually have to process fewer rules than another.) The other main measure is storage efficiency. The memory required for the code to do the ES creation and the ES consultation may both be of interest. Finally, the storage required for the facts and rules is also important. Usually this can be accurately measured, based upon the format and the number of characters used in each. The bottom line is to determine if the expert system can do the required processing within given time and storage constraints.

Maintainability: Expert systems maintainability is also directly dependent upon the amount and complexity of information in the knowledge base. It is advisable to have an automated tool that can be used during the knowledge insertion and modification process that can (independently) assure consistency. This is especially true as the knowledge base grows in size and complexity [Nguy87], [Nguy87a]. Unlike the maintenance of the knowledge base, maintenance of the inference engine would normally much less frequent. With the exception of the ES implementation language considerations, this activity is similar to that of maintaining conventional software. There are important exceptions. For example, LISP allows its code to be self-modifying and if this capability has been employed, it may be impossible to do any realistic verification. Also, it should be remembered that whenever any change is made to the expert system, the library of benchmark test cases should again be run.

VII. RECOMMENDATIONS:

The guidelines for implementing the previously identified evaluation elements can be stated as follows: (1) select the evaluators, (2) identify all the requirements specifications to test, (3) prioritize these for testing (since it will probably be impossible to test them all), (4) formulate the test cases based upon the analysis of the expert system and its specifications, (5) perform the actual tests (keeping in mind that a revised set of priorities may result), (6) document the input, expected output and actual output for each and (7) modify these steps as appropriate during the tests. It is important for all involved to take a positive approach when performing any type of software testing. No evaluation can succeed if participants (e.g., ES developers) are "on the defensive." The remainder of this report will elaborate on the evaluation planning and its execution.

The evaluators should be chosen to include the expertise previously discussed: (a) end-users, (b) a knowledge engineer aided by an expert, (c) programmers, and (d) a manager. With individuals from these four categories, all interests will be represented. These people will prepare the test plan.

Each requirement specification must be tested. The number of tests will depend upon the importance and priority of the requirement. It should also be noted however that some things should be tested that do not necessarily explicitly appear in the requirements. These relate to lower level computer science issues involving the data structures and algorithms (heuristics) used in implementing the expert system. When the benchmark tests are formulated, the following should be kept in mind:

- * Every object (e.g., fact and rule) must be invoked
- * Every possible outcome must be caused
- * Every inference must be correctly explained
- * Every control path must be traversed

- * If certainty factors are used, their boundaries must be tried
- * For mission-critical systems, conditions outside the normal operating limits should be tried

In practice, it may not be possible to do this within the allocated time limits, hence it is necessary to prioritize.

The actual execution of expert systems tests is similar to that of conventional software. The tests are conducted in accordance with the test plan script which dictates the order in which the tests are to be performed together with the test input and expected output. This process may be automated by the use of testing tools. By placing the necessary script information on disk files an automated test "driver" can emulate both the creation and consultation processes through the use of batch mode. This should greatly improve the overall efficiency of the testing process. A log file can then be generated indicating the results of each case together with the corresponding execution time. Automated support is necessary for any realistic ES evaluation and there are some tools available to do this. The CHECK program is used for general knowledge base verification. The design of the ARC program was, in part, based upon experience with CHECK. ARC is used for consistency verification of the production rules for the ART expert system tool. Programs such as CHECK or ARC should be adapted to help evaluate expert systems with similar types of rule bases (e.g., such as CLIPS). Programs like these, augmented by the procedures outlined in this report, should greatly enhance any expert system evaluation.

It should be realized by all parties, that despite the most diligent work by the developers, errors will inevitably occur. Management should convey a positive cooperative spirit that will promote not only better test and evaluation procedures, but solid corrections and improvements in the resulting expert system.

REFERENCES

- Beiz84 Boris Beizer, Software System Testing and Quality Assurance, Van Nostrand Reinhold, New York, NY, 1984.
- Buch84 Bruce G. Buchanan and Edward H. Shortliffe, Ed.s, Rule-Based Expert Systems: The MYCIN Experiments of the Stanford Heuristic Programming Project, Addison-Wesley, Reading, MA, 1984.
- Cont86 Samuel D. Conte, H. E. Dunsmore and V. Y. Shen, Software Engineering Metrics and Models, Benjamin/Cummings, Menlo Park, CA, 1986.
- Gasc83 John Gaschnig, Philip Klahr, Harry Pople, Edward Shortliffe and Allan Terry, "Evaluation of Expert Systems: Issues and Case Studies," Building Expert Systems, Frederick Hayes-Roth, et.al., Ed.s, Addison-Wesley, Reading, MA, 1983.
- Gree87 Christopher J. R. Green and Marlene M. Keyes, "Verification and Validation of Expert Systems," IEEE WESTEX-87 Proceedings, Anaheim CA, Jun 3-5, 1987.
- Hetz84 William Hetzel, The Complete Guide to Software Testing, QED Information Sciences, Inc., Wellesley, MA, 1984.
- McCa83 Thomas J. McCabe, Ed., Structured Testing, IEEE Computer Society, Piscataway, NJ, 1983.

- McCa76 Thomas J. McCabe, "A Complexity Measure," IEEE Transactions on Software Engineering, Vol. SE-2, pp. 308-320, Dec. 1976. (Reprinted in [McCa83], pp. 3-15.)
- Myer77 Glenford J. Myers, "An Extension to the Cyclomatic Measure of Program Complexity," ACM SIGPLAN Notices, pp. 61-64, Oct. 1977. (Reprinted in [McCa83], pp. 98-100.)
- Nguy87 Tin A. Nguyen, Walton A. Perkins, Thomas J. Laffey and Deanne Pecora, "Knowledge Base Verification," AI Magazine, Vol. 8, No. 2., pp. 69-75, Summer 1987.
- Nguy87a Tin A. Nguyen, "Verifying Consistency of Production Systems," Proceedings on The Third Conference on Artificial Intelligence Applications, IEEE Computer Society Press, pp. 4-8, Feb. 23-27, 1987.
- Noye87 James L. Noyes, Considerations in Evaluating Expert Systems, Sponsored by AFOSR Contract F49620-85-C-0013, Aug. 1987. (This report is available from AFWAL/AAI, WPAFB, OH 45433)
- Scam86 Ernest T. Scambos, "A Scenario-Based Test Tool for Examining Expert Systems," Proceedings of the 1986 IEEE International Conference on Systems, Man and Cybernetics, pp. 131-135, 1986.
- Sell85 Peter S. Sell, Expert Systems: A Practical Introduction, Halstead Press (Wiley), New York, NY, 1985.
- Suwa84 Motoi Suwa, A. Carlisle Scott and Edward H. Shortliffe, "Completeness and Consistency in a Rule-Based System," Rule-Based Expert Systems, B. G. Buchanan and E. H. Shortliffe, Ed.s, Addison-Wesley, Reading, MA, 1984.

1987 USAF-UES SUMMER FACULTY RESEARCH PROGRAM/

GRADUATE STUDENT SUMMER SUPPORT PROGRAM

Sponsored by the

AIR FORCE OFFICE OF SCIENTIFIC RESEARCH

Conducted by the

Universal Energy Systems, Inc.

FINAL REPORT

Prepared by:	Noel S. Nussbaum, Ph.D.
Academic Rank:	Associate Professor
Department and	Physiology and Biophysics
University:	Wright State University
Research Location:	Armstrong Aeromedical Research Laboratory Biodynamics and Bioengineering Division, Biodynamics Effects Branch, Wright-Patterson Air Force Base, Ohio
USAF Researcher:	Leon Kazarian, Dr. Ing
Date:	29 September 87
Contract No:	F49620-85-C-0013

Isolation of Osteoprogenitor Cells
from the Trauma-Activated Periosteum

by

Noel S. Nussbaum

ABSTRACT

Closed green-stick rib fractures were produced, by manual pressure, in anaesthetized white New Zealand male rabbits. After 5 days of healing, the enlarged periosteum of the fracture site was collected and subdivided, by sequential collagenase-trypsin digestion, into primary cell cultures. Semi-defined media (BGJ_b, Gibco) supplemented with hydrocortisone and insulin, was used to maintain these non-transformed cells for up to three weeks. Similar cultures were prepared from embryonic chick calvariae. Alkaline phosphatase and glycosaminoglycan secretion into the media was monitored and comparison of data derived from the two species supports the osteogenic identity of the cells isolated from the rabbit periosteum.

ACKNOWLEDGEMENTS

The support of the Air Force Systems Command and the Air Force Office of Scientific Research is gratefully acknowledged. This work could not have been initiated without the interest and intellectual support of Leon Kazarian, Chief, Biodynamics Effects Branch, Armstrong Aerospace Medical Research Laboratory, whose continuing encouragement was always appreciated. The assistance of Pat Roberts and Marvin Souder in coordinating this project with Air Force procedures was of value to its successful completion.

I would like to express my thanks to Maj. J.R. Cooper, Veterinary Services Division, Armstrong Aerospace Medical Research Laboratory, for his assistance in animal acquisition and coordination of support services.

Finally, I acknowledge the valuable technical assistance of Robyn (Butcher) Miller and Jeaninne Lincoln, who performed their laboratory functions with care and speed.

I. INTRODUCTION

Skeletal integrity is maintained by the continuous remodeling of bone, identified by an orderly sequence of events. This sequence is characterized by osteoclastic activation and concludes with osteoblastic production of new bone replacing the resorption lacunae left by osteoclastic action. Bone resorption and new bone formation are closely linked or coupled chronologically and spatially. This process of bone remodeling occurs in discrete units throughout the skeleton at any one time, and current evidence suggests that it is primarily under the control of local factors. Immune cells (lymphocytes and monocytes) appear to be a likely source of the local factors regulating this process (Baron et al., 1983).

One of the functions of the remodeling process is to accomplish repair of micro-fractures accumulating as a result of mechanical stress. The cellular response to micro-injury thus affects the micro-architecture in accordance with Wolf's principle. The details of local control are currently being investigated as examples of the biologic action of a variety of peptide growth factors (Canalis, 1985).

Injury induced healing represents, in part, an accelerated local sequence of events that duplicate many of the specific cellular responses believed operational in normal remodeling. The origin of osteoclasts from reticuloendothelial precursors is now well accepted, but the mesenchymal origins of the osteoblast are still impossible to identify. The size of the mesenchymal cell pool and the rate of cell differentiation combine to determine the condition of bone. Replication of mesenchymal cells is required to replace those lost by injury and

differentiation. Mesenchymal cell replication is essential for skeletal survival and the process is probably a target site for bone active hormones and locally produced paracrine and autocrine factors.

The Biodynamics Effects Branch, AAMRL, has long been involved in basic research efforts directed at determining the nature of bone remodeling control. This work is in conjunction with the role of the Branch in investigating the influences of vibration acceleration, and impact forces and hypokinesia on skeletal integrity. Therefore basic cellular level information relating osteogenic function to physiological control is of direct concern to this effort.

I have been conducting research on skeletal tissue function for the past twenty years. Most recently I have been involved in an effort to establish primary cell cultures from embryonic cartilage and bone, in order to investigate ion transport functions of osteogenic cell membranes. These interests led to my interaction with the Biodynamic Effects Branch and my assignment to this program.

II. OBJECTIVES OF THE RESEARCH EFFORT:

Trauma initiated fracture healing is a model system that has been used to define the microscopic events associated with localized bone repair (Ham and Harris, 1971). The complexity, however, of even this local response, prevents anything other than the morphological aspects of the process, from being investigated in vivo. Accordingly, it was proposed that the activated periosteum, characteristic of the fifth day rib-fracture in the rabbit, be examined in vitro for its osteoblast

potential. The ability to establish a non-transformed cell population derived from such non-embryonic sources, would offer a unique opportunity to examine cellular responses to bone active agents.

The specific objectives for this 1987 Summer Faculty Research Program (SFRP) were: 1) to establish the methodology for the isolation and characterization of osteoprogenitor cells from the mature trauma-activated periosteum and 2) to compare the methods developed with those described for the isolation of similar cell populations derived from embryonic sources.

It was determined that a viable series of primary cell cultures could be prepared from material isolated from the fracture site of adult male rabbits. It was also determined that with respect to two indicator functions e.g., alkaline phosphatase activity and glycosaminoglycan secretion, the rabbit derived cells behaved similarly to embryonic bone cells after five days in vitro.

III. MATERIALS AND METHODS

Male White New Zealand rabbits (4-6 kg) were anesthetized with Ketamine (150 mg, I.M.) and Pentobarbital (32 mg, I.V.). Under anesthesia, two separate rib fractures (ribs 6 & 7) were produced by finger pressure. The animals were allowed to recover and observed for five days for signs of distress or pain. After five days, the animals were again anesthetized with Ketamine and Pentobarbital. The fracture site and contralateral control tissue was collected aseptically and placed in ice-cold, sterile Phosphate Buffered Saline (PBS). The animals were terminated with 0.5 ml of T-61. A total of 3 animals were used to establish fracture sites for tissue collection.

Calvaria were collected from 20 day chick embryos (Carey Farms, Inc., Marion, OH) and stored in ice-cold sterile PBS. Both rabbit and chick material were mechanically trimmed of non-osseous tissue and the appropriate material, (rabbit periosteum or chick bone) was minced and transferred to digestion chambers. Sequential enzymatic digestion with trypsin and collagenase (Cooper Biomedical) according to Cohn and Wong (1979), was employed to prepare separate cell populations at 20 minute intervals. Each separated population was seeded into a 75 cm² culture flask and 10 ml of media added. All cultures were fed with BGJ_b medium supplemented with 10% Fetal Bovine Serum (FBS) and other factors as indicated. All culture media was supplied by Gibco Laboratories, Grand Island, N.Y., and was supplemented with 200 U/ml Penicillin and 200 µg/ml Streptomycin. In addition, insulin, 0.5 units/ml (Squibb) and hydrocortisone acetate, 0.8 µg/ml (United States Biochemical Corp., Cleveland) were added to the BGJ_b medium as supplements for the first 24 hours in vitro. At the first media change after 24 hours in vitro, hydrocortisone was omitted from the medium.

Embryonic cultures were passaged to confluency by release into Trypsin-EDTA (Sigma) and subsequently split 1:3 for subculture. Each media fraction was collected every 2-3 days when media was replaced. Biochemical assays were performed on each culture flask independently.

Protein determinations were performed after Bradford (1976) with reagents supplied by Bio-Rad (Rockville Centre, N.Y.). Alkaline Phosphatase was measured by the hydrolysis of sodium thymophthalein monophosphate (American Monitor, Indianapolis). Enzyme activity is expressed as units/hr/mg protein. Glycosaminoglycans (GAG) were

measured by the method of Whiteman (1973) as modified by Steinberg et al., (1979). GAG concentration is presented as mg/mg protein. All values have been normalized by subtraction of media blanks.

Assay data from concurrent culture flasks were statistically evaluated by a general linear model (SAS), found not to be different, and combined to represent replicate data for determination of mean \pm S.E. as reported.

IV. RESULTS AND DISCUSSION

a. As a result of animal and supply delays the scope of the research planned for this 1987 SFRP was limited to only two cell culture procedures. One involved rabbit and one chick embryo material. In both procedures viable cells were isolated and seeded in five separate culture flasks. The techniques for the initiation of an activated periosteum were validated since comparable numbers of viable cells could be collected from the ribs of one rabbit as are derived from 4 dozen chick embryos by identical methods (Table 1). Fraction number one, composed of primarily blood cells is routinely discarded.

Table 1. Seed cell numbers in each
enzymatically isolated population ($\times 10^5$)

Fraction	Chick Embryo	Activated	Non-activated
Number	Calvariae	Rabbit Rib	Rabbit Rib
2	2.18	2.61	1.95
3	2.60	1.58	1.17
4	1.80	1.85	0.27
5	0.83	0.68	0.38
6	0.27	0.68	0.24

Starting material for embryonic tissue weighed 1.08 gm, and activated rabbit tissue weighed 510 mg. Thus, twice as many cells were isolated from the activated rabbit periosteum on a wet weight basis, indicative of the relatively high growth potential of this material. Non-activated rabbit rib periosteum was also isolated (320 mg net weight) and subjected to enzymatic digestion. Cell yields by fraction number are presented in Table 1.

Although treated identically, non-activated periosteal derived cells did not survive more than 72 hrs in culture and were discarded. This result alone substantiates the hypothesis that events associated with healing in vivo initiate processes that cause activation of a cell population in the periosteum that insures their subsequent continuous survival in vitro. Thus, non-transformed adult mammalian sources can be exploited for the in vitro study of osteogenesis.

b. Embryonic cell cultures, seeded with approximately 2.0×10^4 cells/ 75 cm^2 achieved confluence after 7 days and were subcultured, so as to produce 8 flasks for subsequent analysis. The remaining flasks were used for morphological studies to verify that cultures remained free of multinucleate cells that could represent osteoclastic or transformed elements.

Rabbit cultures initiated with the same cell densities were much slower in mitotic activity and were still sub-confluent after 19 days. A semi-quantitative measurement estimate based on the 2 mm^2 field diameter of the inverted microscope (10x), enabled daily cell density measurements. A density of 2.5 to 13.5 cells/mm^2 at the end of 19 days in vitro, representing a ten-fold increase in cell number was

reached. This relatively slow growth rate is comparable to that of other non-embryonic cell types and suggests that future work could profitably investigate the influence of media supplemented with defined growth factors. Assay results were therefore expressed in terms of normalized media protein for comparison purposes rather than cell number, since growth rates of the two cell types were so distinct.

c. Biochemical assay data reveal that embryonic cells initially retain differentiated function when transferred to culture flasks as indicated by a high alkaline phosphatase activity level in the medium. As growth of this cell population is initiated, this activity drops, reflecting the conversion of cellular activity to division and a reduction in secretory activity (Fig. 1). The rabbit derived cells show a transient increase in alkaline phosphatase secretion, perhaps indicating the continued influence of prior in vivo function, before also converting to growth directed metabolism. After 10 days in culture, both cell populations show identical alkaline phosphatase secretory activity (Fig. 1). This is circumstantial evidence for the osteogenic identity of the rabbit derived population.

Similar, but less convincing evidence for the tissue identity of these separate cell populations is revealed by the GAG assay data. In part, this ambiguity is due to the alcian-blue dye binding technique used in the assay, which assumes uniform molecular weight GAG ligands for detection. Radioactive sulfate tracer studies would be more precise for this purpose, but were beyond the capability of the research facility available. Nonetheless, congruent values for chick and rabbit cells after 8 days in vitro (Fig. 2) support the osteogenic

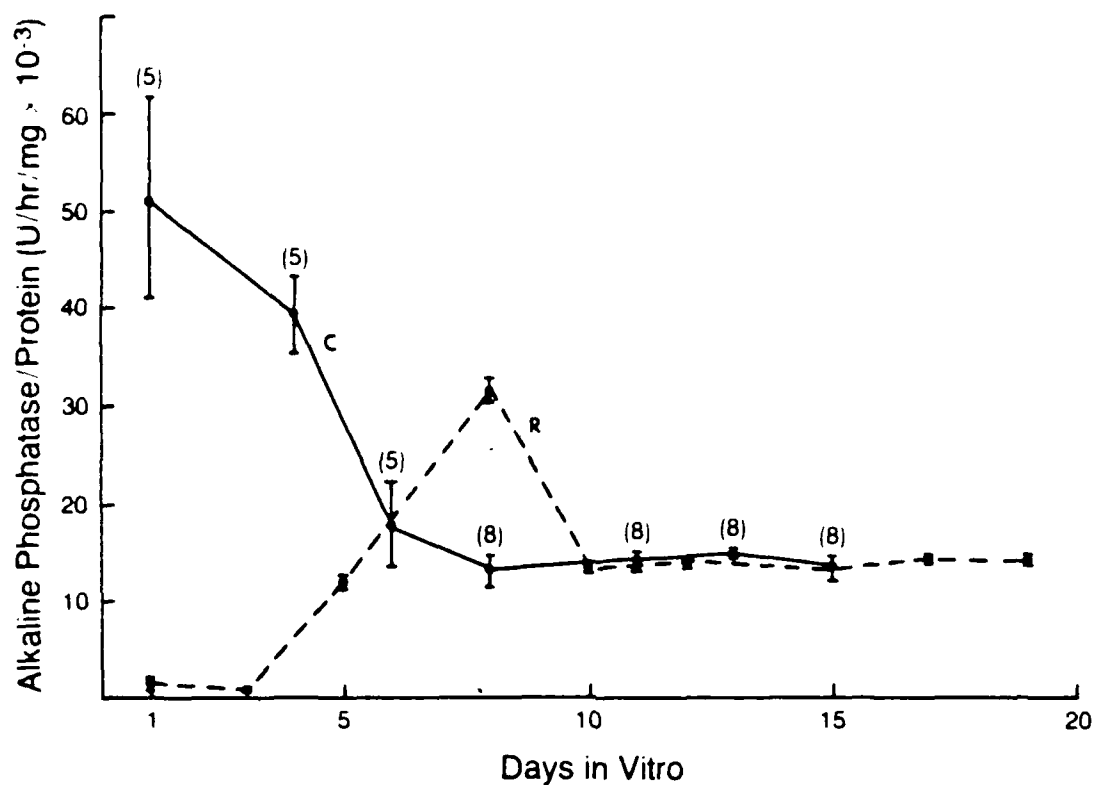


Fig. 1

Alkaline phosphatase activity in media collected during in vitro culture of osteoblastic - like cells. C=chick embryo cells, R=rabbit periosteum derived cells. For rabbit cultures 5 replicates were measured on each collection day. Chick replicates are indicated in parentheses. Mean \pm S.E.

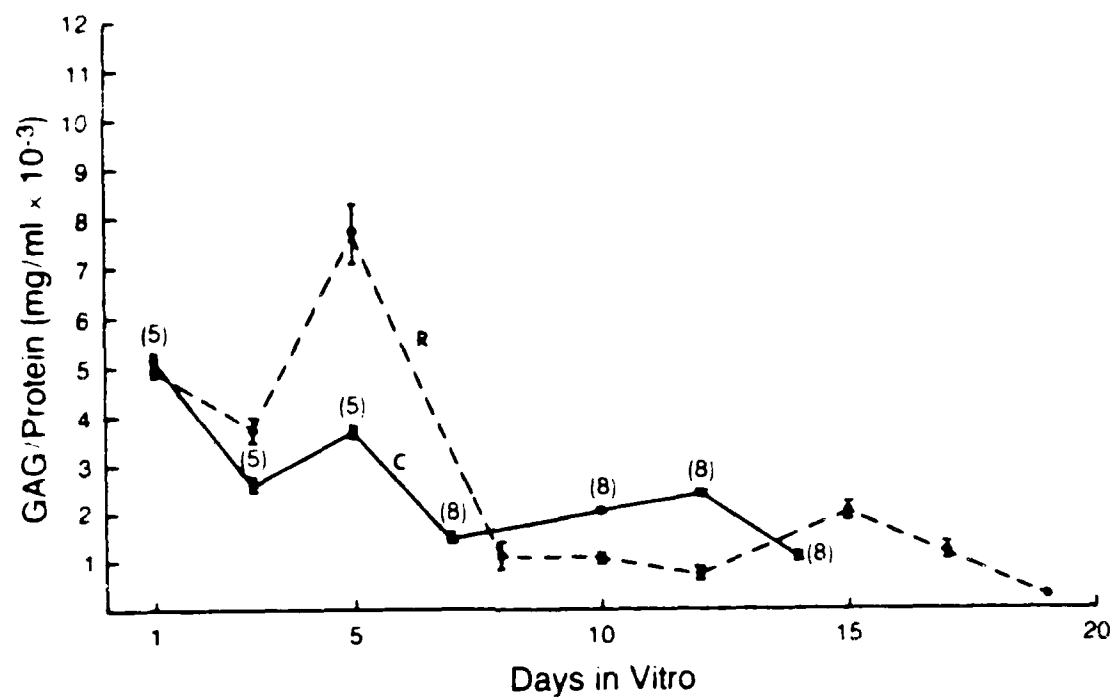


Fig. 2

Glycosaminoglycan concentration in media collected during in vitro culture of osteoblastic - like cells. Symbols as in Fig 1.

tissue identity of these cultures. In both assay techniques, the respectable S.E. values indicate the reliability and internal consistency of the methods.

V. RECOMMENDATIONS

a. The trauma-activated rabbit rib periosteum has been shown to be a useful model for the collection of osteoblastic, non-transformed cells of mammalian origin. This research potential should be exploited, in view of the current interest in metabolic bone disorders, and the relative lack of information on these problems, derived from relevant cell systems. Only one in vivo healing period was tested in this study. It is possible that longer or shorter times may yield larger viable cell numbers; this should be determined.

b. Additional effort should be made to duplicate in vitro the presumed activation process that occurs in vivo by the supplementation of fully defined BGJ_b media with purified growth factors. Platelet derived growth factor (PDGF) and insulin-like growth factor or Somatomedin C have been shown by others to be effective physiological regulators in similar systems (Canalis, 1985; Ross et al, 1986; Mundy, 1987). These agents are now commercially available in highly purified form as a result of recombinant DNA technology.

c. Additional characterization of the cell populations derived from the periosteum could be accomplished by analysis of collagen and non-collagenous protein synthesis and an improved GAG assay system based on radioactive SO_4^{2-} tracer studies.

d. Functional aspects of mono-layer sheets of cells, representing

a simulation of in vivo conditions could be performed utilizing nitrocellulose membrane limited growth chambers (Millipore). Flux experiments measuring Ca^{45} transport through such monolayers would establish base line data for studies involving the examination of Ca^{++} transport regulation.

e. Finally, I must comment on the one negative element in the 1987 program. Standard Air Force procurement policies introduce a four-month delay in the acquisition of expendable supplies. The date of award announcement is too late for the laboratory supporting the research program to assemble necessary supplies in time for adequate work to be accomplished before the end of the award period. The work presented in this report was accomplished only with some difficulty and uncertainty of continuance. I would recommend an accelerated announcement, review and award schedule so as to allow the timely acquisition of supplies or the inclusion of a supply budget, administered by UES, for purchasing purposes.

In all other respects I found the administration of the program by UES satisfactory.

VI. REFERENCES

- Baron, R., Vignery, A., Horowitz, M. 1983. In: Bone and Mineral Research. Vol. 2. Peck, W.A. (ed). Elsevier, pp. 175-242.
- Bradford, M. 1976. A rapid and sensitive method for the quantitation of microgram quantities of protein utilizing the principle of protein - dye binding. Anal. Biochem. 72:248.
- Canalis, E. 1985. Effect of growth factors on bone cell replication and differentiation. Clin. Orthop. 193:246-263.

- Cohn, D.V. and Wong, G.L. 1979. Isolated bone cells. In: Skeletal Research. Vol. 1, Simmons, D.J. and Kunin, A.S. (eds). Academic Press, pp. 3-20.
- Ham, A.W. and Harris, W.R. 1971. Repair and Transplantation of Bone. In: The Biochemistry and Physiology of Bone. Vol. 3. Academic Press. pp. 337-399.
- Mundy, G.R. 1987. Personal communication; Workshop, Annual Meeting of the Society for Bone and Mineral Research, Indianapolis.
- Ross, R., Raines, E.W. and Bowen-Pope, D.F. 1986. The biology of platelet-derived growth factor. Cell 46:155-169.
- Steinberg, J., Sledge, C.B., Noble, J. and Stirrat, C.R. 1979. A tissue-culture model of cartilage breakdown in Rheumatoid Arthritis. Biochem. J. 180:403-412.
- Whiteman, P. 1973. The quantitative measurement of Alcian blue-glycosamino-glycan complexes. Biochem. J. 131:343-350.

1987 USAF-UES SUMMER FACULTY RESEARCH PROGRAM/
GRADUATE STUDENT SUMMER SUPPORT PROGRAM

Sponsored by the
AIR FORCE OFFICE OF SCIENTIFIC RESEARCH

Conducted by the
Universal Energy Systems, Inc.

FINAL REPORT

Assessing the Attributes of Expert Judgment:
Measuring Bias in Subjective Uncertainty Estimates

Prepared by:	Thomas E. Nygren, Ph.D.
Academic Rank:	Associate Professor of Quantitative Psychology
Department and University	Department of Psychology The Ohio State University
Research Location:	AAMRL Wright-Patterson AFB, Ohio
USAF Researcher:	Gary B. Reid
Date:	August 26, 1987
Contract No:	F49620-85-C-0013

Assessing the Attributes of Expert Judgment:
Measuring Bias in Subjective Uncertainty Estimates

by

Thomas E. Nygren

ABSTRACT

It is argued that if our goal is to train individuals to become expert decision makers, regardless of the context of the judgment, it is of paramount importance to understand how non-experts and experts represent uncertainties as subjective probabilities. This paper reports the results of a study that examined the role of the subjective probability function in models of human decision making. Specifically, the study examined the possibility of a dual probability function model similar to that formally proposed by Luce and Narens (1985) and introduced for attractiveness ratings of gambles by Nygren (1981). Results of the study indicated that when subjects were asked to make judgments about risky alternatives, there was a significant trend to give a different estimate or weight to the same probability value in a choice situation when it was associated with the less attractive outcome than when associated with the more attractive outcome. The implications of these biasing effects are discussed in relation to (a) situations where "good" and "bad" outcomes can differentially affect judged probabilities or probability weights and to (b) the study of expert judgment.

Acknowledgments

I wish to thank the Air Force Office of Scientific Research and the Harry G. Armstrong Aeromedical Research Laboratory for sponsoring this research. In particular, I wish to thank Gary B. Reid for his support and concern for this project, and for discussions that led to this productive research effort.

I. INTRODUCTION:

In an age where decisions like those faced by trained Air Force pilots flying new and sophisticated aircraft are becoming more complex and demanding of many cognitive processes, we are relying on these individuals to be more like "experts" in their decision making judgments. However, the decision making literature is full of studies that show how human decision makers choose suboptimal alternatives in decision situations involving uncertainty. It is important, therefore, to understand the mechanism by which we may ultimately be able to efficiently train individuals to become expert decision makers and to exhibit the expertise that their work effort increasingly demands of them.

Related to this effort of understanding how one becomes an expert decision maker is the program of developing expert systems for aiding in the decision making process. An expert system is a complex procedure, usually set in the framework of a computer based program, that has been designed by knowledge engineers (i.e., experts) to solve problems in a specific knowledge domain that cannot be reduced to quantitative formulae. Clearly, these two efforts, the study of expert decision making and the development of expert systems, must be ultimately tied closely together. Both, however, are relatively young areas of research, and as yet few research efforts have tried to bring them together. The Human Engineering Division of the Harry G. Armstrong Aeromedical Research Laboratory has recognized the need for both kinds of efforts and has begun to support both. My summer

research was proposed as an effort to begin to generate questions and ideas to tie human expert judgment and expert systems together.

My research interests can be generally described as two-fold. First, I have been doing theoretical work to develop and enhance different subjective scaling methodologies including multidimensional and conjoint scaling procedures. During the past several years I have begun to expand this interest to a particular applied area of research, the measurement of perceived mental workload. This work has led to a joint effort with personnel at the Harry G. Armstrong Aeromedical Research Laboratory in developing the Subjective Workload Assessment Technique (SWAT), a conjoint measurement approach to the measurement of mental workload. My second area of research interest is judgment and decision making, particularly decision making under uncertainty or risk. My interaction with the scientists at AAMRL has led to the extension of my work in this area to applications that have very important implications for Air Force personnel, and in particular pilots. This is the area of expert judgment and expert systems.

II. OBJECTIVES OF THE RESEARCH EFFORT:

Nowhere has the field of judgment and decision making research expanded more quickly than in the area of expert judgment and expert systems. Moreover the field is visibly multidisciplinary. Recent papers in the decision making literature reflect the increased interest in the study of expert decision making in medical, political, engineering, human factors, chemical, nuclear, business, and military

settings among others. As today's society grows more specialized and complex, so do the vital decisions that must be made by individuals or groups. In addition, with the great advances in the computer science field over the past two decades, we have come to rely on more sophisticated tools to aid people such as pilots in their decision making tasks. Despite the availability of these tools, we still know little about what defines expertise in expert judgment.

There are at least four major problems in research efforts on expert decision making. They are that (a) human experts are limited in their capacities to process all relevant information, (b) it is expensive to train individuals to obtain the level of expertise that is sometimes demanded, (c) experts sometimes disagree and give conflicting judgments, and (d) experts sometimes make mistakes because of inherent cognitive biases about the uncertainty or likelihood of outcomes associated with decision alternatives. Clearly, the study of experts and expert judgment must incorporate each of these issues if we are to establish what makes for a good expert.

It is argued here that a critical dimension of expertise in any judgment situation is the ability to measure or evaluate uncertainties of events without bias or distortion. We make three assertions about these uncertainties. First, all uncertainties are inherently of the same kind. Second, probabilities are useful entities with which to numerically measure uncertainties of events. And, third, probabilities are personal beliefs about uncertain events. That the understanding of uncertainties is central to expert decision making is

clear, since by definition decision making under risk focuses on situations where outcomes are not certain. If these outcomes were associated with clearly determined events, then we would not be developing an expert system but rather a straightforward computer or mathematical algorithm (although, most likely a complex computer algorithm) that would lead to a choice alternative that is always "best" and has no risk or uncertainty associated with it.

My goal as a participant in the Summer Faculty Research Program was to begin to examine the questions of (a) "how do we, both experts and non-experts, relate uncertainties as measured by personal probabilities to our observations of events?", (b) "how should we (or experts whom we must rely on) relate uncertainties to our observations of events so that biases are minimized?", and (c) "what biases exist in our judgments of uncertainties?"

III. A Basis for the Research - The Dual Bilinear Model:

Perhaps the most widely studied current theory of human decision making is Kahneman and Tversky's (1979) prospect theory. The theory proposes that the decision process is completed in two phases. First, the potential prospects or choice alternatives are "framed" for the choice process. This framing often may constitute a preliminary look at the outcomes and this look sometimes results in a simplified and biased representation of the choice alternatives, particularly if the alternatives are complex. Following this initial phase, the prospects are actually evaluated in a manner similar to that suggested by

Subjective Expected Utility (SEU) theory, where the alternative with the highest value (utility) is chosen. The subjective values associated with the outcomes are assumed to be multiplied by decision weights, which are not probabilities, but are monotonic with probabilities. However, the model is a simple bisymmetric model; and hence, it cannot account for an effect found by Nygren and Isen (1985) that suggests differential weighting of an event's probability in winning versus losing or "good" versus "bad" contexts. That is, the model does not allow for the possibility that a decision maker might weight or even evaluate the same probability differently, particularly one that is not explicitly defined, depending on the outcome with which it is associated. Luce and Narens (1985) have presented an alternative representation for utility that would allow for such differential weighting. Their model encompasses the model underlying prospect theory, although it accounts for problematic data by allowing for two subjective probability or weight functions. Luce and Narens (1985) refer to their model as a dual bilinear utility representation where

$$\begin{aligned}
 U(\underline{x} \circ_A \underline{y}) &= U(\underline{x}) * S^+(A) + U(\underline{y}) * [1 - S^+(A)] && \text{if } \underline{x} > \underline{y} \\
 &= U(\underline{x}) && \text{if } \underline{x} \sim \underline{y}, \text{ and} \\
 &= U(\underline{x}) * S^-(A) + U(\underline{y}) * [1 - S^-(A)] && \text{if } \underline{x} < \underline{y}.
 \end{aligned} \tag{1}$$

S^+ and S^- are functions from a set of events \underline{E} into the real interval $(0,1)$ and $U(\underline{x} \circ_A \underline{y})$ is the utility value associated with the risky alternative in which outcome \underline{x} occurs with the probability associated with the event A , otherwise \underline{y} occurs. In the model there are no

constraints on how S^+ and S^- relate to one another or even if they act like probabilities. In order for this model to reduce to the familiar SEU model, S^+ and S^- must be identical.

The major effort of the summer program, then, was to complete an experiment to test the hypothesis that a dual probability process is operational in decision makers. That is, I designed the study to test the hypothesis that non-expert decision makers would make judgments about situations that reflected uncertainty in a nonoptimal manner. Specifically, based on results found by Nygren and Isen (1985), subjects were expected to make preference decisions between pairs of choice alternatives that reflected the assignment of different subjective probabilities to the same event depending on whether the associated outcomes were perceived as being "good" or "bad". It was proposed that two probability functions would be estimated, with distinctly different values assigned to uncertainties associated with good and bad outcomes. A modification of a procedure that was developed by Davidson, Suppes, and Siegel (1957) allowed for a straight-forward, quantitatively-based methodology for estimating these subjective probability functions.

IV. THE EMPIRICAL STUDY:

One hundred and eighteen students at The Ohio State University volunteered to participate in this study in partial fulfillment of the requirements of their introductory psychology course. Subjects were individually seated in front of a computer terminal and were initially

instructed that they would be asked to make choices between pairs of gambles. After they had indicated all of their preferences, the choice situations were randomly sampled and played. Each subject was given 20 poker chips, representing his or her credit for participating and was told that she would be gambling with this credit in the randomly selected gambles. At this point, all subjects were given the opportunity to withdraw from the study without penalty; none did so.

The modification of the procedure used originally by Davidson et al. (1957) to measure utility involved determining the indifference point in sequences of pairs of gambles in order to estimate the subjective utility associated with various outcomes. On each trial, subjects were presented with two two-outcome gambles and were asked to indicate which of two they preferred. The two-outcome gambles were set up as follows: Subjects were told that in each gamble, one outcome would be obtained if the event E occurred and the other outcome would be obtained if the event E did not occur. The event E was never specified, but subjects were informed that it had a true probability of one-half. Pilot data indicated that such instructions produced no bias between these two alternatives of E and not E; subjects indeed weighted the two events equally. On each trial, one gamble had both outcomes fixed and the other gamble had one outcome that was fixed and one that was varied. For each of 14 series of trials, the subject was asked to compare the fixed gamble with the other that was modified each time by changing the variable outcome. The subjects' task on each trial was simply to indicate which gamble they preferred. If the gamble with the variable outcome was less attractive, the variable

outcome was modified to make it slightly more attractive; if this gamble were the more attractive gamble, the variable outcome was modified to make it slightly less attractive. In this way, the variable gamble was modified in a series of steps until the subject indicated that the two gambles were equally attractive. The subjects were then presented with the next gamble in the series of 14. Since events E and $\text{not } E$ had probabilities fixed at .5 and the events were weighted by the subjects as equivalent in probability, we could determine subjective utilities by noting the point at which subjects indicated equality (i.e., the indifference point) between the fixed and variable gambles. That is, we noted the number of points that were assigned to the variable outcome when the subjects reached indifference or subjective equality.

The sequence of pairs of gambles used in this study is presented in Table 1. For example, in the first situation, the subject was faced with one gamble for which she would lose ten points if E occurred and would lose ten points if E did not occur. This, then, was a sure-loss gamble. The alternative gamble in the pair was described as resulting in a loss of A points if E occurred and a gain of ten points if E did not occur. The number of points associated with A was varied in order to find the point at which the subject was indifferent between the gambles $(-10, -10)$ and $(-A, +10)$. In this process we were finding the estimate of the point value of $-A$, the point at which the two gambles in the first series were determined empirically to be equivalent. We assigned a utility of +1 to +10 points and a utility of -1 to -10 points. Then after $-A$ was found, we determined the utility value for

Table 1. Construction Sequence for the Fourteen Trials

Trial	Gamble 1		Gamble 2		Utility	Mean	
	Amt	Prob	Amt	Prob	Value	Points	
A L L	1	-10 (.5)	-10 (.5)	- <u>A</u> (.5)	+10 (.5)	-3	-17.3
	2	+10 (.5)	+10 (.5)	-10 (.5)	+ <u>B</u> (.5)	+3	22.8
	3	-10 (.5)	+ <u>B</u> (.5)	- <u>A</u> (.5)	+ <u>C</u> (.5)	+5	46.3
	4	- <u>A</u> (.5)	+10 (.5)	- <u>D</u> (.5)	+ <u>B</u> (.5)	-5	-32.3
	5	- <u>D</u> (.5)	+ <u>B</u> (.5)	- <u>E</u> (.5)	+ <u>C</u> (.5)	-7	-54.0
	6	- <u>A</u> (.5)	+ <u>C</u> (.5)	- <u>D</u> (.5)	+ <u>F</u> (.5)	+7	79.1
	7	- <u>D</u> (.5)	+ <u>F</u> (.5)	- <u>D</u> (.5)	+ <u>G</u> (.5)	+9	122.5
	8	- <u>E</u> (.5)	+ <u>C</u> (.5)	- <u>H</u> (.5)	+ <u>F</u> (.5)	-9	-85.1
G R O U P 1	9	- <u>H</u> (.2)	+ <u>F</u> (.8)	- <u>E</u> (.5)	+ <u>I</u> (.5)		*
10	+10 (.9)	+ <u>C</u> (.1)	-10 (.5)	+ <u>J</u> (.5)		*	
11	- <u>D</u> (.4)	+ <u>B</u> (.6)	- <u>E</u> (.5)	+ <u>K</u> (.5)		*	
12	- <u>D</u> (.2)	+10 (.8)	- <u>E</u> (.5)	+ <u>L</u> (.5)		59.6	
13	- <u>A</u> (.9)	+ <u>G</u> (.1)	-10 (.5)	+ <u>M</u> (.5)		26.3	
14	- <u>H</u> (.4)	+ <u>F</u> (.6)	- <u>E</u> (.5)	+ <u>N</u> (.5)		68.7	
G R O U P 2	9	- <u>A</u> (.6)	+ <u>C</u> (.4)	- <u>D</u> (.5)	+ <u>I</u> (.5)		*
	10	+10 (.8)	+ <u>C</u> (.2)	- <u>A</u> (.5)	+ <u>J</u> (.5)		*
	11	- <u>H</u> (.1)	+ <u>B</u> (.9)	- <u>E</u> (.5)	+ <u>K</u> (.5)		*
	12	- <u>E</u> (.6)	+ <u>G</u> (.4)	- <u>D</u> (.5)	+ <u>L</u> (.5)		68.1
	13	- <u>D</u> (.8)	+ <u>G</u> (.2)	- <u>A</u> (.5)	+ <u>M</u> (.5)		23.3
	14	- <u>H</u> (.1)	+ <u>B</u> (.9)	-10 (.5)	+ <u>N</u> (.5)		24.9

Note: Letters A - N are the point values being varied and estimated.

$-A$ (which now corresponds to an empirically determined number of points), by substituting in the formula in Equation 1

$$S[.5] * (-1) + S[.5] * (-1) = S[.5] * (+1) + S[.5] * U(-A) \quad (2)$$

making $U(-A) = -3$. That is, $-A$ corresponds to a utility of -3 and we are able to determine for our subjects, how many points (i.e., how great a loss) would be associated with a utility of -3. In a manner comparable to that for Trial 1 in Table 1, a value for $+B$ could be found next, yielding the number of points that are associated with a utility of +3. These utilities of $-A$ and $+B$ were then used in situations 3 through 14 to determine other points on the subjective utility scale.

As shown in Table 1, beginning with Trial 9 one of the gambles in the pair had probabilities other than .5 and .5. For approximately one-half ($n=57$) of the subjects the probabilities associated with winning and losing were (.6,.4), (.8,.2), or (.1,.9) for two of the gambles; for the other group of subjects ($n=61$) the probabilities were just the opposite (.4,.6), (.2,.8), or (.9,.1). In this way each of the probabilities .1, .2, .4, .6, .8, and .9 were associated with winning and with losing on two independent trials. In each case Trials 9-11 were used only as practice and data from these trials were ignored.

The last column in Table 1 presents the mean point values associated with the utilities found on the first eight trials. Once the mean values from these eight trials were obtained, they could be used to

estimate a utility curve for the group data. The best-fitting curve through these points is shown in Figure 1. The curve is based on a polynomial regression analysis using the general linear model procedure (GLM) in SAS. The entire curve was best approximated by the cubic equation

$$\text{POINTS} = 6.159 * U + 0.241 * U^2 + 0.067 * U^3 \quad (3)$$

with an R^2 value of .544. Given this cubic equation, the utility values for the mean point estimates in Trial 12-14 were found for each of the two groups. Once these estimates were obtained they could be used in Equation 1 to solve for two unknowns (the subjective probability estimates) for each group. Table 2 presents the probability estimates that were obtained for the winning and losing events from Trials 12-14.

Table 2
Estimates of Winning and Losing Probabilities

Actual	Prob W	Prob L	Diff
.10	.350	.156	.194
.20	.360	.253	.107
.40	.483	.453	.030
.60	.547	.517	.030
.80	.747	.640	.107
.90	.844	.650	.194

Nonlinear regression in SAS was again used to estimate the best-fitting equations through the two sets of probability estimates. Equations 4 and 5 present the best-fitting cubic curves for the losing and winning probabilities, respectively. Figure 2 provides plots of the actual points and the theoretical curves based on this analysis.

$$SP(\text{lose}) = 2.122 * P - 3.689 * P^2 + 2.511 * P^3 \quad (4)$$

$$SP(\text{win}) = 2.756 * P - 4.881 * P^2 + 3.154 * P^3 \quad (5)$$

where SP is the predicted subjective probability value and P is the obtained probability estimate.

The estimates in Table 2 and the graph in Figure 2 indicate a strong biasing effect. The same objectively stated probability values (.1, .2, .4, .6, .8, and .9) when presented to subjects elicit consistently different subjective values or weights in the subjects' decision process. At all six estimated levels of probability (.1, .2, .4, .6, .8, .9), when the two curves are compared, the estimates that were associated with winning outcomes were consistently weighted higher than the corresponding values for losing. This represents a very strong bias that has important implications for decision research. Clearly, we would not want a decision maker to exhibit such differential weighting behavior. When an event has an established probability associated with it, it should be irrelevant whether that event is associated with a "good" or "bad" outcome. Affective state should not influence the decision process.

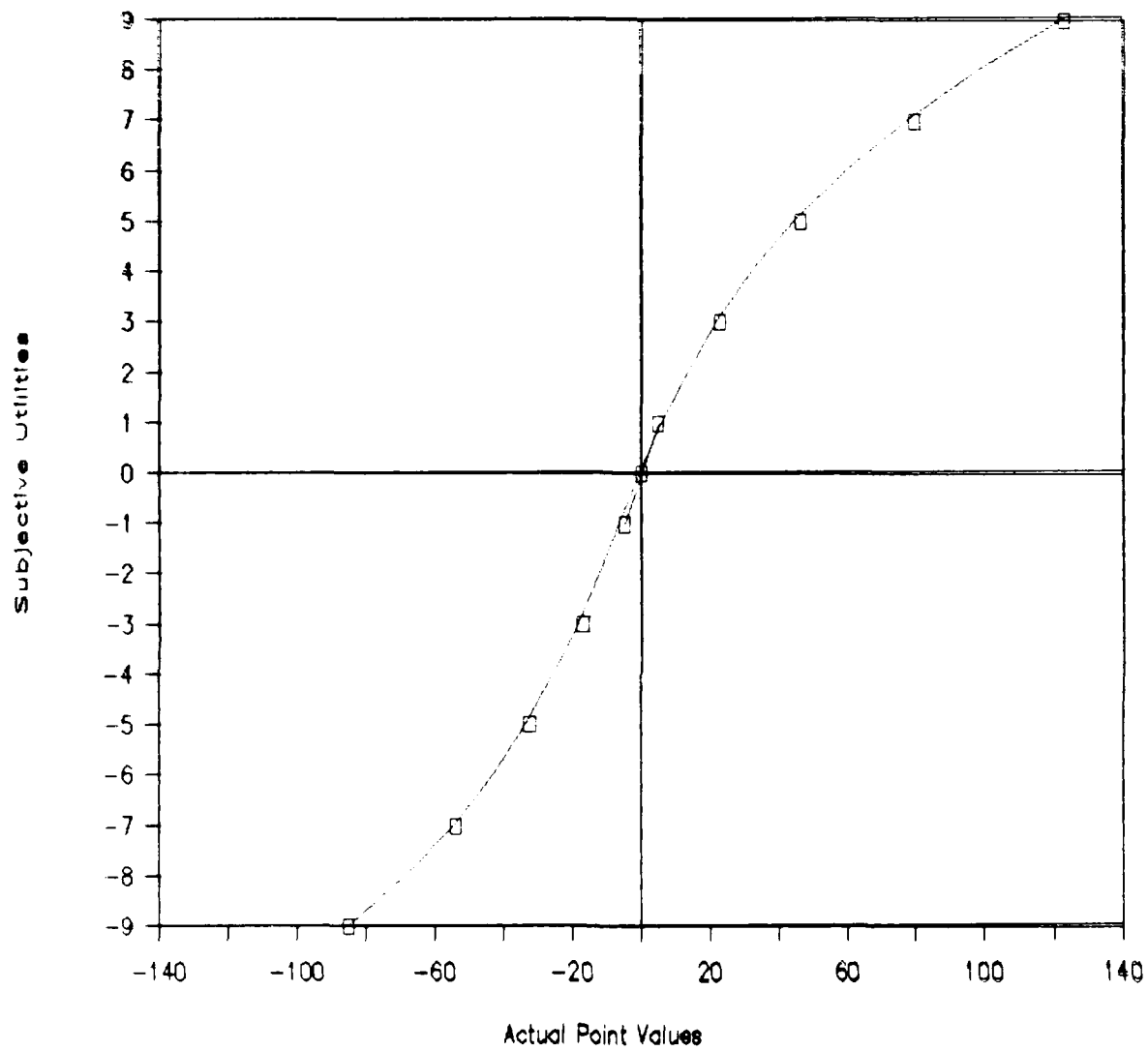


Figure 1. Estimated utility curve for points based on mean estimates from Trials 1-8.

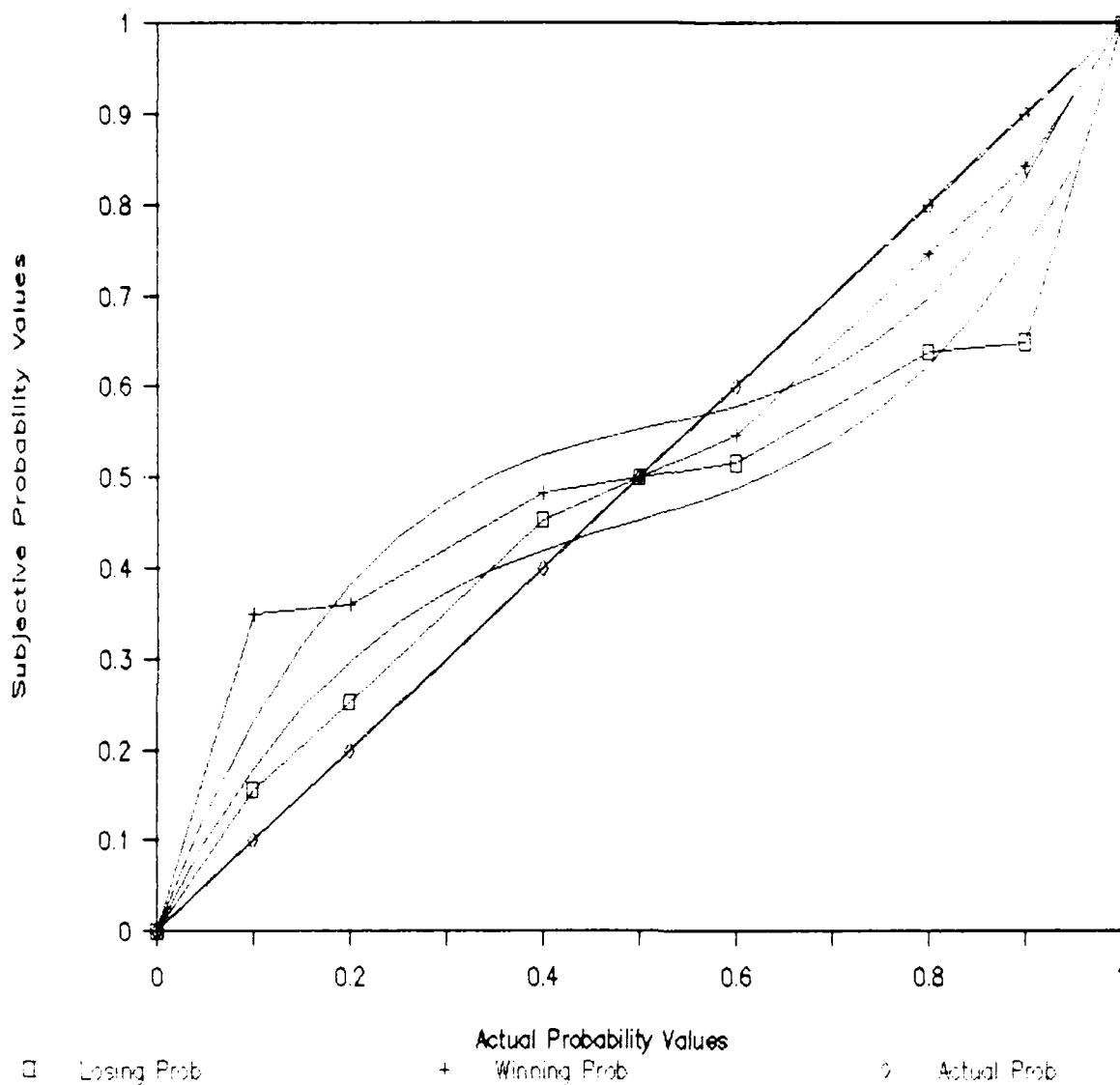


Figure 2. Estimated subjective probability functions for winning and losing probabilities based on mean point estimates from Trials 12-14.

Finally, subjects tend, as has often been found, to exhibit another form of bias; they overestimate low probabilities and underestimate high probabilities. This can be observed in both figures by noting that both the winning and losing curves extend above the 45° line for probabilities below .50 and extend below this line for probabilities above .50.

V. RECOMMENDATIONS FOR FUTURE RESEARCH:

There were two kinds of bias observed in the reported study and these are psychologically very distinct. One, the overestimation vs. underestimation phenomenon, suggests a general misrepresentation and distortion of events that are either quite likely or quite unlikely. It is clearly a property of decision making that is undesirable since it can lead to suboptimal decisions. The second biasing effect that was found, the differential weighting of the same event, is a much more serious undesirable effect and is more interesting from a cognitive perspective. It suggests that there is an affective influence on the judgmental process. Individuals make choices between alternatives by assigning different subjective probabilities or weights to the same explicit event depending on whether it has a positive affective component (winning) or negative affective component (losing).

I have argued that all decision making under uncertainty necessitates that an expert decision maker must somehow associate each relevant uncertainty with a probability value. The study presented here

indicates that humans may introduce a strong affective bias in this process. Clearly, such a bias may lead to suboptimal decisions being made. Since the quality of the design of an expert system hinges on the quality of the experts in the substantive field, further research in this area seems useful. In particular, several issues seems to be initially relevant to continued research:

- a. How strong and how generalizable is the differential weighting effect for probabilities?
- b. What factors influence the strength of this effect, and can decision makers be trained to reduce or eliminate it?
- c. In decisions that involve uncertainties, what is the best way to assign probabilities to uncertain events so as to reduce bias and increase concordance among expert judges (e.g., pilots)?
- d. What expert systems development tools might prove most useful in training individuals to become expert judges in situations involving uncertainty?

Clearly, the demand for individuals, and in particular pilots, to become "expert" decision makers in their work environments will only continue to increase. One aspect of what makes a person an expert decision maker or what is necessary in an expert system is a function of how well probabilities can be assigned to uncertainties that are critical components of the decision situation. It is argued here that the four questions cited above constitute a necessary initial step in better understanding expert judgment.

References

- Arkes, H. R., and Hammond, K. R. (Eds.) Judgment and decision making. New York: Cambridge University Press, 1986.
- Davidson, D., Suppes, P., and Siegel, S. Decision making: An experimental approach. Stanford: Stanford University Press, 1957.
- Kahneman, D., Slovic, P., and Tversky, A. Judgment under uncertainty: Heuristics and biases. New York: Cambridge University Press, 1982.
- Kahneman, D., and Tversky, A. Prospect theory: An analysis of decision under risk. Econometrica, 47, 1979, 263- 291.
- Luce, R. D., and Narens, L. Classification of concatenation measurement: Structures according to scale type. Journal of Mathematical Psychology, 29, 1985, 1-72.
- Nygren, T. E. Examination of a context effect on subjective estimates of probabilities. Paper presented at the Judgment and Decision Group meetings; Philadelphia, PA, November, 1981.
- Nygren, T. E., and Isen, A. M. Effect of positive affect on judgments of likelihoods of events and on gambling behavior. Paper presented at the meeting of the Midwestern Psychological Association, Chicago, IL, May, 1985.

1987 USAF-UES SUMMER FACULTY RESEARCH PROGRAM
GRADUATE STUDENT SUMMER SUPPORT PROGRAM

Sponsored by the
AIR FORCE OFFICE OF SCIENTIFIC RESEARCH
Conducted by the
Universal Energy Systems, Inc.

FINAL REPORT

On the General Existence of Precursor Fields
in a Causally Dispersive Medium

Prepared by: Kurt Edmund Oughstun, Ph.D.
Academic Rank: Associate Professor
Department and Computer Science and Electrical Engineering
University: University of Vermont
Research Location: USAFSAM/RZM
Brooks AFB
San Antonio, Texas 78235
USAF Researcher: Dr. Richard A. Albanese, M.D.
Date: July 31, 1987
Contract No: F49620-85-C-0013

ON THE GENERAL EXISTENCE OF PRECURSOR FIELDS
IN A CAUSALLY DISPERSIVE MEDIUM

by

Kurt Edmund Oughstun

ABSTRACT

A set of conditions on the medium properties under which the Sommerfeld and Brillouin precursor fields can evolve under proper field excitation in a general causal, temporally dispersive medium is obtained. These conditions for the existence of the precursor fields are derived from the asymptotic description of the dynamical field evolution in the dispersive medium due to a given input pulsed electromagnetic field. The only description of the medium employed is that it satisfies the Kramers-Kronig relations. The analysis also provides the requirements on the initial pulse rise-time that are necessary for these precursor fields to be excited in the host medium.

Acknowledgments

The author wishes to express his gratitude to both the Air Force Systems Command and the Air Force Office of Scientific Research for their sponsorship of this research. The author also gratefully acknowledges the assistance provided by Universal Energy Systems with regard to the administrative and directional aspects of this program.

On a more personal note, I would like to thank Dr. Richard A. Albanese of USAFSAM/RZM not only for his support and encouragement throughout this research period, but also for his insightful queries and comments regarding this research both in its formulation and areas of application. I would also like to thank Dr. Arje Nachman of the Applied Mathematics Group of AFOSR for his encouragement to apply for AFOSR support of this research. Finally, I would like to thank the personnel at USAFSAM/RZM who have helped to make my short stay in San Antonio as enjoyable and personally rewarding as could be expected. Of particular note here are Dr. Richard Albanese and his family, Mr. John Penn, Mr. Richard Medina, and Ms. Edith Wood.

I. INTRODUCTION

The dynamical evolution of an electromagnetic pulse as it propagates through a temporally dispersive medium is a classical problem of mathematical physics. If the medium was nondispersive, an arbitrary pulse would propagate unaltered at the phase velocity of the wave field in the medium. In a dispersive medium, however, the pulse shape is modified as it propagates due to two fundamental effects. First of all, each monochromatic component of the initial pulse propagates through the medium with its own phase velocity so that the phasal relationship between the spectral components of the pulse changes with propagation distance. Secondly, each monochromatic component is absorbed at a different rate so that the amplitudinal relationship between the spectral components of the pulse changes with propagation distance. These two effects then result in a complicated change in the structure of the propagated field. For initial pulses with sufficiently rapid rise-times, these effects manifest themselves through the formation of so-called precursor fields whose evolution is completely determined by the dispersive properties of the medium. The precursor fields are readily distinguished in the evolution of the propagated field by the fact that their frequency range of oscillation is typically quite different from that of the input field and their attenuation is typically much less than that at the carrier frequency of the input field.

The Radiation Analysis and Modeling Section of the Radiation Sciences Division of the USAF School of Aerospace Medicine at Brooks Air Force Base has a particular interest in the formation and dynamical evolution of transient fields in biological structures due to external pulsed electromagnetic field sources. Such field sources are commonly employed in the microwave telecommunications industry. At present, the acceptable levels for radiation exposure are set for continuous wave fields. However, because of the transient fields generated by pulsed fields in dispersive media, the level of exposure due to a pulsed field can be significantly different from that due to a continuous wave field of the same carrier frequency and incident electromagnetic energy density. It is, therefore, of critical interest to obtain a complete understanding

of the dynamical evolution of pulsed electromagnetic fields in dispersive media as well as the material conditions under which precursor formation is possible in order that more realistic exposure limits can be set.

My research interest over the past fifteen years has primarily been focused on the uniform asymptotic description of dispersive pulse propagation. This research has led to a correct description of the signal velocity in a dispersive medium and has resulted in a new physical model of the dynamical field evolution that is based on the physical concept of the energy velocity which supplants the previous group velocity description. My keen interest in this area of research was created and has been maintained by both the physical complexity of the problem and the elegant mathematical techniques that need to be derived in its rigorous solution. This background contributed to my assignment to the Radiation Sciences Division.

II. OBJECTIVES OF THE RESEARCH EFFORT

At present, the dynamical evolution of an electromagnetic pulse in a temporally dispersive medium has only been fully described for one specific model of the material dispersion, namely, that given by the classical Lorentz model, and then only for the simplest case of a single resonance frequency. It is then seen to be of critical importance to determine both the medium and source conditions under which precursor formation will occur as well as to categorize this transient field evolution according to the specific medium type. This result will provide an important generalization of the theory of dispersive pulse propagation with wide application.

My assignment as a participant in the 1987 Summer Faculty Research Program (SFRP) was to determine the conditions on the medium properties under which the classical Sommerfeld and Brillouin precursor fields can evolve under proper field excitation in a general temporally dispersive medium that is causal (i.e. a medium whose dielectric permittivity satisfies the Kramers-Kronig relations). Such an existence proof will

also yield a dynamical description of the precursor fields (for the cases in which they exist) that is model independent. This aspect of the problem will (hopefully) be continued with funding from the Mini Grant Program.

III. OVERVIEW

The propagation of an electromagnetic pulse through a medium is profoundly influenced by the presence of any frequency dependence in the medium response. If the medium was nondispersive, an arbitrary pulse would propagate without change at the phase velocity of the wave field in the medium. In a dispersive medium, however, the pulse shape is modified as it propagates. Moreover, the main body of the pulse travels with a velocity that is different from either the phase velocity in the medium at the carrier frequency of the pulse or the vacuum speed of light c , and may be preceded by electromagnetic fields termed precursors or forerunners.

The physical origin of these effects is readily understood through a simple consideration of the principle of superposition for electromagnetic fields and the dispersive properties of the medium. The initial pulse may be expressed as a linear superposition of monochromatic plane waves, each at a given amplitude and satisfying a definite phase relation with respect to the other monochromatic components. Due to the frequency dispersion of the medium response, each monochromatic component propagates through the medium with its own phase velocity and absorption condition. As a consequence, the relative phases and amplitudes of each of these monochromatic components which are present in the initial pulse spectrum change as the pulse propagates through the dispersive medium, and this results in a complicated change in the structure of the total propagated field.

The rigorous analysis of the entire field evolution properties in dispersive pulse propagation critically depends upon the model of the frequency dependence in the medium response. In order to maintain strict adherence to the fundamental physical principle of causality it

is essential that any model chosen for the medium response be causal. An important example of such a causal model is that provided by the Lorentz theory of dielectric media and the associated Drude model for conductors. Because of its applicability in the optical region of the spectrum (along with the fact that it yields a causal response), the Lorentz model has been chosen in much of the rigorous analysis of dispersive pulse propagation. Indeed, it was with the Lorentz model that Sommerfeld [1] and Brillouin [2,3] conducted their foundational research on dispersive pulse propagation and for which the precursor fields were first described. The recent extension of this classical analysis by Oughstun [4] and Sherman and Oughstun [5,6] has provided a complete, uniformly valid description of the entire precursor field evolution and signal arrival for dispersive pulse propagation in a Lorentz medium. This recent analysis has led to a new physical model of the dynamical field evolution [5] that is based on the physical concept of the energy velocity which supplants the previous group velocity description. Although derived explicitly for a Lorentz model medium,¹ this new energy velocity model appears likely to be valid in other lossy dispersive systems; however, this important generalization remains to be proven.

The analysis of the present paper begins this important proof through a consideration of the general conditions under which the so-called Sommerfeld and Brillouin precursor fields may exist. This existence proof will be framed within the exact mathematical formalism of the Fourier-Laplace integral representation of the propagated field in which the phase delay and absorption condition for each spectral component of the initial field are explicitly displayed through a well-defined complex phase function that accounts for the medium response.

There are two different (although related) parts to this general existence proof of the precursor fields. The first is to show under what general conditions a causal dispersive medium will yield those critical

¹A brief description of the Lorentz model of dielectric media and the associated Drude model of conductors may be found in Stratton [7] and Jackson [8]; a detailed description is given in Böttcher and Bordewijk [9].

points (called saddle points) of the complex phase function whose contribution to the asymptotic behavior of the propagated field can give rise to the precursor fields. From the constitutive relations for electromagnetic fields in linear, homogeneous, isotropic, temporally dispersive causal media, admissible models that describe the behavior of the complex dielectric permittivity $\epsilon(\omega) = \epsilon_r(\omega) + i\epsilon_i(\omega)$ in the complex ω -plane must obey the symmetry relation (where the asterisk denotes complex conjugation) [8-10]

$$\epsilon^*(\omega) = \epsilon(-\omega^*) \quad (3.1)$$

Furthermore, due to the analyticity properties of $\epsilon(\omega)$ as expressed by Plemmerson's theorem [10], the complex dielectric permittivity is required to satisfy the relation

$$\epsilon(\omega) = 1 + \frac{1}{\pi i} \int_{-\infty}^{\infty} \frac{\epsilon(\zeta)-1}{\zeta-\omega} d\zeta, \quad (3.2)$$

where the principal value of the integral is to be taken. With Eq. (3.1), the real and imaginary parts of this equation yield

$$\epsilon_r(\omega) = 1 + \frac{1}{\pi} \int_{-\infty}^{\infty} \frac{\epsilon_i(\zeta)}{\zeta-\omega} d\zeta, \quad (3.3a)$$

$$\epsilon_i(\omega) = -\frac{1}{\pi} \int_{-\infty}^{\infty} \frac{\epsilon_r(\zeta)-1}{\zeta-\omega} d\zeta. \quad (3.3b)$$

These well-known relations are called the Kramers-Kronig relations, the Plemelj relations, or simply the dispersion relations. The symmetry relation $\epsilon^*(\omega^*) = \epsilon(-\omega)$ shows that $\epsilon_r(\omega) = \text{Re}[\epsilon(\omega)]$ is an even function of ω , while $\epsilon_i(\omega) = \text{Im}[\epsilon(\omega)]$ is an odd function of ω .

It is important to notice that the above precise form of the dispersion relations for the complex dielectric permittivity must be maintained for proper physical meaning. Of particular importance in this regard is the second relation (3.3b) for the imaginary part of the permittivity. The fundamental point in the derivation of these dispersion relations [8-11] is that it is the polarizability of the medium that is causal. Since the polarizability is linearly related to the electric susceptibility χ_e of the medium, it too is a causal function and is related to the dielectric permittivity by

$$\chi_e(\omega) = \frac{1}{4\pi} (\epsilon(\omega)-1).$$

Hence, it is the quantity ϵ^{-1} , and not ϵ , that is causal, and this fact must be explicitly expressed and maintained in the dispersion relations (3.3). Such care is given by Jackson [8], Nussenzveig [10], and Landau and Lifshitz [11]. Unfortunately, this is not the case with Bottcher and Bordewijk [9], who make use of the mathematical identity

$$\oint_{-\infty}^{\infty} \frac{1}{\zeta - \omega} d\zeta = 0$$

to obtain the relation

$$\epsilon_i(\omega) = -\frac{1}{\pi} \oint_{-\infty}^{\infty} \frac{\epsilon_r(\zeta)}{\zeta - \omega} d\zeta$$

which removes the symmetry with respect to the companion Hilbert transform (1.3a). Although there clearly is no mathematical impropriety in doing this, it can lead to physically nonsensical results when one attempts to extract the approximate behavior of $\epsilon_i(\omega)$ in specific regions of the complex ω -plane. This point is made even clearer when one notices that, for any constant A, either real or complex valued, one can rigorously obtain the relation

$$\epsilon_i(\omega) = -\frac{1}{\pi} \oint_{-\infty}^{\infty} \frac{\epsilon_r(\zeta) - A}{\zeta - \omega} d\zeta$$

which further obscures the inherent symmetry present in the physical nature of the dispersion relations.

The care that must be taken in any determination of the approximate functional behavior of the complex permittivity through the use of the dispersion relations (1.3) is precisely contained in the following paraphrased statement by Landau and Lifshitz [11]: "For any function $\epsilon_i(\omega)$ satisfying the physically necessary condition that $\epsilon_i(\omega') > 0$, Eq. (3.3a) will yield a function $\epsilon_r(\omega)$ that is consistent with all physical requirements, i.e. one which is in principle possible. This makes it possible to use (1.3a) even when the function $\epsilon_i(\omega)$ is approximate. On the other hand, Eq. (3.3b) does not yield a physically possible function $\epsilon_i(\omega)$ for an arbitrary choice of $\epsilon_r(\omega)$, since the condition $\epsilon_i(\omega') > 0$ for finite $\omega' > 0$ is not necessarily fulfilled." Hence, in any attempt at obtaining the approximate behavior of the real and imaginary parts of the complex dielectric permittivity in a given region of the complex

ω -plane, specific care must be given to the precise form and physical meaning of the dispersion relations (1.3) in order that physically meaningful results are obtained.

Even if the medium is such that precursor fields are possible, their actual appearance is also dependent upon the particular form of the initial (or input) field, and this aspect of the problem forms the second part of the existence proof. For the extreme case of a strictly monochromatic field (i.e. a constant amplitude field that oscillates indefinitely at a single definite angular frequency ω_0) there will not be any precursor fields present in the propagated field structure since the spectrum of the field is a delta function at the applied field frequency ω_0 and consequently vanishes at all other frequency values. For the diametrically opposite case of an input delta function pulse, the spectrum is unity at all frequencies; this input field yields the so-called impulse response of the medium and the resultant propagated field evolution is given solely by the contributions due to the saddle points of the complex phase function. This then constitutes the ideal situation in which to observe the dynamical evolution of the field due to the saddle point contributions alone. However, it is only by analogy with other canonical problems that these fields can be termed precursors, and we have finally come round to the important (but unfortunately sticky) question of defining just what a precursor field is. That is, just how does one recognize a precursor field?

From an historical perspective, the synonymic terms precursor and forerunner were first applied in 1914 in connection with general wave propagation phenomena by both Sommerfeld [1] and Brillouin [2,3] with regard to a very specific physical situation. They both treated the canonical problem of the propagation of an input unit step-function modulated field in a Lorentz model medium that is characterized by a single resonance frequency. The initial field at the input plane at $z = 0$ identically vanishes for all times $t < 0$ and oscillates harmonically in time with constant amplitude and fixed frequency ω_0 for all $t > 0$. The resultant field evolution at a fixed, asymptotically distant observation plane at $z > 0$ was found to oscillate predominantly at the applied

signal frequency ω_0 with a steady amplitude only for all times $t > (\theta_0/c)z$, where c denotes the vacuum speed of light and where $\theta_0 \geq 1$ is some fixed number that is determined by the signal frequency ω_0 and the medium parameters. This component of the propagated field is simply given by the input field that has propagated the distance $z > 0$ without dispersion with a definite velocity c/θ_0 and has been exponentially attenuated with the amplitude attenuation coefficient $\alpha(\omega_0)$ as given by the Lorentz model at the signal frequency ω_0 . This steady-state component of the propagated field is then appropriately called the main signal and the velocity $v_0 = c/\theta_0$ is then defined as the signal velocity. The precursor fields then refer to the transient field structure that evolves prior to the arrival and subsequent evolution of the main signal, and hence, is that dominant field structure that evolves over the time interval $z/c \leq t < (\theta_0/c)z$.

The recent, more accurate asymptotic description [4,6] of the field evolution in a single resonance Lorentz medium, however, has shown that the total dynamical evolution of the propagated field is, in a specific frequency domain of the applied signal, more complicated than that originally described by Sommerfeld and Brillouin. In particular, for an applied signal frequency that is sufficiently far above resonance there is the existence of a "prepulse" due to the interruption of the signal evolution by the Brillouin precursor field which becomes asymptotically dominant over the signal for some finite time interval. Hence, this precursor field does not evolve prior to the signal evolution so that the previous definition must be accordingly modified.

One possible generalization is to take the precursor fields as being given by the difference between the actual propagated field in the dispersive medium and a fictitious field that is due to the same initial field propagated the same distance at the energy velocity in a certain nondispersive medium with the same fixed absorption and wave number as that at the applied signal frequency in the dispersive medium. Although physically appealing, this definition breaks down for any field in which the carrier frequency is not fixed (e.g. a frequency-chirped pulse) or

even well-defined as in the case of a delta function input. Nevertheless, for those cases in which the signal frequency is a well-defined constant, this definition is valid and provides a useful numerical technique for determining the resultant precursor field evolution alone.

A generalization that does unambiguously define the precursor fields in all situations may be directly obtained through the asymptotic description of the field. In that description, each contribution to the propagated field is precisely defined according to its source term in the field expansion. The precursor fields are then seen to arise from the saddle points of the complex phase function which depends explicitly upon the medium properties and is independent of the input field structure. The dynamical evolution of the precursor fields is then completely determined by the dynamics of these saddle points in the complex frequency plane. That is not to say that the form of the input field has nothing to do with the precursor fields, for their appearance is certainly dependent upon the spectrum of the input field. This definition is a natural consequence of the asymptotic description of the propagated field and yields the same results as the above physical definition in those situations for which it is applicable. As such, this general definition is adopted in this paper.

IV. GENERAL FORMULATION OF THE DISPERSIVE PULSE PROPAGATION PROBLEM

Consider an arbitrary plane electromagnetic wave that is propagating in the positive z -direction through a linear, homogeneous, isotropic, temporally dispersive medium occupying the half-space $z > 0$. Let $A(z, t)$ represent either the scalar potential or any scalar component of the electric field, magnetic field, or vector potential field. This function $A(z, t)$ then satisfies the scalar wave equation

$$\nabla^2 A(z, t) - \frac{n^2(\omega)}{c^2} \frac{\partial^2 A(z, t)}{\partial t^2} = 0, \quad (4.1)$$

where $n(\omega) = [\epsilon(\omega)]^{1/2}$ is the complex index of refraction of the medium, $\epsilon(\omega)$ is the complex permittivity, and c is the speed of light in vacuum. Under relatively general conditions [7] the wave function $A(z, t)$ may be expressed in either a Fourier or Laplace representation given by

$$A(z, t) = \int_C A(z, \omega) e^{-i\omega t} d\omega. \quad (4.2)$$

The spectral amplitude function $A(z, \omega)$ then satisfies the scalar Helmholtz equation

$$(\nabla^2 + \tilde{k}^2(\omega))A(z, \omega) = 0, \quad (4.3)$$

where

$$\tilde{k}(\omega) = \frac{\omega}{c} n(\omega) \quad (4.4)$$

is the complex wave number at the angular frequency ω .

Consider now the situation in which the field $A(z, t)$ on the plane $z = 0$ is known for all time t and is nonzero only after $t = 0$, so that

$$A(0, t) = f(t) \quad (4.5)$$

for all t , where the function $f(t)$ identically vanishes for all $t < 0$. The integral expression (4.2) for the scalar field $A(z, t)$ is then taken to be a Laplace representation. The frequency spectrum of $f(t)$ is then given by

$$\tilde{f}(\omega) = \int_0^\infty f(t) e^{i\omega t} dt \quad (4.6)$$

provided only that the integral $\int_0^\infty |f(t)| dt$ exists. If $f(t)$ does not vanish properly at infinity, the above integral fails to converge; however, under certain circumstances [7] absolute convergence can be obtained through the introduction of an exponentially decaying factor $e^{-\gamma t}$, where γ is real-valued. The Fourier transform of $e^{-\gamma t} f(t)$ is then given by

$$\tilde{f}(\omega + i\gamma) = \int_0^\infty f(t) e^{i(\omega + i\gamma)t} dt. \quad (4.7)$$

If there exists a real number γ such that

$$\lim_{T \rightarrow \infty} \int_0^T |e^{-\gamma t} f(t)| dt < \infty, \quad (4.8)$$

then $f(t)$ is said to be transformable [7]. The abscissa of absolute convergence is then defined as the lower bound γ_a of the allowable set of values of γ that satisfy Eq. (4.8). For such a transformable function, the inverse transformation is given by

$$f(t) e^{-\gamma t} = \frac{1}{2\pi} \int_{-\infty}^{\infty} \tilde{f}(\omega + i\gamma) e^{-i\omega t} d\omega, \quad (4.9)$$

where $\gamma > \gamma_a$. This expression may be rewritten as

$$f(t) = \frac{1}{2\pi} \int_{-\infty}^{\infty} \tilde{f}(\omega + i\gamma) e^{-i(\omega + i\gamma)t} d\omega,$$

which, under the change of variable $\omega \leftrightarrow \omega + i\gamma$, becomes

$$f(t) = \frac{1}{2\pi} \int_{i\gamma-\infty}^{i\gamma+\infty} \tilde{f}(\omega) e^{-i\omega t} d\omega; \quad \gamma > \gamma_a. \quad (4.10)$$

The contour of integration C appearing in Eq. (4.2) is then seen to be the straight line $\omega = \omega' + ia$ in the complex ω -plane with a being a fixed constant that is greater than the abscissa of absolute convergence for the function $f(t)$ and where $\omega' \equiv R_e(\omega)$ ranges from negative to positive infinity.

The general solution of the Helmholtz equation (4.3) is given by

$$A(z, \omega) = A_+(\omega) e^{ikz} + A_-(\omega) e^{-ikz}, \quad (4.11)$$

where the first term on the right-hand side represents a plane wave disturbance propagating in the positive z -direction while the second term represents a plane wave disturbance propagating in the negative z -direction. For propagation in the positive z -direction alone, the term $A_-(\omega)$ must be zero and Eqs. (4.2) and (4.11) give

$$A(z, t) = \int_C A_+(\omega) e^{i(kz - \omega t)} d\omega. \quad (4.12)$$

Evaluation of this expression at the plane boundary $z = 0$ and application of the boundary condition (4.5) then yields

$$f(t) = \int_C A_+(\omega) e^{-i\omega t} d\omega. \quad (4.13)$$

The inverse transform of this result then gives

$$A_+(\omega) = \frac{1}{2\pi} \int_0^\infty f(t) e^{i\omega t} dt = \frac{1}{2\pi} \tilde{f}(\omega), \quad (4.14)$$

where $\tilde{f}(\omega)$ is the Laplace transform of the initial time behavior of the pulse at the plane boundary $z = 0$ (i.e. the initial pulse spectrum). Therefore, the exact integral formulation that describes the propagation of an arbitrary plane wave pulse through a dispersive medium is given by

$$A(z, t) = \frac{1}{2\pi} \int_{-\infty}^{\infty} \tilde{f}(\omega) e^{i[k(\omega)z - \omega t]} d\omega \quad (4.15)$$

for $z \geq 0$. This form of the solution is most appropriate for numerical simulation that rely on the fast Fourier transform algorithm. With the dispersion relation (4.4) the above expression may be written in the following form that is more suitable for asymptotic methods of approximation:

$$A(z, t) = \frac{1}{2\pi} \int_C \tilde{f}(\omega) e^{(z/c)\phi(\omega, \theta)} d\omega, \quad (4.16)$$

where the complex phase function $\phi(\omega, \theta)$ is defined by

$$\phi(\omega, \theta) = i\omega[n(\omega) - \theta], \quad (4.17)$$

and where

$$\theta = \frac{ct}{z} \quad (4.18)$$

is a dimensionless parameter that characterizes a given space-time point in the field. At a fixed value of $\theta \geq 1$ the observation point is moving along with the field at a velocity c/θ .

From the symmetry relation (3.1), admissible models that describe the behavior of the complex index of refraction in the complex ω -plane must obey the relation

$$n^*(\omega^*) = n(-\omega), \quad (4.19)$$

and hence, from Eq. (4.17) the complex phase function must satisfy the symmetry relation

$$\phi^*(\omega^*, \theta) = \phi(-\omega, \theta). \quad (4.20)$$

Furthermore, for a real-valued initial pulse function $f(t)$ it directly follows from Eq. (4.6) that its spectrum satisfies the relation

$$\tilde{f}^*(\omega^*) = \tilde{f}(-\omega). \quad (4.21)$$

Under the change of variable $\omega \rightarrow -\omega^*$ the integral representation (4.16) becomes

$$\begin{aligned} A(z, t) &= - \frac{1}{2\pi} \int_{i\infty}^{i\infty-\infty} \tilde{f}(-\omega^*) e^{(z/c)\phi(-\omega^*, \theta)} d\omega^* \\ &= \frac{1}{2\pi} \int_{i\infty-\infty}^{i\infty} \tilde{f}^*(\omega) e^{(z/c)\phi^*(\omega, \theta)} d\omega^* \end{aligned}$$

$$= \left[\frac{1}{2\pi} \int_{ia-\infty}^{ia+\infty} \tilde{f}(\omega) e^{(z/c)\phi(\omega, \theta)} d\omega \right]^* = A^*(z, t).$$

Hence, given that the initial field behavior is real, the propagated field behavior must also be real. This fact may be explicitly noted by writing Eq. (4.16) as

$$A(z, t) = \frac{1}{2\pi} \operatorname{Re} \int_{ia-\infty}^{ia+\infty} \tilde{f}(\omega) e^{(z/c)\phi(\omega, \theta)} d\omega \quad (4.22)$$

when $f(t)$ is real.

A case of special interest is that of a pulse-modulated sine wave of constant applied signal frequency ω_c , viz.

$$f(t) = u(t) \sin(\omega_c t), \quad (4.23)$$

where $u(t)$ is the real-valued initial envelope function of the input pulse that is zero for $t < 0$. The spectrum of this field is given by the Laplace transformation (4.6) as

$$\tilde{f}(\omega) = \frac{1}{2i} [\tilde{u}(\omega + \omega_c) - \tilde{u}(\omega - \omega_c)], \quad (4.24)$$

where

$$\tilde{u}(\omega) = \int_0^\infty u(t) e^{i\omega t} dt \quad (4.25)$$

is the spectrum of the initial pulse envelope. Since $u(t)$ is real-valued, its spectrum satisfies the symmetry relation

$$\tilde{u}^*(\omega^*) = \tilde{u}(-\omega) \quad (4.26)$$

Substitution of Eq. (4.24) into Eq. (4.16) then yields the expression

$$A(z, t) = -\frac{1}{4\pi} \left\{ i \int_{ia-\infty}^{ia+\infty} \tilde{u}(\omega + \omega_c) e^{(z/c)\phi(\omega, \theta)} d\omega - i \int_{ia-\infty}^{ia+\infty} \tilde{u}(\omega - \omega_c) e^{(z/c)\phi(\omega, \theta)} d\omega \right\}.$$

Under the change of variable $\omega \rightarrow -\omega^*$ in the first integral of the above expression, one obtains

$$\begin{aligned} A(z, t) &= -\frac{1}{4\pi} \left\{ i \int_{ia-\infty}^{ia+\infty} \tilde{u}(-\omega^* + \omega_c) e^{(z/c)\phi(-\omega^*, \theta)} d\omega^* - i \int_{ia-\infty}^{ia+\infty} \tilde{u}(\omega - \omega_c) e^{(z/c)\phi(\omega, \theta)} d\omega \right\} \\ &= -\frac{1}{4\pi} \left\{ i \int_{ia-\infty}^{ia+\infty} \tilde{u}^*(\omega - \omega_c) e^{(z/c)\phi^*(\omega, \theta)} d\omega^* - i \int_{ia-\infty}^{ia+\infty} \tilde{u}(\omega - \omega_c) e^{(z/c)\phi(\omega, \theta)} d\omega \right\} \\ &= -\frac{1}{4\pi} \left\{ \left[-i \int_{ia-\infty}^{ia+\infty} \tilde{u}(\omega - \omega_c) e^{(z/c)\phi(\omega, \theta)} d\omega \right]^* - i \int_{ia-\infty}^{ia+\infty} \tilde{u}(\omega - \omega_c) e^{(z/c)\phi(\omega, \theta)} d\omega \right\}, \end{aligned}$$

from which it is then seen that

$$A(z,t) = \frac{1}{2\pi} \operatorname{Re} i \int_{ia-\infty}^{ia+\infty} \tilde{u}(\omega - \omega_c) e^{(z/c)\phi(\omega, \theta)} d\omega \quad (4.27)$$

for $z \geq 0$ when $u(t)$ is real.

The integral representations (4.22) and (4.27) form the basis of the problem treated in this paper. These same representations also apply even where the initial field does not identically vanish for times $t < 0$, but rather possess a sufficiently large exponential decay as t approaches negative infinity in order to ensure the existence of the spectrum $\tilde{f}(\omega)$, which is now given by the Fourier transform of the initial field structure. Furthermore, with the use of generalized function theory, these results may be further extended to include, for example, the behavior of strictly monochromatic fields.

An interesting example that employs this formulation is that of an input delta function pulse in a nondispersive medium with fixed complex wave number $k = k_r + ik_i$. With $\tilde{f}(\omega) = 1$, the resultant propagated field is then given by

$$\begin{aligned} A(z,t) &= \frac{1}{2\pi} \int_C e^{i(kz - \omega t)} d\omega = e^{-k_i z} \frac{1}{2\pi} \int_C e^{i((z/v) - t)\omega} d\omega \\ &= e^{-k_i z} \delta(t - (z/v)), \end{aligned}$$

where $v = \omega/k_r$ is the constant phase velocity in the nondispersive medium. It is easy to see from this example that the physical definition of the precursor fields, defined as the difference between the propagated field in the dispersive medium and the above propagated field in the fictitious, equivalent nondispersive medium, is invalid, for the dispersive field evolution in this case is just comprised of the precursor fields.

V. ANALYSIS OF THE COMPLEX PHASE FUNCTION AND ITS SADDLE POINTS FOR A PERFECT DIELECTRIC

By definition, the precursor fields are given by the saddle points of the complex phase function

$$\phi(\omega, \theta) = i\omega[n(\omega) - \theta] \quad (5.1)$$

that appears in both of the integral representations (4.22) and (4.27) of the propagated field. The saddle points are then given by

$$\begin{aligned} \phi'(\omega, \theta) &= i[n(\omega) - \theta] + i\omega n'(\omega) \equiv 0 \\ \therefore n(\omega) + \omega n'(\omega) - \theta &= 0 \end{aligned} \quad (5.2)$$

where the prime denotes differentiation with respect to complex ω . Here $n(\omega)$ denotes the complex index of refraction of the dielectric medium, given by

$$n(\omega) = [\epsilon(\omega)]^{1/2}, \quad (5.3)$$

where the principal branch of the square root is to be taken. Acceptable models for the complex dielectric permittivity $\epsilon(\omega) = \epsilon_r(\omega) + i\epsilon_i(\omega)$ satisfy the dispersion relations

$$\epsilon_r(\omega) = 1 + \frac{1}{\pi} \oint_{-\infty}^{\infty} \frac{\epsilon_i(\zeta)}{\zeta - \omega} d\zeta, \quad (5.4a)$$

$$\epsilon_i(\omega) = -\frac{1}{\pi} \oint_{-\infty}^{\infty} \frac{\epsilon_r(\zeta) - 1}{\zeta - \omega} d\zeta, \quad (5.4b)$$

where $\epsilon_r(\omega) \equiv \text{Re}[\epsilon(\omega)]$ is an even function of ω and $\epsilon_i(\omega) \equiv \text{Im}[\epsilon(\omega)]$ is an odd function of ω ; that is

$$\epsilon_r(\omega' + i\omega'') = \epsilon_r(-\omega' + i\omega''), \quad (5.5a)$$

$$\epsilon_i(\omega' + i\omega'') = -\epsilon_i(-\omega' + i\omega''), \quad (5.5b)$$

where ω' is the real part and ω'' the imaginary part of complex ω .

For a perfect dielectric, the medium absorption identically vanishes at zero frequency. Hence, from Eq. (5.4b) one has that

$$\oint_{-\infty}^{\infty} \frac{\epsilon_r(\zeta) - 1}{\zeta} d\zeta = 0 \quad (5.6)$$

The medium absorption also identically vanishes at infinite frequency, as can easily be seen from the dispersion relations (5.4). Hence, one can safely assume (with little or no loss in generality) that the frequency dependence of $\epsilon_1(\omega')$ along the positive real ω' -axis is such that the loss is significant only within a finite frequency domain $[\omega_0, \omega_m]$, where

$$0 < \omega_0 < \omega_m < \infty. \quad (5.7)$$

For all values of $\omega' > 0$ outside of this domain, the loss is then negligible by comparison. Attention is now focused on two special regions of the complex ω -plane wherein the complex dielectric permittivity is reasonably simple and well-behaved, these being the region about the origin $|\omega| \ll \omega_0$ and the region about infinity $|\omega| \gg \omega_m$.

5.1 The Region about the Origin; $|\omega| \ll \omega_0$

Since $\epsilon_1(\zeta)$ vanishes at $\zeta = 0$, one may then expand the denominator in the integral of Eq. (5.4a) for small $|\omega|$ in a Maclaurin series as follows:

$$\begin{aligned} \epsilon_r(\omega) &= 1 + \frac{1}{\pi} \int_{-\infty}^{\infty} \frac{\epsilon_1(\zeta)}{\zeta} \cdot \frac{1}{1-\omega/\zeta} d\zeta \\ &\approx 1 + \sum_{j=0}^{\infty} \omega^j \frac{1}{\pi} \int_{-\infty}^{\infty} \frac{\epsilon_1(\zeta)}{\zeta^{j+1}} d\zeta. \end{aligned} \quad (5.8)$$

The validity of this expansion procedure hinges upon the fact that when $|\zeta| \leq |\omega|$ and the expansion of $(1-\omega/\zeta)^{-1}$ in the integrand breaks down, $\epsilon_1(\zeta)$ is very close to zero and serves to neutralize this undesirable behavior. Due to the odd parity of $\epsilon_1(\zeta)$, one then obtains the expansion

$$\epsilon_r(\omega) \approx 1 + \sum_{j=0}^{\infty} \beta_{2j} \omega^{2j} \quad (5.9)$$

with

$$\beta_{2j} \equiv \frac{1}{\pi} \int_{-\infty}^{\infty} \frac{\epsilon_1(\zeta)}{\zeta^{2j+1}} d\zeta, \quad (5.10)$$

which is valid for $|\omega| \ll \omega_0$.

Since $\epsilon_r(\zeta)$ does not vanish when $\zeta = 0$, the same expansion technique cannot be used in obtaining an expansion for Eq. (5.4b). However, by use of the symmetry relation (5.5a), that equation may be rewritten as

$$\epsilon_i(\omega) = -\omega \frac{2}{\pi} \int_0^\infty \frac{\epsilon_r(\zeta) - 1}{\zeta^2 - \omega^2} d\zeta, \quad (5.11)$$

which explicitly shows that $\epsilon_i(0) = 0$. For $|\omega|$ small one may then take the approximation

$$\epsilon_i(\omega) \cong 2\delta_1\omega \quad (5.12)$$

where

$$\delta_1 \cong + \frac{1}{\pi} \int_0^\infty \frac{1 - \epsilon_r(\zeta)}{\zeta^2} d\zeta \quad (5.13)$$

is a nonnegative real number.

Hence, for sufficiently small values of $|\omega| \ll \omega_0$, the complex dielectric permittivity may be approximated as

$$\epsilon(\omega) \cong \epsilon_0 + 2i\delta_1\omega + \beta_2\omega^2 \quad (5.14)$$

where

$$\epsilon_0 = 1 + \beta_0 \quad (5.15)$$

is the static dielectric permittivity of the medium. The complex index of refraction in the region about the origin is then given by

$$n(\omega) = [\epsilon(\omega)]^{1/2} \cong [\epsilon_0 + 2i\delta_1\omega + \beta_2\omega^2]^{1/2}$$

$$= \epsilon_0^{1/2} [1 + 2i \frac{\delta_1}{\epsilon_0} \omega + \frac{\beta_2}{\epsilon_0} \omega^2]^{1/2}$$

$$\cong \epsilon_0^{1/2} [1 + i \frac{\delta_1}{\epsilon_0} \omega + \frac{\beta_2}{2\epsilon_0} \omega^2 - \frac{1}{8} (2i \frac{\delta_1}{\epsilon_0} \omega)^2]$$

$$\therefore n(\omega) \cong \theta_0 + i \frac{\delta_1}{\theta_0} \omega + \frac{1}{2\theta_0} (\beta_2 + \frac{\delta_1^2}{\theta_0^2}) \omega^2 \quad (5.16)$$

where

$$\theta_0 = \epsilon_0^{1/2} = n(0). \quad (5.17)$$

With this approximation, valid for $|\omega| \ll \omega_0$, the saddle point equation (5.2) becomes

$$\omega^2 + i \frac{4\delta_1}{3\alpha_1} \omega - \frac{2\theta_0}{3\alpha_1} (\theta - \theta_0) = 0, \quad (5.18)$$

where

$$\alpha_1 \equiv \frac{\delta_1^2}{\theta_0^2} + \beta_2. \quad (5.19)$$

The solutions (roots) of Eq. (5.18) then yield the approximate near saddle point locations $\omega_{sp_N}^{\pm}$, given by

$$\omega_{sp_N}^{\pm} \equiv \pm \frac{1}{3} \left[6 \frac{\theta_0}{\alpha_1} (\theta - \theta_0) - 4 \frac{\delta_1^2}{\alpha_1^2} \right]^{1/2} - \frac{2\delta_1}{3\alpha_1} i \quad (5.20)$$

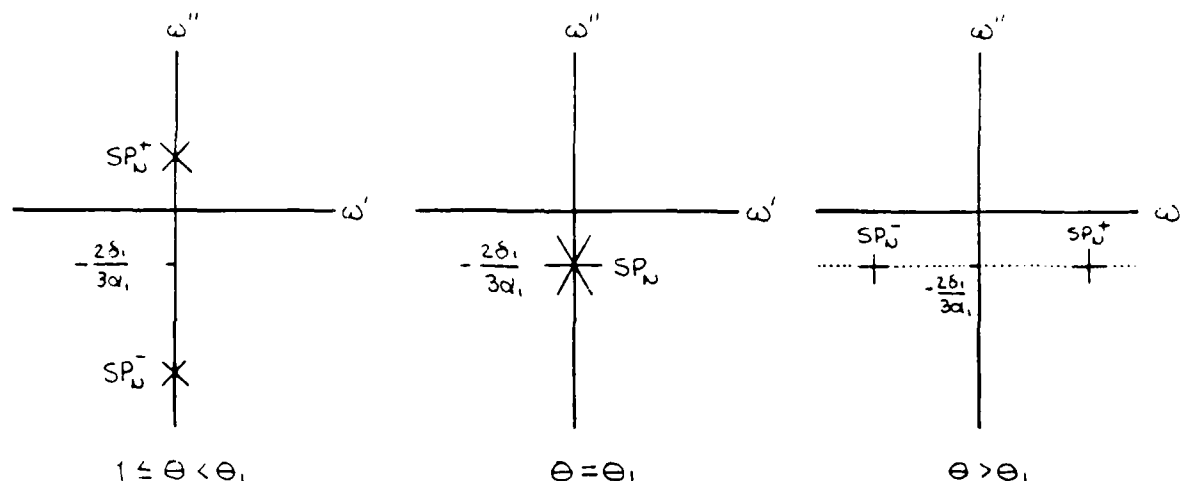
This is precisely the first approximate form obtained for the near saddle point locations in a single resonance Lorentz medium [2-6].

Typically, $\beta_2 > 0$ [as can easily be seen from Eq. (5.10) and the fact that $\epsilon_1(\zeta) \geq 0$ for $\zeta > 0$ and $\epsilon_1(\zeta) < 0$ for $\zeta < 0$] so that $\alpha_1 > 0$ and the following dynamical evolution of the near saddle points is obtained:

For values of θ in the range $1 \leq \theta < \theta_1$, where

$$\theta_1 = \theta_0 + \frac{2\delta_1^2}{3\theta_0\alpha_1} \quad (5.21)$$

the two near saddle points lie along the imaginary axis, symmetrically situated about the point $\omega = -(2\delta_1/3\alpha_1)i$. At $\theta = \theta_1$, the two near saddle points coalesce into a single saddle point of higher order at $\omega = -(2\delta_1/3\alpha_1)i$, and for $\theta > \theta_1$ the two saddle points move off of the imaginary axis and into the complex ω -plane along the line $\omega'' = -2\delta_1/3\alpha_1$. Notice that the accuracy of this approximation for the near saddle point behavior rapidly decreases as θ becomes much different than θ_0 , since $|\omega_{sp_N}^{\pm}|$ will then no longer be small in comparison to ω_0 . A completely accurate description of the saddle point evolution with θ that is valid for all $\theta \geq 1$ can only be constructed once the behavior of $n(\omega)$ is explicitly known in the region of the complex ω -plane about the first absorption peak at ω_0 , as has been done in Refs. [4,6] for a single resonance Lorentz medium.



Dynamical Evolution of the Near Saddle Points

In order to simplify the notation in the remaining analysis of the complex phase behavior at the near saddle point locations, Eq. (5.20) may be rewritten as

$$\omega_{SP_N^\pm}(\theta) \approx \pm \psi(\theta) - \frac{2}{3} \delta_1 \quad (5.22)$$

with

$$\psi(\theta) = \frac{1}{3} \left[6 \frac{\theta_0}{\alpha_1} (\theta - \theta_0) - \frac{4\delta_1^2}{\alpha_1^2} \right]^{1/2}, \quad (5.23)$$

$$\delta = \frac{\delta_1}{\alpha_1}, \quad (5.24)$$

where the positive branch of the square root is to be taken in Eq. (5.23).

For $1 \leq \theta < \theta_1$, the near saddle point locations are then given by

$$\omega_{SP_N^\pm}(\theta) \approx i \left[\pm \psi(\theta) - \frac{2}{3} \delta \right], \quad (5.25)$$

where the quantity inside the square brackets is real-valued. With this substitution Eq. (5.1) yields, with the approximation of Eq. (5.16),

$$\phi(\omega_{sp_N}^{\pm}, \theta) \approx -\left(\frac{2\delta_1}{3} |\psi(\theta)|\right) \left\{ \theta - \theta_0 - \frac{1}{2\theta_0} \left(\frac{2\delta_1}{3} |\psi(\theta)| \right) \left[2\delta_1 - \left(\beta_2 + \frac{\delta_1^2}{\theta_0^2} \right) \left(\frac{2}{3} \delta_1 |\psi(\theta)| \right) \right] \right\}, \quad (5.26)$$

for $\theta \leq \theta_1$. At $\theta = \theta_1$, $\psi(\theta_1) = 0$ and the two near saddle points have coalesced into a single higher-order saddle point at

$$\omega_{sp_N}(\theta_1) \approx -\frac{2}{3} \delta_1 i \quad (5.27)$$

and the approximate phase behavior is given by

$$\phi(\omega_{sp_N}, \theta_1) \approx -\frac{4\delta_1^3}{9\theta_0} \left(\beta_2 + \frac{\delta_1^2}{\theta_0^2} \right). \quad (5.28)$$

Finally, for $\theta > \theta_1$, the two near saddle points have moved off of the imaginary axis and are symmetrically situated in the complex ω -plane with respect to the imaginary axis, where

$$\omega_{sp_N}^{\pm}(\theta) \approx \pm \psi(\theta) - \frac{2}{3} \delta_1 i, \quad (5.29)$$

with ψ real. With this substitution Eq. (5.1) yields, with the approximation of Eq. (5.16),

$$\phi(\omega_{sp_N}^{\pm}, \theta) \approx -\frac{2\delta_1}{3} \left\{ \theta - \theta_0 + \frac{1}{\theta_0} \left[\left(\frac{3}{2} \alpha_1 - \beta_2 - \frac{\alpha_1^2 \delta_1^2}{\theta_0^2} \right) \psi^2(\theta) + \frac{2}{9} \delta_1^2 \left(\beta_2 + \frac{\alpha_1^2 \delta_1^2}{\theta_0^2} - 3\alpha_1 \right) \right] \right\} \quad (5.30)$$

$$\pm i \psi(\theta) \left\{ \theta_0 - \theta + \frac{1}{2\theta_0} \left[\left(\beta_2 + \frac{\alpha_1^2 \delta_1^2}{\theta_0^2} \right) (\psi^2(\theta) - \frac{8}{9} \delta_1^2) + \frac{8}{9} \alpha_1 \delta_1^2 \right] \right\},$$

for $\theta > \theta_1$.

The preceding results remain valid in the special case when $\delta_1 = 0$ (in that case ϵ_1 varies as ω^3 about the origin). The approximate saddle point equation (5.18) is then still correct to $O(\omega^2)$ and, for values of θ not too distant from θ_0 , the approximate near saddle point locations are now simply given by

$$\omega_{sp_N}^{\pm}(\theta) = \pm \left[\frac{2\theta_0}{3\beta_2} (\theta - \theta_0) \right]^{1/2}$$

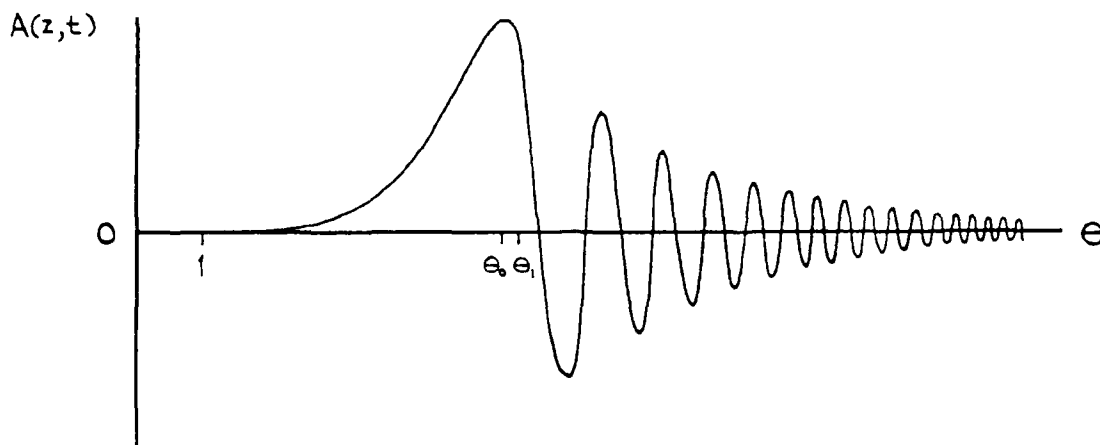
The same dynamical evolution is then obtained but with the two near saddle points now coalescing into a single higher order saddle point at the origin when $\theta = \theta_1 = \theta_0$. Clearly, Eqs. (5.26), (5.28), and (5.30) remain valid in this case with $\delta = \delta_1 = 0$. This is the only special case that can arise here since neither β_0 nor β_2 can vanish for a causally dispersive medium (the trivial case of a vacuum is of course excluded).

Since the above described near saddle point dynamics and complex phase behavior in the region of the complex ω -plane about the origin are completely analogous to that obtained for a single resonance Lorentz medium, as described in Refs. [2] and [3] and by the first approximate expressions in Refs. [4] and [6], the complex phase structure in the neighborhood of these near saddle points is then also the same. The subsequent asymptotic analysis of the contribution to the propagated field from these two near saddle points then exactly follows the procedure described in Refs. [4,6] for a single resonance Lorentz medium. These general near saddle points, when they are the dominant contribution to the asymptotic behavior of the propagated field, then yield the typical Brillouin precursor field evolution. One then has the following result:

Under proper excitation, the classical Brillouin precursor field will evolve in any perfect dielectric medium whose loss is negligible for all values of $\omega' = \text{Re}(\omega)$ such that

$$0 \leq \omega' < \omega_0. \quad (5.31)$$

This precursor field is nonoscillatory for $1 \leq \theta \leq \theta_1$, reaches a peak value at $\theta = \theta_0 < \theta_1$ at which it is unattenuated, and is oscillatory for $\theta > \theta_1$ with an instantaneous angular frequency which increases with increasing θ , as illustrated.



5.2 The Region about Infinity; $|\omega| \gg \omega_m$

Since $\epsilon_1(\zeta)$ vanishes at $\zeta = \pm\infty$, one may then expand the denominator in the integrand of Eq. (5.4a) for large $|\omega|$ as follows:

$$\begin{aligned}\epsilon_r(\omega) &= 1 - \frac{1}{\pi} \int_{-\infty}^{\infty} \frac{\epsilon_1(\zeta)}{\omega} \cdot \frac{1}{1-\zeta/\omega} d\zeta \\ &\approx 1 - \sum_{j=0}^{\infty} \frac{1}{\omega^{j+1}} \frac{1}{\pi} \int_{-\infty}^{\infty} \epsilon_1(\zeta) \zeta^j d\zeta.\end{aligned}\quad (5.32)$$

The validity of this expansion procedure hinges upon the fact that when $|\zeta| \geq |\omega|$ and the expansion of $(1-\zeta/\omega)^{-1}$ in the integrand breaks down, $\epsilon_1(\zeta)$ is very close to zero and serves to neutralize this undesirable behavior. Due to the odd parity of $\epsilon_1(\zeta)$, one then obtains the expansion

$$\epsilon_r(\omega) \approx 1 - \sum_{j=1}^{\infty} \frac{a_{2j}}{\omega^{2j}} \quad (5.33)$$

with

$$a_{2j} \equiv \frac{1}{\pi} \int_{-\infty}^{\infty} \epsilon_1(\zeta) \zeta^{2j-1} d\zeta, \quad (5.34)$$

which is valid for $|\omega| \gg \omega_m$. Notice that the first coefficient a_2 is nonvanishing for any dispersive dielectric.

Since $\epsilon_r(\zeta)-1$ also vanishes at $\zeta = \pm\infty$, the same expansion procedure may then be applied in the integrand of Eq. (5.4b), which may be rewritten in the form (5.11), to yield

$$\begin{aligned}\epsilon_1(\omega) &= \frac{2}{\pi} \int_0^\infty \frac{\epsilon_r(\zeta)-1}{\omega} \cdot \frac{1}{1-\zeta^2/\omega^2} d\zeta \\ &\approx \sum_{j=0}^{\infty} \frac{b_j}{\omega^{2j+1}}\end{aligned}\quad (5.35)$$

with

$$b_j \equiv \frac{2}{\pi} \int_0^\infty [\epsilon_r(\zeta)-1] \zeta^{2j} d\zeta, \quad (5.36)$$

which is valid for $|\omega| \gg \omega_m$.

There are two distinct classes of perfect dielectrics that are distinguished by the value of the zeroth-order coefficient

$$b_0 = \frac{2}{\pi} \int_0^\infty [\epsilon_r(\zeta)-1] d\zeta. \quad (5.37)$$

The first class of perfect dielectrics is distinguished by a nonzero value of this coefficient. In that case, the dielectric permittivity in the region about infinity is given approximately by

$$\epsilon(\omega) \approx 1 + i \frac{b_0}{\omega} - \frac{a_2}{\omega^2} \quad ; \quad b_0 \neq 0. \quad (5.38)$$

An important model which yields this form of the frequency dependence at high frequencies is given by the Debye theory; hence, this class of perfect dielectrics will herein be called the Debye class. The other general class of perfect dielectrics is then distinguished by b_0 being identically zero, in which case one has the superconvergence relation [8,12]

$$\int_0^\infty [\epsilon_r(\zeta)-1] d\zeta = 0 \quad (5.39)$$

In this case, the dielectric permittivity in the region of the complex ω -plane about infinity is given approximately by

$$\epsilon(\omega) \approx 1 - \frac{a_2}{\omega^2} + i \frac{b_2}{\omega^3} \quad (5.40)$$

with

$$b_2 = \frac{2}{\pi} \int_0^{\infty} [\epsilon_p(\zeta) - 1] \zeta^4 d\zeta. \quad (5.41)$$

An important model which yields this form of the frequency dependence at high frequencies is given by the Lorentz theory; this class of perfect dielectrics is accordingly called the Lorentz class. No further classification need be made (at least within the level of approximation of the present analysis) if b_2 also vanishes, since the approximation (5.40) is accurate to $O(\omega^{-3})$. The dynamical evolution of the distant saddle points and the associated complex phase behavior at these points must then be separately developed for these two general classes of perfect dielectrics.

5.2.1. Case I: The Debye Class Dielectric.

In this case, the high-frequency behavior of the dielectric permittivity is given by Eq. (5.38), so that the associated complex index of refraction is given by

$$\begin{aligned} n(\omega) &= [\epsilon(\omega)]^{1/2} = \left[1 + i \frac{b_0}{\omega} - \frac{a_2}{\omega^2} \right]^{1/2} \\ &\approx 1 + i \frac{b_0}{2\omega} - \frac{1}{2} \left(a_2 - \frac{b_0^2}{4} \right) \frac{1}{\omega^2}. \end{aligned} \quad (5.42)$$

With this approximation, valid for $|\omega| \gg \omega_m$, the saddle point equation (5.2) becomes

$$-\frac{1}{2} \left(a_2 - \frac{b_0^2}{4} \right) \frac{1}{\omega^2} + \theta - 1 = 0, \quad (5.43)$$

and the saddle point locations are then simply given by

$$\omega_{sp_D}^{\pm} \approx \pm \left[\frac{a_2 - b_0^2/4}{2(\theta - 1)} \right]^{1/2} \quad (5.44)$$

The behavior of these distant saddle points in the complex ω -plane, as well as their possible contribution to the asymptotic expansion of the propagated field, is then seen to be critically dependent upon the sign of the quantity $(a_2 - b_0^2/4)$. One then has the following subcases:

(i). $a_2 - b_0^2/4 < 0$: Normal Debye Dielectric.

For a simple Debye model medium with high frequency permittivity equal to unity, the complex permittivity is given by

$$\epsilon(\omega) = 1 + \frac{\epsilon_0 - 1}{1 + \tau^2 \omega^2} + i \frac{\epsilon_0 - 1}{1 + \tau^2 \omega^2} \tau \omega,$$

where τ is the macroscopic relaxation time of the medium. In the high frequency limit $\omega \gg 1/\tau$ this expression may be approximated as

$$\epsilon(\omega) \cong 1 + \frac{\epsilon_0 - 1}{\tau^2 \omega^2} + i \frac{\epsilon_0 - 1}{\tau \omega},$$

so that the coefficients appearing in Eq. (5.38) are given by

$$b_0 = \frac{\epsilon_0 - 1}{\tau}, \quad a_2 = \frac{1 - \epsilon_0}{\tau^2}.$$

Clearly,

$$a_2 - \frac{b_0^2}{4} < 0 \quad (5.45)$$

and is equal to zero only when $\epsilon_0 = 1$ [in which case $\epsilon(\omega) = 1$ for all ω and one has the vacuum]. In this important case, which is strictly satisfied by the Debye model, the distant saddle points are symmetrically situated with respect to the origin along the imaginary axis, and

$$\omega_{spD}^{\pm}(\theta) \cong \pm i \frac{k}{(\theta - 1)^{1/2}} \quad (5.46)$$

where $k^2 = (1/2)|a_2 - (b_0^2/4)|$. From Eq. (5.42), the approximate behavior of the complex index of refraction at these two distant saddle points is found to be

$$n(\omega_{sp}^{\pm}) \cong -\theta \pm \frac{b_0}{2k} \sqrt{\theta - 1}, \quad (5.47)$$

and the complex phase function at these points is given by

$$\phi(\omega_{sp}^{\pm}, \theta) \cong \pm 2k \frac{\theta}{\sqrt{\theta - 1}} - \frac{b_0}{2}, \quad (5.48)$$

which is real-valued for all $\theta \geq 1$. At the upper distant saddle point $\phi(\omega_{spD}^{+}, \theta) > 0$ for all $\theta \geq 1$ while at the lower distant saddle point $\phi(\omega_{spD}^{-}, \theta) < 0$ for all $\theta \geq 1$.

In order to obtain the approximate behavior of $X(\omega, \theta) = R_\theta[\phi(\omega, \theta)]$ in a neighborhood about each of the distant saddle points in the complex ω -plane, let

$$\omega = \omega_{sp_D}^\pm(\theta) + re^{i\psi}. \quad (5.47)$$

With this substitution Eq. (5.42) yields the approximate expression

$$n(r, \psi) \cong n(\omega_{sp_D}^\pm) + [2(\theta-1) \mp \frac{b_0}{2k} (\theta-1)^{1/2}] \rho e^{i\psi}$$

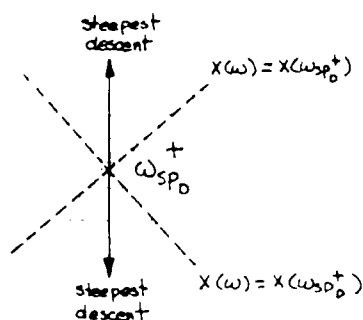
for the complex index of refraction in the neighborhood of each of these two saddle points, where $\rho = r/\omega_{sp_D}^\pm$. With these two substitutions, Eq. (5.1) then yields

$$\phi(\theta, r, \psi) - \phi(\omega_{sp_D}^\pm, \theta) \cong -2ire^{i\psi} \pm \frac{\theta-1}{k} [2(\theta-1)^{1/2} \mp \frac{b_0}{2k}] r^2 e^{i2\psi}$$

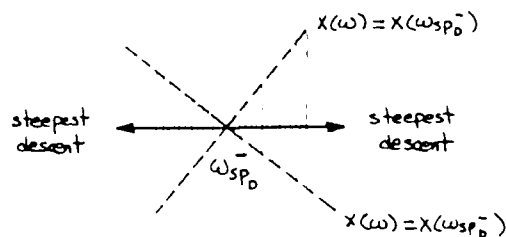
so that

$$\begin{aligned} X(\theta, r, \psi) - X(\omega_{sp_D}^\pm, \theta) &\cong \text{Re}[\phi(\theta, r, \psi) - \phi(\omega_{sp_D}^\pm, \theta)] \\ &\cong 2r\sin\psi \pm \frac{\theta-1}{k} [2(\theta-1)^{1/2} \mp \frac{b_0}{2k}] r^2 \cos(2\psi) \end{aligned} \quad (5.49)$$

It is then seen that $X(\theta, r, \psi)$ attains its maximum variation with r about the distant saddle points $\omega_{sp_D}^\pm$ for $\psi = 0, \pi/2, \pi$ and $3\pi/2$. For the upper distant saddle point $\omega_{sp_D}^+$ the lines of steepest descent through the saddle point are at $\psi = \pi/2$ and $3\pi/2$, while for the lower distant saddle point $\omega_{sp_D}^-$ they are at $\psi = 0$ and π , as illustrated below.



Real Part of the Phase
Behavior about the Upper
Distant Saddle Point



Real Part of the Phase
Behavior about the Lower
Distant Saddle Point

Whether or not either of these two distant saddle points contribute to the asymptotic behavior of the propagated field is of no consequence to the question of the appearance of the Sommerfeld precursor field. For the present situation, there can be no high frequency transient field evolution simply because the distant saddle points have no oscillatory component [i.e. $\phi(\omega_{sp_D}^{\pm})$ is real-valued for all $\theta \geq 1$]. Hence, the Sommerfeld precursor field will be absent for this type of Debye class dielectric. Because of this, a dielectric of this specific type is called here a Normal Debye Dielectric.

(ii). $a_2 - b_0^2/4 > 0$; Inverted Debye-Type Dielectric.

In the previous case of a so-called normal Debye dielectric for which $a_2 - b_0^2/4 < 0$, the real index of refraction $n_r(\omega')$ is seen to approach unity from above in the infinite frequency limit. In the present case with $a_2 - b_0^2/4 > 0$ the opposite is true as $n_r(\omega')$ approaches unity from below as $|\omega'| \rightarrow \infty$, and this is why the modifier "inverted" is used here.

For the inverted Debye-type dielectric, the distant saddle points are symmetrically situated with respect to the origin along the real axis, and

$$\omega_{sp_D}^{\pm}(\theta) \approx \pm \frac{d}{(\theta-1)^{1/2}}, \quad (5.50)$$

where $d^2 = (a_2 - b_0^2/4)/2$. From Eq. (5.42), the approximate behavior of the complex index of refraction at these two distant saddle points is found to be

$$n(\omega_{sp_D}^{\pm}) \approx 2-\theta \pm i \frac{b_0}{2d} (\theta-1)^{1/2} \quad (5.51)$$

and the complex phase function at these points is given by

$$\phi(\omega_{sp_D}^{\pm}, \theta) \approx -\frac{b_0}{2} \mp 12d(\theta-1)^{1/2}.$$

In this case, the phase behavior at the distant saddle points has an oscillatory component that is completely analogous to that obtained for a single resonance Lorentz medium [1-4,6]. These general distant saddle points, when they are the dominant contribution to the asymptotic behavior of the propagated field, will then yield the typical Sommerfeld precursor field evolution with the single exception that the attenuation of this transient is independent of θ (at least to this level of approximation).

(iii). $a_2 = b_0^2/4$; Transition-Type Debye Dielectric.

In the special case when $a_2 = b_0^2/4$ the level of approximation leading to Eq. (5.44) is inadequate and Eq. (5.38) for the high-frequency behavior of the dielectric permittivity must be replaced by the more accurate expression

$$\epsilon(\omega) \cong 1 - \frac{a_2}{\omega^2} + i\left(\frac{b_0}{\omega} + \frac{b_2}{\omega^3}\right). \quad (5.53)$$

The associated complex index of refraction is then given by

$$n(\omega) \cong 1 + \frac{i}{2}\left(\frac{b_0}{\omega} + (b_2 + \frac{1}{2} a_2 b_0) \frac{1}{\omega^3}\right), \quad (5.54)$$

and the saddle point Eq. (5.2) becomes

$$\theta - 1 + i\left(b_2 + \frac{1}{2} a_2 b_0\right) \frac{1}{\omega^3} = 0 \quad (5.55)$$

with solution

$$\omega_{sp_D}^{(\pm n)} \cong \frac{b_0}{2} \left[\frac{1+8b_2/b_0^3}{\theta-1} \right]^{1/3} e^{i[(\pi/2) \pm (2n\pi/3)]}; \quad n = 0, 1. \quad (5.56)$$

In this special case there are three distant saddle points, one along the positive imaginary axis and the other two in the lower-half of the complex ω -plane along lines with angles of $-\pi/6$ and $-5\pi/6$ with respect to the positive real axis. From Eq. (5.42), the approximate behavior of the complex index of refraction at this trio of distant saddle points is readily found to be

$$n(\omega_{sp_D}^{(\pm n)}) \cong 1 - \frac{1}{2}(\theta-1) + \left[\frac{\theta-1}{1+8b_2/b_0^3} \right]^{1/3} e^{\pm i(2n\pi/3)}; \quad n = 0, 1. \quad (5.57)$$

The complex phase function at these three distant saddle points is then given by

$$\phi(\omega_{sp_D}^{(\pm n)}, \theta) \cong -\frac{b_0}{2} + \frac{3b_0}{4} \left[1 + 8 \frac{b_2}{b_0^3} \right]^{1/3} (\theta-1)^{2/3} e^{\pm i(2n\pi/3)} ; n = 0, 1. \quad (5.58)$$

For the saddle point along the imaginary axis ($n=0$), the phase function is purely real, and hence, nonoscillatory, while for the other two saddle points $\omega_{sp_D}^{(\pm 1)}$, the phase function is complex-valued, and hence, will yield an oscillatory component.

In order to obtain the approximate behavior of $X(\omega, \theta) \equiv \text{Re}[\phi(\omega, \theta)]$ in a neighborhood about each of these distant saddle points, let

$$\omega = \omega_{sp_D}^{(\pm n)} + re^{i\psi}.$$

With this substitution Eq. (5.54) yields the approximate expression

$$n(\omega) \cong n(\omega_{sp_D}^{(\pm n)}) + i \frac{2}{b_0} \left[\frac{\theta-1}{1+8b_2/b_0^3} \right]^{2/3} e^{\mp i(4n\pi/3)} \cdot A$$

for the complex index of refraction in the neighborhood of each of these distant saddle points, where

$$A = \left\{ 1 - \frac{3}{2} \left(1 + 8 \frac{b_2}{b_0^3} \right) \left[\frac{\theta-1}{1+8b_2/b_0^3} \right]^{2/3} e^{\mp i(4n\pi/3)} \right\} re^{i\psi}.$$

With these two substitutions, Eq. (5.1) then yields

$$\phi(\theta, r, \psi) - \phi(\omega_{sp_D}^{(\pm n)}, \theta) \cong -\frac{2}{b_0} \left[\frac{\theta-1}{1+8b_2/b_0^3} \right]^{2/3} e^{\mp i(4n\pi/3)} \cdot A \cdot r^2 e^{i2\psi}$$

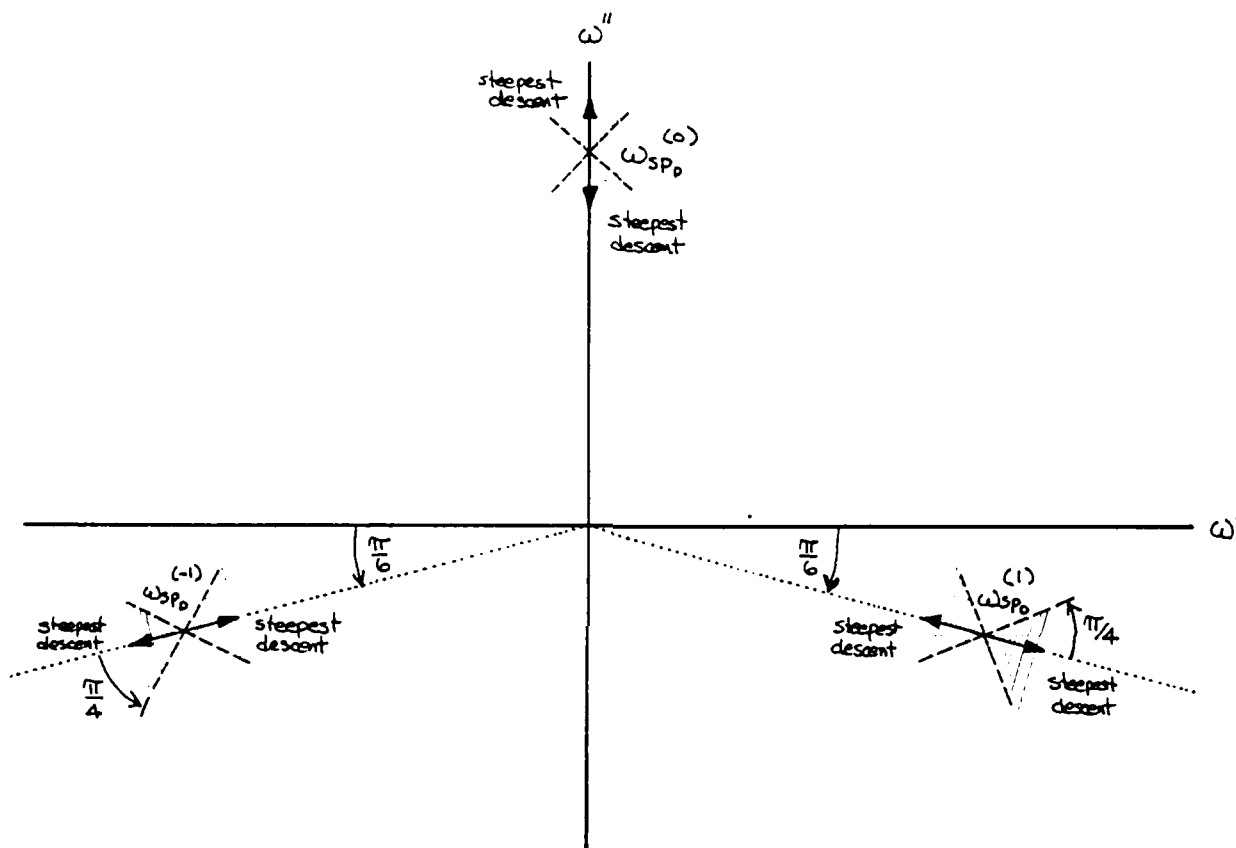
so that

$$X(\theta, r, \psi) - X(\omega_{sp_D}^{(\pm n)}, \theta) \cong \text{Re}[\phi(\theta, r, \psi) - \phi(\omega_{sp_D}^{(\pm n)}, \theta)] \quad (5.59)$$

$$\cong -\frac{2}{b_0} \left[\frac{\theta-1}{1+8b_2/b_0^3} \right]^{2/3} r^2 \left\{ \cos\left(2\psi \mp \frac{4n\pi}{3}\right) - \frac{3}{2} \left(1 + 8 \frac{b_2}{b_0^3} \right) \left[\frac{\theta-1}{1+8b_2/b_0^3} \right]^{2/3} \cos\left(2\psi \mp \frac{2n\pi}{3}\right) \right\},$$

for $n = 0, 1$.

It is then seen that at the distant saddle point along the positive imaginary axis ($n=0$), the paths of steepest descent are along the imaginary axis ($\psi = \pm \pi/2$) and the isotimic contours of $\chi(\omega_{sp_D}^{(0)})$ are at $\psi = \pm \pi/4$.



Real Part of the Complex Phase Behavior about the Distant Saddle Points

For the other two saddle points $\omega_{sp_D}^{(\pm 1)}$, which are along lines with angles of $-\pi/6$ and $-\pi/6$ with respect to the positive real axis, as illustrated, the paths of steepest descent are along these lines and the isotimic contours of $\chi(\omega_{sp_D}^{(\pm 1)})$ are at angles of $\pm \pi/4$ to these lines. These two distant saddle points $\omega_{sp_D}^{(\pm 1)}$, when they are the dominant

contribution to the asymptotic behavior of the propagated field, will then yield the typical Sommerfeld precursor field evolution with the single exception that the attenuation of this transient is independent of θ (at least to this level of approximation).

5.2.2. Case II: The Lorentz Class Dielectric.

In this case, the high-frequency behavior of the dielectric permittivity is given by Eq. (5.40), which may be written as

$$\epsilon(\omega) \cong 1 - \frac{a_2}{\omega(\omega + ib_2/a_2)}, \quad (5.60)$$

so that the associated complex index of refraction is given by

$$n(\omega) = [\epsilon(\omega)]^{1/2} \cong 1 - \frac{a_2}{2\omega(\omega + ib_2/a_2)}. \quad (5.61)$$

With this approximation, valid for $|\omega| \gg \omega_m$, the saddle point equation (5.2) becomes

$$1 - \theta - \frac{a_2}{2\omega(\omega + ib_2/a_2)} + \frac{a_2(2\omega + ib_2/a_2)}{2\omega(\omega + ib_2/a_2)^2} = 0,$$

which may be approximated as [2,3,4,6]

$$1 - \theta + \frac{a_2}{2\omega(\omega + ib_2/a_2)} \cong 0, \quad (5.62)$$

with solution

$$\omega_{spD}^{\pm} \cong \pm \left[\frac{a_2}{2(\theta-1)} - \frac{b_2^2}{4a_2} \right]^{1/2} - i \frac{b_2}{2a_2} \quad (5.63)$$

This is precisely the first approximate form obtained for the distant saddle point locations in a single resonance Lorentz medium [2-6].

These saddle points are then symmetrically situated about the imaginary axis along the line $\omega = -ib_2/a_2$ and, as θ increases from unity, they move in from infinity along this line. From Eqs. (5.61) and (5.63), the complex phase function at these two distant saddle points is found to be given approximately by

$$\phi(\omega_{sp_D}^{\pm}, \theta) \cong -\frac{b_2}{a_2} (\theta-1) \mp i[2a_2(\theta-1)]^{1/2} \left[1 + \frac{b_2^2}{a_2^3}(\theta-1)\right], \quad (5.64)$$

which should be compared with the phase structure given in Eq. (5.52) for an inverted Debye-type dielectric. As in that case, the phase behavior at the distant saddle points again has an oscillatory component that is completely analogous to that obtained for a single resonance Lorentz medium. These general distant saddle points, when they are the dominant contribution to the asymptotic behavior of the propagated field, will then yield the typical Sommerfeld precursor field evolution.

5.2.3. Conclusion.

The results of this section may be summarized by the following statement:

Under proper excitation, the classical Sommerfeld precursor field will evolve in any perfect dielectric medium whose loss is negligible for all values of $\omega' = \text{Re}(\omega)$ such that

$$0 < \omega_m < \omega' \quad (5.65)$$

and provided that the real part of the complex dielectric permittivity approaches its infinite frequency value from below as $\omega' \rightarrow \infty$.

VI. ANALYSIS OF THE COMPLEX PHASE FUNCTION AND ITS SADDLE POINTS FOR AN IMPERFECT DIELECTRIC

If the medium has a nonvanishing static conductivity σ , one speaks of an imperfect dielectric and the complex permittivity $\epsilon(\omega)$ has a simple pole at the origin about which $\epsilon = 4\pi i\sigma/\omega$. The dispersion relations (5.4) are then replaced by

$$\epsilon_r(\omega) = 1 + \frac{1}{\pi} \int_{-\infty}^{\infty} \frac{\epsilon_i(\zeta)}{\zeta - \omega} d\zeta, \quad (6.1a)$$

$$\epsilon_i(\omega) = -\frac{1}{\pi} \int_{-\infty}^{\infty} \frac{\epsilon_r(\zeta) - 1}{\zeta - \omega} d\zeta + \frac{4\pi\sigma}{\omega}. \quad (6.1b)$$

For the behavior in the region of the complex ω -plane about infinity the expansion (5.38) applies so that one obtains the behavior of a Debye class dielectric and the analysis of Section 5.2 directly applies. For a large value of the static conductivity σ the high-frequency behavior of the dielectric permittivity will always exhibit the normal behavior for a Debye type medium and the Sommerfeld precursor will typically be absent. However, if in the absence of the conductivity, the medium is of the inverted Debye type and if σ is sufficiently small, then the imperfect dielectric will also be of the inverted type in which case the Sommerfeld precursor will be present under proper conditions of excitation.

The single major distinction of an imperfect dielectric is due to its behavior about the origin of the complex ω -plane at which it exhibits a simple pole singularity. This singular behavior will clearly have a profound influence upon the dynamical evolution of the near saddle points and the resultant Brillouin precursor field. The expansion (5.9) still applies in the present case but Eq. (5.12) must now be replaced by

$$\epsilon_1(\omega) \cong 4\pi\sigma/\omega, \quad (6.2)$$

for $|\omega| \ll \omega_0$. In the absence of the conductivity, the frequency dependence of $\epsilon_1(\omega)$ along the positive real axis is assumed to be significant only within the finite frequency domain given in Eq. (5.7). Hence, for sufficiently small values of $|\omega|$, the complex dielectric permittivity may be approximated as

$$\epsilon(\omega) \cong \epsilon_0 + i(4\pi\sigma/\omega), \quad (6.3)$$

where $\epsilon_0 = 1 + \beta_0$ is the static dielectric permittivity of the medium in the absence of the conductivity. The complex index of refraction in the region about the origin is then given by

$$\begin{aligned} n(\omega) &= [\epsilon(\omega)]^{1/2} \cong [\epsilon_0 + i \frac{4\pi\sigma}{\omega}]^{1/2} \\ &\cong e^{i(\pi/4)} \left[\frac{4\pi\sigma}{\omega} \right]^{1/2} + \frac{\epsilon_0}{2\pi\sigma} \omega \\ &= e^{i(\pi/4)} \frac{2\pi\sigma}{\omega}^{1/2} + e^{-i(\pi/4)} \frac{\epsilon_0}{2} \omega^{-1/2}. \end{aligned} \quad (6.4)$$

Substitution of this expression into the saddle point equation (5.2)

then yields

$$\begin{aligned} e^{i(\pi/4)} \left(\frac{\pi\sigma}{\omega} \right)^{1/2} + e^{-i(\pi/4)} \frac{3\epsilon_0}{8} \left(\frac{\omega}{\pi\sigma} \right)^{1/2} - \theta = 0 \\ \therefore e^{-i(\pi/4)} \frac{3\epsilon_0}{8(\pi\sigma)^{1/2}} \omega - \theta \omega^{1/2} + e^{i(\pi/4)} (\pi\sigma)^{1/2} = 0. \end{aligned} \quad (6.5)$$

With $\zeta = \omega^{1/2}$, this equation becomes

$$\zeta^2 - e^{i(\pi/4)} \frac{8(\pi\sigma)^{1/2}\theta}{3\epsilon_0} \zeta + e^{i(\pi/2)} \frac{8\pi\sigma}{3\epsilon_0} = 0,$$

with solution

$$\zeta_{\pm} = e^{i(\pi/4)} \frac{4(\pi\sigma)^{1/2}}{3\epsilon_0} \theta \left[1 \pm \left(1 - \frac{3\epsilon_0}{2\theta^2} \right)^{1/2} \right].$$

In terms of the critical value

$$\theta_0 \equiv \left[\frac{3\epsilon_0}{2} \right]^{1/2} \quad (6.6)$$

the above equation becomes

$$[\omega_{spN}^{\pm}]^{1/2} \equiv e^{i(\pi/4)} \frac{2(\pi\sigma)^{1/2}}{\theta_0^2} [\theta \pm (\theta^2 - \theta_0^2)^{1/2}] \quad (6.7)$$

and the near saddle point locations are seen to be given by

$$\omega_{spN}^{\pm}(\theta) \equiv \frac{4\pi\sigma}{\theta_0} [\mp 2\theta(\theta_0^2 - \theta^2)^{1/2} + i(2\theta^2 - \theta_0^2)] ; 1 \leq \theta \leq \theta_0, \quad (6.8a)$$

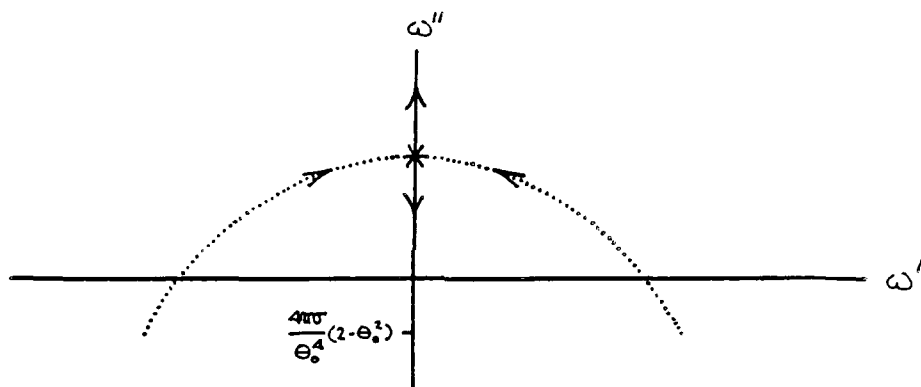
$$\omega_{spN}^{\pm}(\theta) \equiv i \frac{4\pi\sigma}{\theta_0} [2\theta^2 - \theta_0^2 \pm 2\theta(\theta^2 - \theta_0^2)^{1/2}] ; \theta \geq \theta_0 \quad (6.8b)$$

Comparison of these expressions with Eq. (5.20) shows that when the medium has a nonvanishing static conductivity σ , the dynamical evolution of the near saddle points of the complex phase function $\phi(\omega, \theta)$ is essentially reversed from that obtained for a perfect dielectric. In the present case, at $\theta = 1$ the near saddle points are located either in the lower or upper half of the complex ω -plane, dependent upon whether $\theta_0^2 > 2$ or $\theta_0^2 < 2$, respectively, and are symmetrically situated about the imaginary axis. As θ increases to θ_0 , each saddle point moves along an arc toward the point $i(4\pi\sigma/\theta_0^2)$ on the positive imaginary axis and at

$\theta = \theta_0$, the two near saddle points coalesce into a single higher order saddle point at that point. As θ increases above θ_0 , the two near saddle points separate and move along the imaginary axis such that they are symmetrically situated about the point $(4\pi\sigma/\theta_0^4)(2\theta^2 - \theta_0^2)$. As θ goes to infinity, the upper near saddle point $\omega_{sp_N}^+$ goes to $+i\infty$ while the lower near saddle point $\omega_{sp_N}^-$ approaches the origin, so that

$$\lim_{\theta \rightarrow \infty} \omega_{sp_N}^+(\theta) = +i\infty, \quad (6.9a)$$

$$\lim_{\theta \rightarrow \infty} \omega_{sp_N}^-(\theta) = 0. \quad (6.9b)$$



With Eq. (6.7) the approximate behavior of the complex index of refraction (6.4) at the near saddle point locations is found to be

$$n(\omega_{sp_N}^{\pm}(\theta)) \approx \frac{\theta_0^2}{\theta \pm (\theta^2 - \theta_0^2)^{1/2}} + \frac{1}{3} (\theta \pm (\theta^2 - \theta_0^2)^{1/2}), \quad (6.10)$$

which is independent of the conductivity σ . With this substitution, the behavior of the complex phase function $\phi(\omega, \theta)$ at the near saddle point locations is found to be

$$\begin{aligned} \phi(\omega_{sp_N}^{\pm}, \theta) &= i\omega_{sp_N}^{\pm}(\theta) [n(\omega_{sp_N}^{\pm}(\theta)) - \theta] \\ &\approx -\frac{4\pi\sigma}{3\theta_0^4} \theta^2 (\theta \pm (\theta^2 - \theta_0^2)^{1/2}) [2\theta_0^2 - \theta^2 \mp \theta(\theta^2 - \theta_0^2)^{1/2}], \end{aligned} \quad (6.11)$$

which is linearly dependent on the static conductivity σ .

The real and imaginary parts of the complex phase behavior (6.11) at the near saddle points is then given by

$$X(\omega_{sp_N}^{\pm}, \theta) = \operatorname{Re}[\phi(\omega_{sp_N}^{\pm}, \theta)] \approx -\frac{4\pi\sigma}{3\theta_0^4} \theta^3 (3\theta_0^2 - 2\theta^2) , \quad (6.12a)$$

$$Y(\omega_{sp_N}^{\pm}, \theta) = \operatorname{Im}[\phi(\omega_{sp_N}^{\pm}, \theta)] \approx \pm \frac{8\pi\sigma}{3\theta_0^4} \theta^2 (\theta_0^2 - \theta^2)^{3/2} , \quad (6.12b)$$

for $1 \leq \theta \leq \theta_0$, and by

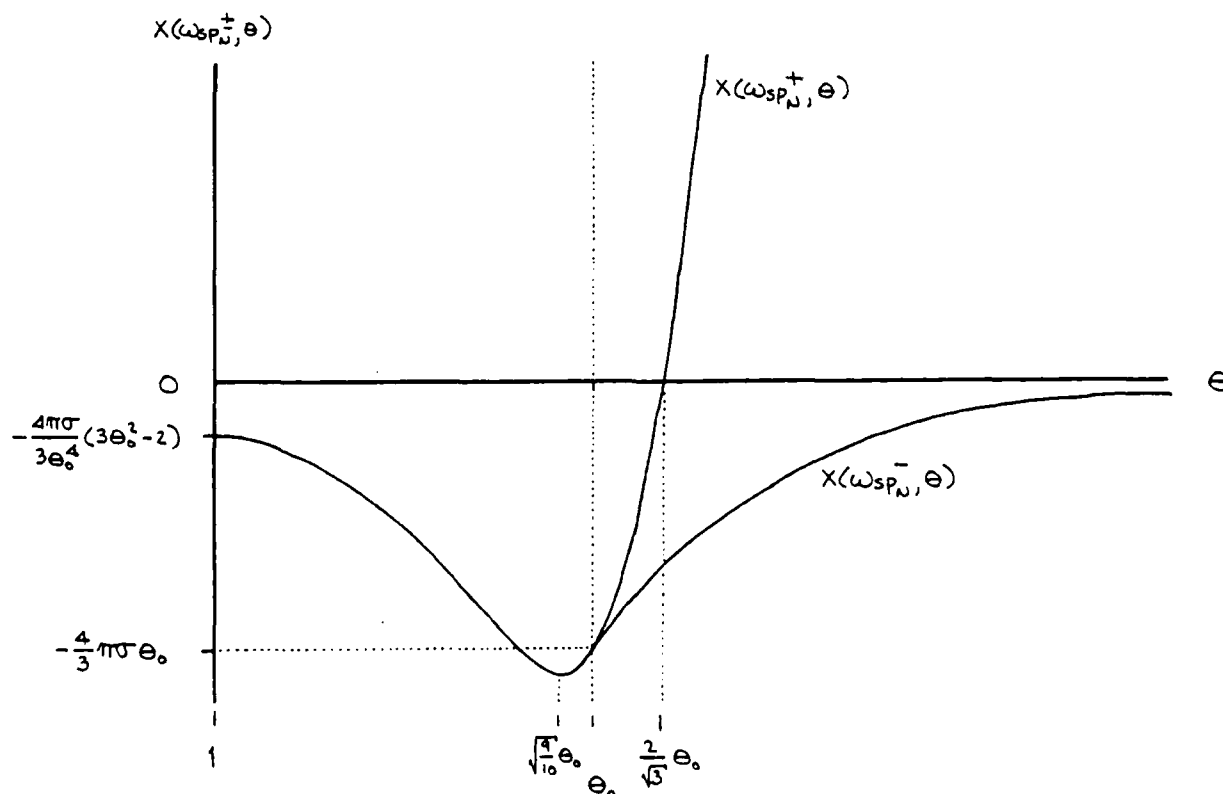
$$X(\omega_{sp_N}^{\pm}, \theta) \approx \frac{4\pi\sigma}{3\theta_0^4} \theta^2 (\theta \pm (\theta^2 - \theta_0^2)^{1/2}) (\theta^2 - 2\theta_0^2 \pm \theta(\theta^2 - \theta_0^2)^{1/2}) , \quad (6.12a)$$

$$Y(\omega_{sp_N}^{\pm}, \theta) = 0 , \quad (6.13b)$$

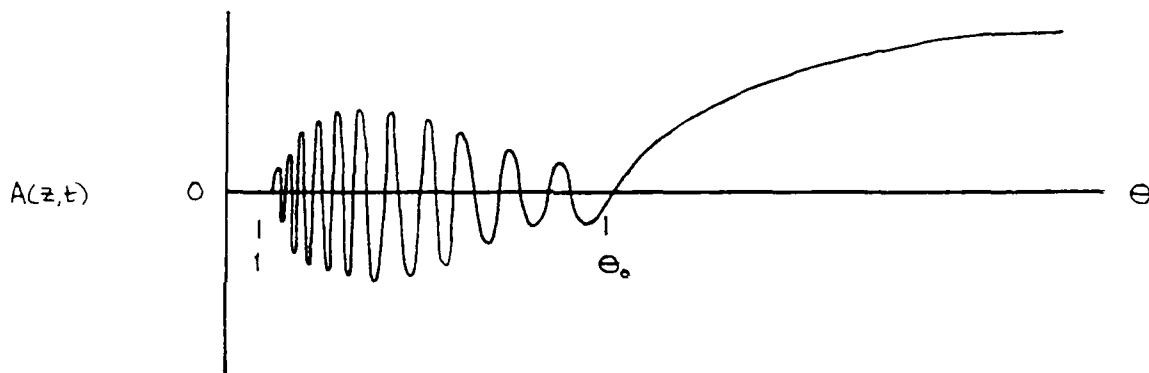
for $\theta_0 \leq \theta$. Notice that in the limit as $\theta \rightarrow \infty$ one has the behavior

$$\lim_{\theta \rightarrow \infty} X(\omega_{sp_N}^{+}, \theta) = \lim_{\theta \rightarrow \infty} \frac{16\pi\sigma}{3\theta_0^4} \theta^5 = +\infty , \quad (6.14a)$$

$$\lim_{\theta \rightarrow \infty} X(\omega_{sp_N}^{-}, \theta) = 0 . \quad (6.14b)$$



The real part of the phase behavior at the near saddle points as a function of θ , illustrated above, is then seen to be essentially the reverse of that obtained for a perfect dielectric medium. Hence, in a dielectric medium with a nonvanishing static conductivity (i.e. an imperfect dielectric), the Brillouin precursor field exists provided that, in the absence of the conductivity, the medium loss is negligible for all values of $\omega' = \text{Re}(\omega)$ such that $0 \leq \omega' < \omega_0$, and evolves in a fashion that is essentially the reverse of that in a perfect dielectric. This precursor field is oscillatory for $1 \leq \theta \leq \theta_0$ with an instantaneous angular frequency that decreases with increasing θ , and is nonoscillatory for $\theta > \theta_0$ with monotonically decreasing attenuation as θ increases to infinity, as illustrated.



VII. INFLUENCE OF THE INITIAL PULSE RISE-TIME ON THE PRECURSOR FIELD FORMATION

The final aspect that needs to be considered in the analysis of the conditions under which precursor field formation will occur in a given temporally dispersive medium is the structure of the initial exciting field itself. The previous two sections have considered at great length the proper medium conditions that are necessary to make possible the evolution of the classical Sommerfeld and Brillouin precursor fields under the assumption that they have been properly excited. Clearly, the ideal excitation is that of an input delta function pulse whose temporal spectrum is unity at all frequencies; in that case the dynamical evolution of the resultant propagated field (i.e. the impulse response of the medium) is entirely described by the dynamical evolution of the saddle

points of the complex phase function for the medium. However, such an idealized excitation is not strictly possible from an experimental point of view and one is forced to consider the conditions under which an experimentally realizable field will excite the precursor fields in such a way that they can be observed.

It is clear that for the precursor fields to be excited, the initial field spectrum must, at the very least, be nonvanishing in those regions of the complex ω -plane wherein there evolves the characteristic saddle points of the dispersive phase function for the medium. It is then seen appropriate to consider the temporal spectrum due to an initial field that identically vanishes for $t < 0$ and which has a finite rise-time envelope function that is continuous in time. An important example of such a field is one with a raised cosine envelope at its leading edge that is monotonically increasing over the time interval $[0, T_r]$ and is constant thereafter. In the limit as the turn-on time T_r goes to zero, this continuous envelope field goes over to the discontinuous limiting case of a Heaviside unit step-function signal which is one of the canonical problems for dispersive pulse propagation [1-4,6]. The raised cosine envelope signal is of a fundamentally different type than the hyperbolic tangent envelope signal considered in Ref. [4] since that initial envelope does not vanish for all times $t < 0$ for finite values of its rise-time. The raised cosine envelope signal can also be used, along with the principle of superposition, to describe a wide variety of finite duration pulses with compact temporal support.

7.1. The Raised Cosine Envelope Signal

The raised cosine envelope function is given by

$$u(t) = \begin{cases} 0 & ; t \leq 0 \\ \frac{1}{2}(1 - \cos(\beta t)) & ; 0 \leq t \leq T_r \\ 1 & ; T_r \leq t \end{cases} \quad (7.1)$$

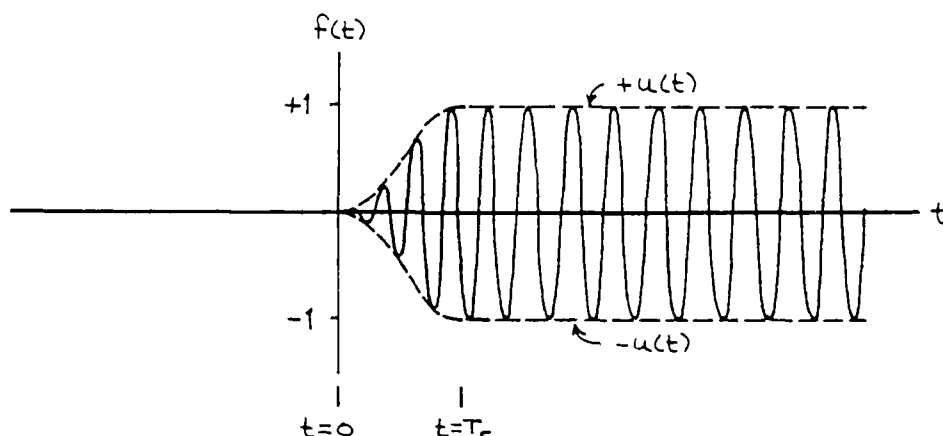
with

$$\beta = \frac{\pi}{T_r} , \quad (7.2)$$

where T_r is the turn-on time of the signal. From Eq. (4.23), the initial field is then given by

$$f(t) = u(t)\sin(\omega_c t) \quad (7.3)$$

where ω_c is the constant signal frequency of the field.



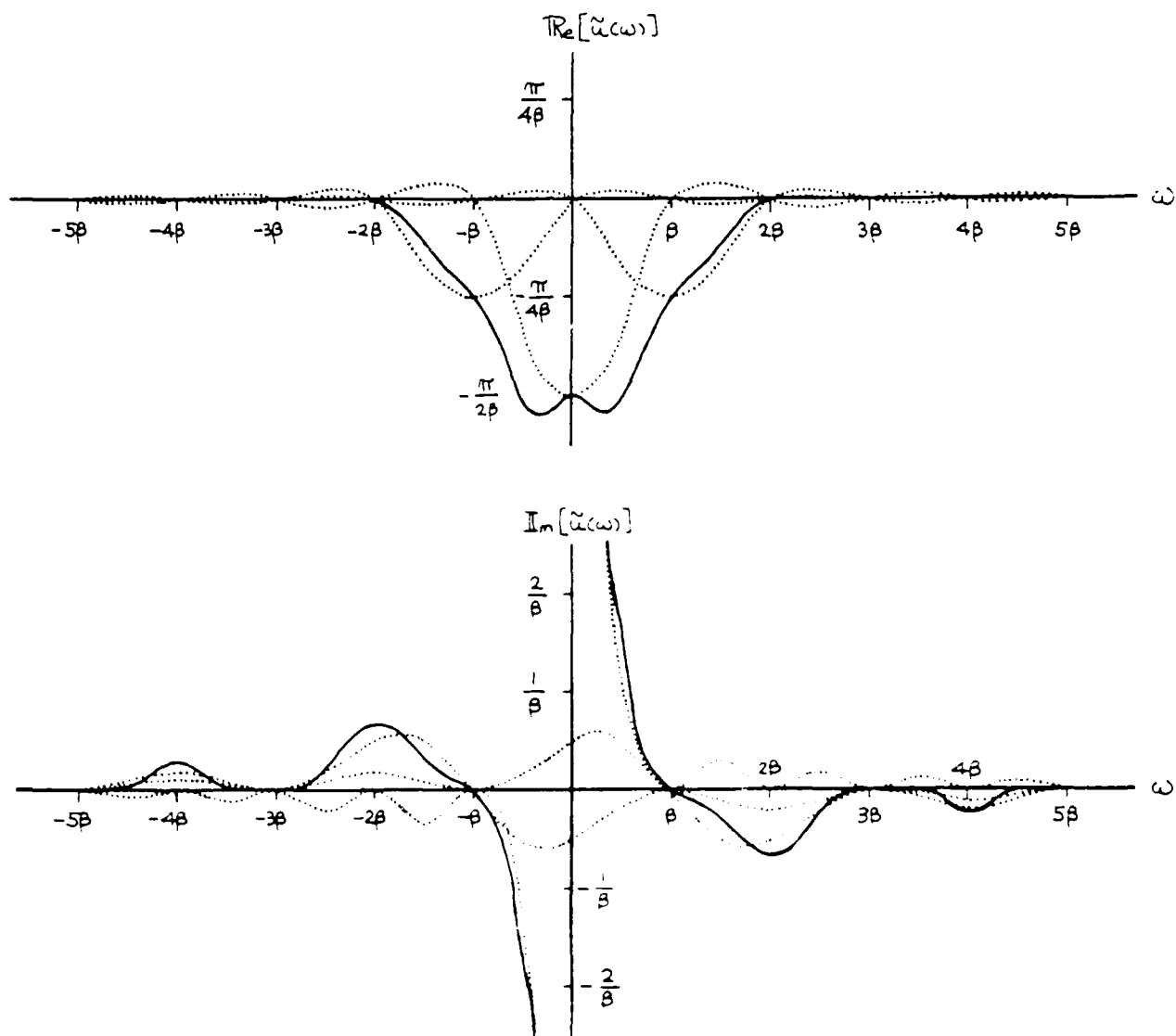
The spectrum of the envelope function (7.1) is given by

$$\begin{aligned} \tilde{u}(\omega) &= \int_0^{\infty} u(t)e^{i\omega t} dt = \frac{1}{2} \int_0^{\pi/\beta} (1 - \cos(\beta t))e^{i\omega t} dt + \int_{\pi/\beta}^{\infty} e^{i\omega t} dt \\ &= \frac{i}{2} e^{i(\pi\omega/2\beta)} \cos\left(\frac{\pi\omega}{2\beta}\right) \left[\frac{2}{\omega} - \frac{1}{\omega+\beta} - \frac{1}{\omega-\beta} \right], \end{aligned} \quad (7.4)$$

with real and imaginary parts (for ω real)

$$\begin{aligned} \text{Re}[\tilde{u}(\omega)] &= -\frac{1}{2} \sin\left(\frac{\pi\omega}{2\beta}\right) \cos\left(\frac{\pi\omega}{2\beta}\right) \left[\frac{2}{\omega} - \frac{1}{\omega+\beta} - \frac{1}{\omega-\beta} \right] \\ &= -\frac{1}{4} \sin\left(\frac{\pi\omega}{\beta}\right) \left[\frac{2}{\omega} - \frac{1}{\omega+\beta} - \frac{1}{\omega-\beta} \right], \end{aligned} \quad (7.5a)$$

$$\text{Im}[\tilde{u}(\omega)] = \frac{1}{2} \cos^2\left(\frac{\pi\omega}{2\beta}\right) \left[\frac{2}{\omega} - \frac{1}{\omega+\beta} - \frac{1}{\omega-\beta} \right]. \quad (7.5b)$$



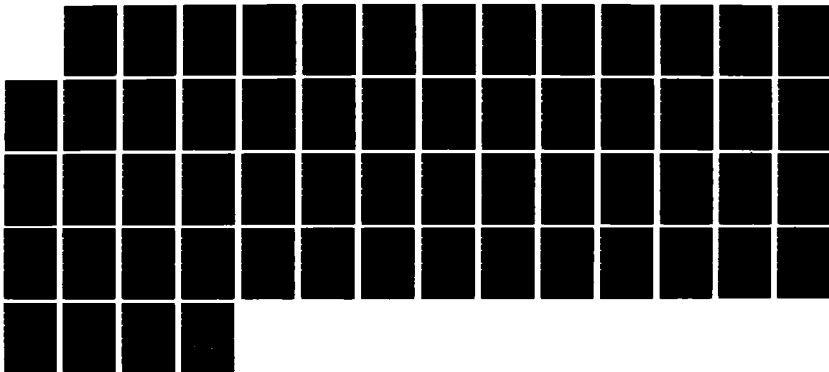
It is well known that the real and imaginary parts of a function are not independent. In fact, they are related by the Hilbert transform. This relationship can be used to find the real part of a function if the imaginary part is known, and vice versa. In this case, the real part of the function is given by the following equation:

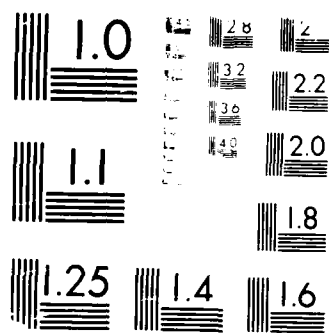
$$\text{Re}[\tilde{u}(\omega)] = \frac{1}{\pi} \int_{-\infty}^{\infty} \frac{\text{Im}[\tilde{u}(\omega')]}{\omega - \omega'} d\omega' \quad (7.93)$$

NO-A191 284

UNITED STATES AIR FORCE SUMMER FACULTY RESEARCH PROGRAM 11/7/
(1987) PROGRAM TE (U) UNIVERSAL ENERGY SYSTEMS INC
DAYTON OH R C DARRAH ET AL DEC 87 AFOSR-TR-88-0213
F49620-85-C-0013 F/G 3/1 NL

UNCLASSIFIED





MICROCOPY RESOLUTION TEST CHART
 NATIONAL BUREAU OF STANDARDS-1963-A

$$\lim_{\beta \rightarrow \infty} \text{Im}[\tilde{u}(\omega)] = \frac{1}{\omega}, \quad (7.6b)$$

so that

$$\lim_{\beta \rightarrow \infty} \tilde{u}(\omega) = \frac{i}{\omega}, \quad (7.7)$$

which is precisely the spectrum for a Heaviside unit step function envelope. In that limit, it is clear that both the Sommerfeld and Brillouin precursor fields will be excited in an appropriate dispersive medium. The opposite limit as $\beta \rightarrow 0$ and $T_p \rightarrow \infty$ is of no interest for this particular envelope function as the entire initial field identically vanishes in this case.²

The initial spectrum of the input field with constant carrier frequency ω_c that appears in the integral representation (4.27) of the propagated field is given by

$$\tilde{u}(\omega - \omega_c) = \frac{i}{2} e^{i(\pi/2\beta)(\omega - \omega_c)} \cos\left(\frac{\pi}{2\beta}(\omega - \omega_c)\right) \left[\frac{2}{\omega - \omega_c} - \frac{1}{\omega - \omega_c + \beta} - \frac{1}{\omega - \omega_c - \beta} \right], \quad (7.8)$$

which has simple pole singularities at

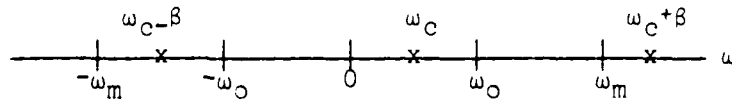
$$\begin{aligned} \omega &= \omega_c, \\ \omega &= \omega_c - \beta, \\ \omega &= \omega_c + \beta. \end{aligned}$$

However, notice that the term $\cos((\pi/2\beta)(\omega - \omega_c))$ that appears in the spectrum (7.8) vanishes at $\omega = \omega_c \pm \beta$, so that these points are removable singularities. Hence, the only pole contribution to the asymptotic behavior of the propagated field is due to that at ω_c . This contribution, when it is the dominant contribution to the asymptotic behavior, yields the main signal evolution which oscillates harmonically in time with the signal frequency ω_c .

²This is not the case for the hyperbolic tangent envelope signal which goes over to a strictly monochromatic field of constant, nonzero amplitude in the limit as the turn-on time goes to infinity. That is the reason why this initial field structure is perhaps more appropriate in investigating the transition of a pulsed field to the continuous wave regime.

Whether or not either the Sommerfeld or Brillouin precursor field is excited by the input field is seen to be strongly dependent upon the value of the carrier frequency ω_c , the rise-time parameter β , and the characteristic frequency values $\omega_0 \gg 0$ and $\omega_m > \omega_0$ wherein the medium absorption is predominantly restricted [see Eq. (5.7)].

The Brillouin precursor field will be allowed to completely form if the

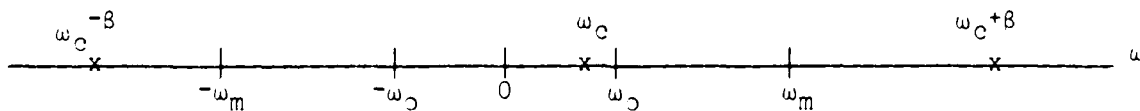


initial pulse spectrum domain $[\omega_c - \beta, \omega_c + \beta]$ encompasses the entire region about the origin wherein the near saddle points evolve. This will certainly be the case if $\omega_c - \beta \leq -\omega_0$, so that one has the condition

$$\beta \geq \omega_c + \omega_0 \Leftrightarrow T_r \leq \frac{\pi}{\omega_c + \omega_0} . \quad (7.9)$$

Obviously this is a stringent condition; however, when it is satisfied, the Brillouin precursor field will be allowed to evolve nearly in its entirety such that it will be difficult to distinguish between the propagated field structure due to this input field and that obtained in the instantaneous turn on case (ignoring the Sommerfeld precursor). If the initial pulse rise-time T_r is increased above $\pi/(\omega_c + \omega_0)$ but is still such that $T_r < (\pi/\omega_c)$, the Brillouin precursor will diminish in its fidelity but will still be observable to some lesser degree. Finally, if T_r is further increased above π/ω_c , the Brillouin precursor will become nearly nonexistent and practically unobservable unless the carrier frequency is placed at a dominant absorption peak of the medium.

The situation for the Sommerfeld precursor field is not quite as accessible since its frequency evolution begins at an infinite frequency (with zero field amplitude) and remains well above the upper edge ω_m of the absorption region of the medium. The Sommerfeld precursor field will be allowed to form to some degree if the initial pulse spectrum



domain $[\omega_c - \beta, \omega_c + \beta]$ at the very least encompasses the negative frequency domain well below $-\omega_m$. Hence, one has the somewhat weak condition that $\omega_c - \beta \ll -\omega_m$, so that

$$\beta \gg \omega_c + \omega_m \Leftrightarrow T_r \ll \frac{\pi}{\omega_c + \omega_m} \quad (7.10)$$

When this condition is well-satisfied, the Sommerfeld precursor field will be allowed to evolve to a certain degree that is dependent upon the value of the applied signal frequency ω_c with respect to ω_m . Clearly, if $\omega_c > \omega_m$, then the Sommerfeld precursor evolution will be greatly enhanced.

As an illustration of the turn-on times demanded by Eqs. (7.9) and (7.10), consider nonconducting water for which

$$\omega_o \cong 1 \times 10^{10}/\text{sec.}$$

$$\omega_m \cong 1 \times 10^{18}/\text{sec.}$$

At microwave frequencies, $\omega_c = 5 \times 10^9/\text{sec.}$ and these conditions yield:

Brillouin Precursor Formation: $T_r \leq 0.2 \times 10^{-9} \text{ sec} = 0.2 \text{ nanoseconds}$

Sommerfeld Precursor Formation: $T_r \ll \frac{\pi}{\omega_m} = 0.003 \text{ femtoseconds.}$

At optical frequencies, $\omega_c = 5 \times 10^{14}/\text{sec.}$ and these conditions yield:

Brillouin Precursor Formation: $T_r \leq \frac{\pi}{\omega_c} = 0.6 \times 10^{-14} \text{ sec} = 6 \text{ femtoseconds}$

Sommerfeld Precursor Formation: $T_r \ll \frac{\pi}{\omega_m} = 0.003 \text{ femtoseconds.}$

Clearly the Sommerfeld precursor will be much more difficult to observe experimentally than the Brillouin precursor.

7.2. The Raised Cosine Envelope Pulse

Using the principle of superposition, the raised cosine envelope signal (7.1) can be used to construct a wide class of pulses of arbitrary duration T_p with different rise and fall times. The analysis of the present section restricts attention to the simplest case of a symmetric pulse with envelope function

$$u(t) = \begin{cases} 0 & ; t \leq 0 \\ \frac{1}{2} (1 - \cos(\beta t)) & ; 0 \leq t \leq 2T_r \\ 1 & ; 2T_r \leq t \end{cases} \quad (7.11)$$

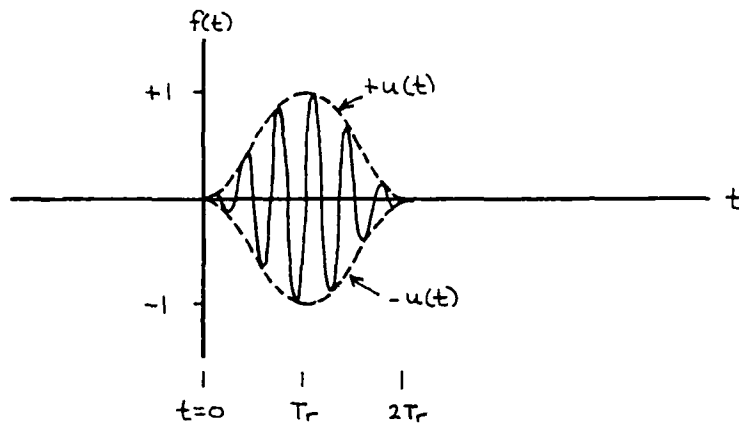
where

$$\beta = \frac{\pi}{T_r}, \quad (7.12)$$

and T_r is the initial rise and fall time of the pulse of temporal width $2T_r$. From Eq. (4.23), the initial field is then given by

$$f(t) = u(t) \sin(\omega_c t) \quad (7.13)$$

where ω_c is the constant signal frequency of the input field.



The spectrum of the envelope function (7.11) is given by

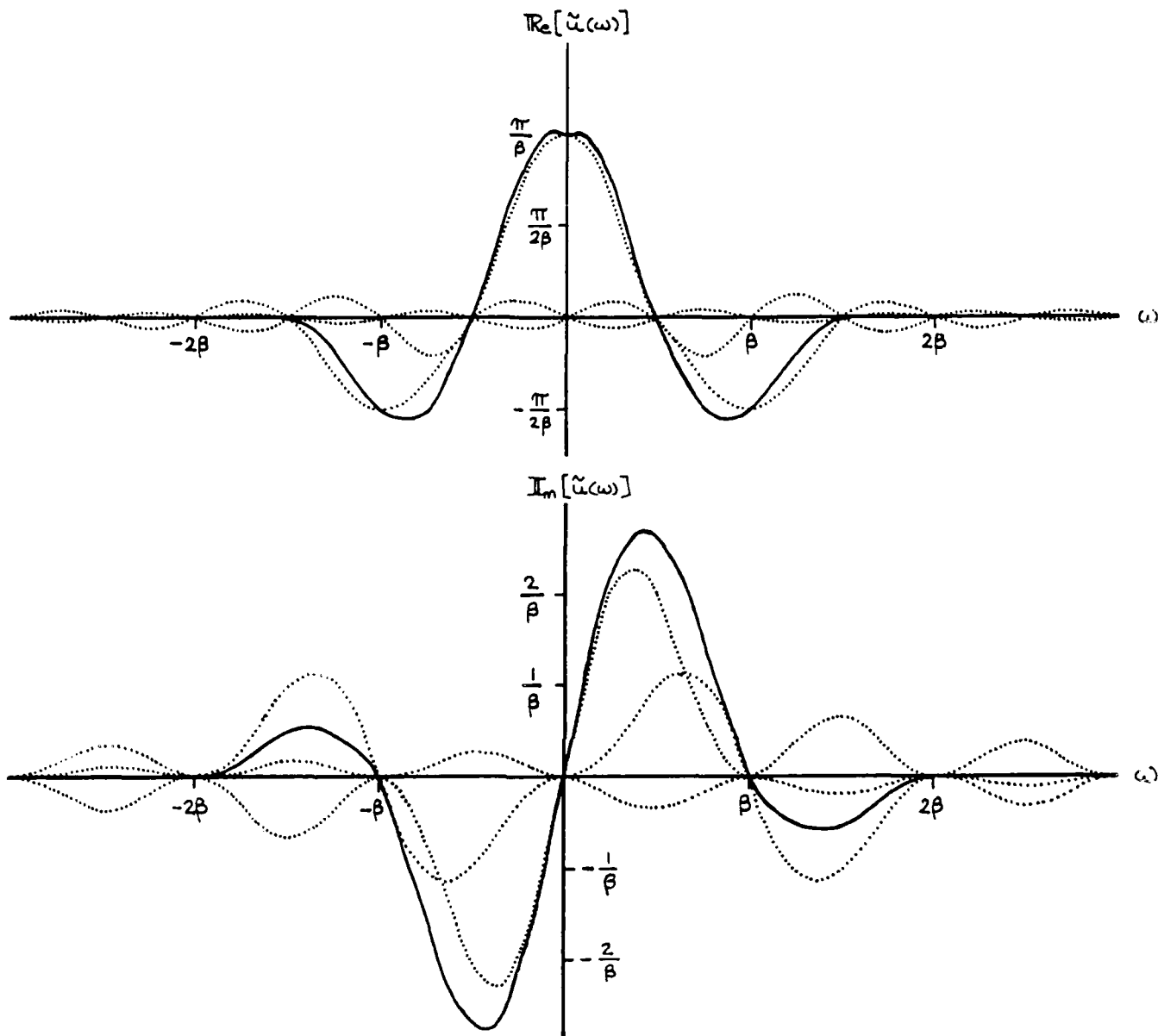
$$\bar{u}(\omega) = \frac{1}{2} \int_0^{2\pi/\beta} (1 - \cos(\beta t)) e^{i\omega t} dt = \frac{1}{2} e^{i(\pi\omega/\beta)} \sin\left(\frac{\pi\omega}{\beta}\right) \left[\frac{2}{\omega} - \frac{1}{\omega+\beta} - \frac{1}{\omega-\beta} \right], \quad (7.14)$$

with real and imaginary parts

$$\text{Re}[\bar{u}(\omega)] = \frac{1}{4} \sin\left(\frac{2\pi\omega}{\beta}\right) \left[\frac{2}{\omega} - \frac{1}{\omega+\beta} - \frac{1}{\omega-\beta} \right], \quad (7.15a)$$

$$\text{Im}[\bar{u}(\omega)] = \frac{1}{2} \sin^2\left(\frac{\pi\omega}{\beta}\right) \left[\frac{2}{\omega} - \frac{1}{\omega+\beta} - \frac{1}{\omega-\beta} \right]. \quad (7.15b)$$

The initial pulse envelope spectrum is then seen to be significant (from a conservative viewpoint) only within the frequency domain $[-\beta, \beta]$.



The initial spectrum of the input field with constant carrier frequency ω_c that appears in the integral representation (4.27) of the propagated field is given by

$$\bar{u}(\omega - \omega_c) = \frac{1}{2} e^{i(\pi/\beta)(\omega - \omega_c)} \sin\left(\frac{\pi}{\beta}(\omega - \omega_c)\right) \left[\frac{2}{\omega - \omega_c} - \frac{1}{\omega - \omega_c + \beta} - \frac{1}{\omega - \omega_c - \beta} \right], \quad (7.16)$$

which has removable singularities at

$$\omega = \omega_c ,$$

$$\omega = \omega_c - \beta ,$$

$$\omega = \omega_c + \beta .$$

The pulse spectrum domain is then $[\omega_c - \beta, \omega_c + \beta]$ and the results of the previous subsection then apply. Hence, the inequality (7.9) must be satisfied in order that the Brillouin precursor field be allowed to form while the inequality (7.10) must be satisfied in order that the Sommerfeld precursor field be allowed to form to some degree.

VIII. RECOMMENDATIONS

The results of this analysis should have general applicability to the generic structure of the transient field structure in a given homogeneous, isotropic, linear dispersive medium. The asymptotic description of the precursor field evolution, to be performed under the Mini Grant, will provide a general understanding of the dynamical field structure in dispersive media that is model independent. These results also provide a convenient means by which a given dispersive medium may be classified according to the types of precursor fields it supports. This is of clear importance to the design of any experiment whose purpose is to observe these transient fields.

Although these general results have broad application to the description of the transient field structure in dispersive media, they cannot provide for a complete description of the entire field evolution since that requires a specific model of the medium response at all frequencies. Such a complete description has only been developed for the simplest case of a Lorentz dielectric. It is critical that this complete description be developed for a more general Lorentz-type dispersive medium with a frequency-dependent conductivity as given by the Drude model in order that the complete dynamical evolution of the field structure for a physically realistic medium be well understood. Not only is this description invaluable for all numerical studies of dispersive

pulses propagation, it also forms the basis for the description of the reflection and refraction of an electromagnetic pulse at a dielectric interface. This latter problem, of extreme practical importance, presents a major extension of our knowledge of electromagnetic wave propagation phenomena and its proper solution will require the development of new asymptotic techniques with broad applicability. This latter research is beyond the scope of a Mini Grant and needs to be continually supported over a period of several years.

REFERENCES

- [1] Arnold Sommerfeld, "Über die Fortpflanzung des Lichtes in Disperdierenden Medien, "Ann. Physik, 44, 177-202 (1914).
- [2] Leon Brillouin, "Über die Fortpflanzung des Licht in Disperdierenden Medien," Ann. Physik, 44, 203-240 (1914).
- [3] Leon Brillouin, Wave Propagation and Group Velocity, (Academic Press, NY, 1960).
- [4] Kurt Edmund Oughstun, Propagation of Optical Pulses in Dispersive Media, PhD thesis, University of Rochester (University Microfilms International, Ann Arbor, MI, 1978).
- [5] George C. Sherman and Kurt Edmund Oughstun, "Description of Pulse Dynamics in Lorentz Media in Terms of the Energy Velocity and Attenuation of Time-Hrmonic Waves," Phys. Rev. Lett. 47, 1451-1454 (1981).
- [6] Kurt Edmund Oughstun and George C. Sherman, "Propagation of Electromagnetic Pulses in a Linear Dispersive Medium with Absorption (the Lorentz Medium)," J. Opt. Soc. Am. B (to be published).
- [7] Julius Adams Stratton, Electromagnetic Theory, (McGraw-Hill, NY, 1941).
- [8] John David Jackson, Classical Electrodynamics, second ed. (John Wiley & Sons, NY, 1975).
- [9] C.J.F. Böttcher and P. Bordewijk, Theory of Electric Polarization, Vol II (Elsevier, Amsterdam, 1978).
- [10] H.M. Nussenzveig, Causality and Dispersion Relations, (Academic Press, NY, 1972), Chapter I.

- [11] L.D. Landau and E.M. Lifshitz, Electrodynamics of Continuous Media,
(Pergamon Press, Oxford, 1960).
- [12] M. Altarelli, D.L. Dexter, H.M. Nussenzveig, and D.Y. Smith,
"Superconvergence and Sum Rules for the Optical Constants," Phys.
Rev. B6, 4502-4509 (1972).

1987 USAF-UES SUMMER FACULTY RESEARCH PROGRAM

Sponsored by the
AIR FORCE OFFICE OF SCIENTIFIC RESEARCH

Conducted by the
Universal Energy Systems, Inc.

FINAL REPORT

Prepared by: Surgounda A. Patil, Ph.D.
Academic Rank: Professor
Department and Mathematics
University: Tennessee Technological University
Research Location: AEDC VKF Instrumentation Branch
Arnold AFS TN 37389-5000
USAF Researcher: Dr Les F. Crosswy
Date: 12 Aug 87
Contract No: F49620-85-C-0013

ESTIMATION OF SPECTRAL DENSITY BY RANDOM SAMPLES

by

Surgounda A. Patil

ABSTRACT

A conditional distribution of the waiting times was utilized to obtain in an ordered random sampling plan and the waiting time relations were used to produce a random sampling plan when the point process followed a Poisson process. A sinusoidal wave process was generated and the process was sampled according to the periodic plan and the random sampling plans. The estimators of the mean velocity, autocorrelation function and spectral density function were defined under each of the sampling plans for a given process. The estimates of these quantities were computed for the simulated sinusoidal wave. The graphs of the autocorrelation function and the spectral density function were presented. The estimators and algorithms for the autocorrelation function and spectral density function for a randomly sampled process were searched in the literature. Among these, the estimators and algorithms which were applicable to randomly arriving data like velocimetry data were identified. An outline of the procedures for these estimators was presented in a usable form.

ACKNOWLEDGMENTS

I wish to thank the Air Force Systems Command and the Air Force Office of Scientific Research for sponsorship of this research. I am grateful to Universal Energy Systems for helping me in all administrative and directional aspects of this program. Also, I wish to thank Mr Marshall Kingery for his assistance in obtaining programming and secretarial help.

My experience at AEDC was very enriching and rewarding to me professionally and personally. There are a number of people who have so willingly helped me in this project, whom I would like to thank. Dr Les Crosswy has helped me to understand the problems of random data arrival with the velocimeter instrument. Mary Craig has given me programming support. I wish also to thank Peter Sherrouse for going through the manuscript and Sharon Russell for typing this technical manuscript. Without the help of these people the project would not have been successful.

1. INTRODUCTION

In taking the measurement of the velocity of particles by the laser velocimeter it is observed that the particles arrive at the velocimeter at random. Entering particles, therefore, form a continuous time random process. The theory developed on the fixed sample size with equal interval sampling is unsuitable for the random phenomenon observed. There is need for the development and testing of methodology based on random sampling plans.

The scientists working in the field of laser velocimetry at AEDC are interested in analyzing the data obtained from the velocimeter and developing statistical inferential procedures based on randomly acquired data. The problems of estimating the average velocity, finding the bias and variance of the estimator, evaluating the turbulence intensity and its variance on the randomly sampled data are being investigated at the AEDC Velocimetry Lab. The related problems of estimating the auto-correlation function and the spectral density with low random data rates based on finite samples are important to the investigation of the flow phenomenon. The scientists are looking for verifiable methods to analyze the data based on the random records available.

My research interests have been in the field of Mathematical statistics and application of statistical methodology to engineering physical and biological problems. I have made investigations in the area of statistical inference, distribution theory and stochastic processes. I have taught courses in random processes and sample functions and worked with homogeneous and nonhomogeneous processes

which should be applicable to the process of collecting the data from the laser velocimeter. In my work simulation procedures for different processes have been used. Knowledge in these areas contributed in my assignment to work with the development and simulation of procedures applicable to randomly acquired samples like velocimetry data.

II. OBJECTIVE OF THE RESEARCH EFFORT

Gaster and Roberts (1975) stated that regularly sampled data has two shortcomings. First, in regularly sampled data aliasing can occur. Second, the spectral estimates are generated at equal intervals in the transformed plane. Also the estimates based on measurements at regular intervals with low data rate (below Nyquist criterion) aren't always reliable. Blackman and Tukey (1959) point out that the use of random sampling might offer an advantage over periodic sampling. Butler and Leneman (1968) have done mathematical investigation on random processes. Butler (1970) has shown that the random sampling prevents aliasing in the estimation of power spectra. Mashry (1978) has shown that the estimates based on random sampling methods are consistent.

There are a number of investigations which discuss the mathematical properties and advantages of random sampling. Only a few papers suggest methods of obtaining random samples and estimating autocorrelation functions and spectral densities. Shipparo and Silverman (1960), Gaster and Roberts (1975), and May, Shay, and Riter (1974) have given various ways of sampling data randomly and estimating the characteristics of the data. Most of these methods, however, are based on acquiring the data by psuedo random triggering. By these methods it is not clear what kind of random process is generated

(Poisson, Nonhomogeneous Poisson). Also explicit estimators of the autocorrelation function and the spectral density functions are not available. Outlines for the algorithms to generate the estimators are presented in their work. The verification of the suitability of the estimators is not clear but could be studied by computer simulation of the algorithms.

My assignment as a participant in the 1987 Summer Faculty research Program (SFRP) was to determine ways to find verifiable estimators of the mean, variance, turbulence intensity, correlation function and spectral density of a known function from which data are randomly sampled. The second purpose was to compare the merits of several algorithms and discuss the suitability of the estimators and algorithms to velocimetry data.

In order to pursue these goals it was decided to design a fixed sample size sampling plan and random sampling plans based on the Poisson process with known sampling rate (λ). There are two random sampling plans possible depending on whether the number of samples are known or unknown. After designing the sampling plans a known sine wave function was sampled in accord with each plan. Estimators of various statistical parameters of the data are discussed. The estimators of autocorrelation and spectral density functions are presented graphically.

The random process generated by the flow velocity may not be periodic process and need to be investigated for its stationarity and ergodicity.

Also testing of the velocimetry data for Gaussian process, acquiring times for poisson process, application of different estimators and

algorithms to the estimation of autocorrelation and spectral density warrants further study.

111a. POISSON PROCESS AND WAITING TIMES

If n events occur in time $(0, t]$ with the probability given by:

$$P(N(t)=n) = e^{-\lambda t} \frac{(\lambda t)^n}{n!}, \quad n=0, 1, 2, \dots \quad (1)$$

(where λ is the rate of events per unit time) then the numbers of events follow a Poisson distribution and the process $N(t)$ forms a Poisson process in continuous time t . A Poisson process exists if the events occurring in time satisfy the following conditions.

i) Events occurring in non-overlapping intervals are statistically independent

ii) The probability of an event occurring in a small interval t is

$$P(N(\Delta t)=1) = \lambda \Delta t + O(\Delta t)$$

$$\text{Where } O(\Delta t) \text{ means limit } \Delta t \rightarrow 0 \quad \frac{O(\Delta t)}{\Delta t} = 0$$

iii) $P(N(\Delta t) \geq 2) = O(\Delta t)$

iv) $P(N(0) = 0) = 1$ (At time zero, zero events occur with probability 1).

Any process satisfying these conditions has the probability given in (1). A few examples of Poisson processes in time t are: i) the number of telephone calls arriving at a switchboard; ii) the number of accidents occurring at a given factory, iii) the number of emissions of gamma ray particles.

In the present study the process of interest $N(t)$ is the process of particles entering the probe region of the laser velocimeter. The particles arriving at random satisfy the above conditions fairly well

hence we can assume the process $N(t)$ formed by incoming particles follows a Poisson process in time. This assumption is made in a number of studies (Masry (1978); Mayo, Shary and Riter (1974); and others).

We are interested in generating a Poisson process $N(t)$ and measuring the velocities at the times dictated. We use the waiting time relations.

Let $T_1, T_2, T_3 \dots$ be the times between the successive events (interarrival times).

The relation between the $N(t)$ process and the interarrival time T_i is given in Ross (1982)

$$N(t) \geq 1 \iff T_1 < t \quad (2)$$

This means that at least one event occurred in time $(0, t]$, if and only if, the waiting time for the first event is less than t . Using Eq. (2) and (1) the distribution function of interarrival time T_1 for the specified rate λ is given by

$$F(t) = P(T_1 < t) = P(N(t) \geq 1) = 1 - e^{-\lambda t} \quad (3)$$

Hence the distribution of T_1 is an exponential distribution with probability density function (pdf).

$$f(t) = \lambda e^{-\lambda t}, \quad 0 < t < \infty. \quad (4)$$

Further it can be shown that the random variables $T_1, T_2, T_3 \dots$ are independent and each has the same distribution as in (3). If we define the waiting time to the n th event

$$S_n = T_1 + T_2 + \dots + T_n \quad (5)$$

then S_n has a gamma distribution with pdf

$$f_n(t) = \frac{\lambda^n e^{-\lambda t}}{(n-1)!} t^{n-1}, \quad 0 < t < \infty. \quad (6)$$

The relation between the $N(t)$ and the waiting time can be written

$$S_n = T_1 + T_2 + \dots + T_n \Leftrightarrow N(t) \geq n \quad (7)$$

$$N(t) = n \Leftrightarrow S_n \leq t < S_{n+1}. \quad (8)$$

The relation (8) is used to simulate the Poisson Process $N(t)$ and associated times of occurrences of the process.

For the given interval $(0, T]$ and the number of events in $(0, T] = n$, it can be shown as in Ross (1982) the random times $t_{(1)}, t_{(2)}, \dots, t_{(n)}$ form the ordered observations from the uniform distribution on $(0, T)$.

The joint pdf of $t_{(1)}, t_{(2)}, \dots, t_{(n)}$ for given $N(T) = n$ is given by

$$f(t_{(1)}, t_{(2)}, \dots, t_{(n)}) = (n!)/T^n, \quad 0 < t_{(1)} < t_{(2)} < \dots < t_{(n)} < T. \quad (9)$$

For given time T and $N(T) = n$, the ordered times $t_{(1)}, t_{(2)}, \dots, t_{(n)}$ are the times of occurrences of n events.

III b. SIMULATION OF POISSON PROCESS AND SAMPLING PLANS

In this section we will discuss the simulation of sample plans.

1) The fixed sample plan: In this plan we divide the time $(0, T]$ into n equal intervals and take the times of occurrences as t_1, t_2, \dots, t_n .

2) Simulation of $N(t)$ Process for given $N(T) = n$

For a given time interval $(0, T]$ and the number of events $N(T) = n$, the arrival times of the events form order statistics from the uniform distribution on $(0, T]$. The joint distribution of these times is given by (9). For the simulation of the times we simulate the random variables u_1, u_2, \dots, u_n from $U(0, 1)$ using the pseudo random variable technique. Using the transform

$$t_i = Tu_i \quad i = 1, 2, \dots, n$$

we obtain t_1, t_2, \dots, t_n , ordering these values we find the

ordered times

$$t(1), t(2), t(3), \dots, t(n). \quad (10)$$

These ordered values represent the times of occurrences of the events.

3) Simulation of $N(t)$ Process for random size

In this section we outline the procedure for finding the occurrence times of the Poisson Process $N(t)$ for given rate of occurrence of events per unit time.

The successive interarrival times $T_1, T_2, T_3 \dots$ are independent, identically distributed exponential random variables. We first generate the times corresponding to these random variables.

The common distribution function of T_i 's is

$$F(t) = 1 - e^{-\lambda t} \quad (11)$$

The distribution of $U = F(t)$ is a uniform distribution on $(0,1)$. The pdf of U is

$$f(u) = 1, \quad 0 < u < 1 \quad (12)$$

The uniform random numbers $u_1, u_2, u_3 \dots$ from the distribution in (12) can be generated by a pseudo random number generator technique.

In order to find the sequence of random times t_i we use the transform

$$u = F(t) = 1 - e^{-\lambda t} \quad (13)$$

or

$$t = (-1/\lambda) (\ln(1-u)) \quad (14)$$

Hence for given λ the random times $t_1, t_2, t_3, \dots, t_n \dots$ are generated by using $u_1, u_2, \dots, u_n \dots$ and

$$t_i = (-1/\lambda) (\ln(1-u_i)), \quad i = 1, 2, 3, \dots \quad (15)$$

The occurrence of events $N(t) = 1, 2, 3 \dots$ are given by

$$N(t_1) = 1, N(t_1 + t_2) = 2, N(t_1 + t_2 + t_3) = 3 \text{ etc.} \quad (16)$$

The process $N(t) = n$ is found from $t_1 + t_2 + \dots + t_n \leq t$ and $t_1 + t_2 + \dots + t_{n+1} > t$. We note that for the given interval $(0, t]$ the number n is random and not predetermined.

IV a. SINE WAVE SAMPLE FUNCTION

In this section we discuss the description of the sine wave function and its various characteristics.

The sine wave function is described by

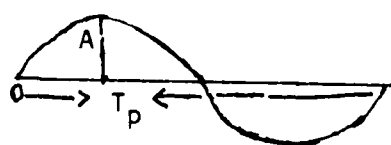
$$X(t) = A \sin (2 f_0 \pi t + \theta) , -\infty < t < \infty \quad (17)$$

where A is the amplitude and f_0 is the frequency which denotes the number of cycles per unit time. Also θ is the initial phase with respect to the time origin in radians and can be regarded as a random variable having uniform distribution on 0 to 2π . However, while analyzing the data, θ is fixed and usually taken to be zero. For this case the sample function $X(t)$ can be written as

$$X(t) = A \sin 2 f_0 \pi t, -\infty < t < \infty. \quad (18)$$

The period of $X(t)$ is T_p and

$$T_p = (2\pi/2\pi)/f_0 = 1/f_0 \quad (19)$$



Sinewave

The mean of the sample function is

$$\int_0^{T_p} X(t) dt = 0 \quad (20)$$

Also the mean of the absolute value is

$$\int_0^{T_p} |X(t)| dt = 2A/\pi \quad (21)$$

The autocorrelation function for the sine wave function $X(t)$ is given by

$$R_X(\tau) = \lim_{T_p \rightarrow \infty} \frac{1}{T_p} \left[\int_0^{T_p} X(t) X(t+\tau) dt \right] \quad (22)$$

$$= (A^2/2) \cos 2\pi f \tau, \quad -\infty < \tau < \infty.$$

The power spectral density is defined in Bendat and Piersol (1971) as the portion of $X(t)$ in the frequency range f to $f + \Delta f$. The power spectral density is denoted by $G_X(f)$ and is expressed as

$$G_X(f) = \lim_{\Delta f \rightarrow 0} \frac{1}{\Delta f} \left[\lim_{T \rightarrow \infty} \frac{1}{T} \int_0^T x^2(t, f, \Delta f) dt \right]. \quad (23)$$

Also the power spectral density in terms of correlation function $R_X(\tau)$ is given by

$$G_X(f) = 4 \int_0^{\infty} R_X(\tau) \cos 2\pi f \tau d\tau. \quad (24)$$

The power spectral of the sine wave $X(t)$ is given by

$$G_X(f) = A^2/2 \delta(f-f_0) \quad (25)$$

where $\delta(f-f_0)$ denotes the Dirac delta function.

IVb. THE ESTIMATION OF SINUSOIDAL WAVE

In this section we find the estimates of various quantities discussed in IV a under the three different sampling plans discussed in Section IIIb.

Plan I: Equal interval fixed sample size

Plan II: Ordered random interval with known sample size

Plan III: Random times with random sample size

The observed mean, variance and turbulence intensity are defined as

$$\bar{X} = (1/N) \sum_{i=1}^N x_i, \quad \hat{\sigma}^2 = (1/N) \sum_{i=1}^N (x_i - \bar{X})^2, \quad I = \hat{\sigma} / \bar{X}$$

For Plan III N is random.

The times under the three plans were generated. The observations were sampled from the sinewave in (18) at these times. The results of the estimates are summarized below.

$$\begin{aligned} \text{I. } N=100 \quad \bar{X} &= 0.000 & \hat{\sigma}^2 &= 0.506 \\ & |\bar{X}| = 0.636 & \hat{\sigma}^2 \bar{X} &= 0.500 & |\bar{X}| &= 0.494 \end{aligned}$$

$$\begin{aligned} \text{II. } N=100 \quad X &= 0.019 & \hat{\sigma}^2 X &= 0.437 \\ & |\bar{X}| = 0.5770 & \hat{\sigma}^2 \bar{X} &= 0.107 & |\bar{X}| &= 0.568 \end{aligned}$$

$$\text{III. } N = 99, \bar{X} = -0.0217 \quad \hat{\sigma}^2 X = 0.518 \quad |X| = 0.659 \quad \hat{\sigma}^2 X^2 = 0.830 \quad |\bar{X}| = 0.937$$

Under these three plans, the estimates are close to each other. They are also in agreement with the true parameters.

The estimated correlation function is defined by

$$R_X(k) = \frac{1}{N} \sum_{i=1}^{N-1} X(t_i) X(t_{i+k}), \quad k=1, 2, \dots, N-1 \quad (26)$$

For the random sample plan

$$R_X(k) = \frac{1}{N(T)} \sum_{i=1}^{N(T)} X(t_i) X(t_{i+k}) \quad k=1, \dots, N(T) \quad (27)$$

where t_i 's are the sampling times.

The estimator of the power spectral density is given by:

$$\sum_{i=0}^{N-1} X(t_i) e^{-j2\pi ki/N} = \sum_{i=1}^{N-1} X(t_i) \cos(2\pi ki) - j \sum_{i=1}^{N-1} X(t_i) \sin(2\pi ki) \quad (28)$$

$$= A - jB$$

then,

$$G_k = (2/T)(A^2 + B^2)^{1/2} \quad (29)$$

Here $j = (-1)^{1/2}$. For the random plan III, N is replaced by observed $N(T)$.

The graphs of estimates of $R(k)$ are given in Figure 1 and the graphs of estimated power spectral densities are given in Figure 2.

V. RELATED ESTIMATORS

In this section we shall discuss the estimators and algorithms discovered by other investigators. The estimators of the autocorrelation function and spectral density function, applicable to random samples are discussed by Shiparo and Silverman (1960) Gaster and Roberts (1975, 1977) Mayo, Shay, and Riter (1974) and Meadows, Whitter, Smith, and Mayo (1974). These estimators are discussed below.

a) We shall first discuss the method discussed by Shiparo and Silverman (1960), and Gaster and Roberts (1975). The estimator of the autocorrelation function is given by:

$$\hat{R}_k = \frac{1}{\lambda T} \sum_{m=1}^{N(T)} X(t_m) X(t_{m+k}), \quad k=1, 2, \dots, N(T)-1. \quad (30)$$

This is the estimator discussed in section III. The spectral density estimator is obtained by the weighted sum of \hat{R}_k . The weights are a function of characteristic function of the waiting time S_i .

The estimator is defined as:

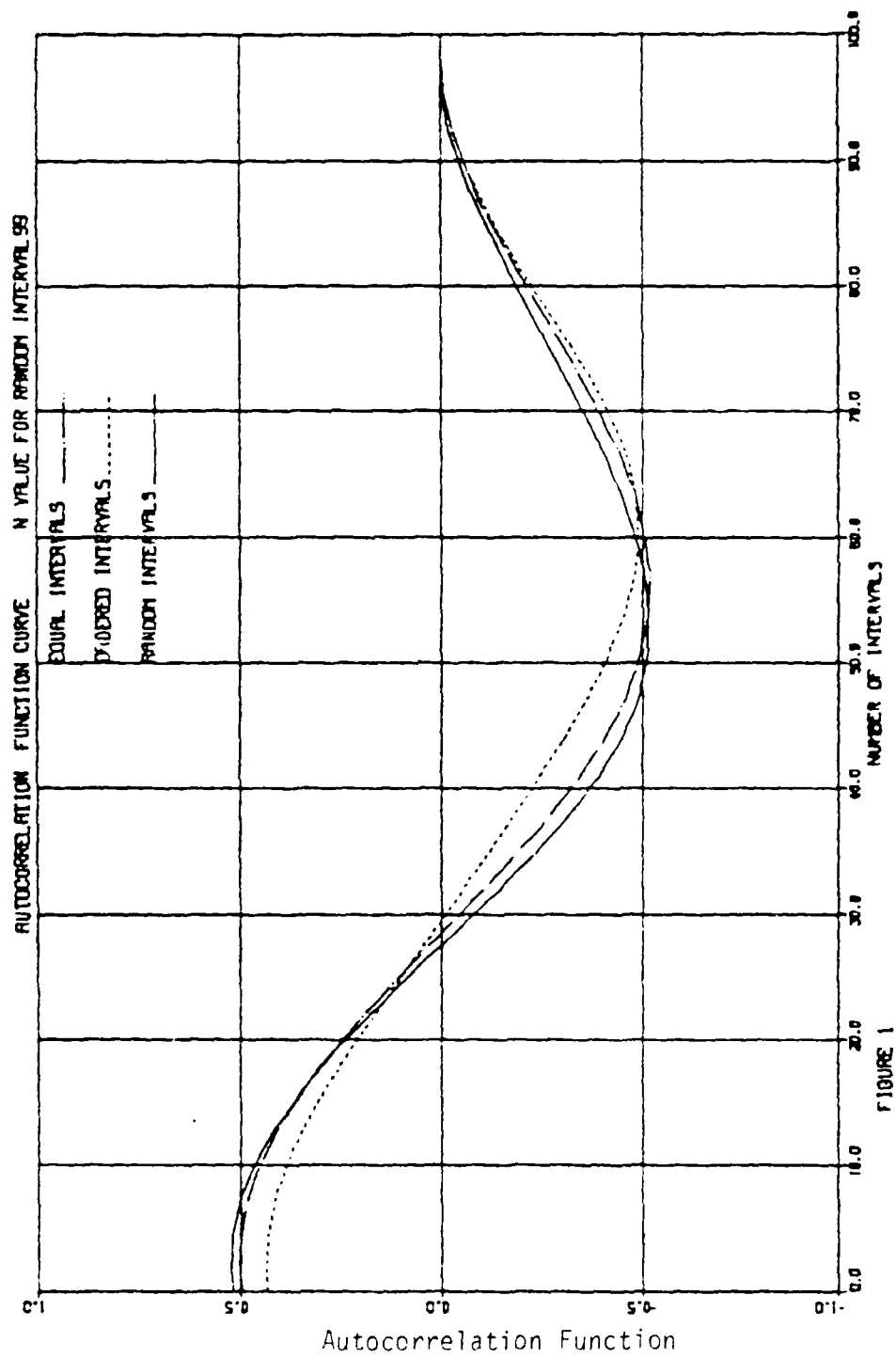
$$G_M(w) = (1/\pi) \sum_{n=1}^M b_n \Psi_n(w), \quad w=1, 2, \dots, M \quad (31)$$

where

$$b_n = (2/\lambda)^{1/2} \sum_{k=1}^{(n-1)} \binom{n-1}{k} (-2)^k \hat{R}_{(k+1)} \quad (32)$$

$$n = \text{Re} \left[-(2\lambda)^{1/2} (jw + \lambda)^{n-1} / (jw - \lambda)^n \right]. \quad (33)$$

$\text{Re}[\]$ denotes the real part of the function. Gaster and Roberts (1975) point out that the variance of the estimator is large and that the



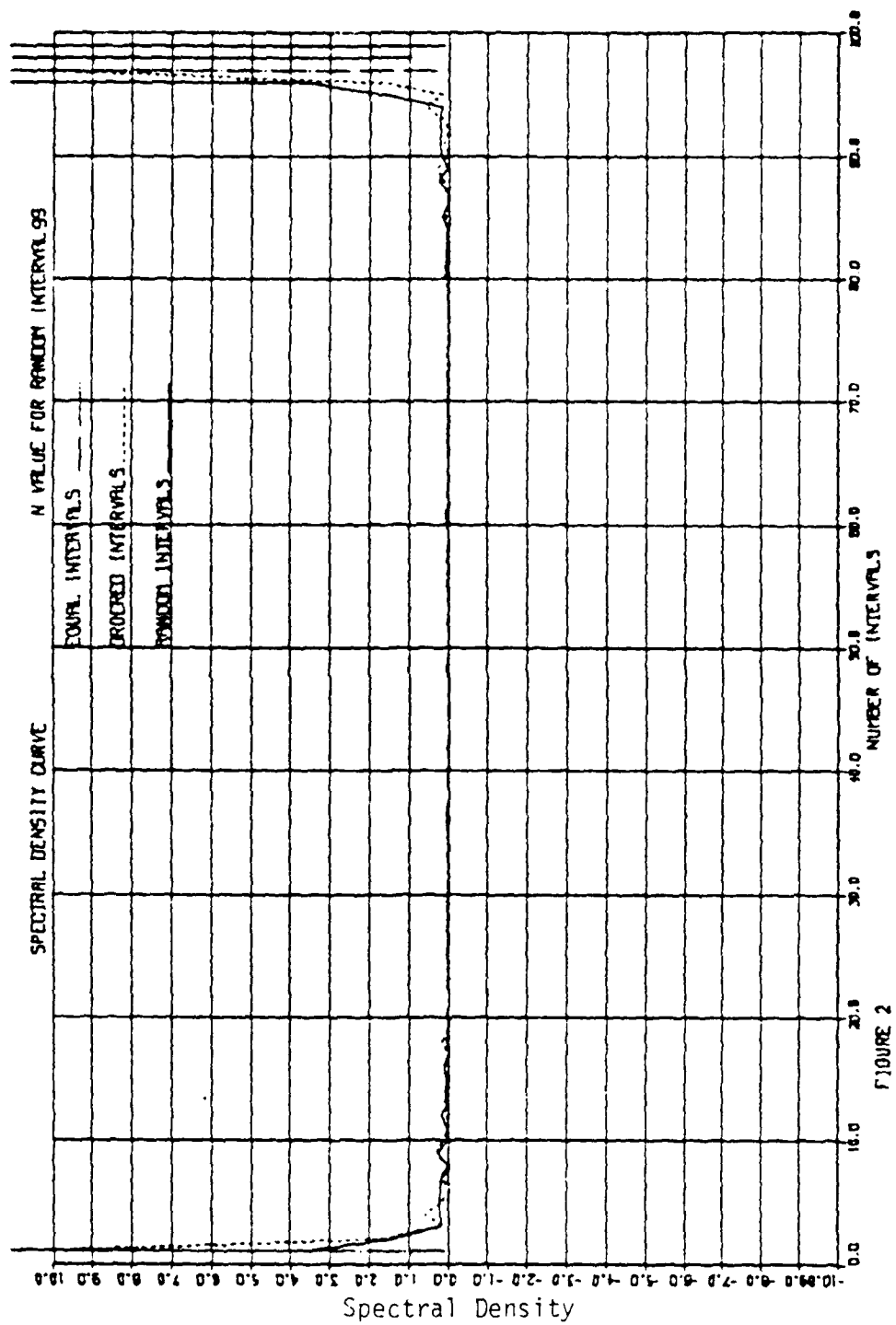


FIGURE 2

method is good for small values of M only.

b) The second method discussed by Gaster and Roberts (1975) utilizes random sampling method II. In this case the sample size N in time $(0, T]$ is known. The estimator is defined by

$$G(w) = \frac{1}{\pi T \lambda^2} \sum_{i=1}^N \sum_{k=1}^N D(t_k - t_i) \cos w(t_k - t_i) X(t_i) X(t_k). \quad (34)$$

Here $D(t_k - t_i)$ is a window function. There are different window functions. One possible window function is the Hanning window defined as

$$D(t_k - t_i) = \begin{cases} (1/2)[1 + \cos \pi (t_k - t_i)/T_m] & 0 \leq t_k - t_i \leq T_m \\ 0 & \text{otherwise} \end{cases} \quad (35)$$

where T_m is the maximum lag in observed times.

If $T \gg 1$ then this estimator is unbiased and its variance is given by

$$\text{Var}(G(w)) = (3T_m/4T) [G(w) + (\sigma^2/2\pi\lambda^2)]^2 \quad (36)$$

Another estimator based on random sampling method III is discussed in Gaster and Roberts (1977). The estimator is similar to one discussed in section III and in Bendat and Peirson (1971). The spectral estimator is based on observed signal. This estimator involves a window function. The performance of the estimator depends on the chosen window, which needs to be studied.

c) The next method of estimation is by Mayo, Shay, and Riter (1974). This method is applicable to random sampling plan III. The method is presented in terms of an algorithm. For given time interval $(0, T]$, $N(T)$ is the observed sample size and $(u_1, s_1), \dots, (u_{N(T)}, s_{N(T)})$ are the velocities and corresponding observed times.

Further, let

$$u_i = u_i - \bar{u}, \quad i=1, 2, \dots, N(T) \quad (37)$$

be the deviations from the mean \bar{u} . We define the interval $(0, T]$ into finer subintervals of length ΔT , where $\Delta T \leq 1/\lambda$, (λ denotes the rate of sampling events). Usually $(1/\lambda)$ is at least 5 times ΔT . The observed times s_i are expressed in terms of Δt as

$$s_1 = k_1 \Delta T, \quad s_2 = k_2 \Delta T, \quad \dots, \quad s_{N(T)} = T \Delta K_{N(T)}. \quad (38)$$

Then to determine the autocorrelation function we find the $\text{Sum}(k)$

$$\text{Sum}(k) = (1/\Delta T) \sum_i \sum_l u_i u_l \quad k=1, 2, \dots, K \quad (39)$$

Sum all i, l such that $[(s_i - s_l)/\Delta T] = k-1$.

Where $[\]$ denotes nearest integer.

Also let $H(k)$ denote the number of terms contained in the above summation $\text{sum}(k)$. Then the autocorrelation function is defined as

$$\hat{R}(k) = \text{Sum}(k)/H(k) \quad k=1, 2, \dots, K. \quad (40)$$

If for some k , $\text{Sum}(k)$ is zero $\hat{R}(k)$ for that k is taken as the average of neighboring $\hat{R}(k)$'s.

The spectral density estimator is given by

$$G(w) = \Delta T [\hat{R}(1) + 2 \sum_{k=2}^K W(k) \hat{R}(k) \cos(w (K-1) \pi / K)] \quad (41)$$

where $W(k)$ is a window function.

This estimator is based on an algorithm containing a window function and requires verification.

d) Another estimator based on an algorithm is by Meadow, Whitfin, Smith, and Mayo (1974). This method is also applicable to random sampling plan III. In this method the time interval $(0, T]$ is divided into a grid with lengths $k_1 \Delta T, k_2 \Delta T, \dots, k_r \Delta T$. The observed velocities and deviations from the mean are found as in (c) above. The autocorrelation function is found as follows:

First, the last element is multiplied by itself and placed in the first

class of the grid. Next, the difference of times between last two elements is classified into one of the classes of the grid and the product of the velocity deviations of the two elements is put into this class and so on. In this way the time differences of each of the previous elements with the last is classified and the corresponding product is put into the proper class. Next, the product of the second to last element with itself is put into the first class. Its time with respect to each of the previous elements is compared and the time differences are classified and product of the elements are put into various classes. The procedure is carried to first element. The autocorrelation function is found as:

$$R(k_m) = \left(\sum_{\substack{i, l \text{ in } (k_m)_{th} \text{ class} \\ m=1, 2, \dots}} u_i u_l \right) / \text{Number in } (k_m)_{th} \text{ class.} \quad (42)$$

The spectral density estimator can be defined as in (c) above. The merits of this estimator can be studied by graphical comparison.

VI. CONCLUSION AND RECOMMENDATION

The estimators for the mean velocity and turbulence intensity and the variances of these estimators are obtained for a sinusoidal wave by using three different plans. The estimators under each plane are close to the theoretical values. The estimators of the autocorrelation function and the spectral density function under each plane are proposed.

These are similar to the estimators proposed by Gaster and Roberts (1975, 1977). The estimates under each plan are computed and presented in a graphical form. The estimators are in agreement with the theoretical results.

There are two methods of estimating the spectral density function of a

random signal. The first method is "The Direct Fourier Transform" or "The Cooley-Tukey method." This method is based on computing the power spectral density via a finite range Fourier transform of the observed signals. The second method is known as "the Blackman-Tukey method." This is based on computing the power spectral density via its Fourier transform relation to the autocorrelation function." In the present development we have used the first method. It is important to study the second method and its agreement with the first method under different sampling plans before applying to the actual data.

There are a number of papers written on the mathematical properties of the spectral density function for a random process. A few of them are concerned with actual estimating procedures from randomly acquired data. Most prominently mentioned procedures are from Gaster and Roberts (1975, 1977) and Mayo et. al (1974). In the present paper we have summarized these methods. These methods need further investigation regarding their merits of relative performance and require determination of the suitability of application to actual data.

The velocity measurements of fluid particles from the velocimeter form a random process. In order to study the statistical properties of the random process. It is required to study the stationarity and ergodic properties of the flow process. Also the point process of acquiring the random data requires investigation as to the homogeneity or nonhomogeneity of the process and its independence from the flow process. These properties can be studied from the spectral density function of the process which could be determined from the procedures discussed in the paper.

REFERENCES

- Bendat and Piersol. Random Data: Analysis and Measurement Procedures 1971. Wiley. Interscience John Wiley & Sons Inc.
- Blackman, R.B. and Tukey, J.W. The Measurement of Power Spectra from the Viewpoint of Communications Engineering, 1959, Dover Publications, Inc. New York.
- Butler, F.J. Alias-Free Randomly Timed Sampling of Stochastic Processes. IEEE Tran. on Inf. Th. 1970 Vol. IT 16, 147-152.
- Butler, F.J. and Leneman O.A. The spectral analysis of impulse processes Information and Control. 1968 Vol. 12, 236-258.
- Gaster, M. and Roberts J.B., Spectral Analysis of Randomly Sampled Signals. J. Ins. Math. Applies 1975, Vol. 15, 195-216.
- Gaster, M. and Roberts, J.B. The spectral analysis of randomly sampled records by a direct transform 1977 Proc. R. Soc. Lond. A Vol. 354 27-58.
- Mashry, E. Alias-Free Sampling: An alternative conceptualization and its application. IEEE Tran. on Inf. Th. 1978 Vol IT-24, 317-324.
- Mayo, W.T., Shay M.T., and Riter, S. The Development of New Digital Data Processing Technique for Turbulence Measurement with a Laser Velocimeter. Technical Report AEDC Contract No. F40600-73-C-0003.
- Meadows, D.M., Whitten, M.C., Smith D.M. and Mayo, W.T. Laser Velocimeter for Supersonic jet Turbulence and Turbulence Spectra Research. Technical Report AFAPL-TR-74-24.
- Ross, S.L. Stochastic Processes (1982) John Wiley & Sons.
- Shapiro, H.S. and Silverman, R.A. Alias-Free Sampling of Random Noise. J. Soc. Indust. Appl. Math 1960 Vol. 8 225-248.

1986 USAF-UES SUMMER FACULTY RESEARCH PROGRAM/
GRADUATE STUDENT SUMMER SUPPORT PROGRAM

Sponsored by the
AIR FORCE OFFICE OF SCIENTIFIC RESEARCH

Conducted by the
Universal Energy Systems, Inc.

FINAL REPORT

COMPUTER SKELETON PROGRAM GENERATOR

Prepared by :	Martin A. Patt
Academic Rank:	Associate Professor
Department and University	Dept. of Electrical Engineering University of Lowell
Research Location:	Geophysics Laboratory, Optical Physics Division
USAF Researcher:	Dr. Donald Bedo
Date:	27 July 1987
Contract No:	F49620-85-C-0013

Computer Skeleton Program Generator

by

Martin A. Patt

ABSTRACT

A skeleton program generator was adapted for use at AFGL. The generator prepares source program text in any of six popular computer languages.

ACKNOWLEDGMENTS

I would like to thank the Air Force Systems Command and the Air Force Office of Scientific Research for sponsorship of my research. In order to be meaningful, scientific research must be conducted in an intellectually stimulating environment. The Geophysics Laboratory provided this environment. The genuine support and encouragement by the scientists and engineers of the Optical Physics Division at AFGL is hereby acknowledged with gratitude.

- M.A.P.

I. INTRODUCTION

One of the nagging problems faced by scientists, engineers, and other occasional computer programmers is the initial tradeoff decision which must be made between software development time and quality of program style. The pressure to "get it working" often leads to the development of programs of such poor style that they are difficult to understand, and indeed nearly impossible to adapt to changing applications without introducing bugs. It was felt that AFGL could benefit from the availability of intelligent programming aids to speed the development of new computer software while, at the same time, improving readability, reliability, and "revisability" (the three R's ?).

II. OBJECTIVES OF THE RESEARCH EFFORT

The objective of the summer research effort was to complete the development of six program generating utilities (one for each of the following languages: Ada, BASIC, C, FORTRAN, Modula-2, and Pascal), and to merge them into a single multilingual intelligent programming aid which could prove useful at AFGL.

III. THE RESEARCH EFFORT

The research effort consisted of completing the work started at the University of Lowell where a number of program skeleton generators were being developed and mass tested by this researcher. The individual generators had all been developed in a common language (C), looking ahead to an opportunity to spend the time required to combine them to form a single, powerful programming aid. Some polishing was done, and a plotting feature was added. All of this resulted in a utility which writes (in the language selected by the user) a main program, an associated

command interpreter routine, a menu generator, and a few "dummy" routines to handle applications. The dummy routines would be expanded later by the user. The command interpreter accepts command mnemonics with or without numerical arguments in a free line format. User entry errors trigger the "BELL" followed by display of the menu. A file is opened for saving output text and data intended to be printed later. A software toggle is provided to activate this save feature. The generated skeleton program is a working program in the sense that it can be compiled, linked and run. Although users will want to expand the dummy routines to meet the requirements of their applications, they are relieved of the burden of writing most of the overhead software needed to enhance their application routines in an elegant manner.

IV. RESULTS AND CONCLUSIONS

The objectives of the summer research effort were met and exceeded. The six program generating utilities were completed and then merged into a single multilingual intelligent programming aid which was installed on the AFGL central VAX computer. A handbook was prepared to inform and instruct potential new users. The existence of the new utility was advertised on the computer's BULLETIN BOARD as well as by word of mouth, and a large number of informal demonstrations were conducted.

V. RECOMMENDATIONS

Although the new multilingual intelligent programming aid can be used to assist in the speedy development of new software in any of six computer languages, only two of those languages (FORTRAN and Pascal) are supported at the central VAX facility at

AFGL. Careful consideration should be given to tremendous improvement in efficiency, clarity, and reliability which could come with the freedom to select the language which best matches the application.

It is respectfully recommended that compilers be obtained to allow users of the AFGL central VAX facility to develop new computer software in languages other than FORTRAN and Pascal. At a minimum, program development in the BASIC and C languages should be supported as soon as possible, and an interdepartmental committee should be formed to recommend further additions to this list.

REFERENCES

Journal Publications

1. M. A. Patt, "THE INS AND OUTS OF PROGRAM-WRITING PROGRAMS", (Interface - The Computer Education Quarterly, Summer 1987)vol.9, no.2.

Internal Publications

2. M. A. Patt, "QUICK_AND_CLEAN USER'S MANUAL" Air Force Geophysics Laboratory, Summer 1987

Technical Manuals

3. M. Patt and R. Dirkman, "PROGRAM DEVELOPMENT ON THE VAX", University of Lowell, 1987.

1987 USAF-UES SUMMER FACULTY RESEARCH PROGRAM/
GRADUATE STUDENT SUMMER SUPPORT PROGRAM

Sponsored by the
AIR FORCE OFFICE OF SCIENTIFIC RESEARCH

Conducted by the
Universal Energy Systems, Inc.

FINAL REPORT

A SUBOPTIMAL FEEDBACK CONTROL FOR WING ROCK

Prepared by:	William N. Patten, Ph.D., PE
Academic Rank:	Assistant Professor
Department and	Mechanical Engineering
University:	University of Iowa
Research Location:	AFWAL/FIGCA Wright Patterson Air Force Base Dayton, Ohio
USAF Researcher:	Dr. Siva Bandi
Date:	9 October, 1987
Contract No.	F49620-85-C-0013

A SUBOPTIMAL FEEDBACK CONTROL FOR WING ROCK

by

William N. Patten

ABSTRACT

An online, suboptimal feedback control strategy is developed for a swept wing aircraft attempting maneuvers at a high angle of attack. A causal model of the aircrafts characteristics that was developed on the basis of free-to-roll wind tunnel experiments, and high order numerical modeling using recent advances in the vortex lattice method.

The control analysis is developed using a weak variational formulation of the classical optimal control problem applied to the nonlinear high angle of attack aerodynamic problem. Quasilinearization, and the finite element method, are combined with a rational feedback procedure to produce an algorithm implementable on a personal computer architecture.

ACKNOWLEDGEMENTS

This work could not have been accomplished had not a most select group of officers, scientists and engineers encouraged the effort without reserve. The advice and interest on the part of the Chief Scientist of the Flight Dynamic Laboratory, Dr. G. Ritchey and his able manager Mr. A. Harris are particularly noted.

Four professionals within the Flight Control Division were especially responsive to and helpful in my endeavors. They were Dr. S. Bandi, Acting Group Leader of the Controls Analysis Group (and scientific focal point), Mr. J. Jenkins, a scientist with the Design Production Group, Mr. C. Suckamul, scientist with the Flying Qualities Division of the Flight Control group and Dr. Hsi-Han Yeh, a member of the Controls Analysis Group. These gentlemen were particularly effective in familiarizing this investigator with many of the physics and controls issues that underlie the research conducted.

In addition, the invaluable day by day support of the various engineers and professionals within the Controls Analysis Group, (including Captains P.J. Lynch, & M.V. Dunbar, Lt. M. Manning, Mr. P. McKeehen and Mrs. L. Johnson) must be cited.

Finally, I wish to thank the Air Force Systems Command and the Air Force Office of Scientific Research for sponsorship of this research, the support and enthusiasm extended by the Air Force Office of Scientific Research, and their Contractor, United Energy Systems is especially acknowledged.

I. INTRODUCTION AND BACKGROUND

The prestall flight maneuverability of certain combat aircraft operating at low Reynold's number conditions, and high angles of attack, is considered marginal. A reduction of control surface effectiveness, and the nonlinear aerodynamics that characterize the plane's response in this domain, can combine to produce a highly unstable dynamical system. The problem is exacerbated by the observation that control actions required of the pilot for stabilization are very often counter-intuitive.

A viable means of providing reliable control during high angle of attack maneuvers must be established if the current operating envelope of certain air frames is to be extended. The work reported on here demonstrates a method of achieving that control objective.

Recently published reports describe research efforts by researchers aimed at unlocking the mysteries of high angle attack aerodynamics. Reports by Nguyen et.al (Ref.5) as well as Hunt (Ref.2) describe experiments that have been conducted in order to establish an understanding of the physics that underlie the process. These two particular sources are noted here because they provide pivotal contributions to the understanding of one of the more problematic aspects of high angle of attack aerodynamics; wing rock.

On the other hand, significant strides have been made in the quest for an explanation of the phenomena that leads to the unstable, limit cycle motion characteristics that accompany

wing rock. There is little evidence that a commensurate level of insight has been gained in the quest to provide a control strategy for an air frame undergoing high angle of attack dynamics.

The discovery of legitimate and reliable control solutions for an aircraft does require, at the very least, a reasonable dynamical model of the coupled fluid, airframe dynamics. A yet to be published paper by Nayfeh, et. al. (Ref 3) describes a low order, nonlinear already numerical state dependent model of the wing rock phenomenon. The work there relied on a novel combination of a predictor-corrector method, coupled with the vortex-lattice method, that was used to simulate wing rock of an aircraft. The computational method was shown to be capable of mimicking the reported wind tunnel experimental results reported in Ref. 5. Most importantly, the authors used regression analysis to identify a low order highly nonlinear physical model of wing rock in terms of the roll angle. That plant model has been adopted here to study the control problem.

While a reliable plant model has been identified, much less progress can be reported in the effort to provide a causal model of the control surface effect on the aircraft's dynamics during high angle of attack maneuvers. It is well known that the conventional control surfaces (including flapper on, ailerons, etc.) at high angles of attack provide little effective control.

Current research (Ref. 1,8,9) appears to indicate that strakes located near the nose of the aircraft do offer

effective control inputs, but at present, there is not available an analytic state dependent input/output characterization of the associated actuator dynamics during high angle of attack.

Finally, a note on the background material used to identify a control solution for the wing rock problem is in order. The tools requisite to the development of a viable feedback control strategy for nonlinear systems have yet to be completely identified. The Engineering community has in the past relied on linear system control theory to provide the bulk of the control analysis for the aerodynamics problem. Nonlinear dynamics were, in general precluded from the operating envelope.

The efforts by this author at developing a simple, low order online feedback control scenario is an extension of a variational method of the solution of the nonlinear control problem offered by Patten (Ref.6).

II. OBJECTIVES OF THE RESEARCH EFFORT

The principal objective of the research conducted under this contract was the development of a reliable, online feedback control algorithm that will provide a stabilizing control for swept wing aircraft during high angle of attack maneuvers. The work sought to develop an algorithm that could conceivably be implemented in the inexpensive P.C. hardware/software environment, in the anticipation that the

onboard closed loop control requirements would be implemented with current systems technology.

III. ANALYSIS:

A procedure is demonstrated in the following section that results in the development of a feedback control strategy for an aircraft undergoing unstable wing rock dynamics. A nonlinear, single degree of freedom model of the roll motion component of wing rock, put forward in Ref. 3, is employed. The effort here was conducted to demonstrate that an almost optimal torque could be identified, that, if applied would attenuate roll motion during a maneuver.

The form of the plant model used was

$$\ddot{\phi} = e_1\phi + e_2\dot{\phi} + e_3\phi^3 + e_4\phi^2\dot{\phi} + e_5\phi\dot{\phi}^2 + u \quad \text{Eq. 1}$$

The dependence of the coefficients e on the angle of attack was described graphically in Ref. 3. A polynomial fit of the data was employed to provide a continuous relationship between the data and the coefficients. In particular,

$$e_i(\alpha) = \sum_{j=0}^3 \beta_j \alpha^j \quad \text{Eq. 2}$$

The data table used to establish the coefficients in Eq. 2 is reproduced in Table 1 (Ref.7). The development is proceeded by first restating the plant dynamics in state variable form.

Defining

$$\bar{x} = \{x_1, x_2\}^t \quad \& \quad x_1 = \phi, \quad x_2 = \phi \quad \text{Eq. 3}$$

then the goal of the analysis is to establish a controlled reaction to a plant's dynamical state in such a way that the weighted energy norm of the system is minimized in some fixed time interval. In functional form, the objective may be stated as;

$$\text{minimize } J = \int_T g(\bar{u}, \bar{x}, \tau) dt; \quad T = (0, T) \quad \text{Eq. 4}$$

where; the convex integrand of the index of performance (IP), has the form

$$g(\bar{u}, \bar{x}, \tau) = \frac{1}{2} \langle \bar{x}, \bar{Q}, \bar{x} \rangle + \frac{1}{2} \langle \bar{u}, \bar{R}, \bar{u} \rangle \quad \text{Eq. 5}$$

and is subject to the pointwise constraint

$$\dot{\bar{x}} = \bar{f}(\bar{x}, \bar{u}, \tau) + \bar{E} \bar{u}; \quad \bar{x}(0) = \bar{x}_0 \quad \text{Eq. 6}$$

The specific form of the right hand side of Equation 6 is defined in equations 1, 2 and 3 above. It is assumed that; the plant remains controllable on the domain, that the state \bar{x} is completely measurable, and that the control vector, \bar{u} is unconstrained and at least piecewise continuous on the interval of domain, while the mxm matrix \bar{R} is constrained to a positive definite form. The solution process proceeds by first establishing an unconstrained form of the IP, and employing the

calculus of variations to discover the first order Euler Necessary Conditions (ENC) associated with the extreamization of the resulting saddle point problem. Defining

$$H = g + \langle \bar{y}, (\bar{f} + \bar{B}\bar{u}) \rangle \quad \text{Eq. 7}$$

Then the augmented IP takes the form

$$J_1[\bar{u}] = \int_T \{ H - \langle \bar{y}, \dot{\bar{x}} \rangle \} dt \quad \text{Eq. 8}$$

The objective here is the identification of weak functional forms that admit approximate solutions to the minimization problem posed. A rigorous development of that procedure has been offered by Patten (Ref.6). The details of that lengthy procedure are abridged for use here. In particular, it has been shown that the forms

$$0 = \int_T \langle \bar{e}_1, \delta \bar{x} \rangle dt \quad \text{Eq. 9a}$$

$$0 = \int_T \langle \bar{e}_2, \delta \bar{y} \rangle dt \quad \text{Eq. 9b}$$

represent the weak inner product functionals sought. It can be shown that

$$\bar{0} = \bar{e}_1 = H_{\bar{x}} + \dot{\bar{y}} \quad \text{Eq. 10}$$

$$\bar{0} = \bar{e}_2 = H_{\bar{y}} - \dot{\bar{x}} \quad \text{Eq. 11}$$

It should also be noted that the relation

$$\bar{u} = -\bar{R}^{-1} \cdot \bar{B}^T \cdot \bar{y} \quad \text{Eq. 12}$$

has been embedded to reduce the problem to the determination of the state and costate vectors only. It is also noted that the solution here presumes

$$\bar{y}(T) = \bar{0}$$

Eq. 13

The nonlinear algebraic form of the ENC suggest the implementation of iterative methods at some point in the solution procedure. Anticipating that fact quasilinearization was introduced before any direct approximation procedure was invoked. The procedure produces an especially attractive computational environment.

Quasilinearization (QL) is a numerical procedure used to achieve solutions to nonlinear boundary value problems. The technique produces a more easily solved linear, though nonstationary approximate form of the boundary value problem. Using the traditional approach, the method requires first a Taylor series expansion of the differential equations (Eq. 10 & 11) about an unknown nominal solution. An initial guess of that nominal solution vector is next supplied. A recursive scheme is then used to establish updated estimates of the solution. The process has been shown to possess a quadratic convergence characteristic, and if the initial guess is, in a measured sense, close to the actual solution, then for a large class of operators and boundary conditions, convergence is also monotonic.

The algorithm suggested here combines the QL procedure with both the finite element method (FEM), and a variable mesh

selection scheme. The combined process results in a set of algebraic equations that are linearly dependent on a set of unknown nodal values that characterize the coefficients in those sequences used to approximate the field variables. In a manner similar to that used in the Newton-Raphson method, the solution is approached iteratively. An absolute error criteria is used from step to step to judge the acceptability of a particular iterate. The variational statements (Eq. 5 & Eq. 6) admit finite element approximations on the domain of the functional if certain, functional constraints are met.

The method requires first a discretization of the time domain and an approximation of the independent field variables on each subdomain. The reader wishing to examine the topological arguments that enable the FEM approximation within the setting of the optimal control problem are referred to Ref(6). Here, it is presumed sufficient to note that a first order Lagrange interpolating function was used as an approximating polynomial on each subdomain. This elemental sequence is particularly attractive in terms of realizability.

The finite element formulation of the control problem and the quasi-variational procedure combines to produce an algebraic evolution operator on the time line with the form:

$$\bar{z} = -\bar{K} \bar{z}_0 \quad \text{Eq. 14}$$

where the vector \bar{z} is a composite of the nodal unknowns associated with future values of the state and costate. The

vector \bar{z} , is composed of known initial and final conditions. The linear mapping (Eq. 14) could conceivably provide a direct solution procedure for the optimal control problem, but would necessarily require the solution of a system of very large dimension. While the resulting system matrix can be shown to be sparse, solutions tend to become problematic due to illconditioning.

As an alternative, an algorithm has been used here that mimics the essence of state feedback control. The procedure is straightforward. First the evolution operator, \bar{K}^- is computed. As the dynamics occur, the current state is used to compute future values of the state and control at a discrete number of future points in time. The solution is used to construct a piecewise linear approximation of the control, that is used for a short period of time, after which the process is repeated.

A key component of the algorithm proposed here is the implementation of a variable mesh gridation of the time domain. Recomputation of the evolution operator and the solution vector occurs when the terminus of the first element has been reached. Three elements were used to span the time domain. Two elements of equal length were packed in the neighborhood of the origin. Their lengths represented a fractional part of the natural period of vibration of the principal linear part of the system. The length of the third element was selected to complete the span of the domain.

RESULTS AND CONCLUSIONS:

A simulation was conducted to test the procedure. In particular, the air frame dynamics are initialized at stable phase plane values. At 1/2 second a rapid maneuver from 15 to 25 degrees (of angle of attack) was initiated, forcing the vehicle into the limit cycle region of Fig. 1. The plane was then subjected to an impulse load at 3 seconds into the maneuver. (The impulse was intended to represent, for example the dropping of wing stores)

The off line, open loop optimal control solution of the problem is shown in Fig. 2 & 3 (see Ref 7 for details). The results of the online suboptimal control application is shown in Fig. 4 & 5. A visual comparison of the open loop versus closed loop results indicates a close correspondence of the solutions. Qualitative observations indicate that the suboptimal online control clearly exhibits chatter, and requires as much as 50% more torque, at isolated points during the simulation. In spite of these short falls, the method does appear to provide a stabilizing control and demonstrates good disturbance rejection. It seems clear then, that results do indicate the utility of the direct methods developed here. Care must be exercised in drawing general conclusions on the suitability of the method. A most significant aspect of the procedure that has not received due consideration here is the computational burden that must be achieved during the execution of the algorithm. Techniques that capitalize on the sparsity of the system equations for example have been explored and will

be reported on elsewhere.

IV. RECOMMENDATIONS:

The results presented here make it clear that the variational formulation does provide a reasonable analytical setting for the development of a suboptimal online, feedback control algorithm applicable to highly nonlinear aerodynamic systems.

Though the work presented is encouraging there remains a number of areas and issues that should be investigated before a commitment is made to implement the technique in a prototype controller for aircraft. The items that deserve immediate interest are:

a) The establishment of dedicated software and hardware that is able to achieve the algebraic solutions required in minimal time. Here, it is proposed that the emerging transputer technology, coupled with a PC based data acquisition system should be combined to port data and process the highly parallel, sparse computations (multiplication and addition) that are required between system updates.

b) In conjunction with the development of "fast", dedicated PC software/hardware systems, a program of experimental verification of the procedure is suggested. That program should proceed first from a least expensive verification methodology. It is expected that the equipment developed in phase a above would be tested using the PC control/transputer architecture by controlling a "Real Time"

model of an aircraft simulated by using a programable analog computer (AC). Here, a companion PC would necessarily be married to the AC to provide "POT" adjustments to the model as the simulation proceeded.

c) Presuming that the analog computer simulations did indeed indicate that the algorithm was implementable in "real time" using the PC architecture described, it would then seem reasonable to embark on a concerted effort at developing the more complex "learning" control algorithm that will ultimately be necessary to control the air frame. A coordinated effort that utilized the highly developed vortex lattice procedure (VLP) is an appropriate test bed for the implementation of the algorithm in the context of learning. In particular, the algorithm should be "piggy backed" on the VLP software. A simulated environment which incorporated various control surface scenarios could be developed that on the one hand assessed the potential suitability of a particular control actuator, and on the other, provide a suitable causal model of that particular actuators input/output characteristic.

d) Having developed a reliable set of actuator dynamics, it would then seem reasonable to attempt an experimental verification of the algorithm/equipment solution. A torque producing controller could be coupled, for example, to NASA's "free to roll" sting mounted delta wing assembly for testing in their low Reynold's number wind tunnel at Langley AFB. Presuming that this procedure provided a plausible set of results, it would then seem prudent to begin the process again,

but now treating the more complicated, coupled, nonlinear dynamical control problem where significant yaw and pitch perturbations accompany the roll dynamics. This later phase would most likely require a similar methodology to that described for the roll problem.

e) Presuming that a complete high angle of attack control methodology was able to be arrived at, it would then seem (consistent with our need to improve the operating envelope of combat aircraft) wise to implement the hardware/ software /technology on a fullsize, piloted air frame.

It is the considered opinion of this investigator that the procedures are "doable" goals, in "real" time, provided a reasonable level of resources are committed to the task. It is hoped that those in a position to pass judgement on the merits of the proposed program concur.

α	a_1	a_2	a_3	a_4	a_5
15	-0.01026	-0.02117	-0.14181	0.99735	-0.83478
21.5	-0.04207	0.01456	0.04714	-0.18583	0.24234
22.5	-0.04681	0.01996	0.05671	-0.22691	0.59065
25	-0.05686	0.03254	0.07334	-0.3597	1.4681

$$\ddot{\phi} + w\dot{\phi} = \mu_1\dot{\phi} + b_1\phi^3 + \mu_2\phi^2 + b_2\phi^2$$

where

$$w^2 = -c_1 a_1$$

$$\mu_1 = c_1 a_2 - c_2 \quad c_1 = 0.354$$

$$b_1 = c_1 a_3$$

$$\mu_2 = c_1 a_4 \quad c_2 = 0.001$$

$$b_2 = c_1 a_5$$

Table 1. Values for Coefficients of EOM

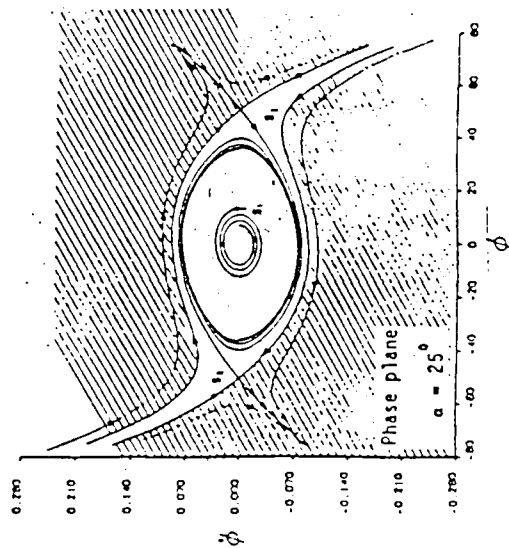


Fig. 1 Phase Plane $\alpha = 25^\circ$

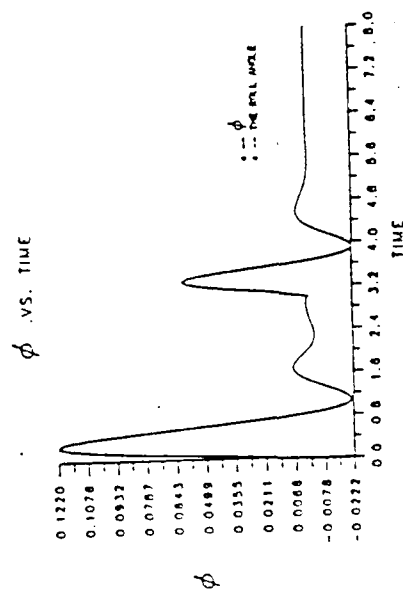


Fig. 2 ϕ vs time;
Open Loop Optimal Control

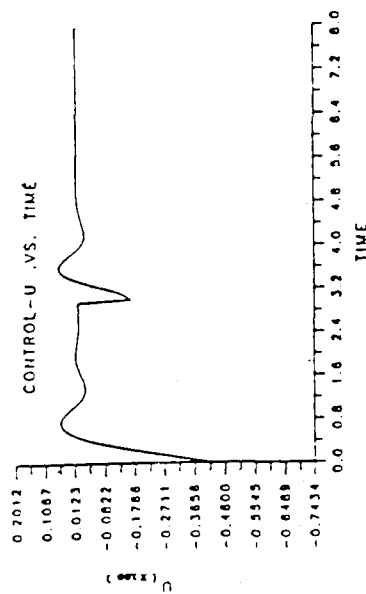


Fig. 3 u vs time;
Open Loop Optimal Control

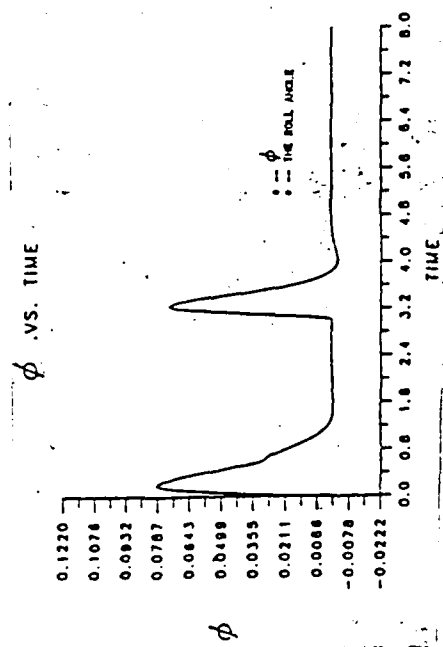


Fig 4 ϕ vs time;
Closed Loop Suboptimal
Control

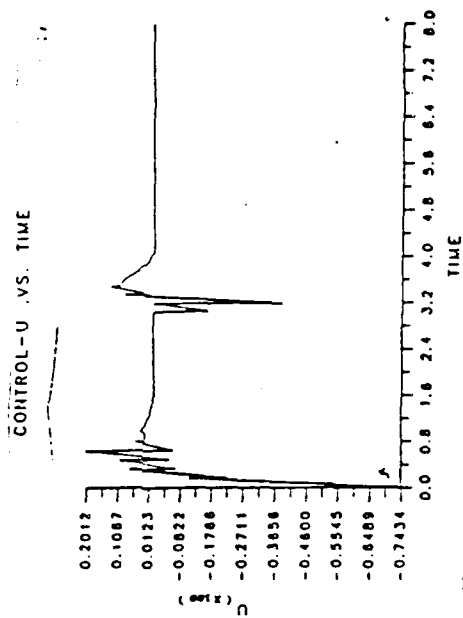


Fig 5 u vs time;
Closed Loop Suboptimal
Control

REFERENCES

1. Brandon, J.M. and Nguyen, L.T., "Experimental Study of Effects of Forebody Geometry on High Angle of Attack Static and Dynamic Stability," AIAA 24th Aerospace Sciences Meeting, Reno, Nevada, AIAA-86-0331, January 6-9, 1986.
2. Hunt, B.L., "Asymmetric Vortex Forces and Wakes on Slender Bodies," AIAA 9th Atmospheric Flight Mechanics Conference, San Diego, California AIAA-82-1336, August 9-11, 1982.
3. Nayfeh, A.H., Elxebda, J.M. and Mook, D.T., "Analytical Study of the Subsonic Wing-Rock Phenomenon for Slender Delta Wings", V.P.I. & S.U., Department of Engineering Science and Mechanics, Unpublished, Work supported by AFOSR under Grant #AFOSR-85-0158.
5. Nguyen, L.T., Yip, L. and Chambers, J.R., "Self-Induced Wing Rock of Slender Delta Wings", AIAA Atmospheric Flight Mechanics Conference, Albuquerque, New Mexico, AIAA-81-1883, August 19-21, 1981.

6. Patten, W.N., "Suboptimal Feedback Control for Nonlinear Dynamical Systems; A Direct Variational Formulation", Submitted to International Journal of Control, 1987.
7. Sierra, C.D., "Optimal Control of the Wing Rock Phenomenon," USAF-UES Summer Faculty Research Program/Graduate Student Summer Support Program, Final Report, July 1987.
8. Stalford, H., "On Robust Control of Wing Rock Using Nonlinear Control", 1987 American Control Conference, FP3, Minneapolis, Minnesota, June 10-12, 1987.
9. Rao, D.M. and Murri, D.G., "Exploratory Investigation of Deflectable Forebody Strakes for High-Angle-Of-Attack Yaw Control", AIAA 24th Aerospace Sciences Meeting, AIAA-86-0333, Reno, Nevada, January 14-19, 1986.

END

DATE
FILMED
5-88

DTIC